

AD-756 564

HYDRAULICS AND HEAT EXCHANGE IN
ELEMENTS OF POWER EQUIPMENT

V. N. Borishanskii, et al

Foreign Technology Division
Wright-Patterson Air Force Base, Ohio

30 October 1972

DISTRIBUTED BY:

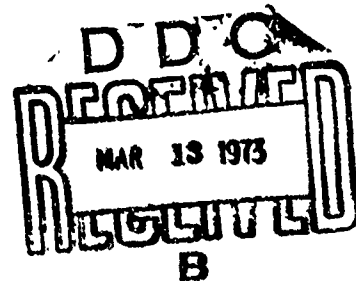
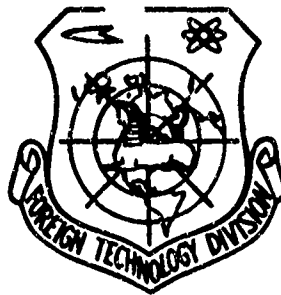
NTIS

National Technical Information Service
U. S. DEPARTMENT OF COMMERCE
5285 Port Royal Road, Springfield Va. 22151

FOREIGN TECHNOLOGY DIVISION



HYDRAULICS AND HEAT EXCHANGE IN ELEMENTS
OF POWER EQUIPMENT



AD 756564

Reproduced by
NATIONAL TECHNICAL
INFORMATION SERVICE
U S Department of Commerce
Springfield VA 22131

Approved for public release;
distribution unlimited.

EDITED MACHINE TRANSLATION

FTD-MT-24-309-72

HYDRAULICS AND HEAT EXCHANGE IN ELEMENTS OF POWER
EQUIPMENT

English pages: 516

Source: Gidravlika i Teploobmen v Elementakh
Energeticheskogo Oborudovaniya,
Leningrad, 1970, pp. 1-343.

Requester: FTD/PDTN

This document is a SYSTRAN machine aided trans-
lation post-edited for technical accuracy by:
Louise Heenan and Francis T. Russell

Approved for public release;
distribution unlimited.

THIS TRANSLATION IS A RENDITION OF THE ORIGINAL FOREIGN TEXT WITHOUT ANY ANALYTICAL OR EDITORIAL COMMENT. STATEMENTS OR THEORIES ADVOCATED OR IMPLIED ARE THOSE OF THE SOURCE AND DO NOT NECESSARILY REFLECT THE POSITION OR OPINION OF THE FOREIGN TECHNOLOGY DIVISION.

PREPARED BY:

TRANSLATION DIVISION
FOREIGN TECHNOLOGY DIVISION
WP-AFB, OHIO.

All figures, graphs, tables, equations, etc.
merged into this translation were extracted
from the best quality copy available.

C

UNCLASSIFIED
Security Classification

DOCUMENT CONTROL DATA - R & D		
(Security classification of title, body of abstract and indexing annotation must be entered when the overall report is classified)		
1. ORIGINATING ACTIVITY (Corporate author) Foreign Technology Division Air Force Systems Command U. S. Air Force		2a. REPORT SECURITY CLASSIFICATION UNCLASSIFIED
		2b. GROUP
3. REPORT TITLE HYDRAULICS AND HEAT EXCHANGE IN ELEMENTS OF POWER EQUIPMENT		
4. DESCRIPTIVE NOTES (Type of report and inclusive dates) Translation		
5. AUTHOR(S) (First name, middle initial, last name) Borishanskiy, V.M.; Andreyevskiy, A.A.; Fromzel', V.N.		
6. REPORT DATE 1970	7a. TOTAL NO. OF PAGES 518 528	7b. NO. OF REFS 437
8a. CONTRACT OR GRANT NO.	8b. ORIGINATOR'S REPORT NUMBER(S) FTD-MT-24-0309-72	
8c. PROJECT NO.		
8d. T69-04-9 T70-02-01B	8e. OTHER REPORT NO(S) (Any other numbers that may be assigned this report)	
10. DISTRIBUTION STATEMENT Approved for public release; distribution unlimited.		
11. SUPPLEMENTARY NOTES Details of illustrations in this document may be better studied on microfiche.		12. SPONSORING MILITARY ACTIVITY Foreign Technology Division Wright-Patterson AFB, Ohio
13. ABSTRACT This collection contains material from the III All Union Conference on heat exchange and hydraulic resistance in the motion of a two-phase flow in elements of power machinery and equipment. The conference was called by resolution of the Soviet AN "USSR" on the problem "High-Temperature Heat Physics" in April 1967 in Leninrad. This collection consists of three main sections. 1. Heat exchange during boiling and critical loads. 2. The hydraulics of two-phase flow. 3. Heat exchange during condensation. The first section includes reports on the intensity of heat exchange, critical loads, and thermal modes in elements of power equipment during the motion of two-phase flow. The second section deals with a study of the hydrodynamics of two-phase steam-water flows, stability, hydraulic resistance, and phase distribution during the motion of two-phase flow in channels of various shapes. The third section includes works on the intensity of heat transfer during film and droplet condensation, the condensation of liquid-metal vapors from a flow of inert gases, condensation on surfaces of various shapes (condensation on ribbed surfaces, vapor condensation during cross-spiral flow around vertical duct banks), as well as the results of a study on steam turbine surface condensers.		

DD FORM 1473
1 NOV 68

UNCLASSIFIED
Security Classification

UNCLASSIFIED
Security Classification

14.	KEY WORDS	LINK A		LINK B		LINK C	
		ROLE	WT	ROLE	WT	ROLE	WT
	High Temperature Heat Treatment Physics Heat Exchange Hydrodynamics						

UNCLASSIFIED
Security Classification

TABLE OF CONTENTS

U. S. Board on Geographic Names Transliteration System..	v
Designations of the Trigonometric Functions.....	vi
SECTION I. HEAT EXCHANGE DURING BOILING AND CRITICAL LOADS.....	1
HEAT TRANSFER AND HYDRAULIC RESISTANCE IN THE MOTION OF A TWO-PHASE STEAM-WATER FLOW IN CHANNELS OF VARIOUS SHAPES, by V. M. Borishanskiy, A. A. Andreyevskiy, V. N. Fromzel', I. B. Gavrilov, G. P. Danilova, and B. S. Fokin.....	2
THE EFFECT OF THE NUMBER OF VAPOR FORMATION CENTERS AND HEATING SURFACE PROCESSING PURITY ON HEAT EXCHANGE DURING THE BOILING OF FREONS, by G. N. Danilova.....	19
STUDY OF EXCHANGE FACTORS AND DROPLET DIFFUSION IN DISPERSED ANNULAR FLOW, by I. I. Paleyev, F. A. Agafonova, M. E. Lavrent'yev, and K. P. Malyus- Malitskiy.....	34
CHARACTERISTICS OF HEAT EXCHANGE DURING THE BOILING OF CERTAIN ORGANIC SOLUTIONS AND DISPERSED MEDIA, by G. M. Pludovskaya.....	43
A STUDY OF HEAT TRANSFER AND THERMAL MODES DURING THE FORCED FLOW OF WATER IN ECCENTRIC ANNULAR CHANNELS, by P. A. Andreyev, N. S. Alferov, and R. A. Rybin.....	49
PROBLEMS OF HEAT EXCHANGE DURING THE COOLING OF CRYOGENIC PIPING, by A. A. Gukhman, L. S. Aksel'rod, V. G. Fron'ko, A. B. Bulanov, D. A. Kazenin, and G. M. Leonova.....	60

CHARACTERISTICS OF HEAT EXCHANGE IN THICK-WALLED HORIZONTAL PIPES AND ANNULAR CHANNELS WITH LAMINAR FLOW OF A VAPOR-WATER MIXTURE, by L. B. Katsenelenbogen and Ya. N. Rudnitskiy.....	75
EXPERIMENTAL RESEARCH ON THE COOLING OF WORKING BLADE ELEMENTS IN A GAS TURBINE ENGINE BY A FINELY DIVIDED AIR-WATER MIXTURE, by L. M. Zysina-Molozhen, I. B. Uskov, and L. V. Zysin.....	89
A STUDY ON THE EFFECT OF FORCED LIQUID MOTION ON HEAT EXCHANGE DURING THE BOILING OF SEA WATER, by V. N. Slesarenko.....	102
CRITICAL THERMAL LOADS IN ANNULAR CHANNELS, by V. I. Polubinskiy, A. K. Litoshenko, and V. L. Shevtsov.....	113
RECOMMENDATION ON CRITICAL THERMAL LOADS IN CYLINDRICAL PIPES, by V. Ye. Doroshchuk and F. P. Lantsman.....	124
A MODEL OF THE BOILING CRISIS DURING FORCED MOTION OF A TWO-PHASE FLOW IN PIPES WITH HIGH OUTPUT VAPOR CONTENTS, by L. S. Kokorev, V. I. Petrovichev, and A. N. Borzyak..	143
AN EXPERIMENTAL STUDY OF CRITICAL LOADS IN STEAM- GENERATING CHANNELS IN THE VICINITY OF BENDS, by O. K. Smirnov and V. S. Polonskiy.....	151
THE MECHANISM OF AMALGAM BOILING, by I. Z. Kopp.....	159
EXPERIMENTAL STUDIES ON THE EFFECT OF DUCT MATERIAL ON THE HEAT TRANSFER OF BOILING MERCURY, by <u>I. I. Gel'man</u> and I. Z. Kopp.....	168
THE EFFECT OF GAS PHASE DISPERSION ON THE INTENSITY OF HEAT EXCHANGE BETWEEN PHASES AND ON THE FLOW PARAMETERS OF A TWO-PHASE FLUID MIXTURE, by D. I. Volkov and N. I. Malofeyev.....	183
THE DYNAMICS OF THE LIQUID BOILING PROCESS IN A FLOW WITH A LARGE PRESSURE GRADIENT, by V. A. Zysin and V. A. Barilobich.....	195
CLASSES OF MOTION FOR A TWO-PHASE DISPERSED FLOW WITH HEAT EXCHANGE BETWEEN PHASES, by N. I. Malofeyev.....	202
DYNAMIC CHARACTERISTICS OF A COUNTERFLOW HEAT EXCHANGE APPARATUS, by V. I. Kochurov and N. I. Tarakanov.....	215
THE SIMULATION OF WEAK GRAVITATIONAL FIELDS FOR STUDYING HEAT EXCHANGE DURING BOILING, by B. I. Verkin, Yu. A. Kirichenko, M. L. Dolgoiy, I. V. Lipatov, and A. I. Charkin.....	224

SECTION II. THE HYDRAULICS OF TWO-PHASE FLOW.....	243
FLOW PULSATIONS IN TYPES OF STEAM BOILERS, by O. M. Baldina, V. G. Zinkevich, R. I. Kalinin, and V. B. Khabenskiy.....	243
STABILITY OF STEAM-WATER FLOW IN A HEATED PIPE IN A SINGLE-LOOP SYSTEM, by G. G. Treshchev.....	259
THE HYDRODYNAMICS OF TWO-PHASE NONEQUILIBRIUM FLOWS, by Ye. I. Nevstruyev, D. A. Khlestkin, T. T. Antidze, and G. M. Dvorina.....	270
AN EXPERIMENTAL STUDY OF HYDRODYNAMIC CHARACTERISTICS DURING THE BOILING OF UNDERHEATED WATER IN VERTICAL PIPES, by G. G. Bartolomey and V. M. Chanturiya.....	279
THE EFFECT OF THERMAL FLUX AND THE GEOMETRIC SHAPES OF A CHANNEL ON THE VAPOR CONTENT PER UNIT VOLUME OF A MEDIUM DURING BOILING, by Z. L. Miropol'skiy, R. I. Shneyerova, A. I. Karamysheva, E. T. Semin, and M. N. Vinogradova...	298
CALCULATING THE VAPOR CONTENT FIELD IN CYLINDRICAL VERTICAL CHANNELS, by I. P. Kornyukhin.....	306
AN EXPERIMENTAL STUDY ON FLOW STABILITY IN STEAM-GENERATING PIPES WITH VARIABLE LENGTHS OF HEATED AND UNHEATED SECTIONS, by V. I. Lezin and O. K. Smirnov.....	313
STRUCTURE OF FLOW OF A STEAM-WATER MIXTURE IN A VERTICAL UNHEATED PIPE AT HIGH PRESSURES, by S. M. Lukomskiy, P. I. Povarnin, and R. I. Shneyerova.....	321
A METHOD OF CALCULATING CRITICAL PARAMETERS DURING PULSATION REGIMES IN THE MOTION OF A STEAM-WATER MIXTURE, by V. S. Polonskiy and Ye. P. <u>Serov</u>	334
EVALUATING CIRCULATION RELIABILITY IN HIGH-STRESS SHIP-BOARD BOILERS, by Yu. V. Aleksandrovskiy.....	343
THE OPERATION OF EVAPORATIVE LOOPS WITH HORIZONTAL AND DESCENDING MOTION OF A STEAM-WATER MIXTURE DURING NATURAL CIRCULATION, by Yu. I. Tseluyko, Ya. N. Rudnitskiy, A. D. Fayershteyn, L. B. Katsenelenbogen, and L. A. Strel'tsov.....	348
A STUDY OF THE HYDRAULICS OF STEAM-WATER FLOW USING AN EXAMPLE OF THE STEAM-GENERATING WELLS IN KAMCHATKA, by O. S. Naymanov.....	357

BASIC CHARACTERISTICS OF TWO-PHASE UNBALANCED STATIONARY FLOWS, by Ye. I. Nevstruyeva.....	371
THE ACCURACY OF CALCULATING WATER CIRCULATION ON ELECTRONIC COMPUTERS, by G. I. Zinger and L. N. Papernaya.....	383
SECTION III. HEAT TRANSFER WITH CONDENSATION.....	388
CALCULATION AND TEST DATA FOR THE HEAT TRANSFER FACTOR DURING THE CONDENSATION OF MOVING STEAM ($Re_{\kappa} < Re_{\kappa \kappa p}$), by L. D. Berman.....	388
THE CONDENSATION OF VAPOR ON RIBBED SURFACES, by N. V. Zozulya and V. A. Karkhu.....	406
HEAT AND MASS TRANSFER DURING CONDENSATION OF STEAM FROM SATURATED AIR IN AN ANNULAR DUCT, by L. S. Bobe, D. V. Pavlov, and D. D. Malyshev.....	414
EXPERIMENTAL STUDY OF HEAT EXCHANGE IN DROPWISE CONDEN- SATION OF STEAM WITH THE USE OF HIGH-SPEED FILMING, by P. F. Vlasov.....	427
QUESTIONS OF THE CONDENSATION OF VAPORS OF ALKALI METALS, by B. L. Paskar' and N. N. Kochurova.....	435
GENERALIZATION OF EXPERIMENTAL DATA ON HEAT TRANSFER DURING CONDENSATION VAPOR OF MOVING INSIDE HORIZONTAL DUCTS UNDER CONDITIONS OF LOW AND MODERATE VELOCITIES, by D. I. Volkov.....	441
A STUDY OF QUESTIONS OF THE KINETICS OF CONDENSATION OF WATER, by N. N. Kochurova.....	459
CONDENSATION OF CESIUM VAPORS FROM A FLOW OF INERT GASES, by K. M. Aref'yev, V. M. Borishanskiy, T. V. Zablotskaya, N. I. Ivashchenko, I. I. Paleyev, and B. M. Khomchenkov.....	467
A STUDY OF THE PROCESS OF CONDENSATION OF A MULTI- COMPONENT MIXTURE OF HYDROCARBON GASES IN A VERTICAL TUBE, by V. D. Dvoyris.....	492

U. S. BOARD ON GEOGRAPHIC NAMES TRANSLITERATION SYSTEM

Block	Italic	Transliteration	Block	Italic	Transliteration
А а	<i>А а</i>	A, a	Р р	<i>Р р</i>	R, r
Б б	<i>Б б</i>	B, b	С с	<i>С с</i>	S, s
В в	<i>В в</i>	V, v	Т т	<i>Т т</i>	T, t
Г г	<i>Г г</i>	G, g	У у	<i>У у</i>	U, u
Д д	<i>Д д</i>	D, d	Ф ф	<i>Ф ф</i>	F, f
Е е	<i>Е е</i>	Ye, ye; E, e*	Х х	<i>Х х</i>	Kh, kh
Ж ж	<i>Ж ж</i>	Zh, zh	Ц ц	<i>Ц ц</i>	Ts, ts
З з	<i>З з</i>	Z, z	Ч ч	<i>Ч ч</i>	Ch, ch
И и	<i>И и</i>	I, i	Ш ш	<i>Ш ш</i>	Sh, sh
Й й	<i>Й й</i>	Y, y	Щ щ	<i>Щ щ</i>	Shch, shch
К к	<i>К к</i>	K, k	Ъ ъ	<i>Ъ ъ</i>	"
Л л	<i>Л л</i>	L, l	Ы ы	<i>Ы ы</i>	Y, y
М м	<i>М м</i>	M, m	Ь ь	<i>Ь ь</i>	'
Н н	<i>Н н</i>	N, n	Э э	<i>Э э</i>	E, e
О о	<i>О о</i>	O, o	Ю ю	<i>Ю ю</i>	Yu, yu
П п	<i>П п</i>	P, p	Я я	<i>Я я</i>	Ya, ya

* ye initially, after vowels, and after ъ, ь; e elsewhere.
 When written as ѣ in Russian, transliterate as yě or ě.
 The use of diacritical marks is preferred, but such marks
 may be omitted when expediency dictates.

FOLLOWING ARE THE CORRESPONDING RUSSIAN AND ENGLISH
DESIGNATIONS OF THE TRIGONOMETRIC FUNCTIONS

Russian	English
sin	sin
cos	cos
tg	tan
ctg	cot
sec	sec
cosec	csc
sh	sinh
ch	cosh
th	tanh
cth	coth
sch	sech
csch	csch
arc sin	\sin^{-1}
arc cos	\cos^{-1}
arc tg	\tan^{-1}
arc ctg	\cot^{-1}
arc sec	\sec^{-1}
arc cosec	\csc^{-1}
arc sh	\sinh^{-1}
arc ch	\cosh^{-1}
arc th	\tanh^{-1}
arc cth	\coth^{-1}
arc sch	sech^{-1}
arc csch	csch^{-1}
<hr/>	
rot	curl
lg	log

This collection contains material from the III All Union Conference on heat exchange and hydraulic resistance in the motion of a two-phase flow in elements of power machinery and equipment. The conference was called by resolution of the Soviet AN USSR on the problem "High-Temperature Heat Physics" in April 1967 in Leningrad.

This collection consists of three main sections.

1. Heat exchange during boiling and critical loads.
2. The hydraulics of two-phase flow.
3. Heat exchange during condensation.

The first section includes reports on the intensity of heat exchange, critical loads, and thermal modes in elements of power equipment during the motion of two-phase flow.

The second section deals with a study of the hydrodynamics of two-phase steam-water flows, stability, hydraulic resistance, and phase distribution during the motion of two-phase flow in channels of various shapes.

The third section includes works on the intensity of heat transfer during film and droplet condensation, the condensation of liquid-metal vapors from a flow of inert gases, condensation on surfaces of various shapes (condensation on ribbed surfaces, vapor condensation during cross-spiral flow around vertical duct banks), as well as the results of a study on steam turbine surface condensers.

Some of the reports from the conference will be published in the coming issues of "Trudy TsKTI."

SECTION I

HEAT EXCHANGE DURING BOILING
AND CRITICAL LOADS

HEAT TRANSFER AND HYDRAULIC RESISTANCE IN THE MOTION OF A TWO-PHASE STEAM-WATER FLOW IN CHANNELS OF VARIOUS SHAPES

V. M. Borishanskiy, A. A. Andreyevskiy,
V. N. Fromzel', I. B. Gavrilov,
G. P. Danilova, and B. S. Fokin

Designations

- q - heat flux, kcal/m²·h;
 p - pressure, atm (abs.);
 w_0 - circulation velocity, m/s;
 w_γ - mass velocity, kg/m²·s;
 γ' - specific weight of liquid phase, kg/m³;
 γ'' - specific weight of vapor phase, kg/m³;
 x - vapor content per unit weight;
 $\gamma_{cm} = \frac{\gamma'\gamma''}{x\gamma' + (1-x)\gamma''}$ - specific weight of two-phase mixture, kg/m³;
 $\Delta p_{полн}$ - full head loss, kg/cm²;
 $\Delta p_{уск}$ - head loss from acceleration, kg/cm²;
 $\Delta p_{тр}$ - head loss from friction, kg/cm²;
 G_{cm} - consumption by weight of two-phase mixture kg/h;
 $w_{cm} = w_0 \left[1 + \left(\frac{\gamma' - \gamma''}{\gamma'} \right) x \right]$ - reduced velocity of two-phase mixture in duct, m/s;
 w_n - reduced velocity of vapor phase, m/s;

w'_n - reduced velocity of liquid phase, m/s;
 ϕ - true vapor content [2];
 ζ - coefficient of friction;
 α - heat transfer factor, kcal/m²·h·°C;
 μ'' - dynamic viscosity factor of saturated vapor, kg/s·m²;
 μ' - dynamic viscosity factor of water on the saturation line, kg/s·m²;
 μ_{cm} - dynamic viscosity factor of two-phase mixture, kg/s·m²;
 ν - kinematic viscosity factor, m²/s;
 r - heat of vaporization, kcal/kg;
 $We = w_{cm} \mu' / \sigma$ - surface tension criterion;
 Re - Reynolds number;
 вых - output;
 вх - input; тр - friction;
 конв - conv.; полн - full;
 расч - calc.; уск - acceleration;
 дф - two-phase; см - mixture;
 тр воды - water friction;
 тр пара - steam friction.

In this article we shall present the results of an experimental study on heat transfer and hydraulic resistance during motion of a two-phase flow in channels of various shapes. Tests were performed on an open circulation loop which consisted of the following basic elements:

- 1) a working section (with electric heating);
- 2) a mixer designed to obtain a steam-water flow with the necessary degree of dryness;
- 3) a system to feed water and steam of the prescribed parameters to the mixer.

This installation and the experimental methodology used, as well as the basic characteristics of the working sections, are presented in reference [1]. Heat transfer and hydraulic resistance were studied during the motion of a two-phase flow in ducts 8, 12, and 18 mm in diameter. Tests were carried out in the following range of basic parameter variations:

heat flux $q = (300-1200) 10^3 \text{ kcal/m}^2 \cdot \text{h}$,

working section pressure $p = 5-36 \text{ atm (abs.)}$,

reduced velocity of two-phase mixture $w_{\text{CM}} = 2.5-200 \text{ m/s}$,

circulation velocity $w_0 = 0.2-5 \text{ m/s}$,

mass velocity $w_\gamma = 180-5000 \text{ kg/m}^2 \cdot \text{s}$,

specific weight of mixture $\gamma_{\text{CM}} = 5-700 \text{ kg/m}^3$,

vapor content per unit weight $x = 0.05-0.99$.

Hydraulic resistance was determined both during isothermal motion of a two-phase mixture and in the presence of heat release in the working section. Pressure loss from friction was calculated from the following expression:

$$\Delta p_{\text{fp}} = \Delta p_{\text{ном}} - \Delta p_{\text{yck}} \quad (1)$$

Pressure loss from acceleration was calculated for two models of flow motion:

a) for a homogeneous model (no slippage between phases)

$$\Delta p_{\text{yck}} = -\frac{G_{\text{CM}}}{3600 g F} (w_{\text{CM}_{\text{max}}} - w_{\text{CM}_{\text{bx}}}) 10^{-4}; \quad (2)$$

b) for a stratified model

$$\Delta p_{\text{str}} = \frac{G_{\text{cu}}^2}{100g\mu^2} \left\{ \left[\frac{(1-x)^2}{(1-x)^2} + \frac{x^2}{x^2} \right]_{\text{max}} - \left[\frac{(1-x)^2}{(1-x)^2} + \frac{x^2}{x^2} \right]_{\text{in}} \right\} 10^{-4}. \quad (3)$$

During isothermal flow losses from acceleration were calculated only for those modes for which the difference in input and output velocities was greater than 5%.

The temperature of the two-phase flow was determined at input and output of the working section. Wall temperature was measured in cross sections (every 100 mm) along the length of the duct. This method of measuring was adopted to determine the local value of the heat transfer factor in any cross section of the working section.

TEST RESULTS

1. Heat transfer to a two-phase steam-water flow moving in ducts. From analysis of numerous experimental works performed both in the Soviet Union and abroad, we find that the main distinction between each transfer during boiling in pipes and heat transfer during boiling on immersed surfaces is the presence in the first case of two factors - circulation velocity w_0 and vapor content x .

Foreign literature contains formulas where the dimensionless heat transfer factor during boiling in pipes is defined as a function of the Martinelli parameter:

$$\frac{\alpha}{\alpha_{\text{hkb}}} = A \left(\frac{1}{X} \right)^n, \quad (4)$$

where

$$\frac{1}{X} = \left(\frac{x}{1-x} \right)^{0.9} \left(\frac{v^*}{v'} \right)^{0.5} \left(\frac{\mu^*}{\mu'} \right)^{0.1}.$$

A substantial disadvantage of functions of this type is the fact that they do not take into account the effect of thermal loading on heat transfer during boiling. To account for the effect of q , it is necessary to introduce a correction factor which is quite difficult to calculate.

The most familiar formulas in the Soviet Union, introduced in the works of S. S. Kutateladze [3] and L. S. Sterman [4], are derived on the basis of an analysis of tests in which there was no significant effect of vapor content on heat transfer (tests were performed at low x). In this case, the value of the heat transfer factor is determined uniquely at constant pressure by the mutual effect of heat flux q and circulation velocity w_0 . The formula proposed by S. S. Kutateladze, for these conditions, has the form:

$$\frac{\alpha_{\text{pac}}}{\alpha_0} = \sqrt[n]{1 + \left(\frac{\alpha_{00}}{\alpha_0}\right)^n}. \quad (5)$$

Here α_{pac} is the heat transfer factor during the development of boiling in pipes; α_0 is the heat transfer factor during the forced movement of liquid (with velocity w_0) without boiling [5]:

$$\alpha_0 = 0,023 \frac{\lambda}{D} \text{Re}^{0,8} \text{Pr}^{0,4};$$

α_{00} is the heat transfer factor during boiling in pipes for the region where the circulation velocity still does not affect the intensity of heat transfer during boiling [5]:

$$\alpha_{00} = 0,7 \alpha_{0,0}; \quad \alpha_{0,0} = 3(\rho^{0,14} + 1,83 \cdot 10^{-4} p) q^{0,7}.$$

However, there are a number of experimental works [6] in which there has been observed an increase in the heat transfer factor along the length of a duct with a growth in vapor content (tests were performed at rather high vapor contents). The amount by which the heat transfer coefficient exceeds (for the case of the vapor content effect) that calculated from the formula

presented above depends both on the value of circulation velocity and the vapor content in a two-phase flow. Under these conditions, circulation velocity w_0 cannot be used as the only parameter accounting for the effect of forced motion on heat transfer. To clarify the parameters on which heat transfer depends in the presence of higher vapor content, experimental data was first processed using the ratio $\alpha/\alpha_{\text{pac}}$ where α_{pac} is the heat transfer factor calculated according to expression (5). The introduction of this ratio enables us to exclude from our examination that effect of circulation velocity and heat flux which appears in the zone of low vapor contents and is accounted for by formula (5). Analysis of the experimental data thus represented indicated that the additional mutual effect of w_0 and x in the zone of increased vapor contents is best accounted for if we take as the determining velocity w_{CM} (reduced velocity of the two-phase mixture).

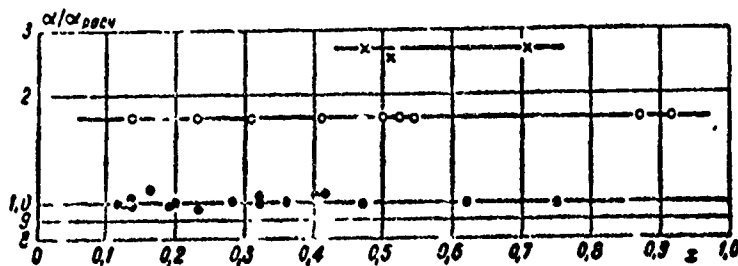


Fig. 1. Heat transfer factor versus vapor content per unit weight ($p = 19$ atm (abs.)):
 $q = 300 \cdot 10^3$ kcal/m²·h):

● - $w_{\text{CM}} = 15$ m/s; ○ - $w_{\text{CM}} = 60$ m/s; × - $w_{\text{CM}} = 115$ m/s.

As an example, Fig. 1 presents the function $\alpha/\alpha_{\text{pac}} = f(x)$ when $q = \text{const}$ and $p = \text{const}$, plotted for several constant values of parameter w_{CM} . From the graph it follows that mixture velocity w_{CM} uniquely accounts for the effect of forced motion on the relative growth of the heat transfer factor in the case examined since neither a change in x nor a change in w_0 when $w_{\text{CM}} = \text{const}$ alters the value of the ratio $\alpha/\alpha_{\text{pac}}$. The mutual effect of thermal flux q and mixture velocity on heat transfer is shown

in Fig. 2. The relative effect w_{CM} is manifest more strongly the less the thermal flux q . For heat flux $q = 300,000 \text{ kcal/m}^2 \cdot \text{h}$ and $w_{CM} = 120 \text{ m/s}$ the value of the measured heat transfer factor exceeds that calculated from formula (5) by a factor of 2.6. In reference [7] it was shown that in the region of elevated vapor contents the mutual effect of q and w_{CM} is best accounted for by introducing the complex $\frac{w_{CM}}{q r_i}$. Figure 3 shows the results of processing in coordinates $\alpha/\alpha_{pac} = f(\frac{w_{CM}}{q r_i})$ of experimental data obtained in this work and also in references [8-14, 19]. Plotted on the graph are both points obtained from tests, where the effect of vapor content on heat transfer was apparent (data of the authors and [13, 14]) and points from such tests where this effect was not noticeable [8, 9, 10, 11, 12]. From the graph it follows that the experimental points are grouped quite satisfactorily along a single averaging curve, which can be described by the following empirical equation:

$$\frac{\alpha}{\alpha_{pac}} = \left[1 + 1.5 \cdot 10^{-8} \left(\frac{w_{CM} r_i}{q} \right)^{3/2} \right]^{1/2}. \quad (6)$$

Here α_{pac} is the heat transfer factor during the development of boiling, calculated from formula (5), proposed by S. S. Kutateladze.

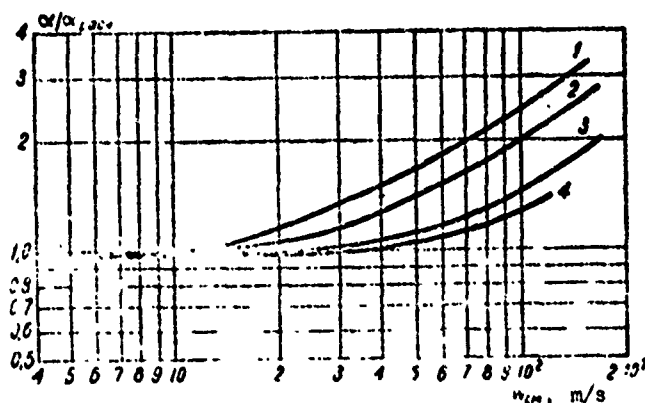


Fig. 2. Heat transfer factor versus mixture velocity and thermal load

($p_{ex} = 19 \text{ atm (abs.)}$):

- 1 - $q = 300 \cdot 10^3 \text{ kcal/m}^2 \cdot \text{h}$; 2 - $q = 500 \cdot 10^3$
- $\text{kcal/m}^2 \cdot \text{h}$; 3 - $q = 800 \cdot 10^3 \text{ kcal/m}^2 \cdot \text{h}$;
- 4 - $q = 1200 \cdot 10^3 \text{ kcal/m}^2 \cdot \text{h}$.

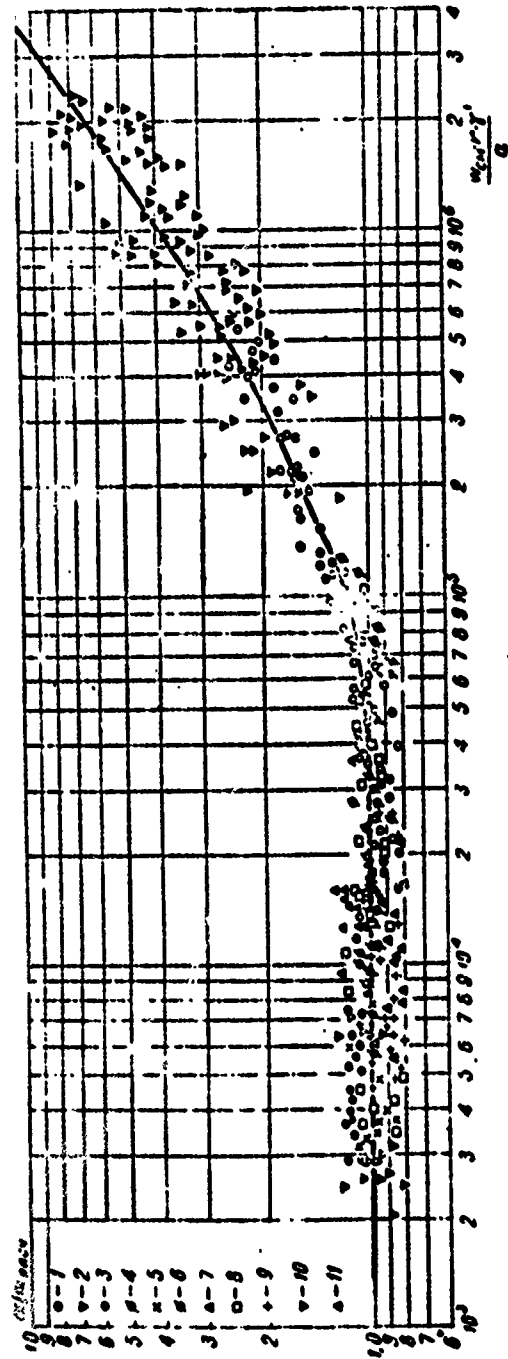


Fig. 3. Heat transfer during the motion of a two-phase flow in pipes and channels (combined graph) $\frac{q}{G} = \left[1 + 1.5 \cdot 10^{-3} \left(\frac{G}{q} \right)^{1.5} \right]^{1/2}$.

- 1 - Pipe \varnothing 8, 12, 18 mm, $p = 5-31$ atm (abs.) (data from this work); 2 - pipe \varnothing 6.95 mm, $p = 2-7$ atm (abs.) [14]; 3 - pipe \varnothing 8 mm, $p = 17$ atm (abs.) [13]; 4 - pipe \varnothing 16 mm, $p = 7$ atm (abs.) [10]; 5 - pipe \varnothing 4 mm, $p = 1-9$ atm (abs.) [8]; 6 - pipe \varnothing 13.75 mm, $p = 20, 40, 60, 80$ atm (abs.) [19]; 7 - pipe \varnothing 10 mm, $p = 80, 100$ atm (abs.) [9]; 8 - slots $d_{\text{эжв}} = 1; 0.5$ mm, $p = 50, 150$ atm (abs.) [9]; 9 - pipe \varnothing 32 mm, $p = 30, 40$ atm (abs.) [12]; 10 - bundle $d_{\text{эжв}} = 9.47$ mm, $p = 50, 100$ atm (abs.) [12]; 11 - slots $d_{\text{эжв}} = 5.76, 3.87$ mm, $p = 50, 100$ atm (abs.) [12].

Expression (6) is substantiated by test data in the following parameter range: $p = 2-170$ atm (abs.), $q = 70 \cdot 10^3 - 5 \cdot 10^6$ kcal/m²·h; $w_{cm} = 1-300$ m/s.

Thus a single formula is obtained for calculating the heat transfer factor during boiling in pipes and channels throughout the range of crisisless modes.

In addition to data with respect to pipes, the graphs also presents experimental points with respect to heat transfer in annular slots [9, 12] and longitudinally streamlined bunches of rods (data of the authors and [12]). It should be noted that as yet there is no single opinion regarding the quantity α_{00} for annular slots and bundles. Thus, based on data in [9], for slots $\alpha_{00} = 0.7 \alpha_{6.0}$ and, based on data in [12], $\alpha_{00} = \alpha_{6.0}$.

For longitudinally streamlined bundles of rods, both V. G. Morozov [12] and the authors of this article have obtained values for α_{00} unlike the values obtained for pipes and equal to $\alpha_{6.0}$. The absence of a sufficient quantity of experimental data makes it impossible to explain the reason for this difference. In connection with this situation, when comparing the examined test data various values of α_{00} ($\alpha_{00} = 0.7 \alpha_{6.0}$ [9], $\alpha_{00} = \alpha_{6.0}$ [12] and our test data) are assumed.

2. Hydraulic resistance during the motion of two-phase flow in pipes. Generally hydraulic resistance during the motion of a two-phase flow in pipes is made up of a number of components. They include losses from the longitudinal acceleration of liquid and vapor phases, losses from wave formation on the phase interface, losses from the separation of droplets from the surface of liquid phase, from the formation and breakup of bubbles, from friction in the boundary layer of liquid, etc. At present it is possible in practice to distinguish from total losses those losses due to longitudinal acceleration (2), (3). Because of this the

majority of authors conditionally define losses from friction in a two-phase flow as the difference between full hydraulic pressure and losses from longitudinal acceleration (1).

Posing the problem in such a manner usually involves two simplified models of two-phase flow: a homogeneous model and a model of two averaged phases. Both models are used in processing experimental data. In the first case, based on analogy with single-phase flow, hydraulic losses from friction can be calculated from formula:

$$\Delta p_{fp} = \zeta_{\Delta\phi} \frac{\gamma_{cm} w_{cm}^2}{2g} \cdot \frac{l}{d}, \quad (7)$$

where $\zeta_{\Delta\phi}$ is the coefficient of resistance for a two-phase mixture. When $w_{\Pi}'' = 0$ or $w_{\Pi}' = 0$, expression (7) changes to the usual formulas for single-phase flow

$$\Delta p_{fp \text{ steam}} = \zeta_1' \frac{\gamma_1' w_1'^2}{2g} \cdot \frac{l}{d} \quad \text{and} \quad \Delta p_{fp \text{ water}} = \zeta_2'' \frac{\gamma_2'' w_2''^2}{2g} \cdot \frac{l}{d}.$$

If we assume that the coefficient of hydraulic resistance for two-phase mixture is equal to the coefficient of resistance for a single-phase flow and does not depend upon the Reynolds number, i.e.,

$$\zeta_{\Delta\phi} = \zeta_1' = \zeta_2'', \quad (8)$$

then expression (7) becomes equivalent to formula:

$$\Delta p_{fp} = \zeta \frac{\gamma_1' w_1'^2}{2g} \cdot \frac{l}{d} \left[1 + \left(1 - \frac{\gamma_1'}{\gamma_2''} \right) \frac{w_2''^2}{w_1'^2} \right]. \quad (9)$$

The last formula is recommended for calculating losses from friction by design standards for water circulation in steam boilers. However, taking expression (8) as a postulate is not well founded (at least for smooth pipes). We can assume that the coefficient of resistance during the motion of a two-phase flow in stainless steel pipes will be a variable quantity over a wide range of velocity variations. Experimental data obtained in

this work confirmed this. Figure 4 presents the dependence of resistance on reduced velocity of a two-phase mixture for experimental data obtained in the pressure range 5-36 kg/m² in pipes 8, 12, and 18 mm in diameter both with isothermal purging and with heat release in the working section.

In Fig. 5 the experimental points, obtained for the entire range of specific thermal loads, pressures, and working section diameters, are compared with the data of other authors [15, 16, 17] for pressures up to 180 kg/cm². A single averaging line with exponent can be drawn through all experimental points at a velocity of $m = 1.75$, i.e., from the graph it follows that the coefficient of friction resistance during the motion of a two-phase mixture in pipes is inversely proportional to velocity to the power $n = 0.25$:

$$\zeta = \frac{\Delta p_{tp}}{\gamma_{cm} \cdot L} \cdot \frac{d}{L} \sim \frac{1}{w_{cm}^{0.25}} \quad (10)$$

Figure 6 shows the coefficient of friction ζ versus w_{cm} , plotted according to the data from this work and [15, 16, 17, 18]. A single averaging line, described by the following empirical equation, can be drawn through all experimental points:

$$\zeta = \frac{0.04}{w_{cm}^{0.25}} \quad (11)$$

The disadvantage of the calculation formula obtained is its dimensioned form. However, reducing function (11) to dimensionless form by a formal introduction of viscosity with respect to formulas of the type:

$$\frac{1}{\gamma_{cm}} = \frac{x}{\mu''} + \frac{(1-x)}{\mu'};$$

$$\rho_{cm} = x\rho'' + (1-x)\rho'$$

was not advisable since these formulas make it possible to generalize the experimental points only in a comparatively narrow pressure range.

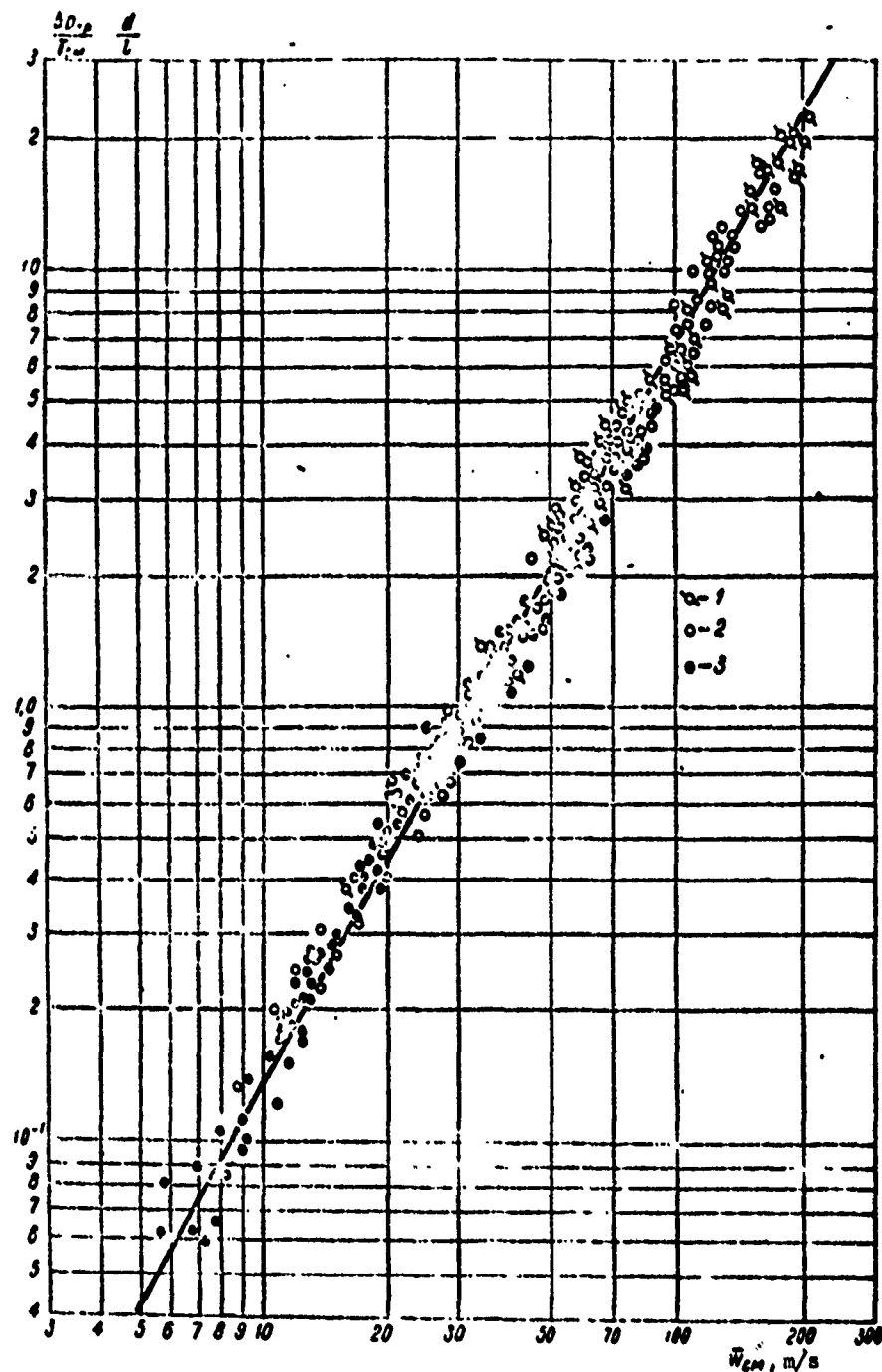


Fig. 4. Friction resistance versus the velocity of a two-phase mixture (pipe \varnothing 8, 12, 18 mm):
 1 - Working section \varnothing 8 mm ($q = 300 \cdot 10^3 - 800 \cdot 10^3$ kcal/m²·h, $p = 5-36$ atm (abs.)); 2 - Working section \varnothing 12 mm ($q = 0-1200 \cdot 10^3$ kcal/m²·h, $p = 5-31$ atm (abs.)); 3 - Working section \varnothing 18 mm, ($q = 0-800 \cdot 10^3$ kcal/m²·h, $p = 5-31$ atm (abs.)).

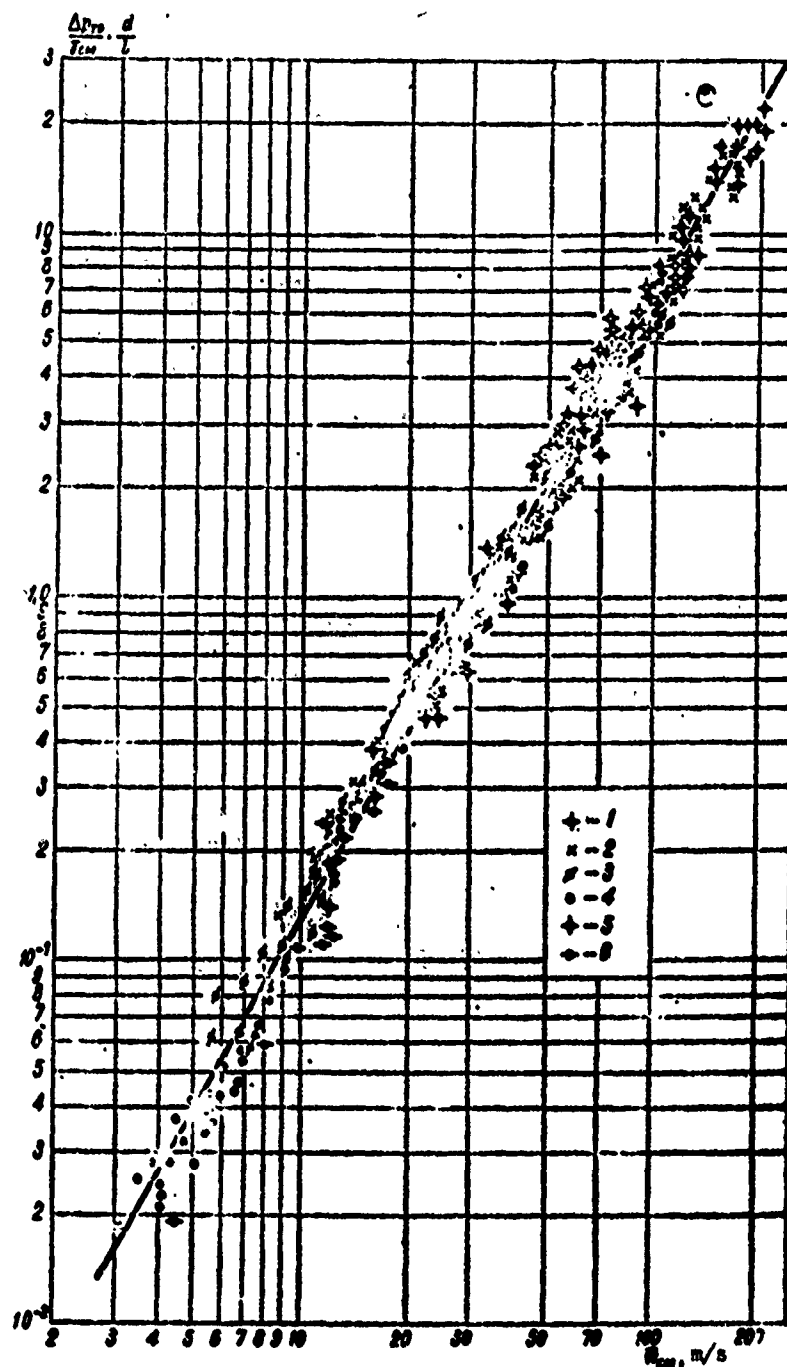


Fig. 5. Friction resistance versus velocity of a two-phase mixture (combined graph):
 1 - Working section \varnothing 8 mm ($q = 300 \cdot 10^3 - 800 \cdot 10^3$ kcal/m²·h, $p = 5-36$ atm (abs.)); 2 - Working section \varnothing 12 mm ($q = 0-1200 \cdot 10^3$ kcal/m²·h, $p = 5-31$ atm (abs.)); 3 - Working section \varnothing 18 mm ($q = 0-800 \cdot 10^3$ kcal/m²·h, $p = 5-31$ atm (abs.)); 4 - Working section \varnothing 8.5 mm ($p = 16-181$ atm (abs.)) [17]; 5 - Working section \varnothing 13 mm ($q = 300 \cdot 10^3 - 1200 \cdot 10^3$ kcal/m²·h, $p = 4$ atm (abs.)) [18]; 6 - Working section \varnothing 29.9 mm ($p = 40-70$ atm (abs.)) [19].

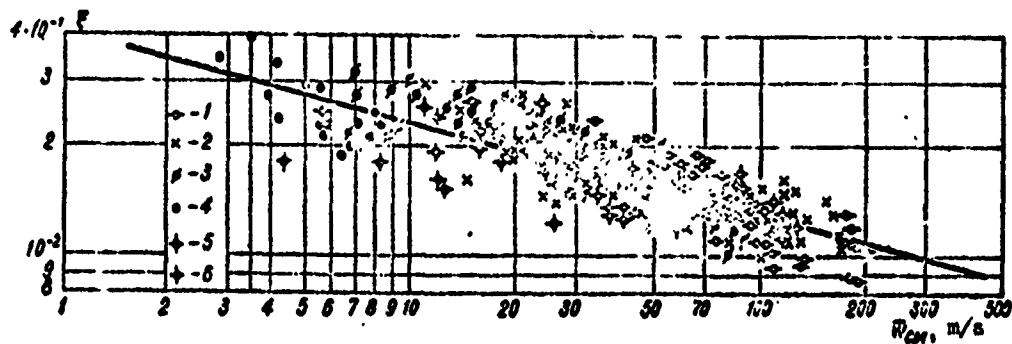


Fig. 6. Coefficient of friction for the mixture versus velocity (combined graph),

$$f = \frac{0.04}{\text{Re}^{0.25}} \dots$$

1 - Working section \varnothing 8 mm ($q = 300 \cdot 10^3$ kcal/m²·h, $p = 5-36$ atm (abs.)); 2 - Working section \varnothing 12 mm ($q = 0-1200 \cdot 10^3$ kcal/m²·h, $p = 5-31$ atm (abs.)); 3 - Working section \varnothing 18 mm ($q = 0-800 \cdot 10^3$ kcal/m²·h, $p = 5-31$ atm (abs.)); 4 - Working section \varnothing 8.5 mm ($p = 16-181$ atm (abs.)) [17]; 5 - Working section \varnothing 29.9 mm ($p = 40-70$ atm (abs.)) [19]; 6 - Working section \varnothing 13 mm ($q = 300 \cdot 10^3-1200 \cdot 10^3$ kcal/m²·h [18].

When using the "two averaged phases" model, each of the phases is characterized by its own average velocity, i.e., the slippage effect is taken into account. When using this model it is proposed that any liquid phase in the form of a ring-shaped layer moves along the walls of the pipe. Because of this, in the processing of the experimental data, the average true velocity of the water (with allowance for slippage) was taken as the determining velocity, while from the physical parameters - the viscosity of the liquid.

The real picture of the motion of a two-phase flow is incomparably more complex than the model studied. On the boundary between liquid and vapor phases wave formation occurs. At certain flow velocities the separation of wave crests and the entrainment of the forming droplets into the main body of the flow occur.

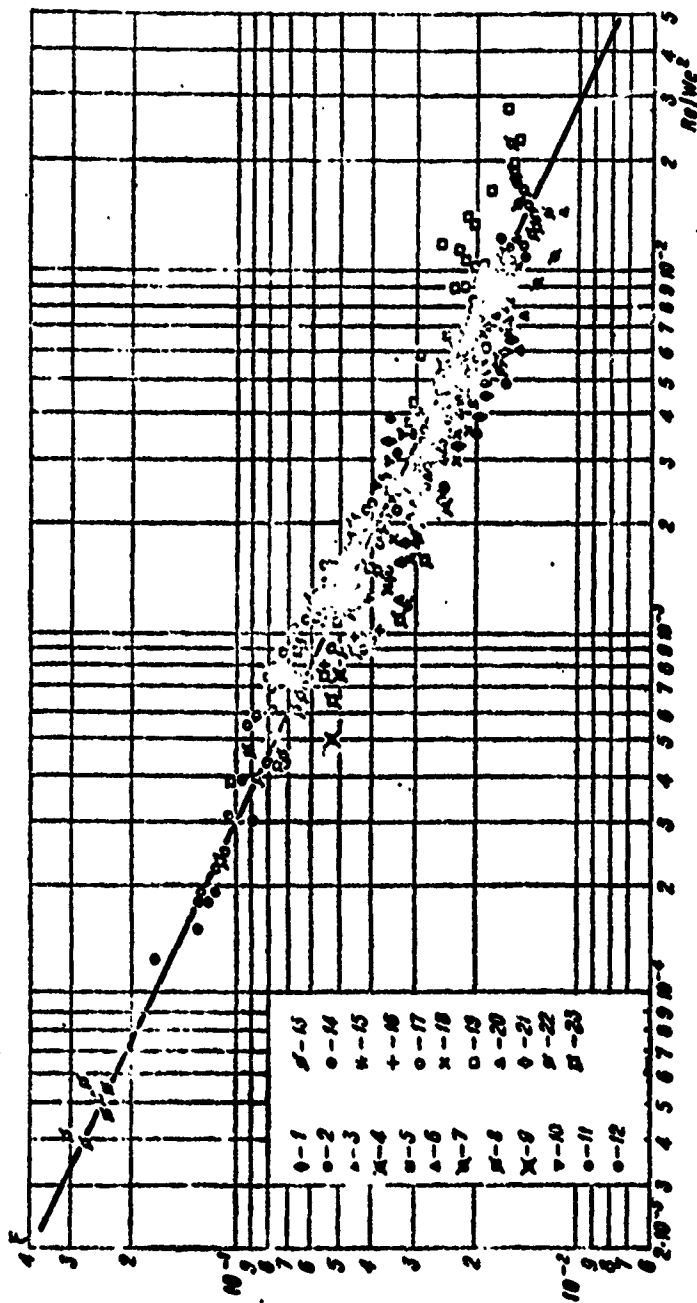


Fig. 7. Hydraulic resistance during friction of a two-phase flow in pipes, $\zeta = 1.7 \cdot 10^{-3} \frac{W_c}{Re^{0.5}}$:

Working section $\varnothing 18$ mm ($q = 0.800 \cdot 10^3$ kcal/m²·h): 1 - $p = 5$ atm (abs.); 2 - $p = 19$ atm (abs.); 3 - $p = 26$ atm (abs.); 4 - $p = 31$ atm (abs.). Working section $\varnothing 12$ mm ($q = 0.1200 \cdot 10^3$ kcal/m²·h): 5 - $p = 5$ atm (abs.); 6 - $p = 11$ atm (abs.); 7 - $p = 19$ atm (abs.); 8 - $p = 26$ atm (abs.); 9 - $p = 31$ atm (abs.). Working section $\varnothing 8$ mm ($q = 0.800 \cdot 10^3$ kcal/m²·h): 10 - $p = 5$ atm (abs.); 11 - $p = 11$ atm (abs.); 12 - $p = 26$ atm (abs.); 13 - $p = 36$ atm (abs.). Working section $\varnothing 8.5$ mm [17] ($q = 0.1000 \cdot 10^3$ kcal/m²·h): 14 - $p = 81$ atm (abs.); 15 - $p = 131$ atm (abs.); 16 - $p = 181$ atm (abs.). Working section $\varnothing 8.22$ mm [15] ($q = 0.1000 \cdot 10^3$ kcal/m²·h): 17 - $p = 26$ atm (abs.); 18 - $p = 100$ atm (abs.); 19 - $p = 170$ atm (abs.). Working section $\varnothing 8$ mm [16] ($q = 0$): 20 - $p = 50$ atm (abs.); 21 - $p = 100$ atm (abs.); 22 - $p = 150$ atm (abs.). Working section $\varnothing 5$ mm [14]: 23 - $p = 4-7$ atm (abs.) ($q = 0$).

The opposite phenomenon also takes place - the precipitation of droplets from the main body of the flow onto the wall. Wave formation, droplet separation, bubble breakup, etc., are connected with the surmounting of surface tension forces. Consequently, among the criteria which characterize the process, along with the Reynolds number there must also be included the surface tension criteria proposed by L. A. Vitman [20]. As a linear dimension in the surface tension criterion the following quantity was assumed [3]:

$$l = \sqrt[3]{\frac{\sigma}{\rho}}. \quad (12)$$

Figure 7 shows the coefficient of resistance ζ as a function of Re/We^2 (ζ was calculated based on true mixture velocity and true specific mixture weight).

It is apparent from the graph that experimental data from various authors agree satisfactorily. A single averaging line, described by the following expression, can be drawn through all experimental points:

$$\zeta = 1,7 \cdot 10^{-3} \frac{We}{Re^{0,5}}. \quad (13)$$

BIBLIOGRAPHY

1. Боришанский В. М. [и др.]. Охлаждение поверхности нагрева двухфазным пароводяным потоком. «Труды ЦКТИ», вып. 86, Л., 1968.
2. Шатерова Р. Н. Экспериментальное исследование истинных паросодержаний и гидравлических сопротивлений в парогенерирующих трубах с применением радиоизотопных методов (Автореферат диссертации на соискание ученой степени к. т. н.). МЭИ, 1965.
3. Кутателадзе С. С. Основы теории теплообмена. Машгиз, 1962.
4. Стерман Л. С. Исследование теплообмена при кипении жидкости в трубах. ЖТФ, т. 24, вып. 2, 1954.
5. Боришанский В. М., Козырев А. П., Свєглова Л. С. Изучение теплообмена при пузырьковом кипении. В сб.: «Конвективная теплопередача в двухфазном потоке». Изд-во «Энергия», 1964.
6. Кичигин М. А., Тобилевич Н. Ю. Экспериментальное исследование теплопередачи при кипении на специальных стендах и заводских выпарных аппаратах. Сб. работ Киевского филиала ЦНИС, 1946—1949, изд. 1951.
7. Боришанский В. М. [и др.]. Теплоотдача к двухфазному потоку. «Теплоэнергетика», 1969, № 5.

8. Аверин Е. К., Кружилли Г. Н. Теплоотдача при кипении воды в условиях вынужденной циркуляции. «Теплоотдача и тепловое моделирование». М., Академиздат, 1959.
9. Андреев П. А., Алферов Н. С., Рыбин Р. А. Теплоотдача при движении кипящей жидкости в трубах и каналах. «Труды ЦКТИ», вып. 78. Л., 1967.
10. Стерман Л. С., Стюшин Н. Г. Влияние скорости движения жидкости на теплообмен при кипении. ЖТФ, 22, 446 (1952), № 3.
11. Морозов В. Г. Исследование теплоотдачи при кипении воды в трубах. В сб.: «Конвективная теплопередача в двухфазном и однофазном потоке». Изд-во «Энергия», 1964.
12. Морозов В. Г., Рыдин Ю. Ю. Исследование теплообмена при кипении в кольцевых каналах и грубых пучках. В сб.: «Конвективная теплопередача в двухфазном и однофазном потоке». Изд-во «Энергия», 1964.
13. Тарасова Н. В., Арманд А. А., Коньков А. С. Исследование теплоотдачи в трубе при кипении подогретой воды и пароводяной смеси. В сб.: «Теплообмен при высоких тепловых нагрузках и других специальных условиях». Энергоиздат, 1959.
14. Paleev I. I., Filippovich B. S. Phenomena of liquid transfer in two-phase dispersed annular flow. «International Journal of heat and mass transfer», 1963—1966, № 9, № 10.
15. Миропольский З. Л., Шидман М. Е., Шисерова Р. И. Влияние теплового потока и скорости на гидравлические сопротивления при движении пароводяной смеси в трубах. «Труды ЦКТИ», вып. 59. Л., 1965.
16. Тарасова Н. В. Гидравлическое сопротивление при кипении воды и пароводяной смеси в обогреваемых трубах и кольцевых каналах. «Труды ЦКТИ», вып. 59. Л., 1965.
17. Полетаевкии П. Г. [и др]. Гидравлическое сопротивление при кипении воды, нагретой до температуры насыщения. «Теплоэнергетика», 1962, № 4.
18. Боришанский В. М. и др. Охлаждение поверхности нагрева двухфазным пузырьковым потоком. «Труды ЦКТИ», вып. 91. Л., 1969.
19. Никонцов А. А., Белокопытов Л. С. Экспериментальное исследование теплообмена при кипении воды в горизонтальных трубах. «Труды ЦКТИ», вып. 58. Л., 1965.
20. Витман Л. А., Палеев Н. Н., Канцельсон Б. Д. Расплавление вязкой жидкости. М. — Л., Энергоиздат, 1962.

THE EFFECT OF THE NUMBER OF VAPOR
FORMATION CENTERS AND HEATING
SURFACE PROCESSING PURITY ON HEAT
EXCHANGE DURING THE BOILING OF
FREONS

G. N. Danilova

Abbreviations:

н = saturation

ст = wall

кр = critical

Experimental and theoretical works of various researchers have established that the processing purity of the heating surface affects heat transfer intensity during boiling in a large volume under conditions of free liquid motion [1-14]. The studied liquids included water, ethyl and methyl alcohol, pentane, ether, carbon tetrachloride, and several others.

Based on Berenson's data [10], for several liquid-heating surface combinations, the heat transfer factor for the same liquid on a surface of the same material ranged from 500 to 600% because of variations in the roughness of the latter.

In the Leningrad Technological Institute of Refrigeration an experimental study was performed on the effect of roughness

on freon heat transfer. Tests were made with pipes of varying roughnesses, on which freons boiled. The experimental apparatus and test results with F-113 at atmospheric pressure $p = 1$ bar, $t_H = 47.7^\circ\text{C}$ and with F-12 at $p = 4.88$ bar, $t_H = 21^\circ$ are described in [15]. Direct-heating steel pipes were used with F-12 and copper and steel pipes with F-113.

The class of surface processing purity was determined in accordance with GOST 2789-59 [ГОСТ = GOST = All Union State Standard]. The height of the roughness R_z in microns was selected as the roughness characteristic.

The results of these tests lead to the following conclusions.

1. An increase in roughness, characterized by an increase in its height R_z in the thermal flux range from 3000 to 30,000 W/m^2 , leads to a decrease in the temperature drop $\Delta t = t_{CT} - t_H$ (wall - saturation) and an increase in the heat transfer factor. This has its greatest effect in the range of low thermal fluxes.

2. Not only the quantity R_z but also the method of obtaining it affects heat transfer intensity: for roughened pipes with $R_z \approx 10-20 \mu\text{m}$ the same values of heat transfer factors are obtained as for pipes having $R_z \approx 50$, which have been shot-blasted and processed on a lathe.

3. There is a quantitative relationship between the heat transfer factor and the microroughness of the surface, which can be represented in the form of a dependence of α on R_z . Figure 1 illustrates the results of tests [15], as well as the data of various authors [16-18] for F-12 at $t_H = -15^\circ\text{C}$ ($p = 1.82$ bar). Works which included information on surface processing purity were examined. The lines on Fig. 1 correspond to the following relationship

$$\alpha \sim R_z^{0.2}. \quad (1)$$

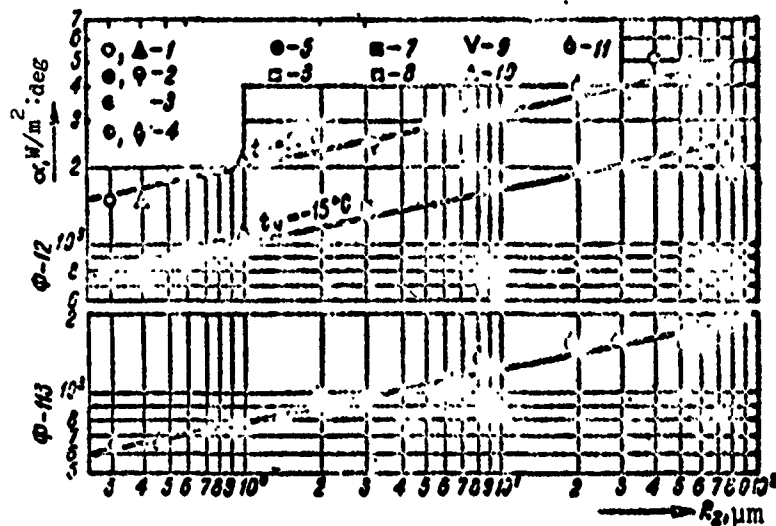


Fig. 1. The effect of roughness on the heat transfer factor of freons

($q = 10^4 \text{ W/m}^2$).

LTIKhP [Leningrad Technical Institute of Refrigeration] tests: 1 - Polished surface; 2 - Industrial preparation; 3 - Large-grained sandpaper; 4 - Shot-blasting surface processing; 5 - Roughened surface. Tests from [18]: 6 - Polished surface; 7 - Industrial preparation; 8 - Shot-blasting surface processing. Tests from [16]: 9 - Polished surface. Tests from [17]: 10 - LTIKHP tests: F-113; 11 - Plate X, *

4. The number of vapor formation centers z ($1/\text{cm}^2$) increases, while Δt decreases with an increase in roughness at the same q and with an increase in q during boiling at the same surface heating (in both cases, the same freon and constant pressure are studied).

Thus, not only heat flux but also the number of vapor formation centers have an effect on the value of the temperature drop and the heat transfer factor. The processing of tests with F-113 showed [19] that

$$\Delta t \sim q^{2/3} z^{-1/3}; \quad (2)$$

$$\alpha \sim q^{1/3} z^{1/3}. \quad (3)$$

Physical concepts concerning the mechanism of heat exchange during boiling and the available experimental material leads us to assume that the number of vapor formation centers must depend upon the physical properties and pressure of the liquid, the roughness of the boiling surface, heat flux, and wettability. Thus, during the boiling of the same liquid on a specific heating surface the effect of pressure on heat transfer intensity must be manifested in terms of a variation in z (at least in the area where q is not too high, where a change in the value of z does not lead to a change in the boiling mechanism).

To check this assumption an experimental study was made on the process of vapor formation in F-12, boiling on a horizontal plate at various pressures. The plate material was 1Kh18N9T steel, length 62 mm, width 2.5 mm, thickness 0.18 ± 0.01 mm. The design of the heating element, the method of sealing the thermocouples, the heating method, and the experimental apparatus in which the tests were conducted were the same as in the tests for determining diameter and frequency of steam bubble separation [20]. Half of the plate (in length) was polished, half processed with abrasive powder (roughened). Processing purity, in the first case, was $R_z = 0.13$; in the second case, $R_z = 7.2 \mu\text{m}$. To determine the heat transfer factor two thermocouples were set up: one in the middle (with respect to length and width) of a section of the roughened surface, the second in the smooth part of the plate.

A number of centers were estimated visually over the area of the friction plate by various observers. The spread between their data did not exceed 15%. The maximum value of the heat flux at which we could still determine z depended on t_H and the roughness.

These tests confirmed the above conclusions concerning the fact that at identical q and p on a roughened surface the number

of vapor formation centers and α is greater, while Δt is less, than on a smooth surface. In addition, tests on a plate showed that with an increase in pressure, z and α increased both on smooth and roughened parts of the plate. The relative effect of pressure in the studied range of parameter variations is approximately the same.

Figure 1 illustrates the experimental values of α for $q = 10^4 \text{ W/m}^2$ with corresponding R_z for both sides of the plate. For the smooth part comparison was made only at $t_H = 20^\circ\text{C}$ since in the case of $t_H = -15$, developed boiling began at $q > 10^4$.

As is apparent from Fig. 1, the results of these tests agree with the results of tests for other heating surfaces.

Figure 2 illustrates graph of function $\alpha = f(q)$, obtained in the experiments, from which it is completely apparent that on the smooth part of the plate and at low saturation temperatures, developed nucleate boiling begins at higher q than on the roughened part of the plate and at high t_H . In the region of developed boiling the logarithmic lines in Fig. 2 are approximated by equations $\alpha = Aq^n$ with $n = 0.75$ and A different for different t_H both for smooth and roughened surfaces.

The experimental results were processed in the form of function (2) (Fig. 3). All data for the smooth and roughened parts of the plate are generalized by the following equation, with an accuracy of $\pm 20\%$:

$$\Delta t z^{1/3} = 35 \cdot 10^{-3} q^{3/4}. \quad (4)$$

From formula (4) it follows that

$$\alpha = 28.5 q^{1/4} z^{1/3}; \quad (5)$$

$$q = 87 \Delta t^{4/3} z^{4/3}. \quad (6)$$

(Here $q - \text{W/m}^2$, $\alpha - \text{W/m}^2 \cdot \text{deg}$, $z - \text{cm}^{-2}$).

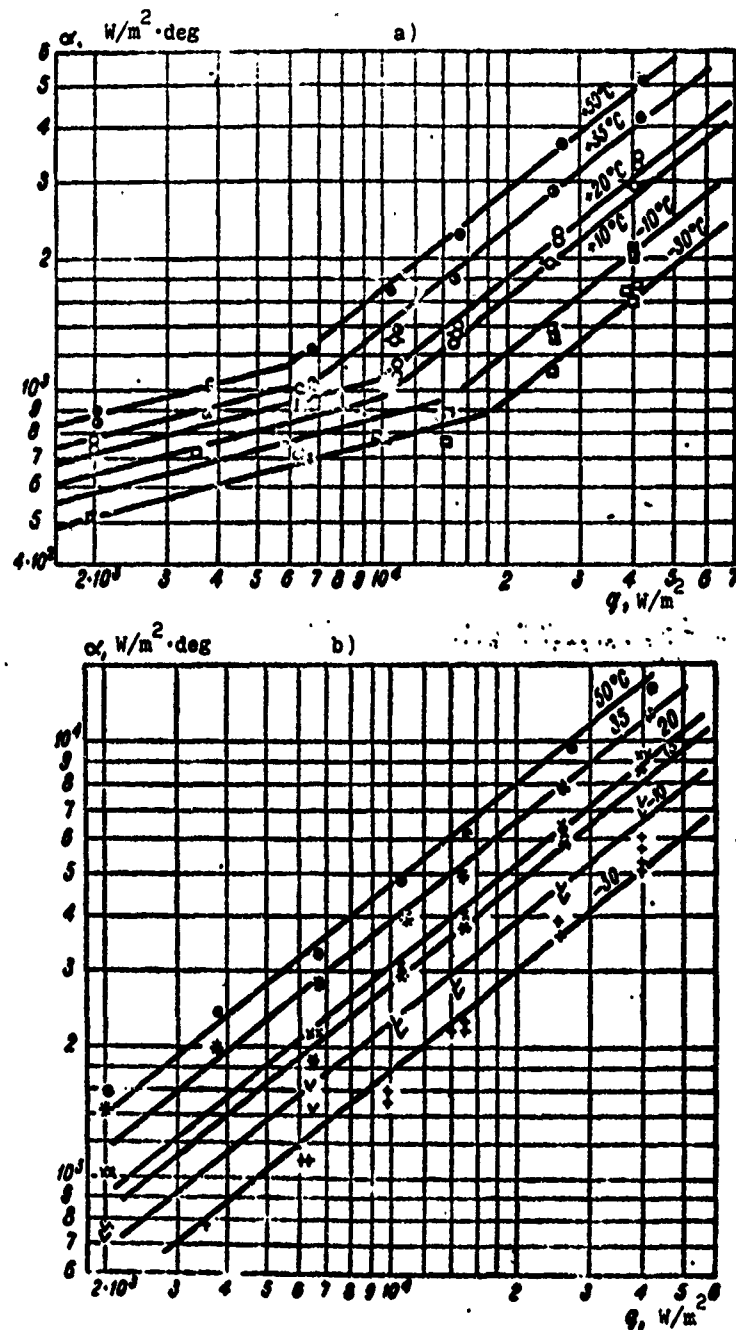


Fig. 2. Heat transfer factors with boiling of F-12:
a - On a smooth plate; b - On a roughened plate.

(1) Пластина	$t_{\text{ж}}, ^\circ\text{C}$					
	50	35	20	10	-10	-30
Гладкая (2)	●	◐	△	-C-	■	□
Шероховатая (3)	○	*	x	*	v	+

KEY: (1) Plate; (2) Smooth; (3) Roughened.

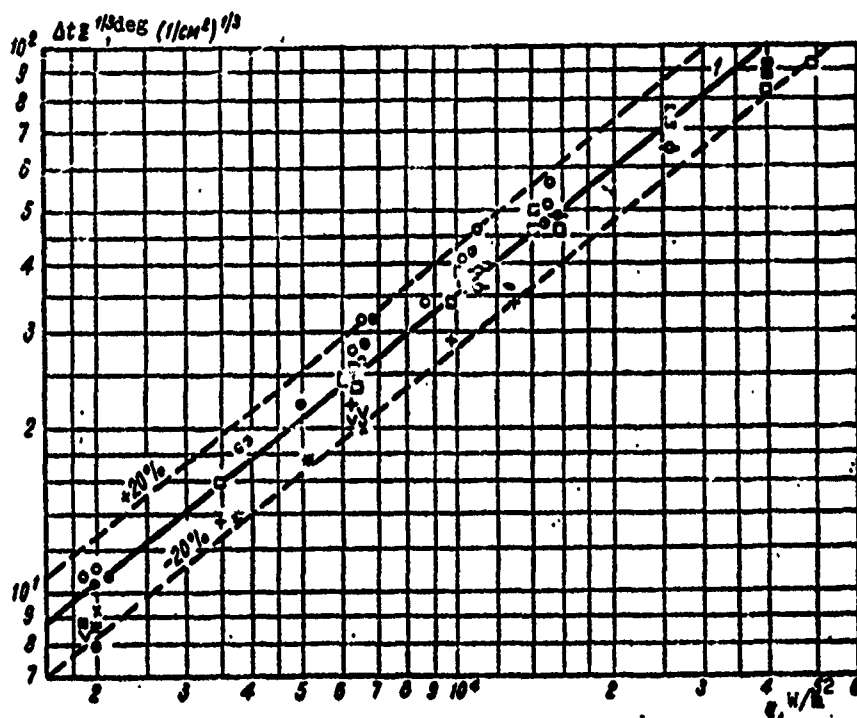


Fig. 3. Relationship between Δt , q , and z for F-12 boiling at $p = 1-11.9$ bar:

1 - $\Delta t = 3.5 \cdot 10^{-3} q^{1/3}$. Designations are the same as in Fig. 2.

Experimental data processed in the form of function $\alpha = f(q^{1/4} z^{1/3})$ are presented in Fig. 4; line 1, corresponding to equation (5), is also plotted there. It generalizes the experimental data in the studied range of pressures with an accuracy of $\pm 20\%$.

Points which correspond to extremely small heat fluxes are dropped (these points do not appear on Fig. 3). Apparently this is connected with the different character of the effect of z and q on Δt and α in this region.

Figure 5 presents the dependence of $z \sim p^k$ on pressure. We can assume that $k = 1.4$ approximately. Similar results for water at $p \approx 1-3$ bar were obtained in [2] with $k = 1$.

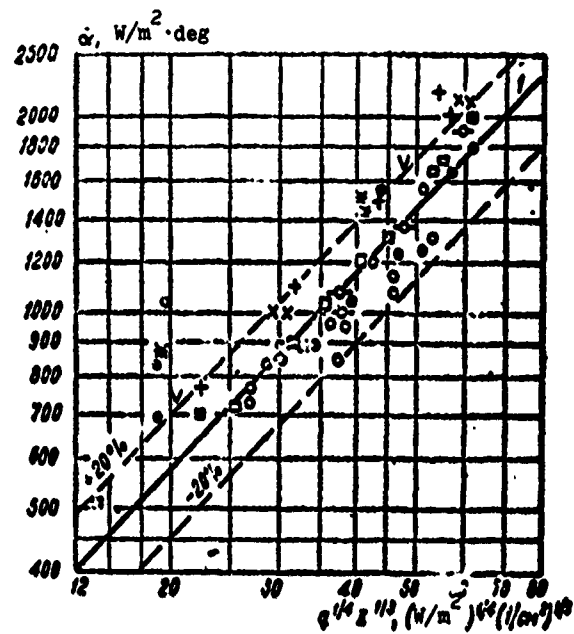


Fig. 4. Relationship between α , q , and z for F-12 boiling at $p = 1-11.9$ bar:
1 - $z \sim q^{1/4}$. Designations are the same as in Fig. 2.

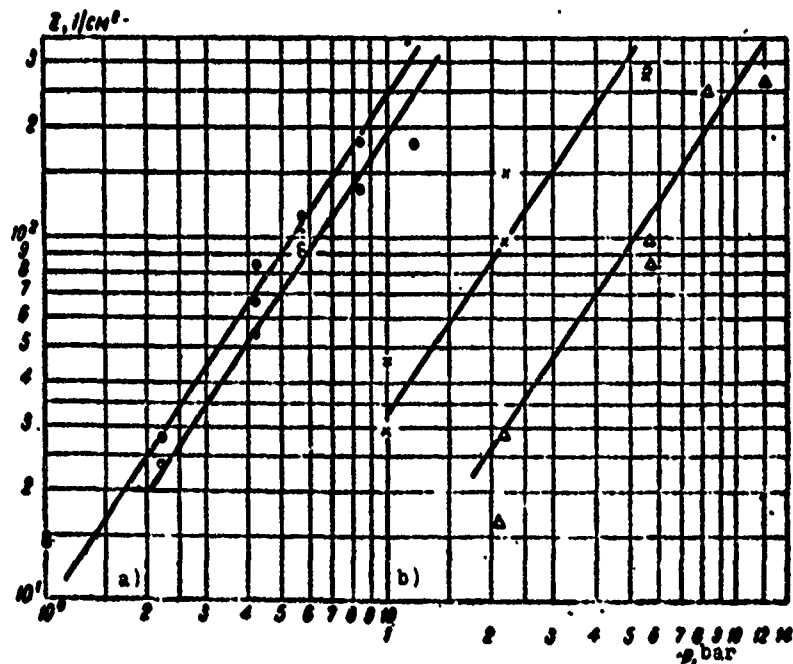


Fig. 5. The effect of pressure on the number of vapor formation centers: a) Smooth plate; b) Roughened plate,
● - $q = 1.5 \cdot 10^4$; ○ - $q = 10.6 \cdot 10^4$; x - $q = 0.65 \cdot 10^4$; Δ - $q = 0.2 \cdot 10^4$ W/m². Lines - $z \sim p^{1/4}$.

The results of these experiments allow us to assume that the effect of pressure on the heat transfer factor is manifested generally through the change in the number of effective vapor formation centers. This assumption agrees with the data from the work of Gol'tseva [27].

The existence of proportionality between α , q , and z was indicated in [1]. Relationships of the type

$$q \sim \Delta t^a z^b \quad (7)$$

were obtained from experiments with liquids having different surface tensions (at $a = 3/2$ and $b = 1/4$) [29], as well as from an examination of the boundary layer [9, 11]. In [9] the values $a = 1$, $b = 0.5$ were obtained; in [11] $a = 2$, $b = 0.25$. And finally, even Zuber [11] obtained relationship (7) with $a = 5/3$ and $b = 1/3$ under conditions of liquid flow dynamics created by growing and separating bubbles and a generalization of experimental material.

In the light of the data obtained in this work, the results are not unexpected. Their peculiarity consists in the fact that they describe tests with different pressures since, as far as we know, all previous studies were carried out at atmospheric pressure. The numerical values for a and b in formula (6) are near the values presented above obtained by Tien [9] and Zuber[11].

The effect of the physical properties of liquids and pressure on the number of vapor formation centers can be evaluated if we examine the conditions necessary for the occurrence of boiling on a hard heating surface. They presuppose, first, the formation of a vapor phase nucleus in liquid phase, which requires the surmounting of a certain energy barrier in the form of the difference in thermodynamic potentials $\Delta\phi$ of the system before and after the nucleus is contained in it and, second, the fact that the dimensions of the nucleus are greater than the value of

R_{\min} , which can be determined by the thermodynamic and mechanical bubble equilibrium conditions.

The quantities $\Delta\Phi$ [22, 5, 12, 25] and R_{\min} [22, 23] are determined by expressions:

$$\Delta\Phi = \Delta\Phi_0\psi; \quad (8)$$

$$\Delta\Phi_0 = \frac{16\pi\sigma^3 T_H^2 A^2}{3(rT_H^2 \Delta t)^2} = \frac{4}{3} \pi \sigma R_{\min}^2; \quad (9)$$

$$R_{\min} = \frac{2A\sigma T_H}{rT_H^2 \Delta t}. \quad (10)$$

Here σ is surface tension; T_H is the absolute saturation temperature of the liquid; r is the heat of vaporization; γ'' is the specific weight of the vapor, $A = 1/427$ kcal/kgf·m; ψ is a quantity depending upon chemical properties of liquid and the examined element of the surface and on the geometric characteristics of the latter [5, 12, 24].

Smaller $\Delta\Phi$ and R_{\min} will correspond to easier conditions for boiling and a larger number of vapor formation centers. Thus, we can assume that the set of physical properties introduced into equations (9) and (10) also determines the number of z , all other things being equal.

In [7] the quantity R_{\min} is taken as the quantity which uniquely determines the number of vapor formation centers in various liquids boiling at various pressures and temperature drops on the same type of heating surface. The processing of their own experiments with ethyl and methyl alcohol and tests [8] with acetone, hexane, CaCl_4 , and CS_2 in the form of function $z = f(R_{\min})$ allowed the authors [7] to assume the assumption introduced by them was correct. An examination of the graph presented in [7] shows that the form of the function obtained is curvilinear. The character of the function for surfaces of different mechanical processing was the same. Labuntsov [12] proposed that we assume

$z \sim R_{\min}^{-2}$. This relationship is confirmed by tests in [2] and [8].

The conclusions in [12] and [7] concerning the effect of R_{\min} on z agree qualitatively and, to a certain extent, quantitatively.

Figure 6 illustrates the function $z = f(1/R_{\min})$ for freon-12 boiling on a plate in the region of developed boiling. In Fig. 6 it is apparent that tests on the same heating surface at different pressures are united by quantity R_{\min} .

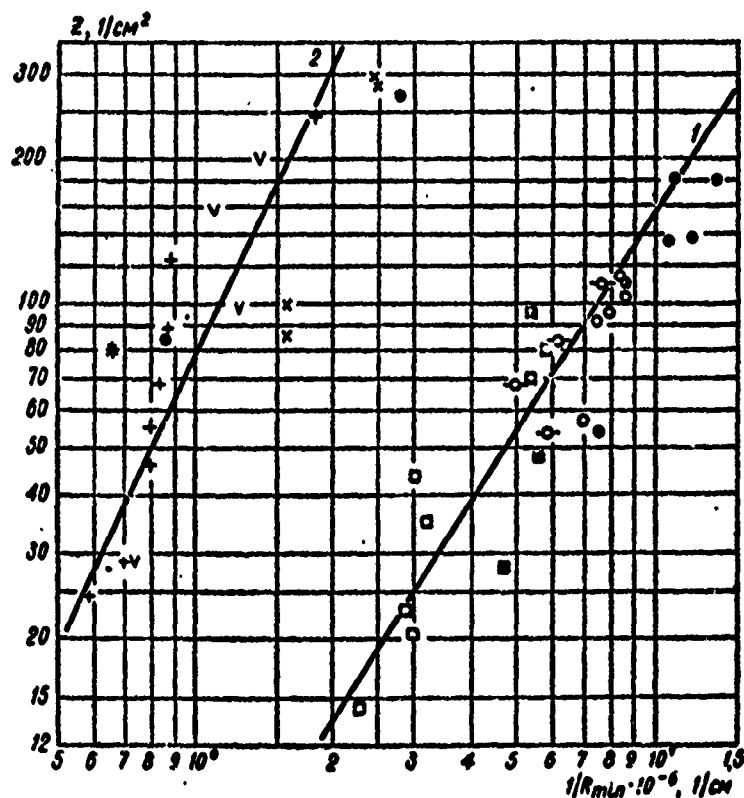


Fig. 6. Relationship between z and R_{\min} for a smooth and roughened plate:

1 - $z \sim R_{\min}^{-1.5}$; 2 - $z \sim R_{\min}^{-2}$. Designations are the same as in Fig. 2.

Experiments on the smooth and roughened parts of the plate are characterized by different values for z at identical R_{\min} and

by the fact that the latter affects Z to varying degrees. In the first approximation we can assume that the effect of pressure, physical properties, and Δt on the number of vapor formation centers can be taken into account with the aid of quantity R_{\min} . As for the effect of the state of the heating surface, it is not reflected by the value of R_{\min} .

As indicated above, the effect of heating surface processing purity on the heat transfer factor of boiling freons can be accounted for with the height of the roughness R_z . Apparently, this quantity does not reflect, to a full extent, the character of the effect of roughness on conditions for the generation and separation of bubbles; for this we must still know the diameter and the flare angle of the recesses. However, a certain evaluation of the effect of roughness, which more precisely defines the condition for comparison of various tests, and calculation formulas for α can be arrived at with the aid of this quantity.

The quantity R_z characterizes the height of the deepest depressions and, to a certain extent, the average depth of the depressions at a given surface processing. As follows from an examination of profilograms, taken from a plate and from several pipes, the form of the depressions is conical, flare angle is somewhat reduced, and the diameter of the depression increases with an increase in R_z .

On the other hand, in narrow conical depressions, considerable overheating on the heating surface is possible for liquid in the depression; consequently, there is a greater probability of the appearance of vapor bubbles due to the flashes of overheating and thermal fluctuations inside the liquid [19, 28]. In addition, the complete filling of such depressions by liquid is difficult [5] and, consequently, there is always the possibility of finding bubbles remaining in them (after the boiling process has ceased) which are equal to or greater than R_{\min} .

And, finally, as theoretical studies [5] and [12] have shown, the dimensions and shape of a depression affect the quantity $\Delta\phi$. The function ψ depends upon the microscopic contact angle θ and flare angle of the depression 2ϕ .

Average macroscopic contact angles for freons, based on the results of our measurements and also data presented in [7] and [13] are $\theta_0 = 30-60^\circ$. With this $\theta > \theta_0$ [26, 12]. If we assume, on the average, $\theta = 70^\circ$, then with an increase in ϕ from 90 to 60° , ψ changes from 0.75 to 0.5 [12].

With a decrease in ϕ and an increase in θ the values of ψ and $\Delta\phi$ are reduced more significantly.

The considerations presented above give a basis for the selection of R_z as the parameter which determines the effect of roughness on heat exchange intensity during boiling. In addition, this selection was dictated by the possibility of determining such a parameter and using it in the practical application of calculation formulas for various heating surfaces.

The effect on the heat release factor of the physical properties and the pressure of freons boiling on a certain surface is reflected by the relationship presented in [21, 30]:

$$\alpha = c_1 q^{0.75} f(p). \quad (11)$$

Heat transfer factors during boiling on another surface can be found by multiplying expression (11) by $(R_z/R_{z.1})^{0.2}$.

It is assumed that the effect of R_z at various p and q is the same. With a known degree of approximation such a conclusion can be made on the basis of results obtained in the above described tests.

The calculation formula for heat transfer during freon boiling in a large volume, under conditions of developed nucleate boiling, assumes the form:

$$\alpha = c_0 q^{0.75} f(p) \left(\frac{R_z}{R_{z,0}} \right)^{0.2}. \quad (12)$$

Here

$$\left. \begin{aligned} c_0 &= 550 p_{kp}^{1.4} T_{kp}^{-1.2} M^{-1.2} (W/m^2)^{1.4} 1/\text{deg} \\ c_0 &= 530 p_{kp}^{1.4} T_{kp}^{-1.2} M^{-1.2} (\text{kcal}/m^2)^{1.4} 1/\text{deg} \end{aligned} \right\} \quad (13)$$

$$f(p) = (0.14 + 2.2(p/p_{kp})) \text{ for } 0.05 \leq \frac{p}{p_{kp}} < 0.5; \quad (14)$$

$R_{z,0} = 1 \mu\text{m}$, R_z is the height of the roughness of the calculated heating surface, μm ; p_{kp} is the critical pressure, bar (or atm (abs.)); T_{kp} is critical temperature, $^{\circ}\text{K}$; M is molecular weight; q is specific heat flux, W/m^2 (or $\text{kcal}/m^2 \cdot \text{h}$).

For industrially prepared pipes processing purity corresponds to class V8-V7 and $R_z = 2-6 \mu\text{m}$; the heat transfer factor is higher by a factor of 1.15-1.4, as compared with a surface having $R_z = 1$.

During boiling in industrially prepared pipes formula (12), for determining the average heat transfer factor, reduces to the form:

for freon-12

$$\alpha = 5.5 q^{0.75} f(p), \quad (15)$$

for freon-22

$$\alpha = 6.2 q^{0.75} f(p). \quad (16)$$

BIBLIOGRAPHY

1. Зысина Л. М., Кутателадзе С. С. К вопросу о влиянии давления на механизм парообразования в кипящей жидкости. ЖТФ, 20, 1950, № 1.
2. Зысина Л. М. Некоторые данные о числе центров парообразования при кипении на технических поверхностях нагрева. В сб.: «Вопросы теплообмена при изменении агрегатного состояния вещества», под ред. Кутателадзе С. С. Энергониздат, 1961, стр. 168.
3. Jakob M. Heat Transfer, v. 1, second Printing. New York, Wiley, 1950.
4. Аверин Е. К. Влияние материала и механической обработки поверхности на теплоотдачу при кипении воды. Известия АН СССР, ОН, 1954, № 3.
5. Бунков С. Г. Вскипание на твердой поверхности в отсутствие растворенной газовой фазы. В сб.: «Вопросы физики кипения». Изд-во «Мир», 1964, стр. 80.
6. Кларк Г., Стренг П., Уэстдотер Дж. Активные центры пузырькового кипения. В сб. переводов: «Вопросы физики кипения», под ред. Аладьева И. Т. Изд-во «Мир», 1964, стр. 138.
7. Гриффитс П., Уоллис Дж. Роль состояния поверхности при пузырьчатом кипении. В сб. переводов: «Вопросы физики кипения», под ред. Аладьева И. Т. Изд-во «Мир», 1964, стр. 99.
8. Kurihara H. M., Myers. Effects of Superheat and Surface Roughness on Boiling Coefficients. Am. Inst. Chem. Eng. Journals, № 6, 1960, с. 83.
9. Tien C. L. A hydrodynamic model for nucleate pool boiling. Int. J. Heat Mass Transfer, v. 5, June 1962, с. 533.
10. Berenson P. J. Experiments on Pool-Boiling Heat Transfer. Int. J. Heat Mass Transfer, v. 5, October, 1962, с. 985.
11. Zuber N. Nucleate Boiling. Int. J. Heat Mass Transfer, v. 6, 1963, № 1, с. 53.
12. Лабунцов Д. А. Теплоотдача при пузырьковом кипении жидкости. Теплоэнергетика, 1959, № 12. Приближенная теория теплообмена при пузырьковом кипении. Известия АН СССР, ОН. Энергетика и транспорта, 1963, № 1, стр. 63.
13. Stephan K. Berechnung des Wärmeüberganges an siedende Kältemittel. Kältetechnik, Bd 15, 1963, № 8, с. 231.
14. Головин В. С., Кольчугин В. А., Лабунцов Д. А. Исследование теплообмена при кипении спирта и бензола на поверхностях из различных материалов. ИФЖ, 1964, № 6, стр. 35.
15. Данилова Г. Н., Бельский В. К. Исследование теплоотдачи при кипении фреонов-113 и 12 на трубках различной шероховатости. Холодильная техника, 1965, № 4.
16. Лаврова В. В. Экспериментальное исследование теплоотдачи при кипении Ф-12. Холодильная техника, 1957, № 3.
17. Stephan K. Einfluss des Ols auf den Wärmeübergang von Siedendem Frigen 12 und Frigen 22. Bd. 16, 1964, № 6, с. 162.
18. Поволоцкая Н. М. Исследование теплообмена при кипении Ф-12. Холодильная техника, 1965, № 3.
19. Данилова Г. Н. К вопросу о влиянии числа центров парообразования на теплообмен при кипении фреона. ИФЖ, т. 11, 1966, № 3.
20. Данилова Г. Н., Бельский В. К., Куприянова А. В. Влияние давления на характеристики парообразования фреона-12. Тезисы доклада на 3-й Всесоюзной конференции по теплообмену и гидравлическому сопротивлению в элементах энергетических машин и аппаратов. Л., 1967.
21. Данилова Г. Н. Влияние давления и температуры насыщения на теплообмен при кипении фреонов. Труды ИКТИ, вып. 57. Л., 1965.
22. Френкель Я. И. Собрание избранных трудов. Т. III. АН СССР, 1959.
23. Кружанин Г. Н. Теплоотдача от поверхности нагрева к кипящей однокомпонентной жидкости при свободной конвекции. Известия АН СССР, ОН, 1948, № 7, стр. 967.
24. Несис Е. И. Кипение жидкостей. Успехи физических наук, т. 87, вып. 3. Изд-во «Наука», 1965.
25. Аладьев И. Т. Теплоотдача при пузырьчатом кипении. В сб.: Конвективный и лучистый теплообмен. АН СССР, 1960, стр. 233.
26. Дерягин Б. В. О зависимости краевого угла от микрорельефа или шероховатости смачиваемой поверхности. Доклады АН СССР, с. 1, 1946, № 5, стр. 357.
27. Гольцева Е. И. Влияние единичного центра парообразования и частоты отрыва паровых пузырей в нем на температуру стенки. ИФЖ, т. IX, 1963, № 4.
28. Розенов У. М. Теплообмен при кипении. В сб.: Современные проблемы теплообмена. Изд-во «Энергия», 1966.
29. Nishikawa K. Studies on Heat Transfer in Nucleate Boiling. Memoirs of the Faculty of Engineering Kyushu University, v. 16, № 1, 1956, с. 1—28.
30. Борншарф В. М. Учет влияния физических свойств и явлений тепло- и массопереноса. Холодильная техника, 1967, № 7.

STUDY OF EXCHANGE FACTORS AND DROPLET DIFFUSION IN DISPERSED ANNULAR FLOW.

I. I. Paleyev, F. A. Agafonova,
M. E. Lavrent'yev, and K. P.
Malyus-Malitskiy

Designations

- w_r - average gas velocity, m/s;
- c - concentration, kg/m³;
- g - specific mass flow, kg/s·m²;
- $g_{пл}$ - flow rate of liquid in film per unit
perimeter of channel, kg/m·s;
- G - full mass flow, kg/s;
- d - diameter, m;
- ρ - density, kg·s²/m⁴;
- D_T - coefficient of turbulent droplet or
particle diffusion, m²/s;
- K - exchange factor;
- $v^* = \sqrt{\tau/\rho_r}$ - dynamic velocity;
- $Re_r = \frac{w_r d r}{\mu_r}$ - Reynolds number for gas.

Subscripts: пл - film, взв - suspension, вым - removal,
вып - deposit, я - core, г - gas, ж - liquid, кр - dye, к - drop,
ч - particle.

With dispersed annular flow of a fluid mixture in channels there is an intense mass exchange of the liquid flowing in the form of a thin film on the channel walls and moving in the form of small drops in the flow core. This mass exchange has a considerable effect on the physical processes which accompany such two-phase flow.

The phenomena of liquid drop transfer in the core of a dispersed annular flow (removal and deposit) are connected, first, with the turbulent pulsations of drops in the gas, i.e., with their turbulent diffusion coefficient. During the turbulent motion of the gas which carries the suspended particles, the latter perform complex pulsation motion.

Since the density of the liquid is greater than the density of the gas ($\rho_{\text{л}} \gg \rho_{\text{г}}$), pulsation frequency, velocity, and mean free path of the drops can differ from the corresponding quantities for pure gas. Droplet size also has a considerable effect. If the drops are small as compared with the scale of the turbulence, they will easily follow behind the components of turbulent gas motion. Certain limiting cases of particle motion in turbulent gas flow are examined by Khintse [1]. We are familiar with a rather limited number of experimental works on the problems of drop (or particle) transfer in gas flow. These are references [2, 3] concerning the measurement of diffusion coefficients and references [3, 4, 5, 6] in which deposit (or removal) of liquid drops from the flow core to the wall is studied. However, quantitative results obtained by various authors disagree considerably. For example, the values of the diffusion coefficients measured in references [2] and [3] differ by approximately two orders.

In our work the turbulent diffusion coefficient for drops in gas D_{T} was determined by the distribution of dye throughout the height of the channel, and the exchange coefficient

$K = g_{\text{BWH}}/cw_r$ by the variation in dye concentration in the liquid film flowing along the lower channel wall.

The experimental apparatus was a channel of organic glass, rectangular cross section 15×20 mm and length 740 mm. A solution of dye (methylene blue) was introduced directly into the liquid film through a slot 0.5×18 mm in the lower channel wall. In order to obtain a uniform feed throughout the channel width the slot was covered with porous plastic. The flow rate of the dye was selected experimentally so that the flow of the film was distorted as little as possible to obtain a good displacement of the dye throughout its width and to insure stable operation of the photocolormeter, with which the concentration of the dye was determined. The dye was introduced for a distance of 400 mm into the working section ($l/H = 27$). Concentration of dye in the film was measured at five points along the length of the channel every 50 mm; reading began from the introduction point (with maximum film thickness $\delta = 0.5$ mm, $l_1/\delta = 100$). The flow rate of the liquid in the film was measured at the end of the working section along each of the channel walls separately. The mass flow of the suspension and the concentration of dye in it along the height of the channel was also measured at the end of the working section.

The equation of turbulent diffusion for the liquid drops separating from the film - dye diffusion equation - can be written approximately in the following form:

$$w_r \frac{\partial c^{xp}}{\partial x} = D_r \frac{\partial^2 c^{xp}}{\partial y^2}. \quad (1)$$

It was assumed that the lateral velocity of the drops upon separation $u_y = 0$, and the longitudinal velocity $u_x = w_r$. The latter can be reduced to a certain overstatement of D_r . The boundary conditions are:

$$c_{x=0}^p = 0; \quad (\partial c^{xp} / \partial y)_{y=\infty} = 0; \quad c_{y=0}^{xp} = c_{\text{ns}}^p. \quad (2)$$

The last condition assumes that the concentration of dye in drops separating from the film is equal to the concentration of dye in the film itself. The second boundary condition can be written in such a form since throughout the tests no dye was detected in the film on the upper channel wall. The solution to equation (1), with allowance for (2), has the form:

$$1 - \frac{c_{np}^{kp}}{c_{n1}^{kp}} = \Phi\left(\sqrt{\frac{y}{2D_t \frac{L}{w_t}}}\right), \quad (3)$$

where L is the distance from the dye introduction spot to the extraction spot at the end of the working section. A comparison of the experimental profile of dye concentration along the height of the channel with the profile calculated by expression (3) makes it possible to obtain a value for the turbulent drop diffusion coefficient in gas D_t for each test. We should note that with the test setup both the average diffusion coefficient along the channel cross section and the average diffusion coefficient for the entire spectrum of drops in the flow were determined.

The expression for determining the exchange coefficient K can be obtained from the balance of dye for an arbitrary section of liquid film:

$$\frac{d(c_{n1}^{kp} g_{n1})}{dx} = c_{np}^{kp} g_{n1} - c_{n1}^{kp} g_{np}. \quad (4)$$

For steady flow $g_{нн} = g_{вн} = \text{const}$, $g_{пл} = \text{const}$, $G_{кр} = \text{const}$.

Under condition $c_{n1}^{kp}(x=x_1) = c_{n1}^{kp}$, from (4) we obtain

$$\ln \frac{c_{n1}^{kp} - c_0^{kp}}{c_{n1}^{kp} - c_{n1}^{kp}} = a(x - x_1), \quad (5)$$

where $c_0^{kp} = G_{кр}/G_{нн}$; $a = \frac{G_{нн} g_{нн}}{g_{пл} G_{вв}}$.

Since the variation in dye concentration in the film along the length of the channel is known from the test, it is easy to

determine quantity a from expression (5) and, consequently, the quantity of separating liquid g_{BH} and the exchange coefficient K .

The values obtained in our tests for the turbulent diffusion coefficients of drops in gas are presented in Fig. 1 as a function of gas velocity. From Fig. 1 it is apparent that the quantity D_T decreases with an increase in gas velocity. We detected no effect of suspension concentration on the drop diffusion coefficient (with the variation $c = 0.1-1.5 \text{ kg/m}^3$). The absolute values of D_T in our tests lay in the range $(1.5-2.2) \times 10^{-3} \text{ m}^2/\text{s}$ and were near in order of magnitude to the turbulent diffusion coefficients of dry gas in pipes, calculated according to Goldenberg's formula [7] for a single-phase flow. On Fig. 2 the same experimental data, presented in the form of the parameter $D_T/w_{\text{r,d}}$ versus the Reynolds number, are compared with the data from other studies. Curve 1 pertains to tests in [3] in which D_T was determined by the deformation of the profile of suspended liquid concentrations along the length of the channel in the initial section of a two-phase stream. (Average drop size was $30 \mu\text{m}$). The relatively overstated values for D_T in these tests are explained by the higher initial turbulence of the gas flow itself in the stabilization section.

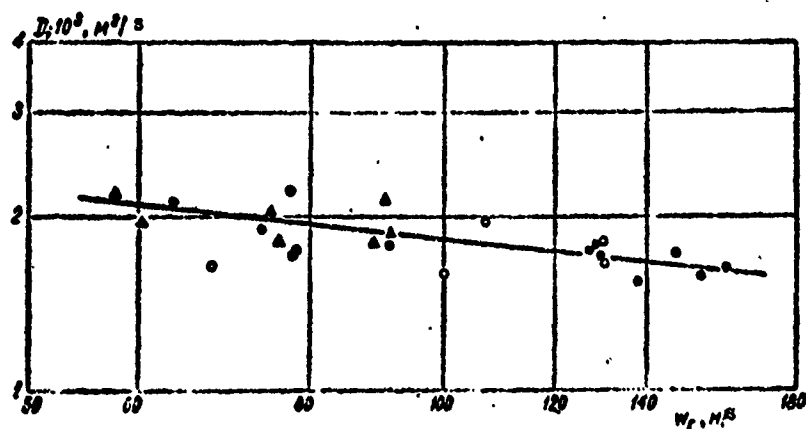


Fig. 1. Turbulent diffusion coefficient of liquid drops in gas versus the Reynolds number of the gas:

○ - $c = (0.10-0.14) \text{ kg/m}^3$; ● - $(0.25-0.39)$;
○ - $(0.43-0.76)$; ▲ - $(0.81-1.50)$.

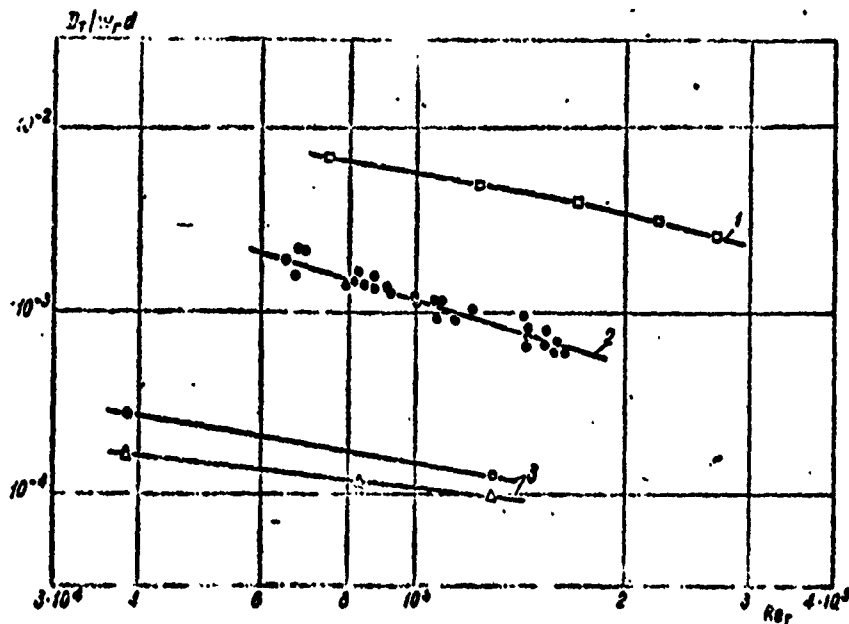


Fig. 2. $D_T/w_r d$ versus Re_r number:

□ - [3]; ● - Our data; ○ - $d_H = 200 \mu m$ [2]; Δ - $d_H = 100 \mu m$ [2].

Curves 3 [2] are obtained for the motion of solid (glass) particles in a gas flow. (Horizontal channel, gas velocity 8-26 m/s). As is apparent, the spread between experimental data from various authors is rather significant.

However, such a method of representing experimental data does not account for particle dimensions, particle density, or the turbulence characteristics of the carrier gas flow. In reference [1] it is theoretically shown that the ratio of turbulent diffusion coefficients for particles D_T and gas D_{T_r} must be a function of the St number $\frac{18\nu_r \tau_L}{\rho_m d_H^2}$ and dimensionless time t/τ_L (τ_L - Lagrange time scale). The character of this relationship is such that with an increase in St and t/τ_L the D_T/D_{T_r} ratio also increases and at the limit tends toward unity. A quantitative evaluation of the parameters St and t/τ_L in our tests

and in tests discussed in reference [2] shows that the character of the divergence between these test data corresponds to theory, i.e., large values of this parameter correspond to large values of D_T (if the values of D_{T_r} were identical).

For calculation of the average turbulent diffusion coefficient of drops during the motion of an air-water mixture in drops we can recommend the following empirical formula:

$$\frac{D_T}{u_d} = 6.4 \cdot 10^2 Re_r^{-1.15}, \quad (6)$$

This formula is obtained with a variation in the Reynolds number $Re_r = 6 \cdot 10^4 - 16.5 \cdot 10^4$ and a per-volume concentration of suspended liquid $c/\gamma_m = 1 \cdot 10^{-4} - 15 \cdot 10^{-4}$.

Test results with respect to determining exchange coefficients are presented in Fig. 3 as a function of the Re_r number. Suspension concentration in the flow is chosen as the parameter on this figure. The effect of the per-volume fraction of suspension in the flow on the exchange coefficient is shown in Fig. 4. With an increase in the liquid load of the flow core the value of K drops. However, with $c/\gamma_m = 8 \cdot 10^{-4}$ the drop rate of K is sharply retarded and with a further increase in the suspension concentration the exchange coefficient changes only slightly. The same effect of the per-volume content of suspension in the flow on the exchange coefficient was noted in references [4, 5].

The test data on exchange coefficients obtained in our work can be approximated as follows:

$$K = 2.61 Re_r^{-0.48} (c/\gamma_m \cdot 10^4)^{-0.72}, \quad \text{when } c/\gamma_m \leq 8 \cdot 10^{-4}; \quad (7)$$

$$K = 1.03 Re_r^{-0.45} (c/\gamma_m \cdot 10^4)^{-0.29}, \quad \text{when } c/\gamma_m > 8 \cdot 10^{-4}. \quad (7a)$$

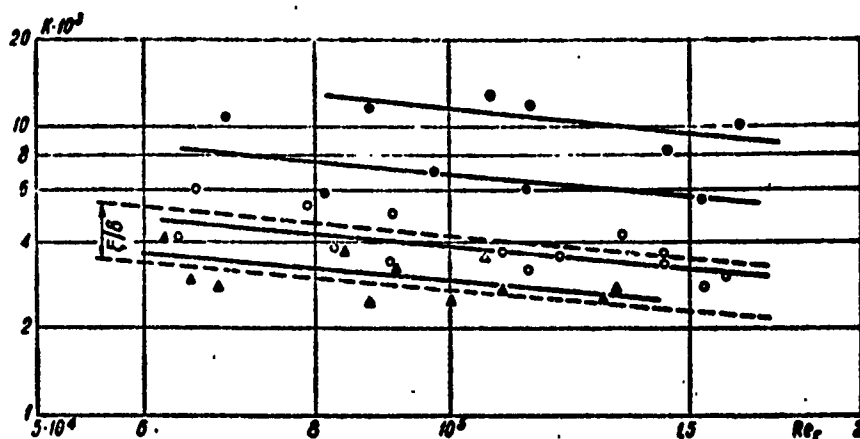


Fig. 3. Exchange coefficient versus gas Reynolds number. (Designations - see Fig. 1).

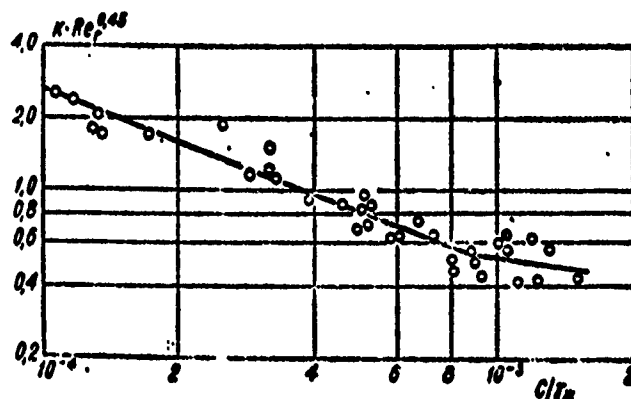


Fig. 4. The effect of the per-volume fraction of suspended liquid on the exchange coefficient.

From the Reynolds analogy between mass transfer and momentum for a single-phase flow there ensues a connection between the exchange coefficient and resistance coefficient which is valid for gases at $Pr = 1$ for gradientless flow:

$$K = \frac{E_{\text{max}}}{cx_r} = \frac{\xi}{8}. \quad (8)$$

Figure 3 illustrates the region of resistance coefficient variation, calculated according to the mean density of the flow

core and the measured pressure drop, without taking into account loss from flow acceleration. It is apparent from Fig. 3 that the character of the dependence on the Re_r number is identical for $\xi/8$ and K . However, for K the dependence on the concentration is expressed more strongly than for ξ .

The values for the exchange coefficients obtained in our work are mean integral values for the entire drop spectrum in the flow. An examination of the experimental data from reference [6] on the deposition of solid particles from gas flow onto a channel wall shows that the rate of deposition depends strongly on particle size if the dimensionless distance through which the particle passes under the effect of turbulent gas pulsation with the Stokes law of resistance $St = 0.9 \frac{v \cdot d_p^2 \rho_g}{\nu_r \rho_r}$, is greater than 3.5.

The research conducted on transfer processes in a dispersed annular fluid flow indicates that these processes have a very complex character. Unfortunately, at this time not enough experimental data have been compiled for a more complete analysis and generalization of the available experimental material.

BIBLIOGRAPHY

1. Хинице И. О. Турбулентность. М., 1963.
2. Soo S. L., Ibrag H. K., El Kouh A. F. Experimental Determination of statistical properties of two-phase Motion. «Trans. ASME», 82D, 3, 1960.
3. Alexander L. G., Coldren C. L. Droplet transfer from suspending air to duct walls. «Ind. Engng. Chem.», 1951, 43, 6.
4. Quant. Mesurement of some basic parameters in two-phase annular flow. «AIChE Journal», 1965, 11, 2.
5. Paleev I. I., Filippovich B. S. Phenomena of liquid transfer in two-phase dispersed annular flow. «Inter. J. Heat Mass Transfer», 9, 1089—1093, 1966.
6. Friedlander J. K., Johustone H. F. Deposition of suspended particles flow turbulent gas streams. «Ind. Engng. Chem.», 1957, 49, 7.
7. Голосенберг С. А. О некоторых экспериментальных закономерностях в области турбулентной диффузии. «Изв. АН СССР, ОТН», 1950, № 4—5.

CHARACTERISTICS OF HEAT EXCHANGE
DURING THE BOILING OF CERTAIN
ORGANIC SOLUTIONS AND DISPERSED
MEDIA

G. M. Pludovskaya

Abbreviations

pacч = calculated

он = experimental

In this work we have made an experimental study on the process of boiling in certain aqueous solutions of organic compounds, which are homogeneous and contain suspended particles. The choice of such media has made it possible to distinguish the qualitative effect of liquid viscosity and heating surface orientation on the intensity of heat exchange during boiling and to obtain certain first recommendations with respect to a quantitative evaluation of heat transfer intensity. These data have great significance in the selection of optimal conditions for industrial thermal processes in the chemical, microbiological, food, and other industries.

The main series of tests were made with a sugar solution of varying concentrations from 20 to 60%, which corresponds to

the liquid viscosity variation from $3.8 \cdot 10^{-5}$ to $34 \cdot 10^{-5}$ kg·s/m².

A sugar solution was selected for the basic tests because there are data available in literature on heat exchange in such media [1].

These data were the starting point in our work for comparing them with the results of tests made subsequently with certain nutrients used in the microbe synthesis industry, particularly in antibiotics.

It should be noted that the above mentioned tests with sugar solution were made for large volumes. However, in our experiments the volume of boiling liquid was quite small. The heat transfer factor during boiling was determined in horizontal and vertical cylinders 100 ml in volume with a heater located inside in the form of a quartz pipe $d = 18$ mm, which emitted heat from an electric spiral passing through it. The heating surface of the pipe was $H = 0.038$ m². The heat transfer factor was calculated from the familiar formula:

$$\alpha = \frac{q}{t_w - t_s},$$

where q is thermal loading, kcal/m²; t_w is heater wall temperature; t_s is the temperature of the boiling medium.

Each series of tests included no less than five measurements of wall temperature and medium temperature after achieving steady state.

The transition to steady state was determined by a preliminary group of control measurements. In all, 13 series of such tests, generalizing data from more than 65 single tests, were conducted. Tests were made on water, on sugar solutions, and on nutrients for the production of penicillin, tetracycline, and streptomycin, containing suspended particles of cornmeal and solutes in the form of glucose, common salt, etc.

In the experiments the thermal load and temperature drop were kept constant.

Thermal load during work with a horizontal heater varied in two limiting values: $19.9 \cdot 10^3 \text{ kcal/m}^2 = 83 \cdot 10^3 \text{ kJ/m}^2$ and $20.1 \cdot 10^3 \text{ kcal/m}^2 = 83.5 \cdot 10^3 \text{ kJ/m}^2$, while during work with a vertical heater $q = 15.5 \cdot 10^3 \text{ kcal/m}^2 = 63 \cdot 10^3 \text{ kJ/m}^2$ and $11 \times 10^3 \text{ kcal/m}^2 = 73.5 \cdot 10^3 \text{ kJ/m}^2$.

The boiling temperature of the studied liquids did not exceed 110°C . For the sugar solution it varied from 100 to 109°C . Within these limits the temperature of the studied media also varied.

The table below presents the average values of the heat transfer factors obtained in the experiments at atmospheric pressure. It is apparent from the table that the arrangement of the heating surface only slightly affects heat transfer during boiling of water and sugar solutions. Reduced values of the heat transfer factors, in those cases with a vertical heater, are determined not as much by its orientation as by the reduced thermal load under which the tests were performed. The recalculation, for example, of the heat transfer factor for water by the increased load with respect to the familiar relationship:

$$\alpha_{\text{pac}} = \alpha_{\text{on}} \left(\frac{q_{\text{pac}}}{q_{\text{on}}} \right)^{0.7} = 7737 \left(\frac{20.1}{15.5} \right)^{0.7} = 9450 \text{ kcal/m}^2 \cdot \text{h} \cdot \text{deg}$$

showed that the quantity α for the case of boiling with a vertical heater becomes very near the value obtained for this coefficient in the case of boiling water with a horizontally arranged heater.

These data agree rather well with the results of M. Jakob's experiments [2], performed for cases of boiling in large volumes of water and carbon tetrachloride.

Table.

(1) № п/п	(2) Исследуемая среда	(3) Тепловая нагрузка, $\frac{\text{ккал}}{\text{м}^2} \cdot 10^{-3}$	(4) Коэффициент тепло- отдачи, $\frac{\text{ккал}}{\text{м}^2 \cdot \text{ч} \cdot \text{град}}$	(5) Температу- ра кипе- ния, °C	(6) Расположение поверхности нагрева
1	Вода (7)	20,1	10610	100	Горизонтальное (12)
2	Вода (7)	15,5	7737	100	Вертикальное (13)
3	Сахарные растворы (8)	19,9	6960	100-109	Горизонтальное (12)
4	Сахарные растворы (8)	15,5	4566	100-109	Вертикальное (13)
5	Питательная среда для тетрациклина (9) .	20,1	10130	100-102,5	Горизонтальное (12)
6	Питательная среда для тетрациклина (9) .	15,5	7400	100-102,5	Вертикальное (13)
7	Питательная среда для пенициллина (10) .	20,1	9620	100-103	Горизонтальное (12)
8	Питательная среда для пенициллина (10) .	15,5	9100	100-103	Вертикальное (13)
9	Питательная среда для стрептомицина (11)	19,9	8225	100-104	Горизонтальное (12)
10	Питательная среда для стрептомицина (11)	15,5	5336	100-104	Вертикальное (13)

KEY: (1) No.; (2) Studied medium; (3) Thermal load

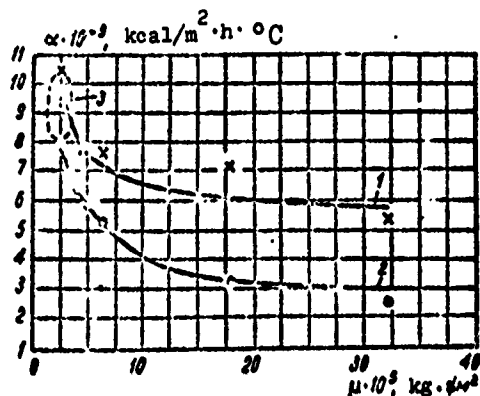
$\frac{\text{kcal}}{\text{м}^2} \cdot 10^{-3}$; (4) Heat transfer factor $\frac{\text{kcal}}{\text{м}^2 \cdot \text{ч} \cdot \text{deg}}$;

(5) Boiling temperature, °C; (6) Arrangement of heating surface; (7) Water; (8) Sugar solutions; (9) Nutrient for tetracycline; (10) Nutrient for penicillin; (11) Nutrient for streptomycin; (12) Horizontal; (13) Vertical.

In all cases, the horizontal arrangement of the heating surface intensified heat transfer during boiling, increasing the heat transfer factor in a ratio of 1.1-1.3.

In a somewhat different respect, while preserving the same character, the orientation of the heating surface affects heat exchange during boiling in nutrients containing suspended particles. The presence of particles in a boiling medium noticeably contributes to the intensification of the boiling process, apparently causing a turbulization of the medium. This situation is illustrated rather well by the figure, on which the relation of the heat transfer factor and the viscosity present in the boiling medium is represented. The upper curve corresponds to the series of tests with water and sugar solutions of different concentrations

during a horizontal heater arrangement and specific thermal load of $q = 20 \cdot 10^3 \text{ kcal}/(\text{m}^2 \cdot \text{h} \cdot \text{deg})$. The lower curve represents the results of tests with a vertical heater arrangement and a specific thermal load of $q = 15 \times 10^3 \text{ kcal}/\text{m}^2 \cdot \text{h} \cdot \text{deg}$.



Heat transfer factor during boiling versus viscosity of the liquid:

1 - Horizontal heating surface

$q = 20 \cdot 10^3 \text{ kcal}/\text{m}^2 \cdot \text{h}$; 2 - Vertical heating surface

$q = 15 \cdot 10^3 \text{ kcal}/\text{m}^2 \cdot \text{h}$; 3 - Order of magnitude of heat transfer factor for dispersed media studied.

As is apparent from the figure, the effect of viscosity on the value of the heat transfer factor is sufficiently perceivable only in the region of insignificant concentrations for the sugar solution, i.e., at low initial variations in its viscosity. With an increase in concentration and, accordingly, solution viscosity, its effect on the value of the heat transfer factor is reduced. The curve, in practice, flattens out.

These results substantiate the conclusions of V. M. Borishanskiy [3] concerning the considerable effect of medium viscosity on the intensity of the boiling process only in regions of low concentrations and small thermal loads. The obtaining of quantitative recommendations, taking this effect into account, is the subject of a separate study. Of particular interest are the data obtained in tests for nutrients, which are two-phase systems with varying degrees of dispersion.

These media contain dissolved and scattered protein components in the form of particles, which give to the solutions the

ability to change their viscosity discretely at certain temperatures.

As the boiling point is approached, clusters are formed which, along with the particles, create noticeable turbulence throughout the liquid. Therefore, for such media it is meaningless to establish the relationship between the heat transfer factor during boiling and the viscosity of the medium.

As is apparent from the figure, in spite of the fact that in such media conditional viscosity becomes substantially higher than for pure water (on the average, for the media $\mu \sim 30 \cdot 10^{-5} \text{ kg} \cdot \text{s}/\text{m}^2$), the heat transfer factor for them is near its value for water under corresponding conditions, i.e., it has a greater value than it would have to have according to the actual medium viscosity. We should, therefore, perform additional research to clarify the effect of the size of the particles suspended in the medium and the medium's degree of dispersion on heat transfer intensity during boiling.

The importance of accumulating further data, particularly on the thermophysical characteristics and peculiarities of heat and energy exchange during boiling, is dictated by the necessity for using them in the engineering development of technological processes and the equipment of enterprises in a number of industrial areas, for the purpose of organizing more effective and economical heat consumption in industrial engineering.

BIBLIOGRAPHY

1. Аверин Е. К. Теплообмен при кипении водных растворов сахара. «Известия Академии наук СССР, ОТН», 1954, № 3.
2. «Современные проблемы теплообмена», перев. с англ. под общей ред. Б. С. Петухова. Изд-во «Энергия», 1966.
3. Борисянский В. М. Автореферат докт. диссертации. МНФИ, 1969.

A STUDY OF HEAT TRANSFER AND
THERMAL MODES DURING THE FORCED
FLOW OF WATER IN ECCENTRIC
ANNULAR CHANNELS

P. A. Andreyev, N. S. Alferov,
and R. A. Rybin

Designations

t - temperature, °C;
 α - heat transfer factor, kcal/m²·h·°C;
 $\epsilon = \frac{e}{d_2 - d_1}$ - relative eccentricity;
 e - eccentricity, m;
 d - channel diameter, m;
 q - thermal flux, kcal/m²·h.

Subscripts:

$ст$ - wall,
 $в$ - water,
 $экв$ - equivalent,
 $расч$ - calculated,
 $пот$ - loss,
 $н$ - external,
 $вн$ - internal.

In the making of heat exchangers of the pipe-in-pipe type there can occur a deviation from the mutually concentric arrangement of the pipes forming the heat exchangers. A deviation from the concentric arrangement and, at the limit, a touching of the pipes can lead both to a change in the heat-exchange characteristics of the channel and to the appearance of a substantial temperature misalignment along the perimeter of the pipes. The latter during independent heating (for example, during nuclear) can cause overburning of the pipes [1].

There have been very few experimental works in this direction in spite of their obvious practical value. In reference [2], based on tests with vertical annular eccentric slots, a formula for heat transfer, averaged along the channel, is obtained, and it is noted that a temperature misalignment occurs along the perimeter of the channel.

In [3] it is indicated that the eccentricity of the pipes forming the annular channel causes a considerable nonuniformity in wall temperature along the channel perimeter.

In our work we have studied heat transfer in an annular channel at $d_2/d_1 = 1.2$ during the flow of water under a pressure of 150 atm (abs.). Tests were made with a relative eccentricity ϵ variation from 0 to ~0.9 in convective heat transfer modes during the turbulent flow of water¹ and during surface boiling.

A more detailed description of the experimental apparatus, which is a closed circulation loop with a forced circulation of water, is presented in reference [4]. The annular slot of the experimental channel was formed by pipes 15 × 1 and 20 × 1 in diameter. With the aid of special adapters in the upper and

¹With a determination of Re based on average water velocity, average temperature, and $d_{\text{снв}} = d_2 - d_1$.

lower sections of the working channel, the internal pipes could be shifted relative to the external. The parallel nature of both pipes was preserved (Fig. 1).

In the upper and lower chambers of the experimental channel four thermocouples each were established in sleeves at diametrically opposite points. Electrical insulation and sealing of the pipes in the upper part of the channel was accomplished with paronite lining, and in the lower section with a stuffing gland. The gland, however, permitted a relative mutual displacement of pipes in an axial direction because of the unlike thermal expansion. The internal pipe was heated by passing electrical current through it. The current was fed to terminals; the lower terminal was detachable.

To remove heat from the ends of the internal pipe which were not cooled by the basic flow of water, these ends were made in the form of tap water-cooled condensers. Thermal insulation and heat-loss compensation were accomplished as in reference [4].

For measuring the wall temperature of the internal pipe of the channel, thermocouples were placed in four sections along its length: in each section four thermocouples were installed. Since the water temperature along the perimeter of the channel and, consequently, at its outlet, due to the eccentricity and constant thermal load¹, could be substantially nonuniform, a mixing cylinder was installed at the channel outlet to determine the average per-volume temperature (see Fig. 1).

The indications of the thermocouples at channel outlet (see Fig. 1) confirmed this assumption. As the tests revealed, the nonuniformity of temperature at channel outlet increased with an increase in the thermal load and eccentricity.

¹In this case, we shall disregard the change in heat release connected with the various dc resistances due to the various wall temperatures along the perimeter of the channel.

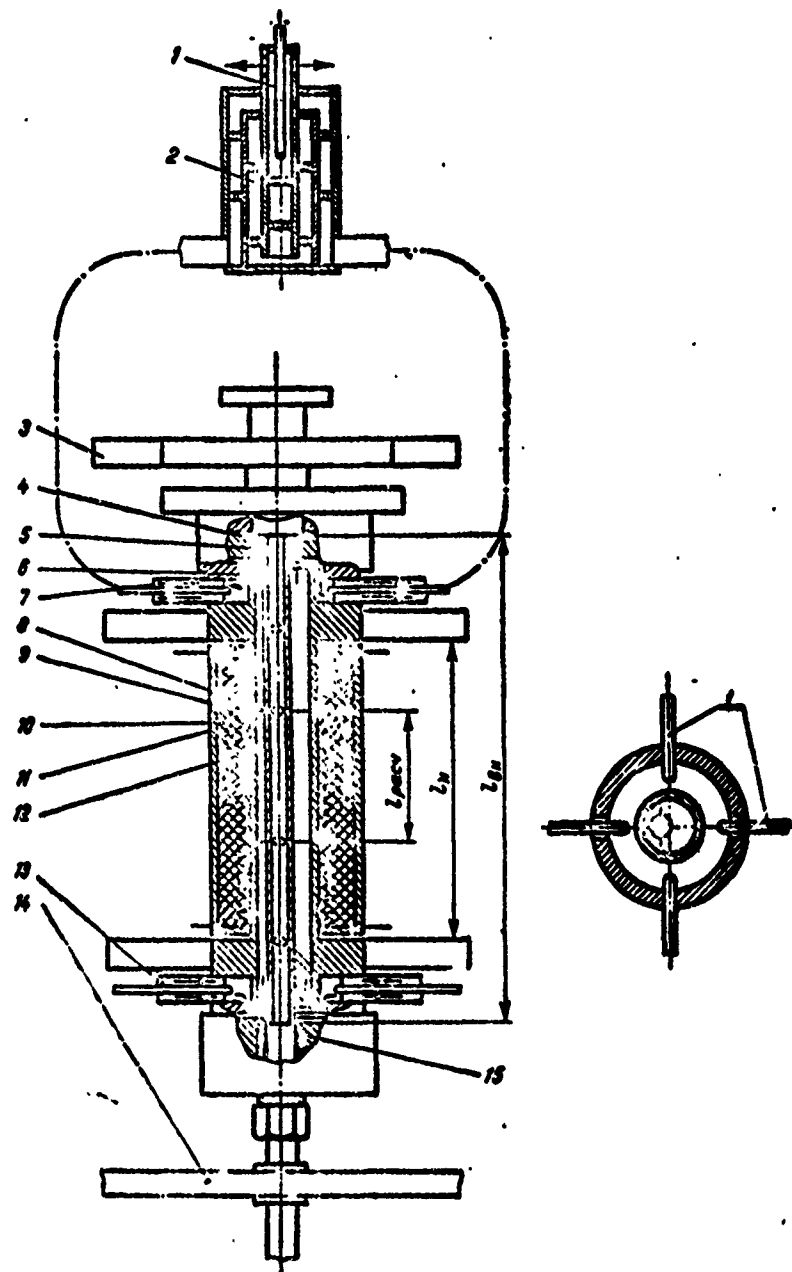


Fig. 1. Experimental installation:

1 - Sleeves for thermocouples; 2 - Mixing cylinder; 3 - Upper end; 4 - Ring; 5 - Paronite lining; 6 - Internal pipe; 7 - Water removal; 8 - Thermocouples; 9 - Compensation heaters; 10 - Asbestos-cement housing; 11 - Metal housing; 12 - External pipe; 13 - Water intake; 14 - Lower end; 15 - Support ring.

The high pressure and small slot width made it impossible to measure the water temperature along the perimeter of the channel and thus determine the local values for the heat transfer factors in the eccentric slot. Because of this only the values of the average heat transfer factors were determined as a function of the value of eccentricity and temperature diagrams along the perimeter were obtained with various eccentricities, thermal loads, and mass velocities in convective heat-exchange modes and surface boiling.

The heat transfer factor α was determined as the average in the segment between section I-II (see Fig. 1) located $l = 23d_{\text{эKB}}$ from input and $l = 20d_{\text{эKB}}$ from output:

$$\bar{\alpha} = \frac{q}{\Delta t}, \quad (1)$$

where

$$\Delta \bar{t} = \bar{t}_{\text{cr}} - \bar{t}_{\text{st}}; \quad \bar{t}_{\text{cr}} = \frac{1}{2} \left[\left(\frac{t_1 + \dots + t_n}{n} \right)_I + \left(\frac{t_1 + \dots + t_n}{n} \right)_{II} \right]; \quad (2)$$

$n = 4$ is the number of thermocouples installed in a given section.

The average water temperature \bar{t}_B was determined by linear extrapolation of the thermocouple readings at input and output of the working channel. For illustration, the test data with heating of the internal pipes are presented on Fig. 2 in coordinates $\frac{\overline{Nu}}{\overline{Pr}^{0.4}} = f(\overline{Re})$ for $\epsilon = 0.4$ and 0.78 . The physical constants were selected based on average water temperature.

As is apparent from Fig. 2, with an increase in eccentricity the average heat transfer factor, determined by formula (1), decreases.

Quantitative relationships for heat transfer to the internal pipe in an eccentric channel can be expressed by formula

$$\overline{Nu} = C \overline{Re}^m \overline{Pr}^{0.4}, \quad (3)$$

where

$$C = 0,0205(1 - \varepsilon)^{0,18} \quad (4)$$

for values of $\varepsilon = 0-0.9$, $d_2/d_1 = 1.2$, thermal fluxes up to 10^6 kcal/m²·h and Reynolds numbers up to 300,000.

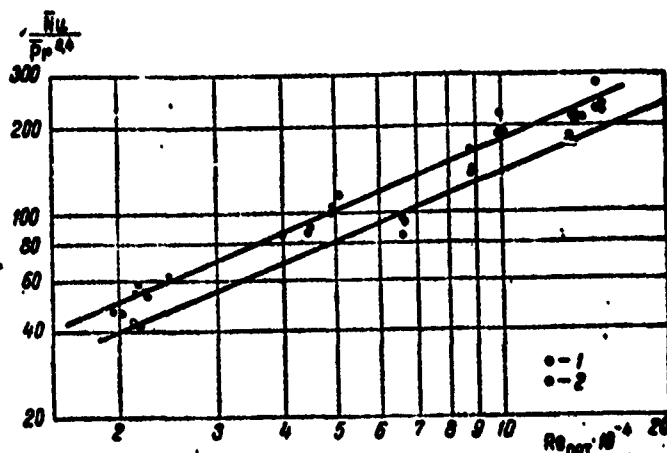


Fig. 2. Function $\frac{Nu}{Pr^{0.4}} = f(Re)$:

1, 2 - When $\varepsilon = 0.4$ and 0.78 , respectively.

If we assume that heat transfer from the internal pipe to the flow along the generatrix of the channel, determined by angle β (Fig. 3), depends only on the velocity in the gap formed by the external and internal pipes, and on the equivalent diameter corresponding to this gap, and if we also assume that there occur along the entire perimeter of the eccentric channel a turbulent flow, equality between the resistances of the eccentric channel and the corresponding concentric channel, full alignment of the water temperature along the perimeter of the channel, then we can estimate the relationship between the average heat transfer along the perimeter of the eccentric channel and the corresponding concentric channel as a function of ε .

The relationship thus calculated can be compared with formula (5) experimentally obtained in reference [4]:

$$Nu = 0,023 \left(\frac{d_2}{d_1} - 1 \right)^{0,12} Re^{0,8} Pr^{0,4}. \quad (5)$$

For an eccentric channel along the generatrix corresponding to angle β , we assume that $d_2 = d_1 - 2\delta$, and $d_{\text{эKB}} = 2\delta$ (see Fig. 3)¹; then

$$Nu = 0,023 \left(\frac{2\delta}{d_1} \right)^{0,12} Re^{0,8} Pr^{0,4}. \quad (6)$$

Assuming, as shown above, that

$$\Delta p = \frac{A}{Re^{0,25}} \cdot \frac{l}{2\delta} \cdot \frac{\gamma w^2}{2g} = \frac{A}{Re_0^{0,25}} \cdot \frac{l}{d_2 - d_1} \cdot \frac{\gamma w_0^2}{2g}, \quad (7)$$

from (7) we find the expression for velocity in an eccentric channel:

$$w = w_0 \left(\frac{d_2 - d_1}{2\delta} \right)^{0,572}, \quad (8)$$

where

$$z = \sqrt{\left(\frac{d_2}{2} \right)^2 - e^2 \sin^2 \beta} - \left(\frac{d_1}{2} + e \cos \beta \right). \quad (9)$$

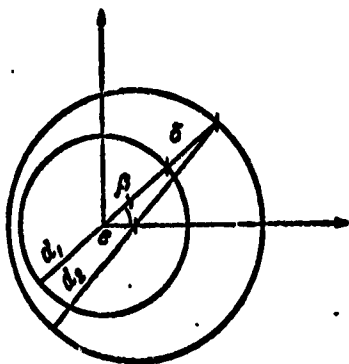


Fig. 3. Calculation diagram for formula (9).

Solving jointly equations (5), (6), (8), (9) and integrating along the channel perimeter, we can obtain the relationship

¹ δ is the gap between the internal and external pipes, corresponding to angle β .

between the heat transfer, averaged along the perimeter, of the eccentric channel and the corresponding concentric channel. It will have the form:

$$\frac{\bar{\alpha}}{\alpha_0} = \frac{1}{\pi} \int_0^\pi \left[\sqrt{\left(\frac{d_2}{d_2 - d_1} \right)^2 - \varepsilon^2 \sin^2 \beta} - \left(\frac{d_1}{d_2 - d_1} + \varepsilon \cos \beta \right) \right]^{0.493} d\beta. \quad (10)$$

After integrating¹ expression (10), we obtain the function $\bar{\alpha}/\alpha_0 = f(\varepsilon)$. This function is illustrated in Fig. 4.

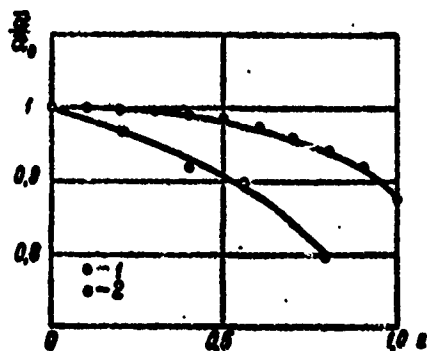


Fig. 4. Graph of function $\bar{\alpha}/\alpha_0 = f(\varepsilon)$:

1 - Calculated points; 2 - Experimental points.

The character of the variation in the average heat transfer factor as a function of ε , evaluated by formula (10) and determined experimentally, agree qualitatively. However, a quantitative comparison would be difficult since, in reality, there occurred a temperature misalignment for the water along the channel perimeter, and in the narrow part of the slot at $\varepsilon > 0.8$ a transition occurred to laminar flow. The wall was heated to a temperature at which surface boiling began, which, accordingly, disrupted one of the conditions on which we based relationship (10). Obviously, this explains the fact that the experimental function $\bar{\alpha}/\alpha_0 = f(\varepsilon)$ differs considerably from the calculated function.

¹Numerical integration of equation (10) was performed on the Ural-2 computer.

In addition to the average values of the heat transfer factor, temperature diagrams were obtained along the circumference of the channel, which were plotted from measurement data taken at four points along the perimeter: $\beta = 0, 90, 180, \text{ and } 270^\circ$.

The characteristic graphs of temperature distribution along the perimeter of the internal pipe for the first section and at various values of ϵ , w_0 , and q are presented in Fig. 5. The temperature maximum virtually agrees with the narrowest section of the channel. From Fig. 5 it is apparent that with the beginning of surface boiling in a channel an alignment of wall temperature along the circumference of the pipe being heated also occurs.

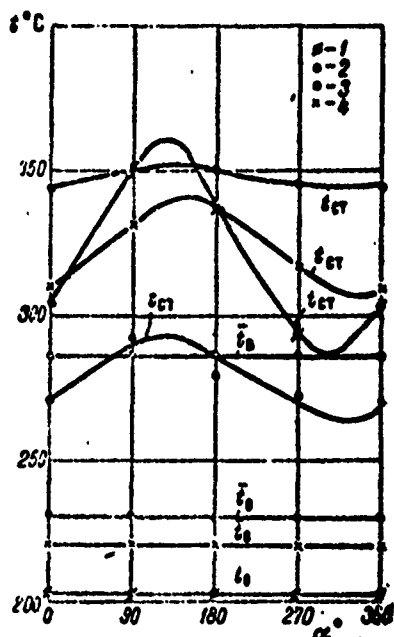


Fig. 5. Distribution of wall temperatures along the perimeter of inner pipe in the first cross section when

$q = 1 \cdot 10^5 \text{ kcal/m}^2 \cdot \text{h}$, $\epsilon = 0.78$:
 1 - $w_0 = 1 \text{ m/s}$; $\bar{t}_b = 203.5^\circ\text{C}$;
 2 - $w_0 = 1 \text{ m/s}$, $\bar{t}_b = 286.3^\circ\text{C}$;
 3 - $w_0 = 3.0 \text{ m/s}$, $\bar{t}_b = 229.5^\circ\text{C}$;
 4 - $\epsilon = 0.56$, $w_0 = 1 \text{ m/s}$,
 $t_b = 220^\circ\text{C}$.

To remove the temperature misalignment of the metal of the eccentric channel it would be necessary to work in the surface boiling mode, i.e., other things being equal, we would have to raise the temperature of the heat-transfer agent.

An increase in velocity reduces, as we would expect, the absolute nonuniformity of temperature along the perimeter of the channel being heated. This is caused, first of all, by a decrease in the thermal head at a prescribed thermal load due to the numerically greater values of the heat transfer factor, as well as the increase in overall flow turbulence, and, in connection with this, the more intensive displacement of the flow along the perimeter of the channel. However, the last assumption is not obvious since the analysis of curves 1, 3 (see Fig. 5) shows that

$$\frac{(t_{cr} - \bar{t}_s)_{\max}}{(t_{cr} - \bar{t}_s)_{\min}} \approx \frac{q_{\max}}{q_{\min}} = 1.8$$

is comparatively equal both for the velocity 1 m/s and for the velocity 3 m/s. Consequently, either water temperature or misalignment along the perimeter is insignificant or the increase in temperature misalignment with a decrease in the water flow rate is compensated by higher values for the heat transfer factor in the narrow section because of an increase in the Re numbers.

A decrease in eccentricity, as we would expect, reduces the temperature misalignment (see Fig. 5, curve 4). At $\epsilon = 0.56$ (4) $\frac{(t_{cr} - \bar{t}_s)_{\max}}{(t_{cr} - \bar{t}_s)_{\min}} = 1.4$, whereas this same quantity at $\epsilon = 0.78$ is 1.8.

All the above relative to temperature distribution along the perimeter of the channel is also valid for the case of two-sided heating. With this, temperature misalignments reach higher values. At $\epsilon = 0.88$, $q_H = q_{BH} = 1 \cdot 10^6$ and $w_0 = 1$ m/s temperature misalignment reaches 100°C. With the beginning of surface boiling at any of the perimeter points, the increase in wall temperature with a rise in q at a given spot was retarded.

BIBLIOGRAPHY

1. Крачеров А. Я., Шевелев Я. В. Инженерные расчеты ядерных реакторов. Атомиздат, 1964.
2. Бек Ф. Теплоотдача и потеря давления в вертикальных кольцевых щелях при вынужденном движении и свободной конвекции. Экспресс-информация. «Теплоэнергетика», 1964, № 27.
3. Субботин В. И., Ушаков П. А., Свириденко Н. П. Исследование теплообмена при турбулентном течении ртути в кольцевом зазоре. «Атомная энергия», октябрь 1964.
4. Алферов Н. С., Рыбин Р. А. Теплоотдача в кольцевых каналах. В сб.: «Конвективная теплоотдача в однофазном и двухфазном потоках». Л., изд-во «Энергия», 1964.

PROBLEMS OF HEAT EXCHANGE DURING THE COOLING OF CRYOGENIC PIPING

A. A. Gukhman, L. S. Aksel'rod,
V. G. Pron'ko, A. B. Bulanov,
D. A. Kazenin, and G. M. Leonova

Designations

- l - length of piping;
- d - internal diameter of piping;
- δ - thickness of pipe wall;
- z - coordinate along the axis of the pipe;
- τ - time;
- τ_* - pipe cooling time;
- j - mass flow rate;
- j_r - mass velocity of the gas (vapor) flow;
- q_w - local heat flux from wall;
- q_w - heat flux from wall, averaged along the length;
- Q_2 - quantity of heat given off by piping to the flow;
- Q_0 - full excess heat content of pipe;
- T_w - pipe wall temperature;
- T_{w0} - initial temperature of pipe wall;
- T_m - temperature of liquid in feeder vessel;

T_s - saturation temperature;
 T_* - temperature of maximum overheating of the liquid;
 $T_{кр}$ - critical temperature;
 T_r - gas temperature (overheated vapor);
 $T_{вх}$ - temperature of flow at input;
 p_0 - pressure at input;
 p - current pressure;
 p_ϕ - pressure in front of liquid front;
 Δp - available pressure drop;
 $\rho_{ж}$ - density of liquid;
 ρ_s - density of saturated vapor;
 ρ_r - gas density (overheated vapor);
 ρ_w - density of pipe wall material;
 c_w - average specific heat capacity of pipe wall material;
 $c_{ж}$ - specific heat capacity of liquid;
 c_p - isobaric heat capacity of overheated vapor;
 r - heat of vaporization;
 ξ - coefficient of hydraulic resistance;
 λ_w - heat conductivity of walls;
 M - mass of piping;
 α - heat transfer factor;
 w - linear velocity.

Abbreviations:

$кр$ - critical
 $п$ - flow
 $ж$ - liquid
 $вх$ - input
 $вых$ - output
 $вн$ - internal

I. PROBLEMS OF HEAT EXCHANGE AND HYDRODYNAMICS DURING THE COOLING OF CRYOGENIC PIPES

The process of heat exchange during the cooling of cryogenic pipes includes a broad group of phenomena. This is explained, first of all, by the fact that the range of pipe wall temperature variations is considerable - from the temperature of the ambient medium, which considerably exceeds the critical temperature of the cryogenic fluid, to the temperature of the fluid itself.

When a cryogenic fluid is fed into an uncooled pipe, the temperature differential between it and the wall is so great that an extremely unique thermal situation is created. Overheating in the zone of contact between the liquid and the wall is considerably higher than the gradient of metastable state stability. Therefore, the existence of liquid phase on the surface of the wall becomes physically impossible and the wall of the pipe is fully blocked by a vapor ring. Inside this ring there is a flow of liquid in which the form of liquid motion can be varied. The phenomenon when liquid at sufficiently high surface temperature can not touch the surface is called the Leydenfrost effect. We call these specific conditions for interaction between the working medium and the wall the Leydenfrost regime.

The problem of determining the boundary of the highest possible liquid overheating was examined theoretically by Doring [1]. In the work of Spugler et al. [2] the following approximate formula was proposed for evaluating the temperature of maximum overheating T_* at pressures far from critical: $T_* = 27/32T_{np}$. For oxygen, nitrogen, and hydrogen this evaluation is 131, 107, and 28.2°K, respectively. After the pipe wall is cooled to temperatures at which moistening begins, the character of the process changes. Heat transfer is forced by the appearance of nucleate boiling. As wall temperature approaches the temperature of the liquid, heat flux decreases, tending toward the value of external heat leak.

The specifics of local heat exchange between the wall and the two-phase flow are closely connected with the hydrodynamic structure of the flow, distinguished by extremely varied forms.

The boundaries between the various regimes of two-phase flow are not clearly defined, all the more so for cryogenic fluids under heat exchange conditions with a solid surface at variable temperature. There are particular empirical methods for determining the regions of the various flow forms, from which we should mention, with respect to cryogenic liquids, the Baker diagram [8].

Recently a number of works have been published in which the results of a visual study on the structure of the two-phase flow of cryogenic liquids have been discussed. Thus, Laverty and Rosenow [9] in tests on the flow of nitrogen in a heatable transparent pipe observed, at low vapor contents, an annular flow regime with a liquid core and a vapor boundary layer - reversed annular regime. With an increase in the vapor content a disruption of the core was observed and a transition to a dispersed structure with a supporting vapor phase. The American scientists Chi and Vetere [7, 14] in tests on the cooling of copper pipes with liquid hydrogen observed, through a transparent section installed behind the experimental section, a shell flow regime ($\phi \approx 0.6$), which we shall subsequently call a liquid shell regime. In addition, with the aid of high-current measurements of flow temperature, the presence of a dispersed liquid phase in the vapor intervals between liquid shells was established in the same work. An analysis of data presented in the above work indicates that, in the range of flow velocity (encountered in problems of cooling cryogenic pipes) the orientation of the pipe does not affect the structure of the flow and the local values for thermal flux.

II. DESCRIPTION OF EXPERIMENTAL EQUIPMENT AND RESEARCH METHOD

The purpose of the experimental research performed at VNIImash [All-Union Scientific Research Institute of Oxygen Machinery] was to determine the most common regularities which are characteristic for the cooling period of cryogenic pipes.

Tests to determine the time required to cool pipes with liquid oxygen and nitrogen were performed on flow test stands with pipes having an internal diameter of $d = 3.4-46$ mm, relative length of $l/d = 30-2800$ and wall thickness of $\delta = 0.25-35$ mm, made of various materials (stainless steel, brass, copper, German silver).

The principal layout of the stands were kept the same in all cases (Fig. 1). Liquid oxygen (or nitrogen) was fed from vessel 1 to the receiving vessel 5 along the experimental piping. The design of vessel 1 made it possible to feed liquid (10-500 l) out of it at a pressure up to 6 atm (gauge). The liquid flow rate was set as a function of the pressure differential in vessels 1 and 5 and was measured with a diaphragm located in the section of the pipe cooled beforehand, in front of the test section or was measured with respect to the increase in the level in the receiving vessel (this vessel was cooled beforehand).

The underheating of the liquid to the saturation state was determined by excess pressure in vessel 1.

The test pipe was a horizontal pipe which was insulated or (in many cases) not insulated against external heat leak. Copper-constantan thermocouples were soldered along the outside of the pipe. In addition, there was a thermocouple for measuring flow temperature at the end of the pipe.

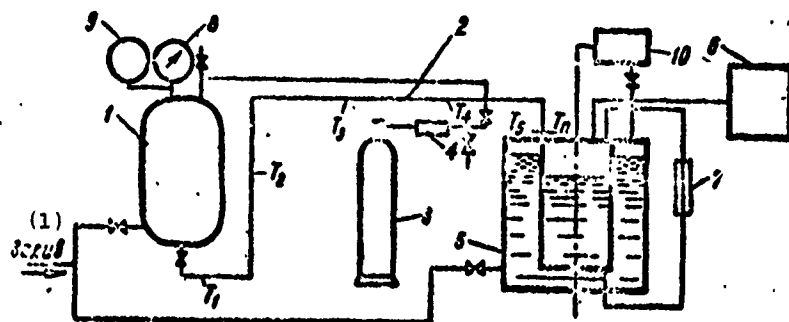


Fig. 1. Experimental installation:
 1 - Vessel for feeding liquid; 2 - Experimental piping; 3 - Gas cylinder; 4 - Reducing gear;
 5 - Receiving vessel; 6 - Gas flow rate meter;
 7 - Level sensor; 8 - Sample manometer;
 9 - MED pressure sensor; 10 - DM pressure sensor;
 T_n - Thermocouple in flow; T_1 - T_5 - Thermocouples on pipe wall.
 KEY: (1) Fill.

In several experiments, the vapor-liquid mixture was separated at input to the receiving vessel; the amount of vapor forming in the pipe was measured by a gas meter.

The stand was equipped with secondary instruments for recording temperature, pressure, liquid level in vessels, and pressure drop on the diaphragm.

Wall temperature was measured with copper-constantan thermocouples with an electrode diameter of 0.1 mm and recorded by an electronic potentiometer EPP-09. The class of instrument accuracy was 0.5, but, due to the nonlinearity of the temperature curve of the thermoelectromotive force, absolute measurement error was different at different points of the temperature range. In the region of oxygen temperatures (90°K) measurement error can reach 2°K. The EPP-09 has a certain time lag. The time required for the carriage to pass through the full scale is 2.5 s; however, in the authors' tests on cooling, which lasted, as a rule, several tens of seconds, this time lag, under the conditions of the

Leidenfrost regime, did not produce any noticeable problem. The time lag of the heat sensor was considerably less than the time lag of the instrument.

Local thermal flows to the cryogenic liquids were evaluated according to formula $q_w = -c_w \rho_w \delta \, dT_w/d\tau$ based on the graphic differentiation of the temperature curve in the cooling process. The terms of the series containing higher derivatives were not applied in calculation due to their smallness and the low accuracy of multiple graphic differentiation.

In the accepted methodology for determining q_w it is assumed that during feeding into a warm pipe, cryogenic liquid obtains heat only from the cooling of the wall. Heat leak to uninsulated pipes, although it exceeded the values in reference [11], nevertheless was one order less than the heat leak to the liquid from wall cooling; in the regime studied $q = 1.5 \text{ kW/m}^2$. Such a correction can have no substantial effect on the value of τ_* .

III. BASIC RESULT OF EXPERIMENTS

The results of these experiments showed that the relative length of the pipe had a considerable effect on the relationship between the time required for full cooling and the time required for liquid to appear at the end of the pipe. Based on this relationship we can subdivide the pipes into long, medium and short.

Pipes in which the liquid reaches the output section in the "initial surge" stage are called "short"; "long" pipes are those in which the full length of the pipe is considerably greater than the length of the "initial surge." The amount of heat transmitted to the flow throughout the entire length of the pipe can be expressed as:

$$Q_1 = \pi d \int_0^{l_1} \int_0^{\tau_1} q_w \, z d\tau. \quad (1)$$

The amount of heat necessary for full evaporation of the liquid is

$$Q_2 = \frac{\pi d^2}{4} \int_0^l (c_A \Delta T_w + r) dz. \quad (2)$$

If the amount of heat entering the liquid flow from the walls is considerably greater than that necessary for its full evaporation, part of the pipe is filled with vapor. As the pipe cools the vapor flow changes into two-phase with an increasing content of liquid phase.

When $Q_1 \ll Q_2$, two-phase flow appears at the end of the pipe at the initial moment. For an evaluation of the length of such pipes we can assume that the average heat flux along the length of the pipe does not vary during cooling (this is confirmed by the results of the experiments), the forming vapor is not overheated, and the mass velocity of the flow remains constant. Then condition $Q_1 \ll Q_2$ can be written in the form:

$$\frac{l}{d} \ll \frac{l(r + c_A \Delta T_w)}{4q_w}. \quad (3)$$

Pipes which satisfy requirement (3) in the cooling period will be called "short." Pipes in which the cooling process has generally ceased by the time the vapor-liquid mixture reaches the end will be called "long"; pipes corresponding to the condition $Q_1 \approx Q_2$ will be called "medium." Such a classification does not claim to be strict but emphasizes, more or less, the qualitative differences which occur during the cooling of pipes of different types. We should stress that the relative length of the pipes l/d in itself is not critical for its classification in a certain category, since the determining factors are not only structural but also the parameters of the regime.

For an approximate evaluation of the operational characteristics of a pipe (short, medium, or long) we can use inequality (3).

The relationship between the cooling time and the time required for liquid to appear, as a function of pipe length, is shown in Fig. 2.

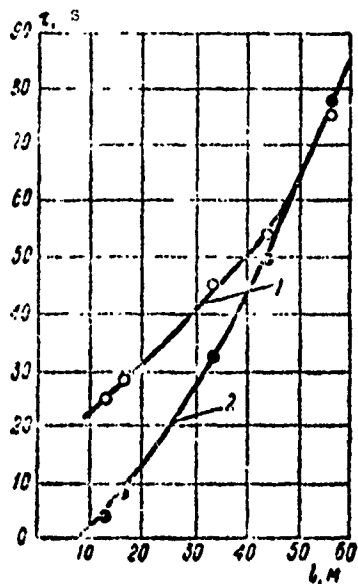


Fig. 2. Time required for liquid to appear at the end of the line and cooling time versus pipe length (pipe St. 1Kh18N9T, $\varnothing 22 \times 1$ mm, $p_{ax} = 4$ atm (abs.), $p_{bux} = 1$ atm (abs.)):
1 - Time of full pipe cooling;
2 - Time of liquid appearance at end of pipe.

Figure 3 shows typical graphs of wall temperature variations during cooling by liquid oxygen; pipe parameters are given, as well as data characterizing the two-phase flow. Temperature T_* corresponds to the sharp change in cooling rate, clearly noticeable on most of the temperature curves. The high intensity of heat exchange after the wall reaches the indicated temperature values attests to the fact that the pipe is cooled in this section by a transition to nucleate boiling. To a considerable extent, the time required for full pipe cooling is determined by the cooling period to temperature $T = T_*$, which, in most cases, is approximately 80-90% of the overall cooling time. Because of this, a knowledge of the value of specific heat flux in the first stage of cooling is of considerable significance in determining cooling time. As an example, Figure 4 shows the variation during cooling of the value of specific heat flux in various sections of the pipe.

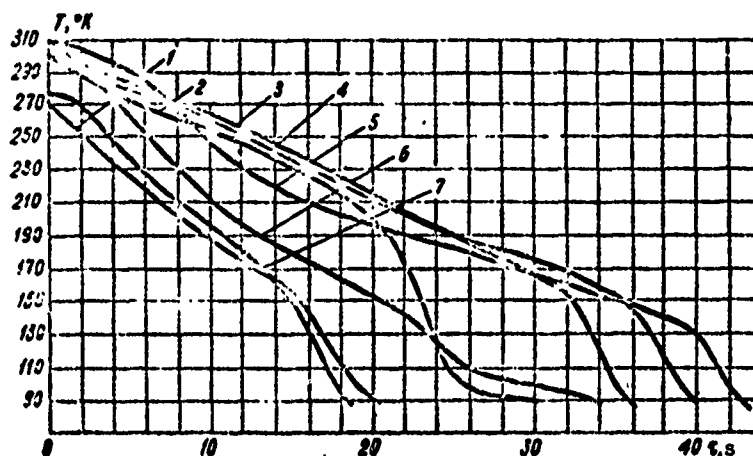


Fig. 3. Typical wall temperature variation during the cooling of a "medium" pipe by liquid oxygen (copper pipe, $\varnothing 45 \times 1.5$ mm, $l = 40$ m, $l/d = 950$, $p_{\text{BX}} = 3$ atm (abs.), $p_{\text{ВЫХ}} = 1$ atm (abs.)):
 1 - In section $z/l = 0$; 2 - In section $z/l = 0.05$;
 3 - In section $z/l = 0.2$; 4 - In section $z/l = 0.35$; 5 - $z/l = 0.5$; 6 - In section $z/l = 0.75$;
 7 - In section $z/l = 1$.

Local specific heat flux changes very little during the first cooling period; its maximum value does not exceed the minimum value more than by a factor of 2-2.5 in spite of the fact that the structure of the flow in medium and long pipes changes from a single-phase flow of superheated or saturated vapor to a reverse annular liquid-shell flow with low vapor content.

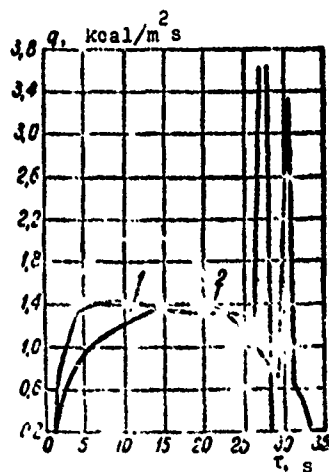


Fig. 4. Local thermal fluxes versus time during cooling by liquid nitrogen (German silver pipe, $\varnothing 3.9 \times 0.25$ mm, $l/d_{\text{ВН}} = 1230$, $p_{\text{BX}} = 1.24$ atm (abs.), $p_{\text{ВЫХ}} = 1.03$ atm (abs.)):
 1 - In section $z/d = 454$;
 2 - In section $z/d = 837$.

In the main part of the pipe the local specific heat removal changes both along the length and over time within such limits that its average value along the length of the pipe can be considered a constant value during most of the cooling time.

IV. GENERALIZATION OF EXPERIMENTAL DATA

Research performed at VNIKimash has shown that in a number of cases the process of cooling a pipe with gas can be examined as the cooling of a concentrated mass with infinitely great heat conductivity. In this case, the process is described by the following equation:

$$\frac{T_w - T_{w\infty}}{T_{w0} - T_{w\infty}} = e^{-At}, \quad (4)$$

where

$$A = \frac{\alpha \pi d l}{M c_z \left(1 - \frac{2 \pi l}{J_1 c_p d} \right)}.$$

The heat transfer factor was determined based on the familiar equation:

$$Nu = 0.023 Re^{0.8} Pr^{0.4}. \quad (5)$$

[First line of paragraph omitted in original Russian document] for average temperature and pressure values along the pipe. The results of the research also show that at high values of q/j , i.e., with considerable vapor content ($\phi \geq 0.9$), the intensity of heat removal, just as the time for cooling by a two-phase flow, can be determined based on the above relationship. The mass velocity of vapor phase, measured in experiments by a test method, is usually unknown in the actual practice of using cryogenic pipes. Because of this, in order to determine the intensity of heat transfer, it is necessary to gather data on the transmission capacity of the pipes.

In the gas escape stage it is characteristic to have three sections of pipe the relationship between which can change as the pipe fills. In the first section the liquid contacts the cooled wall; heat exchange occurs in the second and third sections, filled accordingly with a two-phase mixture and vapor. For "long" pipes the effect of the second section on the cooling rate can be considered insignificant in comparison with the effect of the third section. This is explained by the high vapor content, as well as the insignificant extent of this section when compared with the length of the pipe. To verify the admissibility of this assumption it is sufficient to compare the time of "gas outflow" and the time of "two-phase outflow." The latter can be evaluated based on the time of the initial increase of the liquid level in the receiving vessel and the cooling time of the pipe wall. As has already been noted, this time is relatively short for long pipes.

On the basis of the above, the following outline of the problem is possible. Excess thermal life for a pipe is acquired in the section filled with single-phase flow. The pipe in this section is considered a concentrated mass with infinitely high heat conductivity.

Allowance for the fact that $j = j_r$, $p_\phi = p_0$ and $G_r \Delta i = \text{const}$ makes it possible to propose the following equation for calculating the cooling time of long pipes:

$$\tau = \sqrt{2} \frac{c_{\text{w}} \bar{\epsilon}_{\text{w}} (T_{\text{w}} - T_{\text{m}})}{\Delta i} \left(\frac{1}{r \Delta p} \right)^{1/2} \left(\frac{l}{d} \right)^{3/2}. \quad (6)$$

The results of calculations based on equation (6) agree well with test data.

For average pipes such an outline of the problem is impossible because of the considerable effect of the section with two-phase

flow on heat transfer from the pipe wall. In the general case, for average pipes it is necessary to take into account the vapor content of the flow since this parameter determines the transmission capacity of the pipe and the intensity of the heat exchange.

For work with "short" pipes the instantaneous appearance of liquid in the output section is characteristic. Nevertheless, the problem of cooling such pipes is not a superfluous consideration. The physical picture of the process can be represented in the following manner. In the center of the pipe a liquid core is moving with unique distribution of velocity and temperature. The core is separated from the walls by a layer of vapor thickening along the path of movement. The increase in thickness of the vapor layer is balanced by the heat flux from the walls. Corresponding to this growth there occurs a decrease in the cross section of the liquid core and, consequently, an increase in its velocity. Taking into account losses from friction in the vapor layer, the acceleration of the liquid core is limited by the available pressure drop. Such a diagram is suitable with wall temperatures up to the value at which the wall can be moistened by the liquid. We should note that the motion of the vapor in the boundary layer is due not only to entrainment by the liquid core but also by the presence in the pipe of a pressure gradient caused by core acceleration.

Taking into account all the above, we can obtain the following expression which allows us to evaluate the cooling time of a short pipe based on the known design and physical parameters, as well as the available pressure drop:

$$\tau_* = 7 \left(\frac{l}{d} \right)^{2.9} \left(\frac{T_{w0} - T_s}{2T_s} \right)^{1/3} \left(\frac{\mu_r^2 d}{\rho_s \Delta p} \right)^{1/3} \frac{c_w \rho_w h_w}{\lambda_r} . \quad (7)$$

The values of the physical parameters are taken at average temperature $\bar{T} = T_{w0} + T_s/2$ and average pressure $p = p_0 - \Delta p/2$.

A check indicates that these evaluations correspond to the experimental data of the authors with accuracy up to $\pm 25\%$.

Conclusions

The cooling of cryogenic pipes by liquid oxygen and nitrogen has been studied.

On the basis of the experimental data obtained, which agree well with the results of other studies on hydrogen, the following is indicated.

1) Cooling in a worsening heat exchange regime, when the pipe wall does not directly contact the liquid, covers a large part of the full range of pipe wall temperature variation.

2) Pipes can be subdivided into long, medium, and short, based on the relationship between the time required for full cooling of the pipe and the time in which liquid transport begins.

As a result of the study, we have more precisely defined the physical models of the pipe cooling process proposed earlier and have formulated equations (6) and (7) which can be used for calculating the intensity of heat exchange and the cooling time for long and short pipes, respectively, as well as equation (4) which, with the use of evaluation of vapor phase mass velocity, can be applied for calculating medium pipes.

BIBLIOGRAPHY

1. Döring W. Zeitschrift für physikalische Chemie. Abteilung B. Band 36. Heft 3-6, 1937, s. 371.
2. Spugler, Hopenfeld, Silberberg, Bumpus, Norman. International Journal of Heat and Mass Transfer, 1963, vol. 6, № 11, pp. 987-989.
3. Chi J. W. H. Cooldown temperatures and cooldown time during mist flow. Advances Cryogenic Engineering, v. 10, 1965.
4. Merte M., Clark J. A. Boiling Heat Transfer Data for Liquid Nitrogen at Standard and Near-Zero Gravity. Advances Cryogenic Engineering, vol. 7, 1962.
5. Кутателадзе С. С., Стрыкович М. А. Гидравлика газожидкостных систем. Госэнергоиздат, 1958.
6. Кутателадзе С. С., Боришанский В. М. Справочник по теплопередаче. Госэнергоиздат, 1958.
7. Chi J. W. H., Vetro A. E. Two-phase flow during transient Boiling of Hydrogen and determination of nonequilibrium vapor fractions. Advances Cryogenic Engineering, vol. 9, 1964, p. 243.
8. Bronson I. C., Edeskuty F. I. et al. Problems in cooldown of cryogenic systems. Advances Cryogenic Engineering, vol. 7, 1962, pp. 198-205.
9. Lavery M. F., Rosenow W. M. Film boiling of saturated Nitrogen flowing in a vertical tube. Paper ASME, № NA/HG-26, 1965.
10. Карслоу Г., Егер Д. Теплопроводность твердых тел. Изд-во «Наука», 1964.
11. Р. Френн. Изоляция резервуаров для жидкого водорода в ракетной технике. Сб. переводов: «Жидкий водород». Изд-во «Мир», 1964, стр. 281-296.
12. Chi J. W. H. Forced Convective Boiling Heat Transfer to Hydrogen, «Journal of Spacecraft and Rockets», vol. 3, 1965, № 1, pp. 150-152.
13. Burke J., Byrness W., Post A., Russia F. E. Pressurised cooldown of cryogenic transfer lines. Advances in Cryogenic Engineering, vol. 4, 1960, pp. 378-394.
14. Chi J. W. H. Hug flow and film boiling of hydrogen. «Paper ASME», 1965, № WA/MT-32.
15. Drake E. M., Russia F. E., Ruder I. M. Pressurised cooldown of a cryogenic liquid transfer system containing vertical sections. Advances in Cryogenic Engineering.

CHARACTERISTICS OF HEAT EXCHANGE IN THICK-WALLED HORIZONTAL PIPES AND ANNULAR CHANNELS WITH LAMINAR FLOW OF A VAPOR-WATER MIXTURE

L. B. Katsenelenbogen and
Ya. N. Rudnitskiy

Designations

- $R_1 = 0.5d_1$ - internal radius of pipe;
- $R_2 = 0.5d_2$ - external radius of pipe;
- $R_1 \leq R \leq R_2$;
- $\delta = R_2 - R_1$ - pipe wall thickness ;
- r - radius of insert;
- L, l - length;
- F - area;
- Q - heat removal;
- $q_{\text{нар}}$ - thermal flux on outer surface of pipe;
- $q_{\text{вн}}$ - thermal flux on inner surface of pipe;
- $q^{(p)}$ - thermal flux by spreading along wall of pipes;
- α - heat transfer factor;
- $\alpha_{\text{эKB}}$ - heat transfer factor, equivalent to spread;
- $\alpha_{\text{э}\phi}$ - total heat transfer factor in laminar zone;

λ - coefficient of heat conductivity;
 t - temperature;
 t_{cp} - average wall temperature of pipe outside laminar zone;
 t_{nac} - temperature on saturation line;
 $t_{вepx}$ - temperature of upper generatrix of outer surface of pipes;
 $t_{низ}$ - temperature of lower generatrix of outer surface of pipes;
 $\Delta t = t - t_{cp}$ - overheating of upper generatrix;
 Δt_{cr} - temperature drop in pipe wall;
 Δt_{α} - temperature head corresponding to heat transfer factor;
 c_p - dimensionless overheating of upper generatrix of pipes;
 k_p - indicator of thermal spread;
 $2\theta_0$ - central angle in pipe corresponding to phase interface;
 $0 \leq \theta \leq \theta_0$;
 2Ω - central angle in annular channel corresponding to phase interface;

$$v_n = \frac{2n+1}{2\theta_0} \pi;$$

$$g_n = (-1)^n \frac{2q_{nap}}{v_n \theta_0};$$

$$x_n = (-1)^n \frac{2f_{nac}}{v_n \theta_0};$$

n - summation index, $n = 0, 1, 2, \dots$;
 w - circulation velocity;
 β - flow-rate vapor content per unit volume;
 ϕ - true vapor content per unit volume;
 S'_K - area of vapor segment in ring;
 s'_{kp} - area of vapor segment in circle.

In evaporative cooling devices for continuous heating furnaces of rolling mills the main cooling elements are thick-walled horizontal pipes which form a support bridge along which the metal billets move during their heating in the furnace [1]. To insure the reliable performance of this support, pipe wall

temperature must not exceed the temperature dictated by strength considerations.

Since the temperature drop in the wall of hearth pipes is 50-100°C, the use of the existing calculation function [2] for determining the overheating of the upper generatrix of the pipe during lamination is not admissible since it is valid for the case of a small drop in the pipe wall. In addition, while determining the overheating of the upper generatrix on the internal surface of the pipe, it does not permit the calculation of the external temperature in the overheating zone. (As shown below, the temperature drop in the pipe wall in the laminar zone can not be calculated according to the usual formulas for heat transfer through a cylindrical wall [3]).

In order to apply the method developed by M. A. Styrikovich and Z. L. Miropol'skiy for calculating the overheating of pipes in a laminar zone, for pipes with any wall thickness, Neuman's problem for an annular sector [4] is examined. By annular sector we mean that part of the ring bounded by the two radii (Fig. 1).

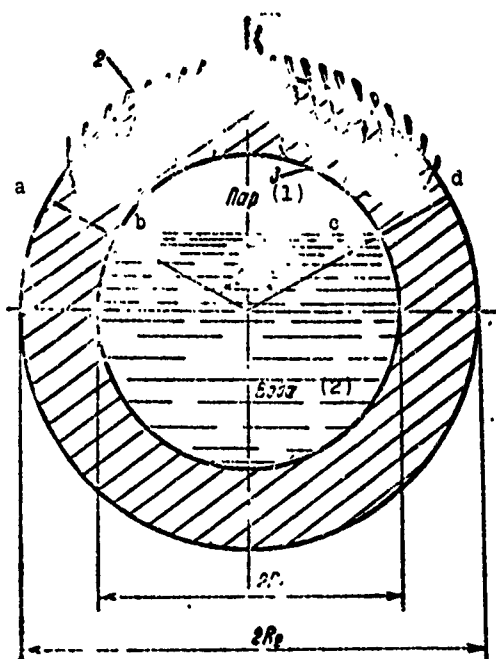


Fig. 1. Diagram of heat removal in a horizontal pipe with laminar motion of a vapor-water mixture: abcd - annular sector in laminar zone; 1 - external heat flux; 2 - heat removal by spreading along wall $q^{(p)}$; 3 - heat removal to vapor.
KEY: (1) Vapor; (2) Water.

On the external surface of the pipe the thermal flux q_{vap} is constant; on the internal surface of the pipe in the laminar zone the coefficient of heat transfer to vapor α is constant; the vapor-water phase interface is assumed to be two-dimensional, and on the sides of the annular sector there is a constant temperature whose value is assumed equal to an average over the thickness of the pipe wall t_{cp} . Vapor temperature is taken as the saturation temperature with pressure in the pipe. For the beginning of reading we take the value for temperature t_{cp} averaged over the thickness of the wall outside the laminar zone. In polar coordinates the equation for heat conductivity has the form:

$$R^2 \frac{\partial^2 t}{\partial R^2} + R \frac{\partial t}{\partial R} + \frac{\partial^2 t}{\partial \theta^2} = 0. \quad (1)$$

Boundary conditions:

$$\lambda \frac{\partial t}{\partial R} \Big|_{R=R_2} = q_{\text{vap}}; \quad (2)$$

$$\lambda \frac{\partial t}{\partial R} \Big|_{R=R_1} = \alpha (t - t_{\text{sat}}); \quad (3)$$

$$t|_{\theta=0} = 0. \quad (4)$$

The general solution to the given problem has the form:

$$t = \sum_{n=0}^{\infty} \left\{ \frac{\left[z_n \frac{aR_1}{\lambda v_n} R_1^{2n} + \frac{b_n R_2}{\lambda v_n} \left(1 + \frac{aR_1}{\lambda v_n} \right) R_2^{2n} \right] R^{2n} + \left[z_n \frac{aR_1}{\lambda v_n} R_1^{2n} R_2^{2n} + \frac{b_n R_2}{\lambda v_n} \left(1 - \frac{aR_1}{\lambda v_n} \right) R_1^{2n} R_2^{2n} \right] R^{-2n}}{\left(1 + \frac{aR_1}{\lambda v_n} \right) R_2^{2n} - \left(1 - \frac{aR_1}{\lambda v_n} \right) R_1^{2n}} \cos v_n \theta. \right. \quad (5)$$

After a series of transformations it can be represented in the following form:

$$t = \sum_{n=0}^{\infty} \frac{z_n \frac{aR_1}{\lambda v_n} \text{ch} \left(v_n \ln \frac{R}{R_2} \right) + \frac{b_n R_2}{\lambda v_n} \text{ch} \left(v_n \ln \frac{R}{R_1} \right) + \frac{b_n R_2}{\lambda v_n} \cdot \frac{aR_1}{\lambda v_n} \text{sh} \left(v_n \ln \frac{R}{R_1} \right)}{\text{sh} \left(v_n \ln \frac{R_2}{R_1} \right) + \frac{aR_1}{\lambda v_n} \text{ch} \left(v_n \ln \frac{R_2}{R_1} \right)} \cos v_n \theta. \quad (6)$$

Formula (6) is the general solution to the equation of heat conductivity (1) under the given boundary conditions (2) - (4) and makes it possible to determine the temperature of any point of the pipe in the overheating zone. Since we have taken the value of temperature t_{cp} for the beginning of reading, it actually determines the value of overheating relative to this quantity. In the particular case $\alpha = 0$ is valid, as shown below, for thick-walled pipes in the region of low vapor contents and low pressures to 20 atm (abs.); formula (6) is considerably simplified and assumes the form:

$$t = \frac{R_2}{\lambda} \sum_{n=0}^{\infty} \frac{\beta_n}{\nu_n} \frac{\operatorname{ch}\left(\nu_n \ln \frac{R_1}{R_2}\right)}{\operatorname{sh}\left(\nu_n \ln \frac{R_1}{R_2}\right)} \cos \nu_n \theta =$$

$$= \frac{8q_{isp} R_2 \beta_0}{\lambda \pi^2} \sum_{n=0}^{\infty} \frac{(-1)^n}{(2n+1)^2} \frac{\operatorname{ch}\left(\frac{2n+1}{2\beta_0} \pi \ln \frac{R_1}{R_2}\right)}{\operatorname{sh}\left(\frac{2n+1}{2\beta_0} \pi \ln \frac{R_1}{R_2}\right)} \cos \frac{2n+1}{2\beta_0} \pi \theta. \quad (7)$$

In the presence of lamination the temperature drop in the pipe wall by the upper generatrix is defined as the difference in the values of overheating for the external ($R = R_2$) and internal ($R = R_1$) surfaces of the pipe and is equal to

$$\Delta t_{cr} = \sum_{n=0}^{\infty} \frac{\beta_n}{\lambda \nu_n} \left[1 - \operatorname{ch}\left(\nu_n \ln \frac{R_1}{R_2}\right) \right] - \frac{\beta_n R_2}{\lambda \nu_n} \left[\operatorname{ch}\left(\nu_n \ln \frac{R_2}{R_1}\right) - 1 \right] - \frac{\beta_n R_2}{\lambda \nu_n} \frac{\operatorname{sh}\left(\nu_n \ln \frac{R_2}{R_1}\right)}{\operatorname{sh}\left(\nu_n \ln \frac{R_2}{R_1}\right) - \frac{\beta_n R_1}{\lambda \nu_n} \operatorname{ch}\left(\nu_n \ln \frac{R_2}{R_1}\right)} \cos \nu_n \theta. \quad (8)$$

When $\alpha = 0$ for a vertical section ($\theta = 0$)

$$\Delta t_{c1} = \frac{8q_{isp} R_2 \beta_0}{\lambda \pi^2} \sum_{n=0}^{\infty} \frac{(-1)^n}{(2n+1)^2} \frac{\operatorname{ch}\left(\frac{2n+1}{2\beta_0} \pi \ln \frac{R_2}{R_1}\right) - 1}{\operatorname{sh}\left(\frac{2n+1}{2\beta_0} \pi \ln \frac{R_2}{R_1}\right)}. \quad (9)$$

As an example, let us determine the temperature drop in the wall of a steel pipe $d = 240 \times 30$ mm when $q_{\text{vap}} = 116.3 \text{ kW/m}^2$, $\phi = 0.05$, $\alpha = 58.15 \text{ W/m}^2 \cdot \text{deg}$ and compare it with the quantity determined from the formula:

$$\Delta t_{\text{cr}} = \frac{q_{\text{vap}} R_2}{\lambda} \ln \frac{R_2}{R_1}. \quad (10)$$

Temperature drop according to formula (6) is 36°C and according to (10) is 86°C .

Heat removal in the section of horizontal pipe washed by vapor phase is accomplished by heat transfer to vapor and the spreading of the heat along the body of the pipe. The relationship between the quantity of heat removed by spreading and by heat transfer to vapor depends upon the part of the perimeter washed by vapor, wall thickness, and the heat transfer factor. To obtain a quantitative evaluation of this relation we shall determine the temperature heads corresponding to the two limiting cases: heat removal only by spreading and heat transfer only to vapor.

In determining the temperature head due to heat removal by spreading, it is necessary to take into account the variable value of thermal flux along the length of the annular sector (see Fig. 1). Since the increase in thermal load along the perimeter is uniform, the average value of thermal flux by spreading $q_{\text{cp}}^{(p)} = 0.5 q_{\text{max}}^{(p)}$, while $q_{\text{max}}^{(p)}$ is determined by the total thermal load Q :

$$Q = q_{\text{vap}} R_2 \theta_0 L; \quad (11)$$

$$q_{\text{max}}^{(p)} = 2q_{\text{cp}}^{(p)} = \frac{Q}{L} = \frac{Q}{(R_2 - R_1)L} = \frac{q_{\text{vap}} R_2 \theta_0}{R_2 - R_1}. \quad (12)$$

The temperature head with heat removal by spreading along an annular sector, in length $l = 0.5\theta_0 (R_1 + R_2)$, is

$$\Delta t_p = q_p^{(n)} \cdot \frac{l}{\lambda}. \quad (13)$$

We shall substitute the value of $q_{cp}^{(p)}$ and l in formula (13)

$$\Delta t_p = \frac{q_{vap} R_2 (R_1 - R_2) \theta_0^2}{4\lambda (R_2 - R_1)}. \quad (14)$$

The temperature head corresponding to heat transfer only to vapor (with error not exceeding 5% when $p < 20$ atm (abs.) and 10% when $p < 40$ atm (abs.)) is equal to

$$\Delta t_s = \frac{q_{sv}}{\alpha} = \frac{R_2}{R_1} \cdot \frac{q_{vap}}{\alpha}. \quad (15)$$

We have disregarded here the temperature drop in the pipe wall since it (Δt_{CT}) is less than Δt_α by a factor of 10-20.

The relationship between heat removal by spreading along the pipe wall and heat transfer to vapor depends upon the values of the temperature heads determined from formula (14) and (15) and is uniquely determined by their ratio, which, therefore, can be considered the spread indicator:

$$k_p = \frac{4\lambda (R_2 - R_1)}{(R_1 + R_2) \theta_0^2 R_1} \cdot \frac{1}{\alpha}. \quad (16)$$

The quantity $\frac{4\lambda (R_2 - R_1)}{R_1 (R_1 + R_2) \theta_0^2}$ in formula (16) represents the heat transfer factor, equivalent to the heat removal by spreading along the pipe wall, related to its internal surface washed by vapor:

$$\alpha_{svs} = \frac{4\lambda (R_2 - R_1)}{R_1 (R_1 + R_2) \theta_0^2}. \quad (17)$$

Accounting for (17), the expression for the spread indicator assumes the form:

$$k_p = \frac{\alpha_{svs}}{\alpha}. \quad (18)$$

High values for the spread indicator $k_p \gg 1$, $\Delta t_\alpha \gg \Delta t_p$ correspond to the predominant heat removal by spreading since the temperature drop along the wall is much less than with heat transfer to vapor, and the heat distribution is inversely proportional to the values

of the temperature heads (similar to the distribution of electrical current between two parallel conductors with varying resistances).

Low values for the spread indicator $k_p \ll 1$, $\Delta t_a \ll \Delta t_p$ correspond to the predominant removal by heat transfer to vapor. Values of the spread indicator for various values of vapor content, pressure, and the wall thickness for a pipe with an internal diameter of 80 mm are presented in Fig. 2.

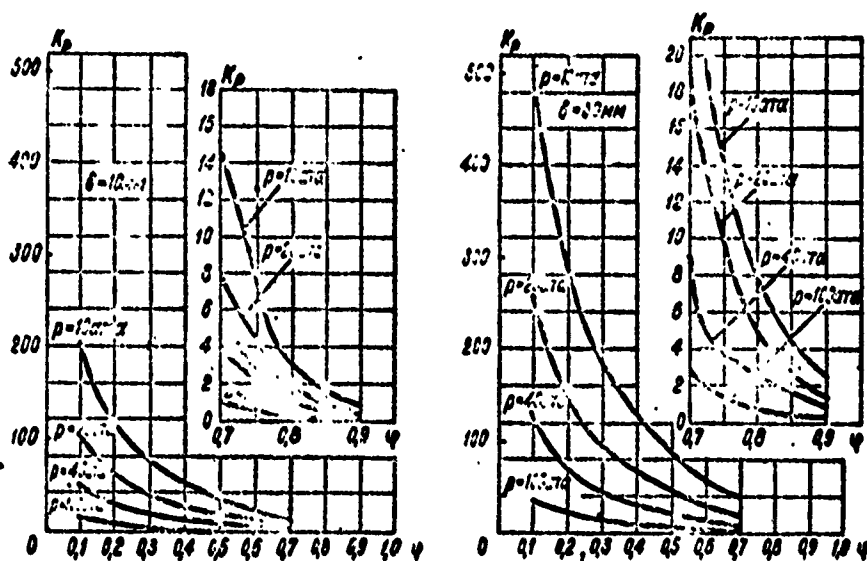


Fig. 2. Heat spread indicator versus vapor content in pipe $d_{BH} = 80$ mm for various values of pressure and wall thickness.
Designation: ata, ama = atm (abs.).

A simplified function is obtained for an approximate evaluation of the overheating of the upper generatrix during lamination, based on analysis of the conditions for heat removal from the section of the pipe washed by vapor.

As shown above, heat removal by spreading along a pipe wall is characterized by a conditional heat transfer factor $\alpha_{\text{ЭНВ}}$, while heat removal to vapor is characterized by the value of α . Since the values of α and $\alpha_{\text{ЭНВ}}$ are related to the inner surface

of the pipe in the zone washed by the vapor, the fractions of internal heat flux $q_{\text{BH}}^{(\alpha)}$ and $q_{\text{BH}}^{(p)}$ corresponding to them are related by simple relationships

$$\frac{q_{\text{BH}}^{(\alpha)}}{q_{\text{BH}}^{(p)}} = \frac{\alpha}{\alpha_{\text{KH}}}; \quad (19)$$

$$q_{\text{BH}}^{(\alpha)} = q_{\text{BH}}^{(p)} = q_{\text{BH}}; \quad (20)$$

hence, with allowance for (18),

$$q_{\text{BH}}^{(2)} = \frac{q}{1 - k_p} = \frac{R_1}{R_1} \cdot \frac{q_{\text{HAP}}}{1 - k_p}, \quad (21)$$

and overheating of the upper generatrix

$$\Delta t = \frac{q_{\text{BH}}^{(\alpha)}}{\alpha} = \frac{R_2}{R_1} \cdot \frac{q_{\text{HAP}}}{(1 - k_p)\alpha}. \quad (22)$$

The quantity $\alpha(1 + k_p)$ in formula (22), equal to $\alpha_{\text{KH}} + \alpha$, is the total heat transfer factor, called the effective heat transfer factor in the laminar zone:

$$\alpha_{\text{eff}} = \alpha_{\text{KH}} + \alpha. \quad (23)$$

Thus, heat removal in the laminar zone is determined not by the heat transfer to vapor, but by the value of the effective heat transfer factor, taking into account total heat removal to vapor and spreading along the wall of the pipe.

To evaluate the accuracy of the calculation of overheating based on this method, we shall compare the result given with the value of overheating from formula (6), for example, of a pipe $d = 76 \times 10 \text{ mm}$ when $q_{\text{HAP}} = 58.15 \text{ kW/m}^2$, $\phi = 0.5$, $\alpha = 58.15 \text{ W/m}^2 \cdot \text{deg}$.

From formula (16) we shall determine the spread indicator k_p :

$$k_p = \frac{4 \cdot 46.5 \cdot 0.01 \cdot 4}{0.028 \cdot 0.008 \cdot \pi \cdot 58.15} = 7.$$

overheating of the upper generatrix, according to (22):

$$\Delta t = \frac{73}{56} \cdot \frac{58150}{8.58,15} = 169^{\circ}\text{C}.$$

From formula (6) we find $\Delta t = 179^{\circ}\text{C}$. Thus, for an approximate evaluation of overheating formula (22) is completely suitable.

The effect of the annular channel on the condition of heat exchange with laminar regime in the region of low vapor contents has been examined. At equal values for true vapor content in the pipe and in the annular channel, when the phase interface goes above the insert (Fig. 3a), the height of the vapor segment in the annular channel is less than in the circular pipe. This is a property of the shape of the annular channel, which has a form of relationship between the vapor segment height and its relative area (Fig. 3b) which is different from that of the circular pipe. Actually, from the inequality of ϕ in the circular pipe and the annular channel it follows that:

$$\frac{S_v^*}{\pi(R_i^2 - r^2)} = \frac{S_{vp}^*}{\pi R_i^2}; \quad (24)$$

$$S_v^* < S_{vp}^*. \quad (25)$$

In calculating the overheating of the upper generatrix of the pipe it is convenient to introduce not the height of the vapor segment but its degree or radian measurement. The relationship between these quantities in the circle and the ring ensues directly from (24):

$$\left. \begin{aligned} \Omega - \sin \Omega \cos \Omega &= \left(1 - \frac{r^2}{R_i^2} \right) (\theta - \sin \theta \cos \theta); \\ \Omega &\leq \arccos \frac{r}{R_i}. \end{aligned} \right\} \quad (26)$$

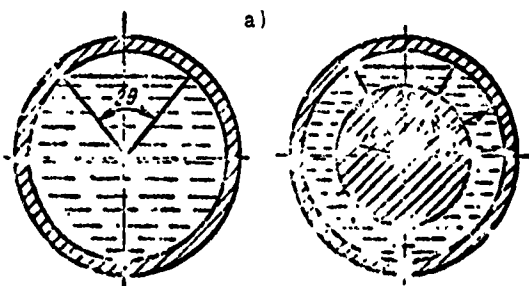
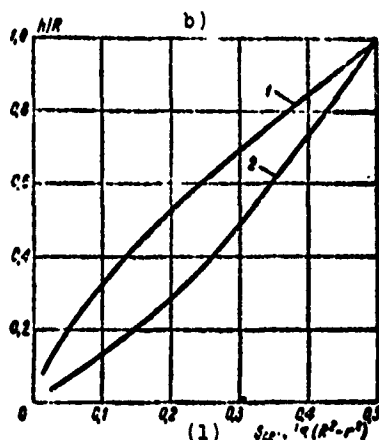


Fig. 3. The relationship between the height and the relative area of the vapor segment in the circle and the annular channel:

1 - In the circle ($r = 0$);
2 - In the annular channel.

KEY: (1) Segment.



On the basis of (22) overheating of the upper generatrix is examined for the pipe and the annular channel, which are represented for equal values in the form of their ratio at different values of the heat-to-vapor transfer factor (Fig. 4).

The data presented show that at low values for true vapor content in the annular channel, overheating of the upper generatrix is less by a factor of 1.6-1.8 than it is in the circular pipe. Since with low vapor contents the average vapor velocity is near the average water velocity [5] both in the pipe and in the annular channel, we can conclude that the lowest value for upper generatrix overheating corresponds to equal circulation parameters in the annular channel.

With evaporative cooling of hearth pipes, because of the underheating of water entering the parts to be cooled, there are

sections of pipes cooled by water which is not heated to saturation temperature, in the presence of surface boiling.

In a horizontal pipe, due to the effect of forces of gravity with surface boiling at the upper generatrix, vapor bubbles can gather and combine and the flow of water can be forced back to the lower generatrix, i.e., lamination can occur which leads to a worsening of heat exchange in the upper part of the pipe and its overheating.

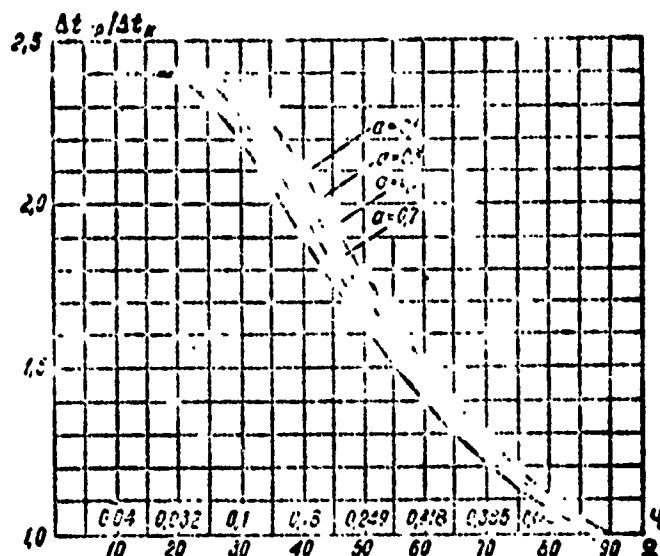


Fig. 4. The relationship between overheating of the upper generatrix of a circular pipe and an annular channel at various values for true vapor content and coefficient of heat transfer to vapor $\left[1 - \sqrt{\frac{2R_1(R_1 - R_2)}{R_1^2 - R_2^2}} \right]$.

Research performed with thermal loads of 50-200 kW/m² in the region of low pressures ($p < 4$ bar) and low underheating (to 15°C) at velocities of 0.5-1.5 m/s for pipes with a diameter of 76 × 10 mm and 144 × 17 mm [6] has established that in the zone of surface boiling, due to lamination, overheating of the upper generatrix occurs. The value of overheating substantially depends

on circulation velocity (increases as it decreases) and on heat flux. There is virtually no effect from underheating and pressure in this range of their variation on the value of overheating.

A similar worsening of heat exchange during surface boiling due to lamination was observed by Z. L. Miropol'skiy. Lamination occurred on the bends of pipes due to the centrifugal effect.

For the practical use of available test data in the entire range of possible pipe diameter and wall thickness variations, the data were processed on the basis of the obtained relationship (7) for overheating during laminar motion of a vapor-water mixture in a horizontal pipe. The essence of this processing is as follows. On the basis of test data on the overheating of the upper generatrix, based on (7) those values of vapor content were determined which correspond to those values of overheating with the locally available values of heat fluxes. Such processing made it possible to establish for each of the pipes the dependence of vapor content on circulation velocity and thermal loading, referred to the internal surface of the pipe, and to represent them in the form:

$$\bar{x} = 2,52 \cdot 10^{-5} q_{sk}^{0.7} w^{-1.7} d_i^{1.3}. \quad (27)$$

With the prescribed values for circulation velocity, heat flux, and pipe diameter, taking into account relationship (10) for Δt_{cr} and

$$\bar{x} = \frac{1}{2\pi} - (2\theta_0 - \sin 2\theta_0) \quad (28)$$

overheating of the upper generatrix can be represented in the form:

$$t_{sup} - t_{ms} = (c_p - 0,5) \Delta t_{cr}. \quad (29)$$

In (29) the quantity c_p :

$$c_p = -\frac{8\theta_{\text{ср}}}{\pi^2 \ln \frac{d_2}{d_1}} \sum_{n=0}^{\infty} \frac{(-1)^n}{(2n+1)^2} \operatorname{cth} \left(\frac{2n+1}{2\theta_0} \pi \ln \frac{d_2}{d_1} \right) \quad (30)$$

is the dimensionless (related to $\Delta t_{\text{ср}}$) overheating of the upper generatrix relative to $t_{\text{ср}}$.

One of the main operational reliability criteria for evaporative cooling installations of heating furnaces is the circulation velocity. From the point of view of ensuring a given temperature regime, permissible circulation velocity depends upon a number of factors including pipe diameter and wall thickness.

Based on relationships (27) and (29), it was possible to determine the value of permissible circulation velocity for pipes with different diameters and wall thicknesses. Calculation was performed based on the condition that with an increase in pipe diameter overheating of the upper generatrix of the pipe must remain constant.

BIBLIOGRAPHY

- 1 Кансвеленборген Л. Б., Рудницкий Я. Н. Работа толстостенных горизонтальных парогенерирующих труб большого диаметра в области низких и средних давлений. «Труды ЦКТИ», вып. 59, 1965.
- 2 Стирикович М. А., Миропольский З. Л. О температурном режиме работы горизонтальных и наклонных парогенерирующих труб при высоких давлениях. В сб. «Гидродинамика и теплообмен при кипении в котлах высокого давления». Изд-во АН СССР, 1955.
- 3 Кутателадзе С. С., Боришанский В. М. Справочник по теплопередаче. Госэнергоиздат, 1959.
- 4 Канторович М. В., Крылов В. И. Приближенные методы высшего анализа. Гостехиздат, 1949.
- 5 Кутателадзе С. С., Стирикович М. А. Гидродинамика жидкостных систем. Госэнергоиздат, 1958.
- 6 Антоньев С. М. [и др.] Непрерывное охлаждение нагреваемых прокатных печей «Сталь», 1955, № 12.

EXPERIMENTAL RESEARCH ON THE
COOLING OF WORKING BLADE ELEMENTS
IN A GAS TURBINE ENGINE BY A
FINELY DIVIDED AIR-WATER MIXTURE

L. M. Zysina-Molozhen, I. B. Uskov,
and L. V. Zysin

Abbreviations:

op = ribbed;
cm = mixture.

The rapid development of power engineering requires that we find new methods for substantially increasing the thermal effectiveness of thermal electric plants.

One possible solution to this problem is the application of high-temperature gas turbines with intensive cooling of flow elements.

The maximum temperature of gas, determined by the thermal stability of materials forming the flow-through section, is a function of heat removal from the surface.

In solving the problem of cooling we generally encounter two approaches in literature: on the one hand, the problem of

protecting the surface from powerful heat flows from the gas side and, on the other hand, the problem of ensuring maximum heat removal from the heated surface. In either case, one of the effective cooling methods examined is the use of humid flows with finely dispersed moisture. In the first case, an air-water mixture fed directly into the gas channel is blown around the outside of the blade [1, 2] and, in the second case, a humid gas flow is blown along the inside of the blade with single-loop cooling or the roots of the blades with double-loop cooling [4, 5]. With respect to the latter case, in the gas turbine laboratory at TsKTI [Central Scientific Research, Planning and Design Boiler and Turbine Institute] and at LPI [Translator's Note: This abbreviation could stand for either the Leningrad Polytechnic Institute or the L'vov Polytechnic Institute] considerable research has been performed, as a result of which an installation has been developed based on the TsKTI-LPI diagram which makes it possible to design for an efficiency on the order of 50% with a working gas temperature of approximately 1200°C [3]. However, we can only obtain the final design data for this layout when we receive reliable recommendations on the intensity of heat exchange in humid flows.

At the present time there is no well defined concept concerning the mechanism of heat exchange in such flows with respect to the above cases, and, therefore, there is no sufficiently well founded theoretical solution to the problem of possible heat removal.

Published results of various studies on heat exchange in moist flows are very contradictory. For example, in some cases they speak of the great intensification of heat exchange from the introduction of moisture (by a factor of several tens) and, in other cases, this intensification only reaches several tens of percents. All this points to the absence of systematic research in a wide range of variation for the determining parameters.

Below we discuss the results of experimental research on the heat transfer, in a moist gas flow, of cascades of blades, cascades of bladed radiators made from ribbed rods, and single ribbed and smooth rods. The experiments were made on stands at LPI and TsKTI.

Figure 1 presents a diagram of a ribbed radiator cascade. Cascades with a fixed rib height of $h = 2.5$ mm were studied at various values of pitch. As the arbitrary characteristic of the ribbing in our tests we took the ribbing coefficient f :

$$f = \frac{F_{op}}{F_0}. \quad (1)$$

Here F_{op} is the surface of the ribbed model; F_0 is the surface of the unribbed model.

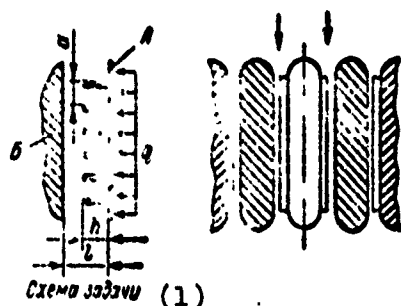


Fig. 1. Diagram of a ribbed cascade of bladed radiators:
1 - Bladed radiator heated by electrical current;
2 - Unheated body.
KEY: (1) Outline of problem.

In the experiments, specific thermal load q , relative humidity \bar{G} , temperature factor ψ , and Reynolds number are varied within the following ranges:

$$q = 4.25 \cdot 10^4 - 4.1 \cdot 10^5 \frac{\text{kcal}}{\text{m}^2 \cdot \text{h}};$$

$$\bar{G} = 1.4 - 14.0\%; \quad \psi = 1.05 - 2.5;$$

$$\text{Re}_x = 3 \cdot 10^4 - 5 \cdot 10^5; \quad G = \frac{G'}{G' + G''} \cdot 100\%;$$

where G' and G'' are the per-unit-weight contents of liquid and gas phases, respectively; $\phi = \frac{T_w}{T_0}$; T_w and T_0 are wall temperatures and gas flow, respectively; $Re_x = \frac{wx}{\nu}$; w is the flow velocity of the cooling mixture at cascade input; ν is the kinematic viscosity of the gas flow, taken with respect to parameters at input; x is the current coordinate read from the leading edge along the contour of the cooled element.

Let us note that the temperature factor in our designations is uniquely related to the criterion $K = \frac{f}{\phi^{1/4}}$ in the definition of reference [4] with respect to the conditions of the problem examined.

Figure 2 illustrates the experimental data on heat transfer in a radiator cascade with a ribbing coefficient of $f = 2.6$ when dry air is flowing around it. The test points are grouped along the curve with a spread of $\pm 15\%$.

$$Nu = 0.043 Re^{0.8} \quad (2)$$

The temperature factor varied within the range of $\psi = 1.18$ to $\psi = 2.7$; however, a clear lamination with respect to ψ was not detected in the tests. Calculations using the following formula are indicated by dashes on this figure:

$$Nu = 0.0434 Re^{0.8} \psi^{0.11} \quad (3)$$

for the limiting values of ψ . Formula (3) was derived by V. I. Lokay for the case of flow in a slotted gap between the blade surface and the deflector.

As is apparent, deviation from this formula does not exceed the spread of our test points. This indicates the practical identity of the formulas. Tests during blowing by dry air with a ribbing coefficient of $f = 3.5$ and a single ribbed rod gave practically the same dependence on the Re number.

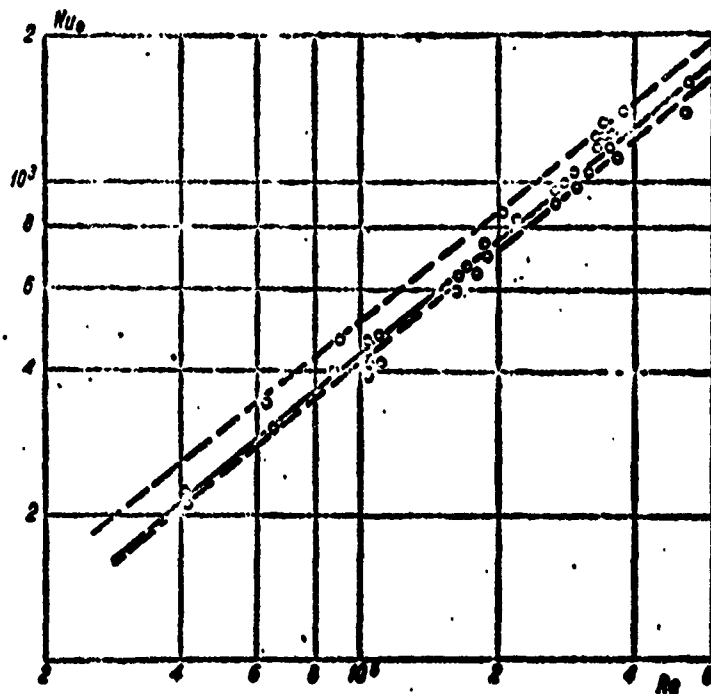


Fig. 2. The function of $Nu = Nu(Re)$ for cascade No. 1 during a flow of dry air around it.

The effect of ribbing in the expression for heat exchange intensity

$$Nu = c Re^{0.8}$$

appears only in terms of the value of coefficient c , connected in our treatment with coefficient f (in the range of f variation from 1 to 3.5) by an empirical relationship of the form:

$$c = 0.034 f^{0.25} \quad (4)$$

As a characteristic of the intensification of local heat transfer values because of the introduction of finely dispersed suspended moisture in the flow, the following value was assumed:

$$N = \frac{Nu}{Nu_0}$$

Here Nu is the intensity of heat exchange during cooling by a two-component humid flow; Nu_0 is the intensity of heat exchange during a flow of dry air around the cooled element.

The introduction of the intensification factor \bar{N} made it possible to formally disregard the effect of the Re number on the heat exchange process in moist flow. Obviously, this is possible only within the limits of a single flow regime in the boundary layer. When the flow velocity exceeds a certain critical value defining the change in the flow regime on the surface, the established regularities can be violated.

The analysis and treatment of test data on heat exchange in humid flows indicated that in the interrib channels of cascades there is a stable uniform flow in the boundary layer and the intensification of heat exchange is varied (as a function of the values of the determining parameters). It is obvious that the greatest intensification of heat exchange is determined by the possibility of a boiling regime. Such conditions occur at values of $\psi = 1.05-1.15$.

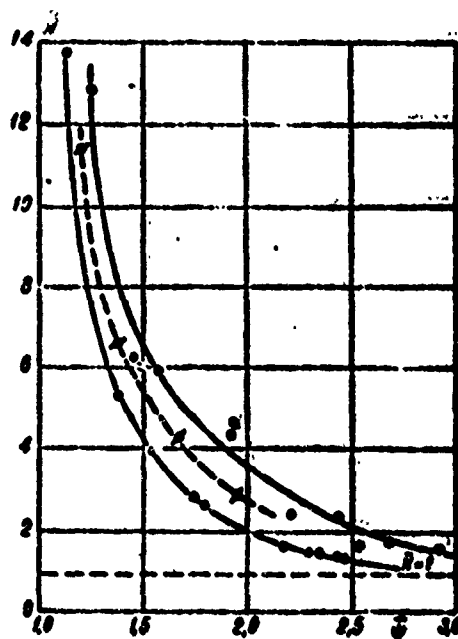


Fig. 3. \bar{N} versus ψ for humid air and vapor flows ($G > 4\%$):
 ● - $q = 1.18 \cdot 10^5$ kcal/m²·h, moist vapor; ⊙ - $q = 1.65 \cdot 10^5$ kcal/m²·h; ⊘ - $q = 1.52 \cdot 10^5$ kcal/m²·h, moist air; ○ - $q = 1.76 \cdot 10^5$ kcal/m²·h, moist air.

As a function of the values of q and \bar{G} , values for $\bar{N} > 10$ can be obtained in these conditions as is apparent, for example, from Figs. 3 and 4. The process of stable boiling in the liquid film forming on the wall, at high gas flow velocity, is considerably hindered [6] and with an increase in ψ it is obviously suppressed entirely. A flow of the dispersed-annular type is established [6]. The intensification of heat exchange, in this case, is achieved from the evaporation of liquid from the surface of the film, which is supplemented by the moisture precipitating from the flow. As ψ increases the evaporating part of the liquid can not be supplemented by that precipitating from the flow and a gradual thinning of the film occurs, with which the intensification of heat exchange decreases. When $\psi \approx 2$ the heat exchange intensification is only 10-40%.

It is apparent from the curves in Fig. 5 that an increase in moisture content in the flow intensifies heat exchange; however, there is a certain limiting moisture content after which a further increase does not affect heat exchange intensity. In our tests this value was on the order of 4-6%. However, in this range of values for \bar{G} , noticeable intensification occurs only when $\psi < 2.0$; the degree of intensification increases when the temperature factor approaches 1. When $\psi > 2$ all curves, regardless of \bar{G} and q , contract toward one limiting value, corresponding to a virtually complete absence of heat exchange intensification, i.e., in essence a heat exchange crisis occurs. The crisis, under our conditions, is not characterized by an abrupt decrease in heat transfer and the approach to it is quite blurred. Apparently this is connected with the specifics of the process at high velocities of the supporting moisture of the flow.

As a result of generalizing the obtained test data, the following relationship was established:

$$\bar{N} = 1 + c q \bar{G}^{0.27} \psi^{-4.63} \quad (5)$$

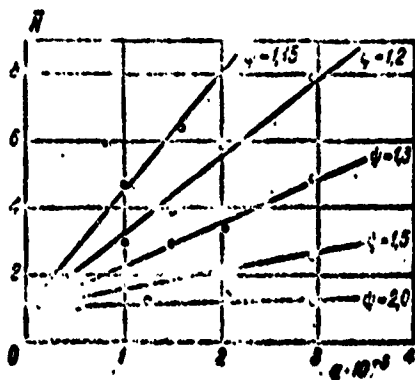


Fig. 4. \bar{N} versus \bar{G} when $q = 3.55 \cdot 10^5$ kcal/m²·h for cascade No. 1.

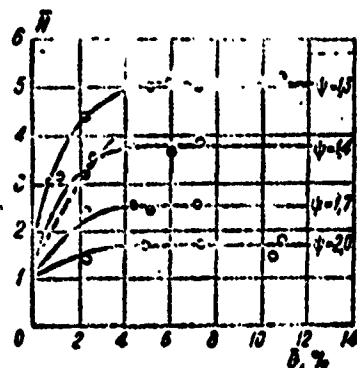


Fig. 5. \bar{N} versus q for cascade No. 1 when $\bar{G} = 6\%$: ----- calculation according to formula (7).

(Here $\bar{q} = -\frac{q}{T_1 - T_2} \sqrt{\frac{T_1 - T_2}{T_1}}$) for a calculation of heat exchange intensification from the introduction of suspended moisture in the flow. The formula was identical for the different cascades; the geometric characteristics of the ribbing affected only the value of coefficient c in formula (5). We should note that the values of \bar{N} for a single rod were the same as for the cascade. This data made it possible to give a general recommendation for calculation in the form of formula (5). To determine the coefficient c with respect to the cases of ribbing we studied, the following experimental relationship was obtained:

$$c = (c)_f f^{-1.1}. \quad (6)$$

Most of the tests were performed on an air-water mixture. A number of experiments were made on moist vapor. These tests were generally pursued for the purpose of obtaining data for comparison. Within the framework of the experiment, as is apparent from Fig. 3, we could not detect a substantial difference between data obtained on moist vapor or air flows.

A comparison of data for single rods with and without ribs shows that when moist flow is used, an increase in the ribbing

coefficient leads to a decrease, all things being equal, in the value of the heat exchange intensification coefficient. This is easy to see, for example, from Fig. 6, which presents the curve for variations in ratio

$$A = \frac{(\bar{N})_{\psi=1}}{(\bar{N})_{\psi=3.5}}$$

as a function of ψ when $q = 1.5 \cdot 10^5 \text{ kcal/m}^2 \cdot \text{h}$.

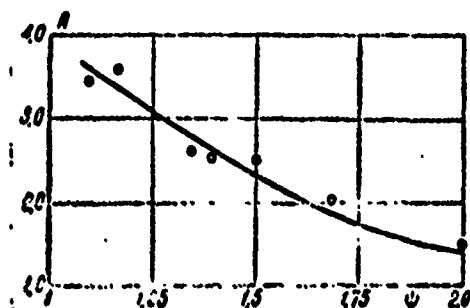


Fig. 6. \bar{A} versus ψ when $q = 1.5 \times 10^5 \text{ kcal/m}^2 \cdot \text{h}$.

Formula (5) is different from the formula of V. I. Lokay for an air-water mixture, obtained relative to a blade with a deflector [5]:

$$\bar{N} = 1 + 0.75 \left(\frac{G_m}{G_n} \right)^{0.8} \psi^{1.65} \text{Re}_{cn}^{0.68}. \quad (7)$$

However, a comparison of formula (5) and (7) shows that in this range, for which formula (7) is obtained ($\bar{G} = 0-2.5\%$; $\psi < 1.4$), it agrees fully with the relationship we obtained. The dashes in Fig. 5 show the results of calculations using this formula.

We should emphasize that formula (5) is invalid when $\psi < 1.15$. In this case, as indicated above, another flow regime occurs in the film.

Tests made on a cascade of turbine blades also revealed a significant intensification of heat exchange during the motion

in the interblade channels of air with finely dispersed moisture [7]. A relationship between the degree of intensification and the determining parameters was detected. Tests with a blade cascade were made in a much smaller volume than those with a radiator cascade; therefore, we could not as yet obtain in them generalized quantitative relationships. However, qualitative relationships are found to be similar in both cases. For illustration, in Fig. 7a we have presented one of the patterns of the variations in the average heat transfer factor in a cascade with a variation in wall temperature. It is apparent from the graph that there are two heat exchange mechanisms: one, corresponding to great intensification in heat exchange, when α reaches values of $\alpha \approx 15 \cdot 10^3$ kcal/m²·h, which can be called the presence of intensive evaporation, and the following decrease in α which corresponds to a change in the heat exchange regime in the boundary layer.

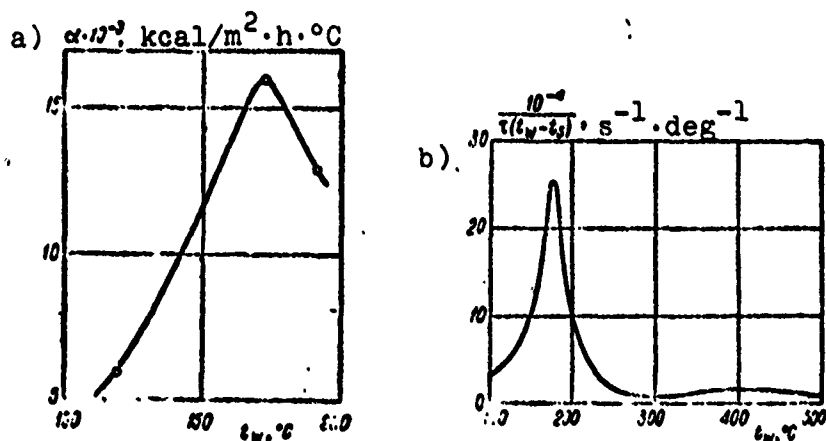


Fig. 7. Average heat transfer factor versus wall temperature during flow around a cascade of turbine blades:

a - Data obtained on a blade cascade; b - Data of V. M. Borishanskiy [9].

Indirect analogy with the pattern examined can be seen in the results of observing vaporization times for the various liquid suspensions on a heated surface presented in reference [8, 9].

The corresponding pattern is presented in Fig. 7b. The ordinate in this figure is proportional to the heat exchange intensity. A comparison of the curves in Figs. 7a and b leads us to assume that in our tests with blades evaporation of drops or separate liquid formations on the surface possibly occurred.

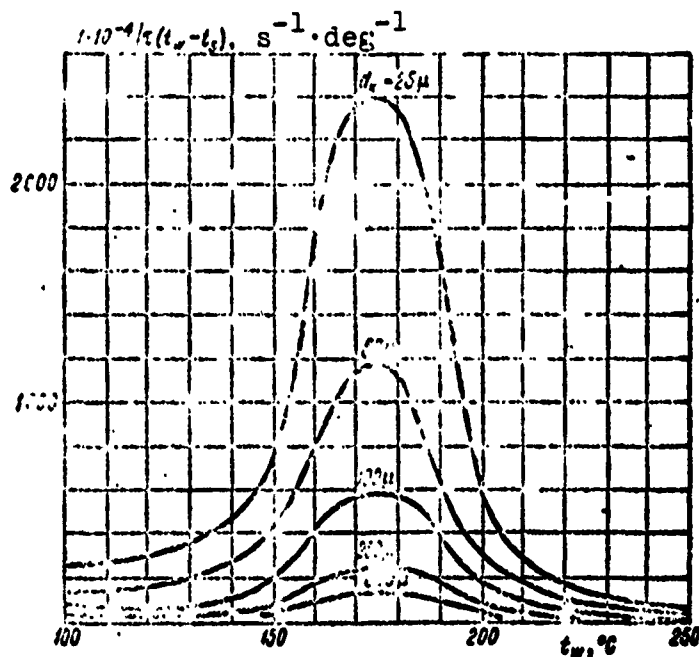


Fig. 8. Intensification of heat transfer as a function of spray dispersion.

In reference [10] it was shown that in the case of the evaporation of separate drops at fixed wall temperature t_w , the ratio of evaporation time to droplet diameter τ/d_k is constant. Taking this regularity into account, similar curves for drops of various diameters were obtained by calculation on the basis of Fig. 7b. The results of these calculations are presented in Fig. 8. As is apparent, in a certain range of surface temperature variation the dispersion of the spray must have a substantial effect on heat exchange intensification.

However, in our tests and in the tests from reference [4] no such effect was detected. Apparently, we did not manage to

achieve sufficient dispersion variation in the tests since the spraying devices in our experimental installations were rather far from the working sections and the dispersion of moisture entering the working section was generally determined by the input conditions.

The effect of dispersion should be the subject of further study.

Special research should also be performed on the effect of curvature and the longitudinal pressure gradient in the interblade channel. There is a basis for assuming that this effect will be quite substantial since, to a certain extent, the amount of moisture precipitating from the main flow in the boundary layer will depend upon it.

To develop an analytical method for calculating heat exchange in flow with finely dispersed moisture it is necessary to set up a study on the mechanism of motion and precipitation of moisture from flow in the boundary layer and its evaporation mechanism.

The quantitative relationships and calculation formulas obtained in this work can be recommended for practical calculation; however, in using them, it is necessary to stay within the above discussed applicability limits.

BIBLIOGRAPHY

1. Полоцкий Л. В., Левин Я. А. Воздушно-водяное охлаждение лопаток газовых турбин. «Энергетическое машиностроение», НИИИИ:ОФМТЯХМАШ, вып. 10, 1965.
2. Зысн Л. В. Высокотемпературные турбины с парциальным подзолом газа и пара. «Труды ЛПИ», № 232, 1964.
3. Зысн В. А., Кириллов И. И., Ошеров С. Я. Высокотемпературная газотурбинная установка с паровым охлаждением. «Труды ЦКТИ», вып. 50, 1964.
4. Бариллов В. А. (и др.) Применение взвешенной влаги для охлаждения высокотемпературных газовых турбин. «Труды ЛПИ», № 286, 1967.
5. Локай В. И. Теплообмен в полой турбинной лопатке. «Труды КАН», XXV. Татарстан, 1951.

6. Агафонова Ф. А., Филиппович Б. С. Исследование критических тепловых нагрузок в высокотемпературном потоке пароводяной смеси при низких давлениях. ИФЖ, т. 10, 1966, № 5.

7. Зыкина-Моложен Л. М. [и др.]. Экспериментальное исследование теплообмена при внешнем воздушноводяном охлаждении лопаток газовых турбин. «Труды ЦКТИ», вып. 91, 1969.

8. Боришанский В. М., Арефьев К. М., Палеев И. И., Тектилов Р. Т. О пленочном кипении жидкости в сферондальном состоянии при свободном растекании по поверхности. «Труды ЦКТИ», вып. 62. Л., 1965.

9. Боришанский В. М. Теплоотдача жидкости, свободно растекающейся по поверхности, нагретой выше температуры кипения жидкости. «Вопросы теплообмена при изменении агрегатного состояния вещества». Госэнергоиздат. М. — Л., 1953.

10. Плещева Н. А., Ребиндер П. А. Закономерности испарения капель жидкостей в сферондальном состоянии. Журнал физической химии, т. 20, № 5, 1946.

**A STUDY ON THE EFFECT OF FORCED
LIQUID MOTION ON HEAT EXCHANGE
DURING THE BOILING OF SEA WATER**

V. N. Slesarenko

Abbreviations:

дист = distillate

м.в = sea water

In the thermal distillation of sea water, rotor installations with boiling in a rotating flow of liquid are being used more and more [1, 2]. The operating regime of such installations is characterized by the formation of a thin rotating film between the heating surface and the boiling liquid. The distinguishing characteristics of rotor evaporators are the low specific flow rate of the heating vapor, good moisture separation, the absence of scum formation, and a high heat transfer factor. However, we should mention that there has been little experimental research on the intensification of convective heat exchange during boiling in thin rotating films.

On an experimental installation [3, 4], the main working element of which was a rotor evaporator, a study was made on the effect of the rotating motion of flow and the thickness of the

boiling film on heat exchange during the boiling of sea water and a distillate.

After the processing of experimental data on the boiling of the distillate, it was found that a change in the number of rotor revolutions with a constant clearance value and specific thermal flux from 11,630 to 116,300 W/m² brings about a significant increase in the heat transfer factor.

Figure 1 gives the graphic functions $\alpha_2 = f(q)$ when $\delta = 1.5$ mm and the variation in the rotor rpm $n = 500, 700, 1000, 1200$ r/min. On this same graph the curve $\alpha_2 = f(q)$ for water boiling in a large volume is plotted. It is apparent from the graph that at the same values for heat flux the quantity α_2 in the presence of flow rotation is significantly higher than for heat exchange conditions during the boiling of water in a large volume.

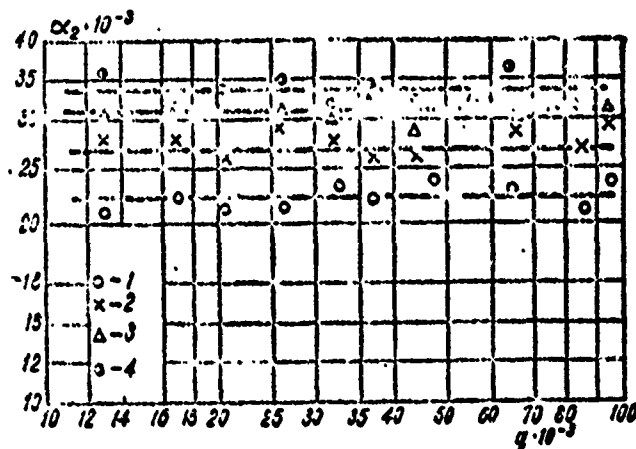


Fig. 1. α_2 versus q for distillate and sea water boiling in a rotating flow: $\delta = 1.5$ mm; 1 - $n = 500$ r/min; 2 - $n = 700$ r/min; 3 - $n = 1000$ r/min; 4 - $n = 1200$ r/min.

In the range of heat fluxes studied an increase in the latter during liquid rotation scarcely affects the value of the heat transfer factor, while with an increase in the rpm, the value of

α_2 also increases. The growth rate (the difference between the values of α_2 at various rpm's) of the heat transfer factor when $q = \text{const}$ drops somewhat with an increase in the rpm. A change in the hydrodynamic regime of liquid motion relative to the heating surface, in our opinion, substantially alters the general picture of the heat exchange process, contributing to an acceleration in the detachment of vapor bubbles and a migration to the boundary layer of new portions of water. At low rpm's ($n = 500, 750 \text{ r/min}$) the frequency of vapor bubble detachment determines the increase in α_2 ; a subsequent change in n (1000, 1200 r/min), obviously, leads to a detachment of liquid from the heating surface and to a certain reduction in the growth rate of the heat transfer factor.

A change in the size of the clearance δ from 0.5 to 1.5 mm leads to a reduction in the coefficient α_2 .

The effect of δ on α_2 at various thermal fluxes can be established from examining Fig. 2.

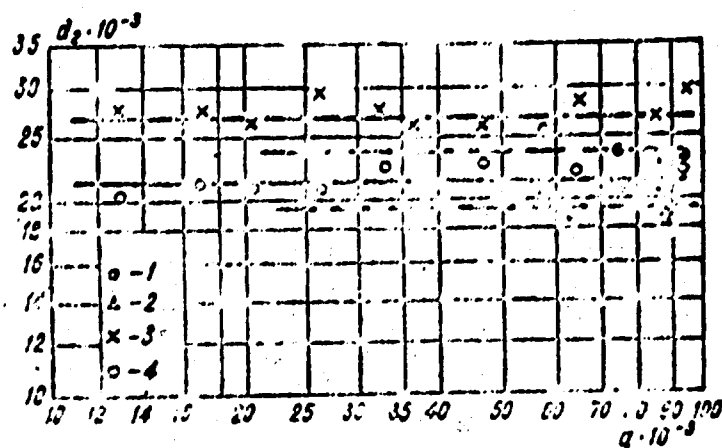


Fig. 2. Variation in the heat transfer factor for distillate with an increase in the thickness of the boiling layer: $\delta = 1.5 \text{ mm}$; N. G. Styushin: 1 - $n = 750 \text{ r/min}$; 2 - $n = 500 \text{ r/min}$; author: 3 - $n = 700 \text{ r/min}$; 4 - $n = 500 \text{ r/min}$.

With small clearances between the rotor and the heating surface ($\delta = 0.5$ mm) the value of α_2 is considerably higher than with large clearances ($\delta = 1.5$ mm). This can be explained by the fact that when $\delta = 0.5$ mm wall temperature is lower than it is with clearances of 1.0, 1.5 mm. The reduction in wall temperature occurs because of the better heat removal from the surface to the liquid and the separation of vapor bubbles of very small dimensions, not yet reaching separation diameter, which, on the whole, leads to an increase in the heat transfer factor α_2 . With an increase in the clearance the heat exchange intensity worsens somewhat.

It follows from the above that forced motion (in the form of rotation) in the heat flux range of $q = 11,630$ to $116,300$ W/m² when $\delta = \text{const}$ enables the intensification of the heat exchange process, causing an increase in the heat transfer factor.

An increase in heat fluxes in this range does not cause a change in the coefficient α_2 . The heat transfer factor depends on the rpm of the rotor (angular velocity) and at large n reaches 23,000-29,000 W/m²·deg.

The growth rate of α_2 drops somewhat with an increase in the angular velocity of rotor rotation. It is possible that when n is too high, the nucleate boiling regime is disrupted and there is a transition to film boiling.

A change in the clearance δ , all other things equal, toward an increase somewhat reduces the value of the coefficient of heat transfer from the wall to the liquid. With the clearance dimensions assumed, α_2 drops 6-8%.

Sea water of constant concentration, boiling in a thin rotating film (see Fig. 1), gives a value for the heat transfer factor 20-25% lower than distilled water boiling under the same conditions. In our opinion, this is explained by the difference

in the physical properties of these liquids since the hydrodynamic regimes of the installation are the same.

An increase in specific heat flux within the assumed range does not change the value of α_2 . This is particularly important for evaporative devices using low-potential heat. Operation at low temperature heads decreases scum formation.

The character of the increase in the heat transfer factor with an increase in the rpm (Fig. 3) and during the boiling of sea water is clearly expressed. In the distillate the effect of angular velocity is less than in the sea water.

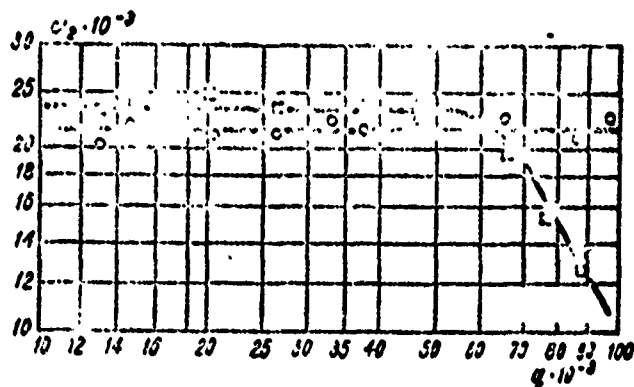


Fig. 3. Heat transfer factor versus rotor rpm:
 \square - $\delta = 0.5$ mm; \circ - $\delta = 1.5$ mm;
 $n = 500$ r/min.

Theoretical treatment of experimental data in connection with the heat transfer factor and the rotor rpm gives the following empirical equations:

$$\alpha_2^{0.7} = 1180n^{0.472}; \quad (1)$$

$$\alpha_2^{0.8} = 685n^{0.815}. \quad (2)$$

A similar character for this relationship is also observed in the works of Hickman et al. [5].

At low concentrations of sea water (1, 5, 3%) with forced motion, a noticeable decrease in the heat transfer factor is not observed as occurs with boiling in a large volume. We can assume that the turbulence of the flow during rotation with low concentrations excludes the supersaturation of the solution in the boundary layer at the heating surface, while with an increase in thermal fluxes during boiling in large volume such a supersaturation is observed and leads to a reduction in α_2 with an increase in concentration.

This position is confirmed by the fact that during tests, the deposition of scum on the heat-transferring surface during the boiling of sea water in a large volume occurs more rapidly than during the boiling of a rotating flow.

With an increase in the concentration (10, 15%) of sea water the value of the coefficient α_2 drops with approximately the same intensity as during boiling in a large volume. In this case, sea water has a considerable salt saturation and a change in the flow hydrodynamics can not substantially change the heat exchange process. It should be mentioned that in the presence of rotation the drop in α_2 at concentrations of 10, 15% begins at a higher range of thermal fluxes (58,000-69,750 W/m²) than with boiling in a large volume (35,000-41,000 W/m²).

In tests with sea water the thicknesses of the boiling rotating layer of liquid varied because of the change in the clearance δ .

Experiments indicated that regularities of the process remained the same as with boiling of the distillate, but the absolute values of α_2 are somewhat lower.

Transition to higher rotor rpm with a decrease in clearance size at $q = \text{const}$ causes an increase in α_2 . But with clearances

of 0.5 and 1.0 mm points are observed for which the value of α_2 drops sharply. A substantial reduction in the heat transfer factor is found with thermal fluxes of approximately 70,000 W/m².

In our opinion, with an increase in rotor rpm at this time the water can not successfully remove heat from the surface, i.e., the process of nucleate boiling is disrupted and the value of α_2 falls.

In the experimental study several characteristics of the scum formation process, which occurs during the rotation of a boiling flow, were studied.

In the presence of rotation in flows of varying thicknesses and constant concentration, taken in our study after 60 h of continuous operation, scum deposit was not observed.

The salt concentration in the boundary layer does not grow infinitely; a reverse transfer of salt to the mass of the solution occurs.

The rotation of the liquid flow obviously contributes significantly to this transfer; with boiling of sea water in a large volume, however, the movement of the liquid masses relative to the surface deteriorates somewhat and with an increase in wall temperature scum begins to appear. An intensive mixing of water near the surface does not allow the salt concentration to increase in the boundary layer and, consequently, the intensity of salt deposit on the surface is reduced. This apparently explains the absence of scum on heating surfaces.

From an analysis of the works of Hadley and Hickman on the boiling of sea water on rotating surfaces it is apparent that they also did not detect the deposition of scum during the continuous operation of an installation for 72 hours. Our

conclusions are valid only at low temperature heads ($\Delta t = 3-10^\circ\text{C}$).

An increase in the temperature head to $15-16^\circ\text{C}$ causes the appearance of scum even with the rotation of flow. An increase in the concentration of sea water for low Δt does not alter these conclusions, but with a rise in Δt scum begins to cover the surface. This once again substantiates the position that the process of scum formation is wholly determined by the values of the temperature head and the concentration of sea water.

From an analysis of the experimental data it is apparent that the disruption in the hydrodynamics of a two-phase flow because of the forced motion of liquid at low heat fluxes (to $116,300 \text{ W/m}^2$) and the value of the heat transfer factor are determined by the velocity of the forced motion. N. G. Styushin [6] arrived at the same conclusions, taking into account the directed motion of the liquid by introducing the criterion $K_w = w^*/w_0$ where w_0 is the velocity of the forced motion, w^* is the rate of vapor formation. We obtained a criterion equation in which the velocity of the forced motion was taken as equal to the angular velocity of the motion of the liquid:

$$\frac{q}{k} \left(\frac{1}{1-\gamma} \right)^{1/2} = A \left(\frac{1}{a} \right)^{n_1} \left(\frac{\omega^2}{a} \right)^{n_2} \left[r \left(\frac{q}{(1-\gamma)\omega^2} \right)^{n_3} \right]^{n_4}. \quad (3)$$

This choice was based on the fact that the forced motion had a rotational shape.

Using the experimental data from our study with distillate and sea water, as well as the data of N. G. Styushin, we attempted to set up the final form of equation (3) and to generalize the experimental data with this equation.

The criteria system which describes the process of liquid boiling in a rotational flow is represented in the form:

$$Nu = f(Pr, Pe_a, K_w). \quad (4)$$

As established during experimentation, a variation in thermal flux (in the range $q = 11,630-116,300 \text{ W/m}^2$) has no effect on the condition of heat exchange during the forced motion of liquid. This enables us to exclude from equation (4) the criterion K_w as not being a determining characteristic of the process in this case.

Then

$$Nu = f(Pr, Pe_a), \quad (5)$$

where $Pe_a = \frac{\omega r^2}{\alpha}$.

The processing of tests (Fig. 4) in coordinates $\frac{Nu Pr^{0.35}}{Pe_a} = f(Pe_a)$ with respect to a distillate in sea water makes it possible to establish the final form of relationship (5)

$$Nu = A Pe_a^{0.6} Pr^{0.35}, \quad (6)$$

where $A = 5.75$ is the distillate; $A = 5.0$ is the sea water.

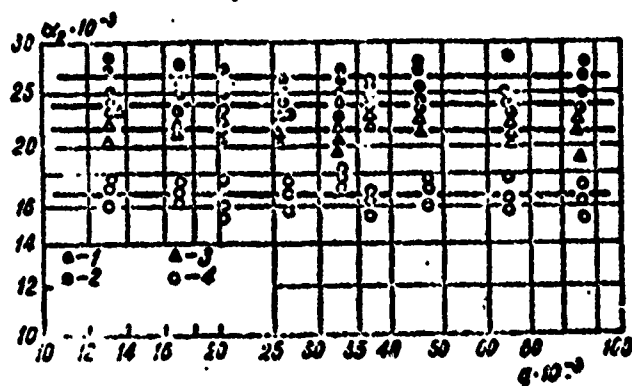


Fig. 4. Processing of experimental data on the boiling of distillate and sea water in a rotational flow in the criterion form:

$\delta = 1.5 \text{ mm}$

Sea water { 1 - $n = 1200 \text{ r/min}$; 2 - $n = 1000 \text{ r/min}$;
 { 3 - $n = 750 \text{ r/min}$; 4 - $n = 500 \text{ r/min}$.

To substantiate the criterion equation (6) we processed the results of the experimental study of N. G. Styushin on the boiling of water during forced motion on various surfaces in the range of q variations which interested us. They were arranged satisfactorily with respect to the averaging curve (Fig. 5). The spread of separate points varied from 0 to 20%. Such a deviation can be explained by the variation in the clearance between the rotor and the heating surface in our test and the tests of N. G. Styushin (2-8 mm).

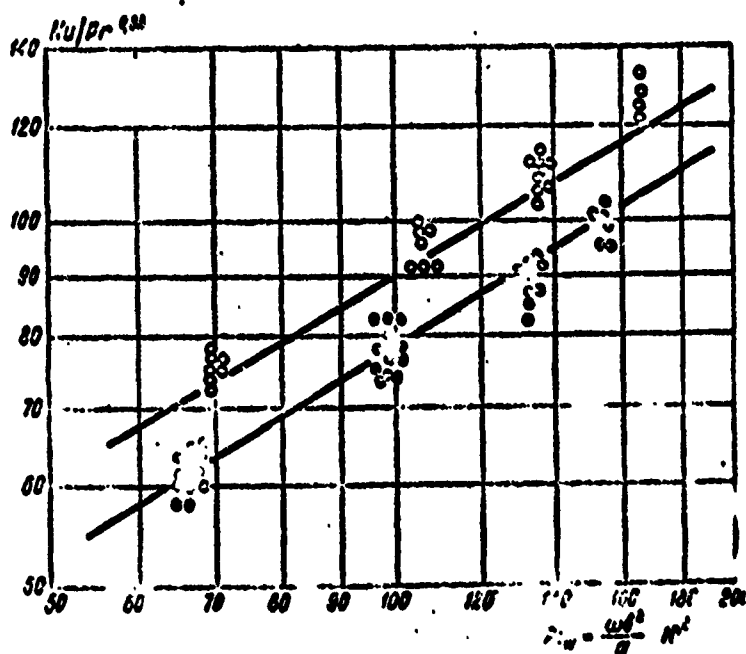


Fig. 5. Generalization of the experimental data of N. G. Styushin on the criterion relationship $Nu = 1.2 \cdot 10^{-3} Re^{0.5} Pr^{0.4}$.

○ - Distillate; ◐ - Sea water: $R_1 - R_2 = 1.5$ mm.

We should mention that the quantity of experimental data on boiling in rotational flows of liquid is very limited, which makes a full check of the derived relationship impossible.

Analysis of the heat exchange process during boiling in a rotational flow leads to the conclusion that an increase in rotor

rpm within the thermal flux range 11,630-116,300 W/m² leads to an increase in the heat transfer factor by 80-85%. The effect of the thickness of the boiling layer is not clearly expressed and, although a certain increase in α_2 at low (0.5, 1 mm) thicknesses is observed, the stability of liquid boiling is disrupted with an increase in thermal fluxes. At the same time, the boiling process, under such conditions, considerably reduces scum formation.

We have based our conclusions on the fact that heat exchange during boiling in the range of thermal fluxes assumed is wholly determined by the angular velocity of the liquid.

BIBLIOGRAPHY

1. Клячко В. А. Сб.: «Оч. и обезсоливание соленых и солоноватых вод». М., Госстройиздат, 1960.
2. Hadley G. T. A mathematical and Experimental study of Climbing Film Evaporation. Industrial and Engineering Chemistry, vol. 52, 1, 1960.
3. Слесаренко В. Н. Исследование процесса теплопередачи при кипении морской воды в судовых и парильных установках. «Труды ЦКТИ», вып. 57, 1965.
4. Слесаренко В. Н. «Труды ДВПИ», т. 64, 1956.
5. Хикман К. К. (и др.). Оч. и обезсоливание соленых вод. М., ИИЛ, 1963.
6. Стюшии Н. Г. ЖТФ, т. 23, вып. 11, 1953.

CRITICAL THERMAL LOADS IN ANNULAR CHANNELS

V. I. Tolubinskiy, A. K. Litoshenko,
and V. L. Shevtsov

Abbreviations

кр = crisis, critical;

нед = underheating.

In various fields of engineering heat exchangers are frequently used in which the motion of the cooling liquid occurs in cylindrical or annular channels where the pipe diameters and slot widths vary from several tens to fractions of a millimeter. Most of these systems in advanced installations use the heat transfer process with surface boiling which does not reach liquid saturation temperature under forced motion conditions. The forcing limit of the heat exchange process with boiling is determined by the critical thermal load at which nucleate boiling changes to film boiling.

Many works have been devoted to the study of the heat exchange crisis. As a result of these efforts, it has been established that the pressure, temperature, and physical properties of the working fluid, the shape and dimensions of the heat-transferring

surface, as well as the velocity of the forced fluid motion affect the value of critical thermal load.

Nevertheless, because of the absence, in a number of cases, of reliable methods of determining critical thermal loads by calculation, it has been necessary to set up special experimental studies.

The purpose of this work has been to study the regularities involved in the appearance of a heat exchange crisis in annular channels 0.2, 0.4, 0.6, 0.8 mm wide under conditions of one-sided external heating in a pressure range from 2.5 to 21.6 MN/m². Mass velocities varied from 50 to 400 kg/m²·s, and underheating of the fluid to saturation enthalpy from 600 kJ/kg to 30% of the per-weight vapor content.

Experiments were performed on a closed circulation loop, all lines of which were made from 1Kh18N9T steel. The cooling fluid was distilled and degassed water. Circulation of the liquid in the system was accomplished with a geared circulation pump in a special housing which would withstand pressure up to 32 MN/m². The pressure in the system was maintained by two NZhR-11 plunger pumps.

The flow rate of the liquid was changed by a diaphragm to which a specially constructed electronic differential manometer was connected [1].

After the diaphragm, the water passed in succession through the heat exchanger, electric heater, experimental section, heat exchanger again, cooler, separator, and, finally, entered the suction pipe of the circulation pump.

In a pipe-in-pipe heat exchanger the water was heated from the heat of the water coming out of the experimental section.

The electric heater was designed for final heating of the water to the required temperature. In the cooler the water was cooled to a temperature of 40-50°C and entered the separator, which was an air-divider tank, during the filling of the system with water.

The test element was a single piece and installed vertically (Fig. 1). The annular channel of the element was formed by two coaxial pipes. The pipes were made together with tightly fitting current-conducting cams. In the lower part the cams were welded at the bottom and were spaced with asbestos-cement insulation at the top, which allowed the thermal expansion of both pipes.

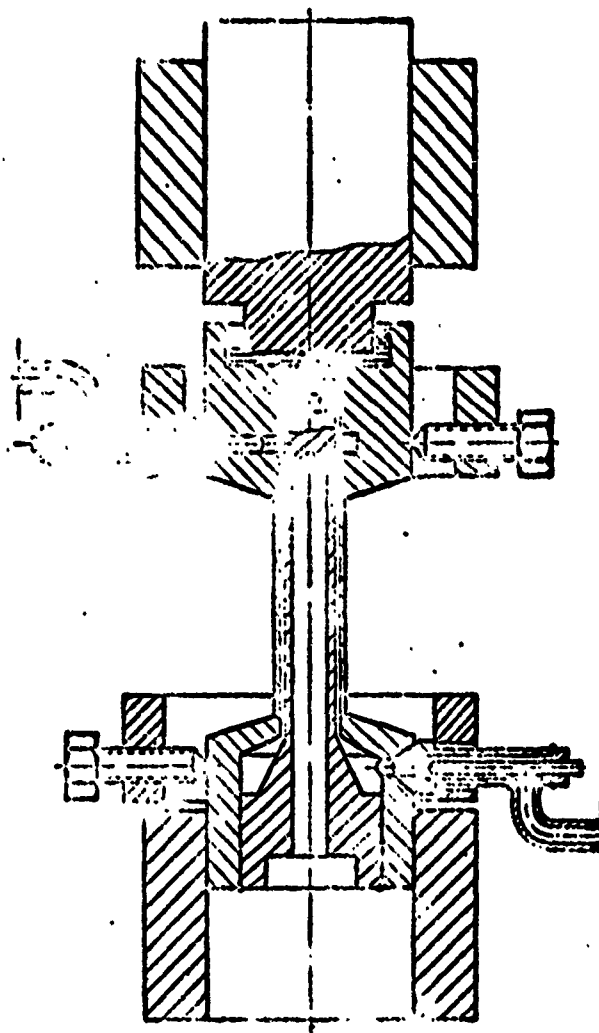


Fig. 1. Test element.

The feed and drain of water was accomplished by clamp nozzles to which thermocouple sleeves were welded. All parts of the test element were made with a high degree of precision and processing purity no lower than the seventh or eighth class. The principal dimensions of the test elements are presented in Table 1.

Table 1.

(1) Ширина канала δ , мм	(2) Диаметр канала, мм		(5) Длина теплоотдающей части l , мм
	(3) $d_{\text{вн}}$	(4) $d_{\text{вн}}$	
0,2	13	12,6	20 40 70 —
0,4	13	12,2	20 40 70 —
0,6	13	11,8	20 40 70 120
0,8	13	11,4	20 — 60 160

KEY: (1) Channel width δ , mm; (2) Channel diameter, mm; (3) External $d_{\text{вн}}$; (4) Internal $d_{\text{вн}}$; (5) Length of heat-releasing part l , mm.

The element was heated by a constant current from an ANG-30 motor-generator, 5000 A, 6 V. The lower current-conducting cam of the test element was set in an expanding contact ring, to the copper nib of which current conducting bus bars were connected. To eliminate from the test element the mechanical stresses which were inevitable with the rigid attachment of both its ends, due to thermal expansions, the upper electrical contact with the test element was accomplished through liquid metal.

The heat exchange crisis was fixed visually by the appearance of an incandescent spot on the outer surface of the heat-releasing part of the element. In the adjustment test the crisis was also fixed with the aid of a balanced bridge. These tests showed good agreement for the quantity $q_{\text{кр}}$ in both cases.

Thermal load on the heating surface was calculated from the force of the heating current and the drop in voltage on the length of the heat-releasing part of the element at the moment

the heat exchange crisis occurred. Liquid flow parameters at the spot of crisis occurrence were calculated based on the thermal balance. Data from the control measurement apparatus made it possible to determine thermal loads with accuracy up to 6-8% and flow parameters with accuracy up to ± 45 kJ/kg.

The increase in thermal load was accomplished by increasing the value of the heating current at prescribed constant values for mass velocity, pressure, and liquid temperature at input to the experimental section. Thermal load rose smoothly. With the appearance of the incandescent spot on the heating surface the load dropped. The next test on the same element was performed with the same values for pressure and mass velocity. Liquid temperature was increased by 20-30°C. A series of tests were performed in the entire possible range of liquid underheating up to saturation enthalpy; the deformed elements were replaced with new ones.

As a result of each series of tests functions $q_{kp} = f(\Delta i_{\text{нед}})$ were obtained at constant values for the width of the annular clearance, mass velocity, and pressure. More than 200 series of tests were made in all.

As studies have shown, the value of critical thermal loading is virtually independent of the underheating of the liquid to saturation enthalpy at mass velocities of 50-200 $\text{mg/m}^2 \cdot \text{s}$; with an increase in mass velocity from 200 to 400 $\text{kg/m}^2 \cdot \text{s}$ the underheating of the liquid affects the value of q_{kp} , which drops with a decrease in underheating. A similar effect of liquid underheating on the value of q_{kp} was detected in [2-5].

The effect of the underheating of liquid to saturation enthalpy on the value of q_{kp} is generally not great and can be taken into account in the following manner:

$$q_{kp}^1 = q_{kp} (1 + 0,12 \omega \cdot 10^{-5} \Delta i_{\text{нед}}) \quad (1)$$

It is apparent that the determination of $\Delta i_{\text{нед}}$ by calculation can not be performed with complete accuracy, especially at low values for $\Delta i_{\text{нед}}$ since, in this case, vapor bubbles, which have separated from the heating surface and have not succeeded in condensing in the boundary layer, are entrained by the underheated flow, while the heat carried by them is not transferred fully to the flow of liquid within the test element. It is safe, however, to estimate the vapor content of the flow as long as it is possible.

Figure 2 presents the function $q_{\text{кр}} = f(p)$ for a clearance of 0.6 mm for the case of liquid heating to boiling temperature. Similar functions were obtained for other clearances, lengths of heat-releasing parts, and mass flow velocities [5]. As is apparent from the graph, the value of $q_{\text{кр}}$ in the pressure range from 2.5 to 21.6 MN/m² first grows with an increase in pressure from 2.5 to 15 MN/m², reaching its maximum values, and then drops with a subsequent increase in pressure from 15 to 21.6 MN/m². The effect of pressure on the quantity $q_{\text{кр}}$ can be expressed by the following equation:

$$q_{\text{кр}} = c_1 p^2 \left(1 + \frac{p^*}{p}\right)^{0.33}. \quad (2)$$

As studies have shown, the critical thermal load, other things being equal, grows with an increase in mass velocity in the studied range of variation. However, mass velocity has a varied effect on $q_{\text{кр}}$ with different clearance widths. With an increase in the width of the annular clearance from 0.2 to 0.8 mm the effect of velocity grows. Partial functions $q_{\text{кр}} = f(pw)$ have the form $q_{\text{кр}} \sim (pw)^n$, where the exponent n depends upon the width of the clearance. In the first approximation, the function $n = f(\delta)$ can be represented by equation:

$$n = 0.6 \sqrt{\delta}. \quad (3)$$

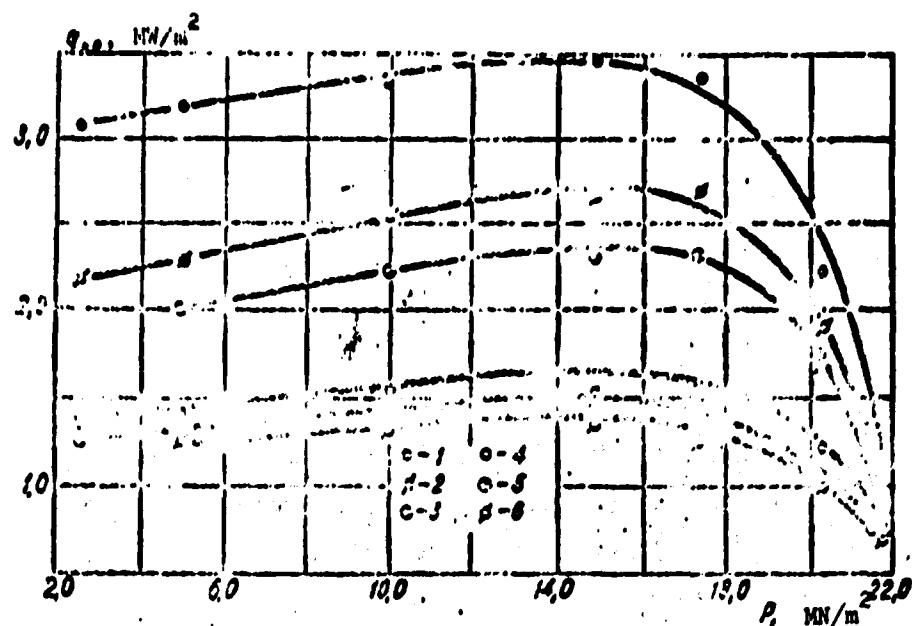


Fig. 2. Function $q_{kp} = t(p)$ for a clearance with width 0.6 mm:

1 - $l = 40$ mm, $\rho w = 400$ kg/m²·s; 2 - $l = 40$ mm, $\rho w = 200$ kg/m²·s; 3 - $l = 40$ mm, $\rho w = 100$ kg/m²·s; 4 - $l = 70$ mm, $\rho w = 400$ kg/m²·s; 5 - $l = 70$ mm, $\rho w = 200$ kg/m²·s; 6 - $l = 70$ mm, $\rho w = 100$ kg/m²·s.

Table 2 presents the values for $n = f(\delta)$ obtained as a result of processing test data, and values for "n" calculated from equation (3).

Table 2.

Ширина кольцевого (1) зазора, мм	$n = f(\delta)$	$n = 0,6 \sqrt{\delta}$
0,2	0,270	0,269
0,4	0,412	0,379
0,6	0,465	0,465
0,8	0,545	0,537

KEY: (1) Width of annular clearance.

Thus,

$$q_{kp} \sim (\rho w)^{0.5} \sqrt{\delta}. \quad (4)$$

The reduction in the exponent n with quantity ρw and an increase in the width of the clearance δ apparently occurs due to the decrease in the turbulence of the liquid flow and its transverse pulsations in the annular channel with a decrease in its width.

Figure 3 presents the function $q_{kp} = f(\delta)$ with $\rho w = \text{idem}$. The value of the critical thermal load increases with an increase in the width of the annular clearance from 0.2 to 0.8 mm, while the partial function $q_{kp} = f(\delta)$, in the studied range of clearance width variation, can be represented in the form:

$$q_{kp} \sim \delta^m, \quad (5)$$

where m varies from 0.5 to 1 and, on the average, can be assumed equal to 0.7. However, as mentioned above, the value of the clearance also enters into the exponent when ρw . Therefore, in the empirical formula which takes into account the joint effect of δ and ρw , the exponent with δ will not be equal to the exponent defined earlier, obtained on the assumption that $\rho w = \text{const}$, although the final result of calculation will reflect the effect of δ in the degree of 0.7.

It is apparent that with a subsequent increase in the width of the clearance above 0.8 mm the value of critical thermal load will tend toward a certain constant.

In the studied range of variation in the determining parameters a decrease in critical thermal load was observed with an increase in the length of the heat-releasing part of the test elements. In the first approximation, we can assume that the quantity q_{kp} , all things being equal, is inversely proportional to the length. In this work the length of the heat-releasing part

of the test element virtually agreed with the geometric length of the channel from liquid input to the spot where the heat exchange crisis occurred.

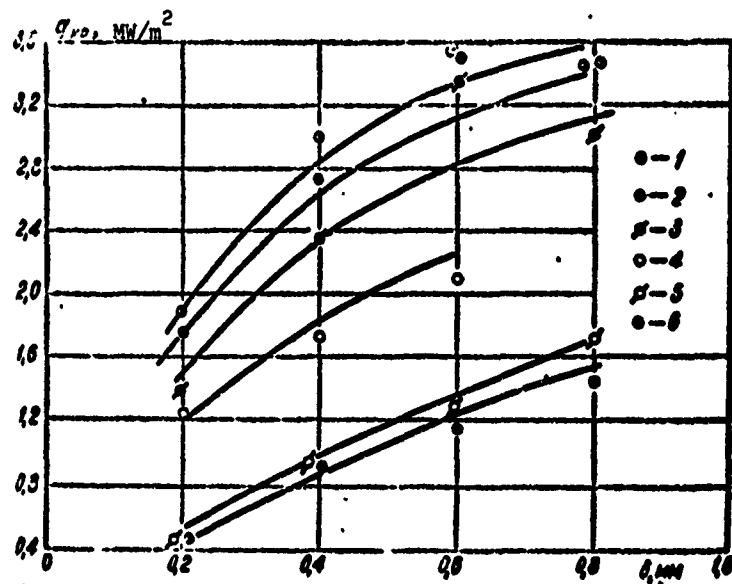


Fig. 3. Function $q_{hp} = f(l)$ when $\rho w = \text{idem}$.

- 1 - $l = 20$ mm, $\rho w = 100$ kg/m²·s, $p = 15$ MN/m²;
- 2 - $l = 20$ mm, $\rho w = 100$ kg/m²·s, $p = 10$ MN/m²;
- 3 - $l = 20$ mm, $\rho w = 100$ kg/m²·s, $p = 5$ MN/m²;
- 4 - $l = 40$ mm, $\rho w = 400$ kg/m²·s, $p = 20$ MN/m²;
- 5 - $l = 80$ mm, $\rho w = 100$ kg/m²·s, $p = 15$ MN/m²;
- 6 - $l = 80$ mm, $\rho w = 100$ kg/m²·s, $p = 17.2$ MN/m².

As a result of clarifying the degree of the effect of separate parameters, the empirical relationship for water heated to boiling point is obtained:

$$q_{hp} = 0.75 \cdot 10^3 \frac{(l w)^{0.61 \sqrt{p}}}{l^{1.31}} r \sqrt{p} \left(1 + \frac{p^*}{p}\right)^{0.38}. \quad (6)$$

Formula (6), as is apparent from Fig. 4, generalizes 83% of all the series of tests with a deviation of $\pm 25\%$. As a result of the research conducted, we make the following conclusions.

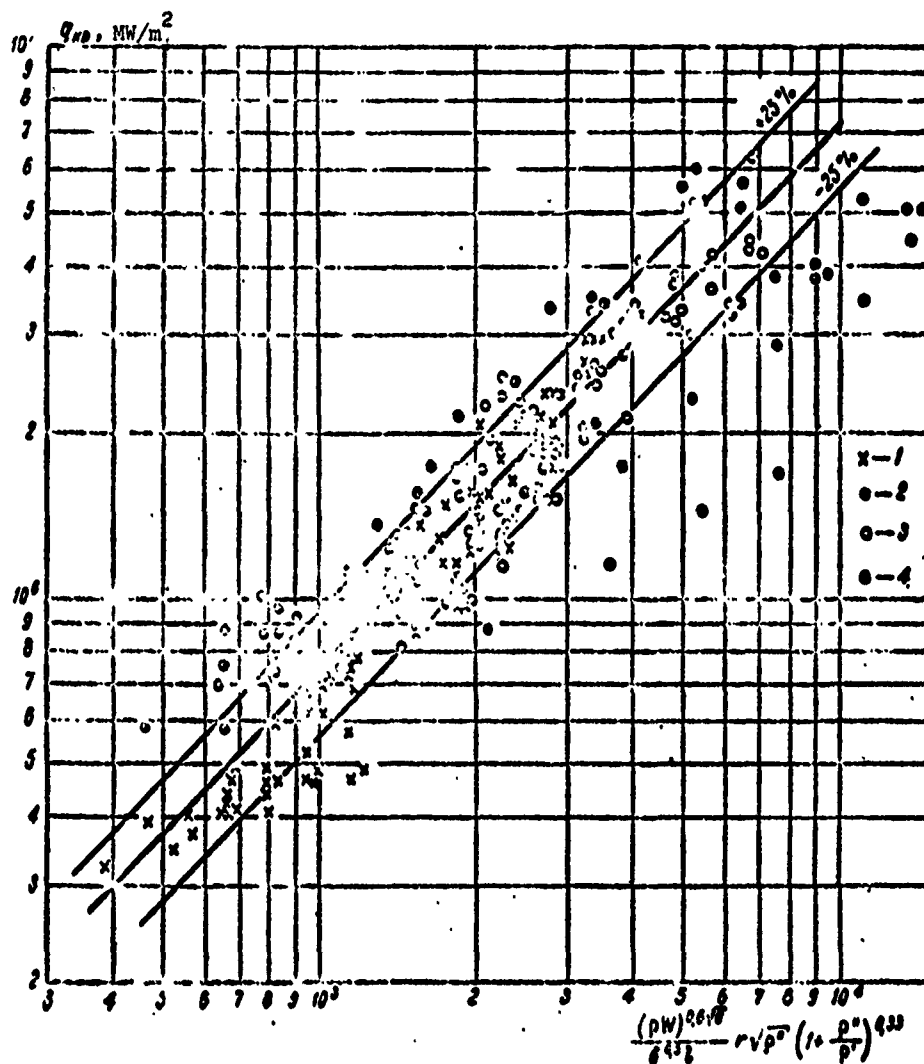


Fig. 4. Processing of experimental data according to equation (6).

1. The effect of critical thermal loads is virtually independent of the underheating of liquid to saturation enthalpy at mass velocities of $pw = 50-200 \text{ kg/m}^2 \cdot \text{s}$. With an increase in pw to $400 \text{ kg/m}^2 \cdot \text{s}$ the value of q_{kp} grows with an increase in underheating.

2. With a rise in mass velocity, critical thermal loads grow; however, in the near-critical region their growth is insignificant.

3. In the studied range of variation in the length of the heat-releasing part and the width of the annular clearance, critical thermal loads rise with an increase in the width of the clearance and fall with an increase in the length of the heat-releasing part.

4. In the pressure range from 2.5 to 21.6 MN/m², $q_{кр}$ achieves its maximum values when $p = 15$ MN/m².

5. For practical calculations we can use equation (6) which is valid for the range of determining parameters indicated in the work.

BIBLIOGRAPHY

1. Литошенко А. К., Чернобай В. А. Кризис теплообмена при кипении в узких кольцевых каналах. «Вестник Киевского политехнического института. Серия—Теплоэнергетика», № 1, 1964.
2. Субботин В. И., Зенкевич Б. А., Алексеев Г. В. Критические тепловые потоки в кольцевых каналах. «Теплоэнергетика», 1963, № 10.
3. Толубинский В. И., Орнатский А. П., Кичигин А. М., Литошенко А. К. Кризис теплообмена при кипении в узких кольцевых каналах. Сб.: «Теплофизика и теплотехника». Изд-во «Наукова думка», 1964.
4. Толубинский В. И., Орнатский А. П., Литошенко А. К. Кризис теплообмена при поверхностном кипении в узких кольцевых каналах. Сб.: «Теплоотдача при изменении агрегатного состояния». Изд-во «Наукова думка», 1966.
5. Толубинский В. И., Литошенко А. К., Шевцов В. Л. Кризис теплообмена в кольцевых каналах шириной 0,4 мм. Сб.: «Теплообмен в энергетических условиях». Изд-во «Наукова думка», 1967.

RECOMMENDATION ON CRITICAL THERMAL LOADS IN CYLINDRICAL PIPES

V. Ye. Doroshchuk and
F. P. Lantsman

Abbreviations

r_p = boundary

κ_p = critical

At the present time, extensive experimental material on heat exchange crises is available both in our country and abroad. To design atomic reactors with water under pressure and, particularly, the boiling type, it is necessary to know the values of critical thermal loads $q_{\kappa p}$, i.e., specific thermal fluxes, at which the nuclear regime of liquid boiling changes to the film regime. As a rule, the surface temperature of the fuel elements rises catastrophically and the reactor enters an emergency state. Unfortunately, test data from various authors on critical thermal loads agree poorly; the spread reaches tens and hundreds of per cents. Naturally, this causes great difficulty in designing reactors.

There is an urgent need to analyze the published experimental material on this question and, based on such an analysis, set up

a table of the most reliable values for q_{kp} . Such a table, which we shall call a "skeleton," can serve the direct needs of planners and can furnish a basis for determining the dependence of q_{kp} on the regime parameters of the heat carrier during the processing of design equations.

To simplify the problem, we have limited ourselves to an examination of critical thermal loads only in circular pipes, for which the greatest amount of experimental data has been published. Circular channels are used in several types of reactors.

It was decided to set up a table based on a channel diameter of 8 mm and the following values for the regime parameters:

- pressure $p = 49, 69, 98, 137, 167, 196 \text{ bar}^1$;
- mass velocity $pw = 750, 1000, 2000, 2500, 3000, 4000, 5000 \text{ kg/m}^2 \cdot \text{s}$;
- underheating of water below boiling $\theta = 0, 10, 25, 50, 75^\circ\text{C}$;
- vapor content per unit weight $x = 0.1, 0.2, 0.3, \dots, x_{rp}^0$, where x_{rp}^0 is the boundary vapor content at which the boundary layer water film dries [19].

In examining the experimental data of various authors, we started with the following assumptions.

1. The material and roughness of the heating surface, the position of the experimental section in space, the direction of flow of the heat carrier, and the frequency of crisis in the same section have no effect on the value of critical thermal load [5, 6].

2. Low-frequency pulsations in flow rate and pressure, which are characteristic to certain diagrams of experimental

¹50, 70, 100, 140, 170, 200 atm (abs.).

installations, can have a considerable effect on q_{kp} [5, 6, 7]. Critical thermal loads in the presence of flow pulsations are reduced by several factors. The necessary conditions for the occurrence of pulsations are the following: the presence of an easily compressible volume (usually a vapor-water mixture) in front of the experimental section, the existence of an "economizer" zone in the experimental section itself, and the presence of a certain minimal thermal load which ensures the formation of a certain amount of steam at the end of the heated pipe (including and because of the surface boiling of water).

3. The channel diameter affects critical thermal loads; in narrower pipes they have high values. To recalculate q_{kp} from one type diameter to another within the range $d = 2-13$ mm, we use the following formulas:

for underheated water

$$q_{kp} \sqrt{d} = \text{const}; \quad (1)$$

for vapor-water mixture

$$(q_{kp})_{d_{\text{нн}}} = q_{kp} - q_0 \left(\sqrt{\frac{8}{d}} - 1 \right). \quad (2)$$

These formulas are borrowed from references [8, 9]. The coefficient q_0 for various pressures has the following values:

p, bar	$q_0 \cdot 10^{-6}$, W/m ²
49	8.20
78	7.58
98	7.29
137	6.71
167	6.28

4. When $l/d > 15$ the length of the heated section of the experimental pipe does not affect the value of q_{kp} [5, 11, 31].

5. The concept of "critical thermal load," related to the so called heat exchange crisis of the first type (a crisis caused by the transition of nucleate boiling to film boiling), has significance only as long as the heating surface is washed by water, including a water film with an annular structure of the vapor-water flow. As soon as the vapor content in the heated pipe reaches a certain boundary value x_{rp}^0 , the water film dries and at this moment a heat exchange crisis of the second type occurs. Thus, the upper boundary of vapor content, at which we can discuss q_{kp} is x_{rp}^0 . Table 1 presents the values of x_{rp}^0 [1].

Table 1.

q_{kp} , $kg/m^2 \cdot sec$	x_{rp}^0 with p in bar					
	49	69	93	137	167	196
750	0.86	0.78	0.64	0.50	0.39	0.28
1000	0.75	0.68	0.58	0.44	0.37	0.22
1500	0.61	0.56	0.47	0.35	0.27	0.19
2000	0.53	0.48	0.41	0.31	0.24	0.16
2500	0.53	0.48	0.41	0.31	0.23	0.15
3000 -- 5000	0.52	0.48	0.40	0.30	0.23	0.15 -

DESIGNATIONS: $kg/m^2 \cdot sec = kg/m^2 \cdot s$

The experimental data on q_{kp} published in [1-6, 9-52] were examined and processed. Not all of the data could be used in setting up the "skeleton" tables, for example:

a) test data obtained at $2 > d > 13$ mm since, in these cases, there are no recommendations for converting the critical thermal loads on a pipe with an 8 mm diameter;

b) experimental stage in which q_{kp} was measured in pulsation regimes [6, 36, 37, 40, 41, 49];

c) measurements of specific thermal loads made at $x \geq x_{rp}^0$, i.e., in the area of heat exchange crisis of the second type [10, 11, 17, 20, 49, 51];

d) studies of P. I. Povarnin and S. T. Semenov [42, 43] made on very thin pipes $d \leq 1.5-3$ mm and generally with underheatings that were too great $\theta \leq 75^\circ\text{C}$;

e) studies of A. P. Ornatskiy and A. M. Kichigin [44-47], which are characterized by a very large spread in experimental points with underheatings of water to 50°C ; moreover, these tests were made on very narrow pipes;

f) references [21, Table 3, 7, 13] containing a limited number of experimental points with a large spread.

When there was no description of the experimental methodology, we were more critical of the test data and after analysis did not use some of them.

To set up tables of critical thermal loads we processed the experimental data of various authors in order to obtain q_{kp} for the skeleton values of p , p_w , θ , x . For this purpose, corresponding graphs were plotted. Interpolation was performed only if there was complete confidence in its regularity.

The experimental data thus processed are presented in summary table 2. In analyzing this table, it was decided not to use the bold faced numbers in Table 2 for further processing of the value of q_{kp} . They include the following:

a) Buchberg's test data [15], obtained at $\theta = 0-10^\circ\text{C}$, with considerable inert gas content; as noted in [34, 39] at $\theta \rightarrow 0$ an abundant liberation of gas bubbles occurs in the flow of water; this leads to unstable flow state and, as a consequence, to a noticeable reduction in q_{kp} ;

b) Becker's test data [13]; this author did not obtain the dependence of critical thermal loading on flow velocity, which,

naturally, causes a certain lack of confidence in his experimental material;

c) our own test data at $x > 0$. The critical thermal loads which we measured in the flow of a vapor-water mixture were somewhat greater than those measured by other authors (Table 2). Apparently this is explained by the severe throttling of the working medium at input to the experimental section (tens and hundreds of kilograms per square centimeter), which ensures the high hydrodynamic stability of the flow and, as a consequence, leads to higher values for q_{kp} [25, 26, 53, 54]. In addition, we performed tests on comparatively thick-walled pipes ($\delta = 2$ mm), which, when they are heated by ac current, could also lead to higher values for q_{kp} (as compared with thinner pipes)[26].

We can assume that the processed recommendations on critical thermal loads, for these reasons, will contain some allowance with respect to q_{kp}

When we dropped the values indicated by bold faced figures, we were able to obtain averaged values of q_{kp} (Table 3). Based on these and the corresponding graphs, the final (leveled off) values of q_{kp} were obtained (Table 4). They are also the final recommendations. After analyzing the deviations in the test data of various authors from these recommendations, we were able to evaluate the accuracy of the proposed values for q_{kp} within $\pm 10\%$.

Table 2.

A, 10 ³ / m ² · sec	Interp- type (1)	P					40 °C						
		h °C					x						
		75	50	25	10	0	0,1	0,2	0,3	0,4	0,5	0,6	0,7
750	27-32					8,14							
	12	9,9		8,43		7,21							
	13												
	14, 26	8,56	8,14	7,79	7,62	7,44	7,19	6,75	5,13	5,62			3,02
1000	27-32					7,68							
	12	9,89	9,19	8,49	7,44	7,21							
	13												
	14, 26	8,91	8,48	8,09	7,89	7,63	6,99	6,34	5,64				3,37
1500	27-32					6,99							
	12	9,89	9,19	8,49	7,56	7,21							
	15					3,13							
	14, 26	9,42	8,84	8,32	8,04	7,73	6,99	6,09					
2000	27-32					6,45		3,55					
	12	9,89	9,25	8,49	7,62	7,21							
	10, 11					3,34					1,43		
	13										0,77		
2500	14, 26	9,77	9,11	8,49	8,07	7,68	6,99						
	27-32					6,05		4,07					
	12	10,00	9,30	8,49	7,68	7,21							
	10, 11					3,58					1,57		
3000	13									1,06			
	14, 26	10,0	9,27	8,48	8,00	7,58	6,99						
	27-32					5,58		3,23					
	12	10,18	9,42	8,43	7,73	7,21							
4000	10, 11					3,64					2,43		
	13									0,7			
	14, 26	10,30	9,34	8,47	7,91	7,44	6,07						
	27-32					5,47							
4000	12	10,81	9,71	8,37	7,79	7,15							
	10, 11					3,58				2,16			
	13												
	14, 26						2,42	1,15					

Table 2 (Continued)

pw. кг/м ² -сек	интервалы	p = 49 бар											
		t °C					x						
		75	50	25	10	0	0,1	0,2	0,3	0,4	0,5, 0,6	0,7	
5000	27-32					5,40							
	12		10,47	8,43	7,85	7,09							
	15					3,79							
pw. кг/м ² -сек	интервалы	p = 69 бар											
		t °C					x						
		75	50	25	10	0	0,1	0,2	0,3	0,4	0,5	0,6	
750	27-32					6,92							2,77
	16, 35						5,12	4,51	3,66				
	12	8,49		7,21		6,16							
	13										3,45		2,71
	14, 25	7,94	7,55	7,14	6,91	6,73	6,43	5,97	5,40	4,93			
1000	27-32			6,61	6,45	6,23							
	16, 35						4,68	3,98	3,47				
	12	8,49	7,91	7,33	6,40	6,16							
	17						5,51	4,56		3,84	3,03		3,00
	18										2,43		
	13										2,83		
1500	14, 25	8,25	7,93	7,32	7,04	6,79	6,20	5,52	4,97				
	27-32			6,33	6,07	5,82	4,24			3,13	2,37		
	16, 35					4,95	4,05	3,31	2,91				
	12	8,49	7,91	7,39	6,45	6,16							
	15					1,98							
	17										3,15		
	18										2,57		
	19					5,95	4,88	4,55					
2000	13						4,45	3,69	3,25	2,04			
	14, 25	8,60	8,19	7,54	7,09	6,77	5,94	5,33					
	27-32			6,00	5,82	5,49	3,72	3,14	2,57	1,84			
	16, 35					4,40	3,72	3,00					
	12	8,55	8,02	7,44	6,57	6,16							
	15					2,08							
	20								3,00	2,04			
	17			6,63	5,86	5,30	4,45	3,69	3,08	2,35			
2000	18						3,84	3,20	2,67				
	13						4,57	3,00		0,21			
	14, 25	9,16	8,43	7,64	7,09	6,72	5,82						

Table 2 (Continued)

Р _{из} , кг/м ² ·сек	Литера- тура	Р - 60 бар										
		t °C					x					
		75	50	25	10	0	0,1	0,2	0,3	0,4	0,5	0,6
2500	27—32			6,02	5,70	5,09	3,61	3,16	2,21			
	16, 35					4,15	3,45	2,73				
	12	8,60	8,14	7,44	6,59	6,16						
	15					2,40			2,36			
	20											
	17						4,66					
	19					5,84	4,65					
	13						4,11					
14, 26	9,32	8,46	7,59	6,97	6,57	5,69						
3000	27—32			6,19	5,61	4,98	3,37	2,80	2,07			
	16, 35					4,05	3,22	2,50				
	12	8,75	8,26	7,50	6,63	6,16						
	15					2,40						
	17					4,95	3,72	3,22				
	18					4,85	3,30	2,66				
	13								0,81			
	14, 26	9,18	8,30	7,44	6,83	6,43	5,40					
4000	27—32			6,51	5,65	4,81	3,20					
	12	9,65	8,66	7,56	6,69	6,16						
	15					2,67						
	20					4,80	3,35	2,83	1,95			
	17			6,60	5,45	4,72	3,26	2,51	1,17			
	18				5,44	4,27	3,02					
5000	27—32					4,88						
	12		9,59	7,79	6,69	6,16						
	15					3,02						
	17					4,70	3,31					
	18					4,54	2,79					

Р _{из} , кг/м ² ·сек	Литера- тура	Р - 98 бар											
		t °C					x						
		75	50	25	10	0	0,1	0,2	0,3	0,4	0,5	0,6	0,7
150	27—32		6,19	5,23	5,35	4,98				2,61	1,91	1,40	0,81
	16, 35					4,16	3,69	3,22	2,77				
	12			5,12	4,36	4,18							
	24							3,37	2,79	2,32	2,09	1,86	
	14, 26	6,01	5,64	5,24	4,99	4,77	4,36	3,95	3,49	3,02			

Table 2 (Continued)

Рав. №2, №3, №4	Литера- тура	Р - 1/2 бар											
		t °C					x						
		75	50	25	10	0	0,1	0,2	0,3	0,4	0,5	0,6	0,7
1000	27-32	5,95	5,88	5,26	4,93	4,59	3,94	3,20	2,37	2,00	1,31		
	16, 35					3,94	3,43	2,85	2,38				
	12	6,60	5,76	4,94	4,42	4,30							
	10, 11										1,38		
	14, 26	6,78	6,22	5,68	5,29	5,06	4,59	3,95	3,37	2,82			
	17								2,47				
1500	27-32		6,19	5,31	4,81	4,36	3,65	2,77	1,97	1,29			
	16, 35					3,69	3,05	2,42	1,72				
	12	7,27	6,22	5,23	4,59	4,42							
	14, 26	7,39	6,75	6,05	5,65	5,35	4,45	3,80	2,93				
2000	27-32		6,22	5,45	5,16	4,16	3,06	2,27	1,51	0,92			
	16, 35	7,73	6,63	5,64	4,88	4,48							
	24						3,37	2,79	2,32				
	10, 11								1,58				
	14, 26	7,62	6,75	5,98	5,54	5,12	4,24	3,39					
	17							3,08					
2500	27-32		6,91	5,56	4,88	3,99	2,84	2,00	1,15				
	16, 35					3,46	2,52	1,72					
	12	8,14	6,98	5,99	5,23	4,77							
	10, 11							2,07	1,28				
	14, 26	8,03	6,98	5,01	5,44	4,92	3,95						
3000	27-32		7,90	5,83	5,01	3,95	2,70	1,80	1,09				
	16, 35					3,43	2,30	1,46					
	12	8,61	7,39	6,34	5,58	4,94							
	10, 11								0,98				
	14, 26	8,55	7,32	6,05	5,35	4,77	3,31						
4000	27-32	9,56	9,06	6,28	5,26	3,92	2,36	1,50	0,80				
	16, 35	9,65	8,37	6,98	6,16	5,23							
	12						2,56						
5000	27-32			6,55	5,51	4,07	2,15						
	16, 35		9,66	7,68	6,40	5,58							

Table 2 (Continued)

ра, кг, м ² ·сек	Темпера- тура	ρ 137 бар									
		t°C					x				
		75	50	25	10	0	0,1	0,2	0,3	0,4	0,5
750	27-32			2,24	2,64	2,50	2,15	1,71	1,45	1,05	0,69
	16, 35					2,33	1,69	1,40			
	12			3,32	2,67	2,56					
	22					1,87					
	21										
	(табл. 8)							2,04	1,51		
	21										
	(табл. 12)			3,65	3,27	2,99	2,52	2,05	1,42		
	14, 26	4,05	3,61	3,14	2,79	2,56	2,21	1,63	1,47	1,16	
1000	27-32	4,59	4,62	3,50	2,79	2,55	2,11	1,63	1,09	0,87	
	16, 35					2,32	1,60	1,19			
	12	4,36	3,84	3,14	2,79	2,67					
	21										
	(табл. 8)						2,26	1,77	1,27		
	22					2,14					
	23			3,62	3,13	2,78	2,22	1,51			
	14, 26	4,42	4,01	3,43	3,02	2,73	2,32	2,03	1,51		
1500	27-32	5,37	4,89	3,86	3,02	2,58	1,93	1,23	0,87		
	16, 35					2,32	1,51	1,01			
	12	5,00	4,42	3,43	3,26	2,91					
	10, 11							1,90	1,05		
	15			3,28	2,56	1,77					
	22					2,43					
	50					2,40	1,87	1,34			
	21										
	(табл. 8)						2,16				
	21										
	(табл. 12)			2,98	2,78	2,70					
	23		4,63	3,84	3,19	2,71	2,09				
	14, 26	5,29	4,65	3,98	3,49	3,12	2,67	1,96	1,63		
2000	27-32	6,19	5,02	4,30	3,42	2,63	1,90	1,26	0,77		
	16, 35					2,32	1,49	1,01			
	12	5,70	5,06	3,84	3,72	3,14					
	10, 11							1,19			
	15			3,64	2,84	1,98					
	21										
	(табл. 12)						2,04				
	22					2,66					
	23			4,37	3,58	2,98	2,05				
	14, 26	6,09	5,23	4,42	3,82	3,26	2,62				

Table 2 (Continued)

ρ_w , кг.м ³ .сек	Литера- тура	$p = 137 \text{ бар}$									
		$\theta^\circ\text{C}$					x				
		75	50	25	10	0	0,1	0,2	0,3	0,4	0,5
2500	27—32		5,70	4,70	3,86	2,73	1,90	1,19			
	16, 35					2,32	1,49				
	12	6,40	5,76	4,30	4,13	3,37		1,50			
	10, 11										
	15			3,85	3,13	2,40					
	22					2,85					
	21										
	(табл. 8)						2,09				
	23			5,07	4,09	3,24	1,67				
14, 26	6,86	5,81	4,65	3,88	3,12	2,32					
3000	27—32		6,13	5,13	4,22	2,97	1,97	1,14			
	16, 35					2,32	1,49				
	12	7,21	6,40	5,12	4,42	3,61					
	10, 11						1,70				
	15			4,37	3,43	2,47					
	22					3,06					
	14, 26	7,44	6,16	4,72	3,72	2,95	1,91				
4000	27—32		7,04	5,92	4,92	3,27	2,22	1,45			
	12	9,48	7,85	5,82	4,65	3,97					
	10, 11						1,22				
	15			5,11	4,01	2,92					
	22					3,35					
5000	27—32			6,71	5,44	3,63					
	13		9,01	6,63	4,65	4,42					
	15		6,92	5,77	4,58	3,42					
	22					3,52					
	21										
	(табл. 12)		6,61	5,23	4,13	3,26					

ρ_w , кг.м ³ .сек	Литера- тура	$p = 167 \text{ бар}$								
		$\theta^\circ\text{C}$					x			
		75	50	25	10	0	0,1	0,2	0,3	0,4
750	27—32		2,86	2,30	1,79	1,69	1,34	0,76		
	12		2,67	2,32	1,98	1,69				
	14, 26	3,02	2,79	2,44	2,30	2,09	1,92	1,74	1,58	1,40

Table 2 (Continued)

G, кг/м²·сек	Интера- тура	p -- 167 бар									
		t °C					x				
		75	50	25	10	0	0,1	0,2	0,3	0,4	
1000	27—32	3,49	3,33	2,52	1,95	1,76	1,41	0,90			
	12	3,66	2,91	2,73	2,27	1,80					
	14, 26	3,49	3,14	2,67	2,48	2,21	2,03	1,74	1,56	1,22	
1500	27—32	4,33	3,84	3,07	2,26	1,83	1,57	1,08			
	12	4,42	3,49	3,26	2,73	2,09					
	10, 11						1,78	1,23			
	14, 26	4,19	3,72	3,14	2,85	2,56	2,19	1,92	1,53	1,28	
2000	27—32	5,12	4,29	3,55	2,63	1,94	1,70	1,19			
	12	5,12	4,07	3,72	3,02	2,32					
	10, 11						1,69	1,34			
	14, 26	4,88	4,28	3,51	3,14	2,77	2,32	1,98	2,09		
2500	27—32		4,76	3,98	2,91	2,08	1,92	1,28			
	12	5,82	4,65	4,07	3,31	2,67					
	10, 11						1,98				
	14, 26	5,63	4,88	3,81	3,33	2,77	2,21				
3000	27—32		5,27	4,41	3,49	2,24	1,94	1,40			
	12	6,51	5,29	4,42	3,66	2,91					
	14, 26	6,63	5,49	4,07	3,33	2,56	1,74				
4000	27—32		6,09	5,08	4,19	2,73	2,49	1,66			
	12		6,75	5,12	4,30	3,49					
5000	27—32						2,62				
	12		8,26	5,99							

рш. кг/м²·сек	Линтера- тура	p = 196 бар						
		t °C					x	
		75	50	25	10	0	0,1	0,2
750	27-32		1,95	1,47	1,29	1,02		
	12		1,45	1,40	1,34	1,34		
	14, 26	2,09	1,92	1,72	1,57	1,43		
1000	27-32	2,32	2,28	1,73	1,41	1,05		
	12	2,21	1,80	1,51	1,45	1,40		
	14, 26	2,42	2,22	2,02	1,80	1,63		

Table 2 (Continued)

ρw, кг/м ³ ·сек	Литература	p = 196 бар						
		θ °C					x	
		75	50	25	10	0	0,1	0,2
1500	27-32	3,37	2,79	2,20	1,66	1,26	1,26	0,93
	12	2,56	2,27	1,86	1,69	1,57		
	14, 26	2,91	2,67	2,32	2,09	1,86		
2000	27-32	4,04	3,26	2,56	1,90	1,34	1,35	1,05
	12	2,91	2,50	2,09	1,86	1,74		
	14, 26	3,26	2,93	2,56	2,30	1,92		
2500	27-32	4,43	3,68	2,87	2,12	1,51	1,45	1,10
	12	3,26	2,85	2,44	2,15	1,86		
	14, 26	3,60	3,29	2,79	2,42	2,05		
3000	27-32	4,75	4,05	3,14	2,31	1,63	1,54	1,23
	12	3,60	3,14	2,67				
	14, 25	3,95	3,58	2,96	2,56	2,13		
4000	27-32		4,77	3,61	2,67	1,95	1,72	1,42

DESIGNATIONS: Литература = Literature; бар = bar.
 кг/м³·сек = kg/m³·s.

Table 3

ρw, кг/м ³ ·сек	p = 49 бар										
	θ °C					x					
	75	50	25	10	0	0,1	0,2	0,3	0,4	0,5	0,6
750	9,22	8,14	8,10	7,62	7,67						
1000	9,42	8,64	8,29	7,66	7,77						
1500	9,65	9,01	8,41	7,79	7,30						
2000	9,83	9,18	8,49	7,84	7,09		3,55			1,11	
2500	10,04	9,28	8,48	7,84	6,94		4,07			1,57	
3000	10,23	9,37	8,44	7,81	6,74		3,23			2,43	
4000	10,51	9,71	8,37	7,79	6,31				2,16		
5000		10,46	8,43	7,85	6,24						
	p = 69 бар										
	θ °C					x					
	75	50	25	10	0	0,1	0,2	0,3	0,4	0,5	0,6
750	8,26	7,55	7,18	6,91	6,61	5,11	4,51	3,66			2,77
1000	8,36	7,92	7,15	6,63	6,40	5,0	4,27	3,47	3,84	2,73	3,00
1500	8,65	8,05	7,67	6,53	5,92	4,40	3,93	3,02	2,70		
2000	8,35	8,22	6,94	6,34	5,62	4,01	3,5	2,48	2,07		
2500	8,96	8,30	7,01	6,42	5,73	4,09	3,94	2,23			
3000	8,98	8,17	7,05	6,37	5,23	3,41	2,79	2,07			
4000	9,65	8,65	6,90	5,82	4,95	3,23	2,67	1,57			
5000		9,57	7,79	6,69	5,09	3,06					

Table 3 (Continued)

ρ , кг·м ² ·сек	$p = 98 \text{ бар}$											
	$\theta, ^\circ\text{C}$					x						
	75	50	25	10	0	0,1	0,2	0,3	0,4	0,5	0,6	0,7
750	6,01	5,92	5,12	4,90	4,52	3,69	3,29	2,78	2,47	2,00	1,63	0,81
1000	6,51	5,95	5,60	4,88	4,49	3,69	3,02	2,41	2,00	1,35		
1500	7,33	5,54	5,53	5,02	4,45	3,35	2,59	1,85	1,29			
2000	7,68	6,52	5,69	5,08	4,58	3,21	2,70	1,80	1,03			
2500	8,12	6,95	5,55	5,18	4,29	2,69	1,93	1,22				
3000	8,58	7,53	6,07	5,63	4,28	2,50	1,63	1,03				
4000	9,51	8,72	6,63	5,70	4,58	2,47	1,50	0,80				
5000		9,65	7,12	5,95	4,82	2,15						

ρ , кг·м ² ·сек	$p = 137 \text{ бар}$										
	$\theta, ^\circ\text{C}$					x					
	75	50	25	10	0	0,1	0,2	0,3	0,4	0,5	
750	4,05	3,61	3,27	2,85	2,47	2,12	1,80	1,49	1,05	0,69	
1000	4,45	4,15	3,42	2,93	2,54	2,05	1,52	1,19	0,87		
1500	5,23	4,84	3,52	3,14	2,67	1,97	1,37	0,95			
2000	5,98	5,11	4,12	3,64	2,82	1,86	1,15				
2500	6,63	5,76	4,51	3,99	2,95	2,37	1,37				
3000	7,33	6,23	4,84	4,12	2,97	1,71	1,14				
4000	9,48	7,44	5,62	4,79	3,61	2,22	1,34				
5000		7,51	6,08	4,75	3,73						

$p = 167 \text{ бар}$											
750	3,02	2,78	2,36	2,02	1,69	1,24	0,76				
1000	3,55	3,13	2,64	2,24	1,78	1,41	0,90				
1500	4,29	3,66	3,14	2,62	2,14	1,67	1,16				
2000	5,03	4,21	3,59	2,93	2,28	1,79	1,26				
2500	5,72	4,73	3,95	3,12	2,51	1,94	1,28				
3000	6,57	5,35	4,30	3,49	2,57	1,94	1,39				
4000		6,42	5,09	4,24	3,12	2,49	1,66				
5000		6,26	5,59			2,52					

$p = 196 \text{ бар}$											
750	2,09	1,78	1,54	1,39	1,27						
1000	2,31	2,10	1,76	1,56	1,36						
1500	2,94	2,57	2,11	1,80	1,52	1,26	0,93				
2000	3,30	2,89	2,41	2,02	1,66	1,35	1,05				
2500	3,77	3,27	2,70	2,23	1,78	1,45	1,10				
3000	4,10	3,59	2,93	2,44	1,88	1,54	1,23				
4000		4,77	3,60	2,67	1,95	1,72	1,42				
5000											

Table 4.

pW, кг·м ² ·сек ⁻²	p = 49 бар									
	θ °C					x				
	75	50	25	10	0	0,1	0,2	0,3	0,4	0,5
750	9,11	8,51	7,94	7,65	7,60					
1000	9,39	8,80	8,24	7,82	7,55					
1500	9,61	8,98	8,34	7,82	7,40					
2000	9,79	9,27	8,37	7,80	7,23	5,34	3,83			
2500	10,00	9,39	8,39	7,64	7,06	5,11	3,60			
3000	10,20	9,50	8,39	7,45	6,94	4,76	3,35			
4000	10,70	9,69	8,39	7,16	6,60					
5000		10,05	8,39	6,95	6,30					

p = 69 бар

750	8,23	7,77	7,06	6,64	6,31	5,23	4,41	3,83	3,37	3,02
1000	8,34	7,91	7,05	6,59	6,20	4,94	4,23	3,68	3,11	2,73
1500	8,60	8,03	7,08	6,60	5,91	4,50	3,72	2,90	2,62	
2000	8,78	8,14	7,08	6,39	5,67	4,14	3,25	2,56	2,09	
2500	9,00	8,30	7,08	6,26	5,50	3,81	2,90	2,32		
3000	9,19	8,40	7,08	6,08	5,34	3,53	2,73	2,09		
4000	9,63	8,70	7,10	5,80	4,99	3,25	2,32	1,63		
5000		9,57	7,25	6,39	5,23					

p = 98 бар

750	6,31	5,69	4,94	4,65	4,41	3,84	3,31	2,84	2,46	2,00
1000	6,54	5,94	5,07	4,82	4,47	3,68	3,07	2,44	1,92	1,35
1500	7,06	6,40	5,35	4,93	4,53	3,56	2,73	1,85	1,29	
2000	7,60	6,55	5,57	4,99	4,56	3,06	2,21	1,51	1,03	
2500	8,10	6,94	5,84	5,05	4,30	2,84	1,93	1,28		
3000	8,55	7,43	6,18	5,10	4,30	2,70	1,63	1,11		
4000	9,52	8,44	6,64	5,56	4,57	2,32	1,51	0,80		
5000		9,63	7,08	5,94	4,83	2,15				

p = 137 бар

750	4,04	3,61	3,14	2,79	2,44	2,21	1,90	1,44	1,04	0,7
1000	4,45	3,86	3,36	2,92	2,51	2,03	1,65	1,23	0,87	
1500	5,21	4,46	3,76	3,13	2,67	1,96	1,39	0,95		
2000	5,98	5,05	4,13	3,44	2,84	2,04	1,28	0,54		
2500	6,74	5,69	4,51	3,67	3,00	2,09	1,21			
3000	7,50	6,27	4,87	3,94	3,18	2,11	1,21			
4000	9,40	7,42	5,69	4,45	3,49	2,21	1,28			
5000		7,50	6,15	5,11	3,73					

Table 4 (Continued)

q, кг/м ² ·сек	p = 167 бар					x				
	t, °C									
	75	50	35	10	0	0,1	0,2	0,3	0,4	0,5
750	3,20	2,77	2,34	2,02	1,69	1,33	0,76			
1000	3,54	3,13	2,56	2,15	1,80	1,41	0,90			
1500	4,25	3,72	3,02	2,52	2,03	1,67	1,00			
2000	5,02	4,27	3,45	2,82	2,29	1,79	1,13			
2500	5,71	4,83	3,84	3,07	2,48	1,94	1,25			
3000	6,45	5,45	4,29	3,48	2,74	2,03	1,39			
4000		6,50	5,08	4,25	3,25	2,36	1,67			
5000		7,85	5,90	4,87	3,76	2,61				

p = 195 бар

750	2,09	1,78	1,58	1,39	1,27					
1000	2,32	2,10	1,75	1,55	1,36	1,25	0,93			
1500	2,88	2,56	2,02	1,80	1,52	1,35	1,04			
2000	3,37	2,88	2,32	2,02	1,66	1,45	1,10			
2500	3,81	3,38	2,70	2,23	1,77	1,53	1,23			
3000	4,15	3,59	2,92	2,44	1,89	1,72	1,42			
4000		7,75	3,60	2,67	1,95					
5000										

DESIGNATION: $\text{кг/м}^2 \cdot \text{сек} = \text{kg/m}^2 \cdot \text{s}$; бар = bar.

BIBLIOGRAPHY

1. Дорошук В. Е. О кризисах теплообмена в испарительной трубе. «Теплофизика высоких температур», т. 4, 1966, № 4.
2. Дорошук В. Е., Фрид Ф. П. Исследование критических тепловых нагрузок. Сб.: «Теплообмен при высоких тепловых нагрузках и других специальных условиях», под ред. А. А. Арманта. Госэнергоиздат, 1959.
3. Субботин В. И. [и др.]. Критические тепловые нагрузки при вынужденной конвекции недогретой до кипения воды в трубах при давлении 140—220 ата. В сб.: «Исследование теплоотдачи и пару и воде, кипящей в трубах при высоком давлении», под ред. Н. А. Доллежале. Атомиздат, 1958.
4. De Bartolli R. A. et al. Forced-convection heat transfer burnout studies for water in rectangular channels and round at pressures above 500 psia. WAFD-188, 1958.
5. Дорошук В. Е., Фрид Ф. П. К вопросу о влиянии дросселирования потока и обогреваемой длины трубки на критические тепловые нагрузки. «Теплоэнергетика», 1959, № 9.
6. Стырикович М. А., Миропольский З. Л., Шницман М. Е. Влияние предвключенных элементов на возникновение кризиса кипения в парогенерирующих трубах. «Теплоэнергетика», 1960, № 5.
7. Дорошук В. Е., Мальтер В. Л. Пульсации потока при больших тепловых нагрузках. «Энергомашиностроение», 1963, № 12.
8. Рыбин Р. А. Исследование влияния диаметра трубы на величину критической тепловой нагрузки при кипении воды. ИФМ, 1963, № 2.
9. Дорошук В. Е., Шницман Ф. П. Влияние диаметра канала на критические тепловые нагрузки. «Теплоэнергетика», 1963, № 8.
10. Смирнов З. Н., Поляков В. Е., Есиков В. И. Экспериментальное исследование кризиса теплоотдачи. «Атомная энергия», май, 1964.

11. Смотин В. Н. [и др.]. О кризисе теплоотдачи в интенсифицирующей трубе. «Атомная энергия», октябрь, 1962.
12. Алабян Н. Т., Долонов Л. Д., Улагов В. С. Критические тепловые нагрузки при течении воды в трубах. «Атомная энергия», 1959, т. 6, вып. 1.
13. Becker K. M. [и др.]. Burnout data for flow of boiling water in vertical round ducts. Annuli and Rod clusters. AS-177, 1965, pp. 1-107.
14. Doroshchuk V. E. and Lantsman F. P. Effect of pressure and mass flow rate on burnout heat fluxes in a water and steam-water mixture flow in tubes. «International Journal of Heat and Mass Transfer», v. 7, № 2, 1964, pp. 187-190.
15. Buchberg H. [и др.]. Heat transfer, pressure drop and burnout studies with and without surface boiling for deaerated and gassed water at elevated pressures in a forced flow system. В сб.: «Heat transfer and Fluid Mechanics Institute». Stanford University. Press, 1961.
16. Алферов Н. С., Рыбин Р. А. Критические тепловые потоки при течении воды и пароводяной смеси в трубах. В сб.: «Конвективная теплопередача в двухфазном и однофазном потоках», под ред. В. М. Борншанского и И. И. Палеева. Изд-во «Энергия», 1964.
17. Lee D. H., Obertelli I. D. An experimental investigation of forced convection burnout in high pressure water. Part II. Preliminary results for round tubes with non-uniform axial heat flux distribution. Winfrith, AEEW-R-309, 1963.
18. Macsner B. Basic experimental studies of boiling fluid flow and heat transfer at elevated pressure. JJD., 18978. (USA), 1963.
19. Hood R. R., Isakoff L. Heavy water moderated power reactors progress report. D. P. 755, June, 1962.
20. Lee D. H., Morris D. I. Burnout and two-phase pressure drop for water at 1000 psia in round tubes with uniform and nonuniform heat flux distribution. Winfrith, AEEW-R-355, 1964.
21. De Bartoli R. A. [и др.]. Forced-convection heat transfer burnout studies for water in rectangular channels and round at pressures above 500 psia. WARD-188, 1958.
22. Jacket H. S., Rourty I. D., Lerbe I. E. An investigation of burnout heat flux in rectangular channels at 2000 psia. Trans. ASME, № 3, 1958.
23. Weatherhead R. I. Heat transfer flow instability and critical heat flux for water in a small tube at 2000 psia ANL 6718, 1963.
24. Миропольский З. Л. [и др.]. Влияние входных условий на критические тепловые потоки при кипении воды в трубах. «Теплоэнергетика», 1959, № 1.
25. Lee D. H. An experimental investigation of forced convection burnout in high pressure water. Part III. Long tubes with uniform and nonuniform axial heating. Winfrith, AEEW-R-355, 1955.
26. Дорошук В. Е. Кризис теплообмена в трубах. Докторская диссертация. ЦКТИ, 1966.
27. Зенкевич Б. А. Критические тепловые нагрузки при вынужденном движении в трубах воды с ядром, не догретым до температуры насыщения, в интервале давлений 100-200 атм. Кандидатская диссертация. ФТИ, 1957.
28. Зенкевич Б. А., Песков О. Л., Субботин В. И. Изучение критических тепловых потоков для трубчатых теплообменных элементов атомных электростанций. «Теплоэнергетика», 1964, № 6.
29. Песков О. Л. [и др.]. Критические тепловые потоки при вынужденном движении пароводяной смеси в трубе. В сб.: «Вопросы теплоотдачи и гидравлики двухфазных сред». Под ред. С. С. Кутателадзе. Госэнергоиздат, 1961.
30. Субботин В. И., Зенкевич Б. А., Песков О. Л. Критические тепловые потоки при вынужденном движении пароводяной смеси в трубах. В сб.: «Конвективная теплопередача в двухфазном и однофазном потоках», под ред. В. М. Борншанского, И. К. Палеева. Изд-во «Энергия», 1964.
31. Алексеев Г. В. [и др.]. Критические тепловые потоки при вынужденном течении воды. «Теплоэнергетика», 1965, № 3.
32. Зенкевич Б. А. К вопросу о законе подобия для критической тепловой нагрузки при вынужденном движении жидкости. «Атомная энергия», № 4, вып. 1, 1958.
33. Epstein H. M., Chastein I. W., Fawcett S. Heat transfer and burnout to water at high subcritical pressures. BM-T-1116, 1958.
34. Bertolotti S. [и др.]. Heat transfer crisis with steam-water mixtures. «Energia Nucleare», v. 12, № 3, 1965.
35. Рыбин Р. А. Исследование критических тепловых потоков при течении пароводяной смеси в обтекании трубок. Кандидатская диссертация ЦКТИ, 1963.
36. Миропольский З. Л. Изучение температурных условий работы парогенерирующей поверхности. Докторская диссертация. МЭИ, 1963.
37. Миропольский З. Л., Шницман М. Е. Допустимые тепловые потоки и теплоотдача при кипении воды в трубах. В сб.: «Исследование теплоотдачи к пару

38. Маронюк С. И., В. И. Сухомов. «Теплоэнергетика», 1959, № 1.
39. Hewitt G. F. [и др.] Burnout and film flow in the evaporation of water in tubes. Harwell, AEE-R 1964, 1965.
40. Стирников М. А., Факторович Л. Е. Влияние длины трубы на величину критических тепловых потоков при вынужденном движении пароводяной смеси. «Трубы АН СССР», т. 120, № 5, 1958.
41. Факторович Л. Е. Исследование влияния длины обогреваемой трубы на величину критических тепловых потоков при вынужденном движении пароводяной смеси. Кандидатская диссертация. ЭНИИ, 1961.
42. Поварнин П. И., Семенов С. Т. Исследования кризиса кипения воды, не догретой до температуры насыщения, при движении ее с большой скоростью в трубах. «Теплоэнергетика», 1959, № 4.
43. Поварнин П. И., Семенов С. Т. Исследования кризиса кипения при течении недогретой воды в трубах малых диаметров при высоких давлениях. «Теплоэнергетика», 1960, № 1.
44. Орнатский А. П., Кичигин А. М. Исследование зависимости критической тепловой нагрузки от весовой скорости, недогрева и давления. «Теплоэнергетика», 1961, № 2.
45. Орнатский А. П., Кичигин А. М. Критические тепловые нагрузки при кипении недогретой воды в трубах малого диаметра в области высоких давлений. «Теплоэнергетика», 1963, № 3.
46. Орнатский А. П. Критические тепловые нагрузки и теплоотдача при вынужденном движении воды в трубах в области сверхвысоких давлений. «Теплоэнергетика», № 6, 1960.
47. Орнатский А. П. Влияние длины и диаметра трубы на величину критического теплового потока при вынужденном движении воды, не догретой до температуры насыщения. «Теплоэнергетика», 1960, № 6.
48. De Bertolli R. A., Masnovi R. Effect of dissolved hydrogen on Burnout for water flowing vertically upward in round tubes at 2000 psia. WAPD-TH-318, 1957.
49. CISE-таблица, отчет RDI (CAW-1), January, 1963, R-73.
50. WAPD-TH-308.
51. Thompson B., Macbeth R. V. Boiling water heat transfer burnout in uniformly heated round tubes. A complication of world data with accurate correlations. Winfrith. AEEW-R-356, 1964.
52. Hunt. An Investigation of the subcooled and quality burnout in circular channels. WAPD, SRM-1, 1955.
53. Becker K. M., Person P. An analysis of burnout conditions for flow of boiling water in vertical round ducts. «Trans. ASME Ser.», № 4, 1964.
54. Levy S. [и др.] Eccentric rod burnout at 1000 lb/in² with hot steam generation. «Int. J. of Heat and Mass Transf.», v. 5, July, 1962.

A MODEL OF THE BOILING CRISIS
DURING FORCED MOTION OF A
TWO-PHASE FLOW IN PIPES WITH
HIGH OUTPUT VAPOR CONTENTS

L. S. Kokorev, V. I. Petrovichev,
and A. N. Borzyak

Experimental research in many laboratories [1-5] has shown that with an increase in vapor content critical thermal fluxes decrease, while the effect of mass velocity and pressure is expressed weakly with low mass velocities w_0 (up to $500 \text{ kg/m}^2 \cdot \text{s}$). Models of the heat transfer crisis at high x [6, 7] are rather contradictory. Generalizing equations based on these models do not make it possible to describe the heat transfer crisis during boiling in pipes in a wide range of variation for the regime characteristics. At the present time there is a limited quantity of experimental data on the heat removal crisis with high vapor contents in the region of low pressures and low mass velocities and calculated relationships for critical thermal fluxes in pipes are not available.

In developing power installations for space equipment one of the main problems is the heat transfer and condensation in variable gravitational fields and under conditions of weightlessness. The mechanism of the gravitational field effect on the heat transfer crisis of a two-phase flow in pipes has been

studied very little. Therefore, the creation of a model of the heat transfer crisis during forced motion of two-phase fluxes in pipes with high vapor contents is of great interest.

A CALCULATION MODEL FOR THE HEAT TRANSFER CRISIS DURING FORCED MOTION IN CHANNELS OF A TWO-PHASE FLOW WITH HIGH VAPOR CONTENTS

The basic regime for a two-phase flow in channels with rather high per-volume vapor contents is an annular regime. In this case, the liquid flows along the walls of the channel in the form of a thin film, and in the core of the flow steam moves with a certain amount of moisture in the form of fine droplets. We can assume that critical thermal flows are determined mainly by the properties of the flow of the liquid film. In the case of film disruption and the appearance of dry spots on any section of the heat-releasing surface, heat exchange in this section is sharply impaired and overheating of the wall can exceed the permissible value during sufficiently high thermal fluxes.

Let us examine first the state of a thin film of liquid on an unlimited horizontal surface (Fig. 1a). Let small harmonic disturbances with wavelengths λ be imposed on the film (amplitude of disturbances A is small as compared with wavelengths λ). The propagation rate of these disturbances can be found from the equation for capillary and gravitational waves in an ideal liquid [9]:

$$a^2 = \frac{\sigma \beta}{\rho'} + g \left(1 - \frac{\rho''}{\rho'}\right) \delta. \quad (1)$$

Here a is the propagation rate of surface waves and a liquid film; $\beta = \frac{2\pi}{\lambda}$ is the wave number; δ is the average liquid film thickness; σ is surface tension; ρ' is liquid density; ρ'' is steam (or gas) density over the film; g is the gravitational acceleration along the normal to the film. The first and second

terms in equation (1) are the squares of the velocities of the capillary and gravitational waves, respectively, in the thin liquid film. The film is assumed thin if the following condition is fulfilled:

$$\frac{b}{\lambda} \ll 1.$$

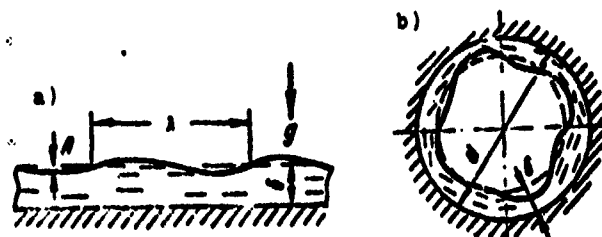


Fig. 1. Liquid film:
a - On a flat surface; b - In a circular pipe.

The liquid flow rate in the film can not exceed the propagation rate of the surface wave:

$$u_i \leq a. \quad (2)$$

Let us examine here the state of the annular liquid film in a circular pipe (Fig. 1b). Let wave disturbances, parallel to the axis of the pipe, be applied to the film. In this case, standing waves exist, with which the integral of wavelengths must be confined to the length of the pipe perimeter.

$$\lambda n = \pi d. \quad (3)$$

On the surface of the pipe a uniformly distributed thermal flux q_F is given. The rate of decrease in wall thickness due to evaporation is

$$u_e = \frac{q_F}{\rho}, \quad (4)$$

where r is the heat of vaporization. The condition for the onset of the heat exchange crisis can be formulated in the following manner: if the rate of decrease in film thickness from evaporation u_q on any section of the surface exceeds the rate of liquid boundary displacement, caused by the effect of capillary and surface waves u_δ , then local drying of the surface is possible on the given section of the surface and, consequently, the onset of the heat exchange crisis. Mathematically, this condition can be expressed in the form:

$$u_q \sim u_\delta \sim a. \quad (5)$$

Using equations (1), (2), and (4), from equation (5) we obtain

$$\frac{q_{vp}}{r\delta} \sim \sqrt{\frac{4\sigma}{\rho} + g\left(1 - \frac{\rho^*}{\rho}\right)\delta}. \quad (6)$$

Hence it follows that the liquid film is most unstable to long-wave disturbances (minimum values of β). From equation (3) the greatest wavelength corresponds to $n = 1$,

$$\lambda = \pi d, \quad \beta = \frac{2}{d}. \quad (7)$$

Then equation (6) is transformed to:

$$\frac{q_{vp}}{r\delta} \sim \sqrt{\frac{4\sigma}{\rho d^2} + g\left(1 - \frac{\rho^*}{\rho}\right)\delta} \sim \left(\frac{1}{d}\right)^{1/2} \sqrt{\frac{4\sigma}{\rho} + g\left(1 - \frac{\rho^*}{\rho}\right)d}. \quad (8)$$

For the annular flow regime relative film thickness can be connected with true vapor content per unit volume

$$\bar{\tau} = \frac{\pi(R-\delta)^2}{\pi R^2}; \quad (9)$$

hence

$$\frac{\delta}{R} = 1 - \sqrt{\bar{\tau}} \approx \frac{1-\bar{\tau}}{2} \text{ for } 1-\bar{\tau} \ll 1.$$

Here $R = \frac{d}{2}$ is the inner radius of the pipe. True vapor content per unit volume ϕ is a function of pressure, vapor content per unit weight, and phase slippage:

$$\bar{\tau} = \frac{1}{1 + \frac{1-x}{x} \cdot \frac{\rho^*}{\rho} \cdot \frac{u^*}{u}} \approx 1 - \frac{1-x}{x} \cdot \frac{\rho^*}{\rho} x. \quad (10)$$

where $\kappa = u''/u'$ is the ratio of vapor and liquid phase velocities. Substituting equations (9) and (10) into (8), we obtain

$$\begin{aligned} \frac{q_{cr}}{r_p} &= K_1 \frac{1}{1-\frac{1}{\kappa}} \sqrt{\frac{4\sigma}{r_p d} - g \left(1 - \frac{1}{\kappa}\right) d} = \\ &= K_1 \frac{1}{\frac{1-x}{x} \cdot \frac{r_p'}{r_p}} \sqrt{\frac{4\sigma}{r_p d} + g \left(1 - \frac{r_p'}{r_p}\right) d}, \end{aligned} \quad (11)$$

where K is the coefficient of proportionality. In a vertical channel in the absence of a gravitational field directed toward the channel walls, the gravitational term in equation (11) can be disregarded as compared with the capillary term. The equation for critical thermal flux assumes the form:

$$q_{cr} = K_1 r_p' \left(\frac{1-x}{x} \cdot \frac{r_p'}{r_p} \right)^{1/2} \sqrt{\frac{4\sigma}{r_p d}}, \quad (12)$$

where the coefficient of proportionality K_1 includes the slippage factor κ .

Figure 2 illustrates the experimental results for critical thermal fluxes during the rectilinear motion of water in a vertical pipe 8 mm in diameter [1]. Tests were made at pressure $p = 1.75$ atm (abs.), mass velocity w_0 variation from 20 to 500 kg/cm²·s, and relative pipe length l/d from 25 to 150. Most of the experimental results are well described by the unique function of vapor content per unit weight x and do not depend upon mass velocity w_0 and relative length l/d in the studied region. The dependence of q_{cr} on x when $x = 0.6-1.0$ is described satisfactorily by

$$q_{cr} \sim \sqrt{\frac{1-x}{x}}.$$

Consequently, the coefficient K_1 in equation (12), in the first approximation, is a constant value. From comparison with tests in [1], $K_1 = 0.275$ is obtained. Thus, equation (12) can be written in the form:

$$q_{cr} = 0.275 r_p' \sqrt{\frac{1-x}{x}} \sqrt{\frac{1}{r_p d}}. \quad (13)$$

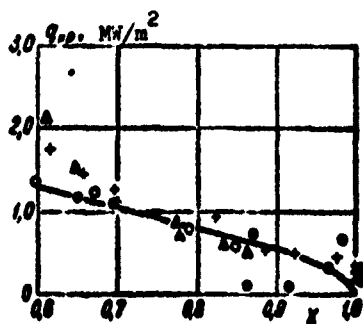


Fig. 2. Critical thermal flux during the rectilinear motion of water in a circular pipe $d = 8$ mm:

$$\left. \begin{array}{l} \circ - l/d = 25; \\ \Delta - l/d = 50; \\ + - l/d = 100; \\ \bullet - l/d = 150; \end{array} \right\} [1] \quad \begin{array}{l} w_Y = 20-500 \\ \text{kgf/m}^2 \cdot \text{s}; \\ p = 1.75 \text{ atm} \\ (\text{abs.}); \text{H}_2\text{O}. \end{array}$$

The dependence of q_{kp} on pipe diameter $q_{kp} \sim 1/\sqrt{d}$ is confirmed by the majority of the experimental works available [3, 4, 10, 11].

THE HEAT TRANSFER CRISIS IN THE TWISTED FLOW OF A HEAT CARRIER WITH LARGE VAPOR CONTENTS

In the twisted flow of a heat carrier, an artificial gravitational field directed along the normal to the pipe wall is created.

With a sufficiently high acceleration of the force of gravity in a twisted flow, we can disregard the capillary term in equation (11) as compared with the gravitational term. Then the equation for critical thermal fluxes in a gravitational field is written in the form:

$$q_{kp} = K_{sp} \left(\frac{1-x}{x} \cdot \frac{p'}{p} \right)^{1/2} \sqrt{gd \left(1 - \frac{p'}{p} \right)}. \quad (14)$$

here g is the gravitational acceleration along the normal to the pipe wall:

$$g = \frac{2w_\phi^2}{d}. \quad (15)$$

where w_ϕ is the rotational component of velocity during the forward motion of the flow.

If we use strips which are twisted lengthwise with step S_n (the distance in which the strip turns 360°) for twisting the flow, expression (15) can be written:

$$g = \frac{2w_z^2 \lg^2 \alpha}{d}, \quad (16)$$

where w_z is the longitudinal component of velocity, and $\lg \alpha = \frac{\pi d}{S_k}$.
In the case of a twisted flow with a large vapor content, we have

$$g = \frac{2x^2 \lg^2 \alpha}{d} = \frac{2}{d} \left(\frac{w_z}{r} \lg \alpha \right)^2. \quad (17)$$

Substituting (17) into (14), we obtain

$$q_{cr} = K_2' r \left(\frac{r}{w_z} \right)^{1/2} w_z x \sqrt{\frac{1-x}{x}} \lg \alpha. \quad (18)$$

Figure 3 presents the experimental results for critical thermal fluxes during the twisted motion of water in a pipe $\varnothing 8$ mm, $S_k/d = 4$; $p = 1.75$ atm (abs.) [1]. As seen from Fig. 3, the experimental results confirm the calculated dependence; the constant K_2' in equation (18), according to tests in [1], is $4.6 \cdot 10^{-4}$.

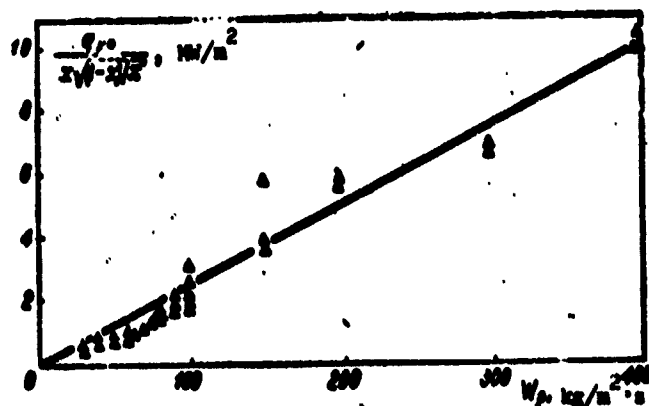


Fig. 3. Critical thermal flux versus mass velocity in twisted flow when $S_k/d = 4$; $p = 1.75$ atm (abs.).

On the basis of a comparison between the calculated dependence and experimental data [1], we can conclude that in the region $w_p > 100$ kg/m².s twisted flow is more effective than rectilinear. If for rectilinear flow the growth in vapor productivity were limited by comparatively low critical flows, then higher vapor

productivity could be obtained in the twisted flow by increasing the thermal flux and, accordingly, mass velocity.

Conclusions

1. A physical model of the crisis at large vapor contents per volume has been created, on the basis of which a generalized theory for the heat transfer crisis during the forced motion of two-phase flows has been developed.

2. The dependence of critical thermal fluxes on the value of the artificial gravitational field in twisted flow in pipes has been obtained.

3. Experimental studies are being performed at the present time to more precisely define the calculated relationships for the heat exchange crisis in two-phase twisted flows.

BIBLIOGRAPHY

1. Селостянов Р. И., Захаров Ю. К., Алазьев И. Т. Влияние типа трубы, поверхности теплообмена и параметров типа «шленк» на критические тепловые потоки в трубах. Сб.: «Теплообмен в элементах энергетических установок», М., 1966.
2. Becker K. Measurements of burnout conditions for flow of boiling water in vertical round ducts. AE-87, AE-114.
3. Becker K. Theoretical and experimental investigation of burnout conditions in vertical round ducts. AE-177, AE-178.
4. Lee D., Obert: III. An experimental investigation of forced convection burnout in high pressure water. AEEW-R-313.
5. Thompson B., Machoth R. Boiling water heat transfer burnout in uniformly heated round tubes. AEEW-R-366.
6. Исбин Г. Физическая модель кризиса в двухфазном пароводяном течении. «Теплопередача», с. С. т. 63, № 2, 1961.
7. Гольдман Н. Явления кризиса в турбулентном потоке. Модель диффузии капель. «Теплопередача», с. С. т. 63, № 2, 1961.
8. Тиняетс Ф. Исследование условий достижения критических потоков при течении кипящей воды под давлением. «Теплопередача», с. С. т. 64, № 1, 1964.
9. Ландау Л. и Лифшиц Г. Механика сплошных сред. М., 1964.
10. Дорожук В. Е., Ланман Ф. П. Критические тепловые нагрузки при течении воды и пароводяной смеси в трубах. Сб.: «Конвективная теплопередача в двухфазных и однофазных потоках». М., 1964.
11. Субботин В. И., Зенкевич В. А., Песков О. Л. Критические тепловые потоки при вынужденном движении пароводяной смеси в трубах. Сб.: «Конвективная теплопередача в двухфазных и однофазных потоках». М., 1964.

AN EXPERIMENTAL STUDY OF CRITICAL LOADS IN STEAM-GENERATING CHANNELS IN THE VICINITY OF BENDS

O. K. Smirnov and V. S. Polonskiy

Abbreviations

rp = load
s = upper
H = lower

In evaluating the operational reliability of steam-generating pipes in the precrisis region, it becomes particularly important to take into account the effect of local phenomena which impair heat exchange. The solution of this problem has been the task of a number of experimental works on the temperature regime of coiled heating surfaces, widely used in contemporary steam generators.

Chief attention has been given to the study of conditions under which the boiling crisis arises in bent elements. Unlike these works, the boundary of developed boiling in the straight sections of pipe adjoining the bend was studied on a MEI [Moscow Power Engineering Institute] stand. The first test results with a mass velocity for the flow of $1100 \text{ kg/m}^2 \cdot \text{s}$ indicated a noticeable reduction in critical thermal loads on the section before the

bend [1]. Then additional tests were made on $w_y = 700 \text{ kg/m}^2 \cdot \text{s}$, the results of which will be discussed in this article.

The experimental stand is a single-loop direct-flow steam generator [2]. All of the steam-water channel is made of 1Kh18N9T stainless pipes. The heated part of the steam generator is divided into three sections: an economizer, an evaporative section, and an experimental section, with independent heating of each of them. Heating is accomplished by sending directly through the pipes low voltage industrial-frequency current. Current-conducting contacts were sliding contacts, because of which it was easy to change the lengths of the working section on the experimental coil. The use of a flexible cable for the feed made it possible for the experimental pipe to freely expand.

As the experimental section we used a three-path loop of pipe $\varnothing 10 \times 2 \text{ mm}$, made from 1Kh18N9T steel. The loop was arranged in the vertical plane. Both bends had relative radius $R/d = 4$. The bends were made by cold bending; therefore, the wall thickness on the internal and external generatrices of the bend was different. Due to this, with the chosen method of heating, the thermal load along the cross section of the bend was nonuniform. Based on evaluation, the thermal flux on the internal generatrix (compressed) can exceed that on the external generatrix (extended) by a factor of 1.5-2.0. However, we can expect that at a relative distance from the bend of $l/d = 15$ and more, where the measurements were made, the nonuniformity of heating is not apparent.

The working part was a pipe with length $l = 600 \text{ mm}$ and a bend at the end. By alternation of the current-carrying contacts the position of the working section on the experimental coil was changed. We could study the effect of the bend on the adjacent straight sections with different directions of motion for the medium in them. In tests with an upper location for the bend, in the previous section there was a rising motion, while in the

section following the bend there was a descending motion. With a lower location for the bend, the direction of motion in the straight sections changes to the reverse.

At input to the economizer section, a regenerative preheater, using the heat of the steam-water mixture used in the stand, is installed. The regenerator was connected in the test with low thermal loads on the experimental section at high mass velocities for the flow.

The water supply was fed by five ND-60 plunger pumps. To the pressurized collector of the pumps a damper is connected with a useful volume of 8 l, 3/4 filled with nitrogen. At economizer input a throttle valve is installed. The flow rate of the water supply through the stand was regulated by a partial bypass of the heated channel. The flow rate of the heat carrier was checked by resistance readings on the measuring disk installed behind the economizer section. Pressure drop was measured with a DM-6 gauge in a set with an EPID-08. In addition, the flow rate was systematically checked by the volume method. The pressure of the medium in the experimental section was maintained at a given level by a valve at the output of the stand.

Temperature was measured with a chromel-alumel thermocouple 0.5 mm in diameter. The hot junctions of the thermocouples were welded to the external surface of the pipe with a step of 25-50 mm; thermoelectrode wires were branched along the isothermal surface. The temperature of the working medium was measured by a thermocouple introduced into the flow without sleeves through a teflon seal. For measuring and recording the emf of the thermocouples, we used PP potentiometers and EPP-09 electronic potentiometers; the latter were equipped with a special filter for reducing induction.

The pressure at various points of the channel was checked with sample manometers, class 0.35 with a scale at 250 atm (tech.).

The electrical load was measured with voltmeters and ammeters, class 0.35 and 0.5. The thermal load and the boundary vapor content were calculated with allowance for thermal losses to the ambient medium. Thermal content at output from the economizer section was checked with a manometer and a thermocouple which was specially calibrated after installation.

Tests were made in the following manner. The experimental section was brought to a given energy level with fixed values for pressure, mass velocity, and thermal load. Then enthalpy at input to the working section was increased in small stages (because of the increase in heat supply on the previous section) during the continuous check of working section wall temperature. A transition to film regime was determined according to the elevation in wall temperature.

The experimental data were obtained at pressure $p = 140$ atm (abs.) in the following range of parameters: mass velocity $w_y = 700-1100$ kg/m²·s, thermal flux $q = 120-600 \cdot 10^3$ kcal/m²·h, boundary vapor content 0.15-0.9, relative distance from bend $l/d = 15-95$.

Tests were made on experimental sections with upper and lower locations of bend.

Figure 1 illustrates the dependence of the boundary vapor content on thermal flux at different distances from the lower bend during mass velocity $w_y = 700$ kg/m²·s.

Relationships $x_{rp} = x(q)$ for the section in front of the bend are located below the relationships corresponding to the section behind the bend. Experimental data at large relative distances from the bend (see Fig. 1, 5) are described by the same relationship regardless of the position of the working section with respect to the bend. The indicated line divides test results obtained in sections before the bend and behind it and satisfactorily describes the experimental material obtained on straight pipes [2-4].

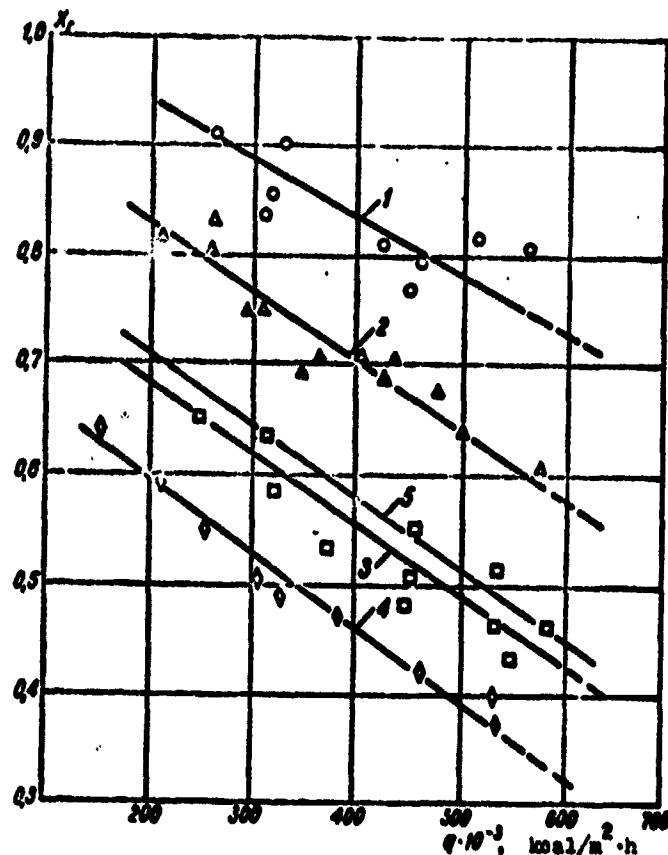


Fig. 1. Boundary vapor content versus thermal flux in tests with mass velocity $w_y = 700 \text{ kg/m}^2 \cdot \text{s}$. Relative distances l/d from bend: 1 - 15; 2 - 45 (behind bend); 3 - 45; 4 - 15 (in front of bend); 5 - 90 (straight pipe).

The effect of the relative distance from the bend on the deviation of critical thermal load is shown in Fig. 2. The value of the deviation in thermal flux with arbitrary l/d from critical thermal flux with $l/d = 90$ is greater the lower the level of boundary vapor content.

The effect of a bend, observed in the test, on conditions for the occurrence of boiling crisis in the adjacent parts can

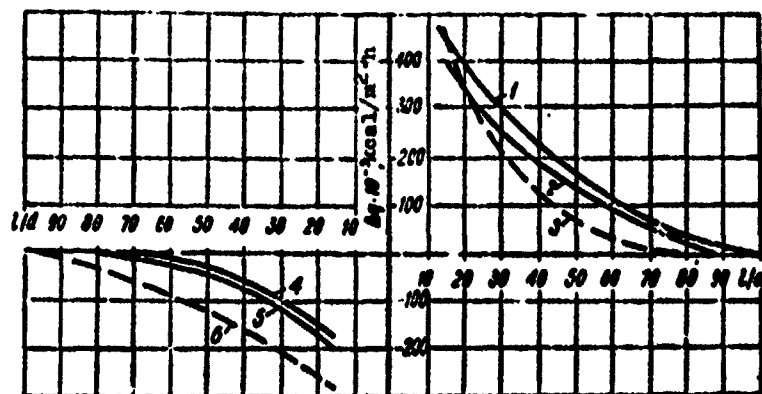


Fig. 2. Increase in thermal flux versus relative distance from lower bend:

when $w_\gamma = 700 \text{ kg/m}^2 \cdot \text{s}$: 1 - $x_{rp} = 0.7$;
 2 - $x_{rp} = 0.85$; 4 - $x_{rp} = 0.6$; 5 - $x_{rp} = 0.4$;
 when $w_\gamma = 11 \text{ kg/m}^2 \cdot \text{s}$: 3 - $x_{rp} = 0.6$;
 6 - $x_{rp} = 0.5$.

obviously be explained in the following manner. With respect to the previous section, the bend acts as additional resistance, retarding the motion of the steam. The portion of the section occupied by steam increases. This reduces the amount of liquid in the film and hampers mass exchange between the core of the flow and the boundary layer, which finally reduces the value of critical thermal load. In the section behind the bend the motion of the steam is accelerated, which is accompanied by a decrease in the portion of the section occupied by the steam and an increase in the thickness of the boundary layer. The cross circulation currents which occur in the bend continue to exist for a certain distance from the bend, intensifying mass exchange between the core of the flow and the liquid film. This leads to the fact that the value of the critical thermal flux increases. Consequently, in design calculations of coil steam-generating heating surfaces it is necessary to introduce a correction factor which takes into account the reduction in critical thermal flux in the section in front of the bend. The principal experiments were made with a lower

location for the bend; a smaller number of tests were made with an upper location for the bend. The change in bend position is accompanied, as mentioned above, by a change in the direction of medium motion in the adjacent section.

Thus, a comparison of the results of these two series of tests enables us to judge the effect of a bend on the condition for the occurrence of boiling crisis with different directions of motion for the heat carrier.

Only one bend design, with a comparatively small relative radius, was studied in the tests. Under such conditions, we can expect that disturbances induced by the bend differ little in the upper and lower positions. Actually, centrifugal forces exceed the force of gravity many times and, obviously, generally determine the character of the bend effect on adjacent sections.

Figure 3 presents a comparison of boundary vapor contents obtained with upper and lower bend positions. The comparison is made in cross sections with the same relative distance from the bend at two mass velocities for the flow $w_Y = 700$ and $1100 \text{ kg/m}^2 \cdot \text{s}$. As is apparent from the figure, deviations in boundary vapor content from the bisector do not have a systematic character and do not exceed $\pm 15\%$ (except for three points).

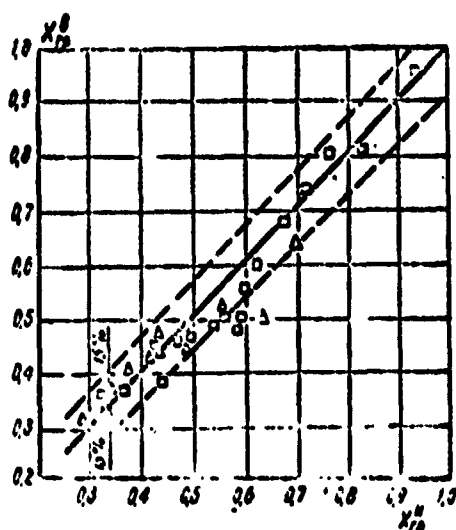


Fig. 3. Comparison of experimental data in tests with upper and lower locations of bend:

$\Delta - w_Y = 110 \text{ kg/m}^2 \cdot \text{s};$
 $\square - w_Y = 700 \text{ kg/m}^2 \cdot \text{s}.$

Thus we can assume that the effect of a bend does not depend upon the direction of heat carrier motion in the adjacent straight sections of a heat-generating pipe.

BIBLIOGRAPHY

1. Серов Е. П., Смирнов О. И., Положский В. С. Экспериментальное исследование температурного режима парогенерирующих труб с гребнем. «Теплоэнергетика», 1966, № 12.
2. Стырковский М. А. (и др.) Некоторые характеристики тепло- и массообмена в парогенерирующих трубах. «Известия Академии наук СССР Энергетика и транспорт», 1964, № 5.
3. Смолин В. Н., Поляков В. К., Есиков В. И. О кризисе теплоотдачи в парогенерирующей трубе. «Атомная энергия», т. 13, вып. 4, 1962.
4. Коньков А. С. Эспериментальное изучение условий ухудшения теплоотдачи при течи пароводяной смеси в обогреваемых трубах. «Труды ЦКТИ», вып. 58, 1966.

THE MECHANISM OF AMALGAM BOILING

I. Z. Kopp

Designations

θ - contact angle;
 σ - coefficient of surface tension;
 ψ - coefficient of friction;
 μ - chemical potential
 ΔS - change in area;
 $\Delta \Phi$ - change in free energy;
 ρ - density;
 r - heat of phase transition.

Subscripts

r - gas phase;
 m - liquid phase;
 s - solid phase;
 ml - melting;
 mc - evaporation.

The possibility of intensifying heat exchange with the boiling of mercury is of considerable interest. Among other methods of heat transfer intensification is the physicochemical method, the

essence of which lies in the addition of amalgamating substances to mercury. The application of boiling amalgams is one of the present problems in the development of certain designs of liquid-metal installations [1].

Reference [2] gives the results of studies on heat transfer during the boiling of potassium amalgams with forced convection in circular vertical pipes, diameter 9.5 mm, wall thickness of approximately 0.72 mm. The data obtained in [2], just as the results of other studies on the boiling of amalgams, do not agree with contemporary ideas on heat transfer during boiling since the characteristics can not be related to either nucleate or film boiling. For this reason it was considered advisable to examine the mechanism of amalgam boiling.

As indicated in [3], the addition of an insignificant amount of potassium or sodium leads to a change in the character of the physicochemical interaction between the melt and the steel heat exchange surface and to a sharp change in the character of melt boiling. If during the boiling of pure mercury the heat transfer factor falls within the range $200-500 \text{ kcal/m}^2 \cdot \text{h} \cdot ^\circ\text{C}$, then during the boiling of amalgams under the same conditions it will reach $2000 \text{ kcal/m}^2 \cdot \text{h} \cdot ^\circ\text{C}$ and more.

M. I. Korneyev studied the boiling of magnesium amalgam [4] where the heat transfer factors in similar conditions reached $5000-7000 \text{ kcal/m}^2 \cdot \text{h} \cdot ^\circ\text{C}$.

According to the conclusion of the authors of reference [3], the intensification of heat transfer to boiling mercury with the addition of amalgamating substances is achieved in three ways:

a) from a reduction in the surface tension of the amalgams as compared with mercury;

b) from the disruption of the oxide film on the heat exchange surface and the creation of a direct contact between the mercury and the wall;

c) the joint effect of both factors.

However, an analysis of the accumulated research material [2, 5 and others] and the conditions for the generation of vapor phase [16] gives no indication that these factors can explain the sharp improvement in heat exchange during the boiling of amalgams when compared with similar processes during the boiling of mercury. It is established by the cited study on heat transfer during the boiling of magnesium amalgam [4, 5] that the heat transfer factor has high values during both the boiling of sodium and potassium amalgams in tests by A. N. Lozhkin and I. G. Izrayelit [3]. However, the surface tension of magnesium amalgam scarcely differs from the surface tension of pure mercury, which is apparent from Fig. 1, and, according to some studies, is even somewhat greater than that of pure mercury [6]. Then from the assumptions discussed in [3] concerning the mechanism of heat transfer intensification during amalgam boiling there remains one moment which provides the probability of oxide film disruption on the heat exchange surface.

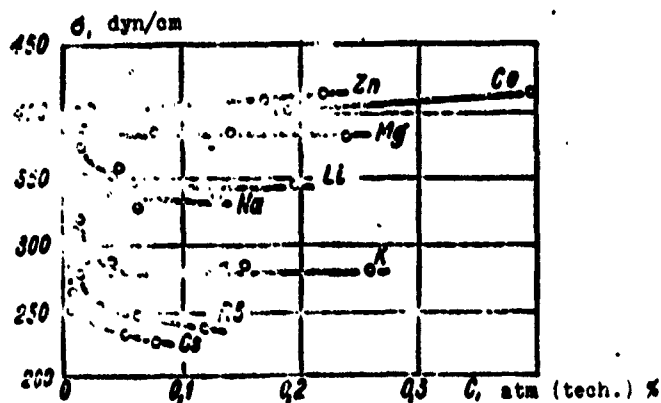


Fig. 1. Surface tension of amalgam based on data from [6].

This argument can explain some observation results. Visual observations of steel surfaces in contact with amalgams and at room temperatures do not reveal any removal of the oxide film from the surface.

Observations show that amalgams moisten well both pure and oxidized surfaces which pure mercury does not moisten. A substantiation of this can be the example of wetting by amalgams of both metal samples and pure glass vessels, which can not be wetted by mercury. Although in [8] the authors discussed the concept that part of the magnesium, during its introduction into the mercury, is expended on reducing the oxides present on the heat exchange surfaces, no direct or indirect proof has been obtained concerning the absence of an oxide film on the surface.

M. I. Korneyev attempted to explain the improvement in the wettability of the heat exchange surface by amalgams as not due to the change in the surface tension of the magnesium amalgam on the boundary with its own vapor, but due to the change in surface tension on the boundary with the wall, i.e., in examining the relationship for the contact angle

$$\cos \theta = \frac{\sigma_{\Gamma T} - \sigma_{MT}}{\sigma_{MT}} - \frac{\sigma_{TP}}{\sigma_{MT}} \quad (1)$$

the determining factors are σ_{MT} and $\sigma_{\Gamma T}$.

It is assumed that the action of the surface-active substance, which is the amalgam with respect to the mercury, affects not only the quantity σ_{MT} but also the quantities σ_{MT} and $\sigma_{\Gamma T}$. Therefore, a decrease in free energy in the isothermal process of droplet spread, described by expression (2), will be of considerable significance:

$$\Delta \Phi = -\sigma_{MT} \Delta S_{MT} - (\sigma_{\Gamma T} - \sigma_{MT}) \Delta S_{\Gamma T} \quad (2)$$

However no qualitative relationships, at the present time, can be obtained and this is the basis for assuming that their

effect is quite small. The foundation for this premise can be the examination of the surface tension of metal on the boundary with its own melt, made in references [9, 10], where it was shown that it is interrelated with the surface tension of the melt by relationship

$$\sigma_{TK} = \sigma_{MT} \left(\frac{\rho_T}{\rho_K} \right)^{2/3} \frac{r_{MT}}{r_{TK}}. \quad (3)$$

It is obvious that if the additions of amalgamating substances are fractions of a per cent, the density ratio is virtually unchanged, while the ratio of the transition heats in all cases refers only to the liquid metal. Thus this assumption does not explain the characteristics of amalgam boiling.

At the same time it is possible to make certain assumptions concerning the mechanism of the physicochemical method of intensifying heat exchange during mercury boiling, i.e., concerning the boiling of amalgams, in connection with the analysis of the behavior of an amalgam film on mercury as a surface-active substance and the mechanism of boiling [16]. It is known [11] that a layer of surface-active substance is continuous and rapidly extends over the entire surface. Since only the surface layer of amalgam can be in contact with the heating surface, in the process of vapor formation there can occur thermal disintegration of the amalgam, the mercury component of which turns into vapor. However, the amalgamating metal immediately comes in contact with the next portion of the mercury and again forms a surface-active substance, approaching the surface of the melt volume. The breakdowns of continuity in the surface layer of amalgams, due to thermal disintegration during boiling, are rapidly eliminated because of the spread of the surface-active layer of amalgam. Based on data presented by V. G. Levich [11], the film spread rate grows as it approaches the source of the surface-active substance, tending toward infinity.

The vapor forming in the process of evaporation during boiling, in spite of the presence of a surface layer of amalgam, contains virtually no impurities. Analysis of the condensate of mercury vapor on the magnesium content, performed by L. I. Gel'man, in a study on the boiling of magnesium amalgam, has shown that with a magnesium concentration of 0.114-0.142% in a boiler, its concentration in the condensate of mercury vapor was 0.00016-0.00031% [7]. This value is less by a factor of ten than the minimum concentration of magnesium in mercury capable of leading to heat exchange intensification during mercury boiling (approximately 0.005%). In the installation in which tests were made and samples were taken for measuring magnesium concentration, there were no separation devices and, consequently, under normal conditions, the magnesium content in steam must be even less than that presented in [7], i.e., near zero.

Based on the results of motion picture studies [12], the reason for the worsening heat exchange during mercury boiling on a contaminated surface lies in the propagation of the steam bubble along the heating surface and the creation of a layer of mercury vapor between the surface and the mercury (the vapor bubble can not overcome the surface tension of the mercury, penetrate into the mercury volume, and collapse). The steam bubble grows because of the evaporation of mercury not from the surface but from the volume of the mercury. However, in the presence of a surface-active layer, heat transfer to the mercury volume can occur only through this layer. Consequently, in the boiling of amalgams, in all cases, the generation and growth of a steam bubble occur not on the heat exchange surface itself but in the volume of the mercury, limited by the surface-active layer of amalgam.

The latter circumstance agrees with the theoretical conclusion that the surface-active layer contributes to a severe attenuation of wave motion on the surface of the liquid [11] and, with a sufficiently high elasticity for the surface layer film, behaves

as an incompressible solid plate. Judging from the test data, concentrations of amalgamating substances in mercury can be very low and can vary over a wide range. For example, in [3] with a change in potassium concentration from 0.0293 to 0.0049% by a factor of six or with a change in sodium concentration from 0.0505% by several factors, the heat transfer factor remained virtually unchanged. In tests [4, 5] using a magnesium amalgam, the beginning concentration varied from 0.01 to 0.04%, which also had no noticeable effect on heat transfer (Fig. 2). Moreover, in the tests described in [3], in one of the installations used for studying heat transfer during the boiling of a potassium amalgam, the boiling of pure mercury was studied. In spite of the fact that, in this case, the concentration of amalgam could be minimum, in the first test period heat transfer to the boiling metal was high, on the level of heat transfer during the boiling of amalgams.

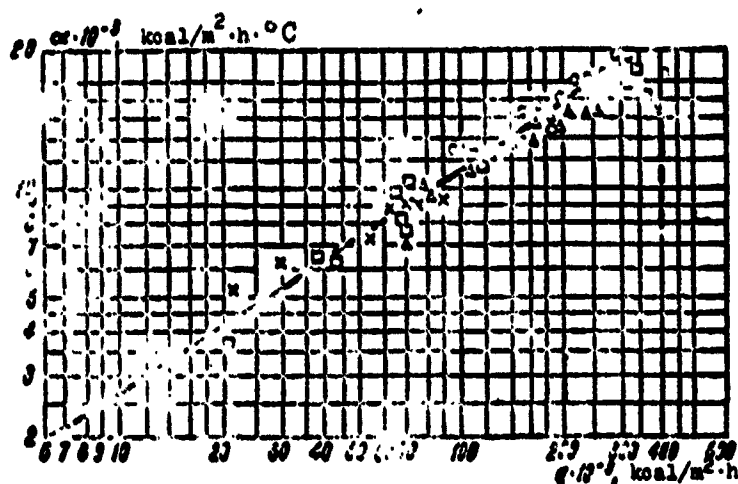


Fig. 2. Heat transfer to magnesium amalgam at various magnesium concentrations [5].

With a high percentage content of surface-active substance-amalgam, the boiling of mercury will occur, in all cases, on the melted metal-additive layer. As shown in reference [13], the overall form of heat transfer regularity during the boiling of liquid on the surface of melted metal does not differ from the

form of the similar regularity during boiling on a solid wall. However, in all cases, for the upper temperature of the calculated temperature head we should take the temperature of the surface on which boiling occurs. Taking this into account, the data in reference [2] can be interpreted in accordance with the known regularities of heat transfer during boiling.

Analysis of the actual function of the variation in thermodynamic potential [14] shows that its maximum occurs not on the surface but at some distance from it, i.e., in the mass of the boiling metal. Hence the possibility of such cases when conditions for the generation of steam bubbles are more favorable at some depth from the wall in the boiling metal. At the same time, in all cases, near the surface conditions are created for local sharp increases in impurity concentration, i.e., the probability increases for the fluctuation of concentrations and, consequently, considerably improves the probability of the formation of vapor phase nuclei. The additional substantiation of the validity of this mechanism can be the examination of critical thermal loads, whose values for amalgams are substantially lower than for mercury, and also the new data on heat transfer during nucleate boiling of mercury [17].

BIBLIOGRAPHY

1. Канаев А. А., Копп Н. З. Судовые и стационарные жидкометаллические энергетические установки. Изд-во «Судостроение», 1968.
2. Tang J. S., Ross P. T., Nicolson R. C., Smith C. R. Forced Convection Boiling of Potassium-Mercury Systems. *AIChE Journal*, 1964, v. 10, No 5, p. 617.
3. Ложкин А. Н., Израелит Н. Г. К вопросу об интенсификации теплообмена между стенкой и кипящей ртутью. *ЖТФ*, т. IX, вып. 24, 1939, с. 2174.
4. Корнеев М. Н. Теплоотдача ртути и амальгам чашки при кипении в условиях свободной конвекции. «Теплоэнергетика», 1935, № 4.
5. Корнеев М. Н. Исследование теплообмена ртути и амальгам чашки при кипении. В сб.: «Жидкие металлы». Атомиздат, 1963.
6. Семенченко В. К. Поверхностные явления в металлах и сплавах. ГИИТЛ, 1957.
7. Гельман Л. Н. Экспериментальное исследование теплоотдачи при конденсации ртутного пара. В сб.: «Вопросы теплоотдачи и гидравлики в жидких средах». ГЭИ, 1961.
8. Ложкин А. Н., Корнеев М. Н., Гельман Л. Н. Особенности эксплуатации ртутно-паровых установок. В сб.: «Комбинированные энергетические установки и циклы». Машгиз, 1952.

9. Крестинский А. Н., Ротин К. М., Вигдорчик В. В. сб. «Поверхностные явления в жидкостях и газах». Металлургия, 1963.
10. Шибанов М., Байбаков В. С. Там же.
11. Тевин В. Г. Физическая гидродинамика. АН СССР, 1952.
12. Тоцкий А. Н., Кроль П. П. О механизме кипения ртути в элементах ртутного парогенератора. ЖТФ, т. 8, вып. 21, 1938, с. 1672.
13. Naračković M., Stefanović M. Int. J. of Heat and mass Transfer, v. 7, № 7, 1964, p. 801.
14. Сирота Н. Н. Состояние и проблема теории кристаллизации. В сб.: «Кристаллизация и фазовые переходы». Минск, 1962.
15. Копп И. З. О границах области возможной реализации пузырькового кипения. В сб.: «Общие вопросы тепло- и массообмена». Минск, 1966.
16. Копп И. З. Анализ условий зарождения паровых пузырьков при кипении жидкостей. «Труды ЦКТИ», вып. 91, 1960.
17. Гельман Л. И., Копп И. З. Теплоотдача при пузырьковом кипении ртути. «Теплофизика высоких температур», 1968, № 3.

EXPERIMENTAL STUDIES ON THE EFFECT
OF DUCT MATERIAL ON THE HEAT
TRANSFER OF BOILING MERCURY

L. I. Gel'man and I. Z. Kopp

Abbreviations

ст - steel;
яac - nucleus;
mac - saturation;
мсн - test;
n - surface [?].

In earlier research on heat transfer during mercury boiling, a summary of which is presented in references [1, 2, 3, 4], the film regime of boiling was observed and possible ways were discussed for intensifying heat transfer of boiling mercury due to the transition to nucleate boiling. In connection with the established possibility of heat transfer intensification due to the achievement of moistening by pure mercury of a heating surface made from low-carbon steel and the achievement of high specific thermal fluxes [5, 6], as well as the observed effect of surface material on heat exchange during the boiling of water and organic liquids [7], the problem was posed to determine the effect of surface material on heat transfer during the boiling of mercury.

Studies were made on an experimental installation, a brief description of which is presented in [3], with high-frequency induction heating by the successive substitution of experimental sections made of various materials.

Along with the study of heat transfer, a check was made of the material of the heat-transferring surfaces, for the wettability of the surfaces by mercury and the content of impurities in the mercury. Analyses were made of the chemical composition of the experimental installation's materials both before tests and after them, as well as a layer-by-layer microspectral analysis of the materials of all sections.

Section No. 1 made from pipe of low-carbon steel, diameter 16 mm, wall thickness 6 mm. Before the tests on mercury, long tests on water were made and the loop was cleansed. The initial chemical composition of the material was characterized by the following indicators: carbon - 0.22%, silicon - 0.20%, manganese - 0.39%, chromium - 0.14%, nickel - 0.18%, sulfur - 0.021%, phosphorus - 0.024%. After the tests were finished, the section was examined and analyzed. The inner surface was uniformly moistened with mercury along the height of the duct.

With immersion into cold mercury in the open air, the mercury wetted the inner surface (concave meniscus) and its form did not change immediately after contact with the mercury ceased. After two or three days, at separate points on the wetted surface breaks in the continuous mercury film appeared. The breaks were rapidly coated with oxides and increased in size. After five or six days, almost all the surface of the duct was covered with oxides and only at certain points were there drops of mercury.

From the middle of the duct two cylinders were cut. One of the cylinders was ground from the ends and used for microspectral analysis in various cross sections along the wall thickness. The second cylinder was used for layer-by-layer chemical analysis in

three different sections, the results of which are presented in Table 1.¹

Table 1. Results of layer-by-layer chemical analysis of the material of Section No. 1.

Layers	Analysis No.	Elements Determined				
		C	Si	Mn	Cr	Ti
Outer (from Ø 26.5 mm to Ø 24.5 mm).....	1	0.30	0.22	0.5	0.11	None
Middle (from Ø 24 mm to Ø 22 mm).....	2	0.23	0.21	0.5	0.12	None
Inner (from Ø 21 mm to internal diameter).....	3	0.23	0.22	0.5	0.12	None

Microspectral analysis was conducted at four points along the wall thickness for determining two impurities only: manganese and silicon (Table 2).

Table 2. Results of analyses on determining impurities in Section No. 1.

Analysis Method	State of Material	Layers	Elements Determined	
			Mn	Si
Chemical	Initial	—	0.39	0.20
	After tests (average)	—	0.5	0.22
Micro-spectral	After tests	Inner	0.47	0.23
		Middle (2 measurements)	0.69	0.33
		Outer	0.87	0.48

¹Metallographic studies were made by G. Z. Khislavskiy.

Section No. 2 was made of new low-carbon steel pipe with a pure inner surface, wall thickness 3.1 mm. Unlike section No. 1 before installation in the loop, section No. 2 did not make contact with the water or other media. After filling the loop with mercury, seven days passed before the heating of the experimental section. During this period mercury temperature did not exceed boiling temperature. Only three times was the mercury heated briefly to a temperature of approximately 200°C for checking and calibrating the measuring equipment. The rest of the time the mercury temperature did not exceed the temperature in the laboratory (below 20°C).

The results of chemical analysis on the material of section No. 2 after tests are presented in Table 3.

Table 3. Results of chemical analysis on the material of Section 2 after tests.

Layers	Analysis No.	Elements Determined				
		C	Si	Mn	Cr	Ti
Outer (from Ø 22 mm to Ø 20 mm).....	4	0.19	0.11	0.45	None	None
Middle (from Ø 20 mm to Ø 18 mm).....	5	0.17	0.11	0.43	None	None
Inner (from Ø 18 mm to interior diameter).....	6	0.15	0.10	0.43	None	None

Here it is more evident, but as for section No. 1, a decrease in carbon content is observed in the surface layer.

The layer-by-layer microspectral analysis of samples from section No. 2 for the content of manganese, silicon, chromium, and nickel is shown in Table 4.

Table 4. The result of layer-by-layer micro-spectral analysis of samples from section No. 2.

Layers	Elements Determined			
	Mn	Si	Cr	Ni
Inner.....	0.64	0.15	Traces	Traces
Middle.....	0.37	0.20	"	"
Middle.....	0.39	0.07	"	"
Outer.....	0.20	0.03	"	"

In all sections of the pipe of section No. 2 complete wetting of the surface by mercury in a cold state was observed.

Section No. 3 was made from a Kh18N10T steel rod, diameter 28 mm. The rod was bored out in the centers to \varnothing 25 mm and then melted with electrodes of low-carbon steel to a diameter of approximately 50 mm. After boring to a clean and smooth surface, the rod was drilled \varnothing 18 mm and bored out in the centers to an outer diameter of 29.2 mm. Such a procedure for preparing the experimental section was adopted for the purpose of ensuring contact of the mercury with the surface of the given material (Kh18N10T steel) and the possibility for induction heating of the experimental section.

However, chemical analysis of the material showed that in the preparation of the section, apparently, there occurred a melting of the stainless steel near the melting zone and a displacement of the material, i.e., the surface on which mercury boiling occurred was substantially different than prescribed (Table 5).

Table 5. Results of chemical analysis on Section No. 3.

Layers	Analysis No.	Elements determined				
		C	Si	Mn	Cr	Ti
Outer.....	7	0.12	0.36	1.07	0.76	None
Inner....-.....	8	0.12	0.53	1.14	6.83	0.038

The microspectral analysis of material in section No. 3 had similar results.

For this reason the test data for section No. 3 was not processed and section No. 4 was prepared to test heat transfer during the boiling of mercury in a stainless steel pipe. To prepare section No. 4 a new pipe of Kh18N10T steel was used, with an inner diameter of 13.4 mm and wall thickness of 2.8 mm. With continuous cooling of the pipe, a layer of low-carbon steel was melted on its surface, after which the surface of the pipe was bored out to a diameter of 29 mm. Before the tests on mercury boiling adjustment operations were performed on this section with respect to heat exchange during the boiling of water.

Before filling the loop with mercury the external form of the inner surface of section No. 4 did not differ from the ordinary surface for Kh18N10T steel.

After filling the loop with mercury and starting the high-frequency heating device of the experimental section, the process of heat transfer to the boiling mercury occurred as in the first period of mercury boiling in section No. 1: wall temperature exceeded mercury saturation temperature by 300-400°C and sharp oscillations in mercury flow rate and pressure occurred in the loop. Such instability of process, indicating the presence of the film regime of mercury boiling, continued for 90 hours of continuous mercury boiling.

After this period, local reductions in the temperature head could be observed at separate points, and after 60 more hours a reduction in the temperature head (wall-flow temperature) was fixed along the entire length of the experimental part and it was possible to increase power input. From this period the study of heat transfer to boiling mercury in section No. 4 was made.

It is obvious that the overall picture of the heat transfer intensification process during the boiling of mercury on a surface of stainless steel does not differ relatively from the similar process of heat transfer intensification from thermomercure processing of low-carbon steel [6]. This agrees with the assumptions made by the earlier discussed authors concerning the principal possibility of achieving nucleate boiling of mercury on the surface of various metals by long purification from products of corrosion, adsorption and chemisorption, which prevent wettability by mercury. The result obtained indicates the possibility of ensuring the wettability of stainless steel by pure mercury with a safe distance of the contaminating impurities from the surface, as with low-carbon steel.

To check the stability of the result obtained, tests on section No. 4 were interrupted for two months, after which a new series of tests were made. During these tests the nucleate regime of boiling was observed.

After dismantling section No. 4 the material was used for chemical and microspectral analyses.

The chemical analysis was made layer by layer and resulted in the data presented in Table 6.

Table 6. Results of the chemical analysis of material from Section No. 4.

Layers	Analysis No.	Elements Determined					
		C	Si	Mn	Cr	Ni	Ti
Outer (melt).....	9	0.05	0.29	0.62	0.41	0.38	None
Middle (from \varnothing 16 mm to \varnothing 14 mm).....	10	0.08	0.34	0.63	1.12	0.77	None
Inner (from 14 mm to internal diameter)	11	0.11	0.53	1.09	18.0	9.8	None

Spectral analysis was performed in ten sections throughout the thickness of the section wall. The results of spectral analysis for determining the five elements are presented in Table 7.

Table 7. Results of the spectral analysis of material from Section No. 4.

Location of Spectra	Elements Determined				
	Mn	Si	Cr	Ni	Ti
Inner layer.....	0.48	—	18.20	10.47	0.47
Middle layer.....	0.81	—	21.80	10.23	0.30
" "	0.85	—	14.45	9.12	0.36
" "	0.72	—	10.72	8.10	0.31
" "	0.66	—	4.89	2.39	0.08
" "	0.75	—	2.08	1.66	0.08
" "	0.56	0.17	1.62	1.20	Traces
" "	0.42	0.27	Traces	0.60	None
" "	0.50	0.20	Traces	Traces	None
Outer layer.....	0.37	0.30	None	None	None

In the initial material for working section No. 4 the following contents were established by microspectral analysis: chromium 9%, nickel 11%, and titanium 0.33%.

It is obvious that the chemical composition of Kh18N10T steel, as a result of continued mercury boiling in a pipe of this steel, was virtually unchanged.

The calculated values of wall thickness in various sections were more precisely defined by direct measurements. In all sections the surface of the pipe in contact with the mercury was uniformly wetted by mercury. With the immersion of segments of the section into mercury at room temperature there was observed complete wetting by mercury of the inner surface of the pipe (the meniscus was concave).

Sections No. 5 and 6 were made from new pipes set up for the pipe system of a high-pressure boiler and characterized by the following data in Table 8 (average composition).

Table 8. Chemical composition of the material of Sections No. 5 and 6.

Sample No.	Chemical composition, %								
	C	Si	Mn	S	P	Cr	Cu	Mo	V
1	0.11	0.20	0.53	0.012	0.012	0.99	0.17	0.28	0.26
2	0.12	0.18	0.50	0.014	0.014	0.11	0.10	0.34	0.22
3	0.13	0.18	0.50	0.014	0.015	0.12	0.11	0.33	0.21

In accordance with TU-257 this composition corresponds to 12Kh1MF steel. Before the tests the material of the section was not wetted by mercury. After the tests the section was uniformly wetted by mercury over the entire surface.

Table 9 presents the geometric characteristics of all experimental sections.

Mercury samples for determining impurities in the mercury were taken directly from the loop through a valve for draining and filling the loop. The necessary measures were taken during sample selection to exclude the possibility of error. For example, part of the mercury was drained past the sample vessel and then the vessel was filled. Samples were taken: 1) before conducting a series of control tests on section No. 1, 2) after conducting tests on section No. 2, 3) before conducting tests on section No. 4.

In all cases, based on total impurity content, the mercury corresponds to brand R-3 according to GOST 4658-49 [GOST = GOCT = All-Union State Standard] (99.9%) (Table 10). According to external appearance, in all cases, in the selected samples the mercury was pure.¹

¹The analyses of mercury were made by N. L. Izanova.

Table 9. Characteristics of experimental sections.

Section No.	Material of the heat exchange surface	Inner diameter of pipe, mm	Outer diameter of pipe, mm	Intermediate diameter of pipe, mm	Calculated wall thickness, mm	Minimum distance of thermocouples from wall, mm	Process for preparing section
1	St.20	16.0	28.0	-	6.0	2.0	New pipe before contact with mercury was in contact with boiling water for approximately a month.
2	St.20	15.8	22.0	-	3.1	3.1	New pipe with clean inner surface protected from corrosion
3	Kh18N10T	18.0	29.2	-	5.6		Bar of Kh18N10T steel \varnothing 28 mm bored out to \varnothing 25 mm. St.30 melted to \varnothing 50 mm, drilled \varnothing 18 mm, bored out to \varnothing 29.2 mm.
4	Kh18N10T	13.4	29.0	19.0	7.8 2.8- 5.0	3.2	New pipe of Kh18N10T steel $\delta_{cr} = 3.0$ mm melted by electric welding St.20 to \varnothing 50 mm and bored out to \varnothing 29 mm. Tests were made previously with boiling water.
5	12Kh1MF	20.2	28.2	-	4.0	4.0	New pipe. After welding and marking, surface strongly oxidized. Wave-shaped bends along length of pipe $l = 100$ mm, $h =$ up to 0.1 mm.
6	12Kh1MF	20.0	28.0	-	4.0	4.0	New pipe. Inner surface strongly oxidized.

Table 10. Results of mercury analyses

Impurities	Before beginning of tests on section No. 1	After tests on section No. 2	Before tests on Section No. 4
Iron.....	$3.5 \cdot 10^{-4}$	$10 \cdot 10^{-4}$	$12 \cdot 10^{-4}$
Magnesium.....	None	-	-
Chromium.....	$2.4 \cdot 10^{-4}$	$0.05 \cdot 10^{-4}$	$0.05 \cdot 10^{-4}$
Nickel.....	$0.094 \cdot 10^{-4}$	None	$0.2 \cdot 10^{-4}$
Copper.....	$0.24 \cdot 10^{-4}$	$0.4 \cdot 10^{-4}$	$2.0 \cdot 10^{-4}$
Titanium.....	None	-	-
Total impurity content	$6.24 \cdot 10^{-4}$	$10.45 \cdot 10^{-4}$	$14.25 \cdot 10^{-4}$

The methodology for determining heat transfer characteristics was as follows: specific thermal fluxes, flow rates, vapor contents, etc., in the processing of measurement results, were similar to those described in [3].

During the tests, regimes were established by changing heater power. The power was gradually increased to permissible surface temperature of the experimental section ($\sim 750^{\circ}\text{C}$) and then gradually reduced until the mercury boiling process degenerated. After this, the regimes were established in an arbitrary order throughout the range of permissible loads. The duration of each regime was no less than 3-4 h.

In the processing we included only those regimes in which the temperature of the outer surface of the steam-generating pipe was below the Curie temperature of the studied material by no less than $30-50^{\circ}\text{C}$ (for pressures corresponding to saturation temperatures up to 600°C).

This report presents the results of experimental studies in the range of specific thermal loads up to $2 \cdot 10^6 \text{ W/m}^2$, which, according to test conditions, correspond to steam content of no more than 20% at section output and a velocity of no more than

50-60 m/s for the steam-mercury mixture, when developed surface nucleate boiling of mercury occurs and the shell or annular flow regime has not yet set in. The chief results of tests made on all experimental sections are presented in Fig. 1. Primarily our attention is turned to the disagreement of data obtained for various sections, as well as the substantial spread in points for each section.

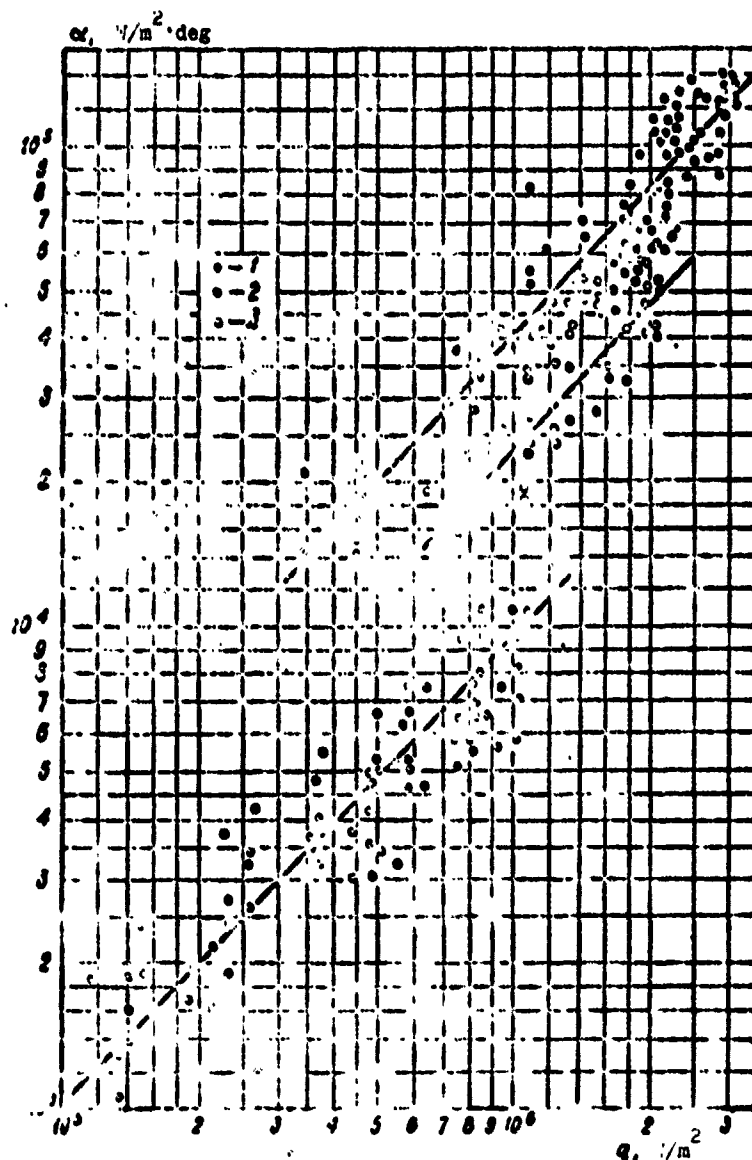


Fig. 1. Results of experimental study on heat transfer during mercury boiling in pipes of various steels: 1 - Low-carbon steel - St.20; 2 - St. 12Kh1MF; 3 - St. Kh18N10T.

GRAPHIC NOT REPRODUCIBLE

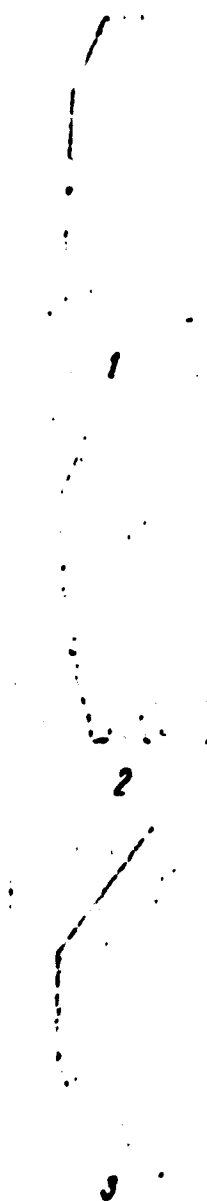


Fig. 2. The structure of actual roughness on the surface of pipes in cross sections (X500):
1 - St. 20; 2 - St. 12Kh1MF; 3 - St. Kh18N10T.

The difference in heat transfer levels during the nucleate boiling of mercury in pipes of various materials can be explained, to a considerable extent, not by the brand of the material but by the effect of the microstructure of the pipe surface. As is apparent from the surface microstructure photograph, several sections of which are presented in the photograph in Fig. 2, the dimensions of the depressions in the roughness of each of the studied surfaces differ considerably. The statistical processing of the series of microstructure photographs showed that the pipes of St.20 steel, used in tests, had an average roughness depression radius of approximately 0.050 mm, while pipes of 12Kh1MF steel had approximately 0.012 mm and pipes of stainless steel had approximately 0.007 mm.

From this point of view, the results obtained agree with the results of tests on the effect of surface roughness on heat transfer during the boiling of nonmetallic liquids [8, 9] and substantiate the analysis of conditions for the occurrence of steam bubble nuclei [10]. All these data show that it is precisely the dimensions of the roughness depressions which determine the dimensions of stable steam bubble nuclei. With an increase in the radius of stable nuclei there is also an increase in the necessary wall temperature head-saturation temperature, which is the main characteristic of heat transfer in accordance with the rule obtained as a result of the joint solution of the Laplace-Gibbs and Clapeyron-Clausius equations, which can be presented in the form:

$$R_{up} = - \frac{2\sigma T_{us}}{r_{ml} \Delta T}.$$

In Fig. 3 our data in coordinates $R = f(\Delta T)$ for mercury with specific thermal load $1 \cdot 10^6 \text{ W/m}^2$ agree with the data from [8] for the boiling of n-pentane with a specific thermal load of approximately $0.5 \cdot 10^6 \text{ W/m}^2$, which are discussed in [9].

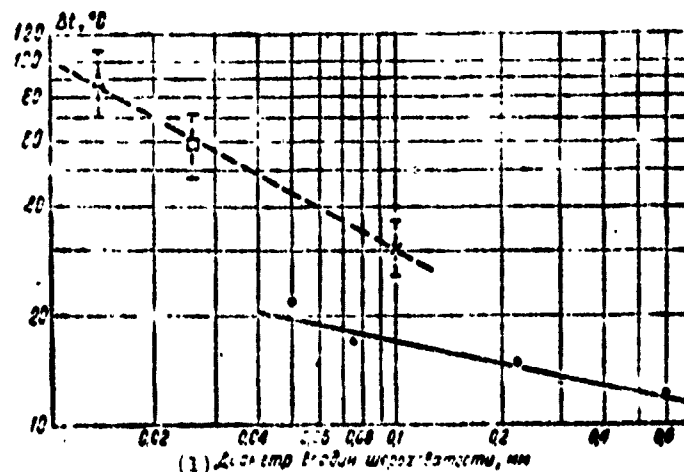


Fig. 3. Temperature head versus dimensions of roughness depressions during the boiling of mercury on various surfaces:
 x - St. 20; □ - St. 12Kh1MF; Δ - St. Kh18N10T;
 ● - Data [8] for n-pentane.
 (1) Diameter of roughness depressions, mm.

For the purpose of clarifying the observed spread in test data with respect to each of the experimental sections studied an additional study of the temperature regimes in steam-generating pipes was set up.

BIBLIOGRAPHY

1. Лопатин А. Н., Канаев А. А. Бинарные установки. Машгиз, 1946.
2. Кутателадзе С. С. и др. Жидкометаллические теплообменники. Атомиздат, 1959.
3. Гельман Л. Н., Копп Н. З. Теплоотдача при пленочном кипении ртути в трубах. Труды ЦКТИ, вып. 78, Л., 1967.
4. Tang J. Heat Transfer with boiling Met. «Nuclear Applications», № 12, 1965, p. 521.
5. Гельман Л. Н., Копп Н. З. Теплоотдача при пузырьковом кипении ртути при тепловых нагрузках до $2 \cdot 10^6$ Вт/м². Теплофизика высоких температур, 1969, № 3.
6. Канаев А. А., Гельман Л. Н., Копп Н. З. Способ интенсификации теплообмена при кипении ртути. Авторское свидетельство СССР № 174613 «Бюллетень изобретений», № 34, 15/XI 1965.
7. Головин В. С., Кольчугин Б. А., Лабунцов Д. И. Исследование теплообмена и критических тепловых нагрузок при кипении жидкостей в условиях свободного движения на поверхностях из различных материалов. Труды ЦКТИ, вып. 58, 1965, с. 35.
8. Corry C., Foust A. S. Chem. Eng. Progr. Symp. Ser., v. 51, № 17, 1955, p. 81.
9. Kuloor N. R., Radhakrishnan V. N. Effect of Surface Roughness on Nucleate Boiling. Chemical and Process Eng., v. 47, № 6, 1966, p. 276.
10. Копп Н. З. Анализ условий возникновения паровых пузырьков при кипении жидкостей. Труды ЦКТИ, вып. 91, 1969.
11. Борншанский В. М., Копп Н. З. К вопросу о правомерности совместного решения уравнений Лапласа—Гиббса и Клапейрона—Клаузуса для определения размеров и роста паровых пузырьков. 3-я Всесоюзная конференция по термодинамике, 1969.

THE EFFECT OF GAS PHASE DISPERSION
ON THE INTENSITY OF HEAT EXCHANGE
BETWEEN PHASES AND ON THE FLOW
PARAMETERS OF A TWO-PHASE FLUID
MIXTURE

D. I. Volkov and N. I. Malofeyev

Abbreviations

ж - liquid
н - beginning
к - end
нач - beginning
из - isotherm
ад - adiabat
кр - critical
г - gas

In various industrial areas two-phase fluid mixtures are used, in which both phases are far from critical states as well as from states which correspond to phase transitions. Some of these mixtures such as, for example, mechanical air foam and others, move along pipes without heat exchange with the ambient medium and with a constant mass composition of each phase.

With high dispersion of the gas phase the motion of the mixture is characterized by the absence of relative phase slippage [1]. In the absence of surface-active salts and structure stabilizers, a fluid mixture of the mechanical air foam type is an elastic porous medium capable of multiple expansion and compression without disruption and coagulation of the gas spheres. The mass of each separately taken gas bubble in the composition of this mixture, during its expansion-contraction, stays constant and, consequently, the thermodynamic laws of ideal gases apply to such a bubble [2]. Therefore, in a number of works [1, 3] there is the concept of isothermal or adiabatic (isentropic) variations in the state of the gas phase during the discharge of the fluid mixture. With adiabatic variations in gas phase state, there is no heat exchange between phases. With isothermal variation in gas phase state heat exchange does occur between phases.

Heat exchange between phases affects the gas phase parameters and, consequently, the parameters of the entire mixture. Let us examine this effect in greater detail.

In the general case, during the motion or discharge of a fluid mixture the temperature of each phase and the value of thermal flux between them are different and variable so that the heat exchange process between phases is nonstationary and occurs under conditions of gradual phase temperature equalization.

Examining a fluid mixture in which the gas phase is a bubble or a sphere with a diameter of less than 25 mm and disregarding the transfer of heat by convection inside the bubble as well as the radiant heat transfer between liquid and gas phases, we can write for a separately taken gas bubble, as for a solid sphere, the familiar Fourier equation of nonstationary heat conductivity. In the heat transfer theory [4] the solution to such an equation with given boundary conditions of the third type is usually reduced to the form:

$$\theta = \Phi(Bi_0, Fo), \quad (1)$$

where $\theta = \frac{\bar{t} - t_m}{t_0 - t_m}$ is the dimensionless temperature of the gas bubble; $Bio = \frac{\alpha R}{\lambda}$ is the Biot criterion for a gas bubble; $Fo = \frac{a \tau}{R^2}$ is the Fourier criterion for a gas bubble; \bar{t} is the temperature on the surface or in the center of the bubble (sphere) at any moment of time, °C; t_m is the constant temperature over time of the liquid surrounding the bubble, °C; t_0 is the temperature, uniformly distributed throughout the volume, of the bubble at the initial moment of time ($\tau = 0$), °C; R is the radius of the bubble (sphere), m; α is the heat transfer factor from liquid phase to the bubble (assumed constant over time), kcal/m²·h·deg; λ is the heat conductivity factor of gas phase, kcal/m·h·deg; a is the temperature conductivity factor of gas phase, m²/h; τ is the heat exchange time, h.

If we know factors α and λ and take into account the Bio and Fo criteria for various values of R and τ , we can, by using the graph of function (1) presented in the handbook on heat transfer [5], determine the dimensionless temperature in the center of the bubble $\theta_{R=0} = \bar{t}_{R=0} - t_m / t_0 - t_m$ or on its surface $\theta_R = \bar{t}_R - t_m / t_0 - t_m$.

Such calculations were made with respect to the following parameters of the air in the composition of the mechanical air foam: $p_0 = 1$ atm (abs.), $t_0 = 20^\circ\text{C}$, $\lambda = 0.0217$ kcal/m·h·deg, $a = 0.0766$ m²/h, $\gamma = 1.164$ kg/m³. Calculations showed that the temperature $\theta_{R=0}$ differs from θ_R only at the beginning of the heat exchange process, i.e., when $Bio \leq 0.1$ and $R \geq 10^{-4}$ m.

The results of calculations in the form of graphs $\tau = f(R)$ for various values of θ_R are presented in Fig. 1.

As follows from Fig. 1, the beginning time τ_H and end time τ_K of the heat exchange process is reduced with a decrease in the bubble radius R according to the law of the power function, namely, $\tau_H = f_1(R^n)$ and $\tau_K = f_2(R^m)$ where n and m are constants.

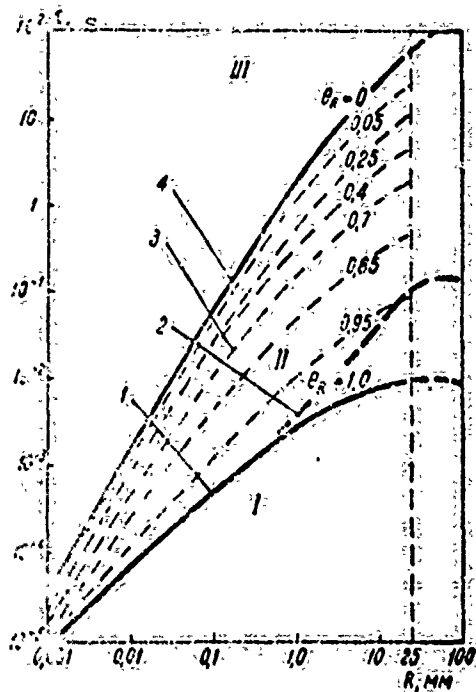


Fig. 1. Time for heat exchange between phases versus dimensions of gas phase bubbles in the flow of a fluid mixture at $p_0 = 1$ atm (abs.), $t = 20^\circ\text{C}$:

1 - Beginning of heat exchange process on surface of gas bubble;
2 - Beginning of temperature variation inside gas bubble;
3 - Process of intensive heat exchange on gas bubble surface;
4 - End of heat exchange process on gas bubble surface.

I - Region of adiabatic flow motion; II - Region of polytropic flow motion; III - Region of isothermal flow motion.

The time of intense heat exchange between phases $\tau = \tau_H - \tau_H$ is determined in Fig. 1 by the segment of the ordinates between the curves of functions $\tau_H = f_1(R, \theta_R = 1.0)$ and $\tau_H = f_2(R, \theta_R = 0)$ corresponding to the beginning and the ending of heat exchange between phases. These curves make it possible to distinguish the following three regions on the graph in Fig. 1.

1. The region of gas phase adiabatic expansion, in which the expansion of this phase during τ occurs without heat exchange with the liquid phase since $\tau_L \leq \tau_H$, where τ_L is the time of the fluid mixture's motion on a segment of the pipe with length l .

2. The region of polytropic expansion in which the gas phase during $\tau_H < \tau_L < \tau_H$ expands with intense heat exchange, occurring at the maximum value and, at the same time, a variable value of the temperature gradient. In this region, partial cases can be the isobaric and isochoric expansion of the gas phase.

3. The region of isothermal expansion in which gas phase during $\tau_l \geq \tau_H$ expands at a minimum and constant value for the temperature gradient, a low value for the thermal flux between phases, and a practically constant temperature head. During the motion of fluid flow the parameters of gas phase p , γ , R , a and λ change continuously and, consequently, their values for the Bio and Fo criteria also change.

The heat exchange time for gas bubbles with liquid phase increases with an increase in pressure p and a decrease in the initial gas temperature t_0 . In this case, the curves for the beginning and end of heat exchange and also the regions of adiabatic, polytropic, and isothermal expansions are shifted upward in the direction of an increase in heat exchange time, while the region of adiabatic expansion is considerably increased due to the increase in the value of τ_H .

The conversion of heat exchange time at new initial parameters for gas phase can be accomplished with formula

$$\tau^{p,t} = k_t k_p \tau^{p_0, t_0} \quad (2)$$

where $\tau^{p,t}$ is the heat exchange time with gas phase parameters equal to $p_0 = 1$ atm (abs.) and $t_0 = 20^\circ\text{C}$, in seconds; k_t is the coefficient which takes into account temperature variations ($k_t = 1.0$ when $t = 20^\circ\text{C}$ and $k_t = 2.5$ when $t = 150^\circ\text{C}$); $k_p = p/p_0$ is the coefficient which takes into account pressure variation.

Using formula (2) and the graph presented in Fig. 1, we can calculate the heat exchange times for the gas sphere (bubble) with variable radius R , increasing with a drop in the pressure of the flow of the fluid mixture from p to p_0 . Such calculations were made for a gas sphere with initial radius $R_{\text{нач}} = 10^{-4}$ m during its expansion along the isotherm and adiabat from pressure $p = 10$ atm (abs.) to $p_0 = 1$ atm (abs.). The values of the radius of the gas sphere during its expansion were determined from formula:

$$R_{01} = R_{02} \sqrt{p/p_0} \quad (3)$$

$$R_{01} = R_{02} \sqrt{(p/p_0)^{1/n}} \quad (4)$$

The results of calculations are presented in Fig. 2. As follows from Fig. 2, the time for the beginning and end of the heat exchange of the gas phase with the simultaneous reduction of its temperature, the drop in pressure of the fluid mixture, and the increase in the gas sphere's radius vary insignificantly. In practice, this time can be considered constant in any flow cross section of the fluid mixture.

We should mention that the time for the beginning τ_H and end τ_K of the heat exchange between phases can be greater, less, or equal to the time for the displacement of the elementary volume of the fluid mixture and the pressure drop in it from hydraulic velocity on length l or the mixture's discharge time into the atmosphere τ_l .

Data on the motion time of mechanical air foam on sections of pipe, nozzle, and free stream are presented in Fig. 3. The motion time for foam τ_l was defined as the ratio of the length of path l to the velocity of foam motion w , measured during the test.

Comparing the time thus determined with the time for heat exchange between phases, calculated from formula (2), we can make the following conclusions.

1. In pipes with length $l \approx 120$ m during the motion of a fluid mixture containing gas bubbles whose radius is a value from 0.001 to 25 mm, condition $\tau_l \geq \tau_H$ is fulfilled. Since the liquid phase has a heat capacity higher than gas phase, its temperature during phase heat exchange remains virtually constant. Under these conditions, the process of gas phase expansion can be considered isothermal with the polytropic indicator $n = 1$.

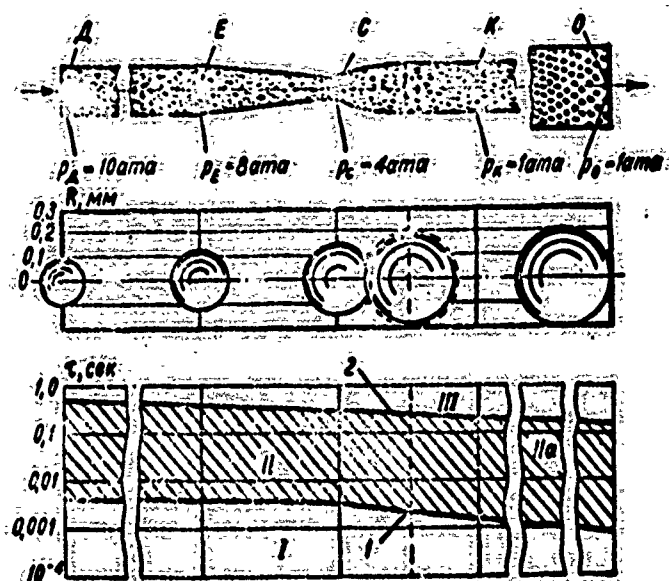


Fig. 2. Times of heat exchange between phases versus pressure drop of mixture and dimensions of gas phase bubbles:
 1 - Beginning of heat exchange process on gas bubble surface;
 2 - End of heat exchange process on gas bubble surface;
 I - Region of flow motion without heat exchange between phases (adiabatic motion); II - Region of flow motion with heat exchange between phases (polytropic motion); IIIa - Zone of polytropic flow motion (isobaric motion in a free stream); III - Region of isothermal flow motion; AE - Pipe section; EC - Nozzle section; CH - Initial section of free stream; HO - Final section of free stream.
 DESIGNATIONS: $\text{сек} = \text{s}$; $\text{ama} = \text{atm (abs.)}$

2. During the discharge of the mixture from the conical nozzle and during the transition of heat from liquid phase to gas phase, the following types of discharge are possible:

- isothermal ($n = 1$) when $R \leq 0.001 \text{ mm}$ and $\tau_1 \geq \tau_H$;
- polytropic ($n = 1.0-1.4$) when $R = 0.01-0.1 \text{ mm}$ and $\tau_H < \tau_2 < \tau_K$;
- adiabatic when $R \geq 0.1 \text{ mm}$ and $\tau_2 < \tau_H$.

With the discharge of a mixture from the conical nozzle and the transition of heat from gas phase to liquid phase the

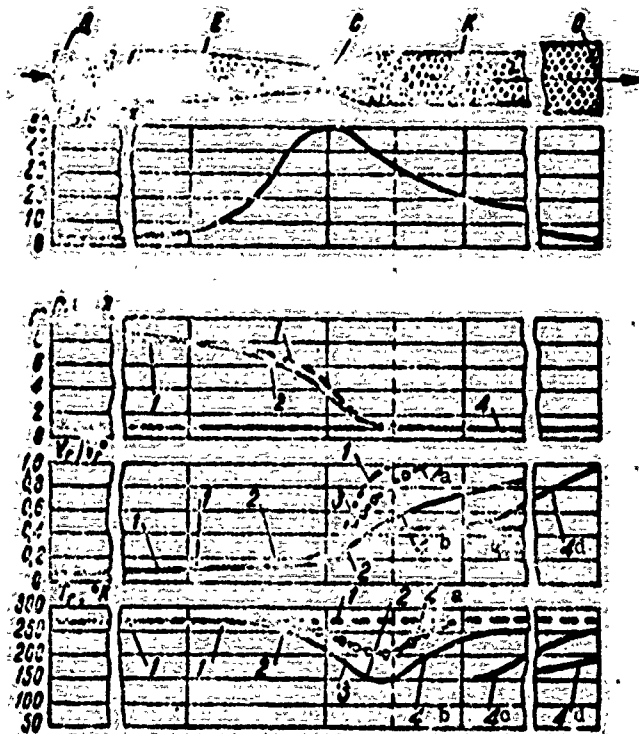


Fig. 3. Variation in gas phase parameters as a function of bubble dimensions (the effect of the dispersion of gas phase on its parameters):

DE - Isothermal motion of a mixture in a section of pipe with length $l_{DE} = 120$ m for $\tau_{DE} = 60$ s, bubble radius $R \leq 25$ mm;

EC - Motion of mixture in nozzle section with length $l_{EC} = 0.05$ m for $\tau_{EC} = 0.001$ s; CH - Motion in initial section of free stream with length $l_{CH} = 0.05$ m for $\tau_{CH} = 0.0001$ s; 1 - Isothermal

motion when $R < 0.001$ mm; 2 - Adiabatic motion when $R > 0.1$ mm; 3 - Polytropic motion when $R = 0.01$ mm; 4, 4a - Isobaric motion

when $R = 0.01$ mm and $R = 0.1$ mm, respectively; HO - Motion of mixture in final section of free stream with length $l_{HO} = 10$ m

for $\tau_{HO} = 1$ s; 4c, 4d - Isobaric motion during $R = 1.0$ mm and

$R = 10$ mm, respectively; - - - - Boundary of gas phase expansion process behind nozzle from p_{HP} to p_0 .

following forms of discharge are possible:

a) polytropic ($n = 1.4 - \infty$) when $R = 0.01 - 0.1$ mm;

b) isochoric ($n = \infty$) when $R < 0.001$ mm.

3. In the free stream of the fluid mixture various forms of mixture motion are possible as a function of the value of R and the ratio between the time of intensive heat exchange τ_l and time (τ_H and $\tau_{H'}$) of the beginning and the end of heat exchange between phases.

Thus, for example, when $R \leq 0.01$ mm and $\tau_l > \tau_H$, the motion of the mixture in the stream flowing from the nozzle will occur without heat exchange between phases and without a change in the state of the gas phase ($p = \text{const}$, $t_g = t_H = \text{const}$) only when such motion is preceded by motion of the mixture in the nozzle under conditions of heat exchange between phases.

When $R = 0.01-10$ mm and $\tau_H < \tau_l < \tau_{H'}$, the motion of the mixture in the stream will occur with heat exchange between phases and with an expansion in the gas phase according to the isobaric law ($n = 0$). The time of gas phase thermal expansion will increase with an increase in gas bubble dimensions.

And, finally, when $R > 10$ mm and $\tau_l < \tau_H$, the motion of the mixture in the stream will occur without heat exchange and without a change in the state of the gas phase; however, with different temperatures for liquid and gas phases ($p = \text{const}$; $t_g = \text{const}$; $V_g = \text{const}$). Nevertheless, such motion must be preceded by motion of the mixture in the nozzle without heat exchange between phases.

The variation in gas phase parameters as a function of the dimensions of the gas bubbles in the mixture is presented in Fig. 3.

From this it follows that the dispersion of fluid flow has a substantial effect on heat exchange between phases and also on such parameters of gas phase as density and specific volume, which, during motion of the mixture and drop in its pressure because of hydraulic losses, change in the process of gas phase expansion. From this point of view, there is a significant difference between

microdispersed and macrodispersed fluid flows. This difference must be taken into account when setting up equations of flow motion which include the density and specific volume of the mixture.

Let us find the dependence of the specific volume of the fluid mixture v on pressure in the presence of heat exchange between phases. For this we shall write first the expression for the specific volume of a two-phase fluid mixture in the following manner:

$$v = V_{\text{in}} + V_{\text{r}} \quad (5)$$

where $V_{\text{in}} = \sum_{i=1}^{n_1} V_{\text{in}}^i = \text{const}$ and $V_{\text{r}} = \sum_{i=1}^{n_2} V_{\text{r}}^i = \text{const}$ are volumes of the incompressible liquid and compressible gas phase, respectively; $V_{\text{in}}^i, V_{\text{r}}^i$ are the elementary volumes of discrete elements of liquid and gas phase, respectively; n_1 and n_2 are the numbers of liquid and gas phase inclusions in 1 kg of the mixture. The per-volume contents of phases will be:

$$\beta_{\text{in}} = V_{\text{in}}/v; \quad \beta_{\text{r}} = V_{\text{r}}/v. \quad (6)$$

Taking expressions (5) and (6) for the volumes of liquid and gas phases in the mixture into account, we can write:

$$V_{\text{in}} = \beta_{\text{in}} v = \beta_{\text{in}}/\gamma = b = \text{const}; \quad (7)$$

$$V_{\text{r}} = \beta_{\text{r}} v = \beta_{\text{r}}/\gamma \neq \text{const}. \quad (8)$$

From expressions (5-8) after transformations it is easy to obtain formulas for specific volume of a two-phase fluid mixture with heat exchange between phases taken into account and as a function of the form of mixture motion.

The table gives the basic characteristics of various forms of motion for a two-phase fluid mixture and formulas are presented for determining the specific volume of the mixture as a function of the form of motion. From the expression for specific volume of the mixture during isochoric motion, it follows that, in this case, the flow is incompressible.

Analysis of the data presented in the table indicates that with different heat exchange intensities between phases and, consequently, with different thermodynamic laws of variation for the state of the gas phase in a moving mixture, density and specific volume of the mixture change as a function of the polytron indicator n . In connection with this, it is obviously expedient to call isobaric, isothermal, adiabatic, isochoric, and polytropic forms of fluid flow motion classes of motion and to study the properties of mixtures separately according to class.

Table. Formulas for the specific volume of a two-phase fluid mixture taking into account heat exchange between phases and the form of mixture motion.

Form of mixture motion and its characteristics	Formula for the specific volume of the mixture
Isobaric motion: $V_1/T_1 = \text{const}; p_1/T_1 = d = \text{const}$	$v = b + d/T_1$
Isothermal motion: $pV_1^{\gamma} = \text{const}; p_1/T_1 = e = \text{const}$	$v = b + e/T_1$
Adiabatic motion: $pV_1^{\gamma} = \text{const}; p_1/T_1^{\gamma} = f = \text{const}$	$v = b + f/p_1^{1/\gamma}$
Isochoric motion: $V_m = p_m/\gamma = b = \text{const}$ $V_r = p_r/\gamma = g = \text{const}$	$v = b + g = \text{const}$

Conclusions

The approximate method of calculating heat exchange between phases in the flow of a two-phase fluid mixture characterized by constancy of mass phase composition indicated that the dispersion of gas phase, to a considerable extent, affects intensity and duration of heat exchange between phases.

Depending upon the time of the beginning and end of heat exchange between phases in the flow of a mixture, the direction

of the thermal flux (from liquid phase to gas or vice versa), the velocity of mixture motion, and the length of the path of motion, there arise isobaric, isothermal, adiabatic, isochoric, and polytropic forms of mixture motions with various gas phase polytropic indicators ($n = 0-\infty$) and various densities and specific volumes for the mixture. This must be taken into account when setting up the motion equation for a fluid mixture.

BIBLIOGRAPHY

1. Кутателадзе С. С., Старикович М. А. Гидравлика газожидкостных систем. Госэнергоиздат, 1958.
2. Титов И. А. М. Техническая термодинамика. Госэнергоиздат, 1952.
3. Гужов А. Н., Медведев В. Ф. Исследование истечения газожидкостной смеси через цилиндрические насадки при критических параметрах. «Теплоэнергетика», № 8, 1966.
4. Михеев М. А. Основы теплопередачи. Госэнергоиздат, 1959.
5. Кутателадзе С. С., Боршанский В. М. Справочник по теплопередаче. Госэнергоиздат, 1959.

THE DYNAMICS OF THE LIQUID BOILING PROCESS IN A FLOW WITH A LARGE PRESSURE GRADIENT

V. A. Zysin and V. A. Barilobich

Abbreviations

np - limiting
H - nozzle
кр - critical
кр.с - critical wall
кр.ц - critical central
np - counterpressure
cp - exit

The discharge of a liquid having an initial temperature near saturation temperature is accompanied by steam formation the intensity of which can significantly exceed the intensity caused by the presence of heat exchange. The process acquires an adiabatic character.

Although the actual process is always accompanied by a disruption of thermal equilibrium, an explanation of the basic regularities of discharge can be obtained from a thermodynamic analysis. In the case of the discharge of a saturated liquid,

boiling must occur with an infinitely small pressure drop, i.e., at input to a convergent nozzle. With underheating of the liquid to saturation temperature the boiling front is shifted downstream. At a certain underheating this front agrees with the minimum cross section of the nozzle. The corresponding regime can be called the "limiting" regime. This regime is characterized by the agreement of the boiling front with the critical cross section, with which vapor formations can develop only in the expanding part of the channel. In the case of a reversible process behind the boiling front the flow must be supersonic. For these conditions, disregarding gravitational forces, we can determine by thermodynamic analysis the velocity in front of the boiling front which responds to the "limiting" regime.

$$w_{np} = \left[\frac{(v')^2 p_0}{v''(v'' - v') c' T_s} \right]^{0.5} \quad (1)$$

Hence we find the corresponding initial underheating

$$\Delta t_{np} = \left[\frac{v' p_0}{v'' c'} \right]^2 \frac{1}{2 T_s} \quad (2)$$

The parameters of the state in (1) and (2) refer to the initial flow state.

In the framework of the assumption made at $\Delta t \geq \Delta t_{np}$, which is characteristic for many technical problems, the flow rate through a nozzle of any shape must be determined by the simple relationship:

$$G = F_H \left[\frac{2(p_0 - p_s)}{v''} \right]^{0.5} \quad (3)$$

where F_H is the area of the minimum cross section; p_0 is the stagnation pressure in front of the nozzle; p_s is the saturation pressure with the temperature at input.

Experience shows that when counterpressure $p_{np} \ll p_s$, the actual flow rate can be substantially different from the values

given in (3). The available data of theoretical analysis does not enable generalization of test material. Therefore, for practical calculations it was proposed to use purely empirical relationships which were far from covering the necessary areas of application.

After thermodynamic analysis taking into account the phenomena occurring in the boundary layer, it was possible to establish a diagram of the process explaining the character of the principal regularities and giving a basis for generalizing test data. According to this diagram, substantiated by special visual observations, with a sufficient pressure drop vapor formation occurs in the convergent part of the channel. However, it is developed in that region of the boundary layer where the velocity does not exceed the quantity from equality (1). Conditions for the limiting flow regime are determined by the local value of full stagnation pressure. Based on this, at "limiting" and "superlimiting" flow regimes, when pressure drop exceeds critical, in the convergent part of the nozzle there occurs a two-layer flow: a two-phase boundary layer and a liquid central layer. At output into unlimited space there occurs a boiling of the central part of the flow and in the free stream a critical section is formed. With discharge from a Laval nozzle with a sufficiently small angle of taper, the expanding section is maintained, apparently a two-layer flow structure; this leads to a very unique character for the discharge process. The peripheral flow, passing into the minimum section through a region of local speed of sound, has a pronounced supersonic character. In the central flow in the expanding part of the channel vaporization occurs. However, this process is limited by the change in channel cross section. Figure 1 shows the distribution of pressure along the axis of the Laval nozzle with various counterpressures and during the discharge of water with constant initial parameters. In all cases, from the point of view of gas dynamics, the discharge regime was supercritical - flow rate remained constant. This is

confirmed by the constant character of pressure distribution up to the minimum cross section of the nozzle. Meanwhile final pressure in the nozzle was dependent on counterpressure. The nozzle's angle of taper affects the value of critical pressure in the minimum section and, as a consequence of this, also affects the flow rate characteristic of the nozzle. A group of studies on the discharge of superheated water in channels of various shapes were made on a special stand. In addition to measuring flow rates and pressure distributions along the channel axis, it was possible to directly measure the reaction of the stream, which enabled us to determine the average discharge rate.

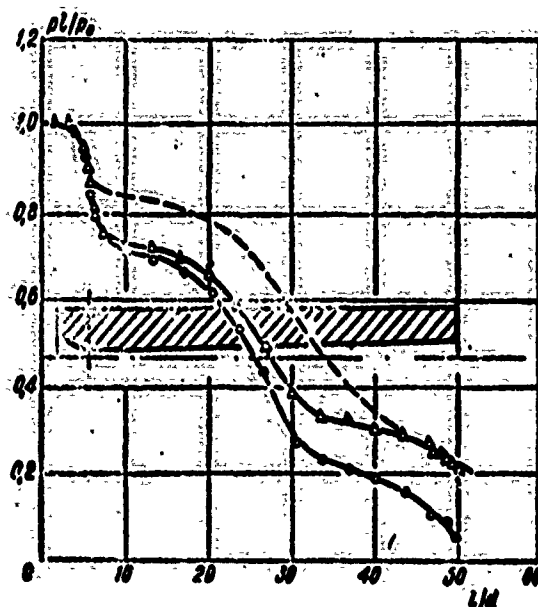


Fig. 1. Pressure variation along a Laval nozzle:
 - - - reversible isentrope.

The most comprehensive generalized characteristics were obtained for cylindrical nozzles. It was possible to establish that there is a certain dimensionless length for the cylindrical part at which the entire vaporization process, up to the blocking of the flow, develops inside the channel. Fittings whose length exceeds the corresponding dimensions are self-similar relative to

the geometry of the channel. Test data for such "long" fittings could be generalized, using the following as the determining criterion

$$K = \frac{r}{\Delta t}, \quad (4)$$

where Δt is the initial underheating of the water up to boiling point.

The results of processing experimental data are presented in Fig. 2. In the tests, initial temperature was varied from 120-170°C and counterpressure from 0.1 to 0.15 bar.

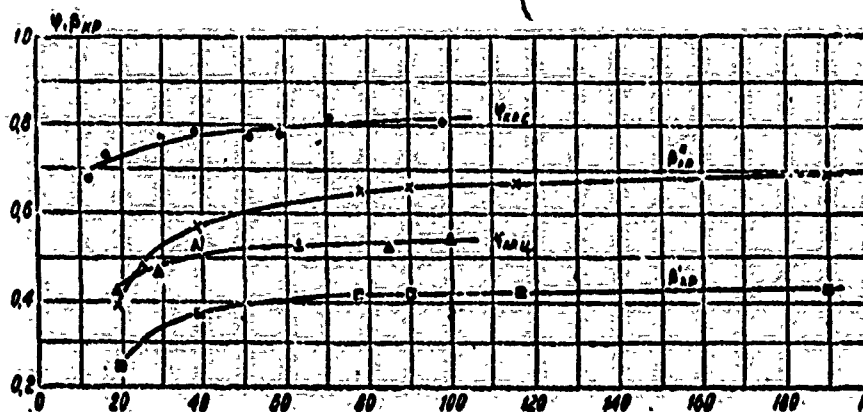


Fig. 2. Generalization of the discharge curve for "long" cylindrical fittings.

Here two critical pressure ratios β_{kp}' and β_{kp}'' are presented. The quantity β_{kp}' determined according to the counterpressure p_{np} at which the following condition was fulfilled:

$$\frac{\partial p_{cp}}{\partial p_{np}} = 0, \quad (5)$$

where p_{cp} is the pressure measured in front of the exit of the output channel section.

The quantity β_{kp}'' was determined according to the counterpressure at which

$$\frac{\partial G}{\partial p_{np}} = 0, \quad (6)$$

where G is the measured flow rate.

We should emphasize that the tests showed the practical impossibility of directly measuring critical pressure in front of the exit. This is explained by the large pressure gradient occurring in the peripheral two-phase flow in front of the blocking front. This agreement between the values of β_{kp}' and β_{kp}'' is found in accordance with the above considerations concerning the mechanism of flow from a Laval nozzle.

By measuring the stream reaction it was possible to determine the average discharge velocity at supercritical regime when flow rate and pressure at the exit was adjusted to depend on the counterpressure; then the velocity factor $\phi_{kp,u}$ was determined from expression

$$\phi_{kp,u} = \frac{w_a}{[2(i_0 - i_{kp})]^{0.5}} \quad (7)$$

Here w_a is the discharge velocity measured according to stream reaction; i_{kp} is enthalpy during isentropic expansion from the initial state (with enthalpy i_0) to the final state p_{kp} .

Pressure p_{kp} was determined from expression:

$$p_{kp} = \beta_{kp}' p_0 \quad (8)$$

As we see, the discharge process is characterized by considerable irreversibility, which is indicated by the very low values of $\phi_{kp,u}$. The degree of irreversibility increases severely with an increase in the initial underheating up to boiling point.

The character of pressure distribution along the output section of a cylindrical channel indicated a sufficiently close agreement with theoretical calculations based on a model of one-dimensional flow. This enables us to assume that mutual phase slippage, to which many authors give a high value, is virtually absent; consequently, the chief factor in the nonequilibrium of

the process must be the difference in the temperatures of liquid and vapor phase. An indirect substantiation of this assumption is the sharp increase in process reversibility with a change from cylindrical fittings to Laval nozzles.

Figure 2 shows the curve of the velocity factor for a Laval nozzle with a taper angle of $\alpha = 4^\circ 28'$, determined from an expression similar to (7), where instead of i_{kp} the value of i_{np} was substituted (i_{np} is the enthalpy during isentropic expansion up to a given counterpressure).

CLASSES OF MOTION FOR A TWO-PHASE
DISPERSED FLOW WITH HEAT EXCHANGE
BETWEEN PHASES

N. I. Malofeyev

Designations

- β - phase content per unit volume;
- h - thickness of liquid layer;
- d - diameter of gas sphere;
- R - radius of gas sphere;
- t or T - temperature in $^{\circ}\text{C}$ or $^{\circ}\text{K}$;
- τ - time;
- p - pressure;
- w - velocity;
- G - flow rate;
- V - specific volume;
- γ - specific weight;
- ρ - density;
- g - acceleration of gravity;
- Ω - cross-sectional area of flow;
- z - geometric head;
- v_* - critical pressure ratio;
- α - ratio of phase contents per unit volume;
- n - polytropic index;

k - adiabatic index;
D - diameter of piping;
L - length;
 μ - coefficient of dynamic viscosity.

Subscripts

г - gas;
ж - liquid;
о - atmospheric conditions;
с - in front of nozzle;
* - in critical cross section;
н - beginning;
к - end, convection;
т - heat exchange;
пр - limiting
из - isothermal
ад - adiabatic;
тр - friction.

In ship building, rocketry, power engineering, the petroleum and chemical industries, various systems are used with two-phase fluid working media moving in an emulsion regime with constant weight composition of phases [1, 2, 3]. Among these media are all fluid dispersed media: air-water emulsions; helium-nitrogen mixtures; flotation, carbon dioxide-water, and mechanical air foams.

In these two-phase flows both phases are far from critical states as well as from states corresponding to phase transition. With a high degree of flow dispersion, which can be ensured by free or forced dispersion methods, there is no relative phase slippage. In the presence of surface-active substances the flow structure is the most balanced and stable.

The absence of successive methods for calculating dispersed fluid flows has meant that, until recently, a calculating device of the hydraulics of incompressible dropping fluids has been used when calculating air-foam systems for ships [2].

With the aim of developing a methodology for the hydraulic calculation of such systems, the author has performed analytic and experimental studies on the processes of motion in a two-phase dispersed flow in pipes, nozzles, and free stream.

The study was made taking into account the compressibility of the two-phase flow, the effect of dispersion on heat exchange between phases, the transformation of phase structure, and the presence of critical parameters which arise during the discharge of a two-phase flow and affect the dynamics of the free stream.

Structural analysis of a two-phase flow has shown that dispersed flow has two flow regions: free-dispersed and connected-dispersed. In free-dispersed flow the gas spheres are not connected to each other and are in a free-suspended state. The initial shear stress, in this case, is zero. In connected-dispersed flow the gas bubbles in the form of polyhedrons with thin films, are connected to a common structural frame which has a certain rigidity (elasticity of shape), because of which the initial shear stresses reach considerable values. The mutual transition of free-dispersed and connected-dispersed flows occurs at a liquid film thickness of $h \approx 0.01$ mm. The value of limiting gas content per unit volume, at which this transition sets in with a given dispersion is determined by expression:

$$\beta_{cr} = \frac{\tilde{n}(1 + \sqrt{2})}{12(1 + \frac{\tilde{n}}{2})^3} \quad (1)$$

The boundary separating the regions of free-dispersed and connected-dispersed motion for a two-phase flow is presented in Fig. 1.

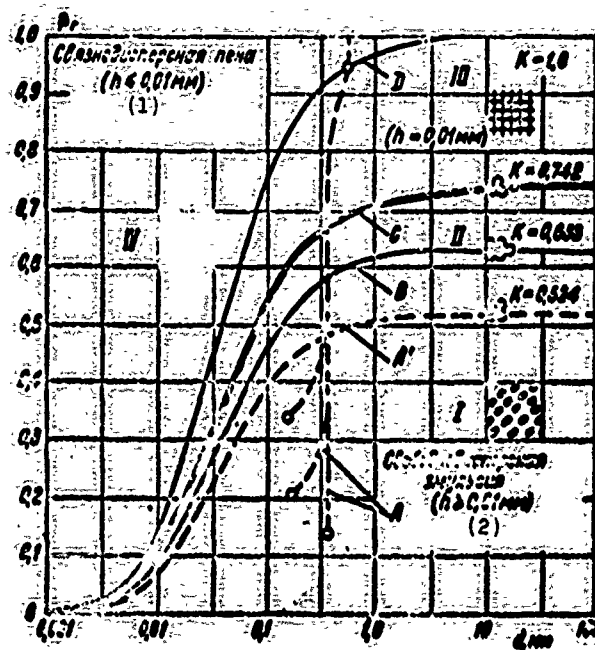


Fig. 1. Regions of free-dispersed and connected-dispersed fluid flow:

A - Curve of gas content variation for emulsion during expansion of gas spheres or phase stratifications;
 B - Curve of gas content for emulsion, corresponding to the beginning of the process of gas sphere recombination at $h = 0.01$ mm; C - Boundary of regions of free-dispersed emulsion and connected-dispersed foam ($h = 0.01$ mm);
 D - Curve of gas content for foam when $h = 0.01$ mm;
 I - Zone of free arrangement of gas spheres in emulsion; II - Zone of gas sphere recombination; III - Zone of gas sphere deformation into polyhedrons; IV - Coagulation zone of foam bubbles and syneresis.
 KEY: (1) Connected-dispersed foam; (2) Free-dispersed emulsion.

A two-phase dispersed flow in the presence of surface-active substances and structural stabilizers is an elastic-porous medium, capable of multiple expansion-contraction without disruption and coagulation of gas spheres. The mass of each separately taken gas bubble during its expansion-contraction is constant and thermodynamic laws of change of state can be applied to it [4].

Heat exchange between phases occurs in the case of a difference in their temperatures or a change in the thermodynamic

state of gas phase during the motion of a two-phase flow with a pressure drop and is nonstationary. In this case, the connection between time and spatial temperature variations at any point of the moving gas medium is determined by the Fourier-Kirchhoff differential equation of heat conductivity [5].

Since most gases and airs are diathermic, radiant heat exchange between phases was not taken into account. The convection of gas phase inside a sphere with a dimension of less than 50 mm was also disregarded since, for these conditions, the product of the Grashof number

$$Gr = 3 \frac{R^2}{\nu^2} \Delta t, \quad (\Delta t = \frac{p - p_0}{\rho \beta})$$

and the Prandtl number

$$Pr = \frac{\nu}{\alpha} \quad (\text{for air } Pr = 0.722)$$

is

$$GrPr < 10^3$$

and the convection factor is $\epsilon_H = 1.0$.

The gas sphere inside the small sphere can thus be assumed immobile. Under this condition, the convective temperature change in the Fourier-Kirchhoff equation is zero and acquires the form of the Fourier equation as in the case of a solid. For discrete elements of gas phase having the shape of a sphere, it assumes the form:

$$\frac{\partial t}{\partial \tau} = a \left(\frac{\partial^2 t}{\partial r^2} + \frac{2}{r} \frac{\partial t}{\partial r} \right). \quad (2)$$

On the basis of the second theorem of thermal similarity (Buckingham's theorem), the unknown function in the form of dimensionless temperature was determined as a function of the Biot number $Bio = \alpha R / \lambda$ and the Fourier number $Fo = \alpha \tau / R^2$. Given the different value for the gas bubble radius R and the time of its heat exchange τ , we obtained the values of Bio and Fo , with

which, based on data from [5], we determined the values of $\frac{p}{p_0}$ and $\frac{T}{T_0}$. With identical values for dimensionless temperatures, a graphic relationship was plotted for heat exchange time and gas phase-air dispersion, $\tau = f(R)$, which is presented in Fig. 2 for conditions $p_0 = 1 \text{ atm (abs.)}$, $t = 20^\circ\text{C}$. Assuming that the parameters of gas phase p , γ , R , a , and λ , as well as the Bi_0 and Fr numbers, change along the flow line, the heat exchange time was corrected by expression:

$$\tau(p, T) = k \frac{p}{p_0} \tau(1 \text{ atm}, 20^\circ\text{C}) \quad (3)$$

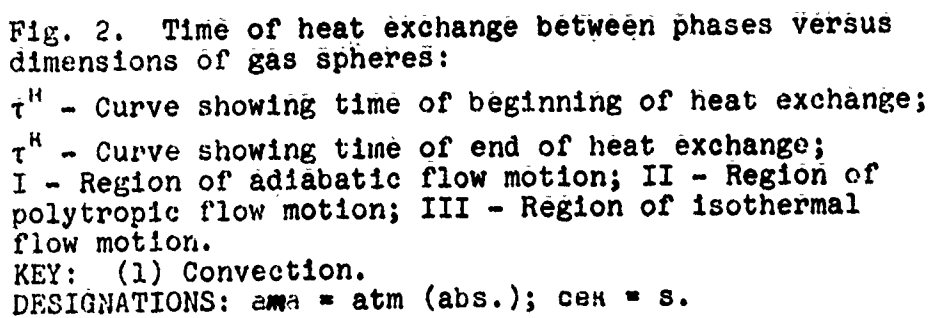
[$1 \text{ atm} = \text{atm (abs.)}$]

where k is the coefficient taking into account temperature variation; p/p_0 is the correction factor taking into account pressure variation in accordance with the first theorem of thermal similarity (Newton's theorem).

Then the time for heat exchange between phases τ_f was compared with the time for the process of two-phase flow motion τ on various sections of the path (pipe, nozzle, stream).

If the time of flow motion τ was less than the time τ_f^H , the beginning of intensive heat exchange between phases, the flow was considered adiabatic ($n = k = 1.4$); if the time for flow motion τ was greater than the quantity τ_f^H but less than the quantity τ_f^H , the time of the end of the heat exchange process between phases, the flow was assumed polytropic ($n = 0-\infty$). If the time of motion of the flow was greater than the quantity τ_f^H , the flow was assumed to be isothermal. When conditions $p = \text{const}$ or $V_f = \text{const}$ were applied, the polytropic process was a particular case of the isobaric or isochoric variations in the state of the gas phase.

This analysis enabled us to distinguish narrower, but sufficiently typical with respect to physical conditions, classes of two-phase flow motion: isobaric, isothermal, adiabatic, and isochoric, for which it was possible to perform mathematical



analysis and derive equations of motion. For the purpose of deriving equations of motion, a number of assumptions were made and the flow itself was taken as a simplified model.

The motion of the flow was considered steady and continuous. Dispersed flow with surface-active substances reducing the surface tension of liquid phase was assumed thermodynamically stable and balanced, i.e., the arbitrary separation of liquid and gas phases under the effect of surface forces and gravity was excluded. The diffusion of gas into liquid and the evaporation of liquid into gas were ignored because of their insignificance, while the weight composition of phases was assumed constant. In addition, we did not take into account the jump in pressure on the phase interface, which, according to the Laplace equation [6] did not exceed 1-2% of the pressure in liquid phase.

In deriving equations of motion for an ideal two-phase flow, the assumption was made that forces of friction and tangential stresses were zero, i.e., there was no dissipation of energy in either phase and the velocity of particle motion at all points of any arbitrarily taken section was identical.

The actual two-phase flow with high phase dispersion was considered a quasihomogeneous flow, whose viscosity and tangential stresses for both phases which were identical, while the density and velocity gradient were continuous functions of the coordinates.

The motion of free-dispersed and connected-dispersed flows was assumed to be translational, nonrotational, or potential.

From the assumptions made it follows that the model of ideal two-phase dispersed flow is similar to the model of steady potential ideal single-phase compressible flow, and a system of combined differential equations with partial derivatives, consisting of

Euler equations, equations of continuity, and the relationship between flow density and pressure, can be applied to it. Integration of the differential equations with the substitution of the dependence of density on pressure gives the following equations of motion for a single-dimension two-phase flow:

$$n=0; (p=\text{const}); \quad \omega_* \Omega_* = \omega_c \Omega_c \frac{1 + \frac{T_r}{T_c}}{1 - \frac{T_r}{T_c}}; \quad (4)$$

$$n=1,0; (T_r=\text{const}); \quad z + \beta_* \frac{p}{\gamma} + \beta_* \frac{p}{\gamma} \ln p + \frac{w^2}{2g} = \text{const}; \quad (5)$$

$$n=k=1,4; (S=\text{const}); \quad z + \beta_* \frac{p}{\gamma} + \beta_* \frac{k}{k-1} \frac{p}{\gamma} + \frac{w^2}{2g} = \text{const}; \quad (6)$$

$$n=\pm\infty; (V_r=\text{const}); \quad z + \frac{p}{\gamma} + \frac{w^2}{2g} = \text{const}. \quad (7)$$

With the use of equations (4), (5), (6), and (7), we analyzed the process of the discharge of a two-phase flow from conical nozzles, which showed that during the discharge of a fluid flow from nozzles there is a critical barrier which is established in a narrow (critical) section of the nozzle owing to the presence of gas phase.

During the critical discharge of a two-phase fluid flow, the discharge velocity, maximum weight-per-second flow rate, and critical pressure ratio are functions of the gas content per unit volume of the flow (or the ratio of phase content per unit volume).

For example, with isothermal discharge of a two-phase dispersed flow (with gas sphere dimensions $R \leq 0.01$ mm), these parameters are determined from the following expressions:

$$w_*^2 = [2g \left\{ \beta_* (1 - v_*) - 2.3 \beta_* \lg v_* \right\}]^{0.5} \sqrt{\rho_c v_c}; \quad (8)$$

$$G_* = \Omega_* \left[2g \frac{\beta_* (1 - v_*^2) - 2.3 \beta_* \lg v_*}{\left(\beta_* + \frac{\beta_*^2}{v_*} \right)^2} \right]^{0.5} \sqrt{\frac{\rho_c}{v_c}}; \quad (9)$$

$$v_*^2 + 4v_* + 4.6 \beta_*^2 \lg v_* - v_c^2 - 2v_c = 0; \quad (10)$$

$$\frac{2v_*}{v_c} - [1 + 1.2 \beta_*^2 (1 + 4.6 \lg v_*)] = 0. \quad (11)$$

With adiabatic discharge of a two-phase dispersed flow (with gas sphere dimensions $R \geq 0.1$ mm), the critical parameters are determined by the following expressions:

$$w_{*c}^0 = \left[2g \left(\beta_{*c}^0 (1 - v_{*c}) + \beta_{*c}^0 \frac{k}{k-1} \left(1 - v_{*c} \frac{k-1}{k} \right) \right) \right]^{0.5} \sqrt{p_c v_c} \quad (12)$$

$$G_{*c}^0 = 2g \left[\frac{\beta_{*c}^0 (1 - v_{*c}) + \beta_{*c}^0 \frac{k}{k-1} \left(1 - v_{*c} \frac{k-1}{k} \right)}{\left(\beta_{*c}^0 + \beta_{*c}^0 \frac{1}{v_{*c} \frac{k-1}{k}} \right)^2} \right]^{0.5} \sqrt{\frac{p_c}{v_c}} \quad (13)$$

$$k \frac{k-1}{k} + 2\beta_{*c} (k+1) v_{*c} + k \beta_{*c}^2 \frac{k-1}{k-1} v_{*c} \frac{k-1}{k} - 2\beta_{*c} \left(1 + \frac{k \beta_{*c}}{k-1} \right) = 0; \quad (14)$$

$$\frac{1}{\beta_{*c} v_{*c}} + \frac{k}{k-1} \cdot \frac{1}{v_{*c} \frac{k-1}{k}} - \left[\frac{k}{2\beta_{*c}^2} + \frac{k-1}{\beta_{*c}} + \frac{k}{2} \cdot \frac{(k-1)}{(k-1)} \right] = 0. \quad (15)$$

Analysis of the discharge formulas indicates that the maximum possible absolute values for discharge velocity and flow rate occur with isochoric discharge of a two-phase flow with heat drain from gas phase to liquid, and the minimum values occur during isobaric discharge of a two-phase flow with heat transition from liquid phase to gas. The first case can occur under the corresponding conditions for discharge in nozzles of American rocket engines operating on liquid and gas nitrogen (or gas helium), because of which the maximum possible thrust is ensured with minimum engine size [3].

Isothermal and adiabatic discharges of a two-phase flow occur in domestic air-foam systems, with which the critical velocity and flow rate in the case of isothermal discharge with heat transition from liquid phase to gas is less than in the case of adiabatic discharge without heat exchange between phases.

These facts are explained by the value of critical counter-pressure established in the nozzle outlet. In the isobaric discharge process $v^* = p_* p_c = 1.0 = \max (\beta_r^c = 1.0)$; in isothermal

$v_* = 0.607$; in adiabatic $v_* = \left(\frac{2}{k+1}\right)^{\frac{k-1}{k+1}}$ ($v_* = 0.528$ for air); in isochoric $v_* = 0$ (during discharge into a vacuum). Thus, the critical parameters during the discharge of a two-phase flow (velocity w_* and flow rate G_*) are determined not by the value of the available potential energy of two-phase flow, but by the value of counter-pressure or the value of critical pressure ratio, which depends upon thermal flux and its direction between phases (from gas phase to liquid or liquid phase to gas).

An experimental study on the motion of real, i.e., viscous two-phase dispersed, flow showed that in the discharge formulas (8), (9), (12), and (13), derived for ideal flow, it is necessary to introduce the flow rate factor $\psi = 0.93-0.96$, which takes into account losses from friction during the discharge of a viscous two-phase flow from conical nozzles.

During isothermal motion of a viscous two-phase dispersed flow in pipes with heat transfer from liquid phase to gas, hydraulic losses can be determined by solving transcendental equations having the form:

$$\frac{(p_n - z_0 p_0)^{nm+1}}{nm+1} - a_0 p_0 \frac{(p_n - z_0 p_0)^{nm}}{nm} - \frac{(p_n - z_0 p_0)^{nm+1}}{nm+1} + \\ + z_0 p_0 \frac{(p_n - z_0 p_0)^{nm}}{nm} = \frac{k_{1p} (k+1)^{-1} (a_0 p_0)^{nm} (w_n \gamma_n)^{3-n}}{2gD^{m+1} (\gamma_n + a_0 \gamma_0)} \Delta l. \quad (16)$$

This equation is obtained by integration of expression

$$-\frac{dp}{dl} = \lambda \frac{w^2}{2gD} \gamma, \quad (17)$$

in which the quantities λ , w , and γ are defined as functions of gas content per unit volume, depending on the absolute value of pressure and changing along the line of flow.

The quantity λ was expressed in terms of variables w , γ , and μ :

$$\lambda = \frac{k_{1p}}{\left(\frac{w}{g\gamma}\right)^m}, \quad (18)$$

where the coefficient of dynamic viscosity μ is connected with the value of gas content per unit volume by functional relationship

$$\mu = k_3 \beta^n \quad (19)$$

Based on the data from an experimental study by the author, the coefficients in equation (16) and formulas (18) and (19) are: $k_{rp} = 64$; $m = 1$; $k_\mu = 0.005$; $n = 2.22$ (when $\beta_r \leq 0.35$); $k_\mu = 0.0126$; $n = 3.24$ (when $\beta_r \geq 0.35$).

The study of isothermal motion of a viscous two-phase flow in pipes, the adiabatic and isothermal discharge processes, and the isobaric motion of a two-phase flow in free stream enabled the author to obtain the relationship necessary for the hydraulic calculation of air-foam systems.

Conclusions

1. It is shown that equations of motion and the relationship between parameters of isobaric, isothermal, adiabatic, and isochoric two-phase flows are varied and in the absence of heat exchange between the ambient medium and the flow and in the absence of phase transition of components, are determined by the thermodynamic law of variation for the gas phase state, which, in turn, depends upon the value of thermal flux and its direction (from gas to liquid or from liquid to gas).

2. It is established that the value of thermal flux depends upon gas phase dispersion.

3. Thermal energy, changing from liquid phase to gas, increases the available energy of two-phase flow and reduces the critical discharge velocity and flow rate. Thermal energy, changing from gas phase to liquid, reduces the value of available energy and increases the critical discharge velocity and flow rate.

4. Critical parameters of two-phase flow during discharge (pressure ratio v_* , velocity w_* , and flow rate G_*) depend on the direction and values of thermal flux and, finally, on the dispersion of gas phase (gas sphere radius R).

BIBLIOGRAPHY

1. Александров А. В. Судовые системы. Судпромгиз, 1962.
2. Андреева Д. А. [и др.]. Собранные средства тушения пожаров на судах во ду и по... Изд-во «Морской транспорта», 1960.
3. Ризз Б., Ризз Л. Равновесие между фазами в сеплах. Латвия. Сб. статей под ред. С. С. Пейтера и Ф. А. Уильямса «Детонация и двухфазное течение». М., Изд-во «Мир», 1966.
4. Лавин А. М. Техническая термодинамика. Госэнергоиздат, 1947.
5. Александров В. Л. Техническая гидромеханика. Гостехиздат, 1964.
6. Кузнецов С. С. и Стирикович М. А. Гидравлика газожидкостных систем. Госэнергоиздат, 1958.
7. Михеев М. А. Основы теплопередачи. Госэнергоиздат, 1947.

DYNAMIC CHARACTERISTICS OF A COUNTERFLOW HEAT EXCHANGE APPARATUS

V. I. Kochurov and N. I. Tarakanov

Abbreviations

ex - input

exx - output

Heat exchangers have found wide application in modern power installations.

The dynamic properties of a heat exchanger which is an element in an overall control system can substantially affect the dynamics of the automated object. The knowledge of dynamic characteristics of heat exchangers is necessary when designing automatic control systems for power installations.

A characteristic peculiarity of heat exchangers is the considerable effect of parameter distribution on the nonstationary processes of heat transfer. This situation, to a considerable extent, makes it difficult to obtain the analytical dynamic characteristics of the equipment. Even after the necessary simplifications, the dynamics of a heat exchanger are described

by a system of differential equations in partial derivatives, whose solution leads to transcendental transfer functions. The use of such transfer functions in studying the dynamics of the object on analog modeling devices is not possible. Because of this, the problem is posed to obtain a simple approximate transfer function for a heat exchanger, which would allow us to determine its transient processes, taking into account the specifics of the physical processes occurring in the object with the necessary degree of accuracy.

Various methods for obtaining an approximate transfer function for a heat exchanger are possible [1, 2].

In this work we use an approximation of the initial transcendental transfer function of the heat exchanger with the application of a method of linear integral evaluation. The results of the solutions obtained are compared with experimental data compiled from a test of a laminated counterflow heat exchanger of the GTK-10 NZL gas turbine type.

A comparison of calculated and experimental dynamic characteristics makes it possible to establish the admissibility of the solutions obtained.

Let us examine a counterflow heat exchanger, whose structural diagram is presented in Fig. 1. Disturbing input actions are the temperature of the hot medium θ_{1BX} and the temperature of the cold medium θ_{2BX} at heat exchanger input; the output parameter is the temperature of the cold medium at heat exchanger output θ_{2BWX} .

In determining the components of the heat exchanger transfer functions

$$W_1(p) = \frac{\theta_{2BWX}(p)}{\theta_{1BX}(p)} \quad \text{and} \quad W_2(p) = \frac{\theta_{2BWX}(p)}{\theta_{2BX}(p)},$$

we make the following ordinary assumptions.

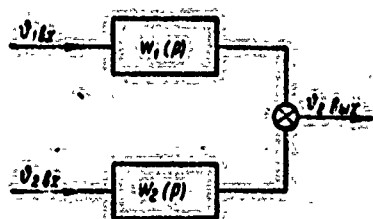


Fig. 1. Structural diagram of heat exchangers.

Let us assume that the physical constants of the working medium are constant, there is no temperature gradient or velocity gradient in the heat exchanger sections, and there is no heat exchange along the axis of the heat exchanger. We shall further assume that the heat exchanger is insulated and heat is transferred from the hot medium to the cold through a dividing wall. Also we assume that the heat exchange coefficients in the transient processes keep their values equal to the values during static regimes and do not depend on coordinates. Let us disregard the thermal inertia of the medium in the heat exchanger channels. We shall examine a single dimensional problem (the axis of the coordinate is directed along the dividing wall of the heat exchanger). Under these conditions, for the heat exchanger element we can set up the following system of equations for thermal balances:

$$\begin{aligned}\frac{\partial \theta_1}{\partial x} &= x_1 (\theta_3 - \theta_1); \\ \frac{\partial \theta_2}{\partial t} &= x_2 (\theta_1 - \theta_3) + x_3 (\theta_3 - \theta_2); \\ -\frac{\partial \theta_3}{\partial x} &= x_4 (\theta_3 - \theta_2),\end{aligned}$$

$$\text{where } x_1 = \frac{\alpha_1 F_1}{C_p G_1}, \quad x_2 = \frac{\alpha_1 F_1}{G_2 C_3}, \quad x_3 = \frac{\alpha_2 F_2}{G_2 C_3}, \quad x_4 = \frac{\alpha_2 F_2}{C_p G_1}.$$

Here θ_1 , θ_2 , θ_3 are the temperatures of the hot medium, cold medium, and dividing wall, respectively; x - relative coordinate ($0 \leq x \leq 1$); G - flow rate of medium; F - heat exchange surface; α - heat exchange factor; G_3 - weight of dividing wall; C_p - specific heat capacity of medium; C_3 - specific heat capacity of wall material. Subscript 1 corresponds to the hot medium and

subscript 2 to the cold. Applying the Laplace transform relative to the variable t at zero initial conditions: $\theta_1(x, 0) = 0$, $\theta_2(x, 0) = 0$, $\theta_3(x, 0) = 0$ and excluding $\theta_3(x, p)$, we find:

$$\frac{\partial \theta_1(x, p)}{\partial x} = A_1 \theta_1(x, p) + A_2 \theta_2(x, p);$$

$$-\frac{\partial \theta_2(x, p)}{\partial x} = B_1 \theta_1(x, p) + B_2 \theta_2(x, p);$$

where

$$A_1 = \frac{x_1 p + x_1 x_3}{p + x_2 + x_3}; \quad B_1 = \frac{x_1 x_2}{p + x_2 + x_3};$$

$$A_2 = \frac{x_1 x_2}{p + x_2 + x_3}; \quad B_2 = -\frac{x_1 p + x_1 x_3}{p + x_2 + x_3}.$$

Next we apply the Laplace transform relative to the variable x under the following boundary conditions:
when $x = 0$

$$\theta_{1,0}(t) \equiv \theta_1(0, p);$$

$$\theta_{2,0}(t) \equiv \theta_2(0, p);$$

when $x = 1$

$$\theta_{2,1}(t) \equiv \theta_2(1, p);$$

$$\theta_2(s, p) = \frac{(s - A_1) \theta_2(0, p)}{s^2 - (A_1 - B_2)s - A_1 B_2 - A_2 B_1} - \frac{B_1 \theta_1(0, p)}{s^2 - (A_1 - B_2)s - A_1 B_2 - A_2 B_1}.$$

Fulfilling the Laplace reverse transform, we obtain unknown transfer functions:

$$W_1^{-1}(p) = \frac{\theta_2(0, p)}{\theta_1(0, p)} = \frac{B_1(e^{s_2} - e^{s_1})}{e^{s_1}(s_2 + B_2) - e^{s_2}(s_1 + B_2)}; \quad (1)$$

$$W_2^{-1}(p) = \frac{\theta_2(0, p)}{\theta_2(1, p)} = \frac{s_2 - s_1}{(s_2 + B_2)e^{s_1} - (s_1 + B_2)e^{s_2}}, \quad (2)$$

where s_1 and s_2 are the roots of the characteristic equation:

$$s^2 - (A_1 - B_2)s - A_1 B_2 + A_2 B_1 = 0;$$

$$s_{1,2} = -\frac{B_2 - A_1}{2} \pm \sqrt{\frac{(B_2 - A_1)^2}{4} + A_1 B_2 - A_2 B_1}.$$

It can be shown that the transfer functions do not change under nonzero initial conditions if we consider deviations of temperatures from their values during the studied heat exchange regime.

With the aid of the transfer functions obtained we can determine the output parameter of the heat exchanger $\theta_{2\text{BX}}(t)$ under various disturbing effects $\theta_{1\text{BX}}(t)$ and $\theta_{2\text{BX}}(t)$. However, finding the analytical functional relationship between these parameters is very difficult as is the use of the dynamic characteristics obtained during the modeling of the transient processes of the heat exchanger. In order to obtain the ordinary transfer functions of the heat exchanger, we shall approximate expressions (1) and (2) of a transfer function of the simplest kind:

$$W^a(p) = \frac{T_2 p + k}{T_1 p + 1}.$$

The parameters of this approximate transfer function are found under the condition that $W^a(p)$ is equal to its exact value $W^m(p)$ at extreme values of p and that the linear integral evaluations are equal to the exact and approximate transfer function, i.e., from the following relationships:

$$\left. \begin{aligned} W^a(p) &= W^m(p); \\ W^a(p) &= W^m(p); \\ \frac{d}{dp} [W^a(p)]_{p=0} &= \frac{d}{dp} [W^m(p)]_{p=0}. \end{aligned} \right\} \quad (3)$$

Performing the necessary transformations according to equalities (3), we obtain approximate transfer functions of a counterflow heat exchanger:

$$W_1(p) = \frac{\theta_{1\text{BX}}(p)}{\theta_{1\text{BX}}(p)} = \frac{k_1}{T_1 p + 1}; \quad (4)$$

$$W_2(p) = \frac{\theta_{2\text{BX}}(p)}{\theta_{2\text{BX}}(p)} = \frac{T_2 p + k_2}{T_2 p + 1}. \quad (5)$$

The parameters of the transfer functions $W_1(p)$ and $W_2(p)$ are found from the following relationships:

$$k_1 = \frac{B_1^0(e^{s_2^0} - 1)}{A_1^0 - B_1^0 e^{s_2^0}}; \quad T_1 = \frac{k_1 N_1 - N_3}{B_1^0(e^{s_2^0} - 1)};$$

$$k_2 = -\frac{s_2^0}{A_1^0 + B_1^0 e^{s_2^0}}; \quad T_3 = e^{-s_2^0} T_2;$$

$$T_2 = -\frac{2(A_1^0 - B_1^0 e^{s_2^0})N_2 + s_2^0 N_4}{(k_2 - e^{-s_2^0})(A_1^0 - B_1^0 e^{s_2^0})^2}.$$

Here

$$A_1^0 = -\frac{x_1 x_2}{x_2 + x_3}; \quad B_1^0 = \frac{x_1 x_2}{x_2 + x_3}; \quad s_2^0 = A_1^0 + B_1^0;$$

$$N_1 = \frac{x_1 x_2 - x_1 x_3}{2(x_2 + x_3)^2}; \quad N_2 = \frac{(x_1 - x_2)^2 x_1 x_2 + x_1 x_2 (x_2 + x_3)^2}{2(x_2 - x_3)^2 (x_1 x_2 - x_1 x_3)};$$

$$N_3 = \frac{x_1 x_2}{(x_2 + x_3)^2} (1 - e^{s_2^0}) + (N_1 - N_2) B_1^0 e^{s_2^0} - (N_1 + N_2) B_1^0;$$

$$N_4 = (N_1 + N_2) (A_1^0 - e^{s_2^0}) + (N_1 - N_2) (1 + B_1^0 e^{s_2^0}) - \frac{x_1 x_2}{(x_2 + x_3)^2} (1 - e^{s_2^0}).$$

The approximate transfer functions obtained have been evaluated on a heat exchanger of the GTK-10 gas turbine type.

An experiment for taking the amplitude-phase frequency characteristics of a GTK-10 heat exchanger was carried out while it was operating in the gas turbine cycle. Therefore, from the experiment we could obtain the total frequency characteristic of the heat exchanger during the simultaneous action of two disturbances: with respect to $\theta_{1\text{BX}}$ and $\theta_{2\text{BX}}$.

The constants of the heat exchanger in the studied GTU operating regime had the following values: $\kappa_1 = 3.15$; $\kappa_2 = 46.9$ 1/h; $\kappa_3 = 53.3$ 1/h; $\kappa_4 = 3.90$.

In determining the constants, the heat exchange factors α_1 and α_2 were found by calculations, using the values for the heat transfer factor of the heat exchanger obtained from the experiment.

For the studied operating regime, the following approximate transfer functions were obtained for the heat exchanger:

$$W_1(p) = \frac{0.063}{115p + 1}; \quad W_2(p) = \frac{3.40p + 0.337}{165p + 1}.$$

Figures 2 and 3 present the calculated values for the amplitude-phase characteristics of the heat exchanger $W_1(i\omega)$ and $W_2(i\omega)$, plotted on the basis of exact and approximate transfer functions. As is apparent from the graph, the obtained approximate dynamic characteristics of the heat exchanger, in spite of their simple form, enable us to indicate very precisely the dynamics of the processes in a wide range of frequencies. Figure 4 illustrates the total frequency characteristics of the heat exchanger, obtained with the aid of expression

$$W(i\omega) = W_1(i\omega) + \frac{W_2(i\omega)}{W_1(i\omega)} W_2(i\omega).$$

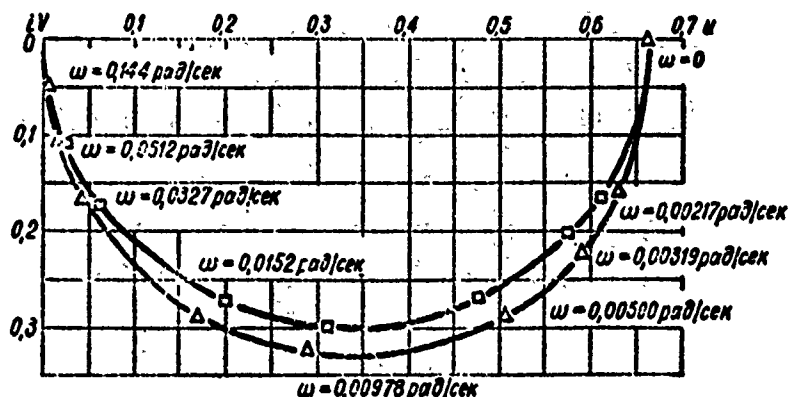


Fig. 2. Amplitude-phase characteristics with respect to the temperature of the cold medium at heat exchanger output and the temperature of the hot medium at input, with constant temperature of the incoming cold medium:

□ - Calculation according to transfer function $W_1^T(p)$, formula (1); Δ - Calculation according to transfer function $W_1^α(p)$, formula (4).
DESIGNATION: $\text{rad/sec} = \text{rad/s}$.

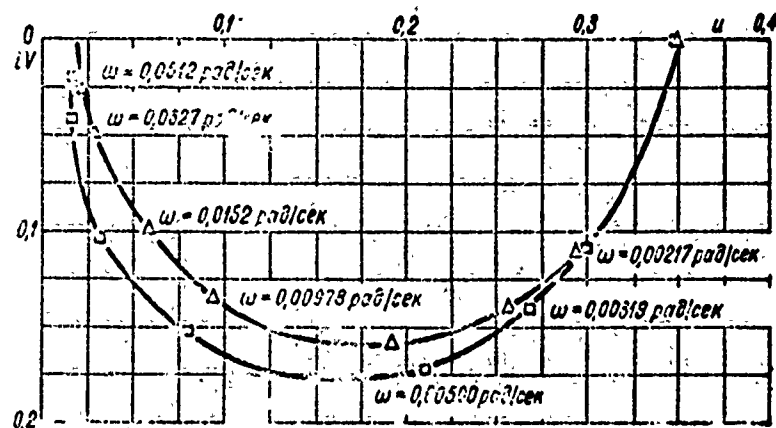


Fig. 3. Amplitude-phase characteristics with respect to the temperature of the cold medium at heat exchanger output and the temperature of the cold medium at input with constant temperature for the incoming hot medium:

□ - Calculation according to transfer function $W_2^T(p)$, formula (2); Δ - Calculation according to transfer function $W_2^\alpha(p)$, formula (5). [$\text{rad/s} = \text{rad/s}$]

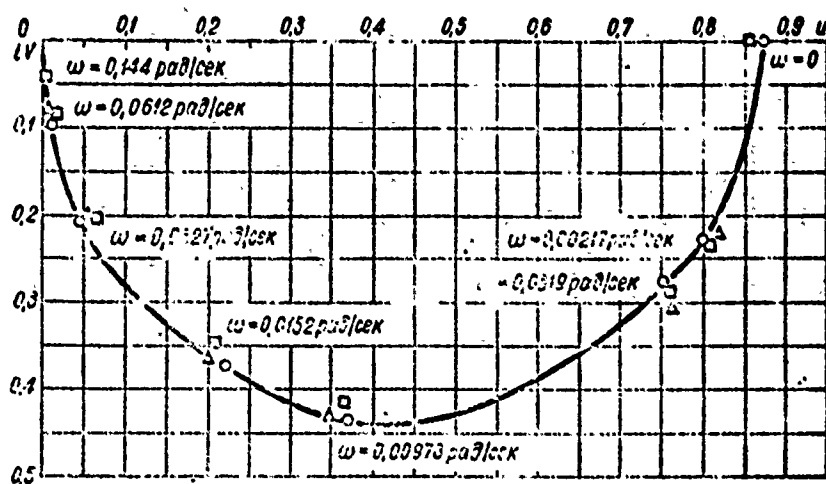


Fig. 4. Amplitude-phase characteristics with respect to the temperature of the cold medium at GTK-10 heat exchanger output and the temperature of the hot medium at input:

○ - Experiment; □ - Calculation according to transfer functions $W_1^T(p)$ and $W_2^T(p)$; Δ - Calculation according to transfer functions $W_1^\alpha(p)$ and $W_2^\alpha(p)$. [$\text{rad/s} = \text{rad/s}$]

The experimental frequency characteristic is also presented there. As follows from the graph, a good correspondence between calculated and experimental frequency characteristics is obtained. The values of exact and approximate frequency characteristics also agree well in the examined frequency range.

The results obtained indicate that the simple approximate transfer functions found can be used for determining the transient processes of heat exchangers.

BIBLIOGRAPHY

1. Девятков Б. Н. Теория переходных процессов в технических аппаратах с точки зрения теории управления. М.: Издательство СО АН СССР, 1964.
2. Девятков А. А., Яковлева Р. В. Упрощенные методы расчета динамических процессов в аппаратах. М.: Машиностроение, 1968.

THE SIMULATION OF WEAK GRAVITATIONAL FIELDS FOR STUDYING HEAT EXCHANGE DURING BOILING¹

B. I. Verkin, Yu. A. Kirichenko,
M. L. Dolgoiy, I. V. Lipatov,
and A. I. Charkin

Abbreviations

п - lift, bubble, flow
с - cohesion
и - inertia
отр - detached
кр - critical
пред - limiting
п кр - critical flux

The study of heat exchange processes in weak gravitational fields, the processes of boiling in particular, is a timely study in connection with the development of new fields of engineering.

Conditions of weightlessness and reduced gravitation (for studying hydrostatic and heat exchange phenomena, etc.) are usually

¹P. S. Chernyakov and V. L. Polunin also participated in this work.

accomplished in laboratories on installations equipped with containers freely falling under the effect of gravity [1, 2]. The main disadvantage of this type of installation is the extremely brief testing time, several seconds in the best of cases. Under these conditions it is very difficult to study processes occurring in liquids or in two-phase media, which require some stabilization in time, for example, heat exchange processes during boiling.

In the Low Temperature Physical Engineering Institute of the Academy of Sciences, USSR, methods have been developed for simulating the conditions of weightlessness and weak gravitational fields, making it possible to perform an experiment for as long a time period as desirable:

- simulation with the aid of a two-dimensional layer of liquid in thin containers and narrow slits;

- simulation with the aid of forces acting on a liquid magnet in a nonuniform magnetic field.

1. SIMULATING WEAK GRAVITATIONAL FIELDS WITH TWO-DIMENSIONAL THIN CONTAINERS¹

In the rather thin layer of liquid (or liquid-gas, liquid-vapor system) located in a narrow inclined slot, only the component of gravity directed along the slot will affect the hydrodynamics and heat exchange processes. In this case, in thin slots we can simulate the conditions of weak gravitational fields for processes occurring in them where the simulated acceleration of gravity g will be equal to (Fig. 1):

$$g = g_n \sin \varphi, \quad (1)$$

where $g_n = 9.81 \text{ m/s}^2$ is the normal acceleration of gravity; φ is the angle of slot slope to the plane of the earth's surface.

¹This method of simulation was proposed by A. D. Myshkis and Yu. A. Kirichenko.

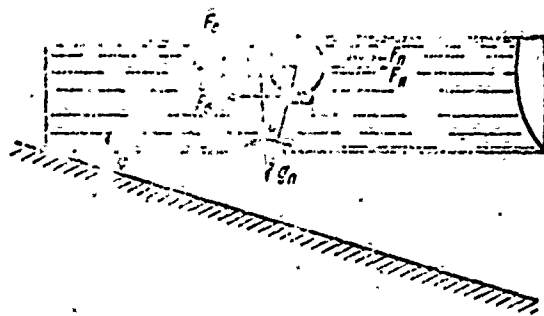


Fig. 1. Simulation of weak gravitational fields in thin containers:

F_n - Lift, acting on the bubble;
 F_c - Cohesive force between bubble and wall; F_d - Drag of liquid; F_μ - Inertia; F_δ - Surface tension.

It is convenient to conduct such studies in thin containers with transparent walls.

If the detached diameter of the bubble D_0 is compared with the distance between the side walls of the container δ so that

$$D_0 \approx \delta, \quad (2)$$

and the bubble touches the side walls at the moment of detachment, only the component of lift directed along the container will affect it. If tests are made with a heater (for example, a resistance heater), located an equal distance from the walls of the slot, the following conditions must be fulfilled:

$$D_0 > \frac{\delta}{2}. \quad (3)$$

For a correct study of boiling under simulation conditions it is necessary that the forces acting on the bubble be either the same as during boiling in a large volume for a weak gravitational field equivalent to that simulated or be small as compared with the simulated lift.

The following forces will act on the bubble at the moment of its detachment from the heater (see Fig. 1): lift F_n , inertia of the liquid F_μ , surface tension F_δ , drag F_d , surface adhesion between the bubble and the wall of the slot F_c . To evaluate the

applicability of the method, we shall find the ratio of forces F_u , F_δ , F_D and F_c to lift F_n :

$$\Pi_1 = \frac{F_u}{F_n}, \quad \Pi_2 = \frac{F_\delta}{F_n}, \quad \Pi_3 = \frac{F_c}{F_n}, \quad \Pi_4 = \frac{F_D}{F_n}. \quad (4)$$

We can see that when condition (3) is fulfilled, the forces acting on the bubble will have the following orders:

$$\left. \begin{aligned} F_u &\sim \frac{4\pi R_0^3 \rho}{\tau_0^2}; \quad F_\delta \sim 8\pi R_0 \sigma; \quad F_D \sim \frac{3\pi^2 R_0^3 \nu}{2\tau_0}; \\ F_c &\sim 4\pi R_0 \sigma (1 - \cos \gamma); \\ F_n &\sim \frac{4}{3} \pi R_0^3 \rho g_n \sin \varphi, \end{aligned} \right\} \quad (5)$$

where ρ is the density of the liquid; τ_0 is the time interval from the moment of bubble generation to its detachment; R_0 is the detached radius of the bubble; σ is the coefficient of surface tension; ν is the kinematic viscosity of the liquid; γ is the contact angle.

We shall designate in terms of R_n and τ_n the detached diameter of the bubble and the time interval between bubble generation and its detachment at $g = g_n$, using the dependence of R_0 on the acceleration of gravity [3]: $\frac{R_0}{R_n} = \left(\frac{g}{g_n}\right)^{\frac{1}{3.5}}$; assuming the detachment time τ_0 , in accordance with the formula of Pleset and Zwick from [4], to be $\tau_0 = \tau_n \left(\frac{g}{g_n}\right)^{-\frac{2}{3.5}}$, we obtain from (5):

$$\left. \begin{aligned} \Pi_1 &= \frac{3R_n}{\tau_n^2 g_n (\sin \varphi)^{1/7}}; \quad \Pi_2 = \frac{6\sigma}{R_n^2 \tau_n g_n (\sin \varphi)^{3/7}}; \\ \Pi_3 &= \frac{3\sigma (1 - \cos \gamma)}{R_n^2 \tau_n g_n (\sin \varphi)^{3/7}}; \quad \Pi_4 = \frac{9\nu}{8R_n \tau_n g_n (\sin \varphi)^{1/7}}. \end{aligned} \right\} \quad (6)$$

The first two expressions in (6) in order are the same as in a large volume [5] (assuming $g = g_n \sin \phi$) and are not needed in the evaluation. To evaluate Π_3 and Π_4 we assume $R_{\text{отр}} = \delta/4$. This is valid for the evaluation calculations of slots with a thickness

of several millimeters since the detached diameters of bubbles in a large volume for the working fluids we used (ether and water), according to published data [6] and the results of our test, are on the order of one millimeter and more. The detachment time was calculated from the formula presented in reference [4].

Given the values of the corresponding physical quantities and assuming $R_n = 0.5$ mm which corresponds to $\delta = 2$ mm, we obtain from condition $\Pi_3 < 1$ for ether and water on glass $\sin \phi < 10^{-3}$ and $\sin \phi < 10^{-4}$, respectively. The contact angle for ether is assumed to be $\gamma = 5^\circ$ and for water $\gamma = 1^\circ$. Evaluations obtained from condition $\Pi_4 < 1$ give even smaller values for $n = g/g_n = \sin \phi$. Thus, on thin slots the simulation of weak gravitational fields during boiling is possible up to overloading¹ on the order of $n = 10^{-3}$.

Experiments were made in thin transparent containers with a clearance width of 1.2-3 mm on ethyl ether, ethyl alcohol, and water. We studied the boiling crisis, as well as heat exchange during nucleate and film boiling on platinum resistance heaters 0.05-0.3 mm in diameter, located in the middle of the container and equal distance from its side surfaces. The heater served, at the same time, as a resistance thermometer. The container was placed in a thermostat in which constant temperature was maintained, near the saturation temperature of the studied liquid. Data on critical thermal fluxes are presented in Table 1 and on Fig. 2, where the solid line indicates the relationship $q_{hp}/q_{n\text{ }hp} = (g/g_n)^{0.25}$. Each point on Fig. 2 and in Table 1 is an average value of three measurements. Based on the results of approximately five hundred measurements of critical thermal fluxes in the overload interval $0 < n < 1$, the following relationship was found by the method of least squares:

¹The ratio of the simulated acceleration to the normal acceleration of gravity ($n = g/g_n$) will be called the "overload."

$$q_{cr} = q_{cr0} \left(\frac{g}{g_0} \right)^k, \quad k = 0.26 \pm 0.01. \quad (7)$$

Taking into account the earlier measurements made on nonthermo-stated containers (approximately 1000 measurements in all)

$$k = 0.24 \pm 0.01. \quad (8)$$

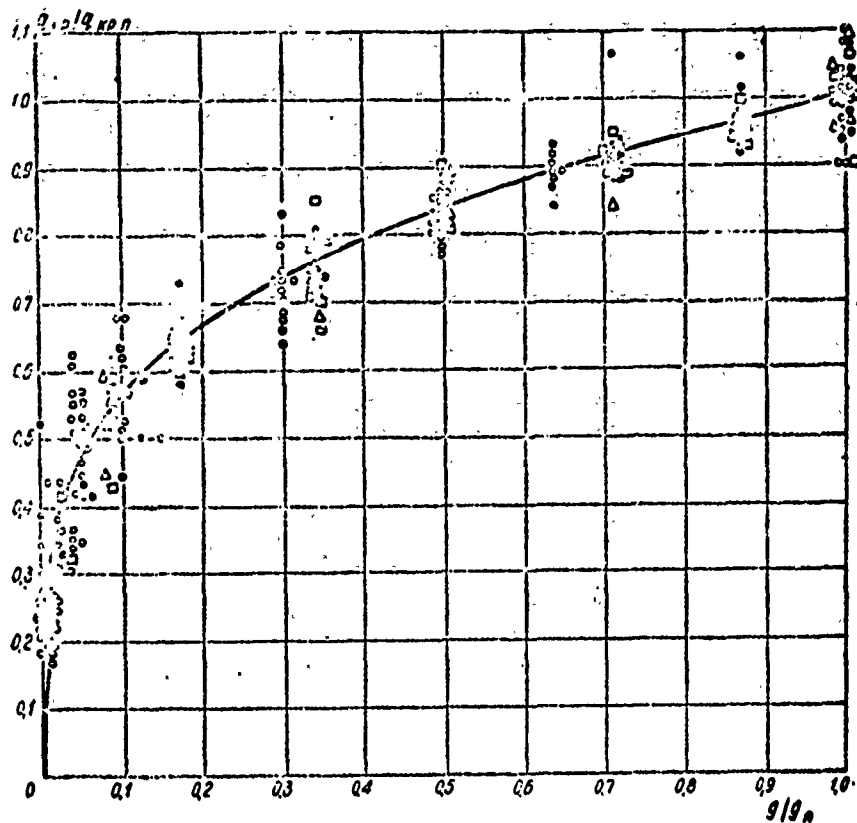


Fig. 2. Critical thermal flux versus modeled acceleration of gravity:
 O - Ether in thin containers; □ - Alcohol in thin containers; Δ - Water in thin containers; ○ - Oxygen in a magnetic field.

Thus, the obtained dependence of critical thermal fluxes on the acceleration of gravity agrees well with the familiar Kutateladze-Borishanskiy-Zubr relationships of the hydrodynamic theory of crises.

Table 1. Critical thermal flux in thermostated containers on platinum heaters.

№ пп	Толщина зазора, мм (1)	Диаметр нагревателя, мм (2)	Жидкость (3)	$q_{н\text{кр}} \cdot 10^{-5}$, Вт/м ² (4)	$q_{н\text{кр}} \cdot 10^{-5}$, Вт/м ² (4)	$\frac{q_{н\text{кр}}}{q_{н\text{кр}}}$	k
1	1,5	0,05	(5) Эфир	4,50	1,54	0,34	0,23
2	2	0,05	Эфир	4,43	2,47	0,56	0,23
3	2	0,05	Эфир	3,66	1,61	0,44	0,21
4	2	0,15	Эфир	3,44	1,51	0,44	0,28
5	2	0,15	Эфир	3,80	0,97	0,26	0,28
6	3	0,05	Эфир	4,91	2,20	0,45	0,285
7	3	0,05	Эфир	3,84	2,04	0,53	0,26
8	3	0,15	Эфир	4,10	0,97	0,24	0,29
9	3	0,15	Эфир	3,24	1,21	0,37	0,27
10	2	0,1	(6) Спирт	7,40	4,1	0,56	0,22
11	2	0,1	Спирт	6,15	2,74	0,44	0,25
12	3	0,15	Спирт	5,37	1,51	0,28	0,28
13	3	0,15	Спирт	5,36	1,68	0,31	0,30
14	1,2	0,1	(7) Вода	4,4	1,61	0,37	0,29
15	2,0	0,1	Вода	4,95	1,97	0,40	0,28
16	2,4	0,1	Вода	5,55	1,78	0,32	0,26
17	1,8	0,3	Вода	5,40	1,59	0,30	0,30
18	2,4	0,3	Вода	5,97	2,12	0,35	0,29
19	3,0	0,3	Вода	5,95	2,03	0,34	0,26
20	1,8	0,1	Вода	4,75	1,8	0,38	0,30

KEY: (1) Clearance thickness, mm; (2) Heater diameter, mm; (3) Liquid; (4) W/m²; (5) Ether; (6) Alcohol; (7) Water.

In the case of an underheated liquid, when condition (3) is not fulfilled, the index k in our tests was considerably less than 0.25.

The average value for relative critical thermal fluxes during weightlessness is

$$\frac{q_{н\text{кр}}}{q_{н\text{кр}}} = 0,38 \pm 0,02, \quad (9)$$

and, taking into account the measurements in a nonthermostated container, is

$$\frac{q_{н\text{кр}}}{q_{н\text{кр}}} = 0,36 \pm 0,01. \quad (10)$$

Table 2. Nucleate boiling in thermostated containers.

N, n	Величина зазора, мм (1)	Диаметр нагревателя, мм (2)	Жидкость (3)	$q \cdot 10^{-5}$, Вт/м ² (4)	Δt_n , град (5)	$\alpha_n \cdot 10^{-4}$, Вт/м ² ·град (6)	$\Delta t(n)$, град (5)	$\alpha(n) \cdot 10^{-4}$, Вт/м ² ·град (6)	$\frac{\alpha(n)}{\alpha_n}$	n
1	3	0.15	Спирт	1.60	24.5	0.667	22.2	0.71	1.03	0.024
2	3	0.15	Спирт	0.702	19.7	0.35	18.7	0.37	1.05	0.018
3	2	0.15	Эфир	0.59	7.7	0.76	6.9	0.86	1.12	0.043
4	2	0.05	Эфир	1.81	25.0	0.73	24.9	0.73	1.005	0.17
5	3	0.05	Эфир	2.29	40.3	0.57	39.9	0.57	1.001	0.17
6	3	0.05	Эфир	1.67	39.3	0.43	37.3	0.44	1.04	0.17
7	3	0.05	Эфир	1.9	40.2	0.48	38.6	0.49	1.02	0.17
8	3	0.05	Эфир	1.32	31.5	0.42	29.0	0.43	1.08	0.17
9	3	0.05	Эфир	2.02	29.3	0.69	30.8	0.65	0.946	0.17
10	1.5	0.05	Эфир	0.93	22.4	0.44	21.8	0.45	1.02	0.17
11	1.5	0.05	Эфир	1.42	23.4	0.6	22.4	0.63	1.04	0.17

KEY: (1) Clearance size, mm; (2) Heater diameter, mm; (3) Liquid; (4) W/m²; (5) Deg; (6) W/m²·deg; (7) Alcohol; (8) Ether.

Tests were made on heat exchange during nucleate boiling in the overload range $0.02 < n < 1$. Certain data on nucleate boiling (11 sets of measurements, 3 series each with 7 measurements in each series) are presented in Table 2. The heat transfer factor α during nucleate boiling with a reduction in the simulated gravitational field increases somewhat. This relationship, calculated by the method of least squares based on the results of more than 200 separate measurements, has the form:

$$\frac{\alpha}{\alpha_n} = 1.04 - 0.04 \frac{g}{g_n}, \quad 0.02 < \frac{g}{g_n} < 1, \quad (11)$$

where $\alpha_n = \alpha$ when $n = 1$.

With weak gravitational fields near weightlessness, we can not fix the region of developed nucleate boiling; following the beginning of vaporization, crisis sets in.

For film boiling the following relationship is obtained:

$$\frac{\alpha}{\alpha_n} = \left(\frac{g}{g_n} \right)^k \quad (k = 0.13 \pm 0.02; \quad 0.03 < \frac{g}{g_n} < 1). \quad (12)$$

The index k in relationship (12) is less than the expected $k = 0.25-0.3$, obviously, because of the heat transfer through the wall of the container and convective heat exchange in the liquid and in the vapor, which does not correspond to simulation conditions. Relationship (12) can be considered the upper boundary of the heat transfer factors during film boiling in the studied range of acceleration.

Figure 3 presents motion picture frames of the boiling process on a thin wire in the container, located at angles 0° ($n = 0$), Fig. 3a, 3b, 3c; 20° ($n \approx 0.35$), Fig. 3d; 90° ($n = 1$), Fig. 3b. There is an apparent tendency for the vapor bubbles to increase and merge during a drop in the overloading.

Under weightlessness simulation conditions the growing bubbles in the boiling process merge into one vapor cavity covering the entire heater.

The same pattern is also observed during the boiling of liquid oxygen in a nonuniform magnetic field when simulating low overloads.

THE MODELING OF WEAK GRAVITATIONAL FIELDS WITH THE AID OF FORCES ACTING ON A PARAMAGNETIC LIQUID IN A NONUNIFORM MAGNETIC FIELD

This method involves placing a paramagnetic liquid (liquid oxygen) in a constant nonuniform magnetic field of such configuration that on each elementary volume of the liquid there acts a force directed against the force of gravity and fully (weightlessness) or partially (weak gravitational field) compensates for it.

If $G_n = \rho g_n V$ is the force of gravity, V is the volume of liquid, F is the force acting on the liquid in the magnetic field,

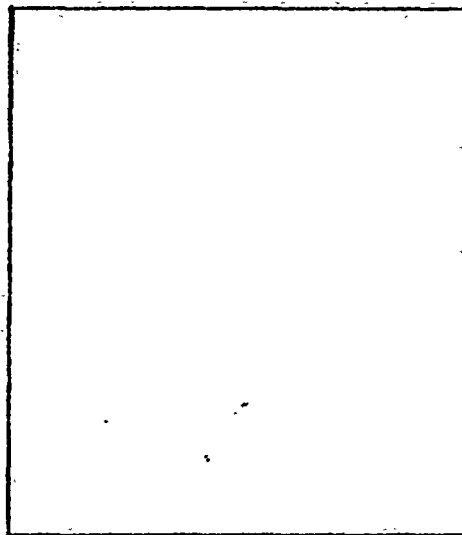


Fig. 3a

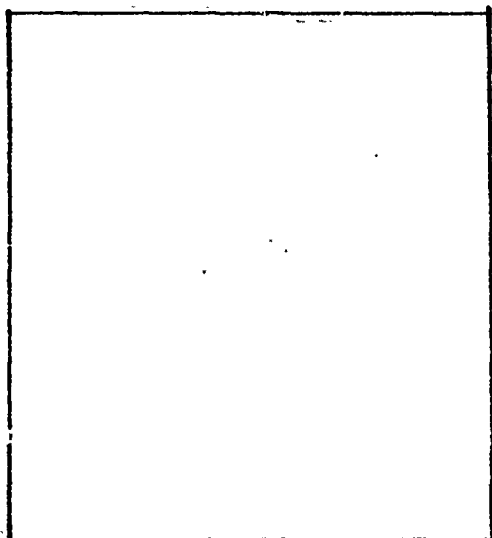


Fig. 3b

GRAPHICS ILLEGIBLE

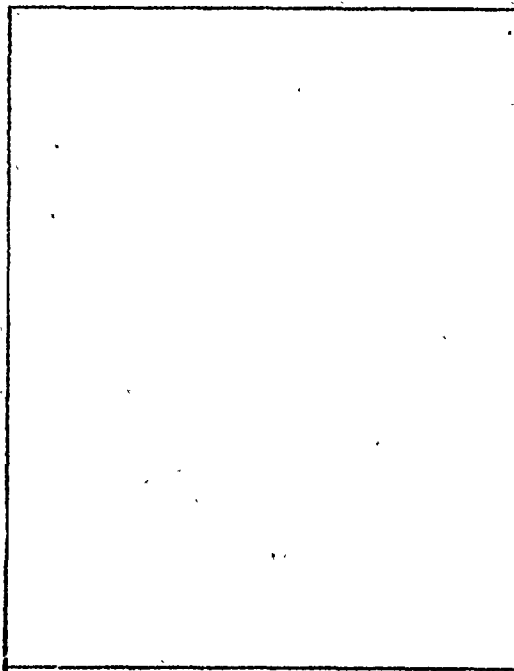


Fig. 3c

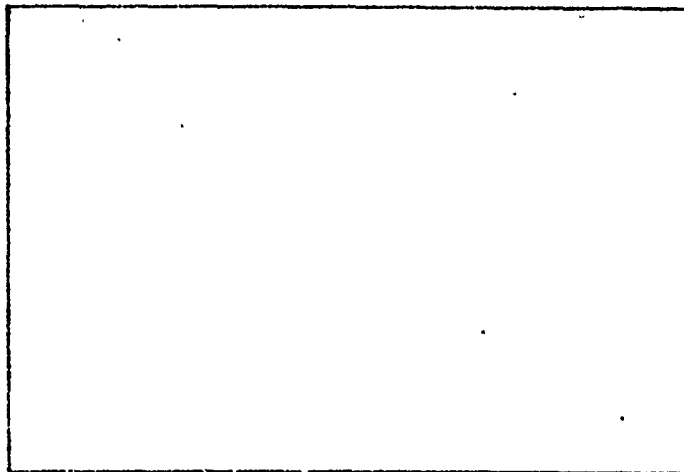


Fig. 3d

GRAPHICS ILLEGIBLE

GRAPHICS ILLEGIBLE

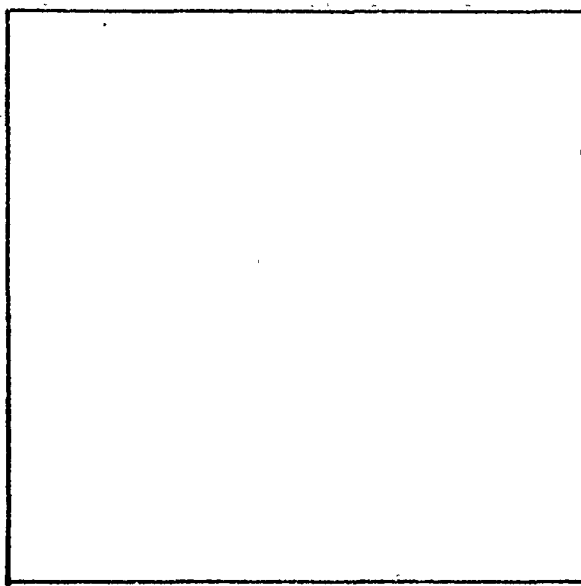


Fig. 3e. The boiling process in a container with various simulated overloads.

then

$$n = \frac{g}{g_n} = 1 + \frac{F}{G_n} = 1 - \frac{|F|}{\rho g_n V}. \quad (13)$$

We can see, using [7], that for a liquid magnet in a uniform magnetic field

$$n = 1 - \frac{1}{2g_n} \chi |\text{grad } H^2|, \quad (14)$$

where H is the intensity of the magnetic field and χ is the specific magnetic susceptibility.

This method is accomplished in the interpolar vertical clearance of an electromagnet with the diameter of the terminals 200 mm and maximum field intensity approximately 10^4 Oe. The polar terminals were designed according to a method similar to [7].

The profile of the polar terminals is presented in Fig. 4 where the dashes indicate the calculated configuration of the terminals, and x_0, z_0 are the cutoff points of the terminal

profile. A constant force compensating the force of gravity acts in the plane of symmetry of the terminals (XY). The volume of the liquid magnet bounded by coordinates $-z_1$, $+z_1$, x_1 , x_2 , and y will be affected by the unstudied vertical components of the compensating force, equivalent to relative overload:

$$\frac{\Delta g_1}{g_n} \approx \Delta n_1 \approx \pm \frac{z_1^2}{(x_1 + x_2)^2}. \quad (15)$$

An evaluation of all errors connected with accomplishing the method shows that it is possible to simulate weak gravitational fields with forces acting on a liquid paramagnet with an accuracy to at least $\pm 0.01 g_n$.

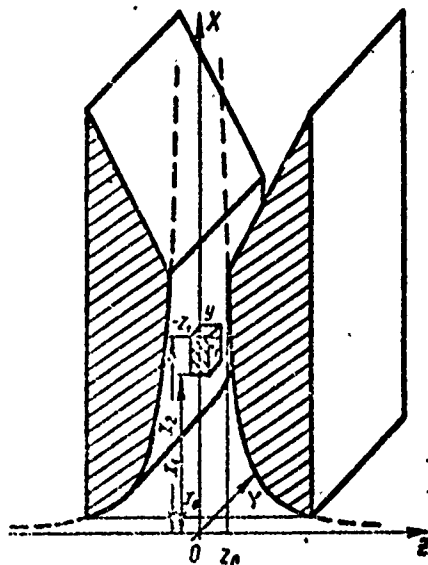


Fig. 4. Profile of polar terminals of a magnet for simulating weak gravitational fields.

The overload for vapor n_n during the simulated overload for liquid can be expressed by the formula:

$$n_n = n + (1 - n) \left| \frac{z_n}{z - z_n} \cdot \frac{\gamma_n - \gamma}{\gamma} \right|, \quad (16)$$

where κ and κ_n are the specific magnetic susceptibilities of liquid and vapor, respectively. The quantity n_n differs insubstantially from n . In the case of weightlessness for liquid

oxygen $n = 0$, while $n_{\text{прд}} \approx 2 \cdot 10^{-3}$.

The most reliable method of checking weightlessness for boiling is the neutral equilibrium of a vapor bubble in the studied region of liquid since in order to simulate the boiling process during weightlessness, it is obviously essential to ensure the weightless conditions for vapor bubbles.

In studying heat exchange there will be additional errors caused by the dependence of magnetic susceptibility on temperature and the appearance of thermomagnetic convection.

The upper limit of simulation in a study of boiling can be found from the relationship:

$$n_{\text{прд}} > \frac{\Delta t}{T + \theta} \cdot \frac{v_M}{v_n}, \quad (17)$$

where T is the average volume temperature of liquid; θ represents the Curie-Weiss points; v_n is the volume of the vapor bubble; v_M is the volume between the bubble surfaces and the heater.

For liquid oxygen when $\Delta t \approx 10$ deg $n_{\text{прд}} = 10^{-3}$. Thus, the presence of thermomagnetic convection does not obstruct the study of heat exchange during boiling. However, thermomagnetic convection makes it impossible to study convective heat exchange with the chosen method of simulating weak gravitational fields. The relationship between the heat transfer factors for thermomagnetic α_M and thermal α_T convections can be written for liquid oxygen in the form:

$$\alpha_M = 2 \cdot \left(\frac{1-n}{0.58n} \right)^{0.25}. \quad (18)$$

If we assume that the study of thermal convection is possible when $\alpha_T \geq \alpha_M$, this gives the evaluation of limiting overload at which it is possible to study thermal convections: $n > 0.6$.

Boiling was studied in a glass Dewar vessel with an internal diameter of 14 mm, placed in the vertical clearance of the magnet on platinum resistance heaters with a diameter of 0.05 and 0.1 mm. The heat transfer factor versus thermal flux for various overloads ($n = 1, 0.64, 0.5, 0.3, 0.1, 0.05, 0.04, 0.02, 0.01, 0$) was studied. Data on boiling are presented in Table 3; some of the boiling curves are given in Fig. 5a and 5b. In addition, critical thermal flux versus the acceleration of gravity was studied (see Fig. 2). The dependence of the heat transfer factor on q , corresponding to convective heat exchange (see Fig. 5), as indicated above, is caused by thermomagnetic convection. In the area of film boiling there is also observed an anomalous dependence of α on q , which is apparently connected with the limited dimensions of the working vessel in which the study was made. For the area of nucleate boiling, which is simulated correctly, we can arrive at certain conclusions relative to the dependence of α on g and α on q in the region of weak gravitational fields. From Table 3, which presents data on heat transfer factors for developed nucleate boiling, reduced to flow $q = 4 \cdot 10^4 \text{ W/m}^2$ and the exponent k for relationship $\alpha = Aq^k$, it is apparent that in weak gravitational fields for developed nucleate boiling the following relationship occurs:

$$\alpha = Aq^{0.7 \pm 0.1}, \quad (19)$$

agreeing with the relationship obtained under normal conditions.

Concerning the heat transfer factor during nucleate boiling under conditions of weak gravitational fields ($0.02 < n < 1$), we can only state that it is not less than under normal conditions. Boiling curves (see Fig. 5) indicate the constriction of the nucleate boiling regions with a decrease in overload. When $n \approx 0$ there is virtually no region of nucleate boiling.

The dependence of critical thermal flux on g was found in the form

$$q_{kp} = q_{nkp} \left(\frac{g}{g_n} \right)^{0.26 \pm 0.01}$$

Table 3. Parameters of the nucleate boiling of liquid oxygen under conditions imitating weak gravitational fields in a nonuniform magnetic field.

n	$\alpha \cdot 10^{-4} \frac{W}{m^2 \cdot \text{deg}}$	k
0,02	4,5*	0,7
0,043	3,9	0,88
0,05	3,9	0,86
0,1	4,2	0,84
0,3	4,6	0,88
0,5	4,1	0,75
0,64	4,2	0,79
1	3,7	0,8

*The value of α corresponds to the moment of crisis during a thermal flux of $3,8 \cdot 10^4 \text{ W/m}^2$.

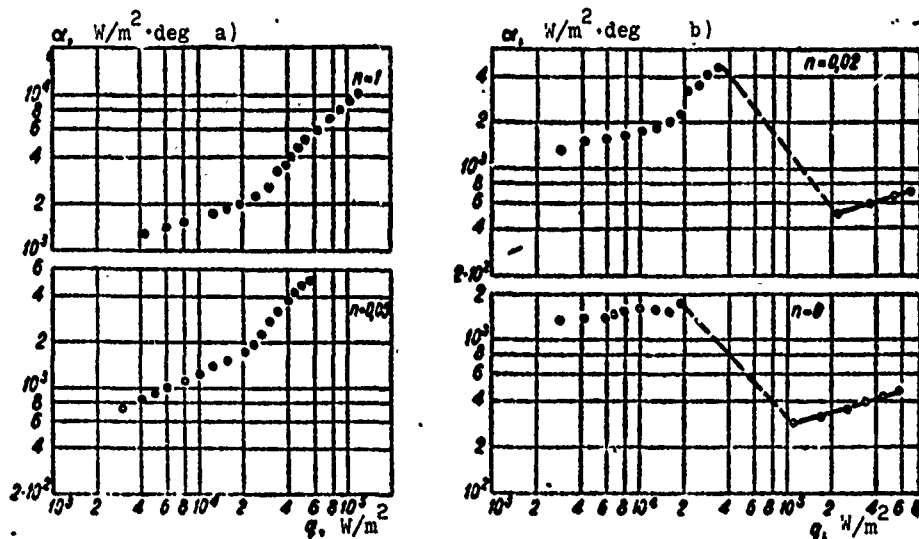


Fig. 5. Curves representing the boiling of liquid oxygen under conditions of weak gravitational fields simulated in a nonuniform magnetic field.

in the range $0.01 < n < 1$. The limiting average value of relative critical thermal flux when $g = 0$ is $q_{кр} / q_{кр0} = 0.26 \pm 0.01$.

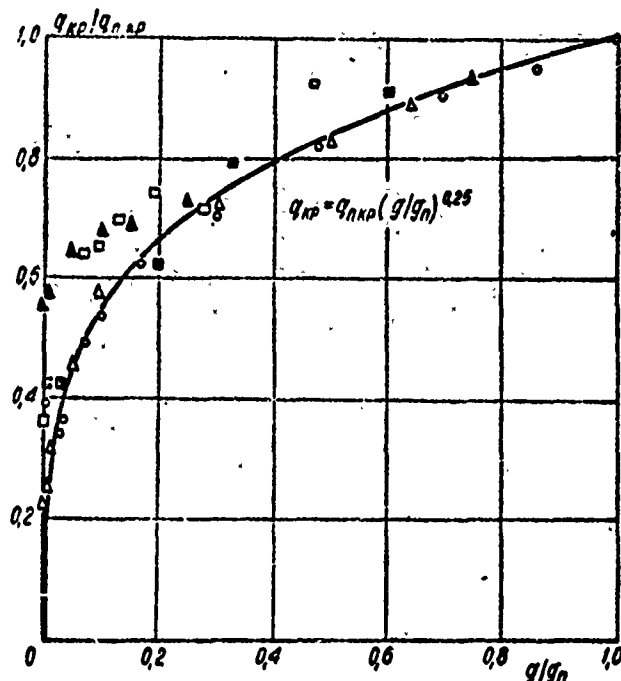


Fig. 6. Critical thermal flux versus the acceleration of gravity based on data from various authors:
 O - Ether in thin container; Δ - Oxygen in a magnetic field; \blacksquare - Based on data from Mert and Clark [8]; \square - Usyskin and Zigel' [3]; \blacktriangle - Lyon [9].

Figure 6 illustrates the relationship $q_{кр} = q_{кр0} \left(\frac{g}{g_n} \right)^{0.25}$ and the experimental points obtained by various authors [3, 8, 9] including the data from our work. Data of Mert and Clark [8], who conducted a very careful study of the boiling of nitrogen from a copper sphere in a falling container, has the best agreement with our dependence of $q_{кр}$ on g in the overload range $0.03 < n < 1$. The elevated values of $q_{кр}$, found by Usyskin and Zigel' [3] during boiling on thin wires in water also in a falling container obviously are explained by the insufficient purity of the weak

gravitational fields and the short testing time. Lyon and colleagues [9], who conducted tests with the simulation of low overloads according to a methodology similar to ours in a magnetic field of a solenoid, also obtained very elevated results in the region of weak gravitational fields. It is possible that intense thermomagnetic convections, caused by the very large surface of the heater, affected the results in reference [9].

Conclusions

1. Methods were developed for simulating weightlessness and weak gravitational fields for studying the process of boiling in the overload range $0.01 < n < 1$.

2. The relationship between critical thermal flux and the acceleration of gravity was found:

$$q_{kp} = q_{nkp} \left(\frac{g}{g_n} \right)^{0.26}; \quad 0.01 < \frac{g}{g_n} < 1,$$

and it agrees well with the familiar theoretical Kutateladze-Borishanskiy-Zuber relationship [10, 11].

3. According to two methods, the limiting average value of critical thermal flux when $g = 0$ was found:

$$\frac{q_{0kp}}{q_{nkp}} = 0.30 \pm 0.05.$$

In the experiments we observed considerably lower values for limiting critical thermal flux ($0.18 q_{nkp} - 0.2 q_{nkp}$).

4. We have shown that the value of the heat transfer factors during nucleate boiling under conditions of weak gravitational fields is no lower than it is under normal conditions.

5. It was found that the dependence of the heat transfer factor during nucleate boiling on the thermal load under conditions of weak gravitational fields remains the same as during normal gravitation.

6. With extremely weak gravitational fields ($g \approx 0$) there is virtually no region of nucleate boiling and after boiling begins crisis sets in.

7. During boiling in weightless conditions there is a tendency toward the formation of a single bubble which surrounds the heater.

BIBLIOGRAPHY

1. Невесомость. Физические явления и биологические эффекты. Под ред. Э. Бенедикт. М., изд. «Мир», 1964.
2. Unterberg W., Congelliere J. ARS Journal, 32, 1962, № 6, 862.
3. Усыскин С., Зигель Р. Экспериментальное исследование процесса кипения в условиях уменьшенной и нулевой гравитации. Сб.: «Невесомость. Физические явления и биологические эффекты». М., изд. «Мир», 1964.
4. Стренг П., Орелл А., Уэстуотер Дж. Микроскопическое изучение роста пузыря при кипении. Сб.: «Вопросы физики кипения». М., изд. «Мир», 1964.
5. Адельберг М., Форстер К. Влияние гравитации на теплопередачу при пузырьковом кипении. Сб.: «Невесомость. Физические явления и биологические эффекты». М., изд. «Мир», 1964.
6. Вопросы физики кипения. М., изд. «Мир», 1964.
7. Ландау Л. Д., Лифшиц Е. М. «Электродинамика сплошных сред». М., ГИИТЛ, 1957.
8. Мерт, Кларк. «Труды Американского общества инженеров-механиков. С. С. Теплопередача», 83, 1961, № 3, 3.
9. Lyon D. N., Jones M. C., Ritter G. Z., Chladacis C. J., Kosky P. G. AIChE Journal, 11, 1965, № 5, 773.
10. Борншанский В. М. ЖТФ, 2, 1956.
11. Кутателадзе С. С. Изв. АН СССР, сер. «Энергетика», 11, 1950.

SECTION II

THE HYDRAULICS OF TWO-PHASE FLOW

FLOW PULSATIONS IN TYPES OF STEAM BOILERS

O. M. Baldina, V. G. Zinkevich,
R. I. Kalinin, and V. B. Khabenskiy

Abbreviations

эк - economizer
пар - steam
вх - input
вых - output
Д - dynamics
мин - minimum
вн - internal

Until recently test data on stability conditions for evaporating parallel flows have been represented in parametric form [1, 2, 3] and made it possible to determine the necessary throttling of boiler pipes only for a heating surface similar to that studied with respect to components and thermal conditions. In the general case, it is very difficult to determine the amount of throttling necessary or the amount of relative throttling Π :

$$\Pi = \frac{\sum \Delta p_{\text{вх}}}{\sum \Delta p_{\text{пар}}}, \quad (1)$$

where $\sum \Delta p_{\text{вх}}$ is the sum of the pressure drop at the input unheated

and economizer sections; Δp_{nap} is the same at the evaporator, reheater, and output unheated sections of the pipe.

Figure 1 is a generalization of test data on the flow stability boundary in a number of industrial and bench test installations as a function of the value of mass velocity w . Certain qualitative regularities in the form of $\Pi = f(w)$ are noticeable only at very low values for w 300 kg/m².s, which are virtually never encountered in steam boilers.

Attempts to use other parameters for the purpose of generalization - pressure, thermal load, output vapor content, etc. - also have not given positive results. Theoretical methods for finding the boundaries of the stability region for the motion of a medium in steam-generating pipe elements, based on the use of the theory of automatic control [4], have not as yet reached the level of engineering design. Available physical concepts have not sufficiently explained the phenomena observed.

For these reasons, a stand was built at the TsKTI [Central Scientific Research, Planning and Design Boiler and Turbine Institute im. I. I. Polzunov] for studying pulsations in parallel pipes at pressures up to 250 atm (abs.) [5]. The study of inter-pipe pulsations on this stand included a study of the nature of the phenomenon and the obtaining of experimental data in the little studied region of high pressures and thermal loads. We studied first two types of horizontal pipe bundles: one of four straight pipes $\varnothing 26 \times 3$ mm, each 7.5 m long, and one of three coils, each 27.5 m and with the same diameter. The pressure drop between the input and output collectors of the pipes was kept constant by a shunting system with a large cross section. The test pipes were heated by steam ($p = 250$ atm (abs.), $t = 500-550^\circ\text{C}$), passing into the furnaces along an annular clearance between the heated pipe and the outer housing. The length of the heated section was: for straight pipes 5.0 m and for coils 4×5.0 m. The stand operated

with a single-flow system and required up to 8 t/h of water. Water was supplied from a high-pressure pump ($p = 300$ atm (abs.)) with a temperature of 100°C and was preheated in surface heat exchangers before entering the test elements.

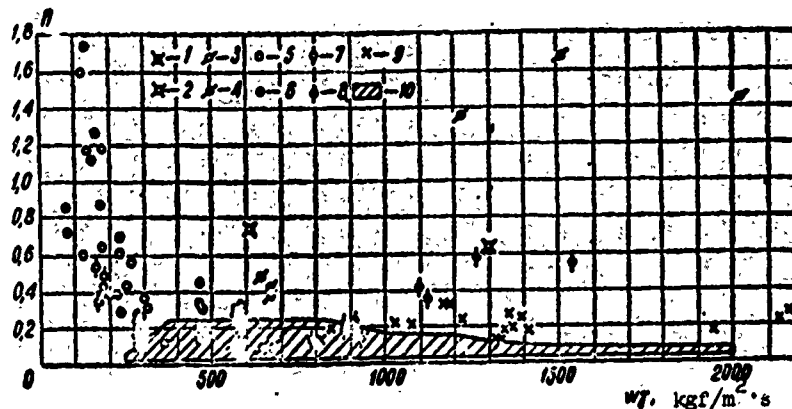


Fig. 1. Test data on the stability boundary in coordinate $\Pi - w_y$:

1 - Davidov's tests, boiler $p = 100$ atm (tech.);
 2 - Kruzhilin's tests, boiler 200-35, $p = 35$ atm (tech.); 3 - Semenovker's tests, boiler 200-35, $p = 35$ atm (tech.); 4 - Shmukler's tests, VTI boiler, $p = 60-140$ atm (tech.); 5 - Golovan's tests, stand, coils $\varnothing 14, 15$, and 17 mm, $p = 15-50$ atm (tech.); 6 - Serov and Lezin's tests, stand, pipe $\varnothing 4$ mm, $p = 30-100$ atm (tech.); 7 - Lavrenov's tests stand, coils $\varnothing 13$ mm, $p = 20-50$ atm (tech.); 8 - Valdina's tests, boiler OKG-100-2, $p = 15-22$ atm (tech.); 9 - Fedorov's tests, stand, pipe $\varnothing 10$ mm, $p = 40-100$ atm (tech.); 10 - Region of the authors' tests, stand, coils $\varnothing 26 \times 3, 28 \times 4, 16 \times 3$, straight pipes $\varnothing 26 \times 3$ mm, $p = 20-200$ atm (tech.).

Horizontal coils $\varnothing 28 \times 4$ and 16×3 mm with dc electrical heating from a GPN-550-750 transformer, 550 kW at a voltage of 85 V, and a vertical coil from pipes $\varnothing 26 \times 3$ mm, heated by steam, were next installed on the stand [6]. Diagrams of these coils are presented in Fig. 2. The horizontal coils were each 24.1 m long and the heated sections 19.6 m each. The vertical coils 26.4 m long could be connected along systems of Π -, N-, and M-shaped motion with the aid of the switching provided. Sections

of each path were heated for a length of 5.0 m.

The pressure in the installation varied from 20 to 240 atm (tech.). The average thermal loads were, with electrical heating, $\bar{q} \leq 400 \cdot 10^3 \text{ kcal/m}^2 \cdot \text{h}$ and, with steam heating, up to $600 \cdot 10^3 \text{ kcal/m}^2 \cdot \text{h}$. Underheating before boiling at water input was $\Delta t_0 = 5-100 \text{ kcal/kg}$.

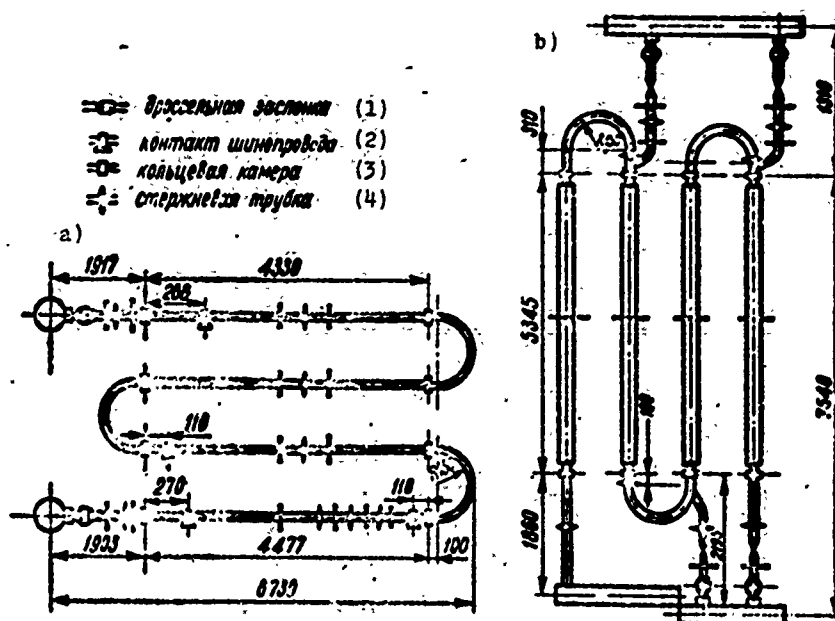


Fig. 2. Diagram of experimental coils:
a - Horizontal $\varnothing 28 \quad 4 \text{ mm}$; b - Vertical $\varnothing 26 \quad 3 \text{ mm}$.
KEY: (1) Throttle gate; (2) Conductor contact;
(3) Annular chamber; (4) Rod pipe.

Variable quantities - water flow rate at input, dynamic head in several cross sections along the pipes, and pressure drops in their sections - were established by the N-700 oscillographs and the single-flow EPP-09, whose signal was fed from syphon sensors through multichannel electronic transformers developed at the TsKTI.

Interpipe pulsations were caused by a change in the parameters of the flow in the coils or by the degree of pipe throttling at

input or output. The flow stability boundary in the studied pipes was determined according to the moment of the sharp increase in vibration amplitude. Several tests have been conducted near it, beginning with stable and up to the appearance of developed pulsations. For example, the appearance of pulsations in horizontal and vertical coils is presented in Fig. 3. The character of the flow process did not depend upon the orientation of the pipes.

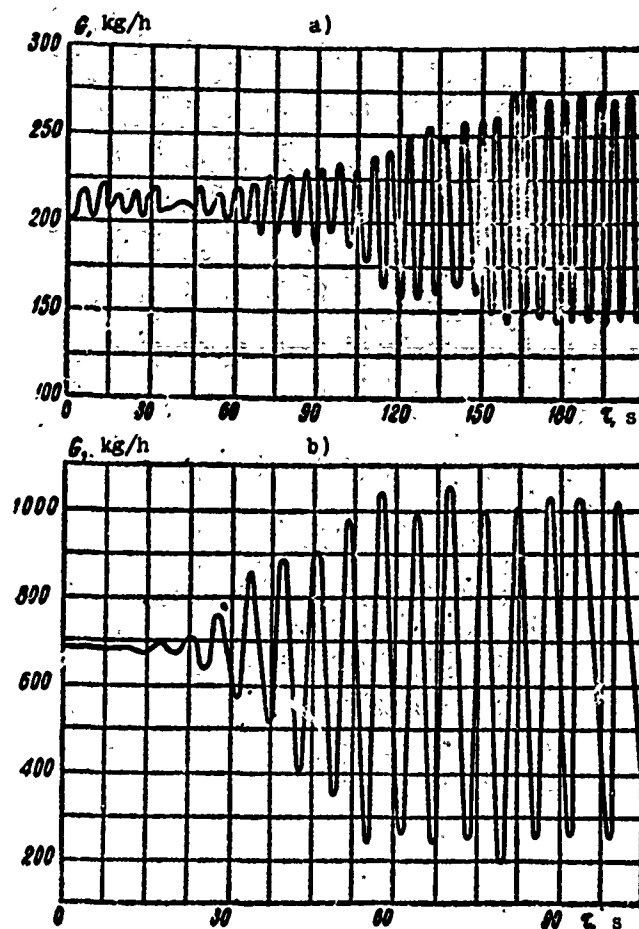


Fig. 3. Development of pulsations during a decrease in flow rate:

a - Horizontal coil $\varnothing 16 \times 3$ mm, $p = 119.8$ atm (abs.),

$q = 129.1 \times 10^3$ kcal/m²·h, $\Delta i_0 = 13.9$ kcal/kg; b -

Vertical lifting pipe, $p = 119.3$ atm (abs.), $q = 389 \times 10^3$ kcal/m²·h, $\Delta i_0 = 84.7$ kcal/kg.

In tests using the markings of a synchronizer, combined diagrams were plotted showing the variations in flow rate G , the dynamic head of the flow on the evaporative part and at output from the coil D , and the pressure drop on its successive input, heated, and output sections (Δp_{BX} , Δp_1 , Δp_2 , Δp_3 , Δp_4 , $\Delta p_{\text{ВВХ}}$) for tests with pulsations (Fig. 4). The combined diagrams showed the identity of the relationship for horizontal and vertical pipes. The pressure drop and the dynamic head of the flow on the water-containing section always vary in opposite phase with the corresponding quantities measured in the output sections of the coil. In the middle section of the pipe these quantities, as a function of the regime, can have any character.

In stable regimes during the forced multiple variation of flow rate, certain opposite-phase variations of dynamic heads at input and output are also noted. However, with a large deviation in flow rate at input the dynamic head at output finally changes in the same direction. With pressure near critical and beyond critical all pressure drops on separate sections of the coil changed synchronously with the change in flow rate at input.

All these peculiarities of the variation in dynamic characteristics of flow along a pipe in nonstationary conditions can be explained if we consider the change in the per-weight capacity of steam-generating pipes during fluctuations in their flow rate. According to the equation for the preservation of matter, flow rates at input G and at pipe output W are connected by relationship:

$$G = W - \frac{dB}{dt}, \quad (2)$$

where dB/dt is the change in the per-weight capacity of the pipe in a unit of time. With subcritical pressure with any small decrease in flow rate, the fraction of space occupied by steam is increased by δG and the per-weight capacity of the pipe is decreased by δB . This part of the per-weight capacity is removed

from the pipe during transient process τ . If the removal rate of part of the per-weight capacity is assumed constant, then immediately after the disturbance the flow rate at output will be:

$$W = G - \frac{2B}{\tau} \quad (3)$$

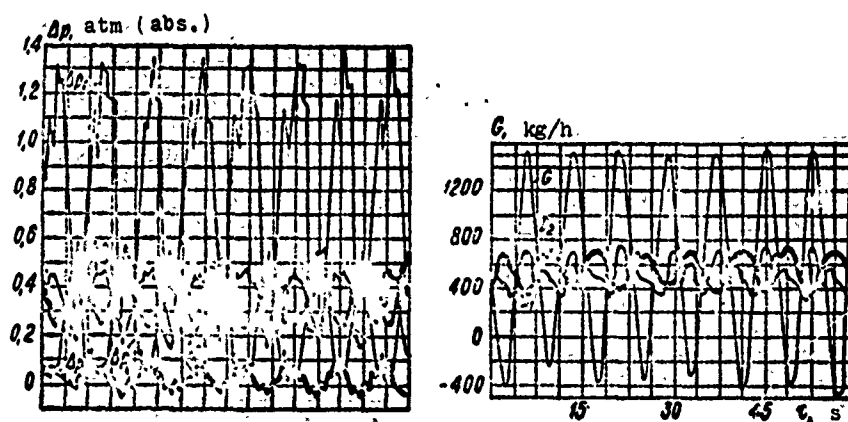


Fig. 4. Combined diagrams showing variations of flow rate in separate sections and pressure drop in the sections of a vertical N-shaped coil:

$p = 96.5$ atm (abs.); $\bar{q} = 345 \cdot 10^3$ kcal/m²·h; $\Delta i_0 = 34$ kcal/kg; G - Flow rate at input; D_1, D_2 - the same at the end of the first and third paths; $\Delta p_{BX}, \Delta p_{BHX}$ - pressure drop at input and output of unheated sections; $\bar{\Delta p}_1, \bar{\Delta p}_2, \bar{\Delta p}_3$ - the same on consecutive heated sections.

If $\left| \frac{2B}{\tau} \right| > \delta G$, then flow rate at output in this period will be greater than the initial quantity. In this case, pressure losses in the steam-containing sections can increase by a greater quantity than losses are reduced in the section before the start of boiling and the reduction in flow rate will continue.

A rise in the pressure drop in the water-containing section increases flow stability. This condition is assumed to be characterized by the coefficient of relative pipe throttling Π , determined by expression (1).

Depending on the dynamic properties of the system, greatly determined by the inconstancy of the filling of the evaporative pipes per unit weight, the necessary value for coefficient Π can vary over a wide range. The intensity of the variation in the per-weight filling of pipes during a decrease in flow rate at input can be characterized by the coefficient called the dynamic coefficient of capacity:

$$B_A = \frac{dB}{dG}. \quad (4)$$

A method for the approximate calculation of the dynamic coefficient of capacity is proposed in [5, 6, 7].

All test data obtained on the stand, concerning the stability boundary of flow in coils, as well as test data from other studies, were processed in coordinates $\Pi - B_A$. A generalized relationship between the necessary relative throttling of the horizontal heated pipes (ensuring the absence of interpipe pulsations in them) and the dynamic properties of the progressing flow is presented in Fig. 5. The region of stable regimes is above the limiting curve. The uniqueness of the relationship is disturbed only at low mass velocities $w_y < 500 \text{ kg/m}^2 \cdot \text{s}$, which was approximately accounted for by introducing a correction factor to the value of the necessary relative pipe throttling, equal to the ratio of mass velocities $500/w_y$ [7]. On Fig. 5 test points at $w_y < 500 \text{ kg/m}^2 \cdot \text{s}$ are plotted with conversion of the relative throttling in reverse relationship. It can be seen that the coordinate chosen made it possible to connect the experimental data obtained on various types of test installations and steam boilers under various flow parameters considerably better than, for example, in Fig. 1.

This generalization was used in the new standards for hydraulic design. The nomogram of the standards is presented in Fig. 6. An evaluation of the necessary value for the relative throttling of evaporative pipes Π_{min} , which ensures the absence of

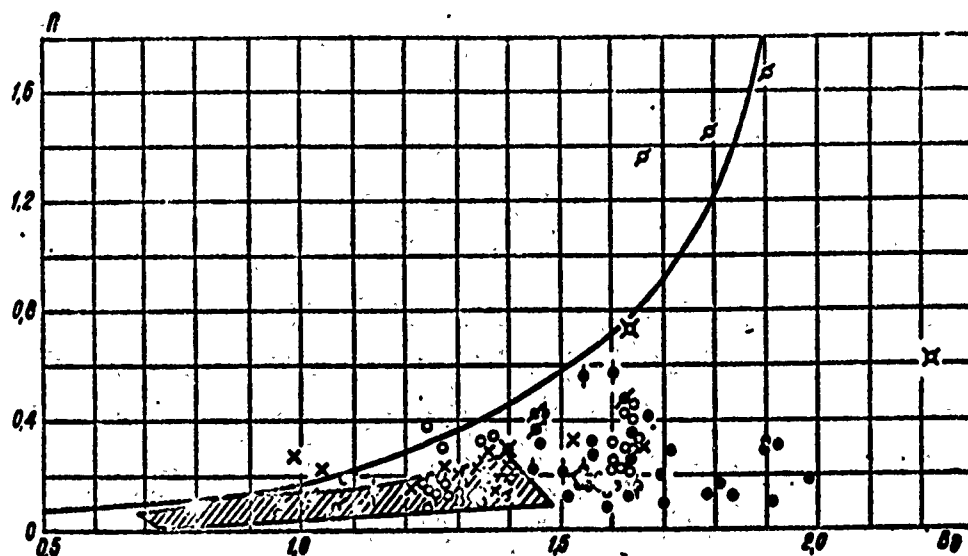


Fig. 5. Generalization of test data on the stability boundary in coordinates $\Pi - B_d$, (see Fig. 1 for designations).

intercoil pulsations, must be made for single-flow boilers at minimum output, when the pressure of the medium in the evaporation zone is minimum, and for boilers with multiple forced circulation, at maximum. For pipes with an orientation other than horizontal, the function of the standards can be applied when the fraction of level pressure drop in them does not exceed 10-20% of the full pressure drop.

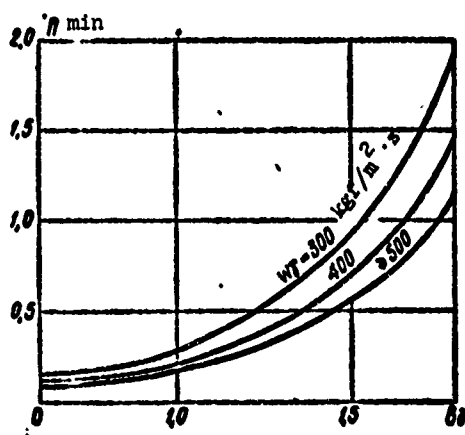


Fig. 6. Nomogram for determining the necessary relative throttling of horizontal pipes.

With a considerable fraction of the level component in the total pressure drop and a strong throttling of flow at input or output sections, a more successful generalization of test data is possible in the coordinates $\Pi - B_d - K$ [18], where

$$K = \frac{\Delta p_{w1} + \Delta p_{12} + \Delta p_{23}}{\Delta p_{w2} + \Delta p_{23}} \quad (5)$$

$\Delta p_{w1}, \Delta p_{w2}$ - pressure drops in throttle devices at input and output from the pipes; $\Delta p_{BX}, \Delta p_{BWX}$ - the same in the input and output unheated sections; $\Delta p_{ЭН}$ - the same in the economizer section.

However, a further refinement of the standard method of determining the value of Π necessary for providing flow stability in a system of boiler pipes is desirable with a more detailed study of the effect of initial parameters on the stability boundary and the mechanism of the nonstationary process in a steam-generating pipe. Nevertheless, an experimental determination of the propagation of a disturbance along a pipe, the rate of change in the mass capacity in its separate sections, the role played by the heat-retaining metal of the power pipe, and other questions is extremely difficult and, in a number of cases, impossible. In order to clarify these problems and the effect on the stability boundary of individual parameters, a method of mathematical modeling was used.

A mathematical model describing a process is a system of equations in partial derivatives, expressing the laws of conservation of energy, mass, and momentum in single-phase and two-phase flows and the heat conductivity equation for the metal of the pipe.

Considerable attention was given to the selection of the experimental relationships necessary for completing the basic differential equations since they have a substantial effect on the course of the nonstationary process. For example, for the pressure

steam content a formula was used which approximates the experimental data generalized in the hydraulic design standards for steam boilers with high accuracy; for the coefficient of friction in a single-phase flow the relationship obtained in [9] was used, which is valid for a wide range of Reynolds numbers. The resistance of friction in a two-phase flow was calculated according to the formula for homogeneous two-phase flow with a factor taking into account the relationship obtained in the standards between losses in actual and homogeneous flows. On the basis of reference [10], this coefficient was defined as a function of the Re number and the ratio of two-phase flow density to water density on the saturation line at a given pressure.

For the most accurate quantitative description of the pulsation process and for tracing the change in parameters over time and along the pipe, the initial system of equations in partial derivatives was numerically integrated on an electronic computer. To solve equations in partial derivatives the method of straight lines was used, with which the derivative with respect to time was retained and the derivative with respect to the spatial coordinate was replaced by finite differences. The obtained system of high-order ordinary differential equations with substantial nonlinearities was solved by the Runge-Kutta method of the fourth order.

The presence of slippage in two-phase flow, the nonuniformity of the thermal load along the pipe, and the need to accurately account for the level component of pressure drop determined the selection of the most convenient system of coordinates in which the equations were presented. The economizer section was described by equations in Lagrange coordinates and the evaporative sections in Euler coordinates. Moreover, such a representation made it possible to eliminate the jump in velocity which occurred during the use of only the Euler system of coordinates.

The numerical integration of the mathematical model was accomplished on a M-220 computer.

The methodology used to derive the pulsation model was similar to the methodology applied in the test. Under determined initial conditions and a large initial flow rate, the pressure drop between the collectors slowly decreased, i.e., imitating the reduction in flow rate in a system of parallel pipes. The pressure drop decreased until the model went into flow pulsation in the pipe, after which flow rate pulsations were fixed at a constant pressure drop between the collectors. When the boundary of instability was reached, a small reduction in flow rate led to a considerable increase in pulsation amplitude. At a considerable amplitude the flow rate pulsations had a pronounced nonlinear character as in the experiments.

The computer calculation program made it possible to change at any instant the throttling at input and output, the thermal load, and the underheating of the water at pipe input.

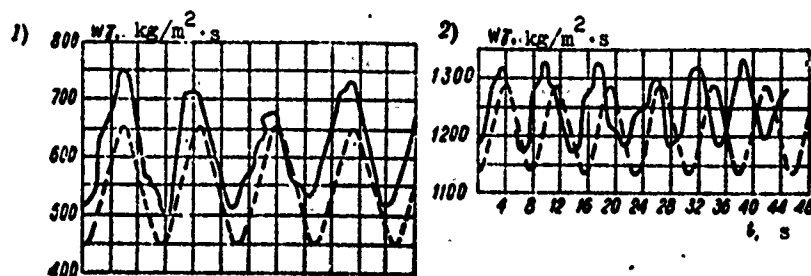


Fig. 7. Variation over time in mass velocity at pipe input in the pulsation process:

———— experiment; ----- theory;

1 - for test conditions $\bar{q} = 355 \times 10^3 \text{ kcal/m}^2 \cdot \text{h}$,

$t_{\text{BX}} = 284^\circ\text{C}$, $p = 57.8 \text{ atm (abs.)}$; 2 - for test

conditions $\bar{q} = 191.5 \times 10^3 \text{ kcal/m}^2 \cdot \text{h}$, $t_{\text{BX}} = 270^\circ\text{C}$,

$p = 100 \text{ atm (abs.)}$.

The theoretical solutions obtained were compared with test data provided on the stand. A good correspondence between theory and experimental results was achieved both with respect to the values of average mass velocity at which pulsations occur and with respect to their period. Figure 7 presents examples of a theoretical and experimental comparison for flow rate fluctuations in the coil $\varnothing 28 \times 4$ illustrated in Fig. 2. The study of pulsations using mathematical modeling is very effective when it is necessary to illustrate, in pure form, the effect of one of the parameters on the stability boundary. During a change of one parameter the others can be maintained within strictly prescribed limits.

Theoretical study of the effect of a specific thermal load on the stability boundary has shown that with its variation during constant underheating, pressure, throttling, and pipe geometry, mass velocity, which corresponds to the pulsation boundary, changes almost proportionally. The slight deviation from the law of direct proportionality is explained by the fact that with an increase in flow rate the ratio of the coefficients of friction in real and homogeneous two-phase flows is reduced. This leads to a reduction in the relative portion of the evaporative section's resistance in the total drop in the pipe and somewhat improves flow stability. Thus with an increase in thermal loading, for example, by a factor of k , boundary mass velocity increases by a factor of Ak . A study of the effect of this phenomenon on the stability boundary has shown that in the range $w_y = 300-1500$ $\text{kg/m}^2\cdot\text{s}$ the coefficient A lies within $0.9 \leq A \leq 1$.

Such regularity for the effect of thermal loading is explained by the fact that the mass capacity of the pipe is kept constant during a synchronous change in w_y and \bar{q} and completely confirms the connection between the value of B_d and the stability boundary [5, 7]. A comparison of the ratios of specific thermal loads and boundary mass velocities for a series of tests conducted on the

stand at near values for the other parameters is presented in Table 1.

Table 1.

p , атм (1)	N п.п. (2)	ΔL , м (3)	Δt , сек (4)	$\bar{q} \cdot 10^{-3}$, ккал/м ² ·ч (5)	B_1 (6)	$\frac{\bar{q}_1}{\bar{q}_2}$ (7)	$\frac{w_{T1}}{w_{T2}}$ (8)	Тип элемента (9)
39	1	24,5	6,9	10,6	86,9	1,13	611	Горизонталь- ный змеевик Ø 28×4 мм (10)
	2	21,5	6,9	10,6	54,7	1,11	411	
58	3	53,3	6,9	10,6	346	1,20	1235	То же (11)
	4	55,2	6,9	10,6	247,5	1,19	962	
	5	56,5	6,9	10,6	216	1,18	830	
100	6	64,3	6,9	2,0	191,8	1,08	645	То же (12)
	7	56,2	6,9	2,0	269,8	1,05	901	
177	8	54,4	7,9	22,8	256	0,72	480	Вертикаль- ная труба Ø 28×3 мм (13)
	9	54,4	7,9	22,8	228	0,75	438	

KEY: (1) atm (abs.); (2) kcal/kg; (3) kcal/m²·h;
(4) kg/m²·s; (5) Type of element; (6) Horizontal coil;
(7) Ditto; (8) Vertical pipe.

To study the effect of pipe diameter on the stability boundary calculations were made for pipes with internal diameters of 10, 20, and 40 mm. Thermal loads were selected so that the output vapor content per unit weight in the initial state was identical in all three pipes. Accordingly, the specific thermal load for a pipe with internal diameter 20 mm was greater by a factor of two and for a pipe with internal diameter of 40 mm was greater by a factor of four than for a pipe with internal diameter of 10 mm. All the remaining parameters (pressure, underheating, throttling at input and output, pipe length) were kept constant. Theoretical

solution has shown that under these conditions the effect of the diameter on the stability boundary is not substantial (Fig. 8).

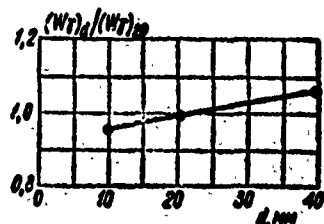


Fig. 8. Variation in the ratio of boundary mass velocities in pipes of various diameters to that in a pipe $\varnothing 20$ mm under identical initial vapor content per unit weight, pressure, underheating, and pipe length.

The validity of this conclusion was checked theoretically for various initial combinations of parameters. The insignificant increase in the boundary mass flow rate with an increase in pipe diameter is connected with the change in the coefficient of resistance during a change in diameter. Thus, we can assume that the effect of pipe diameter on the stability boundary is manifest only in terms of the thermal load, i.e., flow stability does not change if with a change in diameter the specific thermal load changes proportionally or, in other words, the dynamic coefficient of capacity B_d is kept constant. If, however, during a change in diameter the specific thermal load remains constant, an increase in pipe diameter will decrease the boundary value of mass velocity. All other parameters are assumed constant. This regularity is confirmed by experimental data obtained on the stand during a study of horizontal coils with two diameters (Table 2).

Theoretical studies have also shown that the effect of pipe length on the stability boundary during constant parameters is also manifested in terms of the specific thermal load. Thus, for example, with an increase in pipe length by a factor of k and a corresponding decrease in the specific thermal load the pulsation boundary shifts insignificantly toward a flow rate increase. The pulsation period grows significantly.

Table 2.

p , atm (1)	№ п/п	$\Delta t_{\text{н}}$, кал/кг (2)	$\tau_{\text{нз}}$	$\tau_{\text{вмх}}$	$d_{\text{нн}}$, мм	$\bar{q} \cdot 10^{-3}$, ккал (м ² ·с) (3)	B_1	$\frac{w_1}{w_2}$, кг/сек (4)	$\frac{\bar{q}_1}{\bar{q}_2} \cdot \frac{d_2}{d_1}$	$\frac{\bar{w}_1}{\bar{w}_2}$
40	1	24,0	6,9	21,65	20	152,2	1,12	730	—	—
	2	17,2	9,3	15,8	10	62,6	1,05	577	1,236	$\frac{w_1}{w_2} = 1,28$
100	3	34,3	6,9	15,2	20	292	1,01	968	—	—
	4	37,8	9,3	15,8	10	90	1,11	569	1,62	$\frac{w_1}{w_2} = 1,70$
100	5	21,0	6,9	15,2	20	173	0,84	700	—	—
	6	13,8	9,3	15,8	10	90	0,76	676	0,96	$\frac{w_1}{w_2} = 1,03$
60	7	50,5	6,9	21,55	20	347	1,01	1082	—	—
	8	45,0	9,3	15,8	10	95,1	1,12	607	1,82	$\frac{w_1}{w_2} = 1,78$

KEY: (1) atm (abs.); (2) kcal/kg; (3) kcal/m²·h;
(4) kg/m²·s.

BIBLIOGRAPHY

1. Давидов А. А. Исследование пульсаций потока в трубах испарительной части прямоточных котлов. В сб. «Гидродинамика и теплообмен при кипении в котлах высокого давления», АН СССР, 1955.
2. Семеновкер И. Е. Условия исключения межвитковых пульсаций пароводяного потока в котлах. «Труды ЦКТИ», вып. 59, 1965.
3. Голован О. В., Никонов А. А. Экспериментальное исследование условий появления пульсационных режимов в спиральных парогенерирующих змеевиках. «Труды ЦКТИ», вып. 59, 1965.
4. «Труды ЦПН», № 38. «Динамика рабочих процессов прямоточных парогенераторов», под ред. И. И. Морозова. Челябинск, 1966.
5. Балдина О. М., Калинин Р. И. Пульсационные явления в испаряющих трубных элементах. «Энергомашиностроение», 1966, № 7.
6. Балдина О. М., Зинкевич В. Г. Экспериментальное исследование пульсаций потока в парогенерирующих каналах. «Труды СВВМН», № 24. Севастополь, 1967.
7. Балдина О. М. и др. Пульсации потока в горизонтальных элементах парогенераторов. «Теплоэнергетика», 1968, № 8.
8. Балдина О. М. и др. Исследование пульсаций в парогенерирующих горизонтальных и вертикальных трубах. «Труды ВВМНО.У», № 66, 1968.
9. Waggner. Friction Factors for Pressure-Drop Calculations, «Nucleonics», 19, № 11, 1961.
10. Левин С. Расчет падения давления и распределения плотности в двухфазном потоке на основании теории пути перемешивания. «Теплопередача», 85, серия С, № 2, 1963.

STABILITY OF STEAM-WATER FLOW IN A HEATED PIPE IN A SINGLE-LOOP SYSTEM

G. G. Treshchev

Abbreviations

б - container
к - boiling
тр - friction
вх - input
вых - output

In a number of cases, a heat exchanger in which heat exchange occurs with phase transition is connected to a straight-through single-loop system, which can be represented schematically in the following manner.

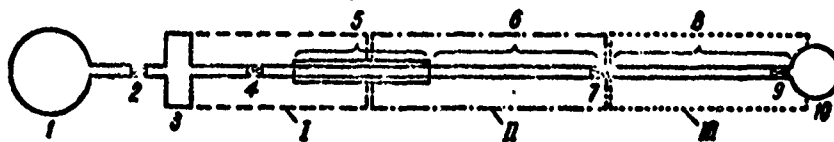


Fig. 1. Diagram of a straight-through single-panel model.

From tank 1 (Fig. 1), in which constant pressure is maintained, liquid moves through throttle 2 with strong throttling, container 3, and throttle 4 with weaker throttling, into section 5 where heat exchange occurs with phase transition. Then the steam-water flow (or steam) through the unheated section of the loop 6 and 8 and chokes 7 and 9 moves to tank 10 in which constant pressure is also maintained.

In spite of the very strong throttling of flow in throttle 2, self-oscillations of steam-water flow can occur in such a loop. The possibility of oscillations is brought about by the presence in front of the heated section of container 3 with a medium which has a compressibility of a sufficient magnitude [1, 2]. Then with relatively small oscillations of pressure in the boiling zone and low resistance for throttle 4 the flow rate of the liquid entering the heated section can change considerably and flow oscillations can occur.

Let us examine what parameters of the system are important in order that strong throttling at input not affect oscillation of the flow in the heated part of the loop. We shall write the equation of motion for zone I, which is indicated by the dashes in Fig. 1. Zone I begins at container 3 and ends at the flow boiling boundary. After integration of the equation of motion with respect to the coordinate along the loop (for simplicity let us assume a system arranged horizontally and disregard the pressure losses from water expansion in the heated part of the loop), we obtain:

$$p_0 - p_k = \int_0^{l_k} \frac{\partial G}{\partial t} dl + \Delta p_{TP} \quad (1)$$

where $G = \rho w$ is mass velocity; p_0 is pressure in container 3; p_k is pressure in the boiling zone; l_k is the length of the channel from the container to the beginning of flow boiling; Δp_{TP} is the pressure loss from friction, involving the resistance of throttle 4.

For an analysis of system behavior at the stability boundaries we can limit ourself to small deviations of flow from stationary flow.

For small deviations, equation (1) is written as

$$\Delta p_0 - \Delta p_k = l_k \frac{\partial \Delta G}{\partial t} + k_{xx} \Delta G; \quad (2)$$

with which it is assumed that ΔG does not change along the coordinate; in this case,

$$\int_0^{l_k} \frac{\partial \Delta G}{\partial t} dl = l_k \frac{\partial \Delta G}{\partial t}.$$

We shall write here the equation of continuity for container 3; in it flows a quantity of liquid FG_0 ; this quantity is constant since it is determined by the drop at throttle 2, which is very large and during small pressure oscillations in the boiling zone and in the container can not vary noticeably (pressure up to throttle 2 is constant). From container 3 flows a quantity of liquid FG (this flow rate is constant per length l_k), consequently,

$$G_0 - G = \beta_0 \frac{\partial p_0}{\partial t}, \quad (3)$$

where $\beta_0 = -\frac{V}{c^2} \left(\frac{\partial v}{\partial p} \right)_t$; let us call this quantity the total compressibility of the examined part of the system; V is the volume of the container per unit cross section of the pipe.

Taking into account the constancy of the flow rate at input to the container (3), during small deviations we obtain from relationship (3):

$$-\Delta G = \beta_0 \frac{\partial \Delta p_0}{\partial t}.$$

Substituting this value of flow rate into the equation of motion (2), we find

$$\Delta p_0 - \Delta p_k = -l_k \beta_0 \frac{\partial^2 \Delta p}{\partial t^2} - \beta_0 k_{xx} \frac{\partial \Delta p_0}{\partial t}$$

or

$$\frac{d^2 \Delta p_0}{dt^2} + \frac{k_{ex}}{l_k} \frac{d \Delta p_0}{dt} + \frac{1}{l_k^2} \Delta p_0 = \frac{\Delta p}{l_k^2} \quad (4)$$

Solution to this equation is found in quadratures and is

$$\Delta p_0 = \frac{1}{\sqrt{\left(\frac{k_{ex}}{l_k}\right)^2 - \frac{4}{l_k^2}}} - \frac{1}{l_k^2} \int_0^t \Delta p_k e^{-\frac{k_{ex}}{l_k}(\tau-t)} \operatorname{sh} \sqrt{\left(\frac{k_{ex}}{l_k}\right)^2 - \frac{4}{l_k^2}} (\tau-t) d\tau.$$

Substituting the value of Δp_0 into the equation of motion (2) and solving relative to ΔG , we obtain

$$\begin{aligned} \Delta G = e^{-\alpha t} \int_0^t \frac{1}{l_k} \left[\frac{1}{\sqrt{\left(\frac{k_{ex}}{l_k}\right)^2 - \frac{4}{l_k^2}}} \times \right. \\ \left. \times \frac{1}{l_k^2} \int_0^t \Delta p_k e^{-\frac{k_{ex}}{l_k}(\tau-t)} \operatorname{sh} \sqrt{\left(\frac{k_{ex}}{l_k}\right)^2 - \frac{4}{l_k^2}} (\tau-t) d\tau - \Delta p \right] e^{\alpha t} dt. \end{aligned} \quad (5)$$

Hence it is apparent that when the quantity $l_k^2 \sqrt{\left(\frac{k_{ex}}{l_k}\right)^2 - \frac{4}{l_k^2}}$ is great, the first term in brackets can be disregarded; then for a deviation of flow rate from the stationary values, the following expression is obtained:

$$\Delta G = -\frac{1}{l_k} e^{-\alpha t} \int_0^t \Delta p_k e^{\alpha t} dt, \quad (6)$$

where $\alpha = \frac{k_{ex}}{l_k}$.

From relationship (6) it is apparent that the change in flow rate is determined only by the pressure oscillations in the boiling zone and the value of the resistance of the system's input section:

$$k_{ex} = \left(\zeta + \xi \frac{l_k}{d} \right) w_{ex},$$

where ζ is the coefficient of resistance of the throttle (4);
 ξ is the coefficient of resistance of a pipe with length l_k and diameter d .

The value of throttling before container 3 does not have a noticeable effect on the change in flow rate ΔG .

To check this experimentally we use a single-loop system consisting of the following elements. Used as tank 1 (see Fig. 1) was a boiler of an experimental heat and power plant, giving steam at a pressure of 300 bar and a temperature of 600°C. A study of pulsations was made at a pressure of 50 bar. Therefore, after cooling the steam in pipe heat exchangers, it was throttled by throttle 2 from 300 to 50 bar. Then container 3 with a capacity of 23 l was connected to the system. The container was filled with a steam-water mixture, which after cooling entered the heated section 5. The container was connected with the section of pipes having an internal diameter of 11 mm and a length of 5.06 m, which then changed into a pipe with diameter 8 mm and a length of 0.5 m. The heated section was made of pipe with a diameter of 12 × 8 mm and a length of 2.4 m. It was heated by dc current from an ASD-50 motor generator. This section was arranged vertically and the water fed into it from the bottom.

Behind the heated section the following were connected in series: a section of pipe \varnothing 8 mm and 0.38 m long, a section of pipe \varnothing 11 mm and 2.62 m long, a throttle ring \varnothing 3 mm, a section of pipe \varnothing 11 mm and 24.82 mm long and then a cooler in which the steam-water mixture was condensed and cooled - two lines of pipe \varnothing 11 mm and 17.6 m long. On the end of the single-loop system was a throttle 9 in which the pressure was reduced to atmospheric (in tank 10).

The resistance between the input end of the heated section and the container was approximately 20,000 N/m² with a mass velocity of water 550 kg/m²·s. The quantity $k_{ex} = \left(\frac{1}{\rho} + \frac{1}{\rho} \frac{d\rho}{dp} \right) \omega$ was equal to 72 m/s.

The value of total compressibility of the medium in the volume of the container, expressed by formula $\beta_0 = -\frac{V}{v} \left(\frac{\partial v}{\partial p} \right)$, was

$0.3 \text{ s}^2/\text{m}$. The value of the product of $t_{\text{in}} \beta_{\text{in}}$ was 22. Consequently, the pressure oscillation in the container was considerably less than in the heated section and its variation can be ignored. During pulsations the pressure oscillations in the boiling zone did not exceed 4 bar. It is clear that the flow rate of water entering the container, determined by the drop of 250 bar in throttle 2, was virtually constant.

Thus, in our single-loop system the small self-oscillations were determined by the input conditions after container 3; however, throttle 2 had no noticeable effect on flow stability.

To investigate the characteristics of the transition of stationary flow to pulsating flow, the above described experimental installations was equipped with IDT quick-response induction pressure gauges. One gauge was installed 0.05 m in front of the heated section and the other 0.05 m behind the heated section.

The temperature of the water flow at input was measured by a quick-response thermocouple. The thermocouple was made of chromel-alumel wire 0.2 mm in diameter, placed in a sleeve 0.8 mm in diameter. The hot junction of the thermocouple and the bottom of the sleeve was a single unit. The emf arising in the thermocouple was intensified by a photoamplifier.

Electrical signals from the pressure gauges, thermocouples, and the heated current of the section (voltage drop) were recorded with a N-105 oscillograph. Along with the recording on the oscillograph, a recording of the parameters of the stationary regimes preceding the regimes with pulsations was made. The transition to pulsations was accomplished either by an increase in the thermal load through an abrupt jump (by 3-30%) or by an increase in the temperature of the water entering the heated section.

Figure 2 presents the oscillograms obtained. If the flow is far from the stability boundary, an increase in thermal load brings about an increase in pressure in the boiling zone, which then drops to a stationary value (Fig. 2a); oscillations do not arise. If flow is in a stable region and near the stability boundary, with an abrupt increase in thermal load attenuating oscillations will occur (Fig. 2b). If, finally, flow is so near the stability boundary that the increase in thermal loading brings about its transition into the unstable region, stable self-oscillations will arise in the flow (Fig. 2c).

An increase in thermal loading causes the additional formation of steam in the zone of the heated section; this leads to an increase in pressure. The pressure impulse affects the flow; the entrance of water into the heated zone decreases and the output of the steam-water mixture increases.

The more the flow is throttled at input and the less at output, the less the flow rate will change at input, the more intensely the steam will be removed from the heated section, and the more slowly the pressure will grow in the boiling zone. As is apparent from a comparison of the oscillograms in Fig. 2a and 2b, as the stability boundary is approached, the rate of pressure growth increases and the pressure impulse grows; this leads to a stronger deviation of flow from stationary. Oscillations occur, but they are attenuating if the dissipation energy for the oscillation period is greater than the input of additional energy as compared with the stationary flow. With a further increase in loading the energy flux into the flow for each oscillation increases; this increased energy input fully compensates energy dissipation and the oscillations become nonattenuating (Fig. 2c). How oscillations arise in flow during a disturbance (growth) in water temperature at input is shown on Fig. 2d.

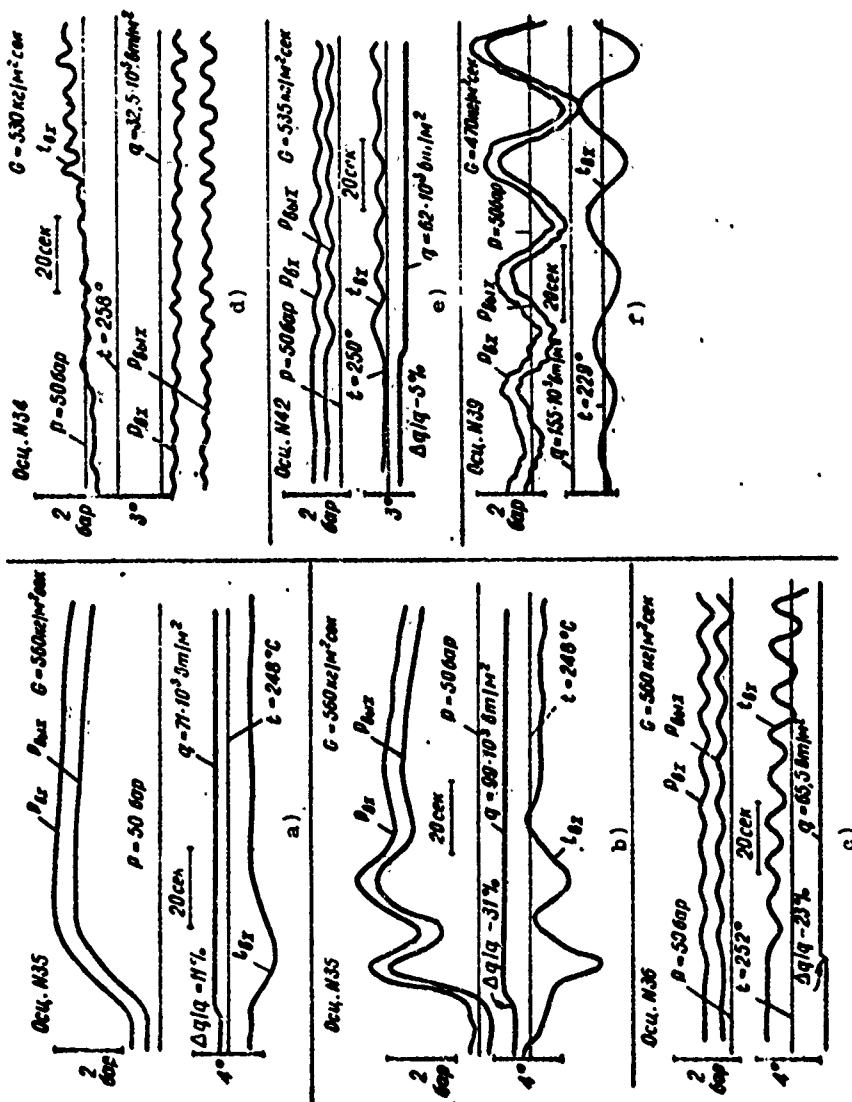


Fig. 2. Oscillograms of experimental regimes.
 DESIGNATIONS: Osc = Oscillogram; бар = bar; $\text{m}^2/\text{m}^2 \cdot \text{cen} = \text{kg}/\text{m}^2 \cdot \text{s}$
 cen = seconds; $\beta \cdot \text{m}/\text{m}^2 = \text{W}/\text{m}^2$.

From the oscillograms it is apparent that when at a given flow rate, pressure, and thermal loading, flow temperature reaches a certain level, oscillations arise which increase with a further rise in temperature. If the temperature increases even more, the oscillations disappear; this begins at the moment the water temperature approaches saturation temperature (underheating less than 2°C).

It should be noted that oscillations can arise not only with an increase in loading but also with a decrease in loading (Fig. 2e). The oscillograms showed that this is connected with the reduction in pressure; this occurs due to a decrease in vapor formation and thus a decrease in pressure loss from friction in the output section and the throttle.

Of course, a reduction in pressure, as a disturbance in the thermal flux, can also cause oscillation (Fig. 2f).

Thus, at the stability boundaries a disturbance of any of the regime parameters can lead to the occurrence of self-oscillations in the flow.

A series of tests were made at constant pressure and flow rate and various underheatings from 2 to 35°C . With a change in underheating in these limits during loadings which are greater the greater the underheating, pulsations whose period changes arise; with an increase in underheating the period grows. However, this connection is not monotonic. Figure 3 presents the values of the square of the oscillation period as a function of the vapor content of the flow.

The circles on Fig. 3 indicate tests in which the transition to pulsation regimes was accomplished by a disturbance of thermal loading, and the triangles indicate the same accomplished by a disturbance of water temperature at input to the heated section.

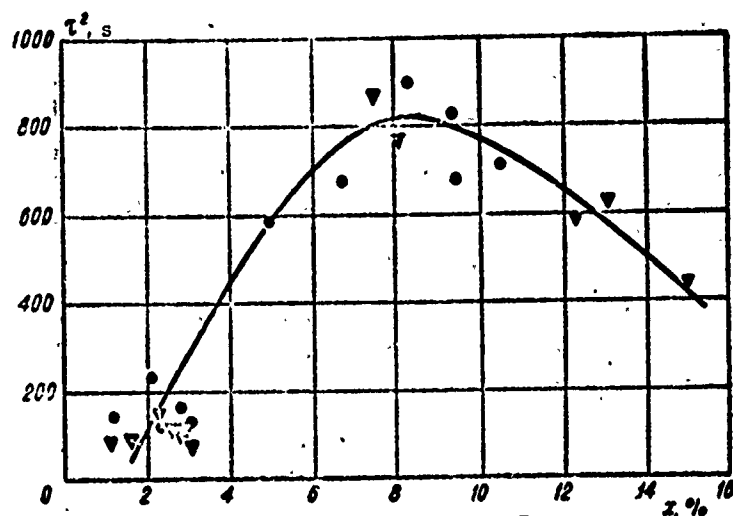


Fig. 3. The square of the oscillation period versus the vapor content of the flow.

In the first approximation we can assume that the oscillation period does not depend upon which parameter is measured for oscillation disturbance: thermal loading or water temperature at input. The spread in points with a low value of vapor content is caused by the low accuracy in this region for both the values of vapor content and oscillation periods. The character of the curve $\tau^2 = f(x)$ - the presence of a maximum - is connected with the fact that the pressure increase in the boiling zone occurs more slowly (the period is greater) the greater the total compressibility of the zone and, consequently, the less the vapor content of the flow. On the other hand, the pressure increase is connected with the rate of steam removal from the zone II (see Fig. 1), and it is less the greater the resistance of the output throttle and, consequently, the greater the vapor content of the flow.

It should be noted that the oscillation period can change somewhat as a function of the pressure oscillation amplitude: with an increase in amplitude it increases somewhat (for example, with an increase in amplitude from 1 to 2.8 bar the period

increases from 24 to 26 s). The amplitude, however, of the oscillations grows with an increase in the abrupt jump of the parameter, which is caused by a disturbance in the flow.

Thus, in a single-loop system self-oscillations can arise; this occurs when the total compressibility of the medium in the part of the system in front of the heating zone is sufficiently great. A large value for the product of the coefficient of input section resistance times the total compressibility of the input part of the system $k_{\text{вх}}\beta$ determines the possibility of pulsations and, on the contrary, a low value for this quantity in the presence of considerable throttling at input ensures flow stability. In the experimental installation described this criterion was 22 seconds.

BIBLIOGRAPHY

1. Миropольский З. Л. Пульсации расхода в испарительных каналах при наличии упругой среды в предвключенных элементах тракта. ИФЖ, 1964, № 8.
2. Мальков В. А., Морозов Н. И. Влияние упругих емкостей на устойчивость рабочего процесса в парогенерирующих трубах. ИФЖ, 1963, № 1.

THE HYDRODYNAMICS OF TWO-PHASE NONEQUILIBRIUM FLOWS

Ye. I. Nevstruyev, D. A. Khlestkin,
T. T. Antidze, and G. M. Dvorina

In most modern steam-generating installations water heated considerably less than saturation temperature is fed to input. With large thermal loads at comparatively short distances from input in the heated channel surface boiling begins. As tests have shown, the steam forming on the heat-transferring surface, even with considerable underheating, does not condense directly on the surface but penetrates the region of underheated liquid and is entrained by the flow. Due to the fact that vapor condensation does not occur instantaneously, but at a finite, frequently rather slow, rate, two-phase flow is thermodynamically unbalanced. Such flow is a mixture of vapor and underheated water; the greater the vapor and the greater the average underheating of liquid phase with the same value for relative flow enthalpy x , determined according to the heat balance, the greater the degree of thermodynamic nonequilibrium.

Furthermore, the process of vapor formation is, in essence, a nonstationary process and is characterized by variable values of basic parameters. Because of this, the processes in steam-generating pipes should be studied not only by measuring the

average values of flow parameters but also by the simultaneous recording of variations in these parameters over time.

A complex study on two-phase nonequilibrium pulsationless flows in heated and unheated pipes is being carried out in the Laboratory of Two-Phase Systems of the Mass Exchange Department of the NIIVT [Translator's Note: This abbreviation could stand for either the Scientific Research Institute of High Temperatures or the Novosibirsk Institute of Water Transportation Engineers.] under the direction of Academician M. A. Styrikovich.

A description of the experimental installation and the research methodology is explained in detail in references [1, 2].

Each series of tests was usually performed with constant average values of pressure, mass velocity, and thermal loading by the gradual increase of temperature at input to the experimental installation. At first pulsationless regimes of flow were studied, and then pulsation regimes up to the onset of crisis. In each series of tests the boundary values of parameters were fixed, corresponding to the beginning of the emergence of self-oscillations in the experimental section. The figure presents the variations in true per-volume vapor content over time in three cross sections along the experimental section (the first two in the heated pipes and the third in the unheated), and it is apparent that, in analogy with pulsationless flow, during pulsation flow regimes the quantity of vapor in the unheated section of the pipes is greater than in the heated.

The figure illustrates various types of pulsation regimes detected in the tests, which can be dependent on the frequency characteristics, and are conditionally called disordered a, ordered b, and low-frequency c.

The term "disordered pulsations" is introduced for the characteristics of regimes in which oscillations of parameters,

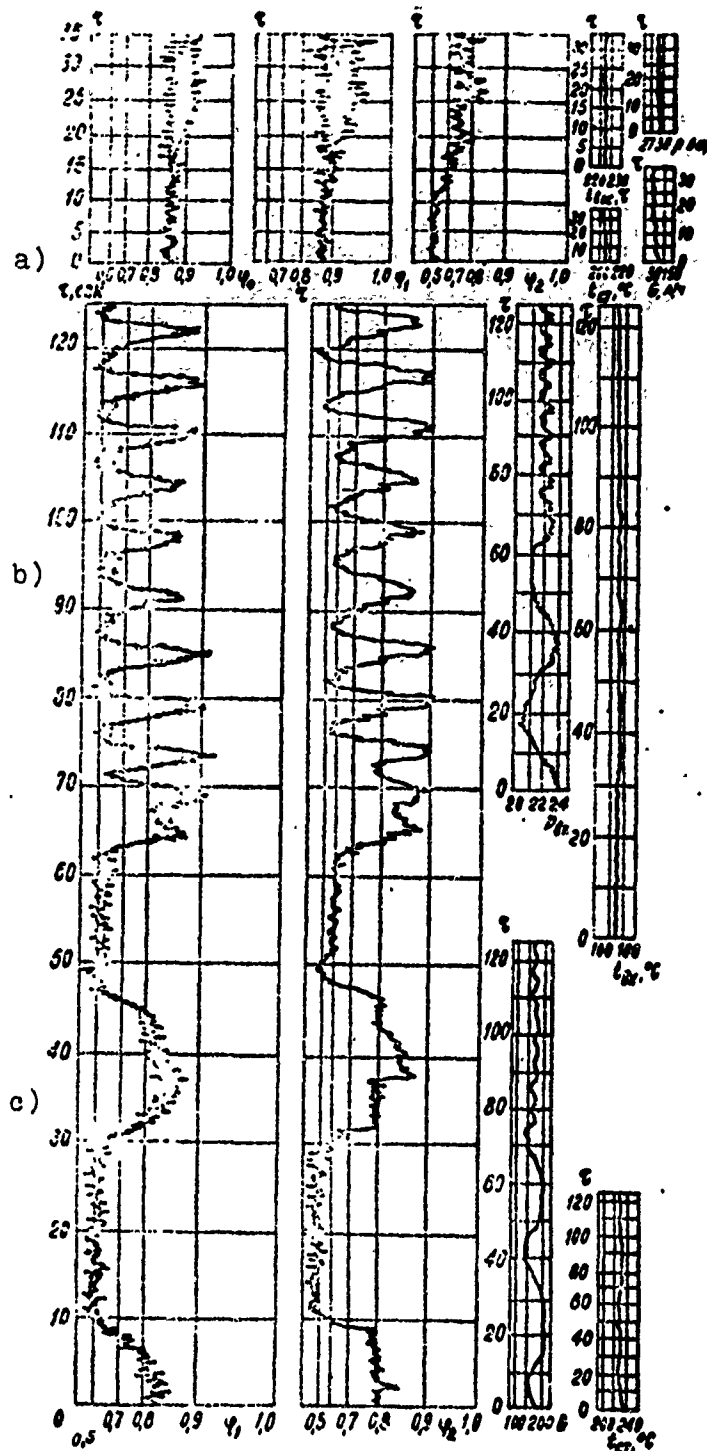


Fig. 1. Regime characteristics of two-phase nonequilibrium flows in the presence of various types of self-oscillations:
 ϕ_0 and ϕ_1 - vapor contents in various cross sections of the heated section of the experimental pipes;
 ϕ_2 - vapor content at output from the unheated section of the experimental pipe.
DESIGNATIONS:
сек = s; бар = bar;
 $n/4 = l/h$; ax = input;
ст = st.

even in short intervals of time, are characterized by variable values of amplitude and frequency, differing by several factors. Such flow regimes occur with large vapor contents and comparatively low thermal loads and, probably, are annular dispersed flow regimes with which part of the liquid phase flows in the form of a film along the channel wall and the other part of the moisture is sprayed in the form of drops in the vapor flow. The character of the film's motion on the heat-transferring surface, as the tests of other authors have shown, can be wave-shaped.

Ordered pulsations are characterized by the almost exact agreement between the frequency and amplitude characteristics of the parameter oscillations and are probably connected with the displacement of large vapor clusters along the channel. With such flow regimes pulsations of vapor contents and pressures, as a rule, agree in phase, while pulsation of flow rate is in opposite phase. The reason for the occurrence of flow rate pulsations in a steam-generating channel is probably the periodic increase in the hydraulic resistance of the channel connected with the periodic increase in vapor content. It should be noted that in installations with powerful pumps and strong flow throttling at channel input (in absence of large compressible capacities) flow rate pulsations do not occur. Under actual conditions in the presence of collectors and multi-pipe systems, increase in the hydraulic resistance in any one of the parallel branches must unavoidably lead to a drop in the flow rate due to the redistribution of flow rates. Thus, the installation used in this study, with a turbine pump apparently imitates rather closely the operation of one branch of a real apparatus, excluding the fact that the pressure drop in the experimental section is not kept constant as occurs under actual conditions.

Low-frequency pulsations (see Fig. 1c) are obviously connected with the periodic temporary increase in pressure in the experimental section. Such a pressure increase and the

corresponding saturation temperature increase lead to a weakening of the boiling process intensity or even to its complete cessation for a certain period of time. The hydraulic resistance of the steam-forming sections falls, flow rate grows, and pressure decreases. The boiling process becomes more intense and vapor formation, hydraulic resistance, and pressure increase, which again leads to a reduction in vapor formation intensity. The period of such pulsations is $\sim 25-30$ s and is commensurate with the time of liquid passage along the entire experimental loop.

Before the appearance of a crisis, whose onset parameters were evaluated earlier, all recording instruments are simultaneously switched on, recording the variations in the basic flow parameters in the period before crisis onset, at the instant of the crisis itself, and after it, i.e., after discharge or reduction of the load. With considerable underheating at input and, accordingly, relatively large critical thermal loads, crisis occurs with pulsationless flow regime and low true vapor contents per unit volume at the spot where the crisis occurs. This type of crisis, arising with comparatively low vapor contents per unit volume, is, of course, similar to the crisis during boiling in a large volume when all the vapor forming at the surface goes into the volume [3].

With moderate underheating at input and, accordingly, average critical thermal loads, crisis occurs in the above examined flow regimes with ordered pulsations. The period for pulsations in vapor content, pressure, and flow rate is up to 2.5 s with a heated section length of 600 mm. The temperature of the heat-transferring surface before onset of crisis does not pulsate in such regimes and remains virtually constant. Only at the instant of crisis is there observed a sharp increase in wall temperature. This points to the fact that before the onset of crisis on the heat-transferring surface even during the approach of large clusters of steam there is a relatively stable film of liquid which ensures the continuous cooling of the surface. Analysis of the regime

characteristics with this type of crisis has shown that the first oscillations (in the direction of increase) in wall temperature are observed when a maximum vapor content per unit volume of 0.95 is reached. Obviously, in this case, the crisis is connected with the fact that the large cluster of vapor at the surface of the liquid film hinders the replenishing of the surface film by liquid from the core of the flow. An evaluation of the liquid film thickness on the heat-transferring surface at the moment crisis occurs indicates that under the examined flow regime a considerable portion of liquid must be in the flow; then it does not greatly affect the intensity of heat transfer from the surface.

With very small underheatings at input to the heated section and, accordingly, low critical thermal loads, a boiling crisis arises during flow regimes with disordered pulsations. Oscillation frequencies during disordered pulsations are approximately one hertz. Variations in vapor content during these regimes as crisis approaches are accompanied by significant oscillations in the temperature of the heat-transferring surface (on the order of tens of degrees, always in the direction of an increase). Since the maximum vapor content with this reaches one, consequently, there is no stable film on the heat-transferring surface, otherwise there would be no such noticeable increases in temperature. Due to the rather high frequency of the oscillations in true vapor content per unit volume, the surface, which is periodically dry, can not be strongly reheated before the entrance of the next portion of moisture either from the core of the flow or from the advancing wave of the boundary layer (on the assumption of the existence of waves on the surface of the liquid film). Only with average vapor content per unit volume equal to 0.95 does crisis arise, accompanied by continuous temperature increase on the heat-transferring surface and by its reddening on the upper output end of the heated section. As visual observations have indicated, the crisis is propagated down to the input section itself.

Thus, based on the studies made, we can state that when investigating the crisis of boiling, the study of the hydrodynamics of two-phase flow by measuring the instantaneous values for vapor contents has great possibilities and is of considerable interest.

By analogy with two-phase gas-liquid or steam-liquid flows in unheated or weakly heated pipes, it is assumed that during passage along the channel of large vapor clusters there occurs a shell flow regime during which the vapor moves along the axis of the vertical pipes while the water moves along the periphery and in bridges between the shells. Moreover experimental data [4, 5] indicate that during the boiling of underheated liquids in the presence of large thermal loads, vapor is concentrated primarily in the boiling boundary layer while the core of the flow not only remains single-phase but also is heated rather weakly. Therefore, we can assume that at sufficiently high vapor contents such flow can be not shell-shaped but ring-shaped; the vapor moves not in the form of shells along the axis of the pipe but in the form of rings. However, the core of the flow can remain single-phased. If such a flow regime actually occurs, then upon the passage of a vapor cluster the main mass of liquid, moving along the axis of the pipe, must have a velocity greater than the velocity of the vapor. The possibility of a vapor cluster on the heat-transferring surface has been demonstrated not only by movie film [6] but also by several analytical studies [7].

As for the bridges of water between the vapor clusters, vapor in them perhaps moves in the form of chains or filaments whose velocity must be greater than the average velocity of the liquid. The problem is particularly complicated when studying nonequilibrium pulsation flows in which the pressure pulsations continuously cause both condensation and boiling. To study such flows, not only new experimental methods are necessary but a completely different approach to analytical studies is required.

Conclusions

1. When a steam-generating channel is fed water which has not reached saturation temperature, the quantity of steam in the sections of this channel is considerably greater, while the temperature of liquid phase is considerably lower, than could be expected in the case of thermodynamic equilibrium.

2. The absence of thermodynamic equilibrium indicates that the condensation of vapor in underheated liquid occurs not instantaneously but at finite, rather low rates.

3. Study of the instantaneous values for pure vapor content per unit volume and other regime parameters has indicated that, as a function of the underheating at input and the thermal load, the existence of various types of pulsationless and pulsation flow regimes is possible for two-phase nonequilibrium flows.

4. The mechanism of boiling crisis in channels is inseparably connected with the hydrodynamics of two-phase flow, and when examining it it is necessary to study not only the heat exchange but also the hydrodynamic characteristics.

5. A study of the heat exchange crisis in two-phase flows must be carried out using quick-response recording equipment due to the transiency inherent in such flows.

6. An analysis of the processes in steam-generating pipes must be performed with the thermodynamic nonequilibrium of two-phase flows taken into account.

7. The research conducted indicated that depending upon the underheating of the liquid at input to the heated channel and, consequently, on the critical thermal load at the same pressures and mass velocities, there are possible at least three completely

different types of boiling crises connected with the structure of the two-phase flow.

8. On the basis of an analysis of the variations in regime parameters of pulsation flow over time, and particularly the instantaneous values of true vapor content per unit volume, we can predict the probable structure of a two-phase nonequilibrium pulsation flow consisting of a rings of vapor and an underheated liquid core.

BIBLIOGRAPHY

1. Невструева Е. И., Хлесткин Д. А. Экспериментальная установка для исследования нестационарных процессов в парогенерирующих трубах. «Труды МЭИ», вып. 63, 1965, стр. 163—171.
2. Невструева Е. И., Хлесткин Д. А. Методика исследования паросодержаний при нестационарных процессах в парогенерирующих трубах. «Доклады научно-технической конференции МЭИ. Секция теплоэнергетическая, подсекция теплофизическая», М., 1965.
3. Стырикович М. А., Невструева Е. И. Некоторые новые методы экспериментального исследования механизма кипения и механизма кризиса кипения. В сб.: «Теплофизика высоких температур», т. 2, № 3, 1954, стр. 437—445.
4. Невструева Е. И., Гонсалес Х. Распределение паросодержаний при поверхностном кипении методом бета-просвечивания. «Теплоэнергетика», 1960, № 9, стр. 34—39.
5. Джи-Джи и Кларк. Пузырьковый пограничный слой и профили температуры при кипении жидкости, движущейся в канале в условиях вынужденного движения. «Теплопередача, серия С», т. 86, № 1, 1964.
6. Сато Т., Хайашида Н., Молода Т. Влияние пульсаций скорости на критическую тепловую нагрузку. «Материалы III Международной конференции по теплообмену», т. IV, 1966, стр. 226—233.
7. Дуклер И. Г. Автореферат диссертации на соискание ученой степени канд. техн. наук. М., МЭИ, 1966.

AN EXPERIMENTAL STUDY OF HYDRODYNAMIC CHARACTERISTICS DURING THE BOILING OF UNDERHEATED WATER IN VERTICAL PIPES

G. G. Bartolomey and V. M. Chanturiya

Designations

- d - internal diameter of working pipe, mm;
- p - pressure at output from working section, bar;
- w - velocity of water at input to working section, m/s;
- (γw) - mass velocity of flow in channel, $\text{kg/m}^2 \cdot \text{s}$;
- q - specific thermal flux, W/m^2 ;
- γ' - specific weight of water on saturation line, kg/m^3 ;
- γ'' - specific weight of vapor on saturation line, kg/m^3 ;
- r - vaporization heat, kcal/kg;
- i' - enthalpy of water on saturation line, kcal/kg;
- i_n - average flow-rate enthalpy of flow, kcal/kg;
- i_{cp} - average flow-rate enthalpy of water in core of flow, kcal/kg;
- i_s - water temperature on saturation line, $^{\circ}\text{C}$;
- t_n - average flow-rate temperature of flow, $^{\circ}\text{C}$;
- t_0 - temperature along axis of flow, $^{\circ}\text{C}$;
- t_n - temperature on interface of viscous sublayer and core of flow, $^{\circ}\text{C}$;

- t_{η} - temperature along the cross section of the flow core, °C;
- t_{cp} - average flow-rate temperature of water in the flow core, °C;
- t_H - temperature of external surface of channel wall, °C;
- t_{BH} - temperature of internal surface of channel wall, °C;
- η - relative radius of working pipe;
- ϕ - average true vapor content along the cross section of the flow;
- x - mass flow-rate vapor content or relative enthalpy of flow;
- x_d - actual mass flow-rate vapor content;
- β - volumetric flow-rate vapor content;
- β_d - actual volumetric flow-rate vapor content.

The hydrodynamic processes which occur during the boiling of underheated liquid under forced circulation conditions, due to their exceptional complexity, are very difficult to subject to theoretical examination, which means that experiment is the chief method for studying these processes in order to reveal their overall regularities. Analysis of published data indicates that the majority of works on one of the most important hydrodynamic characteristics of steam-water flow - pure vapor content during surface boiling - have been performed on channels of rectangular or annular cross sections. As for an experimental determination of this parameter in channels of circular cross section, which is of considerable practical interest in the design of modern thermal apparatuses, only references [1, 2], using the method of labeled atoms, are known to concern this question.

The purpose of our work is the experimental study of true vapor content, averaged along the flow cross section, during the surface boiling of water in vertical heated pipes with internal diameters of 11.7, 15.4, and 24.0 mm by the radiographic inspection of the working channel with a wide beam of γ -rays, along with the

determination of the temperature profile along the flow cross section and the measurement of the external temperature of the channel wall surface. In addition, in a number of supplementary tests, with radiographic inspection of a pipe 15.4 mm in diameter by a narrow beam of γ -rays, the distribution of vapor phase along the cross section of the flow was determined, while the character of the temperature pulsations, measured along the diameter of the working pipe, was studied with oscillographic recordings. Thus, in addition to accumulating test data on true vapor content, our work also included the study of individual characteristics, which enabled us to examine in greater detail the physics of the surface boiling process.

Tests were made at pressures of 15, 30, and 45 bar, thermal loads $(0.4, 0.6, 0.8) \cdot 10^6 \text{ W/m}^2$, and mass velocities of 450, 900, 1800, 2700, and 3600 $\text{kg/m}^2 \cdot \text{s}$. The degree of water underheating at input to the working section varied from 160 to 6°C. At output from this section the value of true vapor content varied from zero to 0.55.

EXPERIMENTAL INSTALLATIONS AND TEST METHODOLOGY

The experimental installation is an open loop connected to the main lines of the MEI [Moscow Power Engineering Institute] heat and electric power plant for the feed water and superheated steam. The diagram of the stand and its description are found in reference [3]. Thin-wall pipes $\varnothing 12.3 \times 0.3 \text{ mm}$, $\varnothing 16.1 \times 0.35 \text{ mm}$, and $\varnothing 26.9 \times 1.45 \text{ mm}$ 2000 mm long, made from 1Kh18N9T stainless steel, were used as the heated channels, which is the main element of the experimental installation. The values for flow temperature along the axis of the pipes at input and output of the working section were measured with chromel-copel thermocouples with alundum wires 0.2 mm in diameter. In addition to this, a similar thermocouple checked the average flow-rate temperature of the working medium one meter from the output section of the experimental section after the flow had passed the elbow.

For measuring the temperature of the external wall surface of the heated channel, five chromel-copel thermocouples were installed along its length and, to avoid induction, were insulated from the current-conducting surface of the channel by a thin layer of mica.

To measure the temperature profile along the flow cross section a specially designed movable thermocouple was used, located 70 mm from the output section of the working pipe. The thermocouple was moved along the channel cross section by a device with a micrometric screw. The position of the hot junction of the thermocouple, diameter 0.4 mm, relative to the axis of the pipe could be determined within ± 0.25 mm. This made it possible to move the thermocouple without liquid leakage at pressures to 60 bar and enabled us to easily replace thermocouples. The moveable thermocouple device is shown in Fig. 1.

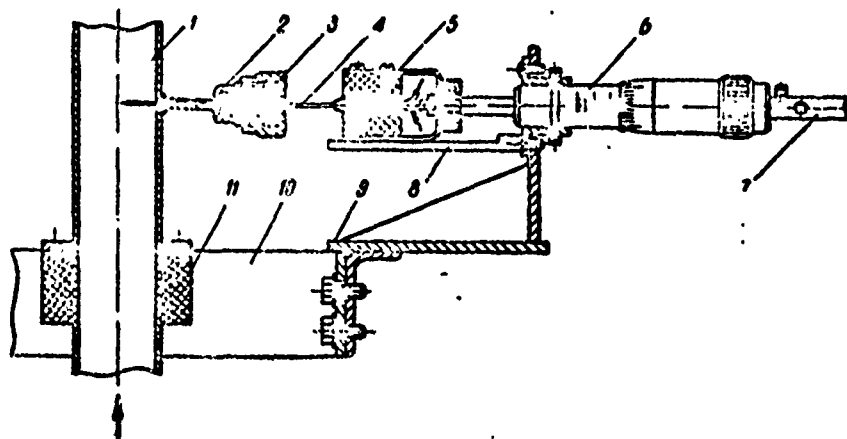


Fig. 1. Moveable thermocouple device:
1 - Working channel; 2 - Fitting; 3 - Teflon recess;
4 - Capillary tube; 5 - Insert piece; 6 - Micrometric
mechanism; 7 - Shaft; 8 - Guide; 9 - Bracket; 10 -
Upper carriage of the radiographic inspection device;
11 - Insulating clamp.

The value of the average radiation intensity, necessary for determining true vapor content, during motion in the channel of

the studied medium was recorded with a special electronic instrument. The isotope $Tu-170$, activity 0.5 g-equiv. Rd , was used as the radioactive source. As the γ -radiation detector we used a $NaJ (Te)$ crystal and a photomultiplier.

The points for measuring radiation intensity during the radiographic inspection of the channel by a wide beam of γ -rays, conditionally designated ϕ_1 and ϕ_2 , were located along the height of the working pipe at various distances from its output section. The signal from output of the measuring system was fed to the indicator or, during a number of tests, to the input of an N-700 loop oscillograph.

Radiographic inspection of the experimental channel by a narrow collimated beam of γ -rays, dimensions $0.5 \times 10 \text{ mm}$, was performed with continuous and uniform movement of the carriage in a direction perpendicular to the axis of the pipe. The measurement cross section for radiation intensity was 300 mm from the output section of the working section.

The order of the basic tests was as follows. According to the test regime assumed, the flow rate, pressure in the working section, and thermal loading on the heated pipe were established. As stationary state was achieved, the simultaneous measurement of the basic thermophysical parameters of the flow was made and also the cross-sectional average radiation intensities were recorded at points ϕ_1 and ϕ_2 . In addition, the external channel wall surface temperature was measured and the temperature was taken by the moveable thermocouple at several points along the flow cross section.

In addition to the main tests, several supplementary experiments were made on a pipe with an internal diameter of 15.4 mm ; the test procedure differed from the above only with respect to parameter recording. The radiation intensity averaged along the flow cross section was measured only at point ϕ_1 .

Tests were made in series. Within each series, several tests were made in both the single-phase liquid flow regime and in the regimes of surface and volume boiling by gradually varying the water temperature at input to the working section. The values of the other parameters were kept as constant as possible. At the measurement point for all recorded values, a condition of thermal and hydrodynamic stabilization was maintained.

EXPERIMENTAL RESEARCH ON TRUE VAPOR CONTENT AVERAGED ALONG THE FLOW CROSS SECTION

The cross-sectional average true vapor content is the basic parameter analyzed in our work. According to the methodology developed earlier for calculating ϕ during the radiographic inspection of an experimental channel by a wide diverging plane beam of γ -rays, the values of the studied parameter in two cross sections of the channel for each of the main tests were determined according to the linear calculation function derived in reference [4]. Maximum absolute errors in determining true vapor content in most tests were within ± 0.035 . The minimum value of ϕ , recorded under experimental conditions, was $\phi_{\min} = 0.015$. The values for relative enthalpy x at the radiographic inspection points were calculated according to the quantity of heat absorbed by the working medium in the section of heated pipes before the given cross section, taking into account losses to the ambient medium in this section. The value of the limiting absolute error in the entire examined range of x variation was less than ± 0.006 .

Figures 2, 3, and 4 are graphs of the true vapor content ϕ versus relative flow enthalpy x , varying from negative values during the boiling of underheated water to positive values corresponding to the beginning of the region of volume boiling. Analysis of the functions obtained makes it possible to illustrate certain regularities in the effect of the regime conditions on the studied parameter. Thus, with a mass velocity of $\gamma w = 900 \text{ kg/m}^2 \cdot \text{s}$

for all three test pipes, an increase in pressure leads to a reduction in true vapor content in the entire studied region of x variation; with a decrease in pipe diameter this relationship noticeably weakens. At higher flow velocities for a test pipe with $d = 15.4$ mm, the noted character of the effect on ϕ is preserved but it is manifested to a lesser degree. However, for a working pipe with $d = 11.7$ mm, with an increase in flow velocity the value of true vapor content at various pressures changes insignificantly, while a disruption in the uniqueness of the effect of pressure on ϕ in the region of negative values for x , in a number of cases, is commensurate with the degree of accuracy involved in determining true vapor content in our work.

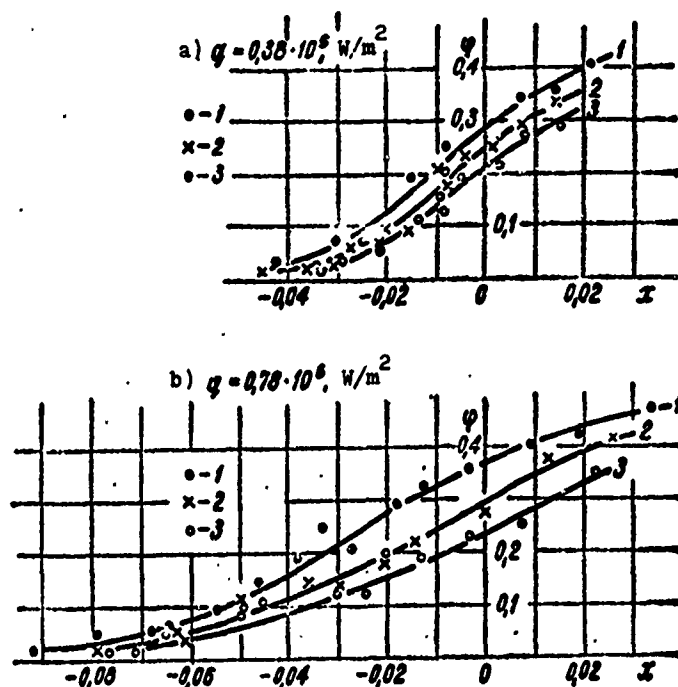


Fig. 2. ϕ versus x for a pipe with $d = 24.0$ mm;
 $\gamma_w = 900 \text{ kg/m}^2 \cdot \text{s}$:
 1 - $p = 15$ bar; 2 - $p = 30$ bar; 3 - $p = 45$ bar.

Within the studied range of parameters an increase in the level of thermal loading, other conditions being equal, as a rule, leads to an increase in ϕ ; the minimum value of true vapor content

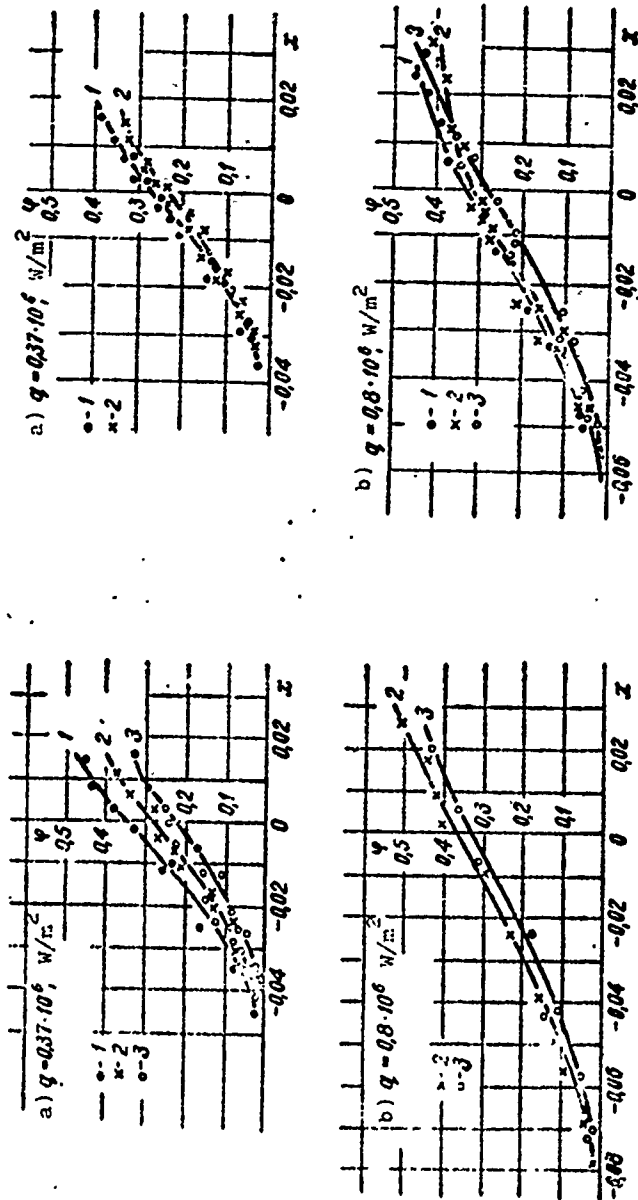


Fig. 3. ϕ versus x for a pipe with $d = 15.4 \text{ mm}$:
 1 - $\gamma w = 900 \text{ kg/m}^2 \cdot \text{s}$, $p = 15 \text{ bar}$; 2 - $\gamma w = 2700 \text{ kg/m}^2 \cdot \text{s}$; $p = 30 \text{ bar}$;
 3 - $\gamma w = 2700 \text{ kg/m}^2 \cdot \text{s}$, $p = 45 \text{ bar}$.

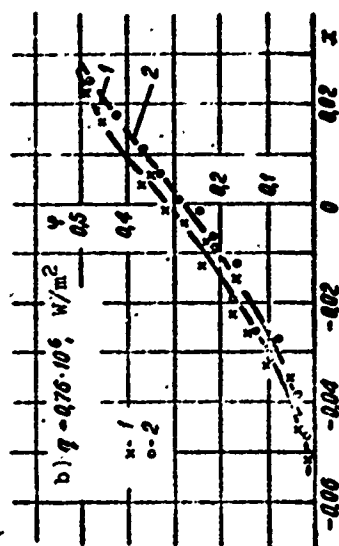
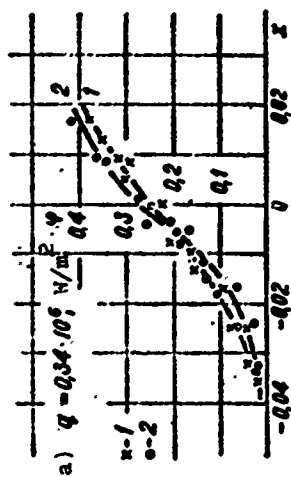
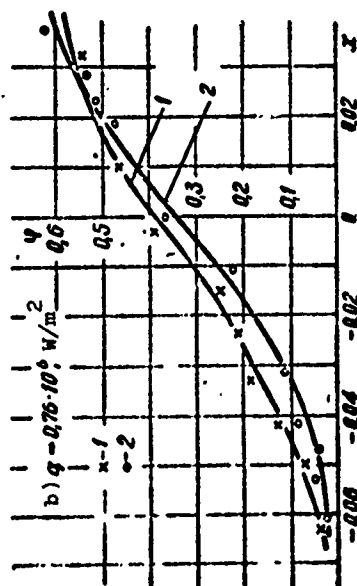
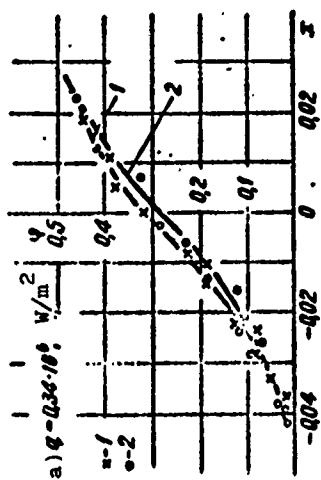


Fig. 4. ϕ versus x for a pipe with $d = 11.6$ mm:
 1 - $\gamma_w = 900 \text{ kg/m}^2 \cdot \text{s}$, $p = 30$ bar; 2 - $\gamma_w = 3600 \text{ kg/m}^2 \cdot \text{s}$, $p = 45$ bar.

recorded in these tests is noted with large negative values for relative enthalpy. Thus, if during $q = 0.8 \cdot 10^5 \text{ W/m}^2$ ϕ_{\min} is recorded approximately when $x = -0.08$, then for the case of $q = 0.37 \cdot 10^6 \text{ W/m}^2$ the minimum possible value of true vapor content occurs only at $x = -0.04$. As relative enthalpy increases, the effect of thermal load on the studied parameter decreases and, to all appearances, gradually disappears in the region of volume boiling.

From a comparison of the test data it is also apparent that in the studied range of variation for the regime parameters, the mass velocity of flow uniquely affects the value of true vapor content; with its increase, ϕ decreases. However, with a decrease in the diameter of the working pipe, all other regime conditions being equal, the value of true vapor content generally increases. However, if the direct relationship $\phi = f(x)$ for a pipe with $d = 15.4 \text{ mm}$ lies above the curve for a pipe with $d = 24.0 \text{ mm}$ throughout the relative enthalpy variation range and the quantity ϕ_{\min} for both cases is noted during near values of x , then for a pipe with $d = 11.7 \text{ mm}$ a noticeable increase in true vapor content is observed only in the region of small underheatings and positive values for relative enthalpy, while the quantity ϕ_{\min} is recorded at smaller negative values for x .

INVESTIGATION OF HYDRODYNAMIC FLOW STRUCTURE AND DETERMINATION OF TEMPERATURE FIELDS ALONG FLOW CROSS SECTION

In our work on the hydrodynamic structure of the flow of a vapor-water mixture during the boiling of an underheated liquid in circular channels, diagrams showing the distribution along the flow cross section of radiation intensities averaged along the chord were recorded on a diagram tape of an EPP-09M2 potentiometer during radiographic inspection by a narrow collimated beam of γ -rays in a series of tests on working pipe with an internal

diameter of 15.4 mm. In processing, the diagrams obtained were broken down into a finite number of chords, for each of which the average value of true vapor content was determined according to a formula for a narrow beam and a source having monochromatic radiation [5]. As a result, diagrams were obtained showing the distribution along the flow cross section of true vapor content averaged along the chord for the region of surface boiling at various values of relative enthalpy (Fig. 5), whose analysis made it possible to give a qualitative evaluation to the character of the structural rearrangement of the flow as the degree of underheating decreases as the working medium moves along the heated pipes.

At large negative values for x the main part of the vapor phase is concentrated near the heated surface. The reduction in underheating of the liquid along the experimental channel is accompanied by the gradual transfer of vapor from the boundary layers to the core of the flow and an overall increase in vapor phase. Our attention is turned to the high concentration of vapor in the central zone of the flow with zero relative enthalpy.

For each of the examined tests the true vapor content, averaged along the radiographically inspected cross section of the channel, was defined as the weighted mean along the chords. The results obtained agree well with the values of ϕ measured by a wide beam of γ -rays under the same regime conditions.

In order to determine the temperature fields along the flow cross sections during the boiling of underheated liquid, temperature measurements were made with a moveable thermocouple at several points at equal intervals along the diameter of the experimental pipe. According to these temperature values, which were averaged over time, temperature profiles were plotted at various values for relative enthalpy; an examination of these profiles made it possible to illustrate the effect of various

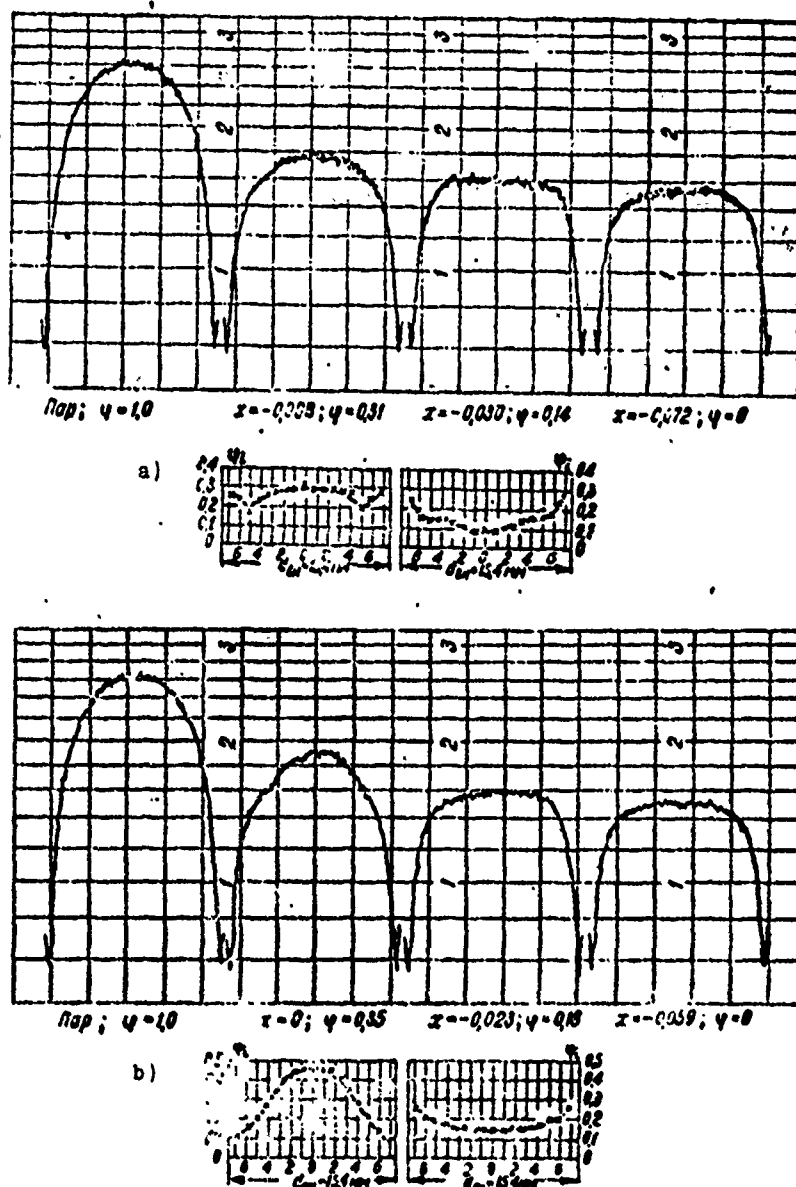


Fig. 5. Distribution of local vapor contents along flow cross section:

$d = 15.4$ mm, $\gamma_w = 900$ kg/m².s, $q = 0.57 \cdot 10^6$ W/m²;
 a - $p = 15$ bar; b - $p = 30$ bar.

DESIGNATION: Π_{ap} = vapor.

regime factors on the character of temperature distribution along the flow cross section. Thus, an increase in pressure within the studied range does not lead to a noticeable restructuring of the examined profiles, while an increase in thermal loading, all other conditions being equal, is accompanied by an increase in the temperature drop between the boundary layers of the flow and its colder core. An increase in mass velocity leads to equalizing of the temperature field due to the higher degree of flow turbulence and, consequently, the more intense transfer of thermal energy from the heated wall to the flow core.

Compared on Fig. 6 are profiles of temperature along the flow cross section, obtained in pipes of various diameters with approximately equal regime conditions. Here there occurs a marked growth in the above noted temperature drop, as well as an increase in the difference between the boundary layer temperature and the average flow-rate temperature of the flow with an increase in the diameter of the experimental pipe. A similar character for the effect of the diameter on temperature distribution along the flow cross section was earlier noted in reference [6]. It should be mentioned that not once did the measured temperature near the heated surface exceed the saturation temperature of the liquid at a given pressure. Attention is drawn to the presence of a certain temperature gradient during values of relative enthalpy near zero. We should note, however, that this design of moveable thermocouple does not exclude the possibility of heat flow along the thermoelectrodes, which leads to a distortion of the temperature profile to be determined and a disruption, in a number of cases, of its symmetry relative to the axis of flow.

In measuring the temperature profiles of the flow throughout the region of studied regime conditions, significant temperature pulsations were observed; to determine the character of these pulsations during supplementary tests on a working pipe with $d = 15.4$ mm, oscillographic recordings of the temperature values

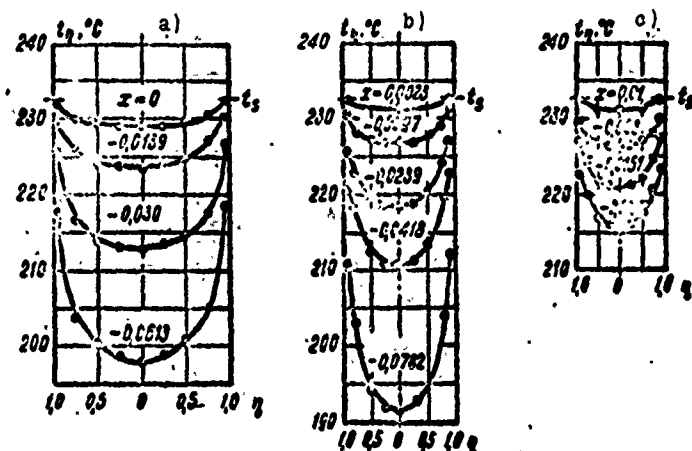


Fig. 6. Temperature profiles along the flow cross section:

$\gamma_w = 900 \text{ kg/m}^2 \cdot \text{s}$, $q = 0.8 \cdot 10^6 \text{ W/m}^2$, $p = 30 \text{ bar}$;
 $a - d = 24.0 \text{ mm}$; $b - d = 15.4 \text{ mm}$; $c - d = 11.7 \text{ mm}$.

at various points along the pipe diameter were made. It can be noted that in the region of large negative values for x , where single-phase or the initial stage of surface boiling occurs, and in the region of small underheatings the character of the change in the examined pulsations is qualitatively different. The noted growth in amplitude as the heating surface is approached, in the latter case, appears more suddenly and is accompanied by a noticeable drop in pulsation frequency. In addition to this, it was established that, all other conditions being equal, an increase in thermal loading leads to an increase in these pulsations.

THE PROCESS OF SURFACE BOILING ALONG THE HEATED CHANNEL

Earlier it was noted that within each of the main series of tests, by varying the degree of water underheating at input to the experimental section, several tests each were performed in both the regime of single-phase flow and the regimes of surface and volume boiling. The values of the remaining regime parameters were kept constant. This enabled us to reduce all the processed

experimental data of each series of tests to one general pattern showing the distribution of temperatures and true vapor contents of the flow, as well as channel wall temperatures as a function of the increase in flow enthalpy along the heated channel at given regime conditions.

For a complex examination of the process of the development and course of surface boiling along a steam-generating channel under forced circulation conditions, the above indicated relationships $t = f(i_n)$ and $\phi = f(i_n)$ are presented, as an example, in the form of graphs obtained from the data from one series of experiments. In plotting these graphic relationships, the values of average flow-rate temperature, temperature along the axis of the flow, temperature of the external channel wall, as well as the values of true vapor content averaged along the flow cross section were successively plotted along the y-axis. The values of the average flow-rate enthalpy of the working medium i_n at the measurement points of the recorded quantities were calculated with the heat balance equation. The average calculated values of the temperature of the inner heat-releasing channel wall surface were determined according to the measured and average values of the temperature of the outer surface of the test pipe and the drop in temperature in the pipe wall. Figure 7 also presents temperature profiles along the flow cross section; in plotting this an additional coordinate was introduced - the current values for the relative radius of the working pipe were plotted along the x-axis.

From an examination of the graph thus plotted it follows that the cross section where the value of ϕ_{min} is recorded virtually agrees with cross section b, beginning with which there occurs a decrease in the difference between the average flow-rate temperature and the temperature along the flow axis, and is considerably removed from the cross section of the formal beginning of surface boiling a where the channel wall temperature reaches

the saturation temperature of the studied medium at the given pressure. This situation agrees well with the pattern, visually observed earlier in reference [7], of the vapor phase distribution along the heating surface during the boiling of underheated water with a clearly distinguished zone of low boundary vapor content (on the order of 0.01) with a subsequent increase in the zone where vapor content grows sharply as the degree of medium underheating decreases. In our case, only the beginning of the second zone is fixed due to the fact that the insignificant vapor contents in the first zone are beyond the sensitivity limits of the meter used for determining true vapor content.

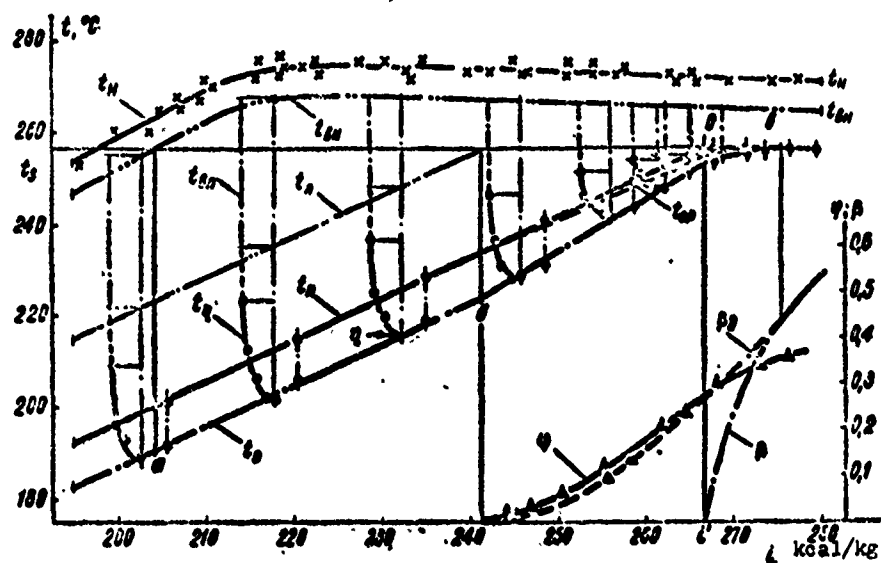


Fig. 7. Temperature, true and flow-rate vapor content versus flow enthalpy:

$d = 15.4 \text{ mm}$; $\gamma_w = 900 \text{ kg/m}^2 \cdot \text{s}$; $q = 0.57 \cdot 10^6 \text{ W/m}^2$;
 $p = 45 \text{ bar}$.

In examining the hydrodynamics of the boiling process for underheated liquid along a steam-generating channel it is expedient to divide the region of surface boiling into a zone of high underheating (from the formal beginning of surface boiling to the beginning of rapid increase in vapor content) and the

zone of low underheating (further from the actual beginning of volume boiling). The generally assumed distinction between the regions of undeveloped and developed surface boiling, in our opinion, is more conveniently used in problems connected with determining the heat transfer factor.

It should be kept in mind, however, that the graphs obtained for the distribution of temperature and vapor content along the working pipes are only approximate. This is generally explained by the fact that each of the analyzed graphs is plotted according to the results of various experiments conducted within a given series of tests under approximately equal regime conditions. Actually, however, the effect of channel length on the course of the process was not directly studied.

An analysis of the approximate graph for the distribution of temperature and true vapor content of flow along a heated pipe makes it possible to assume that the conditions of working medium input to the experimental section must be reflected in the quantity ϕ , measured in any channel cross section. Along with the condition of hydrodynamic and thermal stabilization in the true vapor content measurement section, it is apparently necessary that liquid underheating at input to the working section be at least higher than the values for underheating corresponding to the zone of high surface boiling underheating at the given regime parameters.

Analysis of the graphs presented in Fig. 7 has shown that both in the region of single-phase flow and in the zone of high surface boiling underheating no noticeable restructuring of the temperature field along the flow core cross section is observed since the measured temperature profiles on the noted section of the channel preserve their mutual equidistant nature. This is apparently explained by the fact that in the initial stage of its development along the heating surface the boiling process for

underheated liquid has only a boundary character; therefore, the effect of the turbulizing action of the vapor bubbles which are forming is manifested in the form of a thinning of the viscous sublayer and a more intensive heat transfer because of the motion of molar particles of liquid within this sublayer [8]. Consequently, in the zone of high surface boiling underheating the observed decrease in the full drop between the temperature of the inner heat-releasing surface of the channel wall t_{BH} and the average flow-rate temperature of the flow t_n , characterizing the increase in heat exchange intensity between the channel wall and working medium, is a direct consequence of the decrease in the drop in the viscous sublayer, representing the difference between t_{BH} and the temperature along the interface of the viscous sublayer and the flow core t_n , while the other component of the full drop $t_n - t_n$, generally determined by the character of the temperature distribution in the flow core, remains constant.

After the temperature drop in the viscous sublayer reaches its minimum limiting value, $t_{BH} - t_s$, in the section where the rapid growth of vapor content ϕ begins (see Fig. 7), a subsequent increase in heat transfer intensity in the zone of small surface boiling underheating occurs only from the restructuring of the temperature fields along the flow core cross section, which leads to a gradual decrease in the full temperature drop along the channel.

Conclusions

1. In this work new experimental data were obtained on true vapor content during the boiling of underheated water moving in vertical heated pipes with internal diameters of 11.7, 15.5, and 24.0 mm. The effect of pressure within 15-45 bar, thermal fluxes within $0.4 \cdot 10^6 - 0.8 \cdot 10^6$ W/m², and mass velocities within 450-3600 kg/m²·s on the value of the studied parameter was examined.

2. A calculated relationship was obtained in parametric form for determining true vapor content during the surface boiling of water in a pipe with diameter 15.4 mm for the studied range of regime parameters.

3. The hydrodynamic structure of flow in the region of surface boiling was studied. With values for medium underheating near zero, a high concentration of vapor phase in the central zone of the channel is noted.

4. Temperature profiles along the flow cross section with various degrees of water underheating were measured by a moveable thermocouple. We noted the presence of an underheated flow core and the absence of a state of thermodynamic equilibrium in the flow at zero values for relative enthalpy.

5. A complex analysis was made of the process of surface boiling along a steam-generating channel under forced circulation conditions.

6. The test data obtained make it possible to evaluate the value of the hydrodynamic characteristics in the designing of thermal equipment in which surface boiling is used.

BIBLIOGRAPHY

1. Полетаевкин П. Г., Шапкин Н. А. Водо- и паросодержание при поверхностном кипении воды. «Теплоэнергетика», 1958, № 4.
2. Полетаевкин П. Г. Водо- и паросодержание при поверхностном кипении воды. «Теплоэнергетика», 1960, № 9.
3. Бартоломей Г. Г., Чантурия Е. М. Экспериментальное исследование истинных паросодержаний при кипении нагретой воды в вертикальных трубах. «Теплоэнергетика», 1967, № 2.
4. Бартоломей Г. Г., Харитонов Ю. В. Определение истинного паросодержания в нестационарных режимах. «Теплоэнергетика», 1966, № 11.
5. Миропольский З. Л., Шнейрова Р. И. Исследование течения пароводяной смеси в трубах методом упрочивания. Сб.: «Теплоэнергетика», вып. 1. Изд. АН СССР, 1959.
6. Дорошук В. Е., Мальтер В. Л. О влиянии диаметра канала на критические тепловые нагрузки. «Труды ЦКТИ», вып. 58. Л., 1965.
7. P. Griffith et al., Paper № 38-HT19 ASME-ATChE Heat Transfer Conference, Chicago, 1958.
8. Трещев Г. Г. Сб.: «Теплообмен при высоких тепловых нагрузках и других специальных условиях». Госэнергоиздат, 1959.

THE EFFECT OF THERMAL FLUX AND
THE GEOMETRIC SHAPES OF A CHANNEL
ON THE VAPOR CONTENT PER UNIT
VOLUME OF A MEDIUM DURING BOILING

Z. L. Miropol'skiy, R. I. Shneyerova,
A. I. Karamysheva, E. T. Semin,
and M. N. Vinogradova

Abbreviations

ст - rod
об - course
н - surface
нас - saturation

At the present time a number of works have been published on the study of true vapor content per unit volume during the forced motion of a steam-water mixture in channels of various shapes [1-5]. However, the available data are insufficient for judging the effect of geometric parameters on ϕ , particularly the very little data available for channels of complex configuration such as rod channels with small gaps between the rods ($\delta_{\text{ст.-ст}}$) or between the rods and the unheated course ($\delta_{\text{ст.-об}}$).

Because of this the authors made an experimental determination of the values of ϕ , averaged over a cross section, during the motion of a working medium in a vertical cylindrical

channel with diameter 17.2 mm, inside of which were three heat-releasing rods 5.1 mm in diameter with a spacing of 8 mm. The quantity $\delta_{\text{CT.-CT}} = 2.9$ mm, and $\delta_{\text{CT.-CT}} = 1.4$ mm. The arrangement of the rods was asymmetric along the angles of an equilateral triangle and the equivalent hydraulic diameter of the channel was 6.7 mm. The rods were heated for a length of 400 mm by passing an current along them. The unheated length of the rod at input was 40-155 mm.

The quantity $\bar{\phi}$ was determined by radiographic inspection with a wide divergent beam of γ -rays [6] a distance of 20, 135, and 312 mm from the beginning of the heated section, i.e., l/d_3 was here 3, 20, and 45 respectively. Tests were made at pressures of 30 and 98 bar, mass velocities from 100 to 1000 kg/m².s, and specific thermal fluxes from 0.2 to 2 MW/m². The relative enthalpy of the working medium in the control sections varied from -0.4 to +0.3; the working medium was prepared by preheating deaerated and desalted water from the lines of the heat and power station. After the experimental section the medium was cooled in a heat exchanger and its flow rate was measured by a measuring tank. The enthalpy of the medium in the control sections was determined according to the enthalpy of the feed water at input to the stand, taking into account the heat introduced and the thermal losses determined by special calibration.

For gamma transmission the radioactive isotope Te-127 was used with gamma quanta energy of 0.088 MeV. The maximum absolute error in determining ϕ was ± 0.05 .

Figures 1 and 2 present the results of tests for a cross section located 312 mm from the beginning of heating, in the form of the dependence of true vapor content per unit volume ϕ on relative enthalpy x , specific flow q , and mass velocity w_0 . Here the calculated values are plotted for flow-rate vapor content per unit volume $\beta = \frac{1}{1 + \rho' \rho \frac{1-x}{x}}$ for adiabatic flow in absence of

phase slip. From an examination of these data it follows that in the presence of the heating of rods, values of ϕ other than zero are noted in the zone of negative relative enthalpies and are larger the higher the thermal flux. Accordingly, with equal values for x in this zone, ϕ increases with an increase in q . With an increase in x this difference decreases.

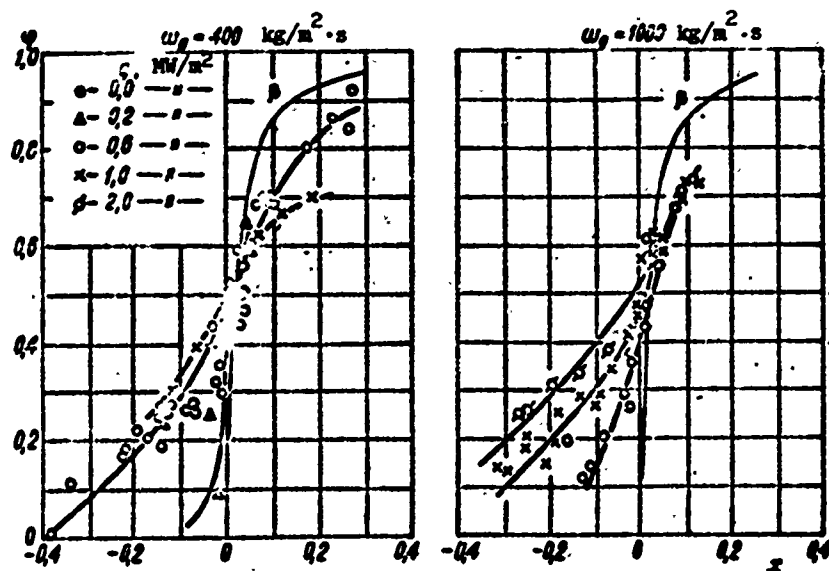


Fig. 1. Dependence of ϕ on x , w_g , and q . A three-rod channel $p = 30$ bar.

When comparing the data obtained with various mass velocities, we can see that in the region of negative relative enthalpies ϕ is reduced with an increase in w_p , while in the region of positive x an inverse relationship is observed.

Relative to the effect of pressure on ϕ , it can be noted that in the region of negative values for x there is observed an increase in ϕ with an increase in pressure; this effect is most strongly manifested at small w_p . With positive values for x and an increase in pressure, ϕ decreases since higher values of β respond to equal values of x at high pressures.

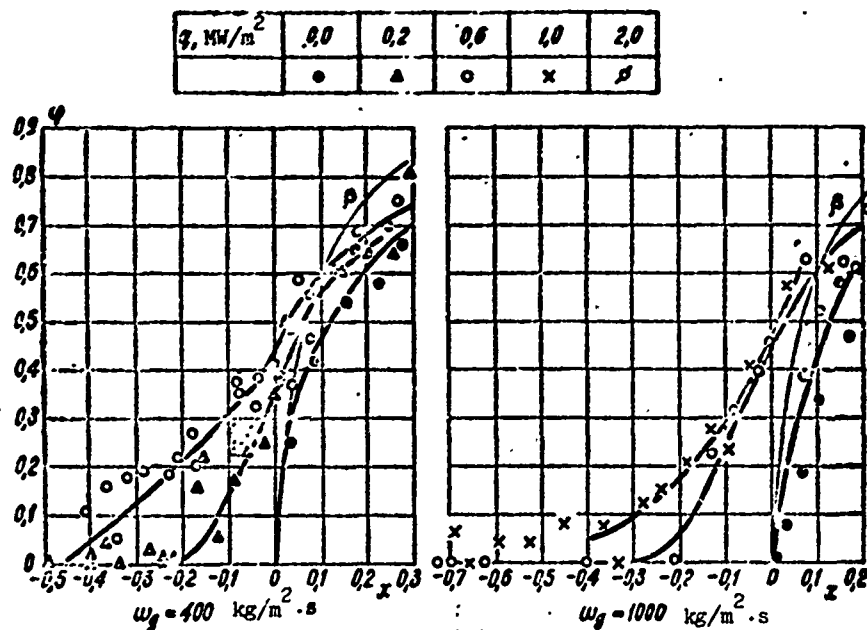


Fig. 2. Dependence of ϕ on x , w_g , and q . A three-rod channel $p = 98$ bar.

The effect on ϕ of the relative length of the section of thermal stabilization is shown in Fig. 3. Here it is apparent that, all other conditions being equal, in the region of negative values for x , ϕ increases with an increase in the length of the connected heated section, particularly in its initial zone since the change in ϕ with a change in the relative length of the section from 3 to 20 is significantly greater than with a subsequent change in l/d_3 from 20 to 45. It should be noted that in pipes and channels with large gaps the effect of the initial section appears to a lesser extent, for example, only when $l/d < 10$. With an increase in relative enthalpy of the medium the effect of the initial section on ϕ decreases and in the region of positive values for x (in practice, when $x \geq 0.05$) in the studied parameter range the effect of the length of the connected sections on ϕ is not noted.

The above mentioned character of the dependence of ϕ on mass velocity, pressure, and the length of the connected sections in the region of negative relative enthalpies of the medium is explained by the following characteristics of the studied process. Surface boiling begins only when surface temperature becomes higher than saturation temperature by several degrees. In the first approximation the beginning of surface boiling can be determined from condition

$$t_n = t_{nsc} - \frac{q}{\alpha}, \quad (1)$$

where α is the heat transfer factor in the absence of boiling.

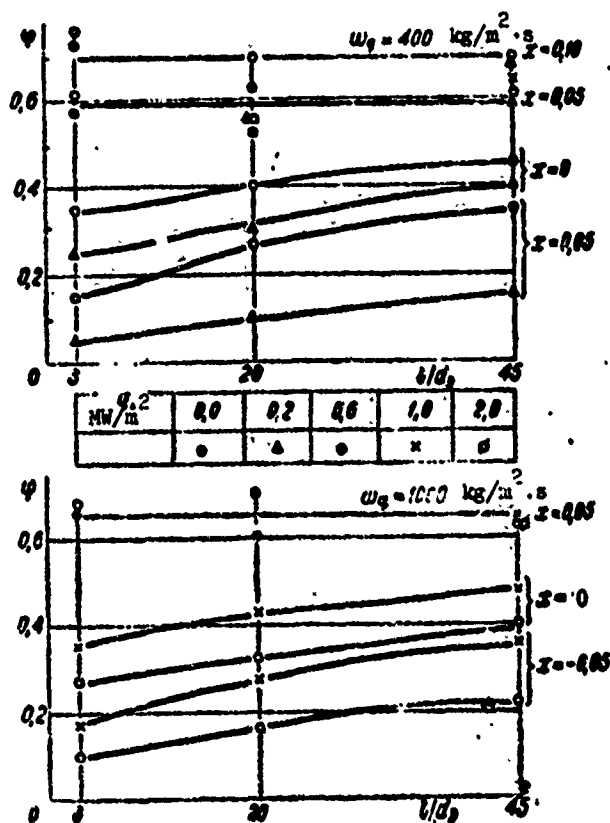


Fig. 3. The effect on ϕ of the length of the connected heated section. A three-rod channel $p = 30$ bar.

With an increase in mass velocity α grows and, accordingly, t_n , t_n , and x increase, in response to the beginning of boiling or a given value of q .

When q and w_p are equal, with an increase in pressure condition (1) is fulfilled at higher t_n , i.e., at somewhat higher values of α (due to the reduction in water viscosity and the increase in the Reynolds number); consequently, the difference in temperature $\Delta i = i' - i_n$ and the difference in enthalpy $\Delta t = t_{\text{hac}} - t_n$ somewhat decrease with an increase in pressure, while $\Delta x = \Delta i / r$ increases since the heat of vaporization decreases more significantly than Δi . The beginning of boiling is shifted to the region of lower values for relative enthalpy.

The reduction in ϕ in the initial section of the channel is also apparently connected with the fact that α here is higher than it is in the presence of thermal stabilization; therefore, boiling begins at higher values for t_n and x . In addition, in the initial sections of the channel the amount of vapor bubbles which enter from the connected heated sections and can not be condensed decreases.

Figure 4 presents experimental data on true vapor content per unit volume obtained by the authors of reference [1] on the same stand during the motion of a working medium in a vertical pipe with an internal diameter of 15.7 mm. The pipe was heated on a length of approximately 500 mm; gamma transmission was accomplished for a distance of 340 mm from the beginning of heating, i.e., l/d was approximately 22. A comparison between this data and that published in [6] for a pipe with a smaller diameter (approximately 8 mm) shows that when $x > 0$ the value of ϕ increases with a decrease in diameter. In reference [2] it is noted that in the zone of negative relative enthalpy the effect of the diameter on ϕ is not detected.

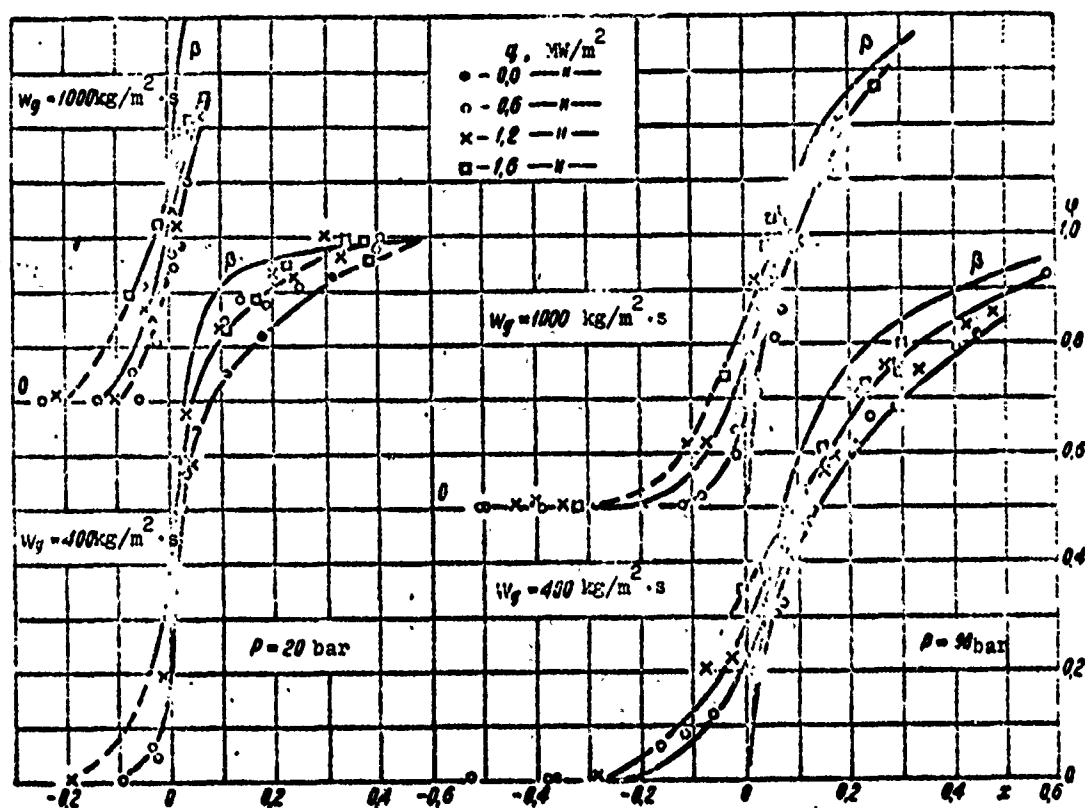


Fig. 4. Dependence of ϕ on x , w_g , and q . Type $d = 15.7 \text{ mm}$.

Since the data presented in Figs. 1, 2, and 4 were obtained in the parameter region where the effect of the length of the connected section is small, they can be compared in order to illustrate the effect of the geometric shapes of a channel section on ϕ with near values for the remaining determining parameters. With such a comparison we see that in the region of negative values for x the vapor content per unit volume in the rod channel with narrow gaps ($\delta_{\min} = 1.4 \text{ mm}$) is noticeably higher than in the pipes and in the region of positive values for x this difference levels off, i.e., surface boiling of liquid in the rod channel begins at lower values of x than in the pipes. Apparently this is explained by the fact that in the narrow gaps between neighboring rods or the rods and the channel wall the velocity of

the flow is considerably less than average while the enthalpy of the medium is higher [7]. The presence of turbulent mass exchange is insufficient for equalizing enthalpy in the cross section of the rod channel and is sufficient for the high condensation of vapor bubbles generated here.

Conclusions

1. In rod channels with narrow gaps between the rods or between the rod and the course (on the order of 1.5 mm and less) surface boiling begins with smaller thermal fluxes or smaller medium enthalpies than in pipes, i.e., in comparable conditions in the region of negative relative enthalpies, ϕ in rod channels is higher than in pipes.

2. True vapor content per unit volume in channel cross sections located at a comparatively small distance from the beginning of heating, all other conditions being equal, can also depend on the length of the connected heated sections, increasing with an increase in this length. With an increase in medium enthalpy the effect on ϕ of the length of connected sections decreases.

BIBLIOGRAPHY

1. Миропольский З. Л., Шнессова Р. И. Исследование фазового состава пароводяной смеси в обогретой трубе при помощи тормозного излучения. «Теплофизика высоких температур», 1963, № 1.
2. Подставка П. Г. Влаго- и паросодержание при поверхностном кипении воды. «Теплоэнергетика», 1960, № 9.
3. Zuber N., Staub F. W., Biwaard G. Proceedings of the III. Int. Heat Transfer Conf., Chicago, 1966, v. V.
4. Petrick M., Rudirka A. A. То же, v. IV (см. [3]).
5. Sher, Neil C., Glenn J., Kangas, Kenneth, F. Neusen. Chem. Engng Progr., Sympos., 1965, 61, № 60, 127-156.
6. Миропольский З. Л., Шнессова Р. И. Исследование течения пароводяной смеси в трубах методом упрощения. В сб.: «Теплоэнергетика», вып. 1. АН СССР, 1959.
7. Баун В. А. К расчету распределения температуры и скорости течения в трубах при критическом режиме. В сб.: «Теплообмен в элементах энергетических устройств». Изд. «Наука», 1966.

CALCULATING THE VAPOR CONTENT FIELD IN CYLINDRICAL VERTICAL CHANNELS

I. P. Kornyukhin

In studying the hydrodynamics of two-phase flow and in certain practical applications it is necessary to know the radial distribution of vapor content $\phi(r)$ in a cylindrical channel. The radiographic inspection of a channel along the chords by a narrow beam of γ -rays enables us to determine only the field of local vapor contents or vapor contents averaged along the chords. (The term "local vapor content" used in many works is unsatisfactory since the concept "local" is usually connected to the value of a function at a point. In our discussion we shall use the term "chordal vapor content" instead.) However, the function of radial distribution can be calculated according to the known field of chordal vapor contents. There are a number of methods for such calculations [1, 2]. The method of K. Schwartz [1] is the most familiar. The function of radial vapor content distribution (or mixture density) in a cylindrical channel under axial symmetry can be represented by the polynomial

$$\varphi(r) = \sum_{k=0}^n a_k r^k, \quad (1)$$

where r is the relative value of the channel radius ($0 \leq r \leq 1$); a_k is the constant coefficient.

The value of the constant coefficients a_k is determined on the basis of the boundary conditions (two boundary conditions) and the results of a radiographic inspection of the channel along chords. The connection between the number of terms of the polynomial $n + 1$ and the number of chords m along which the radiographic inspection is made (in the more general case - the number of node points m for which the values of chordal vapor contents f are known) is expressed by the relationship

$$n + 1 = m + 2.$$

However, in spite of the relative simplicity, the Schwartz method has a substantial disadvantage - it does not give an objective criterion for checking the accuracy of the results obtained. Because of this it is pertinent to examine several possible cases which can be represented when calculating the function $\phi(r)$ according to this method.

1. The coefficients of polynomial (1) do not decrease. The series whose argument varies within $0 \leq r \leq 1$ does not converge and it is difficult to expect a satisfactory correspondence between the calculated vapor content distribution and the actual one.

2. The coefficients of polynomial (1) decrease. In this case, it is not possible to judge the convergence of the series and the question of correspondence between the actual distribution and the calculated distribution remains open.

The accuracy of the method could be improved by increasing the number of nodal points m . At the limit, while increasing to infinity, we can achieve full correspondence between the calculated profile of vapor content and the actual one. However this method involves an enormous amount of calculation and is scarcely advisable.

In addition, a check was made of the reliability of the Schwartz method by comparing the distribution curves when function $\phi(r)$ is given by different equations. Such studies were made for two variants - when $\phi(r)$ is given by a power polynomial (1) and by a trigonometric polynomial

$$\phi(r) = \sum_{k=0}^n a_k \cos \frac{k\pi}{2} r. \quad (2)$$

In both cases, the calculation involved the same values for chordal vapor content obtained in one of the works from ENIN [Power Engineering Institute im. G. M. Krzhizhanovskiy] when $m = 4$. On Fig. 1 curves 1 and 2 in relative form $\phi(r) = \phi(r)/\phi(\bar{\phi})$ (true vapor content per unit volume averaged along the cross section) represent the distribution curves calculated according to equation (1) and (2). The correspondence between them is not satisfactory, another indication of the insufficient reliability of the Schwartz method.

Also known are two methods which make it possible to calculate the true vapor content per unit volume averaged in a certain range of radius variation. One of them was used at the MO TsKTI [Moscow Branch of the Central Scientific Research, Planning and Design Boiler and Turbine Institute im. I. I. Polzunov] by G. I. Aleynikov and Ye. K. Golubev, and the other was used at the ENIN by I. S. Dubrovskiy. However, both these methods make it possible to only approximately determine the form of the function $\phi(r)$. Because of this, the author has developed a strict analytical method for calculating the radial distribution of vapor content, which will be presented below.

As we know, radiographic inspection of a channel by a narrow beam of γ -rays enables us to determine vapor content averaged along the path of the ray. For a cylindrical channel we can thus obtain the vapor content averaged along a chord (diameter), i.e., the chordal vapor content. This quantity can be represented as

the average value of the integral of function $\phi(r)$ along the corresponding chord (Fig. 2):

$$f = \frac{1}{L} \int_L \phi(r) dy. \quad (3)$$

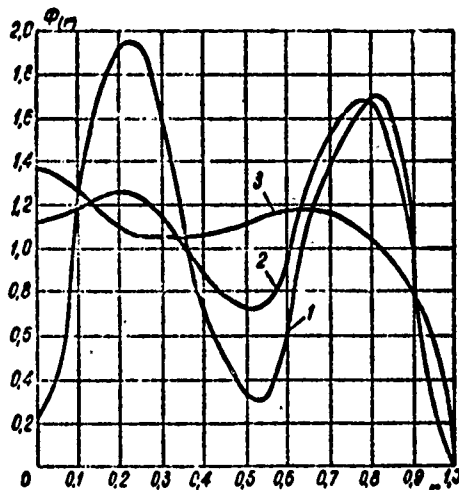


Fig. 1. Curves of radial vapor content distribution: 1 - Schwartz method (equation 1); 2 - Schwartz method (equation 2); 3 - Method used in our work (equations 5-7).

It is assumed that the field of vapor contents is axial. The correctness of this assumption for vertical cylindrical channels is indicated in a number of works [1, 3, 4].

On the basis of (3) we can calculate the average vapor content for any chord of the channel. A generalization of this equation for a chord located at distance x from the axis of the channel ($0 \leq x \leq 1$) and a change of variables give:

$$f(x) = \frac{1}{\sqrt{1-x^2}} \int_x^1 \frac{\phi(r) r dr}{\sqrt{r^2-x^2}}. \quad (4)$$

Function $f(x)$ can be plotted on the basis of the results of a radiographic inspection of the channel along chords and in the subsequent analysis is assumed to be given. In this case, relationship (4) can be considered an equation relative to function $\phi(r)$. This equation is integral. According to the

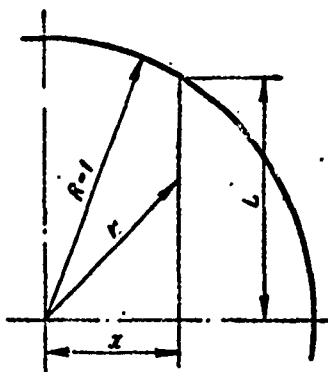


Fig. 2. Diagram of the radiographic inspection of a cylindrical channel by a narrow beam of γ -quanta.

solution method, it is near an integral equation of the Abel type. Its solution gives an analytical expression for calculating the distribution $\phi(r)$ according to the known function $f(x)$:

$$\phi(r) = \frac{2}{\pi} \int_1^r \frac{dF(x)}{dx} \cdot \frac{dx}{(x^2 - r^2)^{1/2}}, \quad (5)$$

where

$$F(x) = f(x) \sqrt{1 - x^2}. \quad (6)$$

Analysis of this expression showed that the necessary condition of boundedness for $\phi(r)$ when $r = 0$ is the equality

$$\left. \frac{dF(x)}{dx} \right|_{x=0} = 0, \quad (7)$$

which, taking into account (6), is transformed to:

$$\left. \frac{df(x)}{dx} \right|_{x=0} = 0. \quad (8)$$

Physically, the condition (8) means that the value of chordal vapor content obtained by radiographic inspection in a diametrical plane must be extremal. With axisymmetric distribution of vapor content such a statement is sufficiently rational.

In deriving equation (5), no limitations connected with the specifics of vapor content are imposed on functions $f(x)$ and $\phi(r)$. Therefore, under conditions of axial symmetry equations (5-7) can be used for calculating the radial distribution of any parameter according to a given field of chordal values.

Several peculiarities in calculating $\phi(r)$ should be mentioned. Both graphic and numerical differentiation of functions $f(x)$ and $F(x)$ can be rather time-consuming and insufficiently accurate. Because of this it is advisable to interpolate beforehand the function $F(x)$ by a polynomial (or several) with the subsequent analytical differentiation and integration. (Interpolation by a polynomial of function $f(x)$ directly would lead to a considerable complication in the calculations). It should be kept in mind that polynomial $F(x)$ must satisfy condition (7).

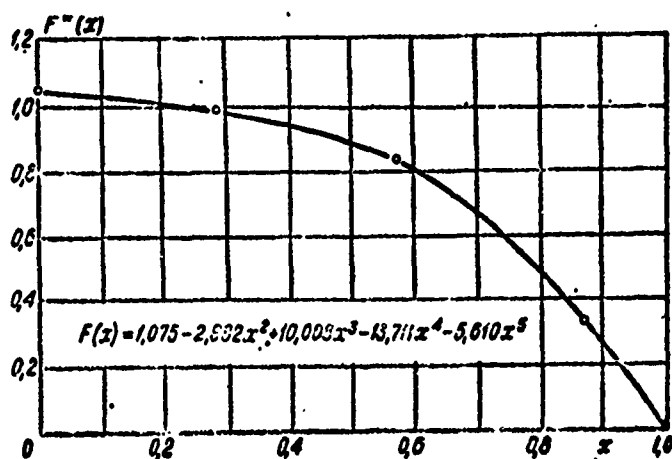


Fig. 3. Interpolation of test values for chordal vapor contents by a polynomial.

The use of this method can be demonstrated by the following example. On the graph in Fig. 3 the points indicate the values of $F^*(x_i) = F(x_i)/\bar{\phi}$ (i -number of chord) calculated according to equation (6) on the basis of the test values for $f(x_i)$. Here the interpolated curve and its equation are presented. The vapor content field $\phi(r)$ was found according to equation (5) on the

basis of the obtained function $F^*(x)$. The results of calculation are presented in Fig. 1 (curve 3). All curves shown on this graph are calculated for identical values of corresponding chordal vapor contents. Comparison of curves 1 and 2 with curve 3 shows that the use, in this case, of the Schwartz method leads to erroneous results.

BIBLIOGRAPHY

1. Schwarz K. Untersuchungen über die Wichterverteilung die Wasser und Dampfgeschwindigkeit für den Reibungsdruck fall in lotrechten und waagerechten Kesselsteigrohren. VDI-Forschungsheft 445, Ausgabe B, Band 20, 1954.
2. Казин И. В. Радиальное распределение пара в восходящем турбулентном потоке. «Теплоэнергетика», 1964, № 1.
3. Bankoff S. G. A variable density single fluid model for two-phase flow with particular reference to steam-water flow. Transaction of the ASME, Series C, Journal of Heat Transfer, v. 82, № 4, 1960.
4. Дементьев Б. А., Лепилин Р. С., Логинов А. А. Исследование гидродинамики водяного объема в условиях больших высот барботажного слоя. «Энергетика», 1959, № 2 (НДВШ).

**AN EXPERIMENTAL STUDY ON FLOW
STABILITY IN STEAM-GENERATING
PIPES WITH VARIABLE LENGTHS
OF HEATED AND UNHEATED SECTIONS**

V. I. Lezin and O. K. Smirnov

Conditions which allow unsteady regimes of heat carrier motion in channels connected in parallel are related to their design characteristics [1, 2].

In this work we shall examine the test results obtained on an experimental installation of the MEI [Moscow Power Engineering Institute] [3], with variations in the length of the heated and unheated sections by a redistribution of the heat supply and a lengthening of the working channel.

The central part of the experimental installation consists of two steam-generating pipes with an internal diameter of 4 mm, joined at input and output by common collectors (Fig. 1). Water at a given temperature is fed from a connected preheater into the input collector and then into the working pipes. After the collector the steam-water flow enters a cooler where it is condensed and the cooled condensate is drained into a supply tank. The water is circulated by three ND pumps.

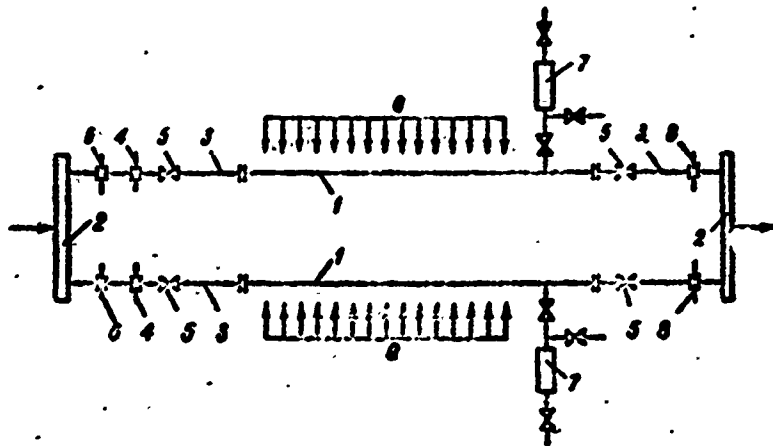


Fig. 1. Diagram of experimental installation:
 1 - Heated section; 2- Collector; 3 - Mounting;
 4 - Throttle washer; 5 - Throttle valve;
 6 - Measuring disk; 7 - Removable vessels;
 8 - Stimulating disk.

The working pipes are heated by passing low-voltage ac current through them. On one of the pipes heat supply is effected on three sections with the independent control of thermal load; on the shunting pipe this is done on two sections. The length of the heated sections varies during the displacement of the sliding current supply.

The overall length of each working pipe is 7.26 m. On the beginning and end sections of the pipes there are removable flange joints to which additional mountings of pipes with an internal diameter of 4 mm are connected.

At the input into each pipe are flow-rate measuring disks and throttles in the form of removable calibration washers or a needle valve. At the output from the pipes there are also throttle washers.

Studies were made in the pressure range 30-100 atm (tech.); mass velocity varied from 200 to 750 kg/m²·s, and thermal loading

on separate sections from 100,000 to 600,000 kcal/m²·h.

The first group of tests was made with variation in the heat supply along the length of the working pipes. In the second group, tests were conducted with a change in the length of the working pipes because of the connection of the unheated mountings. In the third group of tests throttle washers were used on the working pipes in front of the collector.

The effect of thermal load distribution along the length of the channels was studied in tests with a redistribution of the heat supply and disconnection of the heating on part of the evaporative channel during constant, as well as variable, total heat supply. The position of the boiling point was kept constant in all the regimes by the corresponding control of heating power on the economizer channel. Each test involved work with several regimes. In one series of tests the regimes were distinguished by the value of thermal load on the beginning section of the evaporative channel with a constant value of total heat supply, in the other series, by the value of vapor content at output from the pipe during a constant value for thermal load on the initial section of the evaporative channel.

The length of the heated section of the evaporative channel in the various tests was 3.4, 2.55, and 1.7 m. Loss in motion stability was fixed by the appearance of interpipe flow-rate oscillations. Regimes in the immediate vicinity of the motion stability boundary recurred by passage from the stable region to the pulsation region and vice versa.

The effect of the length of the steam-generating pipes was studied with the use of mountings on the unheated sections of the economizer and evaporative channels (see Fig. 1). Mountings 1, 3, and 6 m long with throttle valves were installed at input to the pipes. The same pressure drop was ensured on all mountings by

regulating the valve. The steam-generating pipes were heated uniformly along the length. By gradually increasing the thermal load they passed from stable regimes to pulsation regimes and thus the stability boundary of the heat carrier's motion was determined. Unlike the others, these tests were made with a different temperature at input to the distributing collector.

The same methodology as used in the first group of tests was used in the tests with mountings and throttle washers on the output ends of the pipes, i.e., the length of the economizer channel was kept constant and the uniformity of heating and the total heat supply on the evaporative channel was varied. Mountings 3 and 6 m long covered with thermal insulation were used.

From the test material obtained a clear relationship is apparent between the motion stability boundary and the heat supply distribution along the evaporative channel: An increase in thermal loading on the initial section of the evaporative channels, as with an increase in the overall heating level, leads to the appearance of intercoil pulsations.

An increase in channel length because of the unheated section on the economizer channel improves flow stability. On the other hand, the lengthening of channels due to the unheated section on the evaporative channel reduces flow stability.

Data from all tests were processed with respect to the value of the relative flow throttling, effective vapor content, passage time, and the specific weight of the medium. As a generalizing function we obtained the function in coordinates $\zeta_{\text{ex}} = f(\bar{\gamma})$ where ζ_{ex} is the reduced coefficient of resistance on the economizer section (includes local resistances of the input throttle and measuring disks and the linear resistance of friction of the economizer section), and $\bar{\gamma}$ is the average integral value of the specific weight of the medium in the vapor-containing channel.

Figure 2 presents the generalizing function according to tests at a pressure of 70 atm (tech.) where the most complete data were available.

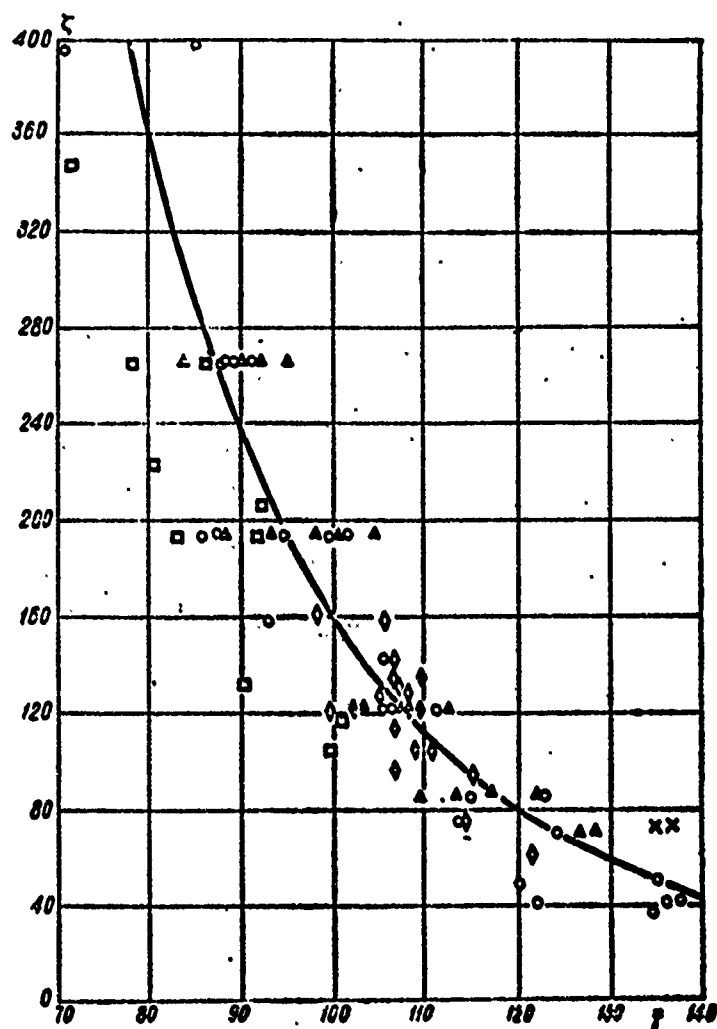


Fig. 2. Boundary value of the reduced coefficient of resistance versus specific weight of the medium in the steam-containing sections when $p = 70$ atm (tech.):
 O - with redistribution of the thermal load along the length of the evaporative channel; Δ - with disconnection of heating on part of the evaporative channel;
 x - with unheated mountings on the economizer channel;
 □ - with unheated mountings on the evaporative channel;
 ◇ - with a variable quantity of heated economizer section.

The experimental points correspond to stable regimes near the boundary of intercoil pulsations. Similar functions were obtained in tests at other pressures.

As is apparent from Fig. 2, the data from tests with a different character of heat supply distribution, including the reduction in the length of the heated section on the evaporative channel, are described by one curve. The relationship obtained also indicates a shifting of the motion stability boundary with a change in the total heat supply on the evaporative channel.

Experimental points corresponding to regimes with mountings on the economizer channel are indicated on the curve in Fig. 2. This means that an increase in channel length because of the heated sections of the economizer channel affects motion stability just as the installation of an additional throttle washer with a resistance equal to the pressure drop on this section. In tests with variable temperature at input to the distributing collector, the length of the economizer channel was changed by a factor of almost two. Experimental points obtained in these tests, for all practical purposes, fall within the general relationship. The effect of increasing the length of the steam-containing channel, as is apparent from Fig. 2, is taken into account, with sufficient accuracy, by changing the specific weight $\bar{\gamma}$.

A series of tests with identical pressure drops on the mountings of the evaporative channel was made in this work. A valve covered the shortest mounting and thus the total pressure drop on this mounting and valve was varied up to a value equal to the pressure drop on the longest mounting. Then by redistributing the heat supply on the evaporative channel, we determined the motion stability boundary of the heat carrier. The processing of tests showed that when the total pressure drops are equal, loss of motion stability occurs under identical conditions. This made it possible to plan a way to evaluate quantitatively the effect on the installations at channel output of the throttle washers used

as stimulating washers during studies on pulsation phenomena. Obviously, in order to determine the boundary of stable regimes we should arbitrarily replace the washer with an equivalent element - an unheated mounting with the same pressure drop; then calculation reduces to the computation of the average specific weight of the medium in the evaporative channel and a determination, according to the curve in Fig. 2, of the necessary reduced resistance for the economizer channel.

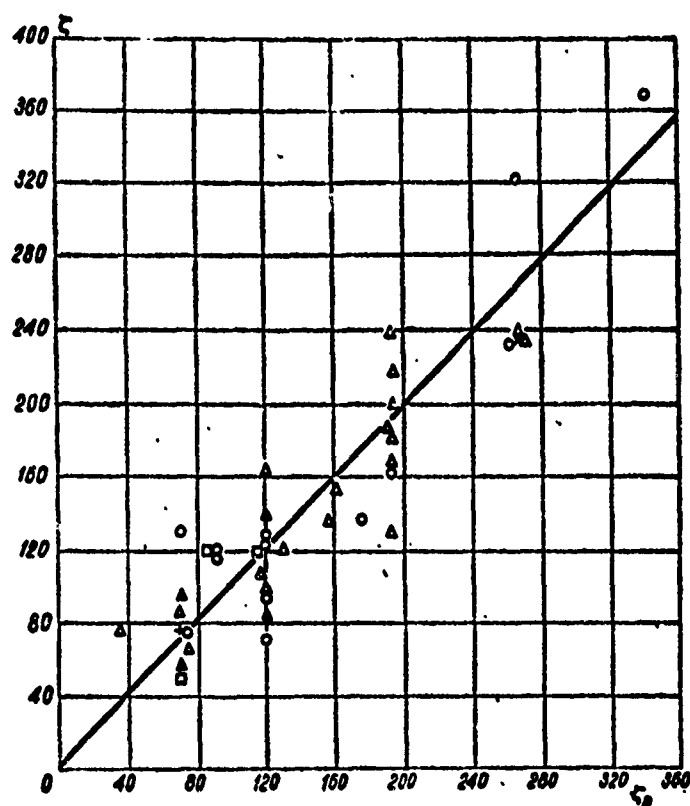


Fig. 3. Comparison of tests and calculated values of ζ on the stability boundary of the heat carrier's motion at pressures 30-100 atm (tech.) and mass velocity of flow 376-565 kg/s with throttle washers at output from the channels:

□ - washers with an opening of 1.5 mm; ○ - washers with an opening of 2 mm; Δ - washers with an opening of 2.5 mm; × - washers with an opening of 3.5 mm; + - washers with an opening of 3 mm.

This method of evaluating the washer effect was checked (Fig. 3) during a comparison of the values of ζ based on the data of this work, and also presented in [3], with the calculated values for $\zeta_{расч}$.

BIBLIOGRAPHY

1. Давидов А. А. Исследование пульсаций потока в трубах испарительной части прямоточных котлов. «Гидродинамика и теплообмен при кипении в котлах высокого давления». АН СССР, 1955.
2. Трещев Г. Г. Пульсации пароводяного потока в обогреваемой трубе «Энерго-машиностроение», 1964, № 3.
3. Серов Е. П., Смирнов О. К., Зыков Л. А. Экспериментальное исследование границ устойчивости потока в параллельно включенных парогенерирующих трубах при неравномерном обогреве поверхностей. «Теплоэнергетика», 1964, № 10.

STRUCTURE OF FLOW OF A STEAM-WATER MIXTURE IN A VERTICAL UNHEATED PIPE AT HIGH PRESSURES

S. M. Lukomskiy, P. I. Povarnin,
and R. I. Shneyerova

In order to observe the structure of flow, a visual section was used on an ascending pipe of a circulation loop and high-speed movie photography was applied.

The loop was made of steel pipes with a vertical section diameter 22.5/36 mm, horizontal section diameter 30/42 mm, total height of loop approximately 6 m. The loop was equipped with a separator for separating the vapor-liquid mixture and a condenser. A throttle gate is located on the descending section of the loop to regulate the flow rate of the working fluid. Visual observation and motion pictures of the cell structure in the pipe were made through a glass viewing section located on the ascending branch of the loop 4 m above the heaters.

The visual section (Fig. 1) consisted of a steel frame in which a pyrex tube is set whose internal diameter (22.5 mm) is equal to the internal diameter of the ascending pipe in order to ensure the constancy of the hydrodynamic conditions in both pipes. There are two holes in the frame for the adjusting screws which have cylindrical glass 14 mm thick installed in them. The main

glass is duplicated by a second safety glass identical in shape and size. The entire device is further provided with protective flanges which are connected by pins passing through from the outside of the section. This adaptation was extremely effective since during heating and the increase in dimensions of the whole section, the tie pins remained cool and provided additional tightening. This construction made it possible to photograph at pressure above 100 atm in the installation.

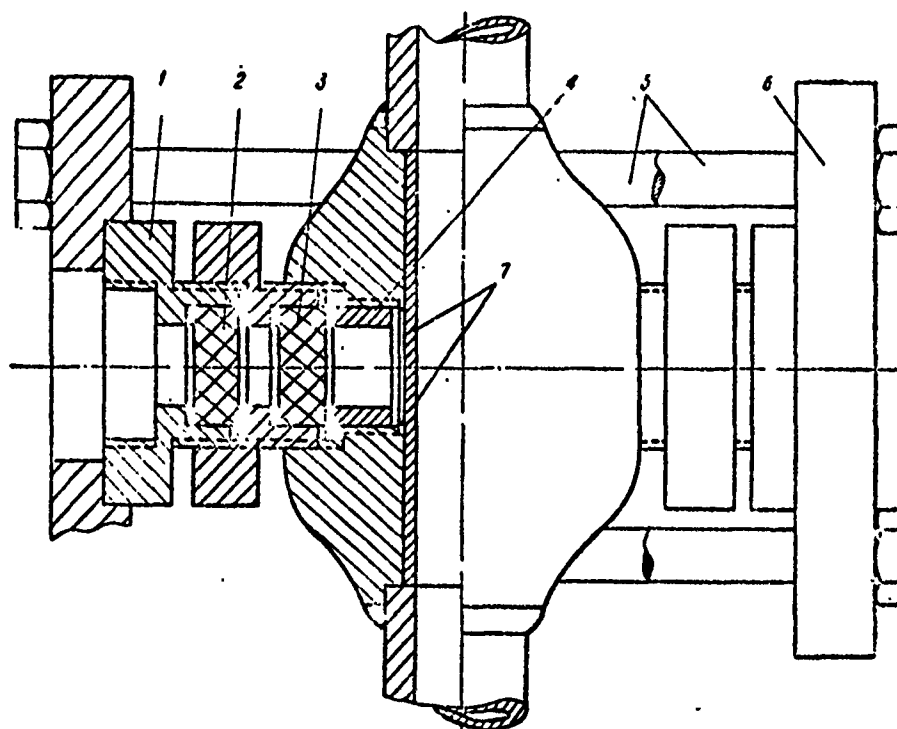


Fig. 1. Overall diagram of installation:
 1 - Safety bolt; 2 - Safety glass; 3 - Working glass;
 4 - Insert; 5 - Tie bolts; 6 - Protective flanges;
 7 - Pyrex tube.

Tests were made on distilled deaerated water. Preheating and partial evaporation of the working fluid was accomplished by the electric heaters. During the tests the following parameters were measured: pressure, temperature in the experimental and descending section, circulation velocity, the capacity on the electric heaters, and exposure speed.

To determine the pressure in the installations a precision diagram [1] was used, consisting of a series-connected differential manometer, filled with mercury, and a compensating standard balance press, which provided measurement sensitivity of ± 5 mm Hg.

Movie photography was performed in the transmitted light of an SKS-1 high-speed camera. The light source was a two-kilowatt lamp with a reflector.

In order to set up an overall representation of the character of the hydrodynamic regimes, film was examined through a 16-NP-6 movie projector with a film advancement speed of 16-24 frames per second which, with an exposure speed of 1000 frames per second, slowed the motion by a factor of fifty. Through marks applied to the film every one hundredth of a second by a neon lamp, we could more precisely define the exposure speed for a given section of film; the quantity of vapor bubbles and vapor locks was measured and the speed of their motion along the axis of the pipe was calculated.

To provide a visual representation of flow structure, we made photoillustrations, conditionally called "pictures of stopped regime," which were compiled as follows: the leading edge of the head of a vapor lock, which was usually clearly outlined, passed through the space of the viewing window during a time corresponding to the passage of n_1 frames. Then on the n_1 frame we had an image of the entire segment of the lock whose length equalled the diameter of the viewing window; after counting off the following n_1 frames, we obtained on the $2n_1$ frames a full image of the next segment of the vapor lock whose length also equalled the diameter of the viewing window.

This operation was performed for the entire segment of film studied - from one lock to another. The frames thus chosen were combined, forming an image or an illustration of this regime.

It should be noted that the picture presented on these frames is, in essence, the unfolding of the process over time on a section $l = 22.5$ mm on which the photography was accomplished. Therefore, when we shall subsequently speak of the "length" of a lock, we shall mean the calculated length obtained as the product of the lock passage time through the viewing window times the speed of its motion.

Series of visual observations and motion picture photography were made at pressures of 10, 30, and 50 atm and single shots were taken at higher pressures - 60, 70, and 80 atm. Generally the photographs were made during a stationary operating mode when, for a long period of time, on the order of 1-2 hours, constant pressure, circulation rate, and vapor content were maintained.

Part of the photography was made at slowly increasing pressure.

However, pressure increased sufficiently slowly, for example, 8-10 atm in one hour; exposure time for one cassette (30 m of film) was approximately 5 s. Thus, we can assume that during the photography pressure was constant. It should be noted that a comparison of the photographic results at identical medium parameters but during stationary regimes and under conditions of slowly increasing pressure indicated complete identity of flow structure.

Table 1 gives the characteristics of some of the films taken, which then were used for subsequent processing and conclusions.

Before describing the results of the motion picture photography, we should pause on the observations made during the tests directly through the viewing window. At low pressures below 3 atm an alternation could be seen in the window between long vapor locks and sections of pure water; in several cases the

Table 1.

№ пленки (1)	$p, \text{кг/см}^2$	$w, \text{м/сек}$	$w_0, \text{м/сек}$
20	9,92	0,515	1,21
18	9,94	1,1	1,51
19	9,94	1,1	0,95
45	10,34	1,06	—
46	10,55	1,1	—
47	10,62	0,49	—
38	20,92	1,1	—
24	29,44	0,52	0,59
23	29,77	0,55	0,49
25	29,1	0,5	0,59
27	26,90	0,56	0,9
28	29,95	0,56	0,91
29	29,95	1,16	0,85
33	48,08	0,58	0,726
40	48,59	1,09	0,596
49	48,82	0,76	—
50	59,38	0,98	—
52	62,85	0,895	—
54	76,4	0,54	—

KEY: (1) Film No.
 DESIGNATIONS: $\text{кг/см}^2 = \text{kg/cm}^2$;
 $\text{м/сек} = \text{m/s}$.

passage time for such a lock could be measured with a stop watch. However, beginning at 5-6 atm and above, a single line of vapor bubbles could be seen in the window, which leads us to speak of the establishment of an emulsion flow regime, i.e., a flow structure where the vapor moves in a liquid mass in the form of more or less uniformly distributed bubbles. However, an examination of the photographic material revealed considerable complexity and variety of structure in the flow which, as mentioned above, during observation by the naked eye appeared to be identical, consisting of a group of "visually emulsion" regimes. The vapor bubbles in the liquid mass have a variety of forms and sizes and a significant portion of the vapor moves in the form of a vapor lock filling almost the entire cross section of the pipe. The presence of such locks of any size can be observed in a

considerable range of pressures and their final disappearance noted only when approximately 80 atm is achieved.

It can be seen that at constant pressure the circulation rate w_0 only slightly affects the character of the flow structure, while a change in the reduced vapor rate w_0'' frequently leads to a considerable change in the observed pattern.

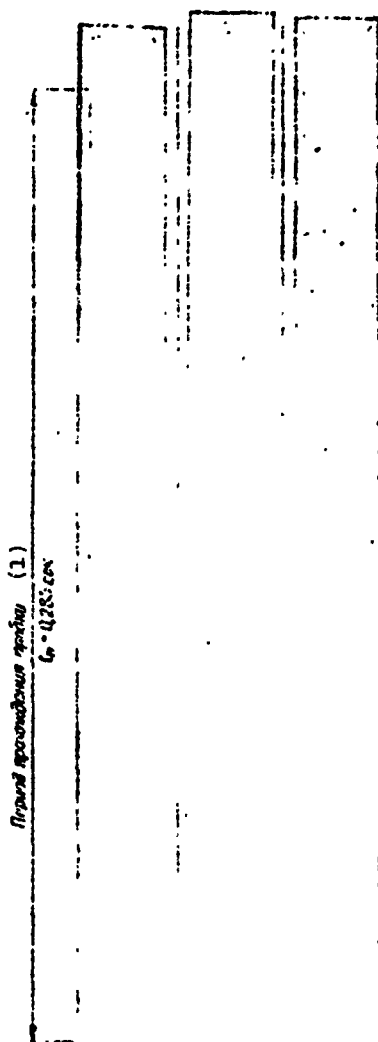


Fig. 2. Flow structure at 30 atm:

No. 24: $p = 29.44 \text{ kg/cm}^2$,

$w_0'' = 0.59 \text{ m/s}$; No. 28:

$p = 29.85 \text{ kg/cm}^2$, $w_0 = 0.55$

m/s , $w_0'' = 0.9 \text{ m/s}$; No. 29:

$p = 29.85 \text{ kg/cm}^2$, $w_0 = 1.15$,

$w_0'' = 0.85 \text{ m/s}$.

KEY: (1) Period of vapor lock passage.

DESIGNATION: $\text{сек} = \text{seconds}$.

The difference in flow structure as a function of vapor content is quite sharply manifested at a pressure of 30 atm. With a circulation rate of $w_0 = 0.5$ m/s and a reduced vapor rate on the order of 0.5 m/s long, sharply outlined vapor locks with foam formation in the stern were observed (Fig. 2); such a structure was seen at a pressure of $p = 10$ atm (abs.) (Fig. 3). When $w_0 = 0.5-1$ m/s and $w_0'' = 1$ m/s (films 24, 28, 29) short locks (50-60 mm) were fixed; such vapor locks frequently do not fill the pipe cross section (see Fig. 2).

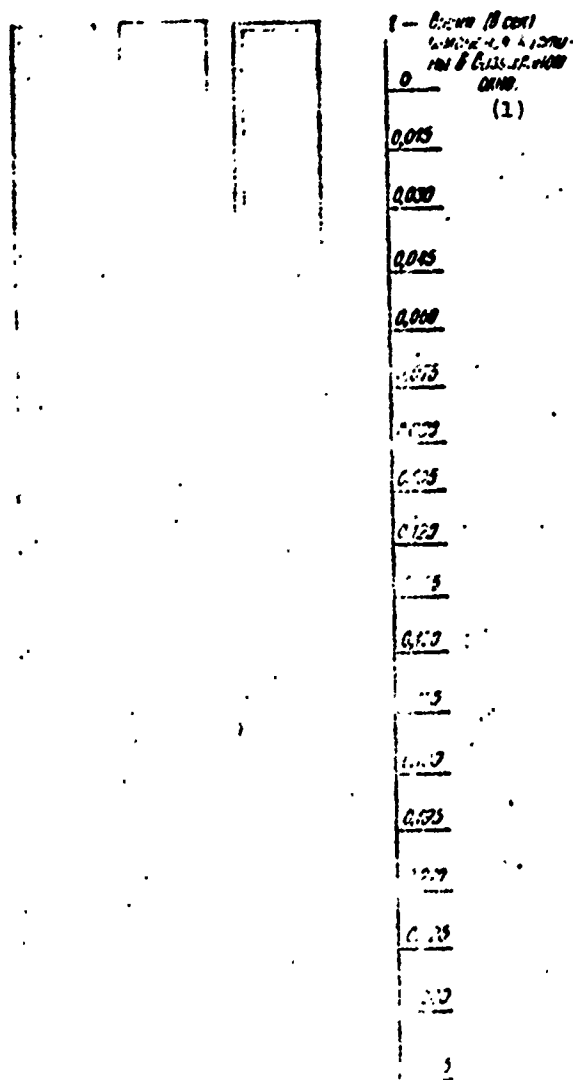


Fig. 3. Flow structure at 10 atm:

No. 18; No. 19, No. 20:

$p = 9.94$ kg/cm², $p = 9.92$

kg/cm², $w_0 = 1.10$ m/s,

$w_0 = 1.10$ m/s, $w_0 = 0.515$

m/s, $w_0'' = 1.51$ m/s, $w_0'' = 0.95$

m/s, $w_0'' = 1.21$ m/s.

KEY: (1) Time (in seconds) of picture change in viewing window.

Extremely intensive foaming occurs at the same time. Large sections of film, hundreds of frames in length, are apparently filled with foam and scarcely let any light through.

At higher pressures the effect of the reduced vapor rate decreases; for example, when $p = 50$ atm (abs.), $w_0'' = 0.73$ m/s and $w_0'' = 0.54$ m/s, identical structure with very small vapor locks was observed (see Table 1).

A comparison of the structure of flow at various pressures, i.e., a photographic picture of the "stopped regime" for pressures of 3 to 80 atm, is given in Fig. 4.

Here, first of all, we can see two different structural groups. The first group, for pressures from 3 to 20 atm, can be characterized as the region of "vapor lock regimes with emulsion." This region is distinguished by fully formed locks 100-200 mm long, occupying almost the entire cross section of the pipe with foam formations in the stern usually reaching dimensions of approximately one third the length of the lock itself.

The liquid intervals between locks are filled with vapor bubbles of various shapes and sizes. With an increase in the amount of vapor the size of the liquid intervals decreases and vapor locks come closer together. Within the described region the vapor lock sizes remain approximately constant with a certain tendency toward reducing as pressure grows. The second region (from 30 to 80-90 atm) can be called the region of "emulsion regimes with passing locks." In this region we can observe a sharp reduction in the size of the vapor locks, which reach 40 and even 20 mm in length; vapor locks 60 mm long are an exception. Behind the locks there is virtually no foaming; many locks occupy less than the cross section of the pipe, partially preserve their axial position, and frequently are deflected toward one of the walls. In this region there is also a tendency

REPORT

$P \cdot 10^5$ atm	394	11.03	15.92	22.04	40.87	64.80	70.1
$W_0 \cdot 10^3$ m/sec	1.0	-	1.0	1.15	0.70	0.035	0.05
$W_0^2 \cdot 10^3$ m/sec	0.0	-	-	0.03	-	-	-

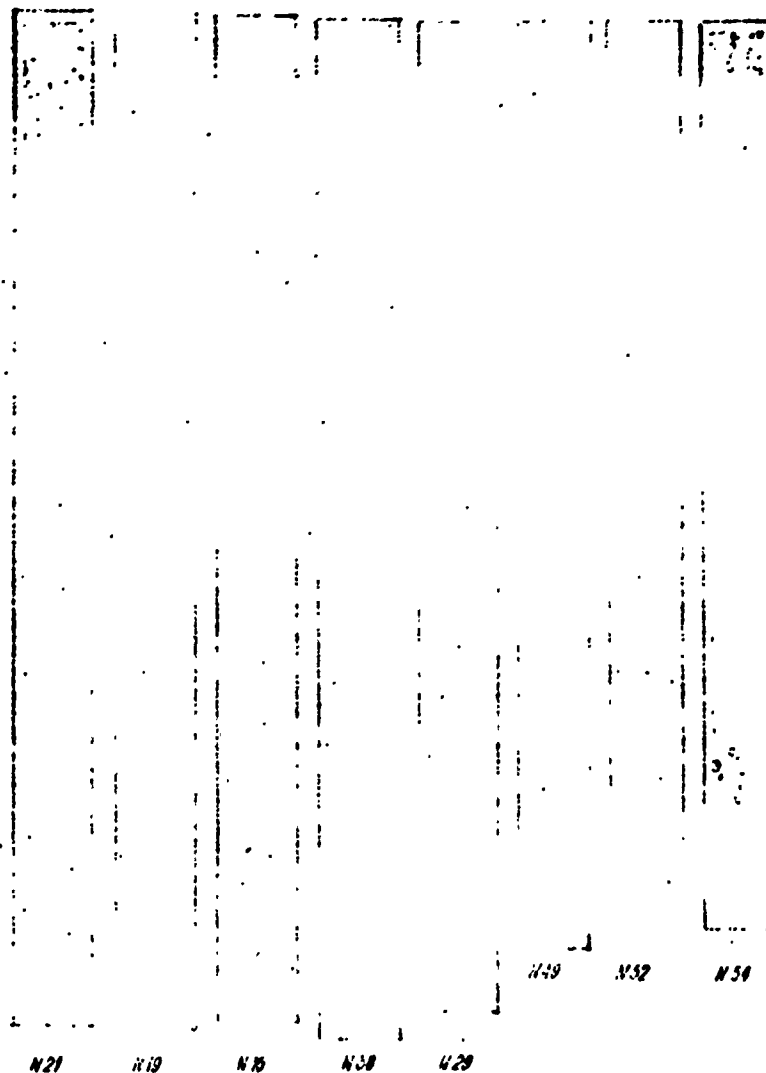


Fig. 4. Variation in structure with pressure.
 DESIGNATIONS: *ama* = atm (abs.); m/sec = m/s.

Reproduced from
 best available copy.



toward a decrease in the size of the locks as pressure grows; at a pressure above 60 atm the locks were observed to degenerate and transform into groups of bubbles.

In the liquid intervals we can see numerous bubbles of very different shapes and sizes; however, fine bubbles up to 4 mm in diameter with the proper outlines of a flattened sphere predominate (Fig. 4).

Finally, at $p = 100$ atm (abs.), which was observed during a showing of films on a screen, vapor locks completely disappear and only groups of separate bubbles remain. Thus, it can be stated that at a pressure of approximately 100 atm (abs.), $w_0 \approx 1$ m/s and $w_0'' \approx 1$ m/s, a transition to a purely emulsion flow regime occurs, where all the vapor is uniformly distributed in the liquid mass.

Regimes at $p = 30$ atm (abs.), undoubtedly of particular interest, can be called transient. As mentioned above, regimes with low reduced vapor rate (w_0'' approximately 0.5 m/s) belong to the first region of "vapor lock regimes with emulsion" (see Fig. 2). Regimes with high reduced vapor rate (w_0'' approximately 1 m/s) belong to the second region "emulsion regimes with passing vapor locks." The main characteristic of regimes with $w_0'' \approx 1$ m/s is the earlier mentioned extremely intensive foaming. Thus, we can assume that at 30 atm it was possible to feel the transition point from structures of one type to another; this transition depends, in the first place, on the quantity of mixture vapor content. Such a conclusion agrees well with the observation of Doctor of the Technical Sciences S. I. Kosterin [2], that with an increase in mixture velocity the dispersion of the structure also increases.

In addition to qualitative observations of the variation of flow structure in a pipe, the method of high-speed motion picture

photography enabled us to find a way of computing the true velocity of vapor bubbles and vapor locks.

We examined locks and bubbles on a section of film corresponding to the stationary regime of motion picture photography, and their velocity was calculated according to the formula:

$$w_{\Pi} = d_{\text{ок}} \frac{n_c}{n_{\Pi}}, \quad (1)$$

where w_{Π} is the true component of the velocity of a vapor lock or a vapor bubble along the axis of the pipe, m/s; $d_{\text{ок}}$ is the diameter of the viewing window, in m; n_c is the exposure speed in frames per second; n_{Π} is the number of frames during which the head of the lock or vapor bubble passed from the lower to the upper edge of the viewing window.

According to the values of w_{Π} obtained for a series of vapor locks or bubbles, we took their average arithmetic value, which was used as the average absolute velocity of a lock or bubble of a given size.

The total error in determining w_{Π} varied from 3% with a low lock velocity and high exposure rate up to 15 and even 20% with a low exposure rate.

Computations made by the method described above have a provisional character; they are necessary for developing a method of processing the photographic material.

The results of calculating w_{Π} for vapor locks according to some photographs are given in Table 2, from which it is clearly established that as yet there is too little data to establish any regularities.

Table 2.

№ пленки	Давление p , кг/см ²	Скорость циркуляции w_0 , м/сек	Приведенная скорость пара w_0'' , м/сек	Скорость смеси $w_{см}$, м/сек	Истинная скорость паровых пробок w_p , подсчитанная по пленкам w_p , м/сек
(1)	(2)	(3)	(4)	(5)	(6)
77	10,283	0,56	1,52	2,08	2,13—2,53
78	10,371	1,20	1,63	2,83	3,0 —3,3
79	27,898	1,03	0,59	1,62	1,75—1,9
80	27,504	0,98	0,40	1,38	1,58—1,78

KEY: (1) Film number; (2) Pressure, p , kg/cm²;
 (3) Circulation rate w_0 , m/s; (4) Reduced velocity of vapor w_0'' , m/s; (5) Mixture velocity $w_{см}$, m/s;
 (6) True velocity of vapor locks w_p computed from films w_p , m/s.

The work performed made it possible to develop a method of observing and fixing, with the aid of a high-speed movie camera, the structure of the flow of a steam-water mixture in a vertical unheated pipe at high pressures.

The complexity of the flow structure was clarified and the relationship between changes in the character of the flow regime and pressure, circulation rate, and the vapor content in the pipes was illustrated.

We could establish that with values of circulation velocity w_0 and reduced vapor velocity w_0'' near 1 m/s and a pipe diameter of 22.5 mm there are two equal regions of hydrodynamic regimes as a function of pressure:

a) the vapor lock regime with emulsion was observed up to 30 atm;

b) the emulsion regime with the passage of fine vapor locks and large bubbles was observed from 30 to 80 atm.

The transition from the first regime to the second was noted at 30 atm during a variation in w_0 from 0.5 to 1 m/s.

The method of high-speed motion picture photography makes it possible to calculate the true velocities of separate vapor bubbles and the vapor locks in a liquid mass and is promising for a determination of instantaneous values of vapor content in the studied section of the pipe.

The material obtained in the motion picture photography of the structure of a two-phase flow made it possible to compile a motion picture film which gives the qualitative picture of the effect of p , w_0 and w_0'' on the structure of flow in a vertical unheated pipe 22.5 mm in diameter.

BIBLIOGRAPHY

1. Лукомский С. М. Прецизионный прибор для измерения высоких переменных давлений с погрешностью, не превышающей 0,05%. «Журнал технической физики», 1943, № 4—5.
2. Костерин С. И. Исследование структуры потока двухфазной среды в горизонтальных трубах, «Известия АН СССР, ОТН», 1943, № 7; Исследование гидравлического сопротивления при движении газожидкостных сред в горизонтальных трубах, «Известия АН СССР, ОТН», 1943, № 11, 12; Исследование влияния диаметра и расположения труб на гидравлические сопротивления и структуру течения газожидкостной смеси, «Известия АН СССР, ОТН», 1949, № 12.

A METHOD OF CALCULATING CRITICAL
PARAMETERS DURING PULSATION
REGIMES IN THE MOTION OF A
STEAM-WATER MIXTURE

V. S. Polonskiy and Ye. P. Serov

Abbreviations

r_p - boundary
H - nomogram
p - calculated
e - experimental

As experimental data show, the value of critical thermal fluxes depends upon the amplitude, frequency, and type of disturbance applied to a system of steam-generating pipes [1, 2].

The period of self-oscillations during intercoil pulsations varies from one or two to several tens of seconds as a function of the type of installation [3], and in order is equal to the passage time of a heat carrier particle through the entire channel [3, 4]. The frequency of forced oscillations, encountered during the operation of steam generators, is of the same order.

In its turn, the process of steam generation is also a periodic process. As experimental data have shown, the frequency

of vaporization depends on the physical properties of the heating surface, the physical constant of liquid, thermal flux, and pressure, and varies within a wide range. In [5] it is shown that the frequency of bubble breakaway is $\omega \approx 35-45$ Hz; in [6] it is $\omega = 30-60$ Hz, in [7] $\omega = 13-17$ Hz, and in [8] $\omega = 15-21$ Hz. From that examined in [9] it follows that a change in the frequency of vaporization was observed within $\omega = 17-55$ Hz. G. G. Treshchev introduces the probable frequency of vapor bubble formation during surface boiling, which is $\omega = 3.0 \cdot 10^3$ Hz [10].

Consequently, the minimum frequencies observed by various authors during boiling in a large volume with moderate thermal loads are 10-15 Hz, while with surface boiling they are two orders greater. It is obvious that the vaporization frequency during the development of boiling in a moving liquid will be nearer the frequency during surface boiling than the frequency during boiling in a large volume.

Mass exchange intensity of liquid phase between the flow core and the boundary layer plays a large role in the onset of the crisis phenomenon. Frequencies of mass exchange processes can be evaluated according to the value of the turbulent pulsation frequency which exceeds 100 Hz [11].

Thus, the frequencies of vaporization processes and turbulent pulsations are at least one or two orders higher than the frequency of forced oscillations or disturbing self-oscillations.

The interaction between the examined periodic processes depends on their frequency relationship. If the pulsation frequency of the flow-rate parameters is the same order as the frequency of vaporization and of turbulent pulsations, there is a direct connection between these processes. On the other hand, if the frequency of these processes differs considerably, each can be examined separately. In this case, the oscillations of

hydrodynamic parameters do not affect the condition of vaporization. Relationships obtained during a stationary regime remain true in dynamic conditions also. This means that in the first approximations the boiling crisis process in steam-generating channels during pulsation regimes can be considered quasistationary.

If in stationary regimes, for example, the value of boundary vapor content or thermal flux for a channel of given form is expressed by relationship:

$$x_{rp0} = f(q_0, (w_1)_0, p_0); \quad (1)$$

$$q_{rp0} = f_1(x_0, (w_1)_0, p_0), \quad (1a)$$

then during oscillations the increase in the boundary vapor content

$$\Delta x_{rp} = x_{rp} - x_{rp0}$$

or thermal flux

$$\Delta q_{rp} = q_{rp} - q_{rp0}$$

is

$$\Delta x_{rp} = \left(\frac{\partial f}{\partial q} \right)_0 \Delta q + \left(\frac{\partial f}{\partial w_1} \right)_0 \Delta w_1 + \left(\frac{\partial f}{\partial p} \right)_0 \Delta p; \quad (2)$$

$$\Delta q_{rp} = \left(\frac{\partial f_1}{\partial x} \right)_0 \Delta x + \left(\frac{\partial f_1}{\partial w_1} \right)_0 \Delta w_1 + \left(\frac{\partial f_1}{\partial p} \right)_0 \Delta p. \quad (2a)$$

This relationship is more accurate the lower the value of parameter deviation. Partial derivatives characterize the degree of the effect of this parameter on the value of boundary vapor content. Corresponding values of the argument increment differ both in amplitude and in phase. The relative amplitude and phase depend on oscillation frequency.

Thus, in finding the region of unreliable regimes, it is necessary to determine: the amplitude- and phase-frequency characteristics of the steam-generating channels, the value of the increment in boundary vapor content or critical load as a function of the frequency and amplitude of the disturbing action, the relationship between the increment of boundary vapor content

Δx_{rp} (Δq_{rp}) and the real increment Δx_2 (Δq) which occurs with a given disturbance.

In general form, during the calculation of the dynamics in channels, a one-dimensional model is usually used, described by the following system of equations: continuity, energy, state, thermal balance or heat conductivity - with corresponding initial and boundary conditions [12].

The equation of heat carrier motion is usually replaced by an algebraic relationship between the equivalent resistance and the flow rate and specific volume. This gives the basis for the model of the boiling crisis during pulsation regimes in the form of a structural diagram recorded for a linear object (see Figure). Here the symbol $w_{\eta\xi}$ designates the corresponding transfer function. Let us examine the purpose of each link during one disturbance, for example, during a disturbance with respect to the input enthalpy. A pulsation of input enthalpy causes a change in output parameters D_2 , i_2 , and γ_2 in terms of the transfer functions $w_{D_2 i_1}$, $w_{i_2 i_1}$. A change in D_2 and γ_2 in terms of transfer functions $w_{p D_2}$, and $w_{p \gamma_2}$ causes a pulsation of pressure in the channel. A pressure pulsation in the channel brings about a pulsation of the medium's temperature and heat transfer factor. Naturally this leads to a pulsation of channel wall temperature, which follows the medium's temperature also with a different amplitude and phase. This causes the appearance of the periodic component of thermal flux from the inside of the channel wall in terms of the transfer function w_{qp} . A change in the periodic component of thermal flux and pressure in terms of transfer functions $w_{D_2 q}$, $w_{i_2 q}$ and $w_{D_2 p}$, $w_{i_2 p}$, respectively, affects the output parameters of the system. The totality of output quantities ΔD_2 , Δp , Δq in the equation (2) modeling unit determines the output quantity Δx_{rp} or the equivalent quantity Δi_{rp} . Comparison of the actual output enthalpy Δi_2 with Δi_{rp} is effected in the comparison unit. If $\Delta i_2 \geq \Delta i_{rp}$,

the boiling crisis begins in the channel; if $\Delta i_2 < \Delta i_{rp}$, the temperature regime of the steam-generating channel will be normal (as for the case when thermal flux is the quantity to be determined).

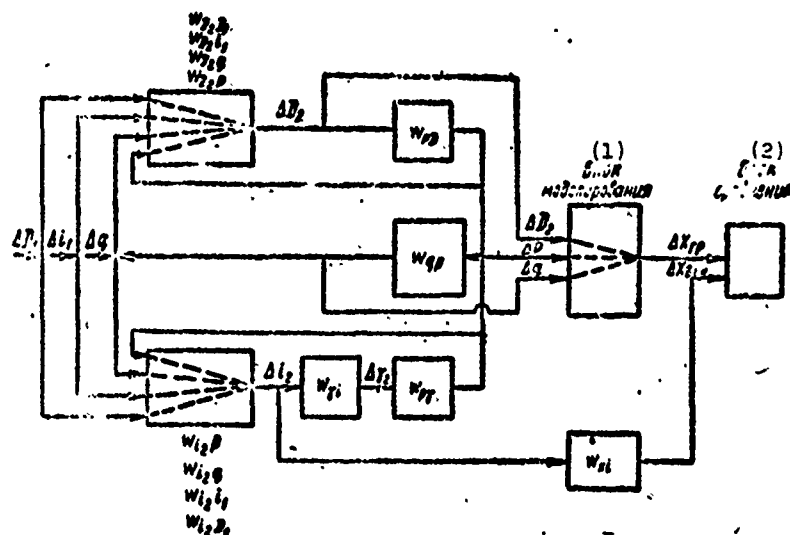


Figure. Structural diagram of the model of a boiling crisis in steam-generating channels during pulsation regimes.

KEY: (1) Modeling unit; (2) Comparison unit.

Table 1 gives a comparison between experimental data and calculation results during a disturbance by the flow rate of the heat carrier ΔD_1 . The static relationship $x_{rp} = x(q, w, p)$ is taken from reference [13] in which it is given in the form of a nomogram.

Table 1 uses the following designations:

- i_{rp} - experimentally determined boundary heat content represented by the authors of [2];
- i_H^0 - heat content determined according to the nomogram in [13], for the average values of flow-rate parameters on the assumption that the process is stationary;

i_H^g - heat content determined with the actual values of output parameters;
 $\Delta i_p = i_{H_0}^0 - i_H^g$ - calculated change in heat content;
 $\Delta i_g = i_H - i_{rp}$ - experimental change in heat content.

Table 1.

p , atm	w , kg/m ² ·сек	T , °K	A_x	$q \cdot 10^{-6}$, kcal/m ² ·h	i_{rp} , kcal/kg	i_H^0 , kcal/kg	i_H^g , kcal/kg	Δi_p , kcal/kg	Δi_g , kcal/kg
100	800	6	0,23	1,1	334	524	342	182	190
100	800	6	0,23	1,0	366	510	400	140	174
100	800	6	0,37	0,8	334	556	377	179	222
100	800	6	0,37	0,7	336	571	461	110	205
100	800	6	0,5	0,7	334	571	380	191	237
100	800	6	0,5	0,6	336	567	451	136	221
100	800	6	0,5	0,88	315	546	340	206	231
100	800	60	0,5	0,59	366	590	487	103	224
100	800	0,6	0,5	2,38	372	454	239	215	32
100	800	0,6	0,5	1,32	404	492	435	57	88
100	2000	6	0,42	1,35	379	454	434	20	75
100	2000	6	0,42	1,27	347	470	363	107	123
100	2000	6	0,42	1,5	318	430	349	46	117
70	800	6	0,5	1,0	340	553	503	50	213

DESIGNATIONS: atm = atm (abs.); kg/m²·сек = kg/m²·s;
сек = s; kcal/m²·h = kcal/m²·h; kcal/kg = kcal/kg.

The increments of heat carrier flow rate and enthalpy were determined according to transfer functions [12]. Thermal loading was assumed constant and equal to the stationary values. The increment of thermal flux was determined according to [14]. For comparison data from [2] were used.

As is apparent from Table 1, the determining parameters varied over a rather wide range. The agreement between calculated and experimental data was fully satisfactory. At low amplitudes for flow rate oscillations the agreement of data was better than at high amplitudes.

For the purpose of a more complete check of the data, a special experiment was set up [15]. Tests were conducted in the following range of factor variation: $p = 100-140$ atm (abs.); $q = 250-550 \cdot 10^3$ kcal/m².h; $w = 700-1100$ kg/m².s. Frequency variation limits were $\omega = 0.8-6.28$ 1/s and relative amplitude for thermal flux was $A_q = 0.25-0.5$.

In the tests examined the amplitude of pressure oscillations did not exceed 5 atm (abs.). The amplitude of pressure oscillations was greater the lower the mass velocity, the higher the average thermal flux level, and the greater the oscillation period. In all tests, oscillations of the heat carrier flow rate were insignificant. A comparison between experimental and calculated data was performed only with respect to the value of boundary enthalpy.

The results of the comparison are presented in Table 2. As is apparent from the table, the agreement between experimental and calculated data was better than during flow rate disturbance. This is explained by the fact that the disturbance along the heating channel obviously is somewhat weaker than a disturbance of the heat carrier flow rate. Consequently, the depth of variation in regime parameters was less.

In performing the calculation of dynamic characteristics, a number of simplifying premises were made; specifically, the feedback with respect to pressure and thermal flux was disrupted. Obviously, a more precise solution within the framework of quasistationary concepts can be obtained with more precise, computerized calculations of the dynamic characteristics of a steam-generating channel.

Table 2.

P , атм	ω , кг, м ² ·сек	$q \cdot 10^{-3}$, ккал, м ² ·сек	A_q	ω , 1, сек	i_2 , ккал, кг	i_p , ккал, кг
100	700	250	0,25	2,09	601	597
100	700	250	0,25	3,14	598	598
100	700	250	0,25	4,65	595	598
100	700	250	0,25	6,28	597	599
100	700	400	0,25	2,09	566	569
100	700	400	0,25	3,14	562	560
100	700	400	0,25	4,83	557	560
100	700	400	0,25	6,28	562	559
100	700	550	0,25	2,09	546	545
100	700	550	0,25	3,14	542	543
100	700	550	0,25	5,04	541	544
100	700	550	0,25	6,28	548	544
140	700	550	0,24	2,09	493	484
140	700	550	0,24	4,19	489	485
140	700	550	0,24	6,28	487	485
140	1100	550	0,28	2,09	475	489
140	1100	550	0,28	3,14	472	489
140	1100	550	0,28	4,19	474	488
140	1100	550	0,28	6,28	475	488
100	700	400	0,25	0,8	569	558
100	700	400	0,25	1,4	568	558
100	1100	400	0,25	2,08	549	552
100	1100	400	0,25	4,18	543	551
100	1100	400	0,25	6,28	549	552
140	700	400	0,5	4,18	486	484
140	700	400	0,5	3,14	489	482
140	700	400	0,5	2,08	492	482
140	700	400	0,5	1,4	495	478
140	700	400	0,5	1,04	497	483

BIBLIOGRAPHY

1. Алашеев И. Т. и др. Кризис кипения в трубах. Сб.: «Теплопередача». АН СССР, 1962.
2. Миropольский З. Л., Шницман М. Е., Пикус В. Ю. Исследование влияния и амплитуды пульсаций расхода на критические тепловые потоки. ИФЖ, т. VII, № 6, 1964.
3. Давидов А. А. Некоторые итоги изучения жидкостной пульсации в прямоточных котлах и направление дальнейших исследований. «Труды ЦКТИ», вып. 59. Л., 1965.
4. Петров П. А. Гидродинамика прямоточного котла. ГЭИ, 1960.

5. Матонора Н. Н. Изучение механизма кипения при больших тепловых потоках. Докл. АН УССР. Сер. Физ.-матем. науки. КИТФ, 1963, № 3.
6. Зиссман-Моллажен Т. М., Кутаепов С. С. К вопросу о влиянии температуры на процесс парообразования в кипящей жидкости. ЖТФ, т. 20, вып. 1, 1950.
7. Ba. Nayak Zubert: «Trans ASME», ser. C, vol. 80, № 3, 1958.
8. I. W. Westwater and I. G. Santangelo. «Industrial and Engineering Chemistry», vol. 47, № 8, 1955.
9. Вопросы физики кипения. Под ред. Н. Т. Азизова. Изд. «Мир», 1964.
10. Тренев Г. Г. Теплообмен при высоких тепловых нагрузках и других специальных условиях. Под ред. А. А. Арманда. ГЭИ, 1959.
11. Шляхтин Г. Возникновение турбулентности. ИИЛ, 1962.
12. Серов Е. П., Корольков Б. П. Динамика процессов в тепло- и массообменных аппаратах. Изд. «Энергия», 1967.
13. Миропольский Э. Л., Шницман М. Е. Критические тепловые потоки при кипении воды в каналах. «Атомная энергия», т. 11, вып. 6, 1961.
14. Серов Е. П., Полонский В. С. Анализ кризиса кипения в парогенерирующих каналах при пульсационных режимах. «Теплоэнергетика», 1967, № 1.
15. Полонский В. С., Серов Е. П. Доклады научно-технической конференции по итогам научно-исследовательских работ за 1965—1967 гг., секция теплоэнергетическая, подсекция тепловых электрических станций. М., МЭИ, 1967.

EVALUATING CIRCULATION RELIABILITY IN HIGH-STRESS SHIPBOARD BOILERS

Yu. V. Aleksandrovskiy

Abbreviations

оп - descent
пол - useful
н - nonstationary
yx - impaired

Shipboard steam boilers, unlike boilers in stationary power plants, operate more frequently in unstationary regimes. During maneuvers, the load of the boiler can change from minimum to full and vice versa. Because of this there is considerable interest in evaluating boiler reliability in unstationary regimes and, particularly, circulation reliability in a boiler during pressure change.

Until recently circulation reliability during unstationary regimes in such boilers has been evaluated according to the method proposed by D. F. Peterson [1]. Studies on the circulation in shipboard high-stress boilers which have unheated descending pipes have shown that an evaluation of the allowable rate of pressure drop in such boilers according to Peterson's formula

gives a significant allowance. The application of the basic assumptions of this method to an evaluation of circulation reliability during a pressure rise in a boiler has shown sufficiently good agreement between calculated and experimental data. The studies have also indicated that a rise in steam pressure in an actual boiler does not lead to a disruption of circulation.

In connection with the development of the "Standard Method of Hydraulic Calculation for Steam Boilers," a check of its assumptions and recommendations was made with respect to the calculation of natural circulation in high-stress shipboard boilers. As a result, it was established that the basic assumptions and recommendations of the method can be used for calculating and evaluating the reliability of shipboard steam boilers. The specifics of such boilers come to light only in an evaluation of the allowable rate of pressure reduction..

As we know, in the "Standard Method" project it was recommended to determine the allowable rate of vapor pressure drop in a boiler (when $w_{\text{on}} \geq 0.8$ m/s) under the condition that circulation reversal and stagnation in the less heated pipes of the loop was not allowable. The danger of stagnation and reversal occurs because of an increase in resistance in the descending pipes. In high-stress shipboard boilers the least heated line of pipes is located in the high-temperature region of gas flow and the specific thermal flux absorbed by it is 150,000-200,000 kcal/m²·h and more. At the same time, the resistance of the descending pipes is not great since the cross section of these pipes is less than 70% of the cross section of the ascending pipes. As a result, as is apparent on the figure, the least heated pipes of the loop in the stationary regime have a multiple reserve with respect to such circulation reversal and stagnation.

Along with this, in the most heated lines of ascending pipes the circulation frequency even in a stationary regime is near the

maximum allowable values. With a drop in steam pressure in the boiler, circulation frequency in the ascending pipe is reduced and reaches values at which heat transfer from the outer surface of the pipe to the working liquid can be impaired [2]. The calculations made indicated that in shipboard high-stress boilers with a pressure drop the circulation frequency in the most heated lines reaches limiting values before circulation reversal and stagnation occurs in the least heated pipes of the loop. Because of this, an additional check on the reliability of circulation during a drop in steam pressure in the boiler is necessary.

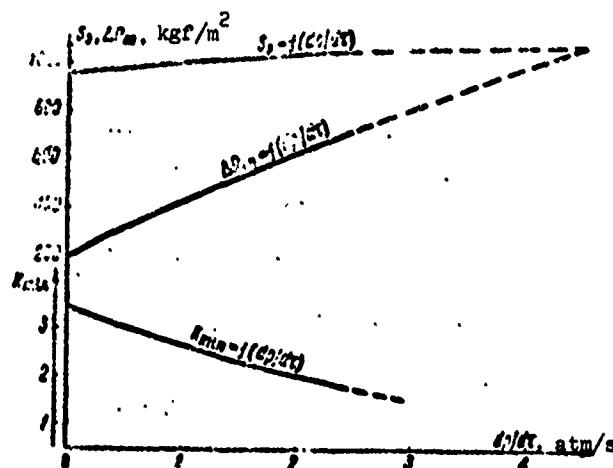


Figure. Variation in the frequency of circulation toward the most heated pipe of the loop K_{min} , stagnation head S_3 , and descent resistance ΔP_{on} during a drop in vapor pressure in a boiler.

Calculations showed that the quantity of heat released to the most heated pipes of the loop during a drop in pressure, going to an increase in vaporization, is not great in them as compared with the quantity of heat absorbed by the pipes from the combustion products. This makes it possible, when evaluating the allowable rate of pressure drop with respect to the value of maximum circulation frequency, to use a diagram of the loop obtained during calculations of the boiler on stationary regime. The hydraulic

curve of the most heated pipe of the loop, as well as the hydraulic curve of the descending system, calculated for various rates of vapor pressure drop in the boiler, should be plotted on this diagram. Assuming that the curves for the ascending part of the loop do not change with a drop in steam pressure, we determine the value of net head in the loop $S_{\text{нон}}$ and the water flow rate at input to the most heated ascending pipe G kg/h. Circulation frequency in it is calculated as:

$$K = \frac{G}{D_H}.$$

where D_H is the quantity of steam generated in the most heated pipe during nonstationary regime, taking into account the additional vaporization due to the release of accumulated heat, kgf/h. Circulation frequencies are calculated at various rates of pressure drop in the boiler. Calculations show that with such an approximate calculation of circulation frequency, error is no more than 1.5% as compared with the values obtained when calculating the loop separately for each of the pressure drop rates.

The allowable rate of pressure drop in high-stress shipboard boilers must be checked further based on the condition that the degree of steam dryness in the most heated pipe during nonstationary regime x_H must not reach the value x_{yx} determined according to the data from the "Standard Method." Taking into account the necessary reserve, the following condition must be fulfilled:

$$\frac{x_{yx}}{x_H} \geq 1.2.$$

The fact that in the most heated pipe of the loop in high-stress shipboard boilers, the circulation frequency is near the maximum allowed, must be taken into account when evaluating the allowable heating surface breakdown. In determining the permissible quantity of jammed pipes in the bunch near the furnace, it is necessary to calculate the circulation frequency in the most heated pipe.

BIBLIOGRAPHY

1. Петерсон Д. Ф. Надежность циркуляции при колебании давления в котле. «Советское котлотурбостроение», 1951, № 3.
2. Локшин В. А. Семеновкер И. Е., Вихрев Ю. В. Температурный режим парогенерирующих труб. «Труды ЦКТИ», вып. 58. Л., 1965.

THE OPERATION OF EVAPORATIVE
LOOPS WITH HORIZONTAL AND
DESCENDING MOTION OF A STEAM-
WATER MIXTURE DURING NATURAL
CIRCULATION

Yu. I. Tseluyko, Ya. N. Rudnitskiy,
A. D. Fayershteyn, L. B. Katsenelenbogen,
and L. A. Strel'tsov

Abbreviations

SH - internal

Experience has been obtained on an evaporative cooling installation of a reheating furnace in one of the modern rolling mills, on the basis of industrial studies and a three-year period of operation, with the performance of hearth pipes having a descending motion for the coolant during operation on evaporative cooling with natural circulation with a pressure range in the drum of 9-17 atm (gauge). A simplified diagram of the installation is presented in Fig. 1.

Heated lateral pipes $\varnothing 114 \times 20$ mm (see Fig. 1, 8) along with longitudinal, which are not shown on the diagram, form the supporting grid on which is placed the metal, heated top and bottom, before rolling. These pipes, which are steam-generating heating surfaces, are connected in parallel to a common

circulation system which provides their cooling. The height of the circulation loop is 21, 25 m. The circulation pump, connected in parallel to a system of descending pipes, is used only during starts and stops of the evaporative cooling installation.

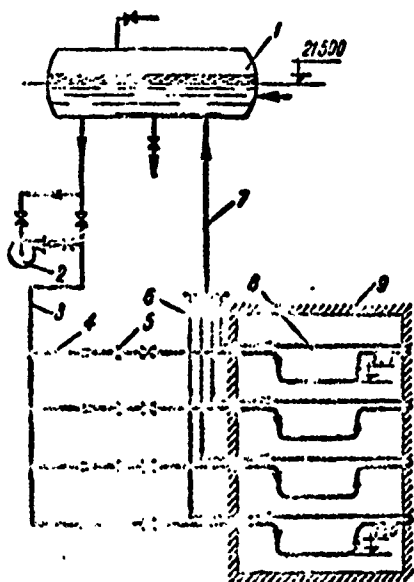


Figure 1. Simplified diagram of evaporative cooling installation:

- 1 - Drum; 2 - Circulation pump for starting and stopping;
- 3, 4 - Descending pipes; 5 - Measuring diaphragm; 6, 7 - Ascending pipes; 8 - Heated loops with descending motion;
- 9 - Boundary of furnace lining.

The use of descending motion makes it possible to cut in half the number of circulation loops of lateral pipes with vertical supports, which substantially reduces the metal content of the installation due to the decrease in the amount of descending and ascending pipes, the number of shut-offs, and meters.

Figure 2 gives the design of a heated loop with descending (up to 2.5 m) motion for the coolant. There are ten such loops in the installation. Thermal stresses, averaged along the heated length of the loop and the perimeter of the pipe, reach 125×10^3 kcal/m².h. As is apparent from Fig. 2, the heated part of the loop consists of horizontal and vertical sections.

Reliable cooling of the horizontal section is determined by excluding lamination of the steam-water mixture. Tests made at

Giprostal' [State Scientific Research and Planning Institute of the Metallurgical Industry] and experience in the industrial operation of horizontal pipes at these pressures and thermal stresses on the order of $(200-240) \cdot 10^3$ kcal/m²·h show that reliable cooling of horizontal pipes with internal diameter up to 75 mm in the zone of surface boiling can be achieved at a circulation rate of 1.2 m/s [1, 2].

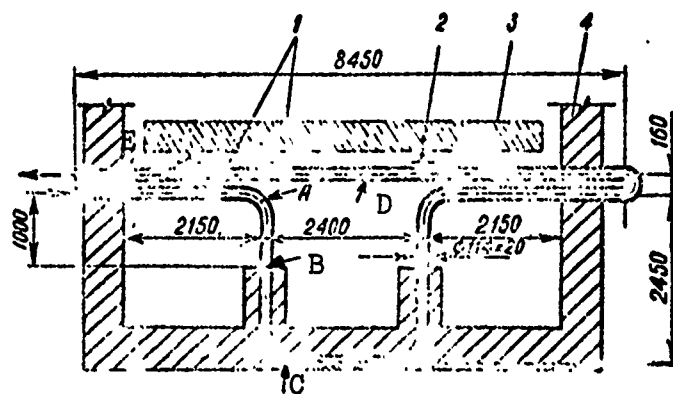


Fig. 2. Heated loop with descending motion:
 1 - Design of support pipe with descending motion; 2 - Longitudinal support pipes;
 3 - Heated metal; 4 - Furnace lining;
 A - Upper (initial) point of the descending section, in the region of which the thermocouples were installed; B - Lower heated point of descending section; C - Lower geometric point of descending section;
 D - Damaged region; E - Output point of heated loop.

With less thermal stress the minimum allowable circulation rate at which there is no lamination in the zone of surface boiling on the horizontal section is accordingly reduced.

Reliable cooling of the vertical heated section with descending motion of the steam-water mixture is determined by the absence of vapor bubble stagnation. Based on data from [3], the circulation rate, which ensures bubble drift is 0.4 m/s; however, these data were obtained on an air-water model under low pressure for pipes with an internal diameter of less than 48 mm.

As shown by special circulation tests on an industrial installation, made on pipes with $d_{BH} = 74$ mm under pressure in the drum of $p = 12$ atm (gauge) with wall temperature measurement by thermocouples caulked-in on the descending part of loop A (Fig. 2, A), the wall temperature of the pipe in the descending region did not increase in the rate reduction range of 1.2-0.55 m/s.

The results of the tests made indicate that with a circulation rate of 0.55 m/s (the flow-rate vapor content per unit volume β with respect to the heated length of the descending section from point A to point B changes from 0.72 to 0.8 - see table) vapor bubble drift is ensured during the descending motion of the flow and the possibility of bubble stagnation is fully excluded. It was not possible to perform tests at rates below 0.55 m/s in industrial conditions.

With low circulation velocities, in order to exclude corrosion effects on horizontal sections, because of the possible stratification of the steam-water mixture, tests at low rates were brief - no more than ten minutes in each regime. However, this time was completely sufficient for studying the steady-state regime.

Thus, the tests allowed us to establish that the minimum allowable circulation rate in a loop with descending and horizontal motions for the coolant is limited not by the conditions of vapor bubble drift on the descending section but by the condition that there be no lamination on the horizontal sections of the loop.

As three-year operational tests on these loops have shown, with thermal stresses up to $125 \cdot 10^3$ kcal/m²·h, the reliable operation of the horizontal sections is ensured at a circulation rate on the order of 1 m/s and above. Vapor content per unit volume β with respect to the heated length of the descending section changes when $w_0 = 1$ m/s from 0.475 to 0.64 (see table).

Table. Characteristics of a loop with descending motion during a total thermal load of 580,000 kcal/h ($q = 125 \cdot 10^3$ kcal/m²·h*, $p = 12$ atm (gauge)).

Regime Designation	Circulation rate, w , m/s	Length of economizer section l_a , m	Vapor content per unit weight (α) and per unit volume (β) along the length of the heated contour (see Fig. 2)					
			Point A, $l = 2.15$ m, heating		Point B, $l = 3.15$ m, heating		Point E, $l = 13$ m heating	
			α	β	α	β	α	β
Circulation rate in descending section, sufficient for vapor bubble drift	0.55	0.67	0.0188	0.72	0.0315	0.8	0.155	0.96
Circulation rate sufficient for reliable cooling of the horizontal section	1.0	1.210	0.0073	0.4750	0.0133	0.64	0.08	0.93
Minimum circulation rate at which boiling is absent in the descending section	2.55	3.15	0	0	0	0	0.02	0.725

*Thermal stress is introduced for the heated part of the loop not covered by masonry.

On the row of loops with descending motion, the furthest from the burners and, therefore, those having the least thermal loads, there was no boiling in the descending sections.

As shown by experience with the parallel operation of loops having boiling and nonboiling descending sections, such a combination does not reduce the reliability of the installation on the whole. The reduction in pressure in the drums to 9 atm (gauge) was caused by pulsation of the flow rate in the most thermally loaded loop ($w_0 = 0.7$ -1.3 m/s). Long operation of the installation revealed the reliability of pipe cooling in such a regime. A reduction in pressure in the drum below 9 atm (gauge) expanded the pulsation range which was bounded by the lower limit of the working pressure on the level of 9 atm (gauge).

Installations with descending coolant motion in the heated pipes have several operational peculiarities.

a) when the installation is filled before the thermal unit (furnace) is started, it is necessary to carefully remove the air from the descending heated sections by the individual flushing of each loop in turn with a rate of no more than 1 m/s.

b) pressure reduction in the installation, when necessary, should be accomplished smoothly, without cutting off circulation, being directed, in each specific case, along the circulation apparatus.

Adjustment and observational tests on evaporative cooling installations with a descending motion of the steam-water mixture has shown that a sharp pressure drop (>0.3 atm (gauge)/min) in the system leads to the formation of vapor locks with a stagnation of circulation in separate loops; after pressure stabilization the stagnation phenomena last longer in the most thermally loaded loops than they do in the others. In the case of such disturbances, it is necessary to eliminate vapor locks by an artificial brief reduction in flow rate to the neighboring loops with the aid of control valves.

Figure 3 shows the characteristic damage to heated pipes, which occurs on the horizontal sections when the operational requirements are not met and which took place in the initial operating period of the first installation with descending motion installed in this country. Damage occurred in the center part of the upper lateral pipe of the loop (Fig. 2D).

As shown by an analysis of the work of loops according to operational manuals and diagrams, as well as by chemical and metalographic studies of damaged pipe specimens, these damages occurred during the formation of vapor locks and long circulation stagnation in the most thermally loaded loops because of the sharp pressure drop in the installation. With long stagnation the metal is damaged under the action of steam-water corrosion,

GRAPHICS NOT REPRODUCIBLE

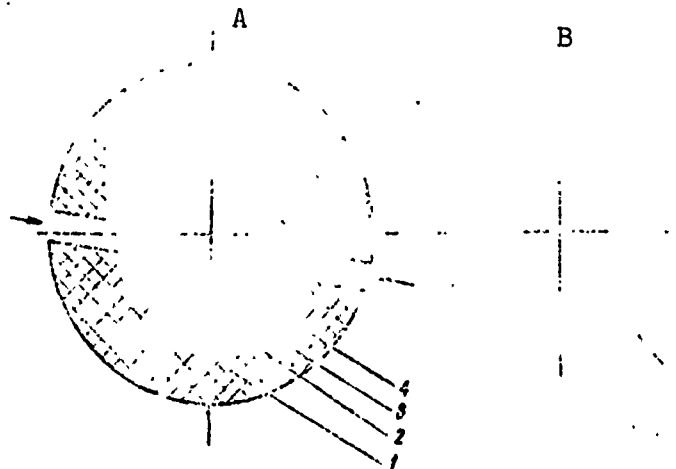


Fig. 3. Damage to the upper lateral pipe $\varnothing 114 \times 20$ mm as a result of the primary effect of steam-water and the secondary effect of the sludge corrosion. The arrows indicate the direction of maximum thermal flux and the spot of hole formation: A - Character of the damage to the insulated pipe in the gap between insulation units; B - Character of the damage to noninsulated pipe; 1 - Insulation; 2 - Pipe; 3 - Dense deposits of corrosion products; 4 - Loose deposits of corrosion products.

which continues with the formation of an oxide layer, and after the restoration of circulation, under the action of secondary sludge corrosion. As is apparent from the figures, the largest damage centers appear in the direction of the action of maximum thermal flux (on Fig 3B from the side of the jet, on Fig. 3A in the gap between the two insulation units covering the top and the bottom of the pipe in the initial period of operation; several months after start-up the insulation was removed).

The effect of metal damage from within under the action of steam-water and sludge corrosion, in the direction of maximum thermal flux, is of interest and, of course, can be used in engineering.

A standardization of the pressure drop regime eliminates pipe damage and provides for the reliable industrial operation of loops with descending motion.

In this country, at the present time, we have in successful operation seven evaporative cooling installations for continuous reheating furnaces, which have heated support pipes with horizontal and descending motion for the coolant. All seven installations operate with natural circulation.

Descending motion is particularly promising for the modern wide furnaces, as well as for redesigning existing ones.

Conclusions

1. A test was made on the reliable operation of pipe elements with descending (to 2.5 m) motion for the steam-water mixture during natural circulation and thermal stresses up to $125 \cdot 10^3$ kcal/m²·h with a pressure range in the drum of 9-17 atm (gauge).

2. It was established that under these conditions the sufficient speed of bubble drift on the descending section of the pipe $d_{BH} = 74$ mm, with flow-rate vapor content per unit volume up to 0.80, is 0.55 m/s. The minimum speed of bubble drift could not be established due to the production limitations on an industrial installation.

3. It was established that the minimum allowable circulation rate in a loop with descending and horizontal motion for the steam-water mixture is limited not by the condition of vapor bubble drift on the descending section but by the lack of mixture lamination on the horizontal sections of the loop. With thermal stress up to $125 \cdot 10^3$ kcal/m²·h in the studied pressure range (9-17 atm (gauge)), reliable operation of horizontal sections is ensured at a circulation rate of 1 m/s and higher.

4. The use of descending motion makes it possible to substantially reduce the number of circulation loops which, in turn, makes it possible to operate with natural circulation in a wider range of thermal loads on the furnace. This also reduces the cost of the installation because of the reduction in the amount of metal used.

BIBLIOGRAPHY

1. Антоньев С. М. и др. Исперительное охлаждение нагревательных прокатных печей. «Сталь», 1955, № 12.
2. Антоньев С. М. и др. Обобщение ряда конструктивных и эксплуатационных показателей установок исперительного охлаждения нагревательных печей. Сборник науч. трудов института «Гипросталь», вып. 7, 1964.
3. Шварц А. Л. и Локшин В. А. Экспериментальное исследование движущих напоров при пусковом движении пароватной массы в вертикальных трубах при давлении до 150 ат. «Теплоэнергетика», 1957, № 6.

A STUDY OF THE HYDRAULICS OF
STEAM-WATER FLOW USING AN
EXAMPLE OF THE STEAM-GENERATING
WELLS IN KAMCHATKA

O. S. Naymanov

Abbreviations

cm - mixture
rp - friction
y - mouth
экс - experimental

At the present time, in the USSR (Pauzhetska GEOTES¹, Kamchatka oblast) the practical use of the Earth's heat for developing electric power has begun. The working medium in these power plants is steam generated from wells drilled to the necessary depth.

The construction, hydrodynamic tests, and regime characteristics of the wells are examined in detail in [1]. Here we shall pause on an explanation of the calculation functions which can be

¹[Translator's Note: The expansion of this abbreviation could not be found; however, the first three letters could stand for the work "geological" and the last three for "thermoelectric power plant."]

recommended for describing the motion of the steam-water mixture in the wells without which it is impossible to analyze theoretically the hydrodynamics of the wells on the whole, its characteristics, and optimum structural dimensions.

Up to the present time, in calculating two-phase flows (in any case, for values of true vapor content per unit volume $\phi = 0.5-0.98$) the only method is the semiempirical method using the true vapor content per unit volume found experimentally. However, the numerical relationship for quantity ϕ of various authors under various initial conditions are different, which gives us no a priori basis for using them in describing the processes involved in the discharge of the mixture from wells.

The process in a well is characterized by the following basic peculiarities.

1. The values for pressure, vapor content per unit weight x , and other parameters of the steam-water flow on the path from the beginning of vaporization to the mouth of the well vary substantially. Thus, for example, x varies from 0 to 0.1-0.15, β from 0 to 0.98-0.99, etc.

2. Since in this article we shall examine wells with constant flow rates and constant pressures at the mouth and in the beginning of vaporization (pulsing wells have not been considered), the flow in separate cross sections can be considered stationary.

3. The steam-water flow passes along a considerable path, counted in tens and hundreds of meters; the diameters of the wells are extremely large (100-200 mm); the pressure zone is 1-10 atm (abs.). The flow is vertical; heat losses to the surrounding rock are insignificant and allow us to consider it isentropic.

We shall write, in general form, on the basis of the Euler differential equation of motion, an expression for the elementary

steam-generating section of the well:

$$dl = \frac{dp - \frac{G^2 d\left(\frac{1}{\gamma_{cm}}\right)}{g}}{\gamma_{cm} + \frac{dp_{rp}}{dl}}, \quad (1)$$

where p is the pressure kg/m^2 ; G is mass velocity of the mixture, $\text{kg/m}^2 \cdot \text{s}$; γ_{cm} is the specific volume of the mixture, kg/m^3 .

Subsequently we shall limit ourselves to a study of the zone $p \leq 2.5$ atm (abs.) and $\phi \geq 0.95$; the component of vapor phase in the familiar expression for the specific volume of the mixture is insignificantly small, which makes it possible to write the simple relationship

$$\gamma_{cm} = \gamma' (1 - \varphi). \quad (2)$$

The drop in pressure going into the acceleration of the flow element (represented in formula (1) by the second term in the numerator), for the indicated pressure zone and when $G \leq 500$ $\text{kg/m}^2 \cdot \text{s}$, as calculations have shown, does not exceed 1-5% of the pressure drop in the well and, therefore, in the subsequent analysis can be disregarded.

We should discuss in somewhat greater detail the value of the resistance by friction occurring as the mixture rises in the well. In general form, we can write

$$\frac{dp_{rp}}{dl} = \frac{\psi k \lambda_0 G^2}{\gamma' 2gD}, \quad (3)$$

where λ_0 is the coefficient of hydraulic resistance, assuming a flow of liquid phase only; k is the additional factor, taking into account the presence of steam-water flow. Several formulas for determining this coefficient have been proposed [2], [3], [10].

In Table 1 we give these formulas. Since in the pressure zone less than 10-15 atm (abs.), which is characteristic for all wells, without exception, the ratio of specific weight $\gamma''/\gamma' \ll 1$,

the original expressions could be somewhat simplified; these simplified formulas are also presented in Table 1. In this same table are given the numerical values for k along one of the wells at three points: at a depth corresponding to the beginning of vaporization, at an intermediate point, and at the mouth of the well.

Table 1.

(1) Необходимая предпосылка для составления формулы	(2) Приближенная формула	(3) Числовые значения коэффици- циента k для давлений p , атм		
		6,5	3,5	1,5
(4) Квазигомогенный поток [2]	$1 - \frac{x\gamma'}{\gamma}$	2,8	28	137
(5) Экспериментальная формула, по- лученная на основе испытаний вер- тикального двухфазного потока [10]	$\frac{(1-x)^2}{(1-\varphi)^{1,53}}$	1,8	16	108
(6) Преобразованная формула Дарси с использованием выражения для среднего динамического напора [3]	$\frac{1}{1-\varphi}$	1,5	6,6	25

KEY: (1) Prerequisite for composing formula; (2) Approximate formula; (3) Numerical values of coefficient k for pressures p , atm (abs.); (4) Quasihomogeneous flow [2]; (5) Experimental formula obtained on the basis of tests on vertical two-phase flow [10]; (6) Transformed Darcy formula using an expression for the average dynamic head [3].

In the high pressure zone where coefficient $\psi = \lambda_{cm}/\lambda_0$ in formula (3), taking into account the difference between the calculated values of Δp_{TP} and experimental, is virtually equal to one, formula (1) has become widely used. However, there are data [4] which indicate that in the zone $\beta > 0.7-0.8$ the value of ψ drops. It is precisely this zone which is characteristic for discharge from a well.

The preliminary calculations we performed (a detailed study of losses from friction during the motion of flow in wells is not the subject of this article) showed that at pressures below 2 atm (abs.) the values of coefficient ψ during calculation according to [2] approach values of 0.1 and less; consequently, formula (3) is more convenient for calculation.

The formula proposed by S. G. Teletov, in our opinion, is more logical in its physical premises and in addition, in the zone of pressures in wells this formula has an extremely simple form. All subsequent calculations were made using this formula.

It should be mentioned that since an analysis of the actual values of ϕ along the wells is the main path, at a given stage of all the experiments on the wells only those were chosen for which the effect of friction on the depth of vaporization was limited to several per cents ($p \geq 2.5$ atm (abs.)). The use of any of the reduced formulas for coefficient k would have an insignificant effect on the final results.

With these remarks taken into account, expression (1) is reduced to a function of p and ϕ only:

$$dl = \frac{\frac{1}{\gamma'} dP}{1 - \epsilon + \frac{A}{1 - \epsilon}}. \quad (4)$$

The parameter

$$A = \frac{\lambda_0}{2gD} \left(\frac{G}{\gamma'} \right)^2$$

for a certain well on a given regime can be considered a known quantity. Assuming the relationship $\phi = f(p)$ under assigned values for pressure, flow rate, and well geometry, expression (4) can be integrated and the calculated value of vaporization depth can be obtained for the corresponding initial conditions of mixture discharge. Unfortunately, there is a large number of different recommendations with respect to finding the quantity ϕ . An illustration of this is Fig. 1, on which in function β the values of $C = \phi/\beta$ are presented according to the data of various authors. Therefore, we should solve the reverse problem, using the experimental values of vaporization depth for determining ϕ . All the available empirical relationships for finding true vapor content per unit volume during the motion of a two-phase medium

in vertical pipes with moderate pressures can be divided into two groups.

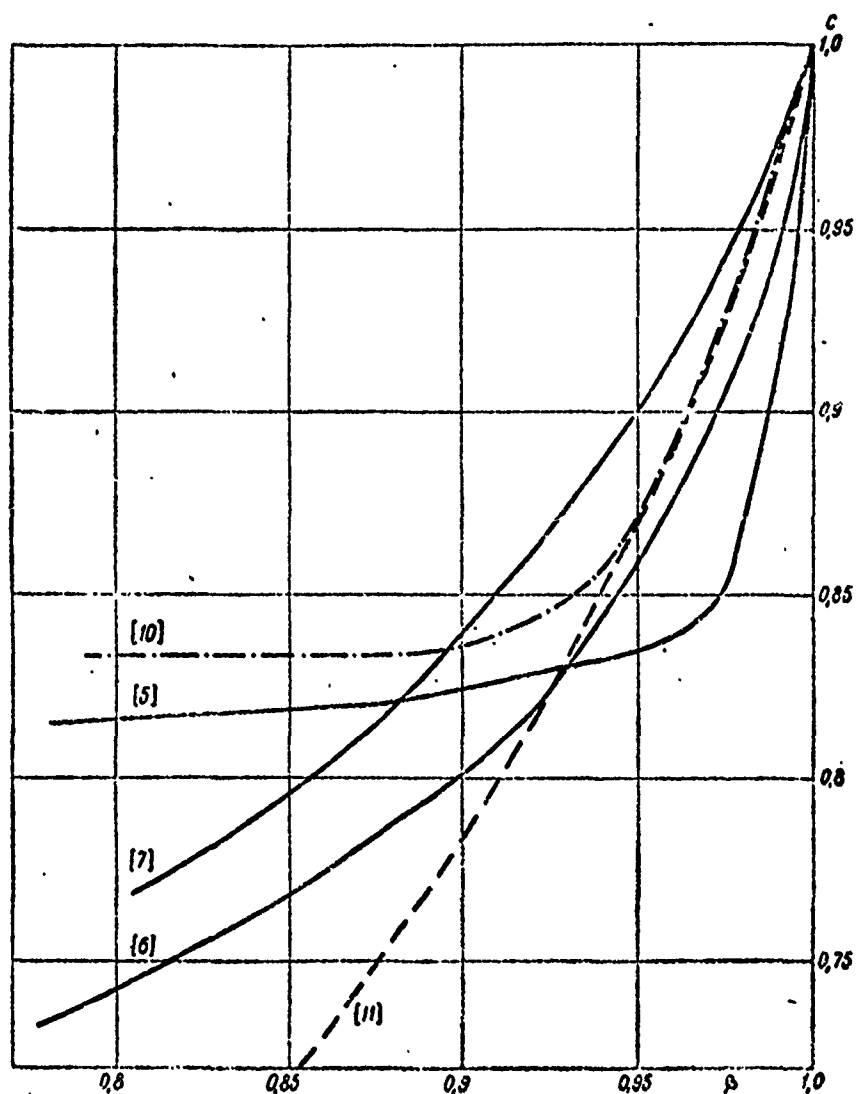


Fig. 1. Function $C = f(\beta)$ according to the data of various authors ($p = 3$ atm (abs.); $G = 10$ kg/s; $D = 132$ mm).

First group. Coefficient C is assumed independent of p , β , Fr_{cm} (Fr_{cm} is the Froude criterion for the mixture) or G . In [5] and [6] ϕ is implicit in the equation connecting the true velocity of vapor phase w'' with the calculated velocity of the

mixture w_{cm} :

$$\alpha'' = a + bw_{cm}^n. \quad (5)$$

G. Ye. Kholodovskiy recommends that we assume $a = 0$, $b = 1.26$, $n = 0.981$ for the reduced velocity of vapor phase $w_0'' \geq 3$ m/s and for $w_0'' < 3$ m/s (the "shell" regime of mixture flow) $b = 1.46$, $n = 0.84$.

Based on the data in [6], where the effect of diameter variation was specially studied, an additional term which takes into account pipe diameter is introduced into coefficient a . The coefficients we obtained according to the graph presented by the authors were equal to

$$a = 0.8 + \frac{4.7}{\exp\left[\frac{D^2 - 5.5}{\sqrt{w_{cm}}}\right]}; \quad b = 1.6; \quad n = 0.92$$

for mixture velocities¹ above 3 m/s; for lower velocities a is equal to as much as in the preceding case, $b = 2.4$, $n = 0.72$.

Cravarollo [7] gives a direct expression for quantity ϕ , obtained purely by the empirical method:

$$1 - \gamma = (1 - \beta) \left[1 + \frac{1.35^{0.9 \cdot 0.45}}{\left(1 + 0.335G \frac{1}{\gamma}\right)^{1/7}} \right],$$

where γ is the coefficient of surface tension. The experimental data from ENIN [Power Engineering Institute im. G. M. Krzhizhanovskiy] [8] for pressures of 40, 70, and 120 atm (abs.), representing $\phi = f(\beta, p, Fr_{cm})$, were replotted by us and extrapolated to a pressure of 1 atm (abs.). With extrapolation accuracy, the results of calculations using these data agreed with the data in [7].

¹When $\beta > 0.8$ the velocity of the mixture w_{cm} differs insignificantly from reduced steam velocity w_0'' .

V. A. Lokshin and A. L. Shvartz [9], after processing the available experimental data on useful moving heads in the pressure range 11-220 atm (abs.), introduce a diagram for finding the quantity C . In the region of developed motion and $\beta \geq 0.91$ coefficient C becomes a function of β only and in the zone $\beta < 0.91$ and $w_{cm} < 3$ m/s a function of mixture velocity (and, consequently, of G). In the pressure zone near atmospheric the following coefficients are assumed in formula (5): $a = 0.75$; $b = 1$; $n = 1$.

Second group. It is assumed that ϕ is a function of β and p only. According to A. A. Armand [10], in zone $\beta < 0.9$ $C = 0.833$; with an increase in β to 1, $C = f(p, \beta) \rightarrow 1$.

According to the results of tests at Cambridge University [10], it is proposed, in pressure zone 1-210 atm (abs.) and $x = 0.03-1$, to calculate

$$\varphi = \frac{x\gamma}{1 + (\gamma - 1)x},$$

where γ - the "slip factor" - is assumed constant at a given pressure. Since the vapor content per unit weight is a function of pressure and vapor content per unit volume β only, the formula introduced is easily reduced to the function $\phi = f(\beta, p)$.

The experimental material available to us on ten wells of two thermal areas (Pauzhetska and Bol'she-Banna), including 29 working regimes on the whole, made it possible to evaluate each of the included calculation functions for determining the quantity ϕ for vertical two-phase flows with respect to actual wells.

The evaluation was carried out as follows. Function $p = f(1 - \phi)$ was represented by a polynomial of the fourth power whose coefficients were found according to each of the examined functions for a network of varying parameter values (beginning transformation pressure p_0 , mass velocity G , well diameter D , pressure at mouth p_y).

Having relationship $p = f(1 - \phi)$ and assuming a constant value for the average specific volume of liquid phase on the vaporization section, expression (4) was integrated, after which it was possible to obtain the calculated value $l = f(G, p_0, p_y)$ for each of the methods.

Extensive calculation was involved; therefore, the basic computations were performed on an electronic computer. The per cent of disagreement between experimental and calculated values for vaporization depths are presented in Fig. 2.

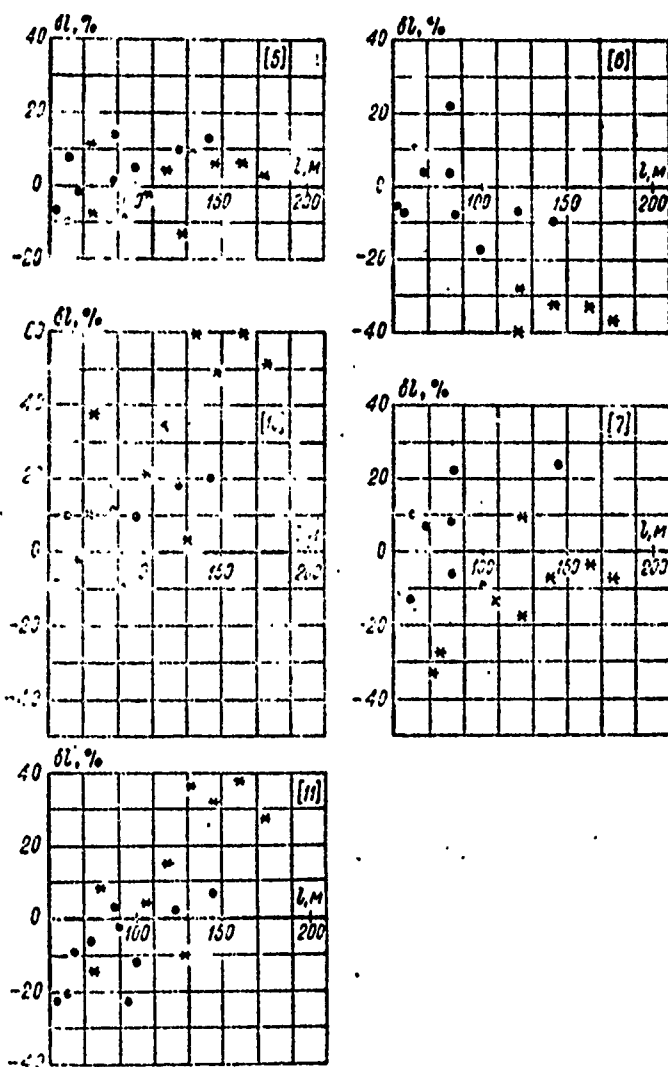


Fig. 2. Per cent of error in the calculated value of vaporization depth as compared with the experiment as a function of vaporization depth according to the data of various authors ($\delta l = \frac{l - l_{\text{exp}}}{l} \cdot 100$, where l_{exp} is experimental vaporization depth).

Table 2 presents the basic data on the tested wells and also the value of l_{tr} which indicates the conditional fraction of decrease in vaporization depth at a given pressure drop and mass velocity caused by energy loss from friction.

Table 2.

	(1) Номер скважины и режима	(2) Давление потока в начале парообразования p_0 , атм	(3) Дебит скважины G , кг/сек	(4) Давление на устье p_y , атм	(5) Расходное объемное паросодержание на устье, %	(6) Экспериментальная глубина начала парообразования $l_{экс}$, м	Δl_{tr} , м
Малодобитные скважины (на рис. 2 обозначены знаком *)	(7) K-2 1 2	9,4	1,7	4,4 5,25	0,963	140 110	2 0
	K-7 1 2	9,8	2,3	4,2 6,35	0,966 0,915	180 80	4 0
	K-8 1 2 3	9,4	3,2	4,4 5,15 6,2	0,956	170 105 75	2 0 0
	K-12	6,6	1,2	5	0,891	40	0
	K-14	6,6	3	2,5	0,978	127	13
Высокодобитные скважины (на рис. 2 обозначены знаком .)	(8) K-4 1 2	8	14	5,4	0,932	88 63	16 12
	K-10 1 2 3	10	8,8	5 5,5 6,3	0,952	140 120 100	15 12 7
	K-11	6,1	8,3	3,2	0,966	90	13
	K-15 1 2	7,5	12,8	4 5,6	0,953	90 50	23 5
	K-29 1 2	8	14 8	5 5,4	0,968 0,916	80 63	16 12

KEY: (1) Well and regime number; (2) Pressure of flow at beginning of vaporization, p_0 , atm (abs.); (3) Flow rate of well G , kg/s; (4) Pressure at mouth p_y , atm (abs.); (5) Flow-rate vapor content per unit volume at mouth, %; (6) Experimental depth at which vaporization begins $l_{экс}$, m; (7) Low-flow-rate wells (designated by * on Fig. 2); (8) High-flow-rate wells (designated by . on Fig. 2).

As we can see, a comparison of the quantities l_{TP} and l illustrates the earlier statement that the method of calculating losses from friction can not substantially affect the degree of agreement between calculated and experimental values of vaporization depth. Of all the analyzed functions for the quantity ϕ , the most satisfactory function, which enabled us to describe all well regimes, without exception, with an accuracy of the experiment itself, was the criterial equation of G. Ye. Kholodovskiy (see Fig. 2).

The results, processed according to [6], disagree considerably with the experiment, which is explained, in our opinion, by additionally taking into account the diameter effect. The correction for diameter, offered by the authors during a transition from $D = 25$ mm to $D = 150-200$ mm noticeably reduces the value of ϕ ; moreover, if it were not taken into account, the results of the calculations according to [6] would agree with [5]. The authors themselves point to the disagreement between their results and the data of several other researchers, who obtained a more moderate effect of the diameter on ϕ . The absence of a noticeable diameter effect up to the value 76-100 mm is obtained in [5] with a constant mass velocity and in [8] with a constant Fr_{CM} . The experimental data on wells indicates that this assumption can be extended to diameters of 150-200 mm. Tests of wells did not indicate a substantial independence effect of diameter.

The effect of the Froude number of the mixture on ϕ has been established by many studies [2], [8]. However, [5], [6], [7], and a number of other authors present the flow-rate velocity as a parameter substantially affecting ϕ . These parameters differ in quantity D (0.8). Since, in absolute value, the diameter enters into the value of Fr_{CM} to the fifth power and the value of ϕ is proportional to the Froude number itself to a power considerably less than one, it is obvious that, taking Fr_{CM} or G as

parameters, we (with different D) will not obtain a noticeable difference in the final results. This situation indirectly confirmed the agreement of calculated values according to [8] and [7] where ϕ is presented as a function of $G\sqrt{D}$.

The substantial inconvenience of using the Froude number of the mixture as a parameter in the practical calculation of wells lies in the fact that by definition it depends on the volume of the mixture and this means also on β . It is, therefore, more convenient to represent the true coefficient of vapor content per unit volume as a function of the separately calculated quantities β and G . In this sense, the expression for ϕ according to [5] has an additional, purely applied advantage in calculating wells.

The use of the method in [7] led to noticeable errors which, obviously, are explained by the inadmissibility of extrapolating the obtained empirical relationships to the region of specific weights less than 40 kg/m^3 and $G < 300 \text{ kg/m}^2 \cdot \text{s}$. (The possible reduction in accuracy was noted by the authors). The function for ϕ in [11] has a simple form; there is a good agreement with Armand's tests with respect to the values of C in the zone $\beta > 0.9$ and with respect to the numerical values of losses from friction. A comparison with the data of well tests indicates a satisfactory agreement of quantities λ for high-flow-rate wells (better than according to [10], possibly because of the reduction of C in the zone of low β and the considerable (up to 40%) disagreement in the quantities for low-flow-rate wells.

Calculation according to Armand's data [10] gave relatively good agreement for high-flow-rate wells, but for low-flow-rate wells the per cent of error exceeded 50%.

According to Lokshin's method when $\beta > 0.91$ the exponent in expression (5) is equal to one, which causes the invariance of C with respect to G . The possibility of reducing C with a decrease in the mixture velocity below 3 m/s was discussed by

the authors for the zone $\beta < 0.91$ only. Since on a larger section of the thermal mixture motion $\beta > 0.85$, the calculated values for vaporization depth according to [9] were independent of mass velocity and agreed with the data in [10].

Examining the entire comparison of calculated and experimental data with respect to the motion of the steam-water mixture in wells, it is easy to see the effect of the character of the mixture motion on the selection of the second parameter (in addition to β) in determining ϕ .

In the case of the annular regime ($w_{cm} > 3$ m/s) the coefficient C depends only slightly on mass velocity. Its numerical values, as calculations for zone p and G show, according to [5] are near those in [9], [10], [11]. This explains the small error for high-flow-rate wells (which have $w_{cm} > 3$ m/s) for all calculation methods. For the "shell" regime of mixture flow ($w_{cm} < 3$ m/s), the effect of mass velocity becomes substantial, which affects the decrease in the exponent with n in [5] and [6]. In this case, calculations according to [10] or [11] give a higher per cent of error and for low mixture velocities are not suitable. Calculation according to [5] gives satisfactory agreement with experiment in the entire zone of real variations in initial data. Calculation according to [6] leads to understated values of l due to the additional reduction in ϕ with a decrease in diameter. Calculation according to [7] and [8] is characterized by a rise in the per cent of error, which indicates nonuniformity of extrapolation of results obtained with large G and γ'' on the condition of mixture discharge from wells.

Conclusions

1. A method is given for calculating vaporization depth in steam-generating wells at $p_y \leq 2.5$ atm (abs.).

2. In order to determine the true vapor content per unit volume, the equation of G. Ye. Kholodovskiy is recommended and gives a satisfactory agreement with the results of tests on all wells.

3. No effect of increasing diameter up to 200 mm on the quantity ϕ was detected.

BIBLIOGRAPHY

1. Паужетские горячие воды на Камчатке. «Наука», 1965.
2. Кутыгеладзе С. С., Стырикович М. А. Гидравлика газожидкостных систем. ГЭИ, 1958.
3. Телетов С. Г. О коэффициентах сопротивления при течениях двухфазных смесей. ДАН СССР, LI, № 8, 1946.
4. Стырикович М. А. Внутрикотловый процесс. ГЭИ, 1954.
5. Холодовский Г. Е. Об анализе опытных данных по циркуляции воды в паровых котлах. «Теплоэнергетика», 1957, № 7.
6. Ellis I. E., Jones E. Lloyd. Sympos. Two Phase Flow. Dept. Chem. Engng. Univ. Exeter, Devon, England, 1965.
7. Cravanello, Hassid. Sympos. two Phase. Flow. Dept. Chem. Engng. Univ. Exeter, Devon, England, 1965.
8. Костерин С. И., Семенов Н. И., Точингин А. А. Относительные скорости пароводяных течений в вертикальных необогреваемых трубах. «Теплоэнергетика», 1961, № 8.
9. Локшин В. А., Шварц А. Л. Расчет движущих напоров и гидравлических сопротивлений при движении пароводяной смеси в вертикальных подъемных трубах. «Теплоэнергетика», 1959, № 8.
10. Армянд А. А. Исследование механизма движения двухфазной смеси в вертикальной трубе. «Известия ВТИ», 1950, № 2.
11. Thom I.R.S. Internat. J. Heat and Mass Transfer, 1964.

Reproduced from
best available copy.

BASIC CHARACTERISTICS OF TWO-PHASE UNBALANCED STATIONARY FLOWS

Ye. I Nevstruyeva

Designations

Z - axial coordinate, channel length;
 Π - heated perimeter;
 F - area of heated surface;
 f - area of cross section;
 G - flow rate;
 V - flow rate per unit volume;
 w_g - mass velocity;
 w - velocity;
 q - thermal load;
 ρ - density;
 i - enthalpy;
 r - heat of vaporization;
 x - relative enthalpy of flow, flow-rate vapor content of balanced flow;
 ϕ - true vapor content per unit volume;
 S - concentration of solutions;
 K - multiplicity of circulation;
 n - steaming coefficient;
 m - recirculation coefficient;

Γ - intensity of change in vapor content,
vaporization, or condensation.

Subscripts and Superscripts

' - water;
" - steam;
исп - evaporation;
под - preheating;
п - vaporization;
н - condensation;
п. с - boundary layer;
я - flow core;
ж - liquid phase;
о, вх - condition at input;
н. з - beginning of intensive boiling
s - parameter on saturation line;
д - actual value, distinct from balanced
value;
** - beginning of unlimited growth of salt
deposits;
нас - condition of solution saturation.

To calculate the characteristics of two-phase balanced flows it is necessary and sufficient to know the pressure gradients and the distribution along the channel of temperatures of the heat-releasing surface and true vapor contents per unit volume. The knowledge of the basic flow parameters and the distribution of thermal load, surface temperatures, true vapor contents per unit volume, and pressures make it possible to determine with respect to the thermal balance the flow-rate vapor content per unit weight, as well as to calculate the reactivity of the reactor and the complete hydraulic design, i.e., to determine the specific weight of the steam-water mixture, the components of losses of head from friction and acceleration, and to calculate the more general hydraulic resistance or moving head of natural circulation.

In real steam-generating installations, water or other liquid which is considerably underheated below saturation temperature is fed to channel input so that two-phase flows, in most cases, are thermodynamically unbalanced [1, 2]. To calculate the basic characteristics of such flows, it is not sufficient to know the basic parameters of the flow at input to the channel and the distribution along the channel of thermal load, true vapor content per unit volume, temperature of heat-releasing surface, and pressure. In order to illustrate what additional data are necessary for calculating the basic characteristics of two-phase unbalanced stationary flows, we shall examine the processes which occur during the boiling of underheated liquid.

The amount of steam forming in a unit of time on a unit of surface is

$$\frac{\Delta G_n}{\Delta F} = \frac{q_{\text{нсн}}}{r}. \quad (1)$$

The multiplicity of the circulation of liquid between the flow core and the boundary layer, which is equal to the ratio of the mass of liquid flowing toward the steam-forming surface from the flow core to the mass of the steam being formed, is

$$K = \frac{\Delta G'}{\Delta G_n}. \quad (2)$$

and the degree of liquid steaming in the boundary boiling layer, which is equal to the ratio of the mass of liquid flowing toward the steam-forming surface from the flow core to the mass of liquid expelled and entrained by the steam from the boundary layer to the flow core, can be expressed in the form

$$n = \frac{\Delta G'}{\Delta G' - \Delta G_n} = \frac{K}{K-1}. \quad (3)$$

The multiplicity of the circulation of liquid between the boundary layer and the flow core, in addition, can be expressed

in terms of the recirculation coefficient which is the ratio of the volume of liquid flowing toward the surface from the boundary layer to the total volume of liquid flowing toward the surfaces, equal to the sum of the volumes of the forming steam and the liquid expelled and entrained by the steam, i.e., if the volume of the forming steam is

$$\frac{\Delta V^*}{\Delta F} = \frac{\Delta G_n^*}{\Delta F_p^*} = \frac{q_{nca}}{r_p^*}, \quad (4)$$

and the volume of the liquid expelled and entrained by the steam is

$$\frac{\Delta V_1'}{\Delta F} = \frac{\Delta G_1' - \Delta G_n^*}{\Delta F_p'}, \quad (5)$$

then, substituting the mass of the flowing liquid from equation (2), we obtain

$$\frac{\Delta V_1'}{\Delta F} = \frac{(K-1)\Delta G_n^*}{\Delta F_p'}. \quad (5a)$$

Then the total volume of liquid flowing from the flow core can be expressed in terms of the recirculation coefficient in the following manner:

$$\frac{\Delta V_1'}{\Delta F} = \frac{K\Delta G_n^*}{\Delta F_p'} = (1-m) \left[\frac{\Delta V_1'}{\Delta F} + \frac{\Delta V^*}{\Delta F} \right]. \quad (6)$$

Substituting (4) and (5) into (6) and limiting ourselves to the quantity of the volume of evaporating liquid, we obtain

$$K = (1-m) \left(K - 1 + \frac{p'}{p^*} \right); \quad (6a)$$

hence

$$K = \frac{1-m}{m} \left(\frac{p'}{p^*} - 1 \right) \quad (7)$$

or

$$m = \frac{1}{K + \left(\frac{p'}{p^*} - 1 \right)}. \quad (8)$$

Thus, the knowledge of any one of the examined quantities (circulation multiplicity in terms of the boundary boiling layer, the degree of steaming of the boiling layer, or the recirculation

coefficient) makes it possible to determine the other two according to formulas (3), (7), or (8) since there is a unique relationship between them (Fig. 1). Furthermore, the knowledge of any of the three examined quantities makes it possible to determine the relationship between the quantities of heat expended during the boiling of underheated liquid on its heating and on evaporation. Actually, the quantity of heat expended on heating liquid flowing to a unit of surface in a unit of time up to the temperature of the boundary layer will be

$$q_{\text{max}} = \frac{\Delta G'}{\Delta F} (t_{\text{n.c}} - t_s) = \frac{\Delta G_n''}{\Delta F} (t_{\text{n.c}} - t_s) = K \frac{q_{\text{ucn}}}{r} (t_{\text{n.c}} - t_s) + \frac{q_{\text{ucn}}}{r} (t_{\text{n.c}} - t_s). \quad (9)$$

It should be noted that the second term in equation (9) takes into account the difference between boundary layer temperature and saturation temperature. If boundary layer temperature is below saturation temperature, heat is expended not only on heating of the liquid up to boundary layer temperature, but also on heating that liquid which then is evaporated, from boundary layer temperature to saturation temperature. If boundary layer temperature is greater than saturation temperature, the heat which was expended on heating the evaporating liquid from saturation temperature to boundary layer temperature then returns to liquid. Thus, the second term in the equation (9) can be either positive or negative. Taking into account the fact that

$$q_{\text{ucn}} + q_{\text{max}} = q, \quad (10)$$

by the simplest transformations we can obtain an expression for the mass of steam forming in a unit of time on an unit of heating surface, as well as an expression for the mass of liquid flowing from the flow core:

$$\frac{\Delta G_n''}{\Delta F} = \frac{\Delta G_n'}{\Delta F} = \frac{q}{r - K(t_{\text{n.c}} - t_s) - (t_{\text{n.c}} - t_s)}; \quad (1a)$$

$$\frac{\Delta G'}{\Delta F} = \frac{Kq}{r - K(t_{\text{n.c}} - t_s) - (t_{\text{n.c}} - t_s)}. \quad (11)$$

If the amount of steam forming in a unit of time on a unit of heating surface area is divided by the cross-sectional area of

the channel and multiplied by its perimeter, vaporization intensity Γ_n , i.e., the amount of steam forming in a unit of time per a unit of liquid flow volume, at the limit will be

$$\Gamma_n = \frac{dG_n^*}{f dz} = \frac{q_n}{r + K(i_{n,c} - i_n) - (i_{n,c} - i_s)} \quad (12)$$

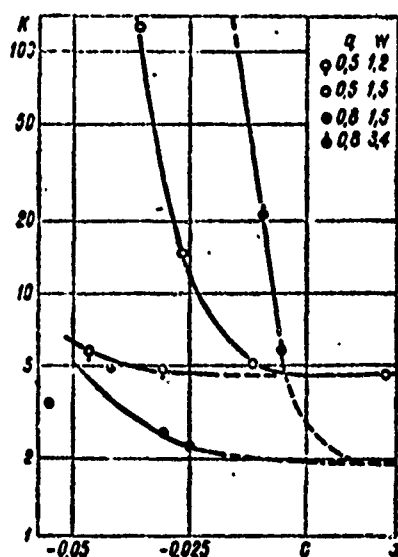


Fig. 1. Circulation multiplicity versus relative flow enthalpy for a pipe 5.4 mm in diameter, 300 mm in length, at a pressure of 1.2 bar.

We should mention that during the boiling of underheated liquid, in the general case, not all the steam is stored in the flow, as occurs with the boiling of liquids heated to saturation temperature, but some of it, in contact with the underheated liquid in the flow core, is condensed. The intensity of steam condensation in the flow of underheated liquid is of independent scientific and practical interests; however, the intensity of steam storage along the channel can generally be expressed in the form

$$\frac{dG^*}{f dz} = \Gamma_n + \Gamma_c \quad (13)$$

In order to find the flow rate of steam in any cross section of the channel, we should integrate equation (13) along the channel from the cross section in which intensive vaporization begins up

to the examined cross section:

$$G'' = f \int_{z_{n,3}}^z (\Gamma_n + \Gamma_k) dZ = f \int_{z_{n,3}}^z \Gamma_k dZ + \\ + f \int_{z_{n,3}}^z \frac{q \Pi}{r - K (t_{n,c} - t_n) - (t_{n,c} - t_s)} dZ. \quad (14)$$

Thus, in order to determine the amount of steam in any channel cross section, it is necessary to know the location of the section in which intensive vaporization begins, the intensity of condensation along the channel, the distribution along the channel of pressure, circulation multiplicity, liquid temperature in the boundary layer, and liquid temperature in the flow core. At the contemporary level of knowledge concerning the boiling processes of underheated liquids, data as yet is insufficient for determining the amount of vapor and, consequently, of liquid.

However, in the first approximation, it is completely acceptable to assume the following.

1. Steam condensation intensity even in the flow of underheated liquid is negligible as compared with vaporization intensity [3, 4]; consequently, it can be disregarded.

2. The pressure drop on the heated section is considerably less than working pressure; therefore, all steam parameters (on the saturation line) and liquid parameters can be considered constant along the channel.

3. The temperature of the liquid in the boundary layer is approximately equal to saturation temperature.

4. Liquid temperature in the flow core is approximately equal (actually it is somewhat lower) to the temperature of liquid phase in the flow.

It should be mentioned that at high thermal loads when the temperature of the liquid in the boundary layer is greater than saturation temperature, the last two assumptions lead to errors which somewhat compensates each other. With the assumptions made, equation (14) takes the following form:

$$\frac{G''}{f} = w'' = \frac{q\Pi}{r} \int_{z_{n,3}}^z \frac{1}{1-Kx_m} dZ. \quad (15)$$

Then the actual vapor content in any channel section can be determined according to formula

$$x_a = \frac{G''}{f} = \frac{q\Pi}{r w_0 \varphi'} \int_{z_{n,3}}^z \frac{1}{1-Kx_m} dZ \quad (16)$$

or

$$x_a = \frac{\Delta x | z_{n,3}^z}{z - z_{n,3}} \int_{z_{n,3}}^z \frac{1}{1-Kx_m} dZ. \quad (16a)$$

Phase velocities can be evaluated according to formulas:

$$w'' = \frac{G''}{f \rho'' \varphi} = \frac{q\Pi}{r \rho'' \varphi} \int_{z_{n,3}}^z \frac{1}{1-Kx_m} dZ; \quad (17)$$

$$w' = \frac{w_0}{(1-\varphi)} = \frac{q\Pi}{r \rho' (1-\varphi)} \int_{z_{n,3}}^z \frac{1}{1-Kx_m} dZ \quad (18)$$

or

$$w'' = \frac{x_a w_0 \rho'}{\rho'' \varphi} \quad \text{and} \quad w' = \frac{(1-x_a) w_0 \rho'}{\rho' (1-\varphi)}. \quad (19)$$

Thus, if we know the distribution of circulation multiplicity along the channel on the basis of any analytical considerations or experimental data, the liquid phase temperature, true vapor content per unit volume, and point of initial intensive vaporization can be evaluated by numerical or graphic integration, as well as the quantity of steam in the channel, the actual vapor content of the flow, and the phase velocity in any section along

the channel. All the above quantities and functions necessary for evaluating the characteristics of two-phase unbalanced flow at the contemporary level of knowledge can be determined only experimentally with the use of completely different study methods.

Circulation multiplicity of the liquid between the boundary layer and the flow core is evaluated on the basis of the salt method [5, 6] according to formula:

$$K = \frac{1}{1 - \frac{S_{\text{ex}}^{**}}{S_{\text{fac}}^{*c}(1 - x_1)}}, \quad (20)$$

where the beginning of unlimited growth of salt deposits S^{**} is determined experimentally in studying the regularity of salt deposition. The salt solubility limit S^{fac} is determined either experimentally or according to handbook data in the first approximation based on saturation temperature on the assumption that the temperature of the boundary layer is equal to saturation temperature. The effective temperature of the boundary layer can be evaluated more precisely by experiment [7]. The actual flow-rate water content of the flow $(1 - x_{\text{a}})$ with low absolute values of vapor content per unit weight, in the first approximation, can be assumed equal to $(1 - x)$ where x is determined according to the thermal balance. Thus, an approximate evaluation of circulation multiplicity is made not according to formula (20) but according to the simplified formula:

$$K = \frac{1}{1 - \frac{S_{\text{ex}}^{**}}{S_{\text{fac}}^{*c}(1 - x)}}. \quad (21)$$

Temperature of liquid phase or the quantity of relative enthalpy of unbalanced flow can be determined by a direct measurement of liquid temperature in a separator installed behind the experimental section. By changing the length of the experimental section, we can, at identical thermal loads and flow parameters

at input, obtain the experimental function of the variation in liquid phase temperature distribution along the channel. These studies should be made simultaneously with the study of circulation multiplicity on the same experimental installation.

The exponential function presented in references [2, 8], proposed for the evaluation of liquid phase enthalpy or temperature distribution, can be represented in the following form by the simplest transformation:

$$x_n = x_{n0} \exp\left(-\frac{A \Delta L}{-x_{n0}}\right), \quad (22)$$

where coefficient A is the increment of vapor content per unit length of the channel:

$$A = \frac{qH}{F w_{\phi} r} = \frac{\Delta x}{Z - Z_{n0}} = \frac{\Gamma_n}{w_g}. \quad (23)$$

It should be mentioned that the selection of the exponential function of distribution is based on formal consideration and is necessary in an experimental check.

The temperature for relative enthalpy of the liquid in the section where intensive vaporization begins or the distance of this section from input to the heated channel can be approximately determined with an examination of the distribution of true vapor content per unit volume along the channel. Relative enthalpy of the liquid and the cross section where intensive vaporization begins is indicated by dashes on the graph showing the dependence of true vapor content per unit volume on relative enthalpy of the flow (Fig. 2). Several empirical relationships are known for evaluating the enthalpy of the beginning of intensive vaporization according to various signs: according to the achievement of saturation temperature or a certain overheating of the wall and according to the beginning of the intensive increase in hydraulic resistance or true vapor content per unit volume. However, all these relationships have a special character [9-13].

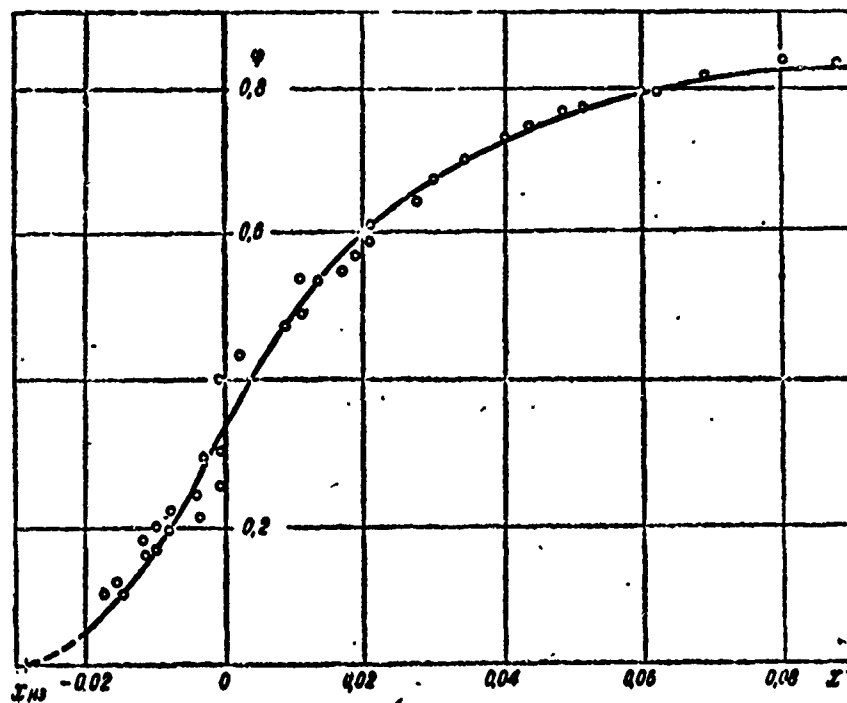


Fig. 2. True vapor content per unit volume versus relative enthalpy of the flow at a pressure of 31 bar and thermal loads from 0.3 to 0.6 MW/m².

The distributions of true vapor contents per unit volume along the channels are mainly studied using the method of radiographic examination and, at the present time, there is a rather large amount of experimental data available [4, 13, 14, 15, etc.]. Recently attempts have been made to analytically solve the problem of the distribution of true vapor content per unit volume [2, 8, 17]. However, even the most successful of them require the knowledge of the location of the point where intensive vaporization begins and the distribution of liquid phase temperatures along the channel, as yet completely unstudied.

Conclusions

A brief analysis of the characteristics of two-phase stationary unbalanced flows has shown that the greatest interest

lies in complex examinations of the hydrodynamics (the beginning of intensive vaporizations, true vapor content per unit volume, pressure gradients), heat exchange (the temperature of the heat-releasing surface, liquid phase, and boundary layer), and mass exchange (circulation multiplicity of the liquid between the flow core and the boundary layer), performed on the same installations under identical conditions.

Such examinations have been performed in recent years at IVT [Translator's Note: The expansion for this abbreviation is not known.].

BIBLIOGRAPHY

1. Styrikovich M. A., Nevstueva E. I. Proceedings of the Third International Heat Transfer Conference, 1966, v. IV, Rep. № 136, pp. 207—215.
2. Zuber N., Staub F. W. and Bijwaard G. Proceedings of the Third International Heat Transfer Conference, 1966, v. V, Rep. № 154, pp. 24—38.
3. Стирикович М. А., Невструева Е. И. Исследование распределения паросодержаний в пограничном кипящем слое методом бета-проецирования. ДАН СССР, т. 130, № 5, 1960.
4. Невструева Е. И., Дворниа Г. М. Экспериментальное исследование паросодержания в пароводяных неравновесных потоках. «Изв. АН СССР. Энергетика и транспорт», № 2, 1967.
5. Невструева Е. И., Романовский И. М. Тепло- и массоперенос, т. II. Минск. (В печати).
6. Стирикович М. А., Невструева Е. И., Мехди А. С. Некоторые новые исследования массообмена при высоких тепловых потоках. Тепло- и массоперенос, т. III, Минск, 1965.
7. Чихладзе Н. М., Невструева Е. И. Закономерности отложения сульфата кальция на поверхности нагрева при низких тепловых нагрузках. «Теплоэнергетика», № 9, 1968.
8. Kroeger P. G. and Zuber N. Int. J. Heat and Mass Transfer, v. 11, 1968, pp. 211—233.
9. Bowring B. W. HPR-29, Inst. of Atomenergi, Holden, Norway.
10. Griffith P., Clark J. A. and Rosenow W. M. Paper № 58-HT-19, ASME—AIChE Heat Transfer Conference, Chicago, 1958.
11. Staub F. W. J. of Heat Transfer, ASME, ser. C, № 11, 1968.
12. Тарасова Н. В. и др. Гидравлическое сопротивление при поверхностном кипении воды в трубе с неравномерной тепловой нагрузкой по длине. «Теплоэнергетика», 1968, № 6.
13. Бартоломей Г. Г., Чантурия В. М. Экспериментальное исследование истинных паросодержаний при кипении подогретой воды в вертикальных трубах. «Теплоэнергетика», 1967, № 2.
14. Ferrell J. K. Sept. 1946, North Carolina State University.
15. Cook W. H. ANL-5621, Nov. 1956.
16. Rouhani S. Z. AE-RTL-768, May 1965.
17. Lev S. Int. J. Heat and Mass Transfer, 10, 951, 1967.

THE ACCURACY OF CALCULATING WATER CIRCULATION ON ELECTRONIC COMPUTERS

G. I. Zinger, and L. N. Papernaya

Designations

- g - projection of the acceleration of gravity in the direction of the pipe, m/s^2 ;
- G - total mass circulation flow rate, t/h ;
- i - heat content, $kcal/kg$;
- l - length, m ;
- p - pressure, atm (tech.) or kgf/m^2 ;
- Q - heat reception of section, $kcal/h$;
- r - heat of vaporization, $kcal/kg$;
- w - circulation velocity, m/s ;
- x - flow-rate vapor content per unit weight;
- z^0 - coefficient of specific hydraulic resistance of pipes;
- β - flow-rate vapor content per unit volume;
- γ - specific weight, kg/m^3 ;
- ρ - density, $kg \cdot s^2/m^4$;
- ϕ - true vapor content per unit volume.

Subscripts and Superscripts

- δ - drum;
- B - beginning of boiling;
- cm - steam-water mixture;
- j - order number of sections convergent to node;
- $'$ - water on saturation line;
- $''$ - steam on saturation line;
- \pm - refer to flows directed toward and away from node.

The calculation of circulation in complex loops consists in determining the circulation flow rate in the system as a whole and the flow rates in individual loops, as well as other parameters characterizing circulation and depending on these flow rates, with given working pressure, thermal fluxes on the heated element, coefficients of hydraulic resistance and the geometric parameters of the circulation loop.

The method of adding characteristics, used in calculations of circulation in boilers [1], is unsuitable when calculating evaporative cooling systems which operate at lower pressures (1-10 atm (tech.)) and are distinguished by the characteristic connection of various groups of unlike individual sections to common intermediate pipes, etc. Calculations using the method from [1], in these cases, lead to results which differ substantially from actual quantities. The method from [2] is used by us in machine computation for calculating stationary regimes; calculation of the economizer sections and determination of the point where boiling begins are performed according to the same formulas as in [1]. The formula for calculating $\phi = \phi(\beta, p, w_{cm})$ [2, 4] is derived by processing the experimental data [3, 5]; the functions $\rho'(p)$ and $i'(p)$ are found by processing the tables in [6]; di/dp is expressed in terms of $\rho'(p)$ and $i'(p)$ according to the Clapeyron-Clausius formula.

For calculating the steam-containing sections, a system of equations for p and x is used:

$$\left. \begin{aligned} \frac{dp}{dl} = -\rho' \frac{\kappa \left[1 - \left(1 - \frac{\rho''}{\rho'} \right) \frac{1}{r} \right] + \frac{w^2}{2} \left[1 + \left(\frac{\rho'}{\rho''} - 1 \right) x \right] + \left(\frac{\rho'}{\rho''} - 1 \right) \frac{dQ}{r dl}}{1 - \frac{\rho' w^2}{2r} \left(\frac{\rho'}{\rho''} - 1 \right) \frac{dl'}{dp}}; \\ x = \frac{1}{r} \left(l_0 + \frac{Q}{G} - l' \right) \end{aligned} \right\} \quad (1)$$

with boundary conditions when

$$\left. \begin{aligned} l = l_0 \quad p = p_0 = p(l_0); \\ l = 0 \quad p = p_0. \end{aligned} \right\} \quad (2)$$

In solving system (1) it is necessary to fulfill conditions $p > p_0$, $x < 1$. We must also fulfill the condition of conjugation at each of the points common for several individual loops (including in the drum):

$$\left. \begin{aligned} p_j &= \text{const}; \\ G^- &= G^+; \\ (Gl)^- &= (Gl)^+, \end{aligned} \right\} \quad (3)$$

expressing pressure balances, material and thermal balance.

The calculation is considered finished if the test flow rate gives at the end of the ascending pipe entering the drum a pressure which differs from p_0 by an allowable discrepancy and the given distribution of flow rate along the individual loops gives a pressure at the end of the converging pipes which differs by the value of the discrepancy. The value of this discrepancy is given in advance by a computer in each specific case. It is actually the accuracy with which system (1) with boundary conditions (2) and (3) is solved. Numerous calculations have shown that the value of the allowable discrepancy rather frequently affects the circulation flow rates, changing them by a factor of 1.5-2. This occurs not only at pressures near atmospheric but also at pressures on the order of 40-50 atm (tech.).

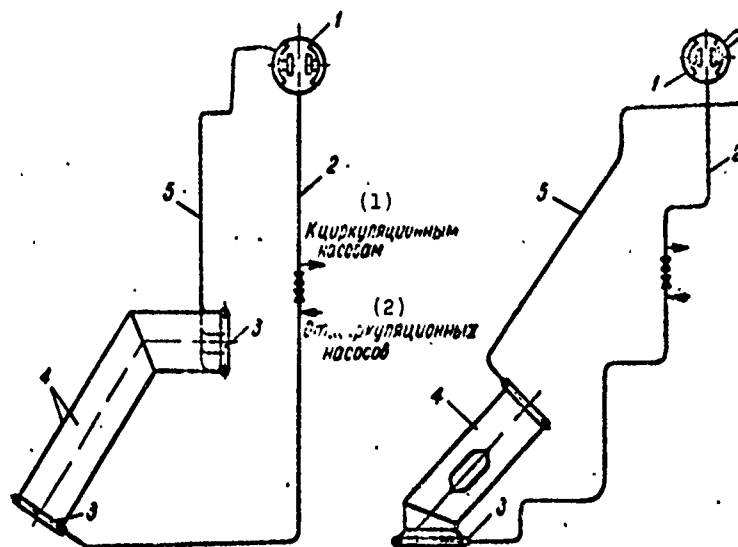


Fig. 1. Assignment to calculate water circulation in the ascending gas duct and the cooling water jacket of a cooler-boiler behind a 250-ton converter from the Karaganda Metal Plant:
1 - Drum; 2 - Descending pipes; 3 - Collectors;
4 - Heated pipes of the water wall; 5 - Steam-transferring pipes.
KEY: (1) To circulation pumps; (2) From circulation pumps.

As an illustration we can use the calculation of circulation in loops of cooler-boilers of converter gases behind a 250-ton converter (Fig. 1). The basic data for calculation is working pressure 48 atm (tech.); thermal stress, for the cooling water jacket $30 \cdot 10^3 - 480 \cdot 10^3$, for the ascending gas duct $14 \cdot 10^3 - 304 \cdot 10^3$, for the descending gas duct $7 \cdot 10^3 - 65 \cdot 10^3$ kcal/m³.h. The heat reception of the bundles of converging pipes is referred to approximately as 1:2:4. The absolute discrepancies are $\Delta_1 = 0.04$ atm (tech.) in version I and $\Delta_2 = 0.005$ atm (tech.) in version II. Accordingly, the graph of reduced circulation velocities are presented in Fig. 2.

A further decrease in the allowable discrepancy did not lead to a decrease in circulation velocities.

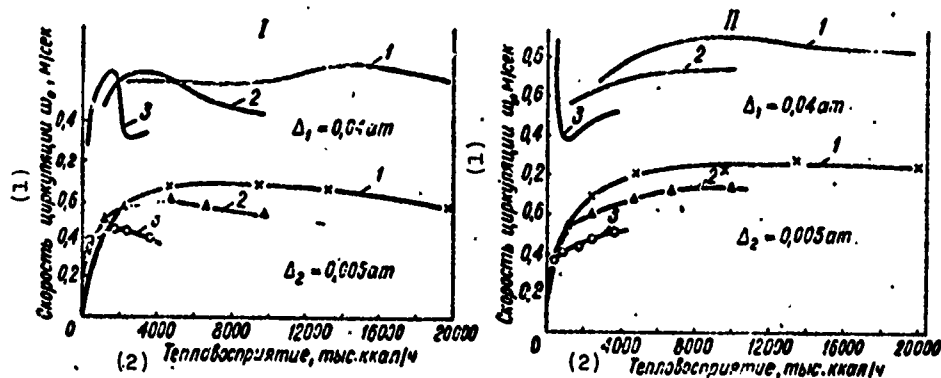


Fig. 2. Circulation rate versus heat reception in the ascending gas duct (II) and the cooling water jacket (I): 1 - Pipe with maximum heat reception; 2 - Pipe with average heat reception; 3 - Pipe with minimum heat reception. KEY: (1) Circulation velocity w_0 , m/s; (2) Heat reception, thous. kcal/h. DESIGNATION: *at* = atm (tech.).

Analysis of the calculations made shows that the allowable discrepancy in calculations must be selected according to the minimum value of the useful head in individual loops and must be one order less. Such calculations are generally rather cumbersome and require computer work.

BIBLIOGRAPHY

1. Петерсон Л. Ф., Балдина О. М. Нормы расчета циркуляции воды в паровых котлах. Труды ЦКТИ, кн. 15, 1950.
2. Лихт М. К., Кузнецкий Р. С., Клаунман И. Л. Расчет циркуляции воды в установках непрерывного охлаждения марганцевых печей на электронной цифровой машине М-3. Сборник научных трудов института «Гипросталь», вып. 5, 114, 1962.
3. Кутателадзе С. С., Стирикович М. А. Гидравлика газожидкостных систем. Госэнергоиздат, 1958.
4. Лихт М. К., Зингер Г. Н. Расчет циркуляции в системах испарительного охлаждения с подпитками параллельными контурами и трубами с запорными на электроных цифровых машинах. Сборник научных трудов института «Гипросталь», вып. 3-4, 185, 1961.
5. Локшин В. А., Шварц А. Л. Расчет движущих напоров и гидравлических сопротивлений при движении парожидкостной смеси в вертикальных подъемных трубах. «Теплоэнергетика», № 8, 73, 1953.
6. Вукалович М. П. Термодинамические свойства воды и водяного пара. Машгиз, 1956.

SECTION III

HEAT TRANSFER WITH CONDENSATION

CALCULATION AND TEST DATA FOR THE HEAT TRANSFER FACTOR DURING THE CONDENSATION OF MOVING STEAM ($Re_H < Re_{H\text{кр}}$)

L. D. Berman

Designations

- c_f - coefficient of friction resistance;
- c_n - specific heat capacity;
- d - external diameter of pipe;
- g - acceleration of gravity;
- $Ga = gl^3/\nu^2$ - Galileo number;
- j - density of the lateral flow of the mass;
- $K = r/(c_p \delta)$ - phase transformation number;
- l - characteristic dimension of the surface in dimensionless numbers
(for the vertical surface $l = 1$
for the horizontal pipe $l = d$);
- L - height of vertical surface;
- $Nu = \alpha l/\lambda$ - Nusselt number;
- p - pressure;
- $Pr = \mu c_p/\lambda$ - Prandtl number;
- r - heat of phase transformation (condensation);
- $Re_n = U_n l/\nu_n$ - Reynolds number for vapor flow;

$Re_H = 4\bar{u}\delta/\nu_H$ - Reynolds for condensate film;
 u - velocity of the medium in the direction of the x-axis;
 U_v - velocity of the basic mass of steam;
 α - averaged (over the height of the vertical surface or along the perimeter of the horizontal pipe) heat transfer factor;
 α_x - local heat transfer factor;
 δ - thickness of condensate film;
 Δ - temperature head (difference between wall and steam temperatures);
 λ - coefficient of heat conductivity;
 μ - coefficient of dynamic viscosity;
 ν - coefficient of kinematic viscosity;
 ρ - density;
 τ - viscous stress.

Subscripts and Superscripts

H - condensate;
 H_p - critical value;
 H - with motionless steam
 v - steam;
 otp - separation;
 x - when $l = X$ (for dimensionless numbers);
 δ - on the interface of liquid and vapor phase.

With film condensation of moving steam, the mechanical interaction between the steam flow and the film condensate changes the flow conditions of the latter, which involves a change in the value of the heat transfer factor as compared with the case of motionless steam condensation [1, 2]. Although Nusselt indicated this more than fifty years ago, there is as yet no single opinion concerning the effect of steam flow on the intensity of heat transfer across a film of condensate when the Reynolds number of the film Re_H is below critical Re_{H, H_p} , which with motionless gas

phase is responsible for the transition to the turbulent regime of the film's flow [3].

The flow of gas (vapor) phase can have a double effect on the flow of the liquid film when $Re_H < Re_{H, \text{кр}}$:

- cause a change in the velocity distribution in the lateral cross section of the film and, consequently, a change in the average velocity and thickness of the film while its laminar flow regime is preserved, owing to the effect of the friction on the interface of liquid and vapor phase;

- be the source of disturbance which causes a more radical restructuring of the flow regime of the condensate film - its transition during relatively low Re_H to a nonregular (three-dimensional) wave regime with separation, under certain conditions, of drops from the liquid surface.

The solution to the problem of the effect of steam velocity on the heat transfer factor during condensation on the vertical surface, proposed by Nusselt [1], pertains to the case when the flow regime of the condensate film is laminar. Viscous stress on the phase interface was defined by him as

$$\tau_i = c_f \frac{\rho_H U_\infty^2}{2}, \quad (1)$$

where the coefficient of friction resistance c_f was assumed constant and equal to 0.00505.

In reference [4] it was proposed to use the results of this solution even for the case of condensation on a horizontal pipe after increasing, in accordance with the test results of the author of this work, the coefficient of friction resistance to $c_f = 0.0085$.

The refined solutions, proposed in references [5-9], for the condensation of moving steam on a vertical surface were intended to account for the fact that the value of viscous stress

$$\tau_s = \mu_s \left(\frac{\partial u}{\partial y} \right)_s \quad (2)$$

or the coefficient of friction

$$c_f = 2\mu_s \left(\frac{\partial u}{\partial y} \right)_s / (\rho_s U_\infty^2) \quad (3)$$

depends on the gradient of steam velocity at the interface, i.e., on the steam flow regimes, and also the fact that during the condensation of steam inside the vertical pipe, the velocity of the steam (or Re_π) decreases as it condensates. In both these references and references [10, 11], for condensation on a horizontal pipe, function $c_f(Re_\pi)$ or the gradient $\left(\frac{\partial u}{\partial y} \right)_s$ were determined according to data for the flow of a gaseous (vapor) medium around an impermeable surface in the absence of condensation.

A number of authors [12-17] have given attention to the circumstance that, in the case of vapor condensation, the transfer of momentum by the lateral flow of the mass (by the condensing steam) affects the value of the gradient $\left(\frac{\partial u}{\partial y} \right)_s$ and, consequently, τ_s . Some of the authors considered it possible to disregard this effect due to its smallness [15]; others, on the other hand, pointed to its significant or even determining role [13, 16, 17].

Although in most of the above works the Nusselt model of laminar flow of a condensate film was maintained as the basis and only the problem of refining the quantity τ_s was posed, in the works of VTI [All-Union Institute of Heat Engineering im. L. E. Dzerzhinskiy] [3, 11, 18, 19] the necessity of changing the basic model itself was discussed. This was based on the assumption that even with low velocities of vapor flow the disturbance caused by it leads to a disruption of the laminar flow of the condensate film, which passes into an irregular wave regime, and to a change, due to this mechanism, in the transfer of heat across

the film. This was manifest in the development of the suggestion discussed earlier in [2, 13] that the external disturbances caused by the precipitating condensate or the moving steam were the reason for the transition, observed in tests, to turbulent condensate film flow even at relatively low Reynolds numbers Re_H (on the order of 200-400 against 1500-2000) in the absence of external disturbances.

Various theoretical relationships for the heat transfer factor during the condensation of moving vapor and the laminar flow of condensate film are compared below to each other and to various test data. They all refer to the condensation of saturated vapor moving downward when $Pr_H \geq 1$, $K \geq 5$, $Re_H < Re_{H,cr}$ when it is necessary to take into account the simultaneous action on the condensate film of both gravity and friction on the phase interface.

CONDENSATION ON A VERTICAL SURFACE

If we assume that during the condensation of the moving steam the film flow remains laminar, then, as was shown in [3], we can use the results of Nusselt's numerical solution even in those cases when the dependence of τ_δ on Re_H and on the transfer of momentum by the condensing steam is taken into account. For this it is necessary to change the quantity τ_δ , accordingly, in the dimensionless number $II_N = \frac{\tau_\delta^2 h}{\rho \mu k} \dots$. If τ_δ depends on α (see below), the quantity τ_δ is more precisely defined by the iteration method. Figure 1 presents some results of calculations thus obtained for the condensation of steam moving downward on a vertical surface (flat plate or surface having radii of curvature along the horizontal which are large enough for us to assume the flow of the thin condensate film is two-dimensional).

On Fig. 1 curve 1 indicates the dependence of α/α_H on U_∞ according to Nusselt with $c_f = 0.00505 = \text{const}$, curve 2 with

Blasius' law of resistance for laminar flow of a gaseous (steam) medium ($Re_{\Pi} \leq 5 \cdot 10^5$) - $c_f = 1.328 Re_{\Pi}^{-0.5}$, and curve 3 with Prandtl's law of resistance for turbulent flow ($Re_{\Pi} \geq 5 \cdot 10^5$) - $c_f = 0.074 Re_{\Pi}^{-0.2}$. Since the examined solution is based on the assumption that a smooth laminar film of condensate is preserved, the increase in c_f , which is observed when a wall is covered with a rippled film of liquid, is not taken into account. All three curves agree well with the approximate equation obtained in [11]:

$$\left(\frac{x_{II}}{x}\right)' + A Re_{\Pi}^n \frac{\gamma_{II}^2}{\gamma_K^2} Ga_K^{-3} (Pr_K K)^{1/4} \left(\frac{x_{II}}{x}\right)^{n/3} - 1 = 0, \quad (4)$$

where for curve 1 $A = 0.0032$ and $n = 2$, for curve 2 $A = 0.92$ and $n = 1.5$, and for curve 3 $A = 0.048$ and $n = 1.8$.

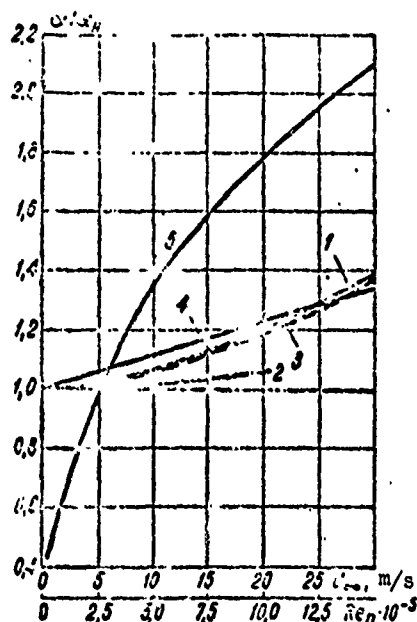


Fig. 1. Calculated values of α/α_H as a function of the velocity of the steam with condensation on a vertical surface (water vapor $p = 1$ bar, $\Delta = 10^\circ C$, $L = 1$ M):
1 - According to Nusselt;
2 - With Blasius' law of resistance; 3 - With Prandtl's law of resistance; 4 - With τ_δ according to formula (5);
5 - With α according to formula (7).

Curve 4 in Fig. 1 is obtained in the same way but with the effect of impulse transfer by the condensing steam taken into account when determining τ_δ . Particles of steam, penetrating from its basic mass through the boundary layer to the phase interface, reduce its longitudinal velocity, while giving corresponding

momentum to the particles of the basic steam flow in the boundary layer. Because of this, the latter are accelerated and the velocity profile in the boundary layer of steam becomes more complete than in the absence of lateral mass flow. The gradient of steam velocity $(\frac{\partial u}{\partial y})_3$, determining the quantity τ_δ , changes accordingly. In addition, with a continuous velocity profile on the phase interface (Fig. 2) connected to the condensate film on an element of its surface, the new portion of liquid has a velocity $u_{\delta x}$ which is higher than the average velocity of the film \bar{u}_x and gives to the film part of its momentum. If we assume that $u_x \ll U_\infty$, we can approximately account for the effect of lateral mass flow, further assuming that¹

$$\tau_\delta = \beta U_\infty = \frac{\alpha \beta}{r} U_\infty \quad (5)$$

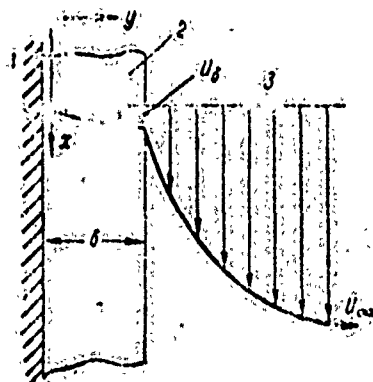


Fig. 2. Velocity profile during condensation of moving steam (descending flow):
1 - Wall; 2 - Condensate film;
3 - Steam.

¹In [13] viscous stress τ_δ is defined as the sum $\tau_\delta = \tau_{\delta \text{ np}} + \tau_{\delta \text{ H}}$, where the component $\tau_{\delta \text{ np}}$ is caused by friction on the phase interface and is determined by a formula in the form of (1), and the component $\tau_{\delta \text{ H}}$ is caused by impulse transfer by the condensing steam and is determined by a formula in the form of (5); in both cases, velocity U_∞ is introduced into the formula. Since $\tau_{\delta \text{ np}}$ actually depends substantially on impulse transfer by condensing steam and the impulse transmitted to the film of condensate, which is again formed by a portion of the condensate during its retardation, depends on velocity u_δ and not U_∞ , it is impossible to agree with such an application of the rule of additivity in determining τ_δ . We should mention that with the practical calculation recommendations it is not used by the authors of reference [13].

This formula, obtained by Meredith and Griffith for longitudinal flow around a plate with uniform exhaust of the boundary layer [20], was used earlier for determining τ_δ in reference [17]. The function for τ_δ obtained in [16] under the condition $u = U_\infty$ when $y = \delta$ also leads to this formula.

The results of our calculations in determining τ_δ according to formula (5) are described well by the equation:

$$\frac{\alpha}{\alpha_H} = 0,125(\sqrt{B+16} + 2\sqrt{B})(\sqrt{B+16} - \sqrt{B})^{1/2}, \quad (6)$$

where

$$B = \text{Re}_n^2 (\text{Ga}_n \text{Pr}_n K).$$

Curve 4, plotted on the basis of these calculations, differs little from curves 1 and 3, i.e., as already mentioned in [3], the change in τ_δ as compared with that assumed by Nusselt did not lead to a substantial change in the values of α/α_H under the examined conditions.

Another result is obtained in reference [21], according to which

$$z = \sqrt{\frac{\lambda_K^2 \rho_K U_\infty}{\mu_K L}} \cdot \frac{\sqrt{2(2+\sqrt{C})}}{\sqrt{1+\sqrt{C}}}, \quad (7)$$

where

$$C = 1 + \frac{16L}{U_\infty^2} \cdot \frac{\mu_K r}{\lambda_K \delta}.$$

Formula (7) answers to curve 5 in Fig. 1. It deviates considerably from the other curves. The reason for this requires clarification especially as in [21] the quantity τ_δ was determined according to the same formula (5) as in calculations represented by curve 4.

As follows from [17], in deriving formula (7) it was assumed, in the first place, that in the case of film condensation

regardless of the nature of the forces acting on the condensate film, the local heat transfer factor is proportional to the square root of the average film velocity in a given cross section of it, i.e.,

$$\alpha_x \sim \sqrt{\bar{u}_x} \quad (8)$$

and, in the second place, that the average film velocities in different cases of condensation are found in the relationship:

$$\bar{u}_{x3} = \bar{u}_{x1} + \bar{u}_{x2} (l^2 m^2), \quad (9)$$

where, taking (8) into account,

$$l = \frac{\alpha_{x1}}{\alpha_{x2}} = \sqrt{\frac{\bar{u}_{x1}}{\bar{u}_{x2}}} \quad \text{and} \quad \bar{m} = \frac{\alpha_{x3}}{\alpha_{x1}} = \sqrt{\frac{\bar{u}_{x3}}{\bar{u}_{x1}}} \quad (10)$$

Here, noted by the subscript 1, are the quantities which relate to the condensation of moving steam when the condensate film is only acted upon by friction on the phase interface (condition of weightlessness), the quantities indicated by the subscript 2 pertain to the condensation of motionless steam during the action of gravity only, and quantities carrying subscript 3 refer to the condensation of moving steam in the field of gravity with the simultaneous action of both forces.

Actually relationship (8) is valid only for weightless conditions and with quantity τ_0 determined by formula (5). It can not be extended to other cases, however, and because of this it is impossible to obtain relationship (10). In addition, for laminar film we actually have, instead of (9),

$$\bar{u}_{x3} = \bar{u}_{x1} + \bar{u}_{x2} \quad (11)$$

Therefore, the formula obtained, based on the above two assumptions, is not well founded theoretically even for the examined case of laminar flow of a condensate film, although, as our calculations indicate, for conditions which respond to the

assumed value of τ_0 , the errors caused by assumptions (8) and (9) have reversed signs and, to a considerable extent, compensate each other. The main reason for the substantial disagreement of curves 4 and 5 is the error which slipped in to the derivation of formula (7). This error means that for the limiting case when $U_\infty \rightarrow 0$, we have, according to this formula, $\alpha \rightarrow 0$ and not toward α_H or, in other words, that $\alpha/\alpha_H \rightarrow 0$ and not toward 1. Such a result contradicts those taken in the derivation of formula (7) as the basic assumption. The introduction of corresponding corrections into the derivation leads to a confirmation of curves 4 and formula (6).

If, taking the above into account, we exclude curve 5 from examination, we can see that on the assumption of a laminar flow of the condensate film and moderate steam velocities, to which Fig. 1 refers, a more precise definition of the quantity τ_0 as compared with that taken by Nusselt is very weakly reflected in the calculated values of α .

For the case of condensation on a vertical surface test data convenient for checking these theoretical relationships are still lacking. Test data for condensation on a vertical two-dimensional plate of freon-113 steam moving downward at $p \approx 1$ bar and $t = 5.5-22^\circ\text{C}$ are presented in the recently published work [9]. However, the test points, presented in this work on a graph, has such a large spread that it is impossible to use them to evaluate the correctness of any theoretical solution.¹ As they only make

¹Hoping to combine the test points for various t on the graph, the author of the work arbitrarily multiplied the obtained values of Nu_x by $(Pr_H K)^{-0.25}$, which according to the data from VTI [22] for condensation of moving steam is inadmissible. This method did not eliminate the large spread of the points.

it possible to establish an approximate (averaged for the studied conditions or for the averaged value of $Pr_K \approx 40$) dependence of the heat transfer factor on steam velocity, which can be represented in the form (Fig. 3 and 4):

$$\frac{\alpha_{\text{an}}}{\alpha_{\text{an}}} = 0.91 Re_n^{0.12} Ga_n^{-0.12} = 0.91 \left(\frac{U_{\infty}}{1.8 \sqrt{g \lambda}} \right)^{0.12} \quad (12)$$

This relationship satisfactorily agrees with the test data from VTI for the condensation of moving water vapor on a horizontal pipe, according to which when $Re_n > 200$ the heat transfer factor is proportional to steam velocity to a degree constituting, on the average, 0.16 against 0.12 in the examined case.

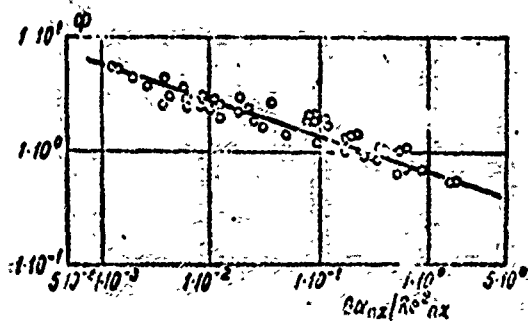


Fig. 3. Dependence of

$$\Phi = \frac{Nu_x}{(Pr_K)^{0.25}} \left(\frac{Re_{n,x}}{Ga_{n,x}} \frac{\nu_n}{\nu_K} \right)^{1/2} \text{ on } \frac{Ga}{Re_{n,x}}$$

during the condensation of freon-113 on a vertical plate according to the tests in [9] ($p \approx 1$ bar, $t = 5-22^\circ\text{C}$).

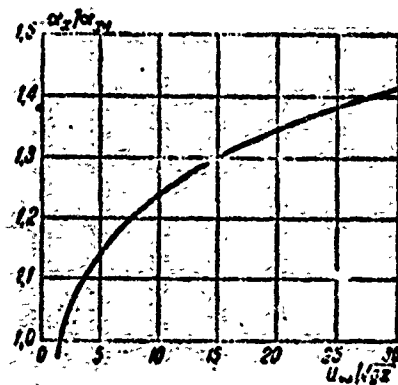


Fig. 4. Dependence of the ratio α_x/α_n on dimensionless steam velocity with the average $Pr_K \approx 40$ (processing of data in [9]).

Other test data described in literature for the condensation of moving steam on a vertical surface were obtained during the motion of steam inside pipes or channels with an annular cross section [23-26]. For the reasons already discussed in [3], the average heat transfer factors obtained with this do not allow us to judge the flow regime of the condensate film.

CONDENSATION ON A HORIZONTAL PIPE

Various calculated data for the case of the condensation of vapor moving downward on a horizontal pipe in lateral flow with a laminar condensate film are presented in the form of α/α_H as a function of the complex

$$\Pi = \frac{l^2 \cdot \alpha_H^2 \cdot \rho_H}{\lambda_H \cdot \mu_H} = Re_H^{2.5n} \cdot \frac{Nu_H}{Gr_H}, \quad (13)$$

represented on Fig. 5.

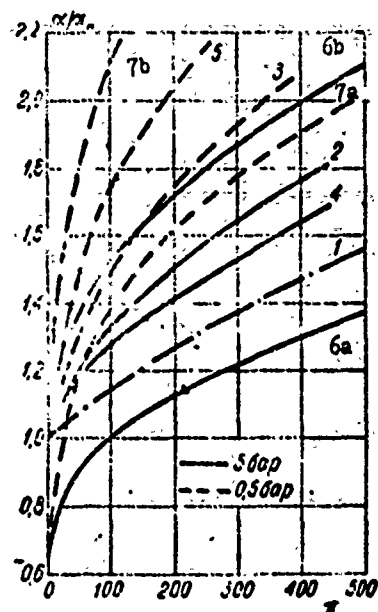


Fig. 5. Calculated values of α/α_H as a function of Π during the condensation of water vapor on a horizontal pipe ($t_s = 10^\circ\text{C}$): 1 - According to [4]; 2, 3 - According to equation (6); 4, 5 - According to equation (14); 6, 7 - According to equation (15) (a - when $\epsilon = 0.42$, b - when $\epsilon = 0.64$). DESIGNATION: 5 bar = bar.

Curve 1, taken from [2, 4] is a modified function as a result of the increase in c_f up to 0.0085, obtained by Nusselt. With the coordinate used in Fig. 5 it remains constant for any p and t_s , while when the dependence of c_f on Re_H is taken into account, the curves for various steam pressures (and temperature heads), plotted on these coordinates, deviate noticeably from each other. This is indicated, for example, by curves 2 and 3 for pressures of 5 and 0.5 bar, respectively, plotted according to and equation in the form of (4) when $A = 1.3$, $n = 1.5$, and $l = d$,

which responds to function $c_f = 4 \operatorname{Re}_n^{-0.5}$ [11]. Up to $\alpha/\alpha_H \approx 1.6$ these curves almost agree with those plotted according to the results of the solution described in [10], while at larger α/α_H they are somewhat higher.

If we assume, as in (5), taking into account the transfer of momentum by lateral mass flow, that $\tau_\delta = jU_n \sin \bar{\phi}$ (where $\bar{\phi}$ is the average equivalent angle of surface slope for a horizontal pipe), then instead of (4) we obtain [3]:

$$\left(\frac{x_n}{x}\right)^4 + 0.79 \operatorname{Re}_n (G_{3n} \operatorname{Pr}_n K)^{-1/2} \left(\frac{x_n}{x}\right)^{5/3} - 1 = 0. \quad (14)$$

According to equation (14), we plot curves 4 and 5 (Fig. 5), pertaining to the same two pressures and diverging even more strongly than curves 2 and 3.

In [17], with the same method of accounting for the effect of lateral mass flow, the following formula is obtained for the average heat transfer factor (when $1/\operatorname{Pr}_n K \ll 1$):

$$\alpha = \epsilon \sqrt{\frac{2.32 U_{in}}{\operatorname{Pr}_n d}} \times \left(1 + \sqrt{1 + 1.69 \frac{K d}{U_{in}^2} \frac{\operatorname{Pr}_n}{\operatorname{Pr}_n K}}\right)^{1/2}. \quad (15)$$

For factor ϵ in this formula two values are given: 0.42 for the flow of steam with boundary layer separation from the surface of the pipe at a polar angle of $\phi_{\text{отр}} = 82^\circ$ and 0.64 for the separationless flow of steam.

In the basis of formula (15) lie the same two basic relationships (8) and (9), just as in the case of formula (7) derivation. Based on the assumption that the variation in the local heat transfer factor along the circumference of a cylinder is the same in various condensation cases, the author of the formula extended

the relationships (8) and (10) to heat transfer factors averaged along the pipe's perimeter. Since this assumption is not precise, it introduces additional error into the solution. This also pertains to the assumption that it is possible to take into account the effect of the location of the boundary layer separation point by changing only the value of factor ϵ in formula (15).

As an argument in favor of the validity of formula (15), sometimes researchers point to the fact that it satisfies two limiting cases: when $g = 0$ it changes into the formula for weightless conditions and when $U_\infty = 0$ into Nusselt's formula for motionless steam. This can not, however, in itself serve as proof of the suitability of formula (15) when $g \neq 0$ and $U_\infty \neq 0$. In addition, for the examined conditions when the forces of friction and gravity act simultaneously, formula (15) is valid only in one limiting case, when during separationless flow $U_\infty \rightarrow 0$. This does not give sufficient basis for the statement that when $U_\infty > 0$, and even more when $\phi_{orp} < 180^\circ$, the formula correctly reflects the effect of steam velocity on the heat transfer factor.

The tentatively evaluated and very wide limits for the variation of the factor ϵ in formula (15) led to the fact that both the theoretical and experimental data obtained by other authors fall between the two curves answering to the extreme values of ϵ for the given conditions (for example, curves 6a and 6b or 7a and 7b on Fig. 5). For this reason it is impossible to consider as a conclusive confirmation of the correctness of formula (15) the fact that a considerable portion of the test points according to data from reference [22] lie in a wide band between the extreme curves plotted according to this formula. At the same time, in comparing the calculated and test data, we should be guided not only by the boundaries of the quantitative discrepancies between them, but also by how much the theoretical dependence based on any model correctly reflects the regularities of the studied process.

In Figs. 6 and 7 the test relationship between α/α_H and Re_n for two series of tests [22] (series I when $p = 0.47$ bar, $\Delta = 7.4^\circ\text{C}$ and series II when $p = 0.031$ bar, $\Delta = 3.1^\circ\text{C}$) are compared with the relationships calculated according to formulas (4), (14), and (15). When computing Re_n according to test data as velocity U_n for a pipe located in a staggered bundle, the steam velocity here is taken in the narrow section of the bundle.

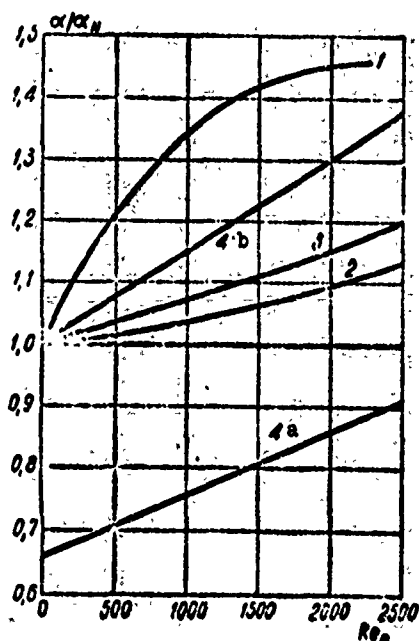


Fig. 6. Dependence of α/α_H on Re_n during the condensation of water vapor on a horizontal pipe ($d = 0.019$ m, $p = 0.47$ bar, $\Delta = 7.4^\circ\text{C}$):

1 - According to tests from [22]; 2 - According to equation [6]; 3 - According to equation [14]; 4 - According to equation [15] (a - when $\epsilon = 0.42$, b - when $\epsilon = 0.64$).

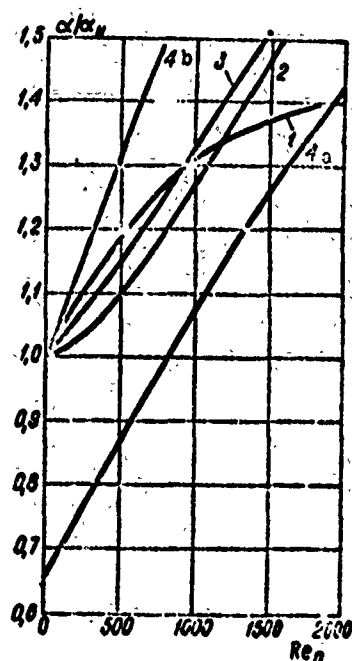


Fig. 7. Dependence of α/α_H on Re_n during the condensation of water vapor on a horizontal pipe ($d = 0.019$ m, $p = 0.031$ bar, $\Delta = 3.1^\circ\text{C}$). Curve designations the same as in Fig. 6.

For $p = 0.47$ bar and $\Delta = 7.4^\circ\text{C}$ (see Fig. 6) the test curve is located noticeably higher than all calculated curves and even

those beyond the limits of the wide band bounded by curves 4a and 4b plotted according to formula (15). Curve 4a, representing the value $\epsilon = 0.42$, describes the test data under the same conditions as curve 3, plotted according to formula (14), but lies considerably below it. Moreover, in the entire region of Re_n covered by the tests, curve 4a lies below line $\alpha/\alpha_H = 1$. This contradicts the basic assumptions of the author of formula (15) and is an attempt to coordinate this formula with test data from reference [22] for other regimes by changing the factor ϵ .

For $p = 0.031$ bar and $\delta = 3.1^\circ\text{C}$ (Fig. 7) the calculated values of α/α_H according to formulas (4) and (14) are near the test values, while those calculated according to formula (15) when $\epsilon = 0.64$ are higher than test values throughout the studied range of Re_n numbers. Formula (15) when $\epsilon = 0.42$, in this case, gives values $\alpha/\alpha_H < 1$ for a rather wide range of Re_n variation. The character of test and calculated curves when $p = 0.031$ bar is also substantially different, due to which in the region of higher Re_n the spread between theoretical and test data increases.

Figures 6 and 7 reveal a substantial spread between calculated and test data with respect to the effect on the heat transfer factor of process parameters, especially steam pressure. The test curves $\alpha/\alpha_H = f(Re_n)$ for the two series of tests examined, encompassing approximately the same range of Re_n , are very near each other; at the highest $Re_n \approx 2000$ the values of α/α_H for series II ($p = 0.031$ bar, $\delta = 3.1^\circ\text{C}$) are only approximately 4% lower than for series I ($p = 0.47$ bar, $\delta = 7.4^\circ\text{C}$), which lies within the limits of experimental accuracy. In contrast to this, at the same Re_n and the same steam parameter variation, the calculated values of α/α_H according to all three theoretical formulas vary substantially and, what is no less important, in the opposite direction; with the change from the conditions of test series I to the conditions of test series II they grow approximately 50% according to formulas (4) and (14) and 65% according to formula (15).

Test data for the condensation of moving steam on a test pipe in lateral flow were also obtained in reference [27], but their accuracy is so low that it is impossible to use them for checking theoretical relationships.

Conclusions

A comparison of calculated and test data for the heat transfer factor during film condensation of moving saturated steam (in the region $Re_K < Re_{K_{кр}}$) indicates that none of the examined theoretical relationships, obtained during various determinations of viscous stress on the interface of liquid and vapor phase, correctly describes the rules of the studied process established experimentally for condensation on a horizontal pipe. Available test data as yet are insufficient for a final judgment concerning the suitability of any of the proposed process models or conditions under which one model should be changed for another. However, they, along with the data available on the flow of liquid films during moving gas phase and on the transfer of matter across liquid films, lead us to believe that the concept of the preservation of a purely laminar flow of a condensate film in the presence of moving steam in the region $Re_K < Re_{K_{кр}}$, which is the foundation of the examined theoretical relationships, on the most part, does not correspond to the actual physical circumstances of the process. These data stand in favor of the assumption, expressed in a number of VTI works, concerning the restructuring of the flow regime of condensate film under the effect of disturbances caused by steam flow, even at relatively low Reynolds numbers Re_K and variations, due to this mechanism, in the heat transfer across the film. Preservation of a purely laminar flow for the film can, obviously, be expected only in a relatively narrow range of Reynolds numbers for vapor flow for very viscous liquids and in the absence of other disturbing factors affecting the film.

BIBLIOGRAPHY

1. W. Nusselt. «Z. d. UDI», 1916, № 27, 28.
2. С. С. Кутателадзе. Теплопередача при конденсации и кипении. Машгиз, 1952.
3. Л. Д. Берман. «Теплоэнергетика», 1966, № 7.
4. С. С. Кутателадзе. «Советское котлоуростроение», 1941, № 1—2.
5. M. Jacob, S. Erk, H. Eck. «Phys. Zeitschr.», 1935, № 5.
6. G. Winkelsesser. Dechema—Monographien. Bd. 20, 1952, № 244.
7. H. Hartmann. «Chemie—Ingenieur—Technik», 1961, № 5.
8. W. M. Rosenow, S. P. Sukhatme. В кн. «Developments in Heat Transfer», MIT Press, Cambridge, Mass., 1964.
9. H. R. Jacobs. Int. J. Heat Mass Transfer, vol. 9, 1966, № 7.
10. S. Sugawara et al. Proc. 6th Jap. Congr. Appl. Mech., III-4, 1956.
11. Л. Д. Берман и Ю. А. Туманов. «Энергомашиностроение», 1964, № 5.
12. A. P. Colburn. Proc. Inst. Mech. Engrs (London), vol. 164, 1951, № 4.
13. E. F. Carpenter, A. P. Colburn. Proc. Gen. Disk on Heat Transfer, Sept. 1951.
14. Г. Г. Черный. ДАН, т. 101, 1956, № 1.
15. W. M. Rosenow, J. H. Webber, A. T. Ling. Trans. ASME, vol. 78, 1956, № 8.
16. R. S. Silver. Proc. Inst. Mech. Engrs (London), vol. 178, 1963—1964, p. 1, № 14.
17. И. Г. Шекриладзе. Сообщения АН ГрузССР., 1964, № 3; Диссертация. ЭНИИ, М., 1964.
18. Л. Д. Берман. «Известия ВТИ», 1953, № 3.
19. С. Н. Фукс. «Известия ВТИ», 1953, № 3.
20. Г. Шлихтинг. Теория пограничного слоя. Изд-во иностр. лит., 1956.
21. И. Г. Шекриладзе и В. Н. Гомеллаурц. Int. J. Heat Mass Transfer, vol. 9, 1966.
22. Л. Д. Берман и Ю. А. Туманов. «Теплоэнергетика», 1962, № 10.
23. A. A. Nicol. Canad. Journ. Chem. Engng, vol. 42, 1964, № 6.
24. В. П. Исаенко, А. П. Солодов и М. А. Тирунариян. Труды МЭИ, вып. 63, 1965.
25. Т. Ф. Пименова. «Холодильная техника», 1964, № 4.
26. J. Borchmann. «Chemie—Ingenieur—Technik», 1966, № 8.
27. H. M. Fishman, S. M. Thesis. Mass. Inst. Technol., 1959 (цит. по [8]).

THE CONDENSATION OF VAPOR ON RIBBED SURFACES

N. V. Zozulya and V. A. Karkhu

Designations

- $x; y$ - coordinates of rib length and height, respectively, m;
 $h; l; \delta(d)$ - height, length, and thickness (diameter) of rib, respectively, m;
 t_s - vapor saturation temperature, °C;
 t_w - rib wall temperature, °C;
 t_0 - rib wall temperature of root, °C;
 $T = t_s - t_w$ - local temperature drop between the temperature of the vapor and the temperature of the rib wall, °C;
 $T_0 = t_s - t_0$ - temperature drop at rib root, °C;
 α - heat transfer factor during vapor condensation, $W/m^2 \cdot \text{deg}$;
 u - perimeter of rib cross section, m;
 f - cross-sectional area of rib, m^2 ;
 λ_w - coefficient of heat conductivity of rib, $W/m \cdot \text{deg}$;
 $\lambda_{\text{ж}}$ - coefficient of heat conductivity of liquid in condensate film, $W/m \cdot \text{deg}$;
 $\mu_{\text{ж}}$ - coefficient of dynamic viscosity of liquid, $kg \cdot s/m^2$;

$\gamma_{\text{ж}}$ - weight density of liquid, kg/m^3 ;
 r - vaporization heat of liquid, J/kg ;
 Q_{TP} ; Q_{P} - quantity of heat removed by smooth pipe and ribbing, respectively, W ;
 G_{TP} ; G_{P} - weight of smooth pipe and ribbing, respectively, kg .

Subscripts

s - vertical;
 r - horizontal.

From an analysis of Nusselt's equation

$$\alpha = \sqrt[4]{\frac{\lambda_{\text{ж}}^3 \gamma_{\text{ж}}^2 r}{4 \mu_{\text{ж}} (t_{\text{с}} - t_{\text{ж}}) x}} \quad (1)$$

it is apparent that the heat transfer factor during vapor condensation on a vertical surface is considerably reduced with a sharp decrease in the coefficient of heat conductivity in liquid phase and the heat of vaporization. These properties characterize the majority of organic low-boiling substances, which have a vaporization heat approximately ten times lower and a heat conductivity coefficient approximately five times lower than that of water. The intensity of heat transfer from the condensing vapor in the condensers for such liquids can be considerably less than it is from the cooling water. In these cases, it becomes advisable to develop the surface on the vapor side by ribbing.

An analysis of the effectiveness of straight longitudinal ribs (continuous and discontinuous) during film condensation is presented in the work of N. V. Zozulya and V. A. Karkhu [1].

In this article, this problem is solved for wire ribbing. Figure 1 shows a pipe with one of the available types of wire ribbing. Such ribbing is widely used in gas heat exchangers. If this ribbing is used for condensing vapor, then, depending upon the pipe arrangement in the condenser (horizontal or vertical),

the ribbing elements can be arranged in three characteristic positions with respect to the direction of the flow of the condensate film formed on the wire ribbing: vertically upward, horizontally and vertically downward. Intermediate positions of a

rib under various angles of slope according to the direction of condensate motion (to or from the root of the rib) can pertain to one of the vertical arrangements.

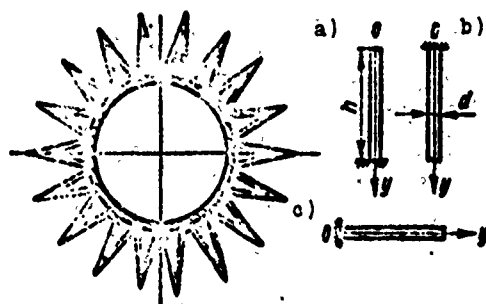


Fig. 1.

For finding the temperature distribution along the height of the wire rib, we shall examine Nusselt's equation (1) for a

vertical plate or its familiar modification for a horizontal pipe and the differential equation of heat conductivity

$$\frac{d^2T}{dy^2} = \frac{aw}{\lambda_w} T \quad (2)$$

with boundary conditions:

$$\begin{aligned} \text{when } y=0 \quad T &= T_0; \\ \text{when } y=h \quad -\lambda_w \frac{dT}{dy} &= aT. \end{aligned} \quad (3)$$

It should be noted that the regularities of the condensation process on such small surfaces as wire ribbing must differ somewhat from the results obtained by Nusselt in solving the above problem. Let us say that in condensation on a horizontal thin wire the forces of surface tension will play a predominant role, while in Nusselt's equation they were not taken into account at all.

In condensation on vertical wire elements the substantial difference from the conditions of Nusselt's problem is the appearance here of temperature gradient along the height of the rib, i.e., along the path of motion of the condensate film.

The local heat transfer factor, in this case, depends not only on the coordinate with respect to height and the temperature at the examined point but also on the temperature at all the points positioned above. Therefore, we can say beforehand that the solution to the problem according to the diagram taken for the rib, cooled from below, gives a somewhat understated result with respect to the quantity of heat removed, while for a rib cooled from above the result is somewhat overstated. In the latter case, for a vertical rib with cooling from above we do not take into account the possible runoff of condensate on the rib from the supporting surface, which would lead to drenching of the rib with liquid and the complete loss of its effectiveness as a surface for vapor condensation.

A vertical rib cooled from below. The differential equation of heat conductivity (2) for a vertical rod of circular cross section, cooled from below (Fig. 1), under conditions of film condensation of vapor, after reduction to dimensionless conditions

$$\theta = \frac{T}{T_0}; \quad \xi = \frac{y}{h}; \quad m_s = \frac{0.70 \lambda_{\text{ж}}^{3/4} \gamma_{\text{ж}}^{1/2} r^{1/4} u h^{7/4}}{\mu_{\text{ж}}^{1/4} \lambda_{\text{ж}} f T_0^{1/4}} \quad (4)$$

has the form:

$$\frac{d^2 \theta}{d\xi^2} = m_s \xi^{-1/4} \theta^{3/4} \quad (5)$$

Turning our attention to the decreasing character of the temperature gradient toward the free end of the rib, in order to facilitate solution of the problem, the boundary conditions has been simplified here and below by the assumption that on the free end of the rib the heat transfer factor is equal to zero, i.e.,

$$\left. \begin{array}{l} \text{when } \xi = 0 \quad \frac{d\theta}{d\xi} = 0; \\ \text{when } \xi = 1 \quad \theta = 1. \end{array} \right\} \quad (6)$$

Equation (5) with boundary conditions (6) was integrated by the numerical method on an electronic computer.

The results of the integration are presented in Fig. 2. The curves of temperature distribution along the rib with various values for parameter m_g can be generalized with sufficient accuracy ($\pm 5\%$) by the following formula:

$$\theta = [1 - 0.07m_g^{2/3}(1 - \xi^3)]^3. \quad (7)$$

Using generalization (7), we determine the amount of heat removed by a single wire rib:

$$Q = - \frac{\pi d^2 \lambda T_0}{4h} \left. \frac{d\theta}{d\xi} \right|_{\xi=1} = \frac{0.16\pi d^2 T_0 \lambda}{h} m_g^{2/3}. \quad (8)$$

A vertical rib cooled from above. With the coordinate system used in Fig. 1, the differential equation of heat conductivity for a vertical rib with cooling from above has the same form as that for a rib cooled from below. The boundary conditions, according to the earlier discussed assumptions, are

$$\left. \begin{array}{l} \text{when } \xi = 0 \quad \theta = 1; \\ \text{when } \xi = 1 \quad \frac{d\theta}{d\xi} = 0. \end{array} \right\} \quad (9)$$

The solution to equation (5) with boundary conditions (9), performed by the numerical method, is presented in Fig. 3. The results of calculating the temperature gradient along the rib in the region $0 \leq m_g \leq 50$ are generalized (within $\pm 5\%$) according to the following formula:

$$\theta = (1 - 0.06m_g^{2/3}\xi^{1-1/3})^3. \quad (10)$$

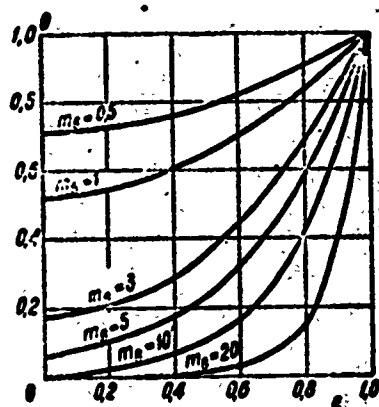


Fig. 2.

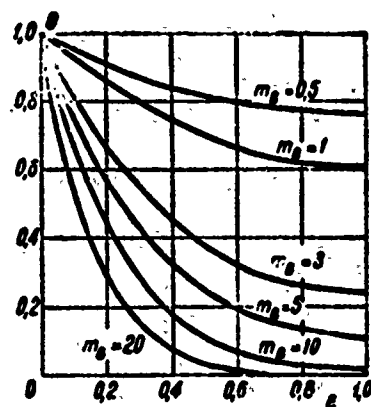


Fig. 3.

We shall calculate the quantity of heat which is removed in the condensation process by a single wire rib with height h :

$$Q = - \frac{\pi d^2 \lambda_m T_m}{4h} \cdot \frac{d\theta}{d\xi} \Big|_{\xi=0} = \frac{0.14 \pi d^2 T_m \lambda_m m_0^{3/4}}{h}. \quad (11)$$

A horizontal rib. To solve the equation of heat conductivity (2) on a horizontal element of wire with finite length, cooled at the root (see Fig. 1), we use the Nusselt equation for the average heat transfer factor during vapor condensation on a horizontal pipe:

$$\bar{\alpha} = 0.724 \sqrt[4]{\frac{\lambda_m^3 g \rho^2 r}{\mu (t_s - t_w) d}}. \quad (12)$$

After substituting (12) into equation (2) and changing variables:

$$\theta = \frac{T}{T_0}; \quad \xi = \frac{y}{h}; \quad m_r = \frac{0.72 \lambda_m^{3/4} g^{1/2} r^{1/2} \mu h^3}{\mu_m^{1/4} \lambda_w \sqrt{T_0} d^{1/4}} \quad (13)$$

we arrive at the differential equation:

$$\frac{d^2 \theta}{d\xi^2} = m_r \theta^{3/4} \quad (14)$$

with boundary conditions:

$$\begin{aligned} \text{when } t=0 \quad \theta &= 1; \\ \text{when } t=1 \quad \frac{d\theta}{dt} &= 0. \end{aligned} \quad (15)$$

An equation of this type is examined in [1] and an approximate analytical solution is obtained for it.

Along with this, a numerical solution to equation (14) with boundary conditions (15) was obtained. The results of integration are presented in Fig. 4 and, within $\pm 5\%$ for $m_p = 0-50$, can be generalized by the following relationship:

$$\theta = (1 - 0.06 m_p^{2.5} t^{1-t})^2. \quad (16)$$

The quantity of heat removed by a single rib in the vapor condensation process is calculated according to formula:

$$Q = - \frac{\pi d_0 T_0}{4h} \left. \frac{d\theta}{dt} \right|_{t=0} = \frac{0.14 \pi d_0 T_0 m_p^{2.5}}{h}. \quad (17)$$

Compared with the analytical solution presented in [1], formula (16) gives a somewhat understated result (with respect to the quantity of heat removed) only at low values for parameter m_p .

When $m_p \geq 5$ both solutions virtually agree. The data in this article and reference [1] make it possible to conduct a concrete evaluation of the effectiveness of various types of ribbing as a function of its working conditions.

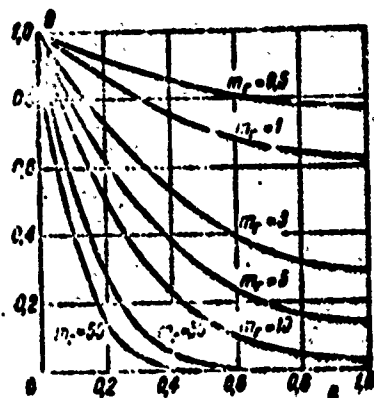


Fig. 4.

For example, ribbed pipes $\varnothing 24/22$, 1 m high, are examined while arranged vertically in the condensers. In [1] a comparison

is made of the effectiveness of smooth and ribbed pipes $\varnothing 24/22$, 1 m high, with longitudinal vertical ribbing. A comparison for

tubes of the same dimensions with looped wire ribbing, characterized by the following data, is given in table two:

Spacing of loop with respect to height..... 4 mm
 Rib height..... 10 mm
 Thickness (diameter) of rib..... 1.0 mm
 Number of ribs..... 36
 Rib material..... Copper

Ribbing effectiveness is calculated for the vapor condensation conditions of two substances - water and carbon tetrachloride - differing sharply in their thermophysical properties. Heat transfer from a smooth pipe is accounted for according to Nusselt's formula. Heat removal from the ribs is calculated according to formula (17).

Table

Working matter	r, kJ/kg	Smooth pipes	Pipe with ribbing		
		Q_T kW	Q_p kW	$\frac{Q_p}{Q_{Tp}} \cdot 100$ %	$\frac{G_p}{G_{Tp}} \cdot 100$ %
H ₂ O	2250	47	24	50	108
CCl ₄	192	4.7	5.9	128	108

The results of calculations lead us to conclude that if, in spite of the high heat conductivity of the selected materials, the use of these forms of ribbing for water vapor condensation is not feasible, then with the condensation of the vapor of low-boiling substances the use of ribbed surfaces can give a noticeable effect.

BIBLIOGRAPHY

1. Н. В. Зозуля, В. А. Карху. Распределение температуры и коэффициент теплоотдачи при конденсации пара на прямоугольном ребре. ИФЖ, т. XIII, № 6, 1967, стр. 853-859.

HEAT AND MASS TRANSFER DURING CONDENSATION OF STEAM FROM SAT- URATED AIR IN AN ANNULAR DUCT

L. S. Bobe, D. V. Pavlov, and
D. D. Malyshev

Designations

- α_{ycn} - conventional heat-transfer coefficient,
 $W/m^2 \cdot \text{deg}$;
 α_{kone} - of convective heat-transfer coefficient,
 $W/m^2 \cdot \text{deg}$;
 q_{cym} - total thermal load, W/m^2 ;
 G - flow rate, kg/s ;
 p - partial pressure, N/m^2 ;
 P_{cm} - total pressure, N/m^2 ;
 t - mean temperature, $^{\circ}C$;
 Δt_{log} - logarithmic temperature difference, $^{\circ}C$;
 ϕ - relative moisture content of air, %;
 r - latent heat of steam generation, J/kg ;
 c_p - specific heat at constant pressure, $J/kg \cdot \text{deg}$;
 $\epsilon_n = p_n/P_{cm}$ - cubic content of steam in mixture;
 β_p - coefficient of mass output relative to the
gradient of partial pressure of steam, l/s ;

$\Pi_g = p_n p_{nrp} / p_{cm}$ - a dimensionless parameter characterizing the cross flow of substance to the surface of condensation;

d_g and d_H - internal and outside diameters of the annular duct, m;

d_g - equivalent diameter, m;

F - heat and mass transfer surface, m^2 .

The remaining designations are conventional.

Subscripts

c. a - dry air; H - condensate; n - steam; rp - phase interface; cm - air-steam mixture; 1 - input; 2 - output; r - gas (air).

The process of condensation of steam from an air-steam mixture is widespread in chemical technology. The condensation of steam from a mixture with cubic content of gas below 50-60% today is sufficiently comprehensively investigated. The heat- and mass transfer during the condensation of steam from a mixture with a large content of noncondensing gas, in particular, from steam-saturated air, at dewpoints of 30-80°C in laminar and transient conditions of motion has been studied less comprehensively. The use, in monographs devoted to air conditioning [1, 2, 3], of calculation procedures in which the coefficient of "dry" heat exchange is multiplied by the conventional coefficient of condensation can lead to large errors. The formula proposed by T. Khobler [4] also agrees insufficiently with experimental data, especially with high steam contents. The condensation of vapor from saturated air should be considered as a combined process of heat- and mass transfer; in this case, as shown in [5], the approximate analogy between heat- and mass transfer can be maintained up to rather high steam contents.

In Zh. F. Sergazin and A. M. Baklastov's recently published work [6] in which a study was made of the process of condensation of an air-steam mixture on a surface under conditions of hydrodynamic stabilized flow, they have shown the existence of an approximate analogy at mean temperature of saturated air up to 45°C.

A matter of independent interest is the research into the effect of the geometric characteristics of the annular duct in conducting the given process in the laminar and transition regions of motion of the mixture. A great many works have been devoted to research on the effect of the geometry of the duct on heat and mass transfer, however, general recommendations for many cases, in particular for the one being examined below, are lacking.

The investigation was conducted with a specially designed laboratory bench. Air free of oil is supplied through a filter to a mixer where it is mixed with steam entering from a vaporizer. From the mixer, the air-steam mixture with steam content deliberately greater than the steam content corresponding to saturation passes through a precondenser and a separator and is superheated 1-2°C in a heat exchanger and it enters into an experimental condenser. In the condenser, part of the vapor is condensed and in the form of condensate flows through a water seal into a graduated container, the air is ejected into the atmosphere. Water from the mains serves as the coolant. Such an organization of the process ensures saturation of the air by steam at a temperature in the separator which is easily controlled. An experimental condenser has been made out of thick-walled Plexiglas. In the cylindrical casing, placed between flanges is the core with a coil made of stainless tubing $\varnothing 2.3 \times 0.1$ wound on it with a pitch of 2.8-3 mm, on the surface

of which condensation occurs; the apparatus is arranged horizontally. In the condenser provision has been made for fittings for the insertion of thermocouples, for the inlet and outlet of air, and for draining the condensate. Apparatuses with the various external and internal diameters of annular duct and ratio L/d_g were used as experimental condensers. The geometric dimensions of the condensers are given in Table 1. The condenser, separator, and the appropriate communications are insulated with "parolon."

Table 1.

(1) № серии опытов	$d_{в.}$ мм	$d_{н.}$ мм	L мм	$d_{г.}$ мм	λ	$\lambda \left(\frac{L}{d_{г.}}\right)^{0.3}$	$\lambda \left(\frac{L}{d_{г.}}\right)^{0.3} \left(\frac{d_{в.}}{d_{н.}}\right)^{1.4}$	Расчетные формулы для массоотдачи при постоян- ном $d_{г.}$ (2)
I	18	26	123	8	0,52	1,11	0,665	$Nu_D = 0,665 Re^{0,6} Pr^{0,85} \varepsilon_g^{-0,4} \times$ $\times \left(\frac{d_{в.}}{L}\right)^{0,3} \left(\frac{d_{н.}}{d_{г.}}\right)^{1,4} \quad (3)$
II	18	26	290	8	0,41	1,11	0,665	
III	18	30,6	120	12,6	0,74	1,41	0,665	
IV	15	50	140	32	1,83	2,78	0,665	
V	18	50	315	32	1,47	2,78	0,665	
VI	9	26	250	17	0,66	1,47	0,332	$Nu_D = 0,332 Re^{0,6} Pr^{0,85} \varepsilon_g^{-0,4} \times$ $\times \left(\frac{d_{в.}}{L}\right)^{0,3} \left(\frac{d_{н.}}{d_{г.}}\right)^{1,4} \quad (4)$
VII	9	50	315	41	2,1	3,68	0,332	

KEY: (1) Series No; (2) Design formulas for mass transfer with constant $d_{г.}$.

The temperature of air-steam mixture on inlet, outlet, and inside the experimental condenser, in the separator, etc., and also the temperatures input and output of the coolant on inlet and outlet were measured by copper-constantan thermocouples in a set with a PPTN-1 potentiometer and an M195/3 galvanometer. In the measurement of the cooling surface temperature, a coil was used as the heat-sensitive element, which served as a resistance thermometer. The internal surface of the

coil in contact with the core was insulated by a thin layer of polyepoxy, grade L-4. To the ends of the coil, copper sleeves were soldered which were led out from the condenser through rubber gaskets. The resistance of coiler was measured by a direct-current bridge of the MO-47 type in a set with an M195/3 galvanometer. The flow rate of the water coolant was measured by a rotameter of the RS-3 type, the air flow rate - by a rheometer of the T2-80 type, and the quantity of condensate - by the volumetric method, and the pressure - by U-shaped differential manometers filled with water. The moisture content of the mixture was regulated by determining the dew point.

Determination of experimental coefficients of heat- and mass transfer was made from the equations usually used for the combined course of these processes:

$$q_{\text{cym}} = \alpha_{\text{KOHБ}}(t_{\text{cm}} - t_{\text{rp}}) + \beta_p r' (p_{\text{a}} - p_{\text{arp}}), \quad (1)$$

where

$$\alpha_{\text{KOHБ}} = \frac{Q_{\text{c.p}} \rho_{\text{c.a}} (t_{\text{cm}_1} - t_{\text{cm}_2})}{F (t_{\text{cm}} - t_{\text{rp}})}; \quad \beta_p = \frac{G_{\text{x}}}{F (p_{\text{a}} - p_{\text{arp}})};$$

$$r' = r_{\text{rp}} + c_{p_{\text{a}}} (t_{\text{cm}} - t_{\text{rp}}).$$

In accordance with the recommendations [7] in determining $\alpha_{\text{KOHБ}}$ only heat transmitted by thermal conductivity ($q = \lambda \frac{dt}{dn}$) was considered.

During vapor condensation from the saturated air-steam mixture with an initial temperature no higher than 80-85°C, the drop in temperature on the film of condensate does not exceed 0.1-1°C, therefore the thermal resistance of the film

can be neglected and it is possible to use for t_{rp} the cooling surface temperature. Only those experimental results were used in analysis, in which the agreement of the thermal load on the part of the air-steam mixture and on the part of the coolant, and also the calculated quantity of condensate with that obtained in the experiments was found to be within limits of 5-10%. Temperatures were averaged according to the logarithmic law $t_{cm} = t_{rp} + \Delta t_{(cm-rp)} \log$. As a controlling linear dimension the equivalent diameter $d_e = d_H - d_B$ was used. The external surface of the coil was taken as the condensation surface. Since the core was made of low heat-conducting material and the contact of the coil with the core passed through the heat-insulating varnish (when using a core of $\varnothing 9$ through the vinyl chloride insulation) the error introduced by this assumption was slight. Maximum error in the experiments is on the order of $\pm 15\%$.

Seven series of experiments were conducted which differed from one another in the geometric characteristics of the duct and in limits of a change in the parameters. The pressure in the condenser varied in series I from $1.0 \cdot 10^5$ to $1.5 \cdot 10^5$ N/m², in the remaining series the pressure did not exceed $1.1 \cdot 10^5$ N/m²; saturation of the air in series I comprised $\phi = 88-100\%$, in the remaining series - about 100%; the rate of the mixture changed from 0.14 to 6.5 m/s, in so doing, the Reynold's criterion was 250-5000; the dewpoint of the air on inlet was kept at 25-80°C, in so doing, the average steam content in the flow comprised 2-38%. The mean log temperature difference between the flow and the condensation surface changed within limits of 3.5-43°C, criterion $\pi_g = (7-324) \cdot 10^{-3}$, the quantity of condensate $(1.7-145) \cdot 10^{-6}$ kg/s, thermal load 400-16,000 W/m², the experimental values of criteria Nu and Nu_D comprised 3.5-95. For the purpose of a change in the condensation surface temperature,

the temperature of the coolant on inlet was changed from 3.5 to 40°C. In series I the flow rate of coolant varied, in the others - it was kept constant. The geometric dimensions of the condensers changed within limits of $L/d_g = 4-36$ and $d_H/d_B = 1.5-5.5$. The cooling surface temperature was kept no lower than 15°C, at lower values the experimental data were not described by the dependences proposed below. This case requires special examination.

Figure 1 depicts (for series IV of the experiments) the dependence of the conditional total heat-transfer coefficient $\alpha_{yc,1} = \frac{q_{cys}}{t_{cu} - t_{fp}}$ on the mean temperature of saturation of the mixture and air velocity in the condenser. As can be seen from the figure, the total heat-transfer coefficient with the same flow rate was the higher, the higher the moisture content of the air, and at one and the same moisture content was the higher, the greater the flow rate. Examination of the dependences for $\alpha_{yc,1}$ gives only a qualitative picture of the process. For development of the calculation procedure it is necessary to examine the general dependences for heat- and mass transfer. Further interpretation of the experiments was conducted using the criterial equations proposed by L. D. Berman for jointly proceeding processes of heat- and mass transfer [5]. Since only one mixture was investigated, the relationship of the physical constants of the components was a constant value, and that of criterion Pr_D also changed insignificantly (0.57-0.59). For saturated air with a saturation temperature up to 85-90°C, the value of gas content ϵ_r is close to one, therefore in the interpretation of the experiments a value of vapor content $\epsilon_n = \frac{p_n}{p_{cm}}$ was used, more accurately describing the process being investigated. For each series of experiments, the experimental data on mass transfer were processed according to the equation:

$$Nu_D = A Re^{m_1} \epsilon_n^{m_2} \quad (2)$$

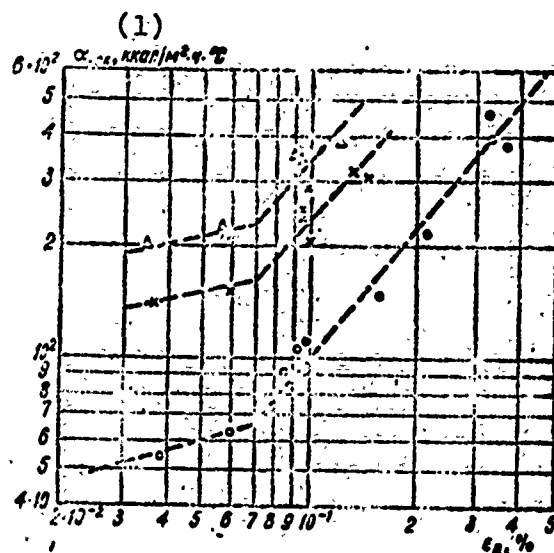


Fig. 1. Dependence of the conventional heat-transfer coefficient (α_{ycn}) on average vapor content of mixture (ϵ_n , %): \circ - $Re = 320$;

\times - $Re = 1000$; Δ - $Re = 2200$.

KEY: (1) $kcal/m^2 \cdot h \cdot ^\circ C$.

By means of successive correlations, using the method of least squares exponents with Re , π_g and ϵ_n and the value of preexponent A for all the series of experiments were determined. The exponents comprised $n = 0.6$; $m = -0.4$; $s = 0.85^{+0.05}_{-0.09}$. Values of preexponent A for equation (2) are given in Table 1. The value of the preexponent, as one would expect, proved different for different geometry of the duct. For short ducts of annular form, the relationships of the length of the duct, the equivalent diameter, and also the external and internal diameters of the annulus are important. By introducing into the dependence the relationships of the geometric dimensions of the duct $(d_g/L)^{0.3}$ and $(\frac{d_H}{d_B})^{1.4}$, it was possible to bring together in one dependence all the experiments conducted at one and the same internal diameter.

Calculation formulas for mass transfer are given in Table 1. It is easy to see that the values of the preexponent are proportional to the relationship of the internal diameters of the annular duct. Figure 2 presents the data on mass transfer. Equations (3)-(4) have been reduced on a graph to one dependence by means of multiplication by the ratio $(d_g/18 \cdot 10^{-3})$.

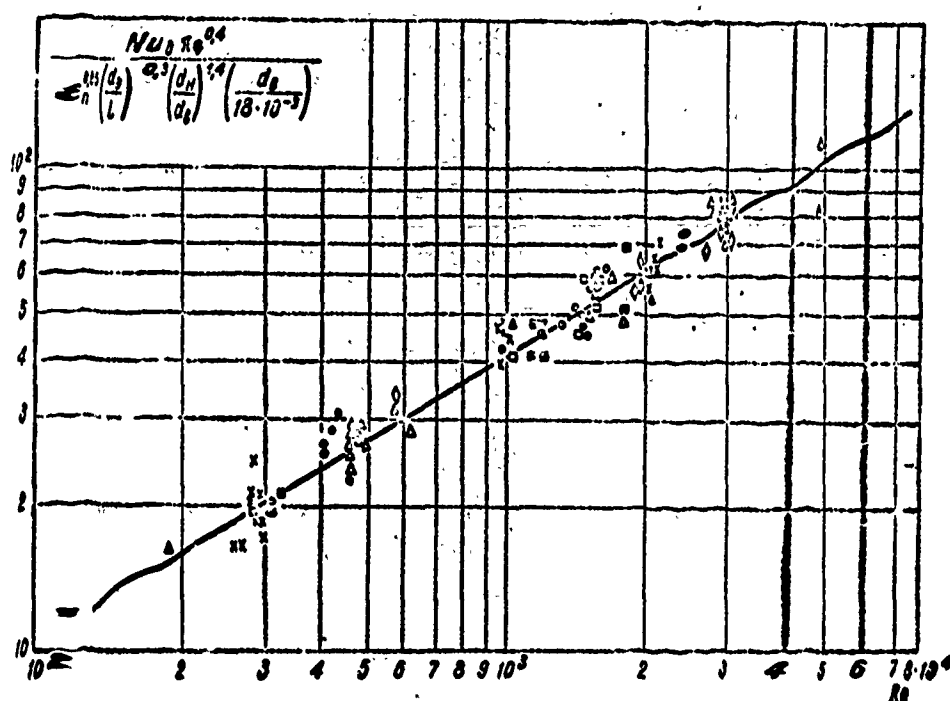


Fig - 2. Generalization of results on mass transfer;
 Δ - series I; \square - series II; \bullet - series III; \times - series IV; \diamond - series V; \circ - series VI; \blacksquare - series VII -

The value of the preexponent in this case comprised 0.665. In the future it is proposed to conduct a special investigation and to eliminate the numerical parameter d_g .

Experimental data on heat exchange and mass transfer for series IV of the experiments processed in the form of dependences $Nu = f(Re)$ and $Nu_D = f(Re)$ up to average vapor contents of 8-9% are given in Fig. 3. Here the results have been represented of experiments in the heat exchange with dry air in the form of the dependence $Nu = f(Re)$. With a moisture content of the air of more than 8-9% (saturation temperature above 48-50°C) approximate analogy between heat- and mass transfer is disturbed and the experimental points are not described by the dependence given in Fig. 3. The use during treatment of the criterion Ar did not lead to a significant decrease in the spread of the experimental data.

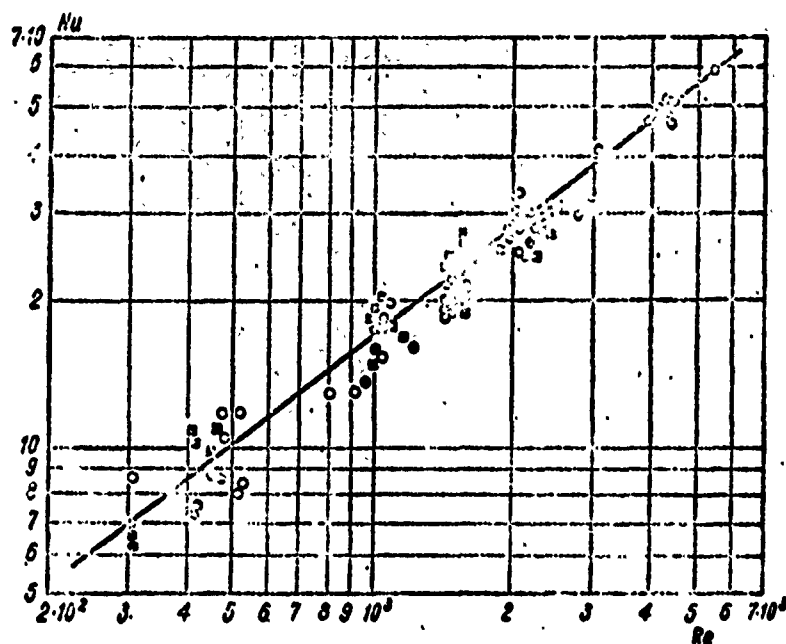


Fig. 3. Dependence of Nu and Nu_D on Re with low vapor contents ($\epsilon_n \leq 9\%$):
 ■ - mass transfer; ● - heat exchange; ○ - heat exchange with dry air.

The best approximation was obtained with treatment of the experiments in heat exchange in the form of dependence (2). The results of the treatment of the experiments are given in Table 2. In the treatment of the experiments the exponents with complexes π_g and ϵ_n proved to be equal respectively to minus 0.7 and plus 0.7, i.e., complex $(\Delta p_n/p_n)^{0.7}$ entered into the equation. For the purpose of extending the obtained dependence to the heat exchange with dry air, the experimental data were treated depending on the value $(1 - \Delta p_n/p_n)$, the exponent in proved to be equal to 0.5. Just as in the case of mass transfer, all the data for one and the same internal diameter of duct were reduced to one dependence with the aid of geometric factors $(d_g/L)^{0.3}$ and $(d_H/d_g)^{1.4}$. The values of the preexponent in dependences (5)-(6) also proved to be proportional to the internal diameter of the annular duct. Figure 4 gives the data on heat exchange processed in the form of equation (5)-(6) and reduced to one dependence by means of multiplication by $(d_g/18 \cdot 10^{-3})$. Here the data have been plotted on heat exchange from dry air, the value of the pre-exponent was 0.16.

In this way, it was possible to describe the coefficients of heat and mass transfer during the condensation of steam from saturated air in short annular ducts with uneven internal surface with $Re = 250-5000$ by single dependences for laminar and transition regions of flow of the mixture.

The obtained generalized formulas are, within the investigated limits, sufficiently precise and can be used for conducting heat engineering calculations.

Table 2.

(1) № серия опыта	d_n мм	d_n мм	L мм	d_s мм	λ	$\lambda \left(\frac{L}{d_s}\right)^{0.3}$	$\lambda \left(\frac{L}{d_s}\right)^{0.3} \left(\frac{d_n}{d_s}\right)^{1.4}$	Расчетные формулы для конвективного теплообмена (2) при постоянном d_s
I	18	26	123	8	0,125	0,263	0,16	$Nu = 0,16 Re^{0.7} \times$ $\times \left(1 - \frac{\Delta p_n}{p_n}\right)^{0.5} \left(\frac{d_2}{L}\right)^{0.3} \left(\frac{d_n}{d_s}\right)^{1.4} \quad (5)$
II	18	26	290	8	0,098	0,268	0,16	
III	18	30,6	126	12,6	0,176	0,338	0,16	
IV	18	50	140	32	0,445	0,67	0,16	
V	18	50	315	32	0,352	0,67	0,16	
VI	9	26	290	17	0,159	0,354	0,08	$Nu = 0,08 Re^{0.7} \times$ $\times \left(1 - \frac{\Delta p_n}{p_n}\right)^{0.5} \left(\frac{d_2}{L}\right)^{0.3} \left(\frac{d_n}{d_s}\right)^{1.4} \quad (6)$
VII	9	50	315	41	0,45	0,8	0,08	
(3) Теплообмен при сухом воздухе	18	26	290	8	0,098	0,263	0,16	$Nu = 0,16 Re^{0.7} \times$ $\times \left(\frac{d_2}{L}\right)^{0.3} \left(\frac{d_n}{d_s}\right)^{1.4}$

KEY: (1) Series No. of experiments; (2) Design equations for convective heat exchange with constant d_s ; (3) Heat exchange with dry air.

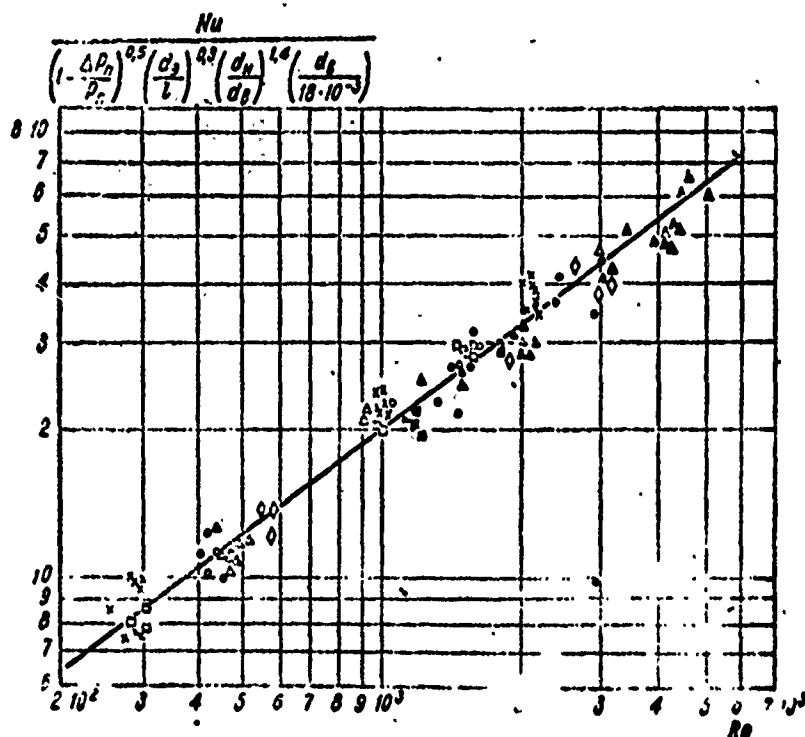


Fig. 4. Generalization of results on heat exchange: Δ - series I; \square - series II; \bullet - series III; \times - series IV; \diamond - series V; \circ - series VI; \blacksquare - series VII; \blacktriangle - heat exchange with dry air.

BIBLIOGRAPHY

1. Дегтярев Н. В. и др. Кондиционирование воздуха. М.-Л., Гос. изд. литературы по строительству и архитектуре, 1953.
2. Гадомский Р. М. Кондиционирование воздуха. М., Пицпроиздат, 1952.
3. Нестеренко А. В. Основы термодинамических расчетов по вентиляции и кондиционированию воздуха. «Высшая школа», М., 1965.
4. Хоббс Т. Теплопередача и теплообменники. М., Госхимиздат, 1931.
5. Берман Л. Д. Об аналогии между тепло- и массообменом. «Теплоэнергетика», № 8, 1955, стр. 10—18.
6. Сергазин М. Ф., Бакластов А. М. Тепло- и массоотдача при конденсации пара из влажного воздуха. «Известия вузов. Энергетика», № 2, 1965.
7. Берман Л. Д. Влияние потока вещества на конвективную теплоотдачу при испарении и конденсации. «Теплоэнергетика», 1956, № 2, стр. 25—30.

**EXPERIMENTAL STUDY OF HEAT EXCHANGE
IN DROPWISE CONDENSATION OF STEAM
WITH THE USE OF HIGH-SPEED FILMING**

P. F. Vlasov

In recuperative heat exchange apparatuses which use the steam being condensed as the warming heat-transfer agent, two forms of removal of the condensate from the condensation surface are possible: in the form of a continuous film - filmwise condensation and in the form of drops - dropwise condensation. The intensity of the transfer of heat during dropwise condensation is significantly higher than in filmwise. The productivity of the apparatus, other conditions being equal, depends upon the heat-transfer coefficient. Therefore, with high values of the heat-transfer coefficient on the part of the cooling agent and low thermal resistance of wall, artificial conversion of filmwise condensation into dropwise will substantially raise the productivity of the heat exchanger. Usually, in industrial heat exchangers filmwise condensation occurs, since all metals are well wet with water. To obtain dropwise condensation it is necessary to create a water-repellent layer on the heat exchange surface with the aid of an appropriate hydrophobizing agent. The period of action of the liquid hydrophobizing agent is

short and at best comprises a few hours [1]. Coating with a silicon varnish is more long-lasting. However, in so doing, the thermal resistances appearing even with the minimum possible thickness of coating are very considerable [2]. In [3] there is a report on the introduction into a closed loop of an experimental installation of copper oleate in the amount of 50 mg/l, which made it possible to maintain a dropwise condensation about 10,000 h.

In this study an extract of the third fraction of petroleum was used as a hydrophobizing agent which in the amount of 1-2 mg/l produced a steady dropwise condensation. Moreover, for maintaining a good hydrophobic action, the necessary concentration is approximately ten times less. For investigating heat exchange during dropwise condensation an installation was used in which the cooling of the condensation surface was accomplished owing to the boiling of the liquid coolant (acetone, benzene, water). The condensation surface consisted of a copper disk \varnothing 92 mm, on which an experimental section 55×55 mm was separated. The remaining part of the disk served as a protective zone. For visual control of the process a sight glass made of stalinite was used. The saturation temperature was maintained automatically by adjustable electric heaters with deviations of not more than $\pm 0.1^\circ\text{C}$. On the installation there were obtained experimental dependences of the specific heat flow on the difference temperature in between the saturated vapor and condensation surface for pressures of $p = 1, 3,$ and 5.2 atm(abs). The maximum heat flows reached were $q = 10^6$ W/m². The filming conducted with a frequency of 600 frames/s and with an enlargement on the negative of 1:1 showed that the rate of the flowing drops depends upon the diameter of the drops.

Research was conducted in parallel on the mechanism for formation and growth of drops during dropwise condensation.

Figure 1 presents a diagram of the installation. Steam from the flask at a pressure close to atmospheric entered condenser 5, where it condensed on hydrophobic surface 3 with \varnothing 20 mm. As the condensation surface plexiglas and glass was used, coated with silicon varnish with a thickness of 0.15-0.30 mm. Cooling of the condenser was accomplished by water with constant temperature and a pressure head from tank 6. The process of dropwise condensation was recorded by a high-speed movie camera 1 hooked up with a biological microscope 2. Photographing was conducted in transmitted light with a frequency of 250-600 frames/s.

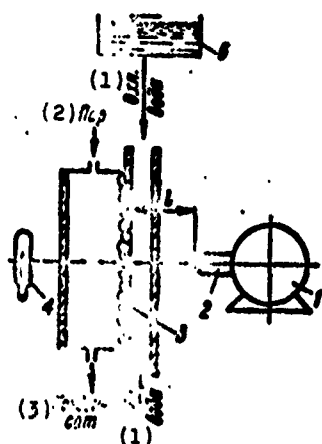


Fig. 1. Schematic diagram of the experimental installation: 1 - high-speed movie camera; 2 - microscope; 3 - condensation surface; 4 - illuminator; 5 - condenser; 6 - tank. KEY: (1) Coolant water; (2) Steam; (3) Condensate.

It is known, that the resolution of a microscope is determined by the objective selected lens, while the eyepiece only increases the obtained image without adding new parts of the object in question. Moreover, the higher the resolving power of the objective lens, the less the distance from it to the object in question. For example, if for an 8^{\times} objective the free distance $l \approx 9$ mm, then for 40^{\times} , $l \approx 0.6$ mm. In connection with this, during the photographing of the process of dropwise condensation in transmitted light the maximum resolution is determined by the structural dimensions of the condenser, and

not by the dimensions of the observed drops, as in photographing in reflected light. Therefore a possibility is created without interrupting the process, to record it at any moment of the time under high magnification.

The cooling regime could be changed by controlling the temperature or flow rate of the water coolant. With a constant cooling regime photographing of the process of the dropwise condensation with one objective was performed, then after reloading the movie camera, without changing the cooling regime, - with another objective. Photographing with other regimes was performed in similar manner.

After the movie films were processed, the following picture of the formation and growth of drops during dropwise condensation was revealed. A drop, achieving separation size, flows down by gravity. Then, in the field of view of the microscope, after a certain time, fine drops appear which, increasing in dimension, come into contact with each other and are united. Part of the surface, in this case, is freed, and on it, in turn, fine drops appear. The process is continued until a united drop does not achieve separating size, after which the cycle is repeated. A drop of separating size, in moving over the vertical surface, picks up all the drops which are encountered on the way, and the width of the track increases. Due to the mutual superposition of the tracks from the moving drops there occurs distribution in the dimensions of the growing drops over the height of the cooling surface. In so doing, only in the upper part does the size of the drops reach separation diameter, decreasing downward in a vertical line.

In [3] the assumption is expressed regarding the presence of a layer between drops, whereby the time from the departure

of a drop from the frame until the appearance in this place of new fine drops is considered to be the critical lifetime of the layer, by which its thickness is determined. However, it turned out that this time depends upon the resolving power of the objective. For example, during a constant cooling regime, the condensation surface which is represented for an 8^x objective free of drops, for a 21^x objective will already be coated by growing drops of a different size. Therefore, up to dimensions determined by the wavelength of visible light, which corresponds to maximum resolution of optical systems, there are no foundations for proposing the presence of a polymolecular layer between drops. Umur and Griffith's experimental data [4], who used elliptical polarization of light to determine the thickness of the layer between drops attest to the absence of a layer greater than one molecule in thickness.

From the photos obtained from the films the quantity of heat per unit of surface $\frac{Q}{F}$ was determined for time τ under the assumption that a 90° contact angle and the condensate have a saturation temperature. As a time reference point there was taken the moment of departure of a drop of separation size covering the entire frame from the field of view under the action of gravity. The error in this case did not exceed a time of 1-2 frames. Then

$$\frac{Q}{F} = \frac{\gamma_{\text{ж}} L \sum V_i}{nF}, \quad (1)$$

where $\sum V_i$ - the total volume of drops on the photo; L - latent heat of steam generation; $\gamma_{\text{ж}}$ - the specific gravity of the condensate; F - the condensation surface on the photo; n - the optical enlargement on the photo.

In this study for research on drop growth we used objectives 8^x, 21^x with water cooling, and 40^x with air cooling of the condenser. In order to determine the actual magnification in the optical system, in each case were conducted the photographs were made of the gauges.

Figure 2 depicts the dependence $\frac{Q}{F} = f(\tau)$ for different cooling regimes. From the graph it is evident that the specific heat flow

$$q = \frac{d\left(\frac{Q}{F}\right)}{d\tau} \quad (2)$$

for a constant cooling regime, i.e., when $\Delta t = [\text{const}]$ (noct), has a constant value.

In [5] there are experimental data on drop growth during dropwise condensation under conditions of slight underheating of the wall. The condensation surface was photographed under the microscope at convenient time intervals. Results were represented graphically in the form of the dependence of the square of the diameter on the time of drop growth. In so doing, all points relating to one and the same growing drop are arranged along a straight line, but the slope angles of straight lines are different: for large size drops the slope angle is greater. If we present McCormick and Baer's experimental data in the form $D = f(\tau)$ (Fig. 3a), then all the straight lines will have an identical slope angle. From (1) it is evident that the value $\frac{Q}{F}$ in the corresponding scale is an averaged diameter of growing drops. In this way, the McCormick and Baer's data also attest to the independence of specific heat flow from dimensions of the drops.

From the mechanism of drop growth it follows that the drops, in coming into contact with each other, are united.

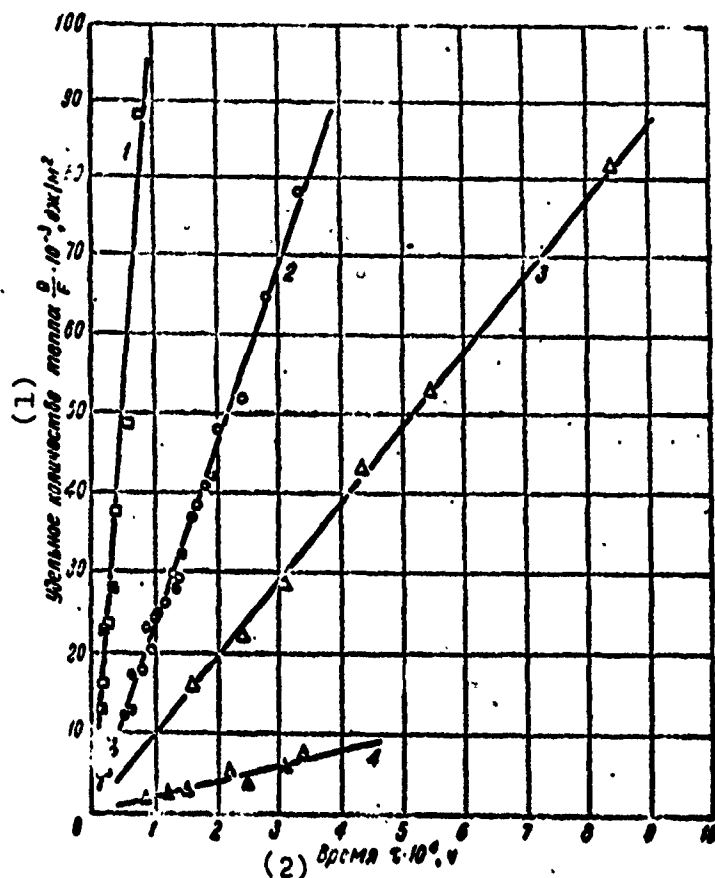


Fig. 2. Dependence of the specific quantity of heat being transferred by the condensation surface on the time of drop growth:
 \square, \circ, Δ - 8 \times objective; $\blacksquare, \bullet, \bullet$ - 21 \times objective; \blacktriangle - 40 \times objective.
 KEY: (1) Specific quantity of heat $Q/F \cdot 10^{-3}$, J/m². (2) Time, $\tau \cdot 10^4$, h.

In so doing, their size suddenly changes. Then growth again follows, etc. If one assumes that the smallest drop in Fig. 3a grew without blending from a nucleus, whose magnitude is determined by the Thompson relationship, then it is possible, having shifted all the points along the time axis up to combination, to obtain a straight line (see Fig. 3b), which represents drop growth without blending. In this case, for $\tau = 0$ we obtain the

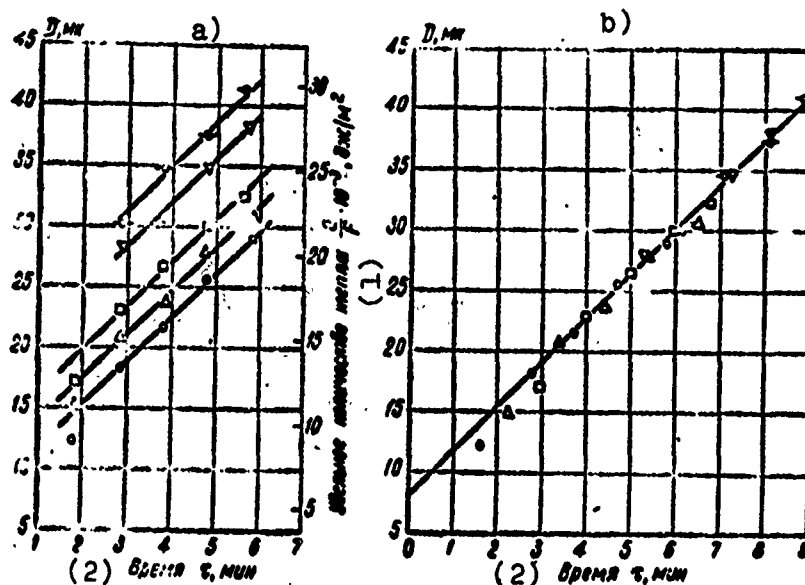


Fig. 3. Correlation of McCormick and Baer's experimental data.

KEY: (1) Specific quantity of heat $Q/F \cdot 10^{-3}$, J/m^2 ; (2) Time τ , min.

dimension of the nucleus from which it is possible to determine the supercooling of the wall:

$$T_s - T_0 = \frac{2\sigma T_s}{L \gamma_{\text{лп}} \rho_{\text{л}}}, \quad (2)[\text{sic}]$$

where T_s and T_0 - respectively, absolute temperatures of saturated vapor at the given vapor pressure and surface of the nucleus; σ , L , $\gamma_{\text{лп}}$ - coefficient of surface tension, latent heat of phase transition, and specific weight of the liquid phase; $\rho_{\text{л}}$ - the critical (smallest possible) radius of curvature of the phase boundary.

BIBLIOGRAPHY

1. H. Hamson, «Engineering», 464-469, 1965.
2. G. K. Kullberg, H. B. Kendall, «Chem. Eng. Progress», v. 56, 1, 82, 1960.
3. I. F. Welch, I. W. Westwater, Microscopic Study of Dropwise Condensation, University of Illinois, 1960.
4. Умур А. и Гринберг И. Груды Американского общества инженеров-механиков, «Технический журнал», № 2, 1935, 135-144.
5. I. U. McCormick, E. Baer, Dropwise Condensation on Horizontal Surface, University of Illinois, 1962.

QUESTIONS OF THE CONDENSATION OF VAPORS OF ALKALI METALS

B. L. Paskar' and N. N. Kochurova

Research on heat exchange during condensation of metal vapors is a new field in thermophysical studies. The first works in this direction showed that the process of heat exchange during the condensation of metal vapors reveals a number of features which are exhibited in a considerable deviation of experimental heat-transfer coefficients from those calculated in Nusselt's theory (with the necessary corrections).

During the condensation of the vapors of metals, a determining role in the total sum of thermal resistances is played by thermal resistance of phase transition [1]:

$$\alpha_{\phi} = \frac{2f}{2-f} \left(\frac{M}{2\pi RT''} \right)^{1/2} \left(\frac{p''-p'}{T''-T'} - \frac{p'}{2T'} \right) [r + c_p(T''-T')], \quad (1)$$

where

f - the coefficient of condensation; M - molecular weight;
 R - gas content; r - the heat of vaporization; c_p - heat capacity;
 T'' , p'' , T' , p' - temperature and corresponding saturation pressures of the vapor and condensate respectively.

All the features of the process of heat exchange during the condensation of metal vapors are caused by the thermal resistance of phase transition. The difficulty in determining the thermal resistance of the phase transition to a considerable degree is connected with the indeterminate form of the coefficient of condensation f .

Usually, the condensation coefficient is determined according to formula (1) [2, 3, 5, 6, 8], using experimental data in respect to thermal conductivity (α_{ϕ}). In this way, the determined coefficient f includes all the unknown features of thermal resistance of phase transition and bears the character of the empirical proportionality factor in formula (1).

In order to investigate the features of heat exchange during the condensation of metal vapors and to determine the true value of the coefficient of condensation, it is necessary to examine in detail the effect of the hydrodynamics of the process, the possibility of the presence of noncondensing gases and their role during heat exchange, the surface condition of the condensate, its purity, etc.

We conducted experiments in the condensation of the vapors of potassium in a vertical tube (Fig. 1). The length of the cooled section of tube was 247 mm, the internal diameter 40 mm. Outside, according to the diagram of countercurrent, the tube was cooled by an NaK alloy. The potassium vapor was fed into the tube from the top. To increase the accuracy of measurement of the wall temperature during high heat flows between the tube in which condensation was accomplished, and the cooling case a copper lining was made with capillaries for thermocouples. Along the axis of the tube from below the junctions of the thermocouples are brought in for measurement of vapor temperature along the length.

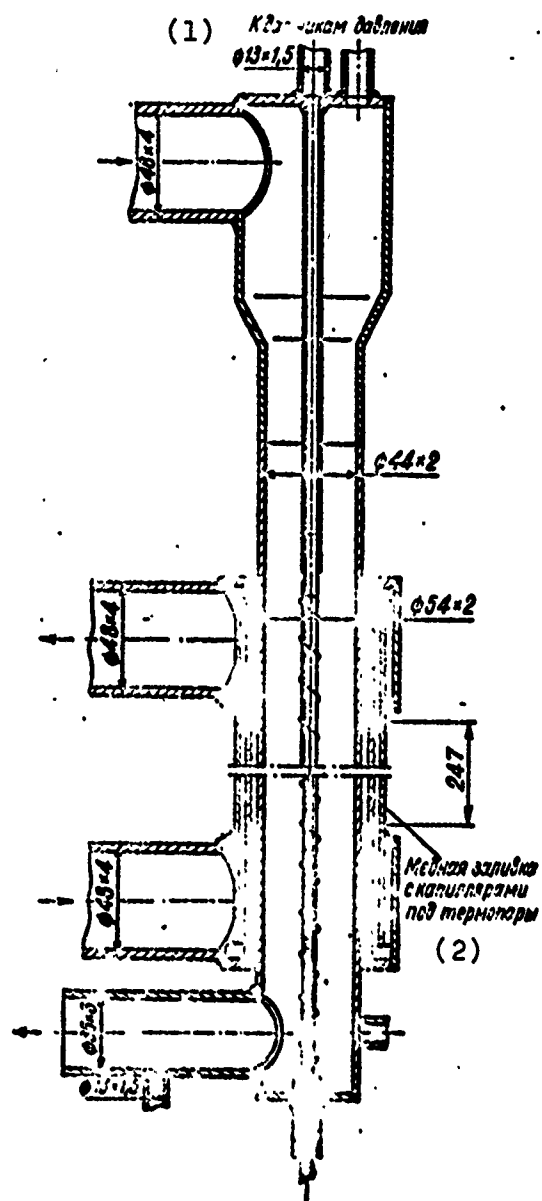


Fig. 1. Test section.
 KEY: (1) To pressure gauge; (2)
 Copper lining with capillaries
 for thermocouples.

Besides the measurement of wall and vapor temperature along the length of the tube, measurement of the temperature of the potassium vapor in the inlet branch pipes was made, and also the temperatures of the NaK on inlet and outlet from the tube; pressure was measured (on potassium) on inlet and outlet from the tube. Chromel-Alumel thermocouples in hermetically sealed stainless capillaries with external diameter of 0.8 mm were used for measurement of the temperature.

Experiments were conducted during partial vapor condensation in the experimental condenser in the range of change in the temperature of potassium vapor on inlet of 520-720°C, the temperature of NaK of 380-530°C, and heat flows of $3.40 \cdot 10^5$ - $10.40 \cdot 10^5$ kcal/m²·h.

The basic problem in the formulated experiments was the obtaining of experimental data during condensation of vapors without the admixture of noncondensing gases. Before beginning the experiment, the hermetic seal of the installation was thoroughly checked. For 5-6 hours at low temperature in the circuit (to 400°C) vacuuming of the entire circuit was performed. Then the vacuuming came to a halt. In the circuit they gradually raised the temperature and set the assigned conditions. A set of experiments was conducted under continuous vacuuming of the condenser (and the entire circuit) while operating in the assigned conditions. Heat transfer in both series of experiments was the same. This was the experiment conducted. After operating at the assigned condition with continuous vacuuming the vacuum pump was disconnected. A check was made as to whether, heat transfer would change in the course of time after disconnection of the vacuum pump (during ~10 h). Heat transfer did not change.

Continuous removal of possible noncondensing gases did not affect heat transfer. Consequently, there were none in the condenser.

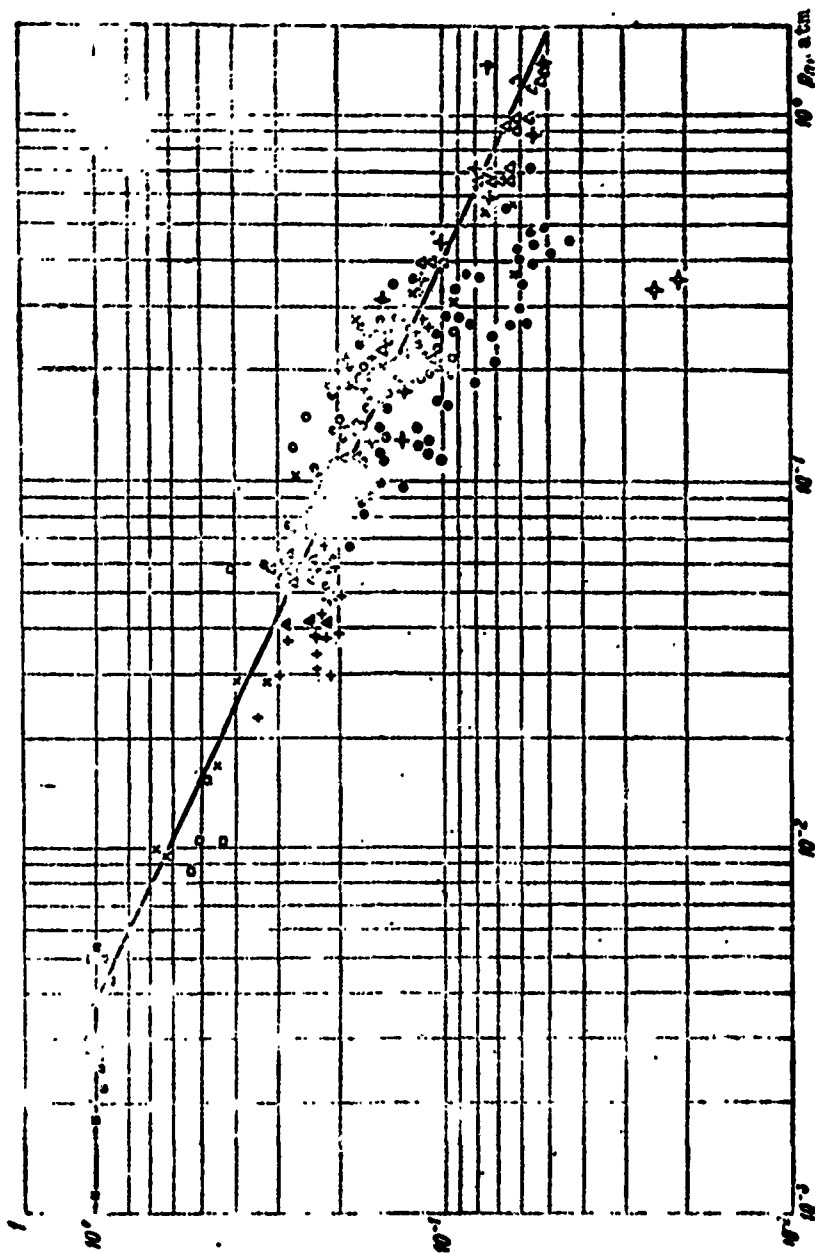


Fig. 2. Dependence of coefficient f in formula (1) on pressure:
 ● - K, this paper (without continuous vacuuming); ○ - K, this paper (with continuous vacuuming); × - K, Kroger [8]; ■ - K, Subbotin et al. [4]; ○ - Na, Barry [6]; ▲ - Hg, Misra, Bonilla [2]; □ - Hg, Sukhatme [7]; Δ - K, Alad'yev et al. [3]; + - K, Labuntsov, Smirnov [5]; • - Na, Labuntsov, Smirnov [5]; -○- K, this paper (in the presence of inert gas).

The supplying of noncondensing argon gas to the circuit sharply lowered the rate of heat transfer.

The conducted measurements of heat transfer made it possible to calculate coefficient f in formula (1). Figure 2 gives the calculated values in the various series of experiments: with continuous vacuuming; only with preliminary, but without continuous vacuuming; with noncondensing argon gas. The first two series of experiments coincide. Values of f in the experiments with gas lie considerably lower than in the others. This figure also gives values of coefficient f obtained by using formula (1) from experiments in heat transfer made by various authors [2, 3, 4, 5, 6, 7, 8]. From Fig. 2 it is evident that a drop in coefficient f is observed with an increase in the pressure of the condensing vapors.

Further experimental and theoretical investigations will make it possible to explain the causes for the experimental dependences obtained.

BIBLIOGRAPHY

1. Кучеров Р. Я., Рикенглас Л. Э. К вопросу об измерении коэффициента конденсации. ДАН СССР, 1960, т. 133, № 5. О гидродинамических граничных условиях при испарении и конденсации. ЖЭТФ, т. 37, вып. 1(7), 1960.
2. B. Misra, C. F. Bonilla. Heat transfer in the condensation of metal vapor: mercury and sodium up to atmospheric pressure. Chem. Engng. Prog. Sym., Ser. 18, 52(7), p. 7-21, 1966.
3. Аладьев И. Т. и др. Доклад на 3-й Международной конференции по теплообмену. Чикаго, Иллинойс, август, 1966. Том II, стр. 313-317. Термическое сопротивление фазового перехода при конденсации калиевого пара.
4. Субботин В. И. и др. «Теплофизика высоких температур», 1964, № 4, стр. 618.
5. Лабунцов Д. А., Смирнов С. Н. Теплообмен при конденсации калиевого пара. Доклад на 3-й Международной конференции по теплообмену. Чикаго, Иллинойс, август, 1966. Том II, стр. 329-336. Теплоотдача при конденсации паров жидких металлов.
6. R. E. Barry, R. E. Balzhiser. Condensation of Sodium at High Heat Fluxes. Proceedings of 3rd Int. Heat Transfer Conf., v. 2, p. 318-328. Chicago, 1966.
7. S. Sukhatme, W. M. Rohsenow. Film condensation of a liquid metal. ASME Journal of Heat Transfer, s. C, v. 83, p. 19-29, 1961.
8. D. G. Kroger, W. M. Rohsenow. Film condensation of saturated potassium vapour. Int. J. of Heat and Mass Transfer, v. 10, p. 1891-1893, Dec. 1967.

GENERALIZATION OF EXPERIMENTAL DATA
ON HEAT TRANSFER DURING CONDENSATION
VAPOR OF MOVING INSIDE HORIZONTAL
DUCTS UNDER CONDITIONS OF LOW AND
MODERATE VELOCITIES

D. I. Volkov

Designations

- α - coefficient of heat-transfer from the vapor to the wall of the duct;
- q - thermal load of condensation surface;
- δ - depth of placement of the hot junction of the thermocouple in the wall of the duct;
- r - heat of vaporization;
- $\lambda, \nu, \alpha, \mu, \gamma$ - coefficients of thermal conductivity, kinematic viscosity, thermal diffusivity, dynamic viscosity, and specific gravity respectively;
- g - acceleration due to gravity;
- w - phase momentum;
- ϵ - relative evaporation on outlet from the zone of condensation, i.e., relationship of the mass flow rates of vapor in sections $x = L$ and $x = 0$;
- $Nu = \frac{\bar{\alpha}d}{\lambda_f}$ - Nusselt's criterion;

$Re = \frac{\bar{q}L}{rgw}$ - Reynolds number of film of condensate at the end of the condensation surface;

$Pr = \frac{\nu_l}{\alpha}$ - Prandtl number of the condensate;

$Ga = \frac{gd^3}{(\nu')^2}$ - Galileo's criterion;

cr - wall;

'(prime) - the value pertains to the liquid phase;

"(double primes) - to the vapor phase.

Contemporary thermal-power engineering, both stationary and transport, needs precise calculation of the heat surfaces of heat exchange apparatuses with condensation of a vapor moving inside horizontal ducts.

Heat transfer during the condensation of vapors of various substances inside single horizontal ducts has been investigated in references [1-6, 10].

However, these studies do not express a unity of opinion in relation to the calculation recommendations for the coefficient of heat-transfer during condensation of vapor with pressure $p = 2-25$ atm(a) inside horizontal ducts under conditions of average and high thermal loads ($\bar{q} = 50 \cdot 10^3 - 800 \cdot 10^3$ kcal/m²·h).

The analytical study of the question made in [7] cannot serve as a basis for engineering calculations. In connection with this, the author conducted a special study of heat transfer during condensation of steam with $p = 1.3-25$ atm(a) inside four horizontal ducts with internal diameter $d = 17.24$ and 35 mm, with length $L = 2.6$ and 3.1 m, made of various materials.

The study was conducted on two installations specially designed for this purpose. A schematic diagram of both test installations is given in [8].

The installations made it possible to study ducts of various diameter and various length over a wide range of change in the regime parameters. The investigated range of parameters and the basic characteristics of the experimental ducts are given in the table below.

Table. Characteristics of experimental ducts and basic parameters of experiments in the condensation of steam inside horizontal ducts.

Duct material	Dimensions of test section		Pressure of condensing steam p, atm(a)	Thermal load \bar{q} , kcal/m ² ·h	Velocity of steam on inlet to duct, w ₁ " , m/s	Mass flow rate of steam on inlet to duct w ₁ " γ " , kg/m ² ·s
	d, d _H mm	L, m				

First stage experiments (low pressure installation)

Brass	35/42	2.6	1.3-7.3	17·10 ³ - 786·10 ³	1.5-66	3-132
Copper	24/32	2.6	1.3-9.3	16·10 ³ - 1160·10 ³	2-145	4-290
Steel 10	17/22	2.6	1.5-7.0	18·10 ³ - 362·10 ³	3-63	6-126

Second stage experiments (raised pressure installation)

Copper	24/32	3.1	5-25	100·10 ³ - 1100·10 ³	13-167	27-335
--------	-------	-----	------	---	--------	--------

In the experiments saturated steam was used with pressure p = 7-28 atm(a) from a marine water-tube boiler. The saturated steam was directed into a separator in which it was dried to a state x = 0.97-0.98 and then its pressure was reduced to a reducing value to that required calculated so that the degree of superheating of the steam would not exceed 5-20°C.

The average heat flow of the condensation surface of the experimental duct was determined from the quantity of condensate of the heated steam, taking into account the heat of superheat of the steam entering the ducts, and the heat of supercooling of the

steam entering the ducts, and the heat of supercooling of the condensate draining from the duct. The condensate of the heated steam was measured by the weight method with accuracy of ± 50 g.

The mean heat-transfer coefficient was determined from the expression:

$$\bar{\alpha} = \frac{1}{\frac{t'' - \bar{t}_{CT}}{\bar{q}} - \frac{\delta_{CT}}{\lambda_{CT}}} \quad (1)$$

Here \bar{t}_{CT} - mean temperature of the wall of the duct at the sites of the thermocouples, °C; t'' - saturation temperature, °C; \bar{q} - average heat flow, kcal/m²·h; $\frac{\delta_{CT}}{\lambda_{CT}}$ - correction for the depth of placement of the hot junctions of the thermocouples, m²·h·deg/kcal.

Wall temperature t_{CT} was measured both around the perimeter and along the length of the duct at 20-24 points in all by copper-constantan thermocouples made of thin wires \varnothing 0.15 mm.

Measurement of the thermal emf of the thermocouples was conducted according to the compensation method with the use of a P 2/1 potentiometer, a standard cell of class I accuracy, and a 4 V dry battery.

The temperature of the steam on inlet to the experimental duct and the temperature of the condensate on outlet from it were measured by copper-constantan thermocouples made of thin wires \varnothing 0.3 mm. The hot junctions of the thermocouples were soldered with silver solder in the bases of the connections of the thermocouples.

The pressure of the condensing steam was recorded by two standard manometers with scale value of 0.08 kg/cm² each.

The results of check tests obtained over various time intervals of operation of the experimental duct coincided well

with each other, which attests to the reliability of the procedure developed for the placement of the thermocouples.

The entire extent of the study was broken into two stages. During the first stage (the low pressure installation) those thermal loads were investigated at which the process of vapor condensation in horizontal ducts $d = 16-35$ mm was not investigated earlier. Tests were made with brass, copper, and steel tubes with a diameter of 35, 24, and 17 mm respectively and with a length of 2.6 m each. Experiments were conducted with pressures of condensing steam $p = 1.3-9.3$ atm (a), thermal loads $\bar{q} = 17 \times 10^3 - 1100 \times 10^3$ kcal/m²·h, momentum of steam on inlet to the duct $w_1'' = 3.5-61$ m/s ($w_1'' \gamma'' = 3-290$ kg/m²·s).

The second stage experiments were conducted with the raised pressure installation, in which, as in the first stage experiments, heat transfer was investigated during complete condensation of steam with pressure $p = 5.5-25$ atm(a) inside a copper duct $d = 24$ mm, $L = 3.1$ m. Experiments were conducted with thermal loads $\bar{q} = 100 \cdot 10^3 - 1100 \cdot 10^3$ kcal/m²·h, momentum of the steam on inlet to the duct $w_1'' = 13-167$ m/s ($w_1'' \gamma'' = 27-335$ kg/m²·s).

In the first stage experiments a study was made of the effect of thermal load, diameter of the duct and the oxide film (experiments with a steel tube) on heat transfer during the condensation of steam inside horizontal ducts. Control of the thermal load was performed by means of changing the quantity and parameters of the condensing steam.

In the second stage experiments the effect of steam pressure on heat transfer was studied. In these experiments regulating of the magnitude of the thermal load of the condensation surface was achieved by means of changing the quantity of steam being condensed in the duct with its pressure constant.

In all, 124 experiments were conducted. For all experiments the mass flow rate of motion of the steam on inlet to the duct w_1 " γ " did not exceed $335 \text{ kg/m}^2 \cdot \text{s}$. Consequently, the mass flow rates of motion of the steam in the conducted experiments were lower than those which were observed in [5, 6, 10] on condensation of fast moving steam in horizontal ducts. For comparison, it may be pointed out that in [5] the mass flow rates of motion of steam on inlet to the duct were $100\text{--}900 \text{ kg/m}^2 \cdot \text{s}$, while in [6] they were higher yet, namely: $400\text{--}2000 \text{ kg/m}^2 \cdot \text{s}$.

In this way, in this work the experiments were conducted with low and moderate mass flow rates of motion of steam in the duct. During the experiments considerable temperature nonuniformity of the wall of the duct was detected both around the perimeter and along the length of the duct.

As an illustration, Fig. 1 gives graphs of the change in wall temperature around the perimeter and along the length of the experimental copper duct $d = 24 \text{ mm}$, $L = 2.6 \text{ m}$.

In previous works [1-3] on heat transfer during condensation of steam and vapors of benzene and toluene in horizontal ducts the existence of an uncommon dependence between $\bar{\alpha}$ and \bar{q} was indicated, namely: $\bar{\alpha} \sim \bar{q}^{0.43\text{--}0.54}$. The experimental data of the present investigation, taking into account the data of experiments made for the first time on brass, copper, and steel tubes with $\bar{q} = 17 \cdot 10^3\text{--}1100 \cdot 10^3 \text{ kcal/m}^2 \cdot \text{h}$, confirmed the fact of the existence of the indicated dependence between $\bar{\alpha}$ and \bar{q} for all four ducts and in the entire range of change in the regime parameters. This is attested to by the results of the initial processing of the experimental data in logarithmic coordinates in the form of the dependence of $\bar{\alpha}$ on \bar{q} given in Figs. 2 and 3.

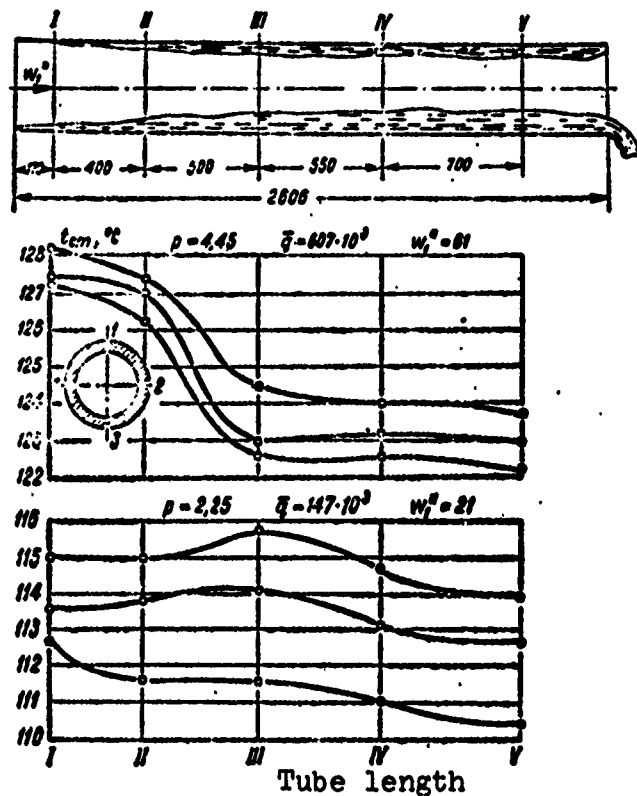


Fig. 1. Graph of change in wall temperature around the perimeter and along the length of an experimental copper tube $d = 24$ mm, $L = 2.6$ m.

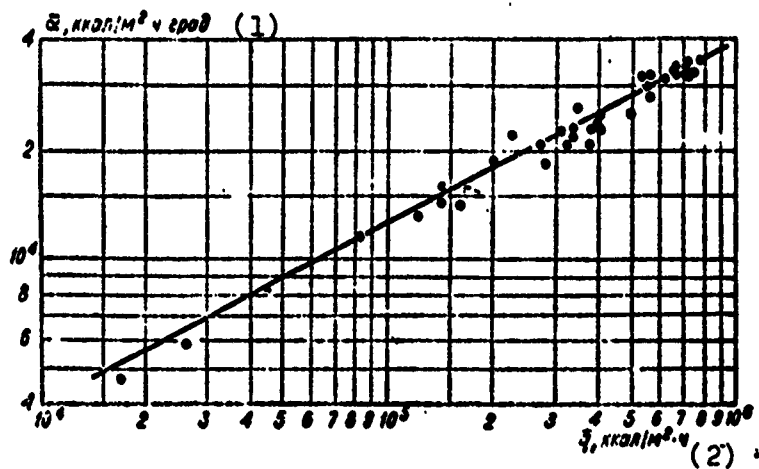


Fig. 2. Graph of dependence of heat-transfer coefficient during steam condensation α on thermal load \bar{q} according to the author's experimental data. Tube, brass, $d = 35$ mm, $L = 2.6$ m.
KEY: (1) α , kcal/m² · h · deg; (2) \bar{q} , kcal/m² · h.

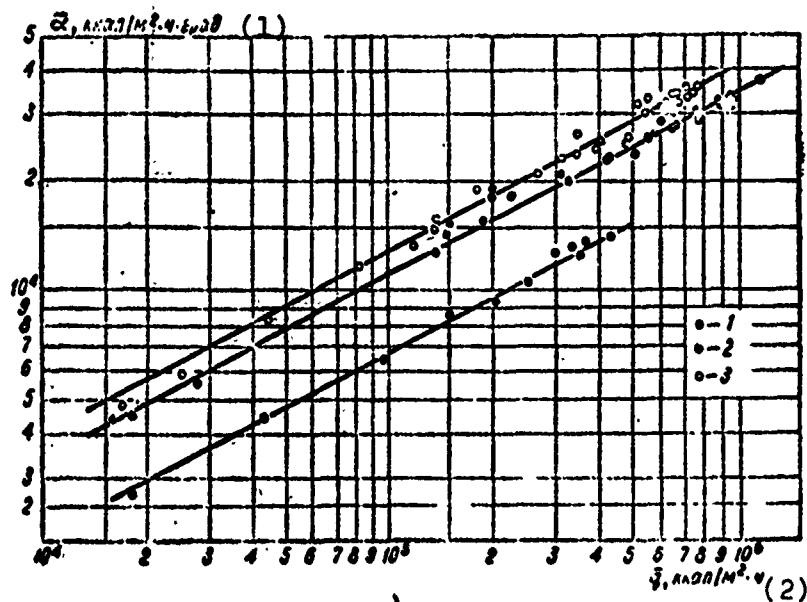


Fig. 3. Graph of dependence of heat-transfer coefficient during steam condensation α on thermal load \bar{q} according to the author's experimental data: 1 - tube, copper, $d = 24$ mm, $L = 2.6$ m; 2 - tube, steel, $d = 17$ mm, $L = 2.6$ m; 3 - tube, brass, $d = 35$ mm, $L = 2.6$ m. KEY: (1) α , kcal/m²·h·deg; (2) \bar{q} , kcal/m²·h.

As follows from these figures, the experimental points for each duct are well placed around logarithmic straight lines conducted with slope equal to 0.5.

The increase in the heat-transfer coefficients with increase in \bar{q} is explained by the effect of velocity of the steam, which for a case of complete steam condensation inside the duct depends upon the thermal load and geometric dimensions of the ducts in the following manner:

$$w_1'' = \frac{4\bar{q}L}{r_1''d} \quad (2)$$

With an increase in velocity of the steam in the initial section of the duct where laminar flow conditions of the condensate exist, the mechanical interaction between the vapor phase and the film of condensate gives rise to a change in average velocity and a decrease in the film thickness, as a consequence of which, there is an increase in heat transfer.

Beginning in some section, external disturbance caused by the flow of steam gives rise to a changeover of the laminar flow conditions of the film to turbulent and, as a consequence of this, to the appearance in the film of molar heat transfer, the intensity of which is the higher, the greater the velocity of the steam and the mechanical interaction between phases.

There are studies in which, at low and moderate speeds of steam inside horizontal ducts there were obtained other dependences between $\bar{\alpha}$ and \bar{q} . Thus, for instance, in [4] the study conducted at low speeds of motion of steam inside two horizontal ducts, with low pressures and thermal loads ($w_1'' = 2-5$ m/s; $w_1''\gamma'' = 2-7$ kg/m²·s; $p = 1-3$ atm(a); $\bar{q} \leq 24 \cdot 10^3$ kcal/m²·h), it was established that $\bar{\alpha} \sim \bar{q}^{0.69}$. This dependence is close to those to those which are observed in experiments on the condensation of fast moving vapors inside ducts. In [5] at moderate velocities of vapor condensing inside a horizontal tube of stainless steel $w_1'' = 0.5-20$ m/s; $w_1''\gamma'' = 40-90$ kg/m²·s; $p = 10-90$ atm(a); $\bar{q} = 50 \cdot 10^3-500 \cdot 10^3$ kcal/m²·h), a dependence of the type $\bar{\alpha} \sim \bar{q}^{0.1}$ was obtained.

Today, in view of the small quantity of experimental data on vapor condensation inside horizontal ducts, it is difficult to establish the causes of the disagreements indicated.

As a result of further processing of the experimental data obtained on ducts of various diameter ($d = 24$ and 35 mm) and

identical length ($L = 2.6$ m) it was established that in the range of the investigated parameters, with an increase in the internal diameter of the duct, the mean heat-transfer coefficient increases in proportion to $d^{0.2}$.

As is known, during the condensation of fast moving vapor inside horizontal ducts, the effect of gravity on heat transfer is slight. Under these conditions, as follows from expression (2), with an increase in diameter of the duct the velocity of the vapor in it decreases, and consequently, heat transfer decreases. During condensation inside the ducts of a vapor which possesses low and moderate velocities, heat transfer is greatly affected by gravity, the force of the surface tension of the film and the floodability of the duct by the stream of condensate flowing in the bottom of the duct. Under these complex conditions an increase in $\bar{\alpha}$ is possible with an increase in \bar{q} . This is contributed to, for example, also by the fact that with an increase in d , other conditions being equal, the floodability of the duct by the stream of condensate and others decreases.

As follows from Fig. 3, with identical length of ducts and identical \bar{q} the heat-transfer coefficient of the steel tube is approximately 40% lower than for copper. The decrease in $\bar{\alpha}$ for a steel oxidized duct, as compared with copper, is explained by the effect of the oxide film covering the surface of the steel tube (the effect of the diameter of the duct on thermal conductivity does not exceed 4-5%). The oxide film, possessing high thermal resistance, considerably decreases the coefficient of heat transfer from the vapor to the wall of the duct. Such a reduction is also contributed to by the fact that the rough oxide film renders a braking action on the flowing film of condensate and causes an increase in the thickness of the laminar sublayer of condensate over the entire surface.

Figure 4 gives the results of processing of the experiments in the condensation of steam with pressure $p = 5.5-25 \text{ atm(a)}$ inside a horizontal copper duct $d = 24 \text{ mm}$, $L = 4.1 \text{ mm}$ (the experiments of the second stage on the raised pressure installation). Earlier it was pointed out that in the experiments of the second stage a study was made of the effect of the pressure of the condensing vapor on heat transfer.

As follows from Fig. 4, in the range of change in pressure of the vapor from 5.5 to 25 atm(a), the effect of the vapor pressure on heat transfer is slight. Only careful analysis of the experimental data makes it possible to observe a certain very insignificant decrease in the heat-transfer coefficient with an increase in vapor pressure from 10 to 25 atm(a). In so doing, it is obvious that the vapor pressure has an effect on the absolute value, but not on the character of the dependence of $\bar{\alpha}$ on \bar{q} . However, it is hardly worthwhile to consider such an insignificant effect of the vapor pressure in practical calculations. As follows from Fig. 4, through the experimental points corresponding to various pressures, it is possible to conduct one averaging logarithmic straight line with a gradient equal to 0.5.

The effect of the vapor pressure on heat transfer during condensation was investigated in more detail and with the inclusion of a greater quantity of experimental data in [9]. According to the data in this source, for water in the region $p/p_{\text{kp}} \leq 0.01$ an increase in vapor pressure gives rise to an insignificant increase in heat transfer, in the region $0.01 < p/p_{\text{kp}} < 0.1$ an increase in pressure has practically no effect on heat transfer, and in region $p/p_{\text{kp}} \geq 0.1$ an increase in pressure gives rise to a decrease in heat transfer.

The results in [9] completely agree with the results of experimental data on vapor condensation inside horizontal ducts [1-6] and with the results of this study, and also with

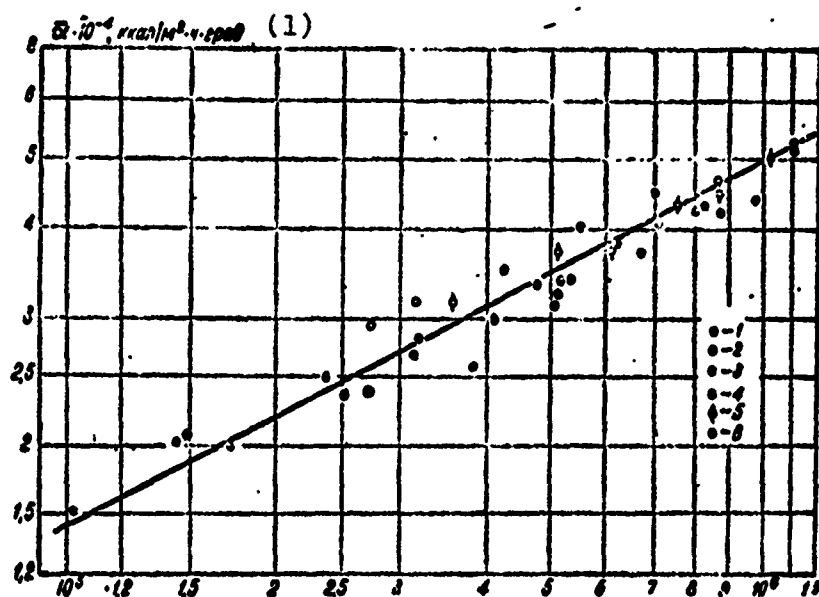


Fig. 4. Graph of the dependence of heat-transfer coefficient during vapor condensation α on thermal load according to the author's test data. Tube, copper, $d = 24$ mm, $L = 3.1$ m: 1 - pressure of condensing vapor $p = 5.5$ atm(a); 2 - $p = 10$ atm(a); 3 - $p = 7$ atm(a); 4 - $p = 17.5$ atm(a); 5 - $p = 20.5$ atm(a); 6 - $p = 24.8$ atm(a). KEY: (1) $\alpha \cdot 10^{-4}$ kcal/m² · h · deg.

the results of a large quantity of experimental data on vapor condensation on the outside of horizontal and vertical ducts.

In this way, with the publication of [9], the question of the effect of pressure on heat transfer during the condensation of vapor with low and moderate speeds of motion can be considered resolved.

A comparison of the experimental data obtained on two copper ducts $d = 24$ mm, with length $L = 2.6$ and 3.1 m made it possible to establish the effect of the length of the duct on heat transfer.

As the results of the processing of the experimental data showed, with an increase in the length of the duct the mean heat-transfer coefficient increases in proportion to $L^{0.3}$. The obtained result agrees well with the experimental data of other authors who conducted an investigation of heat transfer during condensation in horizontal ducts of vapor with low and moderate inlet velocities.

Generalization of the experimental data of the author of the article, and also the experimental data of other authors who investigated heat transfer during vapor condensation in horizontal ducts under conditions of low and moderate speeds of motion, was conducted on the basis of performed theoretical analysis, the results of which have are presented in [7].

From theoretical analysis it follows that

$$\frac{\bar{\alpha}d}{\lambda'} = f\left(\frac{\bar{q}L}{rg\lambda'}; \frac{v'}{a'}; \frac{ga^3}{v'^2}; \frac{\gamma'}{\gamma}; \frac{v'}{v''}; \frac{L}{d}; \epsilon\right). \quad (3)$$

For particular cases of vapor condensation inside horizontal ducts, the form of this dependence is simplified. During complete vapor condensation in horizontal ducts under conditions of low and moderate speeds of motion, the experimental data are generalized by the following dependence:

$$Nu = c Re^{0.5} (Ga Pr)^{1/3} \left(\frac{L}{d}\right)^n$$

or

$$\frac{\bar{\alpha}}{\lambda'} \left(\frac{v'a'}{g}\right)^{1/3} = c Re^{0.5} \left(\frac{L}{d}\right)^n. \quad (4)$$

As the results of the initial processing of the experimental data of this study showed, $\bar{\alpha} \sim \bar{d}^{-0.2}$ and $\bar{\alpha} \sim L^{0.3}$. Therefore, the exponent of the simplex L/d can be taken as equal to -0.2, i.e., $n = -0.2$ (it is considered that the value L enters into the Re number of the film of condensate).

Figure 5 gives the generalized analysis in coordinates

$$\frac{\bar{\alpha}}{k'} \left(\frac{v' a'}{g} \right)^{1/3} \left(\frac{L}{d} \right)^{0.3} = f(Re)$$

of the author's experimental data and the experimental data of [1, 4] in the condensation of steam with pressure $p = 1-25$ atm(a) and at thermal loads $\bar{q} = 8 \cdot 10^3 - 1160 \cdot 10^3$ kcal/m²·h inside clean unoxidized brass and copper ducts (a total of 190 experiments).

As follows from Fig. 5, all the experimental data on the condensation of steam inside copper and brass ducts are satisfactorily grouped around the logarithmic straight line, equation of which takes the form

$$\frac{\bar{\alpha}}{k'} \left(\frac{v' a'}{g} \right)^{1/3} = 0.031 Re^{0.5} \left(\frac{L}{d} \right)^{-0.2}. \quad (5)$$

The data presented in Fig. 5 cover a range of change in Re number, $Re = 20-14,700$, diameters of ducts $d = 24-38$ mm, and lengths $L = 1.15-3.1$ m.

Figure 6 gives generalized analysis in coordinates

$$\frac{\bar{\alpha}}{k'} \left(\frac{v' a'}{g} \right)^{1/3} \left(\frac{L}{d} \right)^{0.3} = f(Re)$$

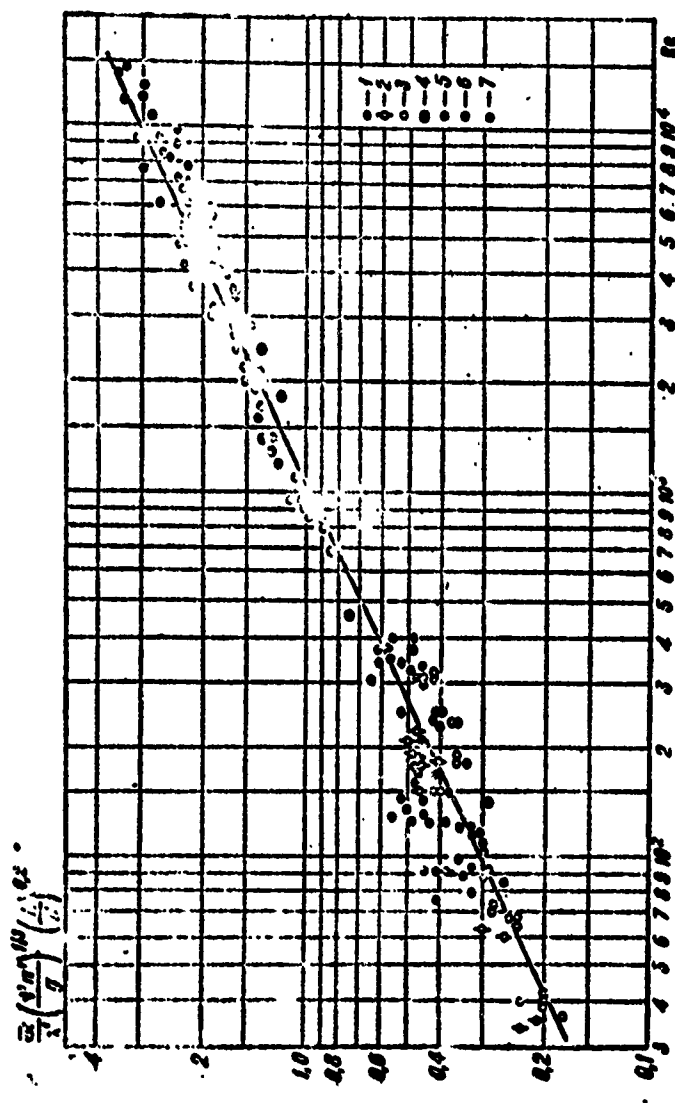


Fig. 5. Generalization of experimental data on heat transfer during condensation of steam inside copper and brass horizontal ducts: 1 - $L = 2.79$ m, $d = 24$ mm; 2 - $L = 1.15$ m, $d = 33$ mm; 3 - $L = 1.15$ m, $d = 24$ mm ($p = 3.1$ atm(a)) - experimental data [1]; 4 - $L = 2.6$ m, $d = 35$ mm; 5 - $L = 2.6$ m, $d = 24$ mm; 6 - $L = 3.1$ m, $d = 24$ mm ($p = 1.3-25$ atm(a)) - author's experimental data; 7 - $L = 2.61$ m, $d = 30$ mm ($p = 1-3$ atm(a)) - experimental data [4].

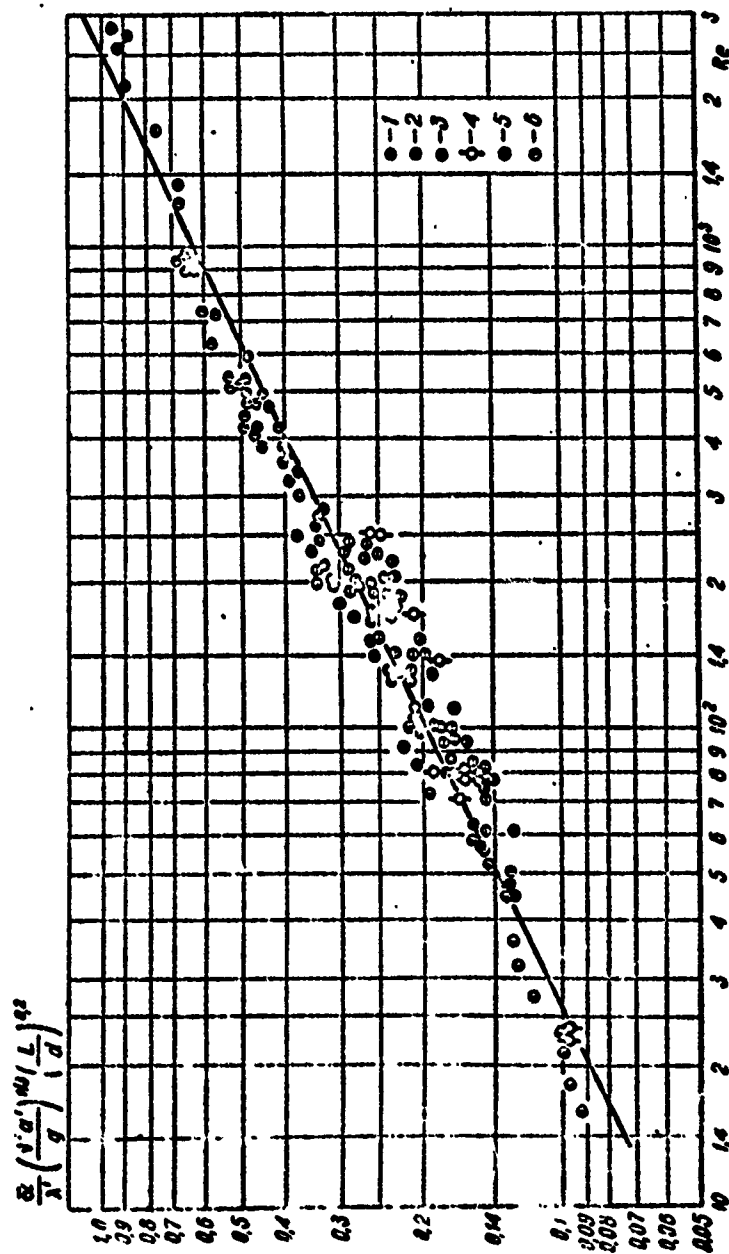


Fig. 6. Generalization of experimental data on heat transfer during condensation of steam, vapors of ammonia and of toluene, inside steel horizontal ducts: 1 - $L = 1.95$ m, $d = 10$ mm; 2 - $L = 1.0$ m, $d = 10$ mm (ammonium vapor $p = 8.11$ and 14 atm(a)) - experimental data [2]; 3 - $L = 1.15$ m, $d = 35.6$ mm; 4 - $L = 4.14$ m, $d = 31$ mm (steam $p = 1-3$ atm(a)) - experimental data [1]; 5 - $L = 2.6$ m, $d = 17$ mm (steam $p = 1.5-7$ atm(a)) - author's experimental data; 6 - $L = 1.0$ m, $d = 12$ mm (toluene vapor $p = 1-20$ atm(a)) - experimental data [3].

of the author's experimental data and those of [1] on the condensation of steam with pressure $\bar{p} = 1.3-7.0$ atm(a) and with $\bar{q} = 8 \cdot 10^3-350 \cdot 10^3$ kcal/m²·h, of the data of [2] on the condensation of ammonia vapor with pressure $p = 8.11$ and 14 atm(a) and with $\bar{q} = 2 \cdot 10^3-26 \cdot 10^3$ kcal/m²·h, and data of [3] on condensation of toluene vapor with $\bar{p} = 1-2$ atm(a) and with $\bar{q} = (3-6) \cdot 10^4$ kcal/m²·h, inside steel oxidized ducts (a total of 210 experiments).

As follows from Fig. 6, the experimental data on the condensation of steam, and vapors of ammonia and toluene inside steel oxidized ducts are also satisfactorily grouped around the logarithmic straight line, the equation of which takes the form:

$$\frac{\bar{q}}{\lambda^*} \left(\frac{\nu' a'}{d} \right)^{1/8} = 0.02 \text{Re}^{0.5} \left(\frac{L}{d} \right)^{-0.2}. \quad (6)$$

The data presented in Fig. 6 cover a range of change in Re number, $\text{Re} = 15-2800$, diameters of ducts $d = 10-17$ mm and lengths $L = 1.0-4.14$ m. The scatter of points around the logarithmic straight lines in Figs. 5 and 6 does not exceed $\pm 20\%$. Formulas (5) and (6) within the limits of the indicated ranges of change in parameters and in geometric dimensions of ducts can be recommended for the calculation of heat transfer during the condensation of steam and vapors of ammonia and also vapors of toluene inside brass, copper, and steel oxidized ducts. In formulas (5) and (6) the physical constants of the condensate are determined from saturation temperature t'' .

BIBLIOGRAPHY

1. Кутателадзе С. С. Теплоотдача при пленочной конденсации пара внутри горизонтальной трубы. Сб.: «Вопросы теплоотдачи и гидравлики двухфазных сред». Госэнергоиздат, 1961.
2. Городническая С. А. К вопросу обобщения опытных данных по теплоотдаче при конденсации внутри горизонтальных труб. «Известия КПИ», т. 18, ГИТЛ, УССР, 1955.
3. Юсуфов В. Д. Экспериментальное исследование процесса теплоотдачи при конденсации бензола и толуола внутри горизонтальных конденсаторов. «Известия АН АССР», т. 2, 1953.

4. Матидеев Л. Л. Автореферат диссертации ЛГПИ, 1953.
5. Консетов Б. В. Экспериментальное исследование теплоотдачи при конденсации чистого насыщенного пара высокого давления внутри горизонтальных и слабонаклонных труб. «Теплоэнергетика», 1960, № 12.
6. Миропольский З. Л. Конденсация пара высокого давления внутри труб. «Теплоэнергетика», 1952, № 3.
7. Волков Д. И. Теплоотдача при конденсации пара внутри горизонтальных труб. «Труды ЦИТИ», вып. 57, Л., 1965.
8. Волков Д. И. Теплоотдача при конденсации пара внутри горизонтальных труб. «Судостроение», 1960, № 11.
9. Борншанский В. М., Кочурова Н. Н. Общий метод учета влияния физических свойств на теплоотдачу при конденсации. Сб.: «Конвективная теплопередача в двухфазном и однофазном потоках». Изд. «Энергия», 1964.
10. Бобков Л. Д., Кружilin Г. Н. Теплоотдача при конденсации пара в трубе. «Изв. АН СССР. Энергетика и транспорт», 1966, № 5.

A STUDY OF QUESTIONS OF THE KINETICS OF CONDENSATION OF WATER

N. N. Kochurova

The condensation rate of vapor is defined by the process of supply of vapor to the condensation surface and by the process of capture of molecules of vapor found on the surface. The latter fact is considered by the so-called "coefficient of condensation" f . Characterizing in essence the surface condition of the condensate and the interaction of the condensing molecules with the condensation surface, the coefficient of condensation, to a considerable degree, defines the kinetics of the process of condensation.

In the table, values are given for the coefficients of condensation for water from the results of measurements made by various authors. The variance in the experimental data obtained is great. The values of f differ from one another 10-100 times.

In measurements of the coefficient of condensation there may be considerable errors which appear as a result of the great experimental difficulties appearing in the measurements of the surface temperature, in the removal or allowing for the presence of air, in considering the various change with time of the temperature of the vapor and of the surface, and in accounting for the appearance of surface contaminations.

Coefficient of condensation	Author
Group I	
0.002	Heidrich [1]
0.003	Silver, Simpson [2]
0.01	Marselin [3]
0.015	Alty and Nicoll [4]
0.02	Prüger [5]
Group II	
0.03	Sayns [6]
0.034	Baranayev [7]
0.036	Alty [8], Silver and Mitchell [9]
0.04	Wyllie [10], Alty and Mackay [11]
0.027-0.042	Delaney et al. [12]
0.045	Hammeke and Kappler [13]
Group III	
0.1	Kappler and Hammeke [14]
0.24-0.42 up to 1	Hichman [15]
0.35	Jamieson [16]
0.35-1	Nabavian, Bromley [17]
∞	Berman [18]

Errors in the measurements of surface are especially numerous. In the surface layer of water, the so-called "thermal boundary layer," with a thickness of water of some tenths of millimeters (~ 0.66 mm) a temperature drop of several degrees is accomplished [5]. The introduction even of fine thermocouples causes a disruption of the surface layer. However, the special procedures used by a number of authors for measurement of the surface temperature of the condensate with the aid of an interferometer, procedures for the removal of noncondensing gases, etc. (see, for example, [15, 16] and others) they make it possible to eliminate or to allow for possible errors of measurement.

All the data in the table with some approximation can be arbitrarily divided into three groups: Group I - $f < 0.03$, Group II - $f \approx 0.04$, Group III - $f \geq 0.1$.

The very low values of the coefficient of condensation of water $f < 0.03$ (Group I) are usually explained by presence on the surface of the water of surface-active substances. According to [27], with a decrease in surface tension to 28 dyn/cm, by introducing surface-active substances, the coefficient of condensation was reduced by 10-60%. In Mackay's experiments, and later in those of Prüger [5] and others, the effect of a solution of glass in water on the rate of evaporation was investigated. It was noticed that with the use of leached glass vessels the rate of evaporation was almost twice that with the use of regular vessels.

The greatest values of the coefficient of condensation $0.1 < f \leq 1$ (Group III) were obtained by researchers in experiments on condensation with streams on a renewed, fast-moving surface of water [15, 16, 17, 18]. In those experiments where the surface of the water was clean and found at rest the coefficient of condensation proved to be equal to $f \approx 0.04$.

Calculation of the coefficient of condensation frequently proves to be difficult due to the absence of data on the structure of the surface layer of condensate and the nature of the vapor-condensate interaction.

The surface layer of the liquid has a special structure and differs in its properties from the volumetric phase.

In water which possesses an especially complex structure caused by hydrogen bonds, dipole-dipole and dispersive forces, one should expect the appearances of different features in the surface layers. Thus, as a result of the strong polarity of the water, on its surface there is observed molecule-dipole orientation, which

can lead to the appearance of a potential jump in the surface layer, to change the character of rotation of the molecules, etc.

The existence of a defined structure of surface layer is confirmed by the sharp distinction of dynamic and static surface tensions of the water. Dynamic surface tension is several times higher than the static surface tension. Dynamic surface tension is measured at the moment of rupture of some volume of liquid, at the moment of formation of the new surface (for example, on streams of fluid issuing at high speed from an opening). A number of authors note that the dynamic surface tension is inversely proportional to the time required for the formation of surface, which is linked with the formation of surface structure. The more rapidly the reorientation of molecules and reorganization occurs on the surface, i.e., the more rapidly the transition from unstable to equilibrium of surface is accomplished, the more rapidly the value of dynamic surface tension approaches the static value.

Anomalies in the changes in surface potential, surface entropy, and in surface tension with a change in temperature attest to the rather complex structure of the water surface. Anomalies were observed, for example, at 15, 30, 45, and 60°C.

There are several attempts at calculating the coefficient of condensation of water on the basis of calculating the structural features of its surface. Thus, Mortensen and Eyring [23], explaining the difference in the internal states of the vapor and condensate by limitation of the rotation of molecules in the condensate as a result of the surface orientation of dipoles, calculated the coefficient of condensation, comparing the statistical sums of rotation for water and nonpolar liquid CCl_4 by the formula:

$$f = \frac{P_{\text{CCl}_4} T_{\text{H}_2\text{O}}}{T_{\text{CCl}_4} P_{\text{H}_2\text{O}}} e^{-\Delta S/R}, \quad (1)$$

where p , T - pressure and temperature of water and CCl_4 , found in corresponding states; δS - the difference in the entropy of vaporization for water and CCl_4 . Calculation according to formula (1) gives a value $f = 0.036$.

Analogous calculations of the coefficients of condensation by comparison of the entropy of water and CCl_4 under certain other assumptions were performed by a number of authors [19, 21]. However, the results of these calculations agree less with the experimental value of the coefficient of condensation for the static surface of water $f = 0.04$.

The coefficient of condensation can be calculated, knowing the moment of inertia and frequency of vibration of the molecules [22]. f also proves to be approximately equal to 0.04.

The coefficient of condensation can be determined from examination of the following sufficiently general model [24].

The coefficient of condensation by definition is the probability of condensation of the molecules which strike the condensation surface. The probability of the course of process (with a clean surface of condensate) depends upon the activation energy, whereby the activation energy during evaporation ϵ_v is connected with the activation energy during condensation ϵ and the heat of vaporization r by the relationship:

$$\epsilon = \epsilon_v - r.$$

If we consider the molecules of the condensate as molecules of vapor located in a potential well $u_0 = r$ and we take the potential interaction energy of the molecules of vapor as equal to zero, then the coefficient of condensation can be determined as the probability of transition of the molecules from one region to another [with $\epsilon = 0$ (Fig. 1a) and with $\epsilon \neq 0$ (Fig. 1b)]. In such a model, $f = \exp\left(-\frac{\epsilon}{kT}\right)$. With $\epsilon = 0$, $f = 1$ with $\epsilon \neq 0$, $f < 1$.

The entire difficulty in calculating the coefficient of condensation consists in determining the activation energy ϵ .

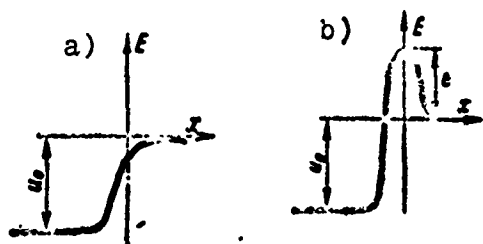


Fig. 1. Model for the calculation of the coefficient of condensation: a - $\epsilon = 0$; b - $\epsilon = 0$.

M. Baranayev [7] assumed that as a result of the orientation of the molecules of water on the surface, a decrease in its surface energy E by the value of δE occurs, which he calculated by means of comparison of the surface energy of water and CCl_4 at corresponding temperatures $T = aT_{\text{кр}}$.

$$\delta E = \Delta r_{\text{H}_2\text{O}}; \Delta = \left(\frac{E}{r}\right)_{\text{CCl}_4} - \left(\frac{F}{r}\right)_{\text{H}_2\text{O}}.$$

M. Baranayev considered that during condensation to water molecules there is required supplementary energy δE for disruption of surface orientation. The value of δE in it was actually the activation energy. Calculating the coefficient of condensation in the formula:

$$f = e^{-\frac{\delta E}{kT}},$$

he obtained $f = 0.034$.

The activation energy can be determined by the difference in dynamic and static tension. Then when $t = 20^\circ\text{C}$, we find:

$$f = \exp\left(-\frac{\epsilon}{kT}\right) = 0.07,$$

where $\epsilon = (\sigma_{\text{дин}} - \sigma_{\text{стат}})S$;

$\sigma_{\text{дин}}$ - the dynamic surface tension is taken as equal to 180 dyn/cm [22];

$\sigma_{\text{стат}}$ - the static surface tension equal to 72.6 dyn/cm;

$S = \left(\frac{M}{N\gamma}\right)$ - the area of one molecule on a surface of the liquid, $\text{cm}^2/\text{molecule}$ [20];

M - molecular weight;
N - Avogadro's number;
 γ - specific weight.

The value $f = 0.07$ is close to the experimental data of group II of the table in definition of the coefficient of condensation for a static clean surface of water. However $\sigma_{\text{дин}} = 180$ dyn/cm, possibly, is not that (greatest) value of dynamic surface tension which corresponds to the true moment of rupture of some volume of the liquid and formation of a new surface, i.e., to the surface condition corresponding to the maximum deviation from static state with minimum surface tension. When $\sigma_{\text{дин}} > 180$ dyn/cm, f will be less than 0.07.

If we take $\sigma_{\text{дин}} = 100$ dyn/cm (which will correspond to lesser deviation of the structure of the surface from the static state, than when $\sigma_{\text{дин}} = 180$ dyn/cm) then we will obtain a value $f = 0.15$.

Of interest also is the following fact. The probability of normal (to the surface) orientation of molecules is equal to $1/3 \approx 0.033$. It can be said that the probability of the appearance of a "feature" on the surface (deviations of its structure from the volumetric structure of the liquid) is equal to 0.033. This value corresponds to $f \approx 0.04$ for a static surface. The correlation of these values is clear, since by the coefficient of condensation are considered all the possible difficulties of the condensation process connected with the structure of the surface.

In this way, the change in orientation of the molecules on the surface, the structure of the surface layer determine the value of the coefficient of the condensation of water. Turning again to the table, it is possible to make the following classification of the experimental data:

- Group I - the values of the coefficients of condensation of water obtained for a static surface in the presence of surface-active

substances decreasing the surface tension and the coefficient of condensation;

— Group II — the values of the coefficients of condensation obtained for a clean, static surface of water;

— Group III — the values of coefficient of condensation obtained under conditions of an increase in the surface tension of water, and disruption of the surface orientation of the molecules.

In this way, the coefficient of condensation for a static surface of water, with sufficient accuracy, can be taken as equal to 0.04.

To obtain reliable data on the kinetics of the process of the condensation of water under various conditions requires research into the change in the structure of the surface layer of the water, depending on the conditions of experimentation.

BIBLIOGRAPHY

1. Heidrich Z. I. Techn. Phys. Bd. 14, 1933, s. 81.
2. Silver R. S. and Simpson H. C. Cw. [15].
3. Marçelin M. R. Comptes Rendus, v. 158, 1914, p. 1674.
4. Alty T., Nicoll F. H. Canad J of Research.
5. Prüger W. Z. I. Phys. Bd. 115, 1940, s. 202.
6. Френкель Я. И. УФН, 1938, 20, № 1, 84.
7. Баранов М. ЖФХ, т. 13, 1939, стр. 1635.
8. Alty T. Prog. Roy. Soc., A-131, p. 554, 1931; Phil. Mag., 15, p. 82, 1933.
9. Silver R. and Mitchell J. A. Trans. NEC Inst., E and S. Dec. 1945.
10. Wyllie L. Prog. Roy. Soc., A, 1949, 197, № 1050, 383.
11. Alty T. a. Mackay C. A. Prog. Roy. Soc., A, 1935, 149, 104.
12. Delaney Z. F., Houston R. W., Eagleton L. C. Chem. Engng. Sci., vol. 19, Febr. 1964, pp. 105—114.
13. Hammeke K. u. Kappler E., Geophys. E. Sonderband (1953), 181.
14. Kappler E. u. Hammeke K. Forschungsber. Wirtschafts und Verkermin, 1955, NRW, 125.
15. Hichman K. C. D. Industr. and Ing. Chem., 1954, 46, № 7, 1442.
16. Jamieson D. T. NEL Report, № 186, Ministry of Technology, 1965.
17. Nabavian K., Bromley L. A. Chem. Engng. Sci., vol. 18, Oct. 1963, pp. 651—660.
18. Берман Л. Д. Процессы фазового превращения в разреженной среде и методы расчета теплохимических аппаратов. «Труды НИИХИМ.Маша», вып. 36. М., 1961, стр. 66.
19. Hildebrand J. H. J. Chem. Phys., 7, 233 (1939).
20. Френкель Я. И. Собрание избранных трудов Т. III. М. — Л., изд. АН СССР, 1959.
21. Pitzer K. S. J. Chem. Phys., 7, 583 (1939).
22. Kincaid J. F., Eyring H. J. Chem. Phys., 6, 620 (1938).
23. Mortensen E., Eyring H. Phys. Chem., 1960, v. 64, p. 846.
24. Кочурова Н. Н. К вопросу о коэффициенте конденсации. ИФЖ, 1964, № 3; О расчете коэффициента конденсации ИФЖ, 1965, № 6, т. 8.
25. Jonsione R. K. M., Smith W. J. Sci. Inst., 1965, 42, 231—235.

CONDENSATION OF CESIUM VAPORS FROM A FLOW OF INERT GASES

K. M. Aref'yev, V. M. Borishanskiy,
T. V. Zablotskaya, N. I. Ivashchenko,
I. I. Paleyev and B. M. Khomchenkov

In the magnetohydrodynamic closed-cycle generators, inert gases - helium or argon are used as working bodies [1]. In order to achieve electrical conductivity, to these gases there are added in small quantities (up to several percentages) vapors of easily ionized substances - cesium or potassium, having the lowest ionization potentials. After the fuel channel of the MHD-generator before the supply of gas to the compressor, the additions must be removed from the flow. This can be achieved (at least partially) because of condensation on the radiator surface during the cooling of the gas [2]. The condensation of small admixtures is determined by the rate of their diffusion through the boundary layer to the cooling surfaces [3]. The thermal resistance of the layer of condensate in the case of alkali metals is very slight due to their high thermal conductivity [4, 5]. Therefore, the temperature of the layer of condensate can be considered as coinciding with the temperature of the cooling surface. The partial pressure of the vapor near the surface will, in practice, be equal to the saturation pressure at this temperature.

Diffusion of the admixtures through the gaseous film bears a molecular nature. Therefore, during calculation of condensation

it is possible to use the regularities of molecular diffusion. The fundamental principles of diffusion for binary mixtures are discussed below and the computed values of diffusion coefficients are given, and also examples of calculations of the condensation of cesium, illustrating the effect of different factors. It is still necessary to bear in mind that at comparatively low surface temperatures and not very small contents of the admixtures being condensed the rate of their diffusion through the boundary layer of the surface (formation of mist) is determined. In this article this question is not examined comprehensively.

1. GENERAL POSITIONS OF THE THEORY OF DIFFUSION. CALCULATION OF THE COEFFICIENT OF DIFFUSION

A strict theory of diffusion phenomena based on the solution of the Boltzmann equation for the distribution function of molecules according to energy, and considering the detailed character of the interaction of molecules, has been developed by Enskog and Chapman [6, 7]. This theory, valid for not very dense gases, gives rise to the following expression for flow g_1 of one of the components of the binary mixture:

$$g_1 = - \frac{n^2}{\rho} m_1 m_2 D_{12} \left[\text{grad} \frac{n_1}{n} + \frac{k_T}{T} \text{grad} T \right], \quad (1)$$

where

n - the total number of molecules per unit of volume;

ρ - the mass density of the mixture;

m_1 and m_2 - the molecular mass of the components of the mixture;

D_{12} - the diffusion coefficient for a binary mixture;

n_1 - the number of molecules of the first component per unit of volume;

T - temperature;

$k_T = \frac{\rho}{n m_1 m_2} \cdot \frac{D_{12}}{D_{12}}$ - thermal diffusion ratio;

D_1^T - the thermal diffusion coefficient for the first component.

Diffusion flow g_1 determines the mass of the first component being transferred through a unit of section in a given time.

The first term in the formula for diffusion flow expresses flow proportional to gradient of the relative partial concentrations (or pressures) and directed counter to this gradient.

The second term determines thermal diffusion flow proportional to $\frac{1}{T} \text{grad} T = \text{grad} \ln T$. The coefficient of thermal diffusion D_1^T , and therefore, the thermal diffusion ratio k_T can be both positive and negative. For mixtures of all the usual gases (not ionized) at not too low temperatures, the heavier molecules (or those having larger dimensions) move because of thermal diffusion in the direction of lower temperatures (i.e., counter to the temperature gradient), while the lighter (or those having smaller dimensions) - in the direction of higher temperatures. This determines the sign of D_1^T and k_T . If we designate the heavier or larger molecules by the subscript 1, then D_1^T and k_T will be positive. With a temperature decrease k_T decreases, and at low temperatures the inversion temperature can be reached, when the sign of k_T changes. Correspondingly the direction of thermal diffusion flows changes.

For the second component of the mixture $D_2^T = -D_1^T$ and thermal diffusion flow is identical in value to the thermal diffusion flow of the second component, but counter directed. Identical in value and opposite in direction are the component diffusion flows, connected with gradients n_1/n and n_2/n , where $n_2 = n - n_1$ - the number of molecules of the second component per unit of volume.

In this way, as a whole, the flow of the second component $g_2 = -g_1$. The equality of the opposite diffusion flows of the

components, being expressed in mass units, satisfies the hydrodynamic continuity equation. The hydrodynamic equation of motion of the medium (Navier-Stokes equation) written in a center-of-mass system is not disturbed due to the diffusion component [7, 8]. However, if the mass of any component in the gaseous environment changes because of physical (condensation, evaporation) or chemical processes, then again supplementary mass diffusion flow appears, usually called Stefanovskiy flow [3 and others]. Below we give the expressions for diffusion flows, taking into account Stefanovskiy flow, first converting expression (1).

We use the relationships for an ideal gas:

$$n = \frac{P}{kT}, \quad n_1 = \frac{p_1}{kT}, \quad n_2 = \frac{P - p_1}{kT},$$

$$\frac{n_1}{n} = \frac{p_1}{P}, \quad N_A k = R, \quad m_1 = \frac{M_1}{N_A}, \quad m_2 = \frac{M_2}{N_A} \text{ and}$$

$$j = m_1 n_1 + m_2 n_2 = m_1 \frac{p_1}{kT} + m_2 \frac{P - p_1}{kT},$$

where

P - total pressure of the mixture, which in our case can be considered as constant;

k - Boltzmann constant;

p_1 - partial pressure of the first component;

$P - p_1 = p_2$ - partial pressure of the second component;

N_A - number of molecules per one mole of ideal gas (Avogadro's number);

R - universal gas constant;

M_1 and M_2 - molecular weight of the first and second components.

Taking into account these relationships we obtain

$$g_1 = - \frac{M_1 P D_{12}}{RT} \cdot \frac{M_2}{(M_1 - M_2) \frac{p_1}{P} + M_2} \left[\text{grad} \frac{p_1}{P} + \frac{k_1}{T} \text{grad} T \right] = -g_2. \quad (2)$$

Flows g_1 and g_2 , passing through a unit of section in a unit of time, will be expressed in units of mass or weight.¹

In the presence of Stefanovskiy flow, full diffusion flow will be written thus:

$$g_1 = - \frac{M_1 P D_{12}}{RT} \cdot \frac{M_2}{(M_1 - M_2) \frac{P_1}{P} + M_2} \left[\text{grad} \frac{P_1}{P} + \frac{k_1}{T} \text{grad} T \right] + w_M \frac{M_1 P_1}{RT}, \quad (3)$$

where w_M - rate of mass flow.

In the case of condensation (or evaporation) the mass flow rate can be found from the condition of impenetrability for the second (inert) component of the phase interface and the condition of constancy of total pressure. During condensation, the diffusion flow of the second component directed from the wall, induced by gradients p_2/P and T , should be compensated by the mass flow directed to the wall. Total flow of the second component should be equal to zero:

$$g_2 = \frac{M_2 P D_{12}}{RT} \cdot \frac{M_1}{(M_1 - M_2) \frac{P_1}{P} + M_2} \left[\text{grad} \frac{P_1}{P} + \frac{k_1}{T} \text{grad} T \right] + w_M \frac{M_2 (P - P_1)}{RT} = 0. \quad (4)$$

Whence we obtain that

$$w_M = g_1' \frac{RT}{M_2 (P - P_1)}, \quad (5)$$

where

g_1' - flow of the first component without Stefanovskiy flow, expressed by formula (2) (taking the sign into account).

Substituting (5) in (3), we obtain

¹This depends on the accepted dimensionality of R . In the SI system of units $R = 8.32 \cdot 10^3$ J/kmole·deg, while in the technical system $R = 848$ kgm/kmole·deg.

$$g_1 = g_1' - g_1' \frac{M_1 g_1}{M_2 (P - p_1)} = g_1' \frac{(M_1 - M_2) \frac{p_1}{P} + M_2}{M_2 (1 - \frac{p_1}{P})},$$

or

$$g_1 = - \frac{M_1 P D_{12}}{RT} \cdot \frac{1}{1 - \frac{p_1}{P}} \left[\text{grad} \frac{p_1}{P} + \frac{k_T}{T} \text{grad} T \right]. \quad (6)$$

Computing Stefanovskiy flow during condensation (and evaporation) led to reduction of the value $[(M_1 - M_2) \frac{p_1}{P} + M_2]$ in the formula for flow g_1 , but there appeared the factor $\frac{1}{1 - \frac{p_1}{P}}$, giving a correction for Stefanovskiy flow.

In the case interesting us of small admixtures, this factor is close to one. For example, when $\frac{p_1}{P} = 0.02$, the value of $\frac{1}{1 - \frac{p_1}{P}}$ is equal approximately to 1.02. For the sake of simplicity in the calculations, this correction may not be considered and it can be taken that

$$g_1 = - \frac{M_1 P D_{12}}{RT} \left[\text{grad} \frac{p_1}{P} + \frac{k_T}{T} \text{grad} T \right]. \quad (7)$$

In the absence of thermal diffusion, Stefanovskiy flow can be considered and formula (6) can be rewritten thus:

$$g_1 = \frac{M_1 P D_{12}}{RT} \text{grad} \ln \left(1 - \frac{p_1}{P} \right). \quad (7a)$$

The closeness of the values of $\frac{1}{1 - \frac{p_1}{P}}$ to one still does not mean that the contribution of Stefanovskiy flow to the transfer of mass is negligible. The portion of Stefanovskiy flow in general comprises:

$$\frac{w_1 \frac{M_1 p_1}{RT}}{g_1} = \frac{M_1 \frac{p_1}{P}}{(M_1 - M_2) \frac{p_1}{P} + M_2}.$$

For the case of a mixture of cesium with helium with $p_1/P = 0.02$, due to the great difference in molecular weights it results in the portion in question being equal to 0.41. For a mixture, for example, of potassium with argon with small p_1/P , the portion of Stefanovskiy flow is small.

If in formula (3) we express the first term in terms of w_m with the aid of (5), then we obtain

$$g_1 = \frac{M_1 p_1 - M_2 (P - p_1)}{(M_1 - M_2) \frac{P}{p} + M_2} w_m = \rho w_m. \quad (6a)$$

Flow g_1 remains constant at various distances from the flat wall. In proportion to proximity to the wall, in the case of the use of a mixture of cesium with helium, the mixture density ρ drops and the mass flow rate increases.

For further calculations, data are necessary on the diffusion coefficients D_{12} and thermal diffusion ratio k_T . Enskog and Chapman's theory makes it possible to determine these values. For the diffusion coefficient in a binary mixture D_{12} the following expression is obtained in first approximation [7]:

$$D_{12} = 0.002628 \frac{1}{P_{12}^2} \frac{T^{\frac{1}{2}} \frac{M_1 - M_2}{2M_1 M_2}}{\epsilon_{12}^{1/2} \Omega_{12}^{(1,1)}(T_{12}^*)}, \quad (8)$$

where $T_{12}^* = \frac{kT}{\epsilon_{12}}$ - reduced temperature;

ϵ_{12} and σ_{12} - parameters of the potential energy of interaction of the molecules of the first and second components;

$\Omega_{12}^{(1,1)}(T_{12}^*)$ - reduced integral of collisions considering the interaction of molecules during diffusion in two-component mixtures.

In the given formula the temperature T is entered in $^{\circ}\text{K}$, pressure P in atm, and the parameters σ_{12} and ϵ_{12}/k in \AA and $^{\circ}\text{K}$, respectively. Then coefficient D_{12} will be obtained in cm^2/s . Coefficient D_{12} in first approximation does not depend upon the component content in the mixture. Parameters ϵ_{12} and σ_{12} characterize the potential energy of interaction of the molecules. For nonpolar molecules, the Lennard-Jones potential is usually used [7]:

$$\varphi_{12}(r) = 4\epsilon_{12} \left[\left(\frac{\sigma_{12}}{r} \right)^{12} - \left(\frac{\sigma_{12}}{r} \right)^6 \right], \quad (9)$$

where r — the distance between molecules; when $r = \sigma_{12}$, $\phi_{12} = 0$.

At close intervals, the force of interaction of the molecules $f_{12} = -\partial\phi_{12}/\partial r$ is positive, molecules are repelled. At distant intervals $f_{12} < 0$, molecules are attracted. At a distance of $1.12\sigma_{12}$ the potential energy reaches minimum, repelling and attraction forces are balanced. The depth of the potential well is equal to ϵ_{12} .

Integral $\Omega_{12}^{(1,1)*}(T_{12}^*)$ for the Lennard-Jones potential has been calculated. In [7] there are tables of its values. The values of the other analogous integrals are given for other transfer coefficients. Therefore, with the known parameters σ_{12} and ϵ_{12} , calculations of the diffusion coefficient are performed rather simply. A general form of formula (8) without integral $\Omega_{12}^{(1,1)*}(T_{12}^*)$ can be obtained on the basis of the simplest model in which the molecules are considered as solid spheres undergoing elastic collisions. Integral $\Omega_{12}^{(1,1)*}(T_{12}^*)$ gives a correction for the actual interaction of molecules.

The parameters σ_{12} and ϵ_{12} can be approximately estimated according to the parameters σ_{11} , σ_{22} , ϵ_{11} and ϵ_{22} , relating to the gases of the mixture. Usually the combination rules are used [7]:

$$\sigma_{12} = \frac{\sigma_{11} + \sigma_{22}}{2} \quad (10)$$

and

$$\epsilon_{12} = \sqrt{\epsilon_{11}\epsilon_{22}}. \quad (11)$$

For gases, rule (11) for the most part leads to satisfactory results. However, as we shall see from what follows, for mixtures of vapors of alkali metals with an inert gas, rule (11) gives large errors. It is possible to use another method for determination of ϵ_{12} [7, 9, 10]. For the attracting forces (dispersion forces) acting at great distances between nonpolar molecules, according to London [11] we have:

$$\phi_{12}(r) = -\frac{3}{2} \alpha_1 \alpha_2 \frac{U_1 U_2}{U_1 + U_2} \cdot \frac{1}{r^6}, \quad (12)$$

where α_1 and α_2 - the polarizability of the molecules;

U_1 and U_2 - characteristic energies of molecules.

According to London, energies U_1 and U_2 are close to ionization energies. However, more detailed examination shows that the differences between these energies can be considerable [11, 12].

Substituting in (12) the value $\phi_{12}(r)$ for large r expressed with the aid of (9) in terms of ϵ_{12} and σ_{12} , we obtain

$$\epsilon_{12} = \frac{3}{8} \cdot \frac{\alpha_1 \alpha_2}{\alpha_{12}^2} \cdot \frac{U_1 U_2}{U_1 + U_2}. \quad (13)$$

If we take

$$\sigma_{12} = \sqrt{\sigma_{11}\sigma_{22}}, \quad (14)$$

which differs slightly from (10), and determine U_1 and U_2 from relationships of the type

$$\epsilon_{11} = \frac{3}{16} \cdot \frac{\alpha_1^2}{\alpha_{11}^2} U_1; \quad \epsilon_{22} = \frac{3}{16} \cdot \frac{\alpha_2^2}{\alpha_{22}^2} U_2. \quad (15)$$

emanating from (13) for the interaction of identical molecules, then we obtain

$$\epsilon_{12} = 2 \frac{U_1^{1/2} U_2^{1/2}}{U_1 + U_2} \sqrt{\epsilon_{11} \epsilon_{22}}. \quad (16)$$

Hence, it is apparent that only when $U_1 = U_2$ rule (10) obtained. In the case of the use of mixtures of vapors of alkali metals (subscript 1) with an inert gas (subscript 2) U_1 is much less than U_2 , since in alkali metals the low ionization energy, and the high ionization energy of the inert gas (despite the differences U_1 and U_2 are close in order to ionization energies). In this way, rule (10) for the case in question should give rise to large errors.

Values of σ_{11} and ϵ_{11} for cesium can be found from the processing of experimental data on the viscosity of vapors of cesium, using the expression emanating from Enskog and Chapman's theory for the viscosity of gases. Processing the experimental data on the viscosity of vapors of cesium [13] gives $\sigma_{11} = 5.7 \text{ \AA}$ and $\epsilon_{11}/k = 167^\circ\text{K}$. During the processing it was assumed (in the future we will also so assume everywhere) that the vapors of cesium consist of monatomic Cs molecules. The content of diatomic Cs_2 molecules is small. It is still necessary to note that the atoms of cesium (and the other alkali metals) interact with each other with potential energies corresponding to two different types of dependences on distance [13 and others]. One fourth of the collisions occur in atoms in singlet state $^1\Sigma$, when the atoms are attracted and only at short distances (less than 0.5 \AA) are repelled. The depth of the potential well turns out to be great, corresponding to the value of dissociation energy of diatomic molecules. Three fourths of the collisions occur in atoms in triplet state $^3\Sigma$, when atoms are only repelled. Attraction is obtained only at great distances because of dispersion forces. In this way, the Lennard-Jones potential can be used only conditionally to describe the interaction of atoms of alkali metals. Nevertheless, from the experimental data on the viscosity of vapors of cesium it is possible to select values of parameters σ_{11} and ϵ_{11} , which remain unchanged in the experimental temperature range ($600\text{--}1100^\circ\text{K}$).

The values of parameters σ_{22} and ϵ_{22} for helium and argon, also selected from the data on viscosity, are given in [7]. These values, just as the values of σ_{11} and ϵ_{11} mentioned in the text for cesium are given in Table 1. There also are given the polarizability values from [14] and calculated values of σ_{12} and ϵ_{12} for mixtures of cesium with helium and argon found with the aid of formulas (14), (15), and (16).

Table 1: Values of polarizabilities and parameters of the Lennard-Jones potential function.

(1) Вещество или смесь	$\alpha \cdot 10^{24}$, cm ³	σ , Å	ϵ/k , °K
Cs	36	5,7	167
He	0,207	2,56	10,2
Ar	1,63	3,47	116
Cs—He	—	3,82	20
Cs—Ar	—	4,45	63,5

KEY: (1) Substance or mixture.

Having the values of σ_{12} and ϵ_{12} , it is possible to calculate the diffusion coefficient for Cs-He and Cs-Ar mixtures with the aid of formula (8). The results of the calculations are presented in Table 2 (for atmospheric pressure; for other pressures, the diffusion coefficient is inversely proportional to the pressure and is easily determined by recalculation). Table 2 also gives the experimental values of the diffusion coefficient. At a temperature of 723°K the experimental values of the diffusion coefficient for Cs-He and Cs-Ar mixtures were determined by the Stefan method, i.e., by the rate of evaporation of cesium in an atmosphere of helium or argon [15]. Error in the experiments is estimated at $\pm 15\%$. For a temperature of 299°K, the experimental values of the diffusion coefficient have been borrowed from [16]. These values have been

Table 2. The calculated and mean experimental values of the diffusion coefficient D_{12} cm²/s with $p = 9.81 \cdot 10^4$ N/m².

Температура, (1) °K	(2) Значения коэффициента диффузии	(3) Смесь	
		Cs — He	Cs — Ar
723	(4) Расчетные	2,13	0,47
	Опытные [15] (5)	2,06	0,69
299	(4) Расчетные	0,50	0,11
	Опытные [16] (6)	0,37	0,19

KEY: (1) Temperature; (2) Values of diffusion coefficient; (3) Mixture; (4) Calculated; (5) Experimental [15]; (6) Experimental [16].

determined by optical measurement of relaxation times of nonequilibrium populated Zeeman levels of hyperfine structure of cesium atoms. Error in determining the diffusion coefficient amounts to $\pm 30\%$.

From Table 2 it is evident that for the Cs-He mixture the experimental and computed values of the diffusion coefficient are sufficiently close. If we introduce correcting factor K into formula (8), equal in this case to 0.97, then at a temperature of 723°K the calculated and experimental values of the diffusion coefficient will coincide, while at a temperature of 299°K the differences will be slight (not emerging beyond the margins of error of determining the diffusion coefficient). The analytic curve with correction factor $k = 0.97$ is given in Fig. 1. Experimental points are also shown. It is still necessary to note that the values of σ_{12} and ϵ_{12} for a Cs-He mixture were determined by Robinson [9, 10] from the processing of experimental data in regard

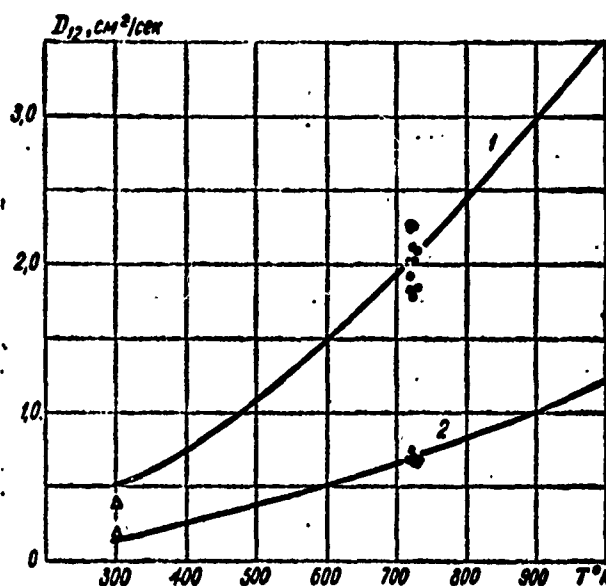


Fig. 1. Diffusion coefficient D_{12} for Cs-He and Cs-Ar mixtures depending on temperature with pressure $P = 9.81 \cdot 10^4 \text{ N/m}^2$:
 1 - analytic curve for Cs-He mixture;
 2 - analytic curve for Cs-Ar mixture;
 ● - authors' experimental points [15]; Δ - experimental points from reference [16].

Designation: $\text{cm}^2/\text{сек} = \text{cm}^2/\text{s}$.

to displacement of a hyperfine structure of cesium atoms in an atmosphere of helium. There was obtained $\sigma_{12} = 3.39 \text{ \AA}$ and $\epsilon_{12}/k = 40.8^\circ\text{K}$. Calculation of the diffusion coefficient by formula (8) using these values of parameters for a temperature of 723°K leads to somewhat overstated results. For atmospheric pressure there is obtained $D_{12} = 2.4 \text{ cm}^2/\text{s}$. The calculated results presented in Table 2 are closer to experimental

From Table 2 it is also evident that the calculated and experimental values of the diffusion coefficient for the Cs-Ar mixture differ from one another more strongly than for the Cs-He mixture. In the case of the use of a Cs-Ar mixture, the experimental values of the diffusion coefficient are higher than

calculated. For agreement of the calculated and experimental values of the diffusion coefficient at a temperature of 723°K it is necessary to introduce into formula (8) the correction factor $k = 1.47$. The analytic curve taking this factor into account is also given in Fig. 1. Experimental points have also been plotted. At a temperature of 299°K, the divergence of the calculated and experimental values of the diffusion coefficient do not fall outside the limits of error of the experimental determination of the diffusion coefficient.

Let us still note that calculated determination of diffusion coefficients was also made for K-He and K-Ar mixtures [15]. It again turned out that for the K-He mixture the experimental and computed values of the diffusion coefficient are close, while for the K-Ar mixture the experimental values are higher than the calculated. In this way, the calculation for mixtures with argon needs refinement.

It was stated earlier that formula (8) answers to the first approximation of the Enskog and Chapman theory for low-density gases. In the second and following approximations the diffusion coefficient begins to depend upon the content of components in the mixture. Higher approximations give [7]:

$$|D_{12}|_k = |D_{12}|_1 / f_{D_{12}}^k. \quad (17)$$

Here the subscript k signifies the number of the approximation. Correcting function $f_{D_{12}}^k$ depends upon the content of components, their molecular weight, viscosity, and also on the temperature. The values of this function usually differ very slightly from one. For the majority of two-component mixtures the values of $f_{D_{12}}^{(2)}$ calculated using the Lennard-Jones potential change within limits of from 1.0 to 1.03 [7].

For the following approximations $f_{D_{12}}^{(k)}$ is still closer to one. For a mixture of cesium with helium under our conditions $f_{D_{12}}^{(2)} = 1.003$. So small are the values of $f_{D_{12}}^{(k)}$ for the mixture of cesium with argon. In this case, with such corrections it is possible to be not considered.

For dense gases the value of the diffusion coefficient can be determined by the formula [7]:

$$D_{12} = \frac{D_{12}^0}{Y_{12}}, \quad (18)$$

where D_{12} - the diffusion coefficient determined from formula (13). Correcting value Y_{12} is given by the relationship:

$$Y_{12} = 1 + \frac{2}{3} \pi n_1 \sigma_{11}^3 \left(\frac{z_{11} - 4z_{22}}{4z_{11} + 4z_{22}} \right) + \frac{2}{3} \pi n_2 \sigma_{22}^3 \left(\frac{4z_{11} + z_{22}}{4z_{11} + 4z_{22}} \right) + \dots \quad (19)$$

The value of Y_{12} begins to differ noticeably from one only at comparatively high pressures (at large n_1 and n_2). For the mixture of cesium with helium with atmospheric pressure the value is practically equal to one.

2. CALCULATION OF THERMAL DIFFUSION RATIO

The Enskog-Chapman theory makes it possible to calculate the thermal diffusion ratio [7]. For two-component gaseous mixtures in first approximation

$$[k_T] = \frac{x_1 x_2}{6 [\lambda_{12}]_1} \cdot \frac{S_{x_1}^{(1)} - S_{x_1}^{(2)}}{X_A + Y_A} (6C_{12}^* - 5), \quad (20)$$

where $x_1 = \frac{n_1}{n} = \frac{p_1}{p}$ and $x_2 = \frac{n_2}{n} = \frac{p_2}{p}$ - molar fractions of components in the mixture;

$[\lambda_{12}]_1$ - coefficient of thermal conductivity of the mixture in first approximation;

$S^{(1)}$ and $S^{(2)}$ - functions of the molecular weight of the components, of coefficients of thermal conductivity $[\lambda_{12}]_1$, $[\lambda_{11}]_1$ (for $S^{(2)}$) and reduced temperature $T_{12}^* = Tk/\epsilon_{12}$;

$[\lambda_{11}]_1$ and $[\lambda_{22}]_1$ - coefficients of thermal conductivity of first and second components in first approximation;

C_{12}^* - function of T_{12}^* ;

X_λ and Y_λ - functions of $[\lambda_{11}]_1$, $[\lambda_{22}]_1$, $[\lambda_{12}]_1$, x_1 , x_2 , and T_{12}^* .

In [7] relationships and tables are given which determine the values necessary for calculations according to formula (20) (for the Lennard-Jones potential and other potentials). Thermal diffusion ratio k_T depends substantially on the concentrations of components in the mixture and the difference in their masses (molecular weight). With small x_1 (or x_2) the thermal diffusion ratio is small. The thermal diffusion ratio is also small with a small difference in the masses of the components. The value of k_T should be rather large for the mixture of cesium with helium (with a not very small content of cesium). For the mixture of argon with helium, k_T should be less, while for the mixture of potassium with argon, k_T should be very small.

With an increase in the content of cesium in helium or argon the value of k_T increases, then, passing through the maximum value, it decreases. With an increase in temperature, k_T increases. However, this increase for temperatures, considerably exceeding

inversion, is slight. The inversion temperature to which the value $T_{12}^* = kT/\epsilon_{12} = 0.95$ corresponds, for the mixtures interesting us turns out to be rather low¹). Within the limits of the theory in question, k_T does not depend on pressure.

For the mixture of cesium with helium, the values of k_T were calculated using values of σ_{12} and ϵ_{12} found by Robinson ($\sigma_{12} = 3.39 \text{ \AA}$ and $\epsilon_{12}/k = 40.8^\circ\text{K}$). The use of data on the parameters σ_{12} and ϵ_{12} from Table 1 does not give rise to any noticeable differences. The values of k_T depend very slightly on the value of the parameters σ_{11} and ϵ_{11} for cesium (with small contents of cesium). Calculated values of k_T for small contents of cesium (up to $x_1 = 0.1$) and temperatures exceeding 400°K (when k_T practically stops increasing with an increase in temperature) are given in Fig. 2. For a mixture of cesium with argon under comparable conditions of value, k_T is approximately 2.5 times less. For a mixture of potassium with argon when $T = 773^\circ\text{K}$ and $x_1 = 0.02$, the thermal diffusion ratio is negative and very small in value ($k_T \approx -3 \cdot 10^{-6}$).

It should be specified that the Enskog and Chapman theory, which leads to good results in calculations of the diffusion coefficient and other analogous transfer coefficients, is not sufficiently precise for calculations of the thermal diffusion ratio k_T , especially in first approximation. Calculation of the following approximations is extremely awkward. Great deviations are obtained in the region of inversion temperature [17]. However, the temperatures interesting us are far from the inversion temperature. At such temperatures, theoretical calculation gives a correct order of magnitude of k_T .

¹The Enskog and Chapman theory gives rise to an even lower second inversion temperature at which the sign of k_T is again changed. However, in experiments the second inversion was not observed.

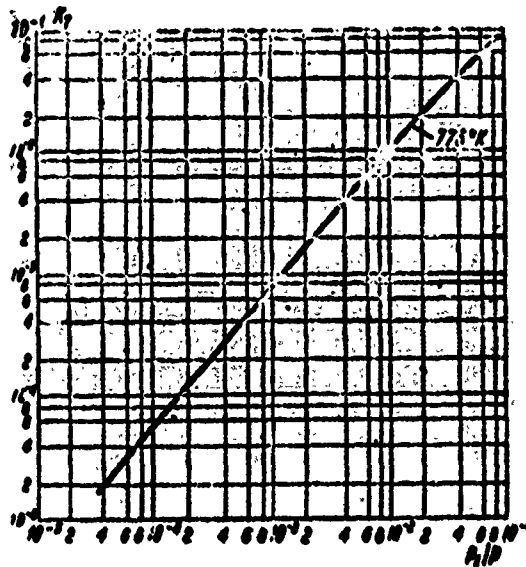


Fig. 2. Thermal diffusion ratio k_T for Cs-He mixture depending on cesium content $p_1/P = x_1$ for temperatures above 400° .

3. ANALOGY BETWEEN DIFFUSION AND HEAT EXCHANGE

Between the phenomena of diffusion (mass transfer) and heat exchange there is a known analogy widely utilized in experiments and calculations [18-22 and others]. On the basis of it rests the analogy between the expressions for diffusion flow (in the simplest case) and heat flow transferred because of thermal conductivity. During heat exchange, Nusselt's thermal criterion $Nu = \frac{\alpha d}{\lambda}$ represents a function of the Reynold's criterion $Re = \frac{wd}{\nu}$ and the thermal Prandtl number $Pr = \frac{\nu}{a}$. Here α - heat-transfer coefficient; λ - coefficient of thermal conductivity; d - determining dimension; w - flow rate; ν - kinematic viscosity; a - coefficient of temperature conductivity. For mass transfer, Nusselt's diffusion criterion $Nu_D = \frac{\alpha_D d}{D_{12}}$ (α_D - the coefficient of diffusion exchange or mass transfer) depends upon the Reynold's criterion Re and diffusion Prandtl number (or Schmidt's criterion) $Pr_D = \frac{\nu}{D_{12}}$.

Due to the analogy of dependence $Nu=f(Re, Pr)$ and $Nu_D=f(Re, Pr_D)$ they should be identical. Therefore, the experimental results in heat exchange generalized by a criterional function can be transferred to mass transfer. Similarly, from the results obtained from the mass transfer it is possible, using a criterial function, to calculate heat exchange. These methods are widely used in the study of heat and mass transfer. The analogy has been repeatedly checked by experiment. It is natural that under the simplest conditions it is well confirmed. Deviations are caused by the effect of Stefanovskiy flow in mass transfer. Usually in formulas on mass transfer the criterion p_1/P is additionally introduced, characterizing the role of Stefanovskiy flow. In the case being examined by us the analogy can still be disturbed by thermal diffusion. Furthermore, according to the Enskog and Chapman theory, heat flow not only is not transferred because of thermal conductivity and is proportional to the temperature gradient (as this was accepted in substantiation of the analogy), but is still caused by the concentration gradient [7] (the Dufour effect, a phenomenon, the reverse of thermal diffusion). In addition, a certain quantity of heat is again transferred with diffusion flow of molecules. The full expression for heat flow q (taking into account Stefanovskiy flow) takes the form¹).

$$q = -\lambda \text{grad } T + RTh_1 \frac{K_1}{P M_1} + \frac{5}{2} RT \frac{K_1}{M_1}. \quad (21)$$

The second and third terms exactly define the indicated heat flows. The third term has been written for the monatomic gas moving to the wall (cesium or potassium), the specific heat of which for one mole is equal to $5/2 R$ (with constant pressure).

¹The expression given below for q differs from the corresponding expression in [7], since Stefanovskiy flow has been taken into account (in this case $g_2 = 0$).

However, estimates show that the supplementary heat flows in question are small as compared with the flow being transferred by thermal conductivity. Even for a mixture of cesium with helium when there can be considerable thermal diffusion, the second and third members in (20) together comprise less than 3% of the first member with cesium content $p_1/P = 0.02$. In this way, it is impossible to expect a noticeable disturbance of the analogy induced by the supplementary components of the heat flow.

4. CALCULATION OF CONDENSATION OF CESIUM FROM A FLOW OF INERT GAS. EXPERIMENTAL RESEARCH ON CONDENSATION

Let us examine, as an example, the condensation of cesium from a flow of helium during transverse flow of a single tube. Let the diameter of tube equal 40 mm. For calculation of coefficients α and α_D we will use the following criterial formula [19]:

$$Nu = A Pr^{0.35} Re^n. \quad (22)$$

The coefficients A and n entering into this formula have different values in different ranges of Re numbers. For example, with $Re = 100-5000$, $A = 0.665$ and $n = 0.47$.

With small molar additions of cesium to helium (i.e., in the case of relatively small number of molecules of the addition) coefficients λ , and ν and α can refer to pure helium.

Diffusion flow of vapor to the surface of tube, induced by concentration diffusion (without thermal diffusion), is equal to¹).

¹For small concentrations of cesium the correcting factor $\frac{1}{1 - \frac{p_1}{P}}$ is practically equal to one.

$$g_{\text{кон}} = \frac{M_1 P_{sD}}{RT} \left[\left(\frac{p_1}{P} \right)_{\text{ог}} - \left(\frac{p_1}{P} \right)_{\text{нос}} \right] = \frac{M_1 P \text{Nu}_D D_{12}}{R d T} \left[\left(\frac{p_1}{P} \right)_{\text{ог}} - \left(\frac{p_1}{P} \right)_{\text{нос}} \right], \quad (23)$$

where d - diameter of the cylinder;

$\left(\frac{p_1}{P} \right)_{\text{ог}}$ and $\left(\frac{p_1}{P} \right)_{\text{нос}}$ - relative partial pressure of cesium in gas volume (in the flow) and at the surface of the tube.

The pressure of the cesium at the surface can be considered equal to the saturation pressure at surface temperature $T_{\text{нос}}$. For the temperature, in the denominator of the entity $\frac{M_1 P_{sD}}{RT}$ or the entity $\frac{M_1 P \text{Nu}_D D_{12}}{R d T}$ one should take that determining temperature, to which it is recommended to refer the physical properties in the criterial formula used (22) (mean temperature in the gas boundary layer, the temperature of incident flow, etc.). The fact is that the dependence of the ratio $\frac{D_{12}}{T}$ on the temperature is approximately the same as the dependence of the coefficient of thermal conductivity λ on the temperature. Therefore, when λ is considered a constant value with a change in the gas temperature (as is usually done), it is rational to consider also as constant the ratio $\frac{D_{12}}{T}$ [3].

In Fig. 3 the calculated values are given for the flow of concentration diffusion for the surface of tubes with diameter of 40 mm depending on number Re with cesium content in the flow of from $1 \cdot 10^{-4}$ to $4 \cdot 10^{-4}$. Temperature in the flow $T_{\text{ог}}$ is taken as equal to 873°K, and the surface temperature of the tubes - 373°K.

Diffusion flow to the surface of tube must still grow because of thermal diffusion.

For an approximate estimate, the temperature gradient at the surface of the tubes can be taken as equal to $\frac{T_{\text{ог}} - T_{\text{нос}}}{\delta_{\text{т}}}$, where $\delta_{\text{т}} = \frac{d}{\text{Nu}}$ - the thickness of the thermal reduced film. The temperature flow of cesium to the surface (the cesium, because of thermal diffusion, moves to the colder surface of tube, condensation is increased)

can be estimated, using the relationship

$$G_{\text{diff}} = - \frac{M_1 D \left(\frac{D_{12}}{T} \right)}{R} \cdot \frac{k_T}{T} \cdot \frac{T_{\text{об}} - T_{\text{ноб}}}{\delta_T} \quad (24)$$

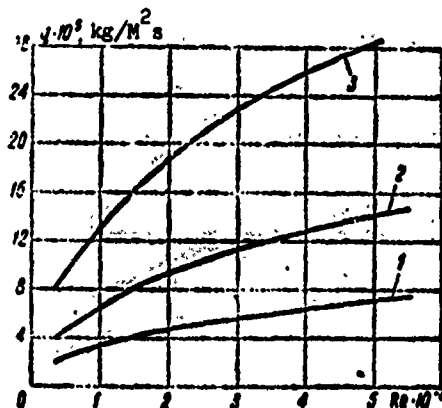


Fig. 3. Calculated values of flow of concentration diffusion of cesium from a mixture with helium on the surface of a tube under transverse flow depending on the Reynolds number ($T_{\text{об}} = 730^\circ\text{K}$;

$T_{\text{ноб}} = 373^\circ\text{K}$): 1- $\left(\frac{p_1}{p}\right)_{\text{об}} = 1 \cdot 10^{-4}$; 2- $\left(\frac{p_1}{p}\right)_{\text{об}} = 2 \cdot 10^{-4}$; 3- $\left(\frac{p_1}{p}\right)_{\text{об}} = 4 \cdot 10^{-4}$.

According to the data in Fig. 2, the value of k_T with small contents of cesium depends practically linearly upon the relative fractions of cesium $x_1 = \frac{p_1}{p}$. If we make use of the data in Fig. 2 and refer the value of k_T/T to conditions in the middle of the diffusion reduced film, then it is found that thermal diffusion flow will comprise about 30% of the concentration diffusion flow. In this way, for the case of condensation of cesium from a mixture with helium, thermal diffusion is considerable and must be considered. For the case of condensation of cesium from a mixture with argon, the effect of thermal diffusion is much weaker, since the thermal diffusion ratio is less (approximately 2.5 times).

In the example examined a low cesium concentration in helium is taken $\left[\frac{p_1}{p} = (1/4) \cdot 10^{-4}\right]$. With higher cesium concentrations, the vapors within the limits of the boundary layer of the surface of the tubes, can become supersaturated (due to the temperature decrease) and the formation of fine drops of mist can begin [23].

Condensation on the surface of the tube is reduced. Part of the drops of mist will be carried out by the flow from the limits of boundary layer, and another part of the drops will reach the surface under the action of forces of thermophoresis (proportional to the temperature gradient and moving the drops to the colder surface [24]. As the flow cools, formation of mist will begin in the flow. The case of condensation of cesium additions from gases with formation of mist in the boundary layer and in the flow requires special examination.

Of practical interest is the research on the condensation of alkali metals from a flow of inert gases during flow around bundles of tubes placed after the channel of an MHD-generator. These can be either heat exchangers or special condensers intended for purifying the gas of ionizing additives.

Calculations were made and experimental investigations were conducted on the condensation of cesium from a flow of argon during transverse flow past a bundle with staggered arrangement of tubes with a diameter of 12 mm and a height of 140 mm. The total number of rows was 32.

Calculation of diffusion precipitation induced by concentration diffusion was performed using the analogy between heat and mass transfer. The coefficients of mass transfer were found by using the formula from [21]:

$$Nu_{\text{diff}} = 0,35 Re^{0,6} Pr_{\text{diff}}^{0,34}. \quad (25)$$

Calculations showed that, within the limits of heat exchanger with the selected regime parameters, supersaturation of the vapors of cesium sets in and the zone of volumetric formation of mist, in which the mechanism for precipitation differs from that of diffusion, occupies a considerable part of the length of the heat exchanger.

In order to find the quantity of precipitated cesium in the vapor zone and in the zone of mist formation experiments were conducted in the study of condensation in a bundle of tubes and a comparison was made with the results of calculation. The experiments were conducted at an inlet gas temperatures of 270-370°C, with concentrations of cesium in argon of $(2-11) \cdot 10^{-4}$ kg/kg, and Reynolds numbers 1200-3000. The concentration of cesium in argon on inlet and outlet from the heat exchanger was determined with the aid of gas sampling by chemical methods.

The experiments showed that the quantity of cesium which was being condensed on the surface of the heat exchanger comprised a value on the order of 40% of the quantity put in. Comparisons of the calculated and experimental data are given in Fig. 4. One should note the satisfactory agreement of the results of calculation and experiment. Consequently, under conditions of the conduct of the experiments the main contribution to the process of precipitation was made by diffusion condensation. A certain excess of experimental data over calculated can be caused by the precipitation of cesium in the zone of mist formation.

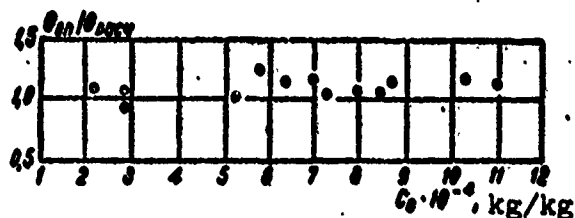


Fig. 4. Comparison of the calculation and experimental data on precipitation on the cooled surface of the bundle: G_{on} - experimental value of precipitation; G_{pac} - calculation value of precipitate.

I. G. Kholmiskiy took part conducting the calculations presented in the article.

BIBLIOGRAPHY

1. Магнитогидродинамические траторы Обзор Г. В. Скворцова и Э. П. Зимина. Сб.: «Магнитогидродинамический метод преобразования энергии», ГИФМЛ, 1963.
2. Стырикович М. А., Годик Н. Б. Методика расчета массообмена в низкотемпературных теплообменниках МГД-установок. «Известия АН СССР, Энергетика и транспорт», 1966, № 5.
3. Франк-Каменецкий Д. А. Диффузия и теплопередача в химической кинетике. Изд. АН СССР, 1947.
4. Субботин В. И. и др. Теплообмен при конденсации казевого пара. «Теплофизика высоких температур», т. 2, № 4, 1964.
5. Бонилла Ш. Сб.: «Жидкометаллические теплоносители». ИИЛ, 1958.
6. Чепмен С., Каулинг Т. Математическая теория неоднородных газов. ИИЛ, 1962.
7. Гиршфельдер Дж. и др. Молекулярная теория газов и жидкостей. ИИЛ, 1961.
8. Ландау Л. Д., Лифшиц Б. М. Механика сплошных сред. Москва, Гостехиздат, 1954.
9. Robinson L. B. «Phys. Rev.», 117, 1275, 1960.
10. Робинсон Л. Б. Сб.: «Термоядерное преобразование энергии», 1. Атомиздат, 1964.
11. Гельман Г. Г. Квантовая химия. ОНТИ, 1937.
12. Pitzer K. S. «Adv. in Chem. Phys.», 2, 53, 1959.
13. Дэвис Р. Х., Мейсон Е. А., Мани Р. Т. Прямое преобразование тепловой энергии в электрическую и топливные элементы. вып. 2:43, 1966.
14. Fontana P. R. «Phys. Rev.», 147, 1275, 1960.
15. Арефьев К. М. и др. К вопросу о выделении из потока газа малых добавок конденсирующихся веществ. Сб.: «Тепло- и массоперенос», т. 2 Минск, изд. «Наука и техника».
16. Legovski S. «Journ. Chem. Phys.», 41, 1313, 1964.
17. Grew K. E., Jounson F. A., Neal W. E., Proc. Roy. Soc., A224, 1158, 1954.
18. Гребер Г., Эрк С., Григуль У. Основы учения о теплообмене. ИИЛ, 1958.
19. Берман Л. Д. Испарительное охлаждение воды. Госэнергониздат, 1957.
20. Шорин С. Н. Теплопередача. Изд. «Высшая школа», 1964.
21. Кутателадзе С. С., Боришанский В. М. Справочник по теплопередаче. Госэнергониздат, 1959.
22. Исаченко В. П., Осипова В. А., Сукомен А. С. Теплопередача. М. — Л., «Энергия», 1965.
23. Амелин А. Г. Теоретические основы тумана при конденсации пара. М., «Химия», 1966.
24. Харт А. и др. Некоторые аспекты восстановления добавки. Сб.: «Магнитогидродинамическое преобразование энергии», Труды международного симпозиума. Париж, 1964, ч. 2. Изд. ВИННИТИ, 1966.

A STUDY OF THE PROCESS OF CONDENSATION OF A MULTICOMPONENT MIXTURE OF HYDRO- CARBON GASES IN A VERTICAL TUBE

A. D. Dvoyris

The process of condensation of mixtures has extensive application in installations for the separation of natural and by-product oil gases by the cooling method. The heat-transfer condensation apparatus in such installations in regard to metal content comprises up to 60-70% of the total metal investment and, as a rule, works under conditions of aggregate conversion of the state of the mediums. The gases being treated are basically complex in composition, multicomponent mixtures of maximum hydrocarbon-homologs of the methane series (from methane to the pentanes, inclusive), whereby the predominant component is methane. The remaining components, depending on the specific conditions, can be distributed in various ratios. In a number of cases, nitrogen (up to 15% by volume is present in the initial mixture).

In this way, the natural and by-product oil gases being treated under industrial conditions are multicomponent vapor-gas mixtures which contain, depending on the cooling temperatures, one or several noncondensing components (nitrogen, or nitrogen, methane, and ethane).

During condensation of multicomponent vapor-gas mixtures in the cross sections of the condenser temperature and concentration gradients appear, i.e., as compared with the case of condensation of a pure substance, there appear additional resistances to heat and mass transfer in the vapor phase. These effects can significantly limit the intensity of the process of condensation as a whole, and disregard of their effect can give rise to the errors in designing appropriate equipment. The intensity of the process of condensation proves to be, in this way, dependent on the intensity of two interdependent transfer processes: heat transfer and mass transfer. The experimental data available in literature on the study heat and mass transfer during the condensation of multicomponent mixtures are extremely limited, while the generalized calculation equations practically do not exist.

This paper is devoted to the study of the concurrent heat and mass transfer during direct-flow condensation of multicomponent hydrocarbon gases for the purpose of developing the design procedure for condensers of complex mixtures.

Description of the Pilot Plant and Conduct of the Experiment

A single-tube vertical condenser was adopted as an experimental model. The length of the working zone of tube comprised $l = 0.88$ m, the internal diameter $d = 6$ mm, the wall thickness was 1 mm. The tube was made of 1Kh18N9T stainless steel. Condensation of the mixture occurred on the interior surface because of boiling liquified propane in the intertube space. The condenser was divided into four sections; in the four sections provision was made for measurements of the wall temperature and flow core by height. Temperatures were measured

by copper-constantan thermocouples to within 0.1°C . For measurement of the wall temperature the thermocouples were placed in grooves specially drilled to a depth of up to 0.5 mm and were covered with epoxy resin. The electrodes of the thermocouples were embedded in an isothermal section from the place of insertion. The depth of the insertion of the thermocouple was taken into account in determining the inner-surface temperature of the tube. To measure temperature in the core of the moving mixture, a constantan wire was strung axially along the tube. In the same sections where provision was made for measurement of the wall temperatures, thin copper wires were soldered, forming a row of thermocouples over the height of the tube. Recording of the thermal emf of the thermocouples was performed with the aid of an R-306 low-resistance potentiometer in a set with a type G 17/1 mirror galvanometer. The flow of the uncondensed mixture and condensate after their separation was generated by GKF-6 gas meters with accuracy to within 0.3%. In so doing, the vapor and liquid phases were first throttled down to a small excess pressure and were heated in the heat exchanger (the condensate was completely vaporized); the temperature and pressure of the flows before the meters were recorded.

The initial mixture was prepared in a special mixer by means of enrichment of natural gas delivered at a pressure $p = 20$ and 30 atm by heavy hydrocarbons (propanes and butanes) and entered the experimental condenser in practically saturated state. Experiments were run at pressure of 20 and 30 atm. The initial mixture contained from 59.6 to 81.4% methane, from 1.5 to 4% ethane, from 10.1 to 34.89% propane, and from 2.47 to 13.8% butanes (total of normal butane and isobutane)¹. The methane and ethane were the noncondensing components of the mixture.

¹Here and in the future the composition of the mixture is indicated in percents by volume.

The average speed of the mixture was changed from 0.72 to 3.6 m/s, the degree of condensation (volumetric) - from 0.103 to 0.396, the pressure of the boiling propane in intertube space - from 0.1.3 to 5 atm. In connection with the fact that the experiments were run at reduced temperatures (the temperature of the mixture on outlet from the tube changed from 0 to -30°C), the condenser and the phase separator were thoroughly insulated. The experiments were conducted in the following manner; at a determined pressure and with a fixed composition of the initial mixture (the latter was achieved by maintaining the appropriate pressure and temperature during the bubbling of the natural gas through liquified hydrocarbons in the mixer) a specified flow rate of mixture on inlet to the tube was established. After stabilization of conditions, the temperatures of the flow core and wall were taken, the readings of the manometers and gas meters were recorded and samples were taken of the initial mixture, the vapor residue, and the condensate for analysis. Then the flow of the mixture was changed. Analyses of the hydrocarbon composition were performed on a KhPA-4 chromatograph having sensitivity of 0.02%.

In order to determine temperature at the interphase interfaces during condensation of the mixture it is necessary to know the thermal resistance of the condensate film. In connection with this, on a given test stand, as a preliminary stage, a study was made of thermal conductivity during filmwise condensation of vapors of propane. Experiments were conducted with propane with 95-99.5% purity (0.5-5% was made up of non-condensing impurities - methane and ethane) at a pressure of 6 atm in a range of input flow rates from 2.5 to 10 m/s.

A STUDY OF THERMAL CONDUCTIVITY DURING CONDENSATION OF PROPANE VAPORS

The intensity of the heat transfer through the film during condensation of the moving vapor is greatly affected by the flow rate. The question of quantitative estimation of this effect at present has not been completely resolved; the results of available analytical solutions proposed by various authors often disagree with experimental data. Analyzing the possible reasons for these divergences, L. D. Berman showed that they are connected with the practical impossibility of considering by analytical methods the effect being exerted by the motion of the vapor on rearrangement of the flow conditions of the film, which is characterized by transition from laminar flow into random-wave and turbulent [1]. In practice, the effect of the rate of the vapor on the heat-transfer coefficient during condensation must be estimated on the strength of experimental data. We did not have such data available in conducting the present study (condensation in vertical tubes of dense hydrocarbon vapors at speeds of from 1 to 10 m/s.). The latter necessitated preliminarily investigating the process of thermal conductivity during the condensation of a moving hydrocarbon vapor. The effect of rate on the heat-transfer coefficient has been examined in an example of the condensation of propane since it was the basic condensing component of the mixture. Experiments were conducted at $p = 6$ atm during the concurrent flow of phases. The experimental data are provided in Table 1. The heat-transfer coefficient was determined as averaged from the formula:

$$\alpha_k = \frac{q}{\Delta t},$$

where

α_k - the experimental value of the heat-transfer coefficient, kcal/m²·h·°C; q - specific heat flow, kcal/m²·h; Δt - the mean

Table 1.

Forward flow pressure, atm(abs)	Pressure in column, atm(abs)	Total flow rate V_0 , Nm ³ /h	Flow rate for liquid V_M , Nm ³ /h	Flow rate for vapor V_n , Nm ³ /h	Specific thermal load q_0 , kcal/m ² ·h	Temperature difference be- tween flow core and wall Δt , °C	Initial mixture, % by volume				Liquid % by volume	
							CH ₄	C ₂ H ₆	C ₃ H ₈	C ₄ H ₁₀	CH ₄	C ₂ H ₆
6	3.93	2.87	1.06	29.900	18.61	1.16	0.78	0.51	97.97	0.09	0.19	
6	3.755	2.76	0.995	28.600	16.92	0.88	0.72	0.45	98.45	0.06	0.22	
6	2.468	1.49	0.938	15.400	12.913	0.38	0.48	0.28	99.16	—	0.24	
6	2.566	1.59	1.047	16.100	12.13	0.54	0.63	0.22	99.83	—	0.23	
6	4.245	1.35	2.895	14.050	6.485	0.39	0.58	0.29	99.03	—	0.23	
6	4.333	1.414	2.919	14.850	6.612	0.35	0.4	0.28	99.25	—	0.18	
6	1.784	0.795	1.008	8.080	7.306	0.46	0.77	0.25	98.77	—	0.17	
6	1.617	0.626	0.991	6.520	7.331	0.31	0.63	0.16	99.06	—	0.11	
6	1.653	0.576	1.11	6.040	5.641	0.009	0.49	0.17	99.42	—	0.05	
6	1.64	0.536	1.104	5.600	5.218	0.009	0.46	0.14	99.45	—	0.11	
6	1.667	0.505	1.162	5.250	4.903	0.31	0.38	0.18	99.31	—	0.2	
6	1.644	0.488	1.156	5.100	5.125	0.16	0.51	0.28	99.33	—	0.38	
6	3.681	2.55	1.131	26.500	15.38	1.1	0.75	0.43	97.9	0.25	0.23	
6	2.413	1.414	1.00	14.750	15.164	1.38	0.78	0.4	97.59	0.25	0.28	
6	2.177	1.266	0.891	13.450	17.665	1.51	0.81	0.36	97.38	0.30	0.19	
6	2.488	1.393	1.095	14.700	10.99	0.87	0.71	0.29	98.18	0.24	0.27	
6	4.26	3.26	1.00	34.300	17.73	0.5	0.6	0.39	93.65	0.25	0.25	
6	3.749	2.699	1.05	28.500	17.575	0.59	0.65	0.32	98.51	0.25	0.2	
6	3.45	2.47	0.98	26.000	16.275	1.22	0.89	0.53	97.71	0.18	0.2	
6	4.184	2.33	1.854	24.200	13.066	1.54	3.08	1.0	94.94	0.44	0.97	
6	4.316	2.462	1.854	25.700	14.01	1.54	3.08	1.0	94.94	0.44	0.97	
6	2.632	1.622	1.01	17.000	18.03	1.8	1.31	0.92	94.11	2.78	1.0	
6	3.55	2.49	1.06	26.000	17.82	1.8	1.31	0.92	94.11	2.78	1.0	
6	5.48	2.46	3.02	26.000	12.75	0.5	2.2	1.0	96.8	0.5	0.4	
6	6.22	4.24	1.98	44.700	17.605	0.6	2.6	1.0	96.3	0.5	0.4	
6	2.397	1.301	1.036	13.550	12.112	0.4	2	0.6	97.1	0.5	0.4	
6	6.156	1.963	4.193	20.500	8.422	0.65	2.04	0.71	95.45	1.86	0.45	
6	1.391	0.921	0.47	10.420	11.01	0.6	1.29	0.71	95.19	2.92	0.31	
6	1.738	1.074	0.632	11.210	12.47	0.5	1.27	0.52	95.9	2.33	—	
6	1.626	1.004	0.622	10.503	11.95	0.6	1.45	0.64	95.55	2.4	0.21	
6	2.03	1.162	1.463	12.110	10.69	0.43	1.88	0.72	97.49	0.2	0.94	
6	2.505	1.055	1.441	11.110	9.18	0.67	0.75	5.05	99.19	0.39	2.1	
6	1.207	1.643	2.564	17.200	9.132	1.20	0.64	2.03	97.7	0.46	1.7	
6	6.077	2.534	3.543	25.400	11.43	0.38	1.62	0.66	97.74	0.26	0.9	
6	6.119	2.235	3.851	23.700	11.035	0.96	1.69	0.41	97.15	0.2	0.78	
6	3.49	2.69	0.8	28.100	17.09	0.60	1.47	0.9	97.43	0.24	0.54	
6	1.67	1.23	0.44	12.800	19.023	1.15	1.74	0.97	98.88	0.23	—	
6	6.32	3.54	2.78	36.000	14.025	0.8	1.6	0.91	97.5	0.1	0.53	
6	5.515	5.01	0.511	52.200	25.304	0.76	0.97	0.73	97.23	1.04	0.42	
6	5.442	4.828	0.514	51.205	23.955	0.44	0.94	0.53	97.53	1.09	—	
6	5.641	4.937	0.704	51.400	24.42	0.59	0.70	0.66	97.61	1.10	0.52	
6	5.613	4.917	0.696	51.400	24.98	0.66	1.17	0.97	94.53	1.44	0.50	
6	5.802	1.266	1.516	44.400	22.67	3.3	1.73	1.34	92.31	2.6	1.15	
6	3.49	1.49	2.00	15.600	9.37	1.45	1.28	0.6	97.17	0.1	0.48	
6	6.349	2.883	3.466	30.180	13.5	0.94	1.79	0.71	97.04	0.23	0.46	

Table 1 cont'd

Liquid % by volume		Vapors, % by volume				Content in vapor (CH ₄ + C ₂ H ₆) on inlet to tube	Degree of condensation, % by volume	Heat transfer coefficient during condensation α_w , kcal/m ² ·h·°C	Flow rate on inlet to tube w_g , m/s	Reynold's number on inlet to duct Re_{ax}	Ratio, α/α_{N_4}	Prandtl number Pr
C ₃ H ₈	C ₄ H ₁₀	CH ₄	C ₂ H ₆	C ₃ H ₈	C ₄ H ₁₀							
98.74	0.56	1.87	1.73	98.4	—	1.94	0.732	1600	5.69	45800	2.06	2.55
99.1	0.23	2.03	1.66	98.28	—	1.6	0.736	1630	5.6	43500	2.11	2.55
99.48	—	1.27	1.3	97.43	—	0.84	0.599	1190	3.71	25800	1.38	2.48
99.58	0.09	0.88	0.96	98.26	—	1.17	0.596	1325	3.69	30300	1.5	2.46
99.41	0.08	1.00	1.84	98.10	—	0.97	0.9186	2170	6.34	49300	2.17	2.45
99.51	0.08	0.58	0.72	98.7	—	0.75	0.322	2250	6.55	50900	2.25	2.45
99.58	—	0.6	0.92	98.78	—	1.23	0.438	1105	2.67	20800	1.13	2.46
99.73	—	0.59	0.55	98.47	—	0.94	0.366	890	2.42	18800	0.91	2.46
99.78	—	0.18	0.73	99.09	—	0.58	0.341	1070	2.52	19600	1.03	2.44
99.75	—	0.19	0.57	99.24	—	0.55	0.327	901	2.45	19100	0.893	2.44
99.62	—	0.35	0.65	98.99	—	0.69	0.302	1065	2.5	19450	1.012	2.45
99.34	—	0.49	0.76	98.75	—	0.67	0.297	965	2.46	19150	0.95	2.45
99.97	0.37	3.15	1.2	95.56	0.09	1.85	0.693	1720	5.45	42800	2.15	2.62
98.87	0.45	2.01	1.03	95.78	0.18	2.16	0.584	973	3.59	28000	1.17	2.59
99.01	0.45	2.5	1.17	95.15	0.18	2.23	0.591	1155	3.24	25300	1.45	2.5
98.98	0.48	2.11	1.66	95.51	0.12	1.58	0.553	1335	3.7	28900	1.48	2.53
99.04	0.32	2.83	1.55	95.18	0.07	1.1	0.786	1635	6.3	49100	2.42	2.5
99.18	0.3	1.87	1.37	96.68	0.08	1.24	0.72	1625	5.56	43500	2.03	2.5
99.0	0.27	3.05	1.43	95.41	0.11	2.11	0.695	1600	5.1	39600	1.98	2.5
97.53	0.5	3.13	4.05	92.47	0.35	4.62	0.557	1850	6.25	43600	2.16	2.5
97.53	0.5	3.13	4.05	92.47	0.35	4.62	0.571	1726	6.45	50200	2.08	2.48
95.96	3.12	1.95	2.39	94.03	1.63	3.11	0.617	944	3.93	30600	1.21	2.5
95.96	3.12	1.95	2.39	94.03	1.63	3.11	0.701	1455	5.33	41200	1.87	2.5
97.8	0.8	2.8	3.3	93.7	0.2	2.7	0.45	2040	8.13	63200	2.38	2.48
97.9	0.7	0.9	3.6	95.4	0.1	3.2	0.682	2510	9.24	71800	3.18	2.5
98.3	0.7	0.6	2.6	95.6	0.2	2.4	0.558	1120	3.52	27200	1.27	2.5
91.86	4.28	0.76	2.06	95.54	1.04	2.69	0.710	2440	9.16	82000	2.57	2.46
95.67	3.41	0.49	2.16	96.16	1.19	1.89	0.662	947	2.09	11450	1.052	2.5
95.31	4.17	0.29	2.01	95.01	1.69	1.77	0.619	893	2.62	23800	1.03	2.5
95.8	3.35	0.51	2.16	96.02	1.24	2.15	0.616	830	2.14	21700	1.00	2.5
97.84	0.5	1.85	2.61	95.76	0.09	2.31	0.442	1132	3.91	35900	1.26	2.5
92.13	0.3	1.3	2.02	95.4	0.28	1.32	0.425	1210	3.71	33200	1.29	2.5
97.62	3.77	1.94	2.14	95.76	0.14	1.54	0.341	1555	6.25	55100	2.01	2.5
98.02	0.42	1.33	3.0	95.5	0.17	2	0.412	2318	9.11	81100	2.64	2.43
95.13	0.3	0.65	2.97	95.21	0.14	2.65	0.371	2150	9.15	81100	2.4	2.5
93.33	0.23	2.05	3.8	94.03	0.1	2.33	0.771	1645	5.2	46300	2.06	2.53
93.8	0.23	1.75	3.30	94.95	—	2.89	0.737	672	2.49	22100	0.86	2.53
93.56	—	1.04	3.40	95.47	0.09	2.4	0.56	2630	9.36	84000	3.13	2.52
97.71	1.14	1.32	2.72	95.54	0.14	1.73	0.491	2630	8.2	73400	2.79	2.62
98.33	1.14	1.1	2.62	95.02	0.25	1.38	0.924	2133	8.1	72400	2.84	2.62
97.04	1.78	0.92	1.94	95.83	0.11	1.29	0.875	2133	8.37	74800	2.81	2.62
95.4	2.04	3.42	2.13	93.51	0.58	2.03	0.88	2133	8.4	74500	2.79	2.62
94.51	3	1.81	3.72	93.54	0.93	5.06	0.736	1950	8.34	77500	2.6	2.56
98.76	0.15	1.79	0.59	97.46	0.16	2.73	0.423	1952	5.33	46000	1.78	2.52
94.41	0.42	0.78	2.33	96.71	0.18	2.73	0.455	2332	9.42	81400	2.82	2.59

temperature difference between flow core and wall, °C.

The value of specific heat flow was defined as

$$q = \frac{G_H r}{F_{tp}},$$

where

G_H - the quantity of condensate forming on the tube, kg/h;
 F_{tp} - the internal surface of the tube, m^2 ; r - latent heat of condensation of propane, kcal/kg; at 6 atm $r = 89$ kcal/kg.

The mean temperature difference was determined from the readings of the thermocouples in four sections over the height of the tube. Experiments on the convergence of heat balance up to 15% were used in the processing. In order to estimate the effect of the flow rate on the heat-transfer coefficient it is necessary to have data obtained on absolutely pure propane. Under our conditions, the purity of the initial propane varied from 95 to 99.5% (0.5-5% was made up of noncondensing impurities of methane and ethane). Figure 1 gives the dependence constructed from experimental data of the absolute value of the heat-transfer coefficient α_H and its relative reduction from a total impurity content of 6% at inlet flow rates w_0 of from 2.54 to 9.31 m/s (Re numbers from 21,500 to 80,000). For comparison, in this same figure experimental data have been plotted for the vapor-air mixture from reference work [2]. From Fig. 1 it is evident that an increase in speed of flow reduces the negative effect the inert gas and at rates of $w_0 = 7.34$ -9.31 m/s it becomes minimum. The reduction in the effect of the action of components on thermal conductivity with an increase in speed of flow is explained by the decrease

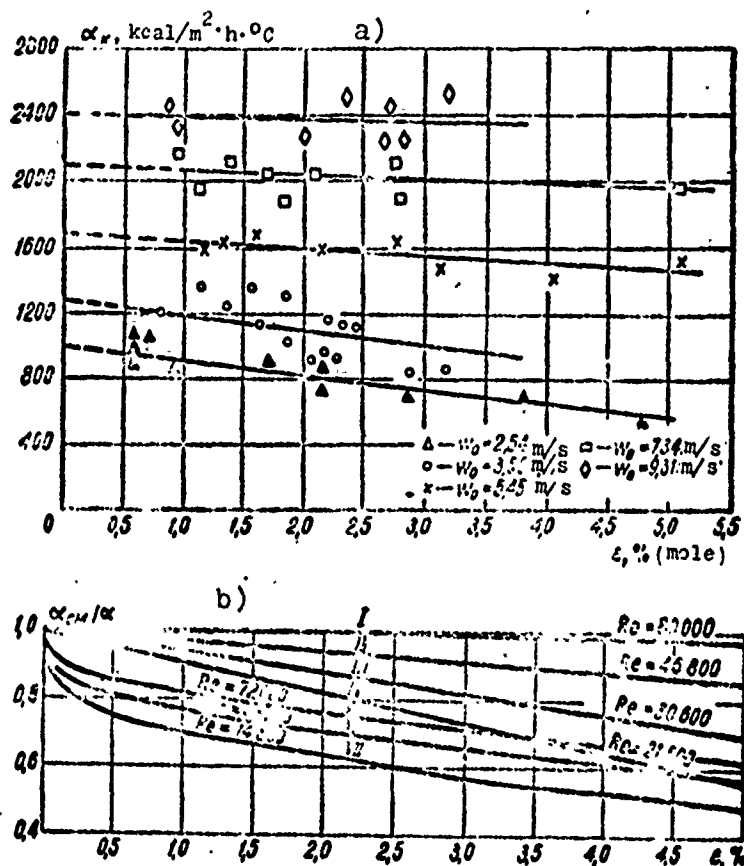


Fig. 1. Dependence of coefficient α_H and its relative reduction on total impurity content: I, II, III, IV - the author's data: V, VI, VII - the vapor-air mixture - Renker's data.

in this case of the resistance to mass transfer of the condensing components in the gas phase. The presence in steam of even negligible admixtures of air, as can be seen from Fig. 1, leads to a sharp reduction in the heat-transfer coefficient. This fact is characteristic for both vertical and horizontal ducts. Our experimental data do not reveal such a sharp dependence. The latter is connected with the considerably higher absolute values of the heat-transfer coefficient during condensation of pure steam as compared with the vapors of pure hydrocarbons.

Other conditions being equal, the higher the heat-transfer coefficient during filmwise condensation of pure vapors of one substance or another the more sharply is expressed the negative effect on the heat transfer of the noncondensing admixtures with very small concentrations of them.

It should also be noted that the methane, ethane, and propane are adjacent substances in the homologous series of saturated hydrocarbons. Because of this, methane and ethane dissolve relatively well in liquified propane. The thermal effect of absorption of the inert admixtures of methane and ethane by the condensing propane is very insignificant, since the heat of absorption of these hydrocarbons under the given conditions is lower than the latent heat of condensation of propane, and their quantity by weight in the condensate did not exceed 2% of the total amount of the forming liquid phase. Therefore, in determining the coefficient α_H , the heat effect of absorption was not examined separately. However, the higher solubility of the admixtures in the condensate under our conditions also, in some measure, smoothed their negative effect on heat transfer.

Reference work [2] shows that, with the exception of the very high percents of vapor contents and low flow rates, the type of admixtures has less effect on the heat-transfer coefficient during condensation than their content in the mixture. Extending conclusion reached to our experiments, it can be assumed that the effect of methane, ethane, or their mixture, on the condensation of propane, other conditions being equal, (identical rates and one and the same content of propane in the mixture) is approximately equivalent.

Figure 2 depicts graphs of the dependence of heat-transfer coefficient α_H on temperature difference Δt . As can be seen from these graphs, with inlet velocity $w_0 = 2.54$ m/s, the

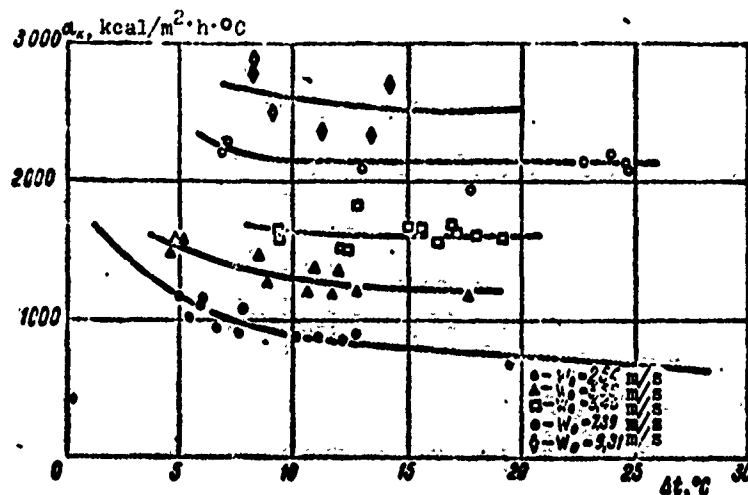


Fig. 2. Dependence of coefficient α_k on temperature difference.

experimental heat-transfer coefficients practically coincide with the calculated in Nusselt's equation for a motionless vapor (lower curve). At higher speeds, α_k becomes almost independent of Δt . The connection between the averaged values of heat flow, the heat-transfer coefficient, and inlet velocity for a pure vapor can be presented in the following equation:

$$q = \frac{(w_0 \rho_v) N r d}{4l} \quad (1)$$

or

$$\alpha = \frac{(w_0 \rho_v) N r d}{4l \Delta t}, \quad (2)$$

where w_0 - input flow rate, m/s; ρ_v - vapor density, kg/m³; l - length of the working zone of the tube, m; d - diameter of the tube, m; N - degree of condensation.

The value of N is defined as $N = \frac{G_H}{G}$, where G - the overall mass flow rate, kg/h.

As a result of experiment, it came to light that a change in heat flow q at constant inlet velocity of the vapor (when $w_0 > 2.54$ m/s) leads to a proportional change in the values of N and Δt , i.e., the mean heat-transfer coefficient α_H remains constant. In order to estimate the effect of the flow rate on coefficient α_H , the experimental data of this paper were compared with that calculated according to Hartmann's equation (Fig. 3). This equation was obtained on the assumption that the motion of the film of condensate is laminar and the flow of the vapor turbulent, and takes the following form [3]:

$$Nu = 0,36 Re_n^{0,6} \left[K Pr \frac{d}{l} \right]^{0,333} \times \left[\frac{\rho_n}{\rho_H} \left(\frac{v_n}{v_H} \right) \right]^{1,2}. \quad (3)$$

Here

$$Nu = \frac{\alpha_H d}{\lambda_H}, \quad Re_n = \frac{w_0 d}{\nu_n}, \quad Pr = \frac{c_{pH} \mu_H}{\lambda_H}, \quad K = \frac{r}{c_{pH} \Delta t},$$

where λ_H , c_{pH} , μ_H - in accordance with the conventional designations for thermal conductivity, heat capacity, and viscosity of the condensate; ρ_n , ρ_H - density of vapor condensate respectively; ν_n , ν_H - kinematic viscosity of vapor and condensate respectively.

The experimental points in Fig. 3 are located significantly higher than those calculated by equation (3), i.e., the effect of velocity on the heat-transfer coefficient α_H under actual conditions is expressed to a greater degree than is predicted by

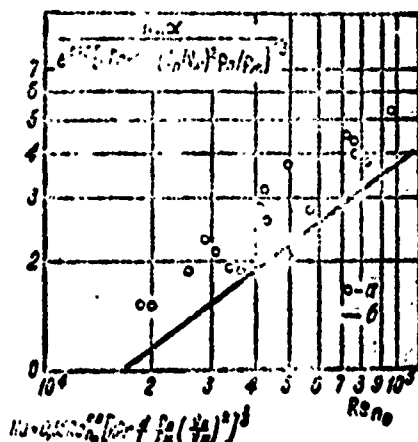


Fig. 3. Comparison of experimental data with that calculated by Hartmann's equation [3]:
a - experimental points; b - according to Hartmann's equation.

by equation (3). Let us note that these disagreements can be connected with the assumption accepted in [3] in regard to the laminar conditions of motion of the condensate film. For a quantitative estimation of the effect of velocity, the experimental data were treated in the form of the dependence of the ratio of the heat-transfer coefficients of moving and motionless vapors α_K/α_{Nu} on the complexes:

$$\Pi_w = \frac{w^2 \rho_n^2 Nu}{g \rho_c^2 d} \quad \text{and} \quad \Pi_d = \frac{w^2 \rho_n}{g \rho_c d}.$$

Let us note that both these complexes are connected with each other by the relationship:

$$\Pi_w = \Pi_d Nu_{nn}.$$

where $Nu_{nn} = \frac{\alpha_{Nu} d}{\lambda_K}$ - Nusselt's criterion for a motionless vapor;
 α_{Nu} - the heat-transfer coefficient for a motionless vapor, determined from Nusselt's theoretical formula. Analysis of the obtained dependences separately from the complexes Π_w and Π_d

showed the possibility of single valued treatment only from the complex Π_d . The results of this treatment are represented in Fig. 4. The spread of the experimental points on the graph in Fig. 4 does not exceed $\pm 25\%$. From Fig. 4 it follows that with values of the complex $\Pi_d \leq 2.6$, the effect of velocity on the heat-transfer coefficient can be disregarded, taking it as equal to the heat-transfer coefficient for a motionless vapor α_{Nu} .

With $\Pi_d > 2.6$, the effect of the flow rate can be taken into account according to the equation describing the experimental data dependences depicted in Fig. 4:

$$\alpha_k / \alpha_{Nu} = 0.68 \Pi_d^{0.43} \quad \text{with } \Pi_d = 2.6 - 30. \quad (4)$$

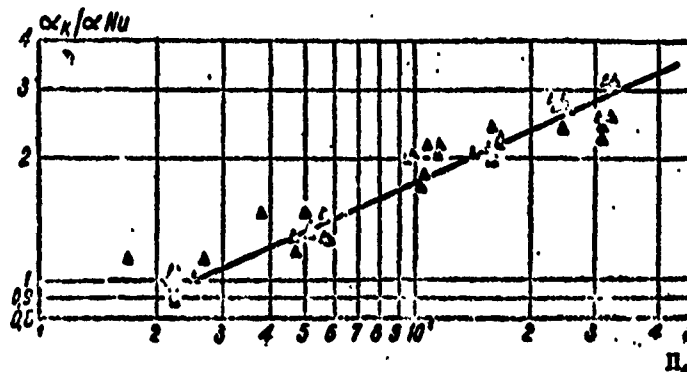


Fig. 4. Dependence of α_k / α_{Nu} on the complex Π_d .

A STUDY OF HEAT TRANSFER DURING CONDENSATION OF A MULTICOMPONENT HYDROCARBON MIXTURE

During the condensation of a multicomponent mixture, the total heat flow from the vapor side (without allowing for the heat of the cooling of the condensate) is determined by the following equation [4]:

$$q = \alpha_L \Delta t_{s-sa} + \frac{\lambda_s \Delta t_{s-sa}}{x_s} r_{cu}. \quad (5)$$

where α_L - the heat-transfer coefficient characterizing the transfer of the physical heat of cooling of the mixture, kcal/m²·h·°C; β_K - the coefficient of mass transfer of the condensing component of the mixture, m/h; $\Delta t_{\text{ж-пл}}$ - the difference in temperature in the bulk of the mixture and on the condensation surface, °C; Δc_K - the difference in mole concentrations of the condensing component in the bulk of the mixture and on the condensation surface, kmole/m³; x_K - the mole fraction of the condensing component in the condensate forming in a given section, kmole/kmole; r_{cm} - the latent heat of condensation of the mixture, kcal/kmole.

In this way, for determining the required surface during the designing of condensers for complex mixtures, it is necessary to estimate the values of coefficients α_L and β_K . In connection with this, the treatment of the experimental data obtained as a result of the study of condensation of multicomponent mixture was reduced to determining the actual coefficients of heat transfer and mass transfer (as applied to the condensing components of the mixture) and development of the effect on them of the basic determining factors. Let us note that the latter includes the mean mass flow rate of the longitudinal and cross flows of the substance, the composition of the mixture and its thermal and diffusion properties. In [4] it is shown that the criterial equations for describing the concurrent processes of heat and mass transfer during condensation of multicomponent vapor-gas mixtures should take the following form:

for mass transfer as applied to the condensing component of the mixture

$$Nu_{D_K} II_K = f(Re_x, Ar, Re_y, Pr_{D_K}), \quad (6)$$

for heat transfer

$$Nu = G(Re_{\infty}, Ar, Pr, K_t). \quad (7)$$

In equations (6) and (7) the criterion Re_y and complex K_t reflect the effect of the cross flow of mass on the fields, of velocities, temperatures, and concentrations. The complex Π_K in equation (6) characterizes the distribution of the condensing component between the condensate and the equilibrium vapor.

Below the results are noted on the research on heat exchange during condensation of multicomponent hydrocarbon mixtures. The data taken for processing were those for which the material balance was reduced to within 10%, and the heat balance - to 15-18%. The convergence of material balance was checked component-wise. The specific heat flow was determined from the equation:

$$q = \frac{G_1 I_1'' - (G_2 I_2'' + (G_1 - G_2) I_2')}{F_{\text{tp}}},$$

where G_1 - the weight quantity of the initial mixture, kg/h;

I_1'' - the enthalpy of the initial mixture on inlet to the tube, kcal/kg; G_2 - the weight quantity of the vapor-gas mixture on outlet from the tube, kg/h; I_2'' - the enthalpy of the vapor-gas mixture on outlet from the tube, kcal/kg; I_2' - the enthalpy of the condensate, kcal/kg.

For each experiment diagrams were constructed of the change in the temperature of the flow core and wall of the tube over its length, from which the mean-integral temperature differences $\Delta t_{\text{R-CT}}$ were determined. In this way, for each experimental

condition it was possible to determine the conditional heat-transfer coefficient α_{ycl} by the equation;

$$\alpha_{ycl} = \frac{q}{\Delta t_{n-cl}}.$$

Subsequently, the components of the overall heat flow were estimated from the following equations:

$$\begin{aligned} q &= q_{снр} + q_{рвн.г} + q_{рвн.ж}; \\ q_{снр} &= \frac{(G_1 - G_2) r_{сн}}{F_{np}}; \\ q_{рвн.г} &= \frac{G_1 + G_2}{2F_{np}} (I_1' - I_2''); \\ q_{рвн.ж} &= \frac{G_1 - G_2}{2F_{np}} (I_1' - I_2'). \end{aligned}$$

where $q_{снр}$ - the flow of latent heat of condensation of the mixture, kcal/m²·h; $q_{рвн.г}$ - the flow of the apparent sensible heat of cooling of the mixture, kcal/m²·h; $q_{рвн.ж}$ - the heat flow being taken away from the condensate during its cooling, kcal/m²·h; I_1' - the enthalpy of the condensate at the dew point of the mixture, kcal/kg.

From the overall heat flow q taking into account the effect of flow rate (see Fig. 4) the heat-transfer coefficient through the film α_n was determined. In so doing, the thermophysical properties of the condensate (viscosity, thermal conductivity, specific weight) were calculated taking into account its fractional composition. The heat-transfer coefficient α_L was defined as $\alpha_L = \frac{q_{рвн.г}}{\Delta t_{n-ж}}$, and the value of the mean temperature difference between the flow core and phase boundary $\Delta t_{я-пл}$ was calculated

from the total temperature difference Δt_{R-CT} and the mean temperature difference in the film $\Delta t_{\Pi n-CT}$:

$$\Delta t_{R-nA} = \Delta t_{R-CT} - \Delta t_{nA-CT},$$

where

$$\Delta t_{nA-CT} = \frac{q}{\alpha_k}.$$

The treatment of experimental data on the heat exchange in final form was reduced to development of a criterional function according to equation (7). The treatment of the experimental data on mass transfer has not been finished at the present time, and therefore the results of the study in this direction are not examined. For each experiment, in accordance with (7) the following criteria and parametrical complexes were determined:

$$Re_x = \frac{w_{cp} \rho d}{\mu}; \quad Re_y = \frac{J d}{\mu g}; \quad Pr = \frac{g \mu c_p}{\lambda}; \quad Pr_{D_1} = \frac{\mu}{\rho D_1};$$

$$K_i = \sum_{i=1}^n \frac{\Delta z_i}{Pr_{D_1}} \cdot \frac{c_{p1}}{c_p}; \quad Nu = \frac{\alpha_L d}{\lambda},$$

where w_{cp} - the average speed of the vapor-gas mixture in the tube, m/s; J - the density of cross flow of the substances, kg/m²·h; Pr_{D_1} - Prandtl's diffusion number; Δz_i - difference in mass concentrations of the i -component of the mixture in the flow core and on the interface, kg/kg; c_{p1} - heat capacity, kcal/kg·°C, i - component of the vapor-gas mixture; c_p - heat capacity of the vapor-gas mixture, kcal/kg·°C; ρ , μ , λ - in accordance with the conventional designations, density, viscosity,

and thermal conductivity of the vapor-gas mixture; g - gravity acceleration, m/s^2 ; n - number of components in the mixture.

The value of J was determined from the quantity of forming condensate, i.e., $J = G_1 - G_2 / F_{TP}$. Determination of the coefficients of molecular transfer (thermal conductivity, viscosity, and the generalized diffusion coefficients), and also certain thermophysical properties (specific heat, density, enthalpy) of the multicomponent hydrocarbon mixture was made on the basis of the thermodynamic law of corresponding states according to the methods expounded in [5], at the mean temperature on tube of the mixture in the flow core and according to its averaged working composition.

To estimate the effect of condensation of the mixture on coefficient α_L first a series of experiments was conducted without condensation ("dry" heat exchange) on natural gas containing from 2.7 to 3.72% propane and butane. The results of these experiments are given in Table 2.

The obtained heat-transfer coefficients during "dry" heat exchange α_c are generalized criterially in the form of the dependence:

$$Nu Pr^{0.33} = f(Re_x).$$

In Fig. 5 data are also plotted for conditions of simultaneous condensation. The results of experiments in thermal conductivity during condensation are given in Table 3. From Fig. 5 it is evident that condensation of the mixture leads to a considerable increase in the heat-transfer coefficient α_L at the same mean flow rates. The latter is connected with the effect on the

Table 2.

Pressure, atm(abs)	Total flow, Nm ³ /h	Rate, m/s	Dry gas composition				q_{cp} , kcal/m ² ·h	Temperature difference $\Delta t_{n.ct}$, °C	Heat-transfer coefficient α_L , kcal/m ² ·h	Nu number	Pr number	Re _x number
			CH ₄	C ₂ H ₆	C ₃ H ₈	C ₄ H ₁₀						
20	2.0	0.59	92.0	4.28	2.19	1.53	2120	22.04	96.1	26.4	0.803	8230
20	2.02	0.6	93.32	3.7	2.19	0.79	2030	25.57	79.9	23.7	0.892	8500
20	3.92	1.17	91.91	4.21	2.0	1.88	3860	22.27	170	46.7	0.806	16000
20	6.0	1.81	93.3	3.88	2.05	0.77	6060	23.7	236	68	0.778	23600
20	7.9	2.35	93.1	3.9	2.0	1.0	6350	21.05	302	82.8	0.813	31000
20	3.95	1.2	93.32	3.6	2.29	0.79	3770	23.237	162.5	47.3	0.87	16700
20	5.95	1.78	92.74	3.67	2.27	1.33	6030	25.79	233	67.6	0.89	24300
20	7.99	2.37	94.5	2.8	2.04	0.66	7650	27.54	278	80.6	0.91	31600

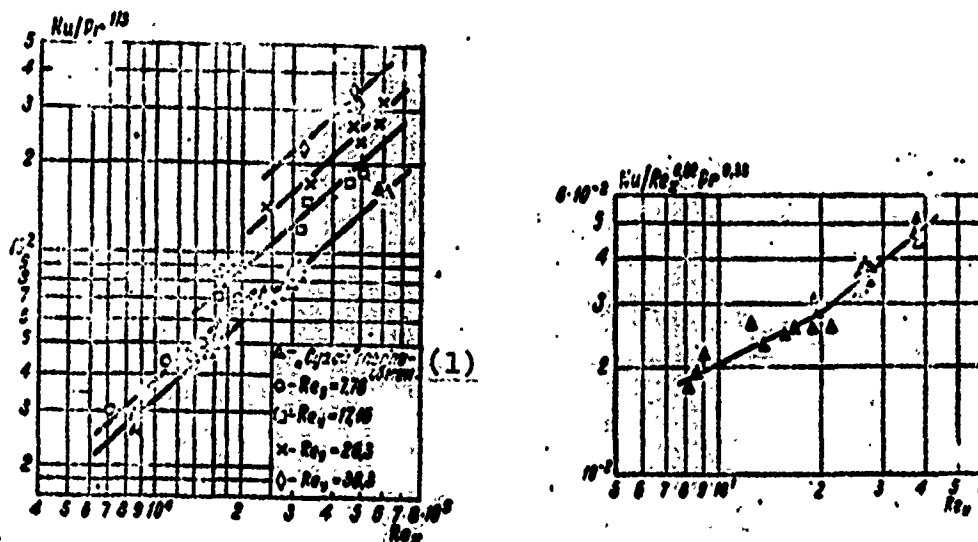


Fig. 5. Dependence of complex $Nu/Pr^{1/3}$ on Re_x and of complex $\frac{Nu}{Re_x^{0.82} Pr^{0.38}}$ on Re_y .

KEY: (1) "Dry" heat exchange.

intensity of heat transfer of the cross flow of the substance approaching the phase interface. Other conditions being equal, the higher the density of cross flow of the substance J , the greater the heat-transfer coefficient α_L . Let us note that the change in the total density of cross flow is determined by the corresponding change in the composition of the initial mixture and the inlet flow rate. The straight lines in Fig. 5 were divided into layers according to the constant values of the criteria of cross flow $Re_y = \text{const}$ and were arranged parallel to lines characterizing "dry" convective heat exchange.

In this way, the effect of the Re number of the longitudinal flow during condensation was kept the same as in the case of "dry" heat exchange. For development of the degree of effect of the criterion of cross flow, there was constructed a generalized graph of the dependence of $\frac{Nu}{Re_x^{0.82} Pr^{0.38}}$ on Re_y depicted on right

side of Fig. 5. From this graph it is evident that the effect of the density of cross flow on coefficient α_L is exhibited

Table 3.

Forward flow pressure, atm(abs)	Total flow rate, V_0 , Nm ³ /h	Flow rate for liquid V_M , Nm ³ /h	Degree of condensation N	Initial mixture, % by volume				Liquid, % by volume				Average velocity w_{CD} , m/s
				CH ₄	C ₂ H ₆	C ₃ H ₈	C ₄ H ₁₀	CH ₄	C ₂ H ₆	C ₃ H ₈	C ₄ H ₁₀	
20,4	4,01	1,14	0,386	59,6	3,04	34,89	2,47	14,85	4,78	74,35	6,02	1,375
20	7,17	1,36	0,190	67,94	4,01	23,65	4,4	14,09	4,7	65,7	15,55	2,66
20	7,79	1,34	0,172	68,1	3,34	26,0	2,64	12,84	4,7	73,32	9,14	2,96
20	8,5	1,83	0,215	71,32	2,74	20,58	5,36	14,95	4,76	61,6	18,79	3,07
20	2,833	0,823	0,291	66,1	2,64	25,91	5,35	17,35	4,63	61,52	16,5	0,97
20	3,013	0,97	0,323	64,3	2,64	27,12	5,94	16,85	4,77	63,65	14,73	1,02
20	5,954	1,961	0,33	64,1	3,55	25,98	6,37	12,0	4,14	55,51	28,35	2,04
20	5,945	0,95	0,16	76,23	3,24	14,69	5,84	15,3	5,05	46,08	33,57	2,22
20,2	5,79	0,79	0,136	78,5	3,62	11,5	6,3	16,5	6,05	38,95	38,5	2,21
20	7,974	1,166	0,147	70,55	3,04	20,83	5,58	10,22	4,42	49,59	35,77	2,96
20	9,39	1,319	0,14	69,98	2,89	22,98	8,15	11,6	3,98	53,14	31,28	3,6
30	1,291	0,25	0,194	72,18	2,93	21,19	4,7	18,51	5,75	57,62	18,12	0,32
30	9,098	0,972	0,107	79,56	3,41	8,5	8,53	15,4	6,03	35,98	42,59	2,35
30	9,052	0,933	0,103	81,39	3,28	8,38	6,95	15,11	5,55	36,39	42,95	2,35
20	2,23	0,428	0,184	65,25	3,07	24,88	6,8	20,22	2,14	53,37	23,57	0,864
20	2,188	0,513	0,246	55,72	2,68	29,69	11,91	8,62	3,09	55,76	32,53	0,83
20	2,013	0,686	0,34	58,4	2,12	30,14	9,34	7,4	2,78	61,3	28,52	0,72
21	1,995	0,361	0,181	66,1	1,5	21,55	10,85	8,96	2,34	47,42	41,1	0,755
21	8,29	1,16	0,14	69,0	1,48	15,72	13,8	10,7	2,68	40,62	46,0	3,4
21	8,14	1,71	0,21	63,2	3,34	22,05	11,41	10,2	3,29	40,71	45,8	3,07
20	3,426	0,413	0,12	77,6	2,6	14,4	5,4	10,9	3,74	62,8	22,56	1,31
21	5,103	1,122	0,22	58,6	3,0	25,56	12,84	8,09	2,69	51,78	37,44	2,01

Table 3. cont'd

Specific thermal load $q_{\text{нш}}, \text{kcal/m}^2 \cdot \text{h}$	$q_{\text{ср}}, \text{kcal/m}^2 \cdot \text{h}$	$q_{\text{нш}}, \text{kcal/m}^2 \cdot \text{h}$	Mean temperature difference $\Delta t_{\text{н-ср}}, ^\circ\text{C}$	Mean temperature difference $\Delta t_{\text{н-ср}}, ^\circ\text{C}$	Mean temperature difference $\Delta t_{\text{н-пн}}, ^\circ\text{C}$	Heat-transfer coefficient $\alpha_{\text{нш}}, \text{kcal/m}^2 \cdot \text{h} \cdot ^\circ\text{C}$	Heat-transfer coefficient $\alpha_{\text{н}}, \text{kcal/m}^2 \cdot \text{h} \cdot ^\circ\text{C}$	Heat-transfer coefficient $\alpha_{\text{л}}, \text{kcal/m}^2 \cdot \text{h} \cdot ^\circ\text{C}$	Nu number	Pr number	Re _x number	Re _y number
14950	9545	5290	28,38	17	11,38	527	883	465	119	0,785	23200	27,4
19300	10680	7420	27,51	15	12,51	700	1270	595	178	0,77	40000	26,3
19640	9250	9530	23,99	15	8,99	820	1335	1048	250	0,797	47000	26,7
26900	14564	12100	30,54	20	10,54	882	1300	1150	304	0,8	48200	37,9
10850	5805	4140	29,31	12	17,31	370	870	257	66	0,775	16200	16,8
12100	6570	4960	29,44	14	15,44	412	850	321	82	0,781	16600	19,1
23000	14420	7130	29,068	20	9,068	791	1090	792	202	0,765	32500	36,5
15400	6607	8430	28,36	12	16,36	544	1250	516	132	0,8	32300	19,45
13600	5580	7700	28,14	10	18,14	483	1330	424	109,2	0,813	31200	15,8
23000	9300	12500	30,708	15	15,708	750	1440	795	203	0,793	47000	25,5
27900	9350	16300	31,84	16	15,84	877	1825	1028	286	0,9	57000	26,9
4070	1659	2180	22,632	3,1	19,532	180	1290	112	29	0,96	6920	5,35
19300	7210	11400	30,54	14	16,54	634	1370	690	178	0,85	51000	21,3
17100	7497	9300	30,695	15	15,695	555	1130	592	152	0,77	46100	19,2
4160	2851	1220	10,73	4	6,73	398	1192	182	45	0,73	14500	8,6
9750	4136	4750	30,5	10,2	20,3	320	960	234	59,5	0,752	13800	12,6
9830	6008	3120	23,17	10,6	12,57	424	920	296	64,5	0,75	11100	13,9
5750	2614	2570	22,26	5	17,26	258	1140	149	37,9	0,785	12400	8,1
21500	9054	11820	24,52	12,5	12,32	665	1730	960	245	0,762	52500	26,2
30700	13620	15300	32,13	20,7	11,13	955	1480	1340	312	0,835	44000	38,8
8900	3241	5440	29,85	9	20,85	298,5	1060	261	67	0,8	19500	9,02
19800	8665	9840	33,38	18	15,38	581	1060	640	163	0,736	33000	25,2

dissimilarly: to a lesser degree in the range of Re_y from 8 to 20 and to a greater extent in the range of Re_y from 20 to 40. The experimental data obtained on heat transfer during condensation of the mixture can be described by the following criterial equations:

$$Nu = 0,0068 Re_x^{0,42} Re_y^{0,48} Pr^{0,33} \quad \text{with } Re_y \text{ from 3 to 20;} \quad (8)$$

$$Nu = 0,00242 Re_x^{0,62} Re_y^{0,78} Pr^{0,33} \quad \text{with } Re_y \text{ from 20 to 40.} \quad (9)$$

In equations (8), (9) the Re_x number changed from 7000 to 57,000, the Pr number - from 0.73 to 0.9. Complex K_t for all experiments changed very insignificantly, therefore its effect on the intensity of heat transfer as yet has not been examined.

Equations (8) and (9) can be converted if we separate the dependence on the determining criteria only of the ratio α_L/α_c . In this case, the obtained equations will take the following form:

$$\alpha_L/\alpha_c = 0,313 Re_y^{0,19} \quad \text{with } Re_y \text{ from 8 to 20;} \quad (10)$$

$$\alpha_L/\alpha_c = 0,112 Re_y^{0,70} \quad \text{with } Re_y \text{ from 20 to 40,} \quad (11)$$

where α_c - the corresponding heat-transfer coefficient during "dry" heat exchange.

Let us note that the portion of the apparent heat of cooling of the mixture can, during the condensation of hydrocarbon mixtures, reach 50% and more of the overall heat flow (see Table 3). Therefore, the calculation of this component of heat flow in determining the required surface of the condenser is very important.

BIBLIOGRAPHY

1. Л. Э. Берман. О кинетике при высокой температуре диссоциации газа. Тетраэдрон, 1949, № 7.
2. Renker, Chem. Technik, VIII, Bd. 7, 1938, № 8.
3. H. Hartmann. Chem. — Ing. — Technik, Bd. 33, 1961, № 3.
4. А. Д. Двойне, О. А. Беньячинович. Труды ВИННИГАЗа, 1968, в печати.
5. В. М. Платонов, Я. Д. Монко. Прикладная термодинамика смесей легкого углеводорода. ГосИИТИ, 1959.

Reproduced from
best available copy.